4/6

~~CONFIDENTIAL~~
~~RESTRICTED DATA~~
~~Atomic Energy Act - 1954~~

RECORD COPY

SNPO-C

WANL-TNR-199

April 1965

Westinghouse Astronuclear Laboratory

NOTICE
This report was prepared as an account of work sponsored by the United States Government. Neither the United States nor the United States Energy Research and Development Administration, nor any of their employees, nor any of their contractors, subcontractors, or their employees, makes any warranty, express or implied, or assumes any legal liability or responsibility for the accuracy, completeness or usefulness of any information, apparatus, product or process disclosed, or represents that its use would not infringe privately owned rights.

Prepared by :

L. BOMAN

Reactor Analysis Department

EXCLUDED
UNCLASSIFICATION

Classification cancelled ~~or changed to~~ _____
by authority of
H.A.C. SEP 1973

~~INFORMATION CATEGORY~~
~~CR~~
~~B~~ 5-5-65
~~Authorized Classifier~~ Date

WANL-TNR-199

DISTRIBUTION OF THIS DOCUMENT IS UNLIMITED

ANALYSIS OF NRX-A2

MASTER

REACTOR TEST RESULTS

(Title Unclassified)

~~CONFIDENTIAL~~
~~RESTRICTED DATA~~
~~Atomic Energy~~

RECORD COPY

DISTRIBUTION OF THIS DOCUMENT UNLIMITED

ACKNOWLEDGMENTS

The following members of Reactor Analysis contributed directly to the preparation of this document.

C. R. Blivin
L. Boman
M. A. Capo
G. E. Cort
R. A. Doncals
J. C. Guzek
W. L. Howarth
W. L. Knecht
A. Y. Lee
E. E. Menge
A. I. Miller
A. L. Mowery
L. Ortenberg
T. P. Speis
L. D. Stephenson
H. Woodsum

CHAPTER 1 *INTRODUCTION*

CHAPTER 2 *BACKGROUND*

CHAPTER 3 EXPERIMENTAL PLANS I, II, & III

THERMAL and FLUID FLOW 3-3

Gaseous Hydrogen Test 3-3
Test Chronology and Description 3-3
Reactor Performance 3-6
Core 3-8
Reflector System 3-8
Nozzle 3-8

Liquid Hydrogen Test 3-12
Test Chronology and Description 3-12
Reactor and Feed System 3-14
System Temperatures 3-17
System Pressures 3-17
Reflector Material Temperatures 3-24

Temperature Coefficient Test - EP II 3-24
Test Chronology and Description 3-24
Temperatures 3-24

NUCLEAR 3-27

EP-1A Test 3-27
Approach to Criticality 3-27
Peripheral Poison Wire Removal 3-27
Central Poison Wire Removal 3-36
Differential and Integral Drum Bank Worth 3-44
Delayed Critical Drum Bank Position Without Nozzle 3-48
Worth of Individual Drums 3-53
Effect of Paraffin Block on Drum Worth 3-53
Reflector System Material Symmetry 3-56
Further Study 3-56
Conclusion 3-62
Calibration of Control Drum Number 2 3-62

EP-1B Test 3-63
Cold Critical Drum Position 3-63
Gaseous Hydrogen Test 3-63
Evaluation of Hydrogen Worth 3-67
Evaluation of Initial Offset 3-69
Liquid Hydrogen Test 3-71

EP-II Test 3-71
Delayed Critical Position 3-71
Neutronic Power Calibration 3-71
Wire Calibration 3-71
Rabbit Calibration 3-77
Neutronics Tank Calibration 3-78
Temperature Coefficient Measurements 3-79
Calibration of Control Drum 2 3-83

EP-III Test 3-83
Delayed Critical Position 3-83
Temperature Coefficient 3-83

CHAPTER 4 EXPERIMENTAL PLAN IV-POWER TEST

TEST DESCRIPTION 4-1

PRECHILL 4-8

Thermal and Fluid Flow 4-8
Reactor 4-8
Core 4-10
Reflector 4-10
Nuclear 4-18
Delayed Critical Bank Position 4-18

HIGH POWER HOLDS 4-18

Thermal and Fluid Flow 4-19
Power Determination 4-19
Reactor and Feed System Conditions 4-25
Core 4-25
Core Inlet Temperatures 4-28
Core Pressure Measurements 4-31
Core Temperature Measurements 4-32
Thermocouples 4-32
Thermal Capsules 4-35
Multiple Regression Fit of Measured Core Temperatures 4-45
Post-test Calculation of Core Operating Conditions 4-55
Pressure Drop and Axial Temperature Distribution Calculation 4-55
Radial Temperature Variation 4-66
Maximum Calculated Fuel Temperatures 4-71
Tie Rod Temperatures 4-73
Reflector 4-80
Reflector System Coolant Temperatures and Pressures at the Highest Power Hold, CRT 14085 4-82

Reflector System Power Comparison at Various Power Holds 4-88
Reflector Inlet and Outlet Plenum Temperature Azimuth Measurements 4-91
Material Temperatures 4-91
Lateral Support System 4-101
Nozzle 4-105

Nuclear 4-107
Feedback Reactivity 4-107
Implications of Differences Between Measured and Calculated Drum Bank Position 4-109
Reactor Power 4-109
Correction Factors 4-109
Estimated Accuracy of the Data 4-115

STARTUP AND SHUTDOWN 4-118

Thermal and Fluid Flow - Startup 4-118
Reactor 4-118
TNT Calculations and Measured - Startup 4-123
Core - Startup Period 4-124
Reflector - Startup 4-124

Thermal and Fluid Flow - Shutdown 4-130

Nuclear 4-140

Shutdown 4-140

COOLDOWN 4-141

CHAPTER 5 EXPERIMENTAL PLAN V

LOW POWER MAPPING TEST

TEST OBJECTIVES, DESCRIPTION AND CHRONOLOGY STEADY STATE OPERATING CONDITIONS - THERMAL 5-1

Thermal and Fluid Flow - Analysis of Data 5-5

Thermal and Fluid Flow - Comparison with TNT Calculations 5-10

FIXED DRUM TEST TRANSIENT REACTOR OPERATION - THERMAL 5-12

Thermal and Fluid Flow - Comparison of Data with TNT Calculations 5-12

NUCLEAR CONSIDERATIONS 5-14
Delayed Critical Bank Position 5-14
Feedback Reactivity 5-14

CHAPTER 6 REVIEW OF NUCLEAR DATA

ANTICRITICALITY SYSTEM 6-1
CONTROL WORTH 6-1
CRITICALITY MEASUREMENTS 6-1
Pretest Conditions 6-1
Material Loss in EP-IV 6-2
Apparent Reactivity Loss in EP-V 6-4
Accuracy of Critical Bank Measurements 6-5
Operating Reactivity Changes 6-5
HYDROGEN WORTH 6-6
TEMPERATURE COEFFICIENT 6-6
NUCLEAR PROBLEM AREAS 6-7

CHAPTER 7 REVIEW OF THERMAL DATA

PERFORMANCE 7-1
EP-IV Test 7-1
EP-V Test 7-2
CORE 7-2
Core Material Temperatures 7-2
Core Pressure Drop 7-3
Tie Rod Exit Gas Temperatures 7-4
REFLECTOR, SHIELD AND LATERAL SUPPORT 7-4
NOZZLE 7-5
THERMAL PROBLEM AREAS 7-6

CHAPTER 8 DOSIMETRY

EXPERIMENTAL PROGRAM 8-1

Dosimetry Methods 8-2

Dosimetry Placement 8-3

ANALYTICAL METHODS 8-10

Gamma Ray Dose Rates 8-10
Surface of the Pressure Vessel 8-10
Meridian Ring and Radial Traverse 8-11
Below the Privy Roof 8-12
Privy Roof Capture Gamma Rays 8-12
Wall Capture Gamma Rays 8-14
Gamma Rays Scattered from the Test Cell Wall and Pad 8-16
Direct Beam Dose Rates 8-17

Fast Neutron Fluxes and Dose Rates 8-18
Surface of Vessel, Meridian Ring, and Radial Traverse 8-18
Under the Privy Roof 8-19
Neutron Scattering From the Wall and Pad 8-20
Air Scattered Neutrons 8-20

Thermal and Epithermal Neutron Data 8-22

COMPARISONS OF EXPERIMENTAL AND CALCULATED GAMMA RAY DATA 8-25

Pressure Vessel Surface 8-25

Equatorial Ring 8-27

Meridian Ring 8-29

Radial Midplane 8-33

Below Privy Roof 8-35

Additional Locations 8-37

COMPARISONS OF EXPERIMENTAL AND CALCULATED FAST NEUTRON FLUX AND DOSE RATE 8-37

Pressure Vessel Surface 8-37

Equatorial Ring 8-42

Meridian Ring 8-46

Radial Midplane 8-52

Below Privy Roof 8-54

Additional Locations 8-60

COMPARISONS OF EXPERIMENTAL AND CALCULATED THERMAL AND EPITHERMAL FLUXES 8-62

CONCLUSIONS AND RECOMMENDATIONS 8-72

Gamma Ray Environment 8-72

Fast Neutron Environment 8-73

Thermal and Epithermal Neutron Data 8-75

Correlation of High Power vs Low Power Data 8-75

CHAPTER 9 POST-OPERATIVE EXAMINATION

RADIOCHEMISTRY 9-1

Radial Power Distributions from Post-Run Calculations, Measurements and Radiochemistry 9-1

Calculated and Measured Cold to Hot Power Change 9-3

Power Gradients Across Peripheral Fuel Elements Derived from Predictions, Radiochemistry and NRX-A2 PAX Measurements 9-14

Measured and Predicted Axial Power Distributions 9-15

RADIATION EXPOSURE FOR MAJOR REACTOR COMPONENTS 9-15

CORE ELEMENT EXAMINATION 9-22

Summary of Core Element Corrosion 9-22
Internal Fuel Elements 9-22
Peripheral Fuel Elements 9-25
Unfueled Elements 9-25

Summary of Cluster and Seal System Component Examination 9-26
Support Block 9-26
Pyrographite Insulating Sleeves 9-26
Pyro Cups, Stainless Steel Liner Tubes, Cluster Plates, Tie Rods and Orifices 9-26

LIST OF ILLUSTRATIONS

Figure		Page
	Frontispiece	
3-1	EP I Flow Test - Flow Rates	3-2
3-2	Temperature Coefficient Test Power Flow and Temperature	3-4
3-3	Ambient GH_2 Flow Test - Flow, Pressure and Control Drum Position	3-7
3-4	EP IB Ambient GH_2 Comparison of Pressures	3-9
3-5	EP IB Ambient GH_2 Comparison of Component Pressure Drop	3-10
3-6	EP IB Ambient GH_2 Nozzle Tube Inlet Pressure	3-11
3-7	Liquid H_2 Flow Schematic, Test Cell A	3-15
3-8	EP I-B 2nd LH_2 Test Flow Rate	3-16
3-9	NRX-A2 EP IB LH_2 Run Span of Reflector Inlet and Outlet Temperature: Time Histories	3-18
3-10	Core Inlet Temperature vs. Time, Second LH_2 Run EP I-B	3-19
3-11	Core Inlet Temperature vs. Azimuthal Position at Beginning and End of Flow Ramp, Second LH_2 Ramp	3-20
3-12	Reflector Inlet and Outlet Temperature vs. Azimuth at End of Prechill EP IB (CRT 26583.5)	3-21
3-13	NRX-A2 EP IB 2nd LH_2 Run: Reflector and Core Inlet and Exit Pressure Time Histories	3-22
3-14	NRX-A2 EP IB 2nd LH_2 Run: Core, Shield, and Reflector Pressure Drop Time Histories	3-23
3-15	NRX-A2 EP IB LH_2 Run Typical Outer Reflector Material Temperature Time Histories	3-25
3-16	EP II Temperature Coefficient Test, Axial Temperature Distribution in Core	3-28
3-17	Core Material Temperature EP II CRT 28000	3-29

LIST OF ILLUSTRATIONS (Continued)

Figure		Page
3-18	Core Material Temperature EP II CRT 28350	3-30
3-19	Poison Wire Loading Pattern for the NRX-A2	3-31
3-20	Reactor-Source-Detector Geometry for EP-IA of NRX-A2	3-32
3-21	Inverse Multiplication Versus Number of Peripheral Poison Wires Removed	3-34
3-22	Reactor-Source-Detector Geometry for PAX	3-35
3-23	Inverse Multiplication Versus Number of Poison Wires Remaining	3-39
3-24	Critical Drum Positions During Final Poison Wire Removal	3-41
3-25	Reactivity Worth of Poison Wires at the Core Center Circle	3-42
3-26	Shutdown of NRX-A2 Versus Number of Poison Wires Remaining in Center of Core With Drum Bank at 180°	3-43
3-27	NRX-A2 Control Drum Bank Differential Worth	3-46
3-28	NRX-A2 Integral Control Drum Bank Worth	3-47
3-29	Source Effects on Indicated Criticality	3-50
3-30	Effect of Paraffin Block on Drum Worth	3-55
3-31	NRX-A2, EP-1A Drum Worth Symmetry	3-62
3-32	Control Drum Number 2 Differential Worth	3-64
3-33	NRX-A2, EP-1B GH_2 Profile Measured Control Drum Bank Position Versus Time	3-66
3-34	NRX-A2 EP-1B Drum Bank Rotation Versus GH_2 Mass Flow Rate	3-68
3-35	NRX-A2, EP-1B Second LH_2 Run Control Drum Bank Position Versus Time	3-73
3-36	NRX-A2, EP-II, Measured Nuclear Average Temperature for Major Components	3-80

LIST OF ILLUSTRATIONS (Continued)

Figure		Page
3-37	NRX-A2, EP-II Control Drum Bank Rotation During Temperature Coefficient Tests	3-81
3-38	NRX-A2, EP-II Drum Bank Rotation Vs. Change in Nuclear Average Core Temperature	3-82
4-1	Power, Flow, and Temperature EP-IV	4-4
4-2	NRX-A2 EP IV Prechill and Startup Typical Reflector Inlet and Outlet Temperature Time Histories	4-11
4-3	Typical Core Temperatures vs. Time (Prechill)	4-12
4-4	Core Inlet and Dome End Temperatures vs. Azimuthal Position at End of Prechill (CRT 13693)	4-13
4-5	Reflector Inlet and Outlet Temperature vs. Azimuth at End of Prechill (CRT 13693)	4-14
4-6	NRX-A2 EP IV Control Drum, Vane, and Sector Temperatures at End of Prechill (CRT 13693)	4-15
4-7	NRX-A2 EP IV Inner Reflector Material and Seal Chamber Temperatures at End of Prechill CRT = 13693	4-17
4-8	NRX-A2 Cycle Conditions at Time CR 14085 Seconds	4-26
4-9	NRX-A2 Shimming Distribution and Instrumentation Placement	4-34
4-10	NRX-A2 EP-IV Core Material Temperature Histories	4-36
4-11	NRX-A2 Unfueled Element Thermal Capsule Family With Axial Temperature Distribution	4-39
4-12	X-ray of Unfueled Element Showing Fused Thermal Capsules	4-43
4-13	NRX-A2 Thermal Capsule Data Preliminary 19 Radial Positions in Core Central Region	4-44
4-14	NRX-A2 Thermal Capsule Data Preliminary 34 Radial Positions in Core Periphery	4-46
4-15	NRX-A2 Thermal Capsule Data Unfueled Element Temperature at 45 - Inches	4-47

LIST OF ILLUSTRATIONS (Continued)

Figure		Page
4-16	NRX-A2 Thermal Capsule Data Unfueled Element Temperature at 45 - Inches Sector - 1	4-48
4-17	Radial Plot of Station 45 Thermal Capsule Readings	4-49
4-18	NRX-A2 Filler Strip Thermal Capsule Family with Axial Temperature Distribution	4-50
4-19	Comparison of NRX-A2 Thermal Capsule Results with Post Run Calculations at High Power Hold	4-53
4-20	NRX-A2 EP IV Post-Test Calculated Flow Schematic CRT-14085 (1096 MW)	4-60
4-21	Axial Temperature Profile in Average Fueled and Unfueled Element CRT-13790 (581 MW)	4-62
4-22	Axial Temperature Profile in Average Fueled and Unfueled Element CRT-13900 (953 MW)	4-63
4-23	Axial Temperature Profile in Average Fueled and Unfueled Element CRT-13985 (1051 MW)	4-64
4-24	Axial Temperature Profile in Average Fueled and Unfueled Element CRT - 14085 (1096 MW)	4-65
4-25	NRX-A2 EP IV Calculated and Measured Radial Temperature Profile CRT-13900 (953 MW)	4-67
4-26	Tie Rod Exit Gas Temperature Profile EP IV	4-75
4-27	Location of Tie Rod Exit Gas Thermocouple	4-79
4-28	Typical Damaged Tie Rod Exit Gas Thermocouple	4-81
4-29	Reflector System Fluid Temperatures and Pressures for NRX-A2 EP-IV at CRT 14085	4-84
4-30	Temperatures, Flows, and Radiation Heating Rates in Shield and Support Plate at CRT 14085	4-85
4-31	NRX-A2 EP IV Inner Reflector Temperatures at CRT 14085	4-87

LIST OF ILLUSTRATIONS (Continued)

Figure		Page
4-32	Reflector Inlet Temperature vs Azimuth for the Four Power Holds of NRX-A2 EP IV	4-92
4-33	Reflector Outlet Temperature vs. Azimuth for the Four Power Holds on NRX-A2 EP IV	4-93
4-34	Outer Reflector Sector Material Temperature vs. Axial Position	4-94
4-35	Azimuth Sector Temperature Variation in NRX-A2 EP IV	4-95
4-36	Control Drum and Boral Vane Temperatures for NRX-A2 EP IV	4-97
4-37	NRX-A2 EP IV Inner Reflector Axial Temperature Variation	4-99
4-38	Comparison of Measured and Calculated Inner Reflector Temperature	4-100
4-39	NRX-A2 EP Lateral Support Hydrogen and Material Temperature at High Power Hold CRT 14085 (Measured and Calculated)	4-103
4-40	NRX-A2 EP IV Normalized Seal Chamber Pressure Distribution at High Power Hold CRT 14085	4-104
4-41	NRX-A2 EP IV Control Drum Bank Position During the High Power Test, Measured Calculated	4-110
4-42	Startup LH_2 Flow Lag	4-119
4-43	Power, Flow and Temperature Demands	4-120
4-44	NRX-A2 EP IV Startup Power and Nozzle Chamber Temperature	4-121
4-45	Core Material Temperatures and Tie Rod Exit Temperatures During Startup	4-122
4-46	Core Inlet Pressure and Core ΔP vs Time	4-125
4-47	NRX-A2 EP IV Prechill and Startup Reflector Inlet, Outlet and Differential Pressure Time Histories	4-126

LIST OF ILLUSTRATIONS (Continued)

Figure		Page
4-48	Pressure and Temperature to Illustrate Assembly at Reflector Inlet	4-127
4-49	Core Inlet Azimuthal Temperature Variation at CRT-13720 and CRT 13780	4-129
4-50	NRX-A2 EP IV Prechill and Startup Selected Inner Reflector and Control Drum Material Temperature Time Histories	4-131
4-51	NRX-A2 EP IV Prechill and Startup Selected Outer Reflector Material Temperature Time Histories	4-132
4-52	NRX-A2 Shutdown Nozzle Chamber Temperature	4-134
4-53	Shutdown Variables and Demands	4-135
4-54	Core Inlet Temperature Versus Time	4-136
4-55	Reactor Shutdown History	4-137
4-56	NRX-A2 EP IV Shutdown Station 45 Temperature Spike Anomaly	4-138
4-57	NRX-A2 EP-IV Shutdown Reactivity	4-139
4-58	NRX-A2 EP IV Cooldown Predicted and Actual Coolant Flow Rates	4-142
4-59	NRX-A2 EP IV Cooldown - Predicted and Actual Coolant Usage	4-144
4-60	Comparison Between Experimental And Calculated Decay Power During Cooldown Following EP IV	4-146
5-1	EP-V Low Power Mapping Test Low Power Performance Map	5-2
5-2	EP-V Low Power Mapping Test: Power, Flow, and Control Drum Position vs. Time	5-4
5-3	EP-V Low Power Mapping Test: Fixed Control Drums Power and Flow	5-13
5-4	EP-V Low Power Mapping Test: Fixed Control Drums Nozzle Chamber and Tie Rod Temperatures	5-15

LIST OF ILLUSTRATIONS (Continued)

Figure		Page
5-5	EP-V Low Power Mapping Test: Fixed Control Drums Reactor Plenum Pressures	5-16
5-6	Control Room Time-Seconds NRX-A2 EP-V Low Power Mapping Test	5-18
8-1	NRX-A2 Reactor Showing Meridian and Equatorial Ring and Dosimeter Placement on Vessel	8-5
8-2	Cross Sectional View, at Horizontal Midplane (Station 26) Looking Toward Dome	8-6
8-3	NRX-A2 Cross Sectional View Locating Dosimeter Positions on the Meridian Ring and on the Vessel Surface (Axial Placement)	8-8
8-4	Cross Sectional View at Horizontal Midplace (Station 26) Looking Toward Dome	8-9
8-5	Experimental and Calculated Gamma Ray Dose Rate on the Surface of the Pressure Vessel (Axial Traverse)	8-26
8-6	Experimental and Calculated Gamma Ray Dose Rate on the Surface of the Pressure Vessel (Circumferential Traverse)	8-28
8-7	Experimental and Calculated Gamma Ray Dose on the Equatorial Ring	8-30
8-8	Experimental and Calculated Gamma Ray Dose Rate on the Meridian Ring	8-32
8-9	Experimental and Calculated Gamma Ray Dose Rate as a Function of Distance from the Reactor	8-34
8-10	Experimental and Calculated Gamma Ray Dose Rates Under the Privy Roof Shield and at Test Car Location	8-36
8-11	Experimental and Calculated Fast Neutron Flux on the Surface of the Pressure Vessel (Axial Traverse)	8-39
8-12	Experimental and Calculated Fast Neutron Flux on the Surface of the Pressure Vessel (Circumferential Traverse)	8-41

LIST OF ILLUSTRATIONS (Continued)

Figure		Page
8-13	Experimental and Calculated Fast Neutron Flux on the Equatorial Ring	8-43
8-14	Experimental Fission Foil Data on the Equatorial Ring	8-45
8-15	Experimental and Calculated Neutron Sector 5 Feet from the Center of the Core on the Midplane, Reactor $\theta = 345^{\circ}$	8-47
8-16	Experimental and Calculated Fast Neutron Dose Rate on the Equatorial Ring	8-48
8-17	Experimental and Calculated Fast Neutron Flux on the Meridian Ring	8-49
8-18	Experimental Fission Foil Data on the Meridian Ring	8-50
8-19	Experimental And Calculated Fast Neutron Dose Rate on the Meridian Ring	8-51
8-20	Experimental and Calculated Fast Neutron Flux as a Function of Distance from the Reactor	8-53
8-21	Experimental Fission Foil Data ($0.004 < E < 0.75$ Mev) as a Function of Distance from the Reactor	8-55
8-22	Experimental Fission Foil Data ($0.75 < E < 1.5$ Mev) as a Function of Distance from the Reactor	8-56
8-23	Experimental Fission Foil Data ($1.5 < E < 2.5$ Mev) as a Function of Distance from the Reactor	8-57
8-24	Experimental and Calculated Fast Neutron Dose as a Function of Distance from the Reactor	8-58
8-25	Experimental and Calculated Fast Neutron Flux under the Privy Roof Shield and at Test Car Location	8-59
8-26	Comparison of Calculated and Measured Reaction Rates for Cobalt at the Surface of the Pressure Vessel ($E > 0.4$ ev)	8-64
8-27	Comparison of Calculated and Measured Reaction Rates for Copper at the Surface of the Pressure Vessel ($E > 0.4$ ev)	8-65

LIST OF ILLUSTRATIONS (Continued)

Figure		Page
8-28	Comparison of Calculated and Measured Reaction Rates for Gold at the Surface of the Pressure Vessel (E > 0.4 ev)	8-66
8-29	Comparison of Calculated and Measured Reaction Rates for Cobalt at the Surface of the Pressure Vessel (E < 0.4 ev)	8-67
8-30	Comparison of Calculated and Measured Reaction Rates for Copper at the Surface of the Pressure Vessel (E < 0.4 ev)	8-68
8-31	Comparison of Calculated and Measured Reaction Rates for Gold at the Surface of the Pressure Vessel (E < 0.4 ev)	8-69
9-1	Comparison of the Measured and Predicted Power Distributions Through Traverse 008 to J4M, Fissions Per Gram	9-4
9-2	Comparison of the Measured and Predicted Power Distributions Through Traverse 008 to J5L, Fissions Per Gram	9-5
9-3	Comparison of the Measured and Predicted Power Distributions Through Traverse 008 to J8D, Fissions Per Gram	9-6
9-4	Comparison of the Measured and Predicted Power Distributions Through Traverse 008 to J9T, Fissions Per Gram	9-7
9-5	Comparison of the Measured and Predicted Power Distributions Through Traverse 008 to J4M, Fissions Per CC	9-8
9-6	Comparison of the Measured and Predicted Power Distributions Through Traverse 008 to J5L, Fissions Per CC	9-9
9-7	Comparison of the Measured and Predicted Power Distributions Through Traverse 008 to J8D, Fissions Per CC	9-10
9-8	Comparison of the Measured and Predicted Power Distributions Through Traverse 008 to J9T, Fissions Per CC	9-11
9-9	Azimuthal Power Variations in the Peripheral Fuel Elements, Measurements and Predictions	9-12
9-10	Comparison of the Predicted and Observed (Cold PAX-Hot NRX-A2) Ratio of the Cold to Hot Power Distributions	9-13

LIST OF ILLUSTRATIONS (Continued)

Figure		Page
9-11	Peripheral Element Power Gradient, Element J3H	9-16
9-12	Peripheral Element Power Gradient, Element J4M	9-17
9-13	Peripheral Element Power Gradient, Element J5K	9-18
9-14	Peripheral Element Power Gradient, Element J6D	9-19
9-15	Comparison of the Measured and Predicted Axial Power Distributions	9-20
9-16	Predicted Radial Fission Distribution at 90° and 103.2°	9-21
9-17	NRX-A2 Region Description Showing Major Components	9-24
Appendix		
C-1	NRX-A Sleeve Type	C-4
E-1	Temperature Distribution in Unfueled Element at Station 32 With Flow Around Thermocouple	E-3

LIST OF TABLES

Table		Page
3-1	EP IB Ambient Hydrogen-Selected Test Chronology	3-5
3-2	Selected Chronology EP I-B LH_2	3-13
3-3	EP II Selected Chronology Temperature Coefficient Test	3-26
3-4	EP IA Poison Wire Removal Sequence	3-37
3-5	EP IA Inverse Multiplication Data	3-38
3-6	Differential Control Drum Bank Worth Data and Critical Bank Positions Following Poison Wire Removal for EP IA	3-45
3-7	Selected Drum Bank Measurements During EP IA	3-49
3-8	Factors Affecting the Critical Bank Position Expected in Other Tests	3-52
3-9	Drum Symmetry Verification, Method 2	3-54
3-10	Control Drum Cylinder	3-57
3-11	Outer Reflector Sectors	3-58
3-12	Control Plates	3-59
3-13	Drum Symmetry Verification, Method 1	3-60
3-14	Selected Drum Bank Measurements During EP IB	3-65
3-15	Comparison of Calculated and Measured Drum Rotation in the EP IB, GH_2 Test	3-70
3-16	Possible Effect of Pressurization	3-72
3-17	K Factors for Calibration of NRX-A2 Channels 12 and 13	3-75
3-18	NRX-A2 Neutronics Calibration Run EP II Uranium-Aluminum Wire Analyses	3-76
3-19	EP III Temperature Coefficient	3-84

LIST OF TABLES (Continued)

Table		Page
4-1	Limits Established for NRX-A2 Operation	4-3
4-2	Chronology NRX-A2 EP IV	4-5
4-3	NRX-A2 Extreme Operating Conditions	4-7
4-4	Reactor Conditions at the End of Prechill (CRT 13693) Predicted and Measured	4-9
4-5	EP IV High Power Test LH_2 Flow Rates and Nozzle Chamber Temperature	4-20
4-6	Details of Heat Balance Reactor Power Calculation, EP IV	4-23
4-7	EP IV Reactor Thermal Power at Steady State Holds	4-24
4-8	Average Core Inlet Temperature as Measured, After Heating Correction, and Calculated Based on Shield Dome End Measured Temperatures	4-30
4-9	Test Values and Post Test Calculations at Four Steady State Holds	4-33
4-10	List of Thermal Capsule Metals and Alloys	4-38
4-11	Thermal Capsule Family Distribution	4-40
4-12	Filler Strip Thermal Capsules	4-41
4-13	Multiple Regression Analysis of NRX-A2 Thermocouples, Station 45	4-54
4-14	Sample MCAP Printout - Sheet 1	4-56
4-15	Sample MCAP Printout - Sheet 2	4-57
4-16	Sample MCAP Printout - Sheet 3	4-58
4-17	Hot Channel Factors Considered in Analysis of Element to Element Temperature Variation	4-70
4-18	Hot Channel Considerations	4-72
4-19	Maximum Fuel Temperatures at High Power Hold CRT 14085 (1096 MW)	4-74

LIST OF TABLES (Continued)

Table		Page
4-20	Nominal Unfueled Element Thermal - Hydraulic Data, EP IV Test Conditions (14085 CRT)	4-76
4-21	Tie Rod Exit Gas Temperature Uncertainty Analysis EP IV Full Power Hold	4-78
4-22	Reflector System Hydraulic Model - Dimensional Data and Loss Coefficients	4-83
4-23	Comparison of Experimental and Calculated Pressures and Differential Pressures in the Reflector System	4-89
4-24	Calculated Reflector Heating Rates from ΔH and Flow Rate and Comparison to Nuclear Heating Rates	4-90
4-25	NRX-A2 EP IV Control Drum and Control Vane Temperatures	4-98
4-26	Miscellaneous Component Temperatures	4-102
4-27	Comparison of Test and Post Test Calculated Nozzle Tube Pressures and Temperatures at Holds	4-106
4-28	Comparison of Measured and Calculated Control Bank Position	4-108
4-29	Correction Factors for EP IV A for Buildup of Decay Gammas and Betas	4-112
4-30	Correction Factors for EP V For Buildup of Decay Gammas and Betas	4-112
4-31	Neutronic Power Indications During EP IVA	4-114
4-32	Comparison of Integrated Energy Release During NRX-A2 Tests	4-116
5-1	EP-V Low Power Mapping: Steady State Test Data	5-7
5-2	EP-V Low Power Mapping Test Comparison Between TNT Predictions and Test Data	5-11
5-3	Comparison of Calculated and Measured Control Drum Bank Position	5-17
6-1	Summary of Critical Control Drum Bank Positions	6-3

LIST OF TABLES (Continued)

Table		Page
8-1	Dosimeter Placement During Low and High Power NRX-A2 Runs	8-4
8-2	Experimental and Calculated Gamma Ray Dose Rate at Additional Locations	8-38
8-3	Experimental and Calculated Fast Neutron Flux at Additional Locations	8-61
8-4	Calculated and Measured Reaction Rates on the Lateral Surface of the Pressure Vessel at the Core Midplane	8-70
8-5	Calculated and Measured Cadmium Ratios Along Lateral Surface of the Pressure Vessel	8-71
9-1	Maximum Integrated Radiation Exposures for Neutrons (E > 1.0 mev) and Gamma Rays for Major Reactor Components	9-23
Appendix		
A-1	NRX-A2 Reactivity Equations	A-2
D-1	"U"-Tube S/N 9 Geometrical and Heat Transfer Data Supplied by Aerojet	D-2

Frontispiece. NRX-A2 Reactor Test Run
24 September 1964

CHAPTER 1

INTRODUCTION

The NRX-A2 reactor was tested at NRDS from 12 August 1964 to 15 October 1964. To determine operating conditions during the test and verify or upgrade analytical methods used in reactor thermal and nuclear design, an analysis of the test results was made. The test series consisted of experimental plans (EP's) as follows:

- EP IA. Initial criticality and control drum worth measurements
- EP IB. Initial automatic startups and ambient GH_2 and liquid hydrogen flow tests
- EP II. Neutronics calibration and temperature coefficient test
- EP III. Scaled-down power test
- EP IV. High power test
- EP V. Restart and low power mapping test

Maximum reactor operating conditions were 1096* MW reactor thermal power, 75.6 lb/sec LH_2 flow rate, and 3815°R average core exit gas temperature. Total energy generated during the high power test was 3.41×10^{11} watt-seconds or an average of 813 MW over the 7 minute test. Total energy generation for the test series was 3.81×10^{11} watt-seconds.

Chapters 6 and 7 of this report contain a review of the analysis of the thermal and nuclear test results, while Chapter 8 contains a review of dosimetry measurements and analysis.

---

* Calculated from heat balance

CHAPTER 2

BACKGROUND

The NRX-A2 Test Series as described in the NRX-A2 Test Specification[1] was c[illegible] out at NRDS in Test Cell A. Initial criticality was achieved on 12 August 1964, the high power test was performed on 24 September 1964 and the final test was completed on 15 October 1964. The major objectives of the test were to verify design analysis and to determine the adequacy of the design to operate at the steady state power level required for the experimental engine system.

The calculation of heat transfer and fluid flow characteristics and nuclear characteristics of the reactor are essential to establish proper test conditions in future reactor tests and to properly assess and improve future reactors. This report presents an analysis and diagnosis of the measured experimental reactor data from the NRX-A2 tests and a comparison of this data with calculations. An evaluation of these comparisons and the associated mathematical models which are used in the computer programs is made. In appropriate cases a description of improvements in the calculation models which resulted are described.

Preliminary tests are considered in Chapter 3, the high power test in chapter 4, and the restart in chapter 5, while chapters 6 and 7 contain reviews or summaries of the nuclear and thermal results, respectively. Chapter 8 contains dosimetry analyses and chapter 9 post-operative examination results.

A summary of the operational history of the NRX-A2 test assembly including NTO operating description, observations, and test assembly and test facility data is available.[2]

---

1 WANL-TNR-153, NRX-A2 Test Specification, as updated by the NRX-Test Specification and Procedure Review Board and The Test Review Board

2 NTO-R-0008, NRX-A2 Site Test Report, 20 November 1964

The post-operative instrumentation disassembly condition was reported[3] and data discrepancies during the NRX-A2 test series have been listed and analyzed.[4] Post-operative disassembly and inspection results have been documented by NTO.[8]

Mechanical performance of the NRX-A2 reactor has also been documented.[5] Analysis of core radial growth data, tie rod loadings, control drum torques, strain gage and accelerometer data is included with evaluation of noncorrosive damage. A report of the post-operative inspection of the NRX-A2 reactor components has also been published.[6] A comprehensive NRX-A2 Test Report will be issued.[7]

A supplement to this report is planned. It will include an analysis of post-operational data which has recently become available and an extension of the analysis presented herein. Items to be considered include an analysis of corrosion data, an improved Reactor Model for System Analysis (TNT) based on test results, additional thermal analysis of core material temperatures, and additional nuclear analysis of feedback reactivity.

---

3 WANL-TME-1079, NRX-A2 Instrumentation Disassembly and Post-Operative Report, by G. Chambers, 8 January 1965
4 NTO-R-0010, Data Discrepancy Report NRX-A2 Test Series, by H. Norkin, 2 November 1964
5 WANL-TME-1075, NRX-A2 Postmortem Analysis, by G. Downs, P. Stancampiano, P. Warner, January 1965
6 WANL-TME-1071, NRX-A2 Post Operative Mechanical Component Evaluation, by J. Karbowski, February 1965
7 WANL-TNR-193, NRX-A2 Test Final Report, to be issued in April 1965
8 NTO-R-0018, NERVA Program NRX-A2 Post Test Report, February, 1965

CHAPTER 3

EXPERIMENTAL PLANS I, II, AND III

In this chapter experimental data from the experimental plans which preceded the high power test is presented and in appropriate cases compared to calculated values. In this first section the thermal and fluid flow test results are considered for the GH_2 and LH_2 cold flow tests and the temperature coefficient test. In the next section the nuclear results are reviewed for the initial criticality, cold flow tests, calibration and temperature coefficient tests.

The NRX-A2 test sequence was developed by NERVA Test Operations according to the requirements set forth in NRX-A2 Test Specifications[1] and changes which were approved by the Test Review Board. A brief description of the tests which preceded the high power test are given below. Operational history of the NRX-A2 test assembly is contained in NTO-R-0008, NRX-A2 Site Test Report, 20 November 1964.

EP-1A (EXPERIMENTAL PLAN I A) INITIAL CRITICALITY

This EP was completed on 12 August 1964 when poison wires were removed from the core and initial criticality achieved. Control drum integral and differential worths were obtained. The reactor was operated at ambient temperature with an approximate maximum power of 500 watts.

EP-1B (AMBIENT AND LIQUID HYDROGEN FLOW TEST OF 4 SEPTEMBER 1964)

Initial automatic startups were achieved and an ambient GH_2 flow test and two LH_2 flow tests were completed at low power in order to obtain hydrogen reactivity worth data and verify reactor flow and chilldown characteristics.

The ambient GH_2 test consisted of a programmed flow ramp to 12 pounds per second with constant power of 100 watts. The test flow ramp which closely reproduced the programmed flow is shown on figure 3-1.

---

1 WANL-TNR-153, NRX-A2 Test Specification, as updated by the NRX Test Specification and Procedure Review Board and Test Review Board

REFERENCE	[redacted]	PREPARED BY	APPROVED BY	Astronuclear

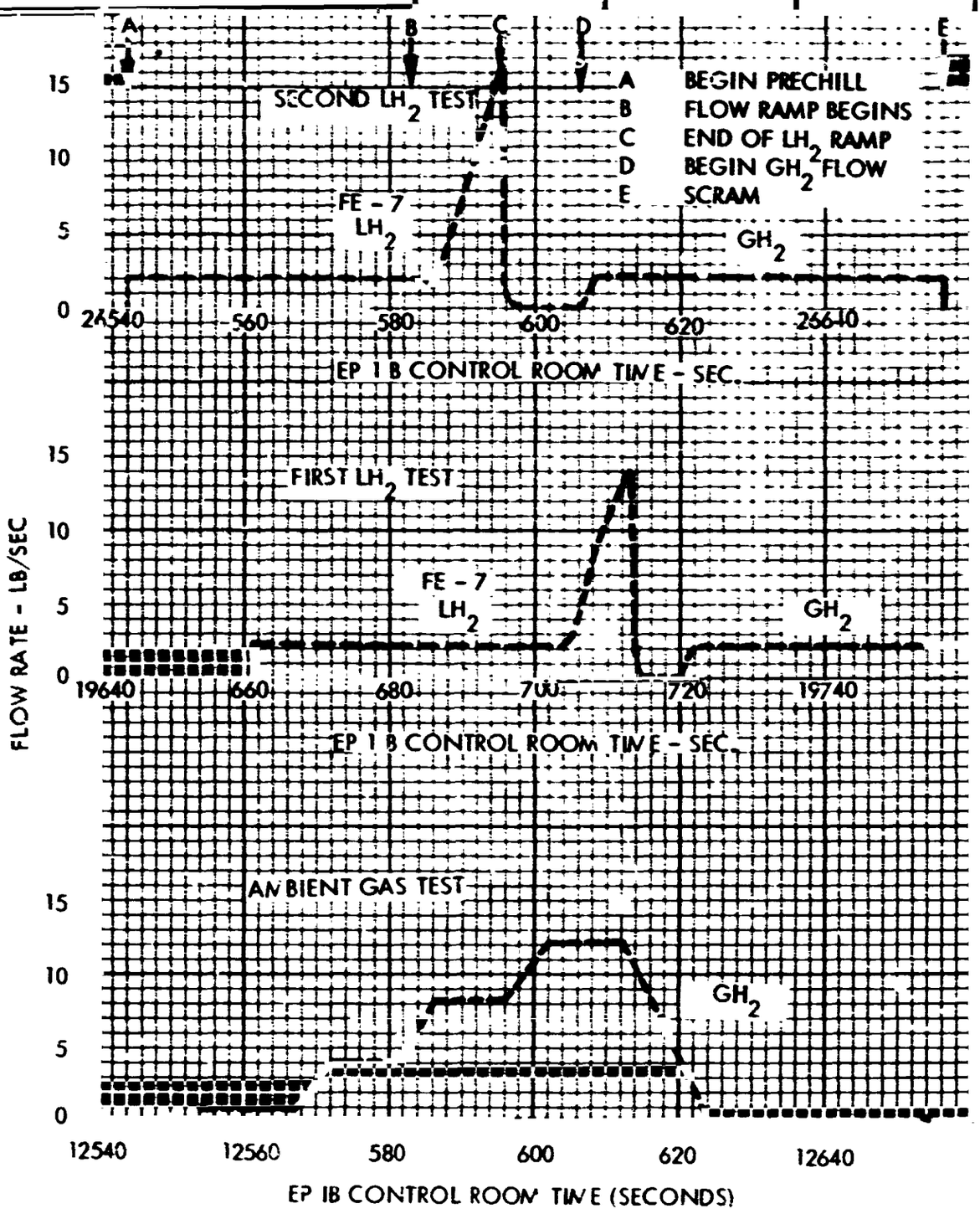

EP I FLOW TEST - FLOW RATES

CURVE NO.	FIGURE NO.
II-1	3 - 1

The LH_2 test consisted of a prechill with approximately 2 lb/sec reactor flow until core inlet temperature had been decreased 90°F below ambient, followed by a 1.25 lb/sec^2 flow ramp to a maximum flow rate of 16 lb/sec. A rerun of this test was performed because the observed control drum motion was less than predicted in the first test. The LH_2 flow rate measured at the venturi meter is given in figure 3-1 for these tests.

EP II - (NEUTRONIC CALIBRATION AND TEMPERATURE COEFFICIENT TEST OF 16 SEPTEMBER 1964)

Neutronic instrument calibration was obtained by irradiating U-Al wires in the core during this test. The reactor was then operated with core temperatures up to about 1000°R to obtain temperature coefficient of reactivity data and verify proper operation of the power control system temperature trim loop. Gaseous helium coolant was used as necessary and maximum reactor power was about one MW. Power and two typical core material temperature traces are given in figure 3-2.

EP III - (SCALED-DOWN POWER TEST)

On 18 September 1964 the reactor was operated using the power test profile scaled down by a factor of 1000 as a check-out for the power test. Ambient helium was the only coolant used.

THERMAL AND FLUID FLOW

Gaseous Hydrogen Test

TEST CHRONOLOGY AND DESCRIPTION

A chronology of the ambient gas flow test, Experimental Plan IB is given in table 3-1. From an initial condition of minimum ambient hydrogen flow and the reactor in power control at 100 watts, the programmed 1 lb/sec^2 GH_2 ramp to a maximum flow of 12 lb/sec with intermediate steady state holds was run. The decreasing flow also followed a 1 lb/sec^2 ramp.

REFERENCE	PREPARED BY	APPROVED BY	Astronuclear

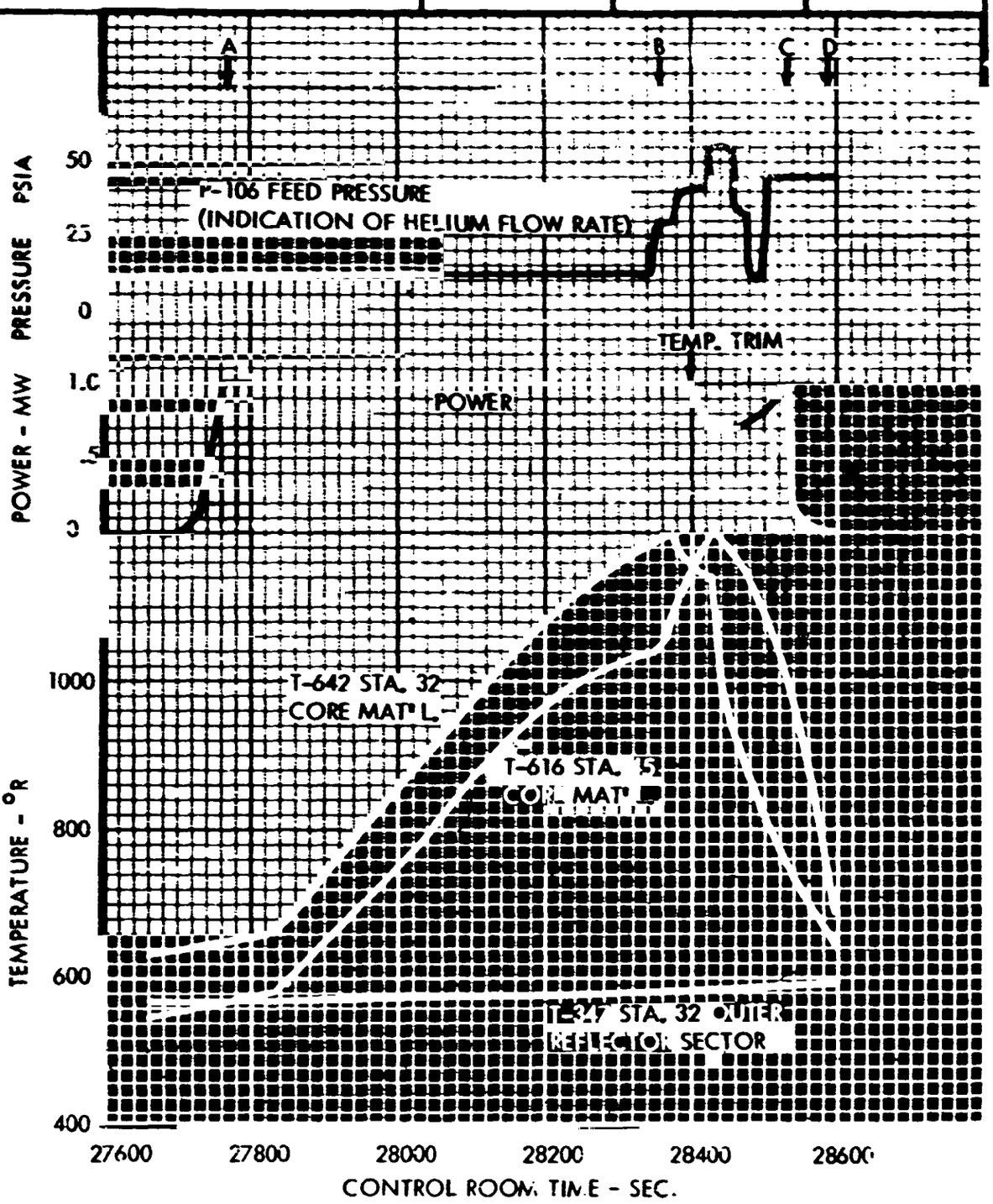

TEMPERATURE COEFFICIENT TEST POWER FLOW AND TEMPERATURE

CURVE NO.	FIGURE NO.
	3 - 2

TABLE 3-1

EP IB AMBIENT HYDROGEN-SELECTED TEST CHRONOLOGY

Key	Event	EP IB Control Room Time (Seconds)
	Automatic startup to 1 KW	12157
	Reduce power to 100 watts	12485
	Establish minimum GH_2 flow	12547
A	Start GH_2 run	12568
	4.05 ± 0.69 lb/sec selected time for data analysis	12576
	8.15 ± 0.70 lb/sec selected time for data analysis	12590
	12.18 ± 0.71 lb/sec selected time for data analysis	12608
B	Start downward flow ramp	12612
	Scram	12686

REACTOR PERFORMANCE

In this test the pressure-flow characteristics of the reactor components and the hydrogen reactivity effect were verified by comparison to predictions. The reactor flow rate, selected reactor system pressures from Calcomp data, and average control drum position from digital printout are presented graphically on figure 3-3 as a function of time. The reactor flow rate was calculated from the pressure measured upstream of the ambient hydrogen venturi FE-10. Hydrogen temperature was determined from measurements downstream of this venturi because the temperature measurement upstream of FE-10 was faulty. For the test flow rates, choked flow occurred at the venturi throat. The 2σ accuracy of the flow rate has been evaluated on the basis of the possible error in the venturi coefficient, the pressure measurement, and the temperature measurement. This accuracy range is indicated on the figure by the vertical line through the calculated flow rates. The 2σ accuracy (95 percent confidence level) is indicated by the length of this line. The method used in evaluating the data accuracy is presented in Appendix G.

In this subsection the system pressures and differential pressures are compared to the pre-run predicted values given in the Test Prediction Report[1] for the ambient GH_2 test. The experimental data for these comparisons is taken during the steady state holds of the flow profile at the times indicated in table 3-1 and the comparisons are presented as a function of flow rate in figures 3-4, 3-5, and 3-6. As for the majority of the experimental data presented in this report a 2σ accuracy range has been calculated as described in Appendix G for the pressure measurements. This accuracy range is represented by the length of the vertical line extending from the data points while the flow rate accuracy range is given by the horizontal line. A more detailed comparison and description of the pressures measured during the ambient test follows. Ambient hydrogen reactivity effects which caused the control drum to move inward as flow increased are discussed in the Nuclear section of this chapter under Experimental Plan 1B.

---

1 WANL-TME-887, NRX-A2 Test Prediction Report, July 1964

REFERENCE	PREPARED BY	APPROVED BY	Astronuclear

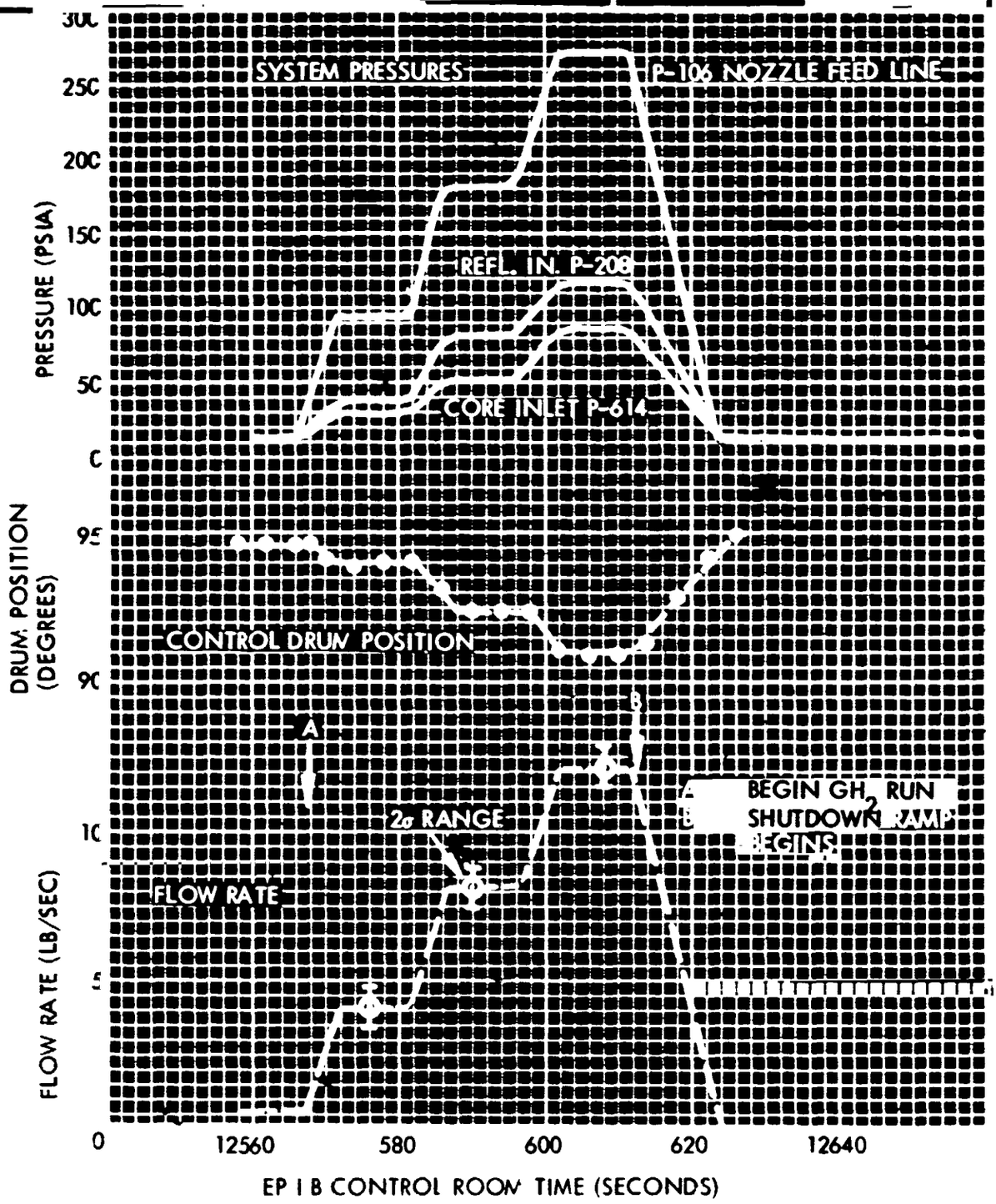

AMBIENT GH_2 FLOW TEST - FLOW, PRESSURE, AND CONTROL DRUM POSITION

CURVE NO.	FIGURE NO.
[redacted]	3 - 3

CORE

Predicted and experimental values of core inlet and exit pressure are given as a function of flow in figure 3-4 for the EP I-B ambient GH_2 test. A similar curve on figure 3-5 gives the core pressure drop. The predicted values on these figures are from pre-test calculations using the TNT code.[1,2] Also included on figure 3-5 is the range of core ΔP data obtained from the NRX-A1 test. In all cases the pre-test predicted value is within the rectangular area which defines the range of the 2σ error band on the experimental data, although at the upper edge of this range for the core ΔP. NRX-A orifice test data and its application to ambient hydrogen are described in detail in appendix C. The temperature of the hydrogen propellant and reactor materials was assumed to be 540°R for the predictions shown in the figures. During the test, plenum temperatures varied from 530 to 550°R.

REFLECTOR SYSTEM

Reflector inlet pressure, reflector outlet pressure, shield ΔP, inner reflector ΔP, and radial graphite barrel ΔP are given on figures 3-4 and 3-5. As was done for the core, experimental and pre-test TNT values are compared. In all cases excepting inner reflector ΔP the predicted values are within the 2σ range of the experimental data.

NOZZLE

Nozzle tube inlet pressure as a function of GH_2 flow rate is given in figure 3-6. The calculation was based on the available geometrical AGC U-tube nozzle information. Ambient gas nozzle inlet pressure is a strong function of minimum nozzle tube flow area and independent of reflector inlet pressure, because choking flow occurs at the minimum tube area. The high calculated pressure may have been the result of using a tube area less than the true area. Nozzle geometrical configuration data and heat transfer coefficient data used in the TNT analyses are given in appendix D.

---

1 WANL-TME-887, NRX-A2 Test Prediction Report, July 1964
2 WANL-TME-483, NRX-A Reactor Model for System Analysis, 31 July 1963

REFERENCE		PREPARED BY	APPROVED BY	Astronuclear

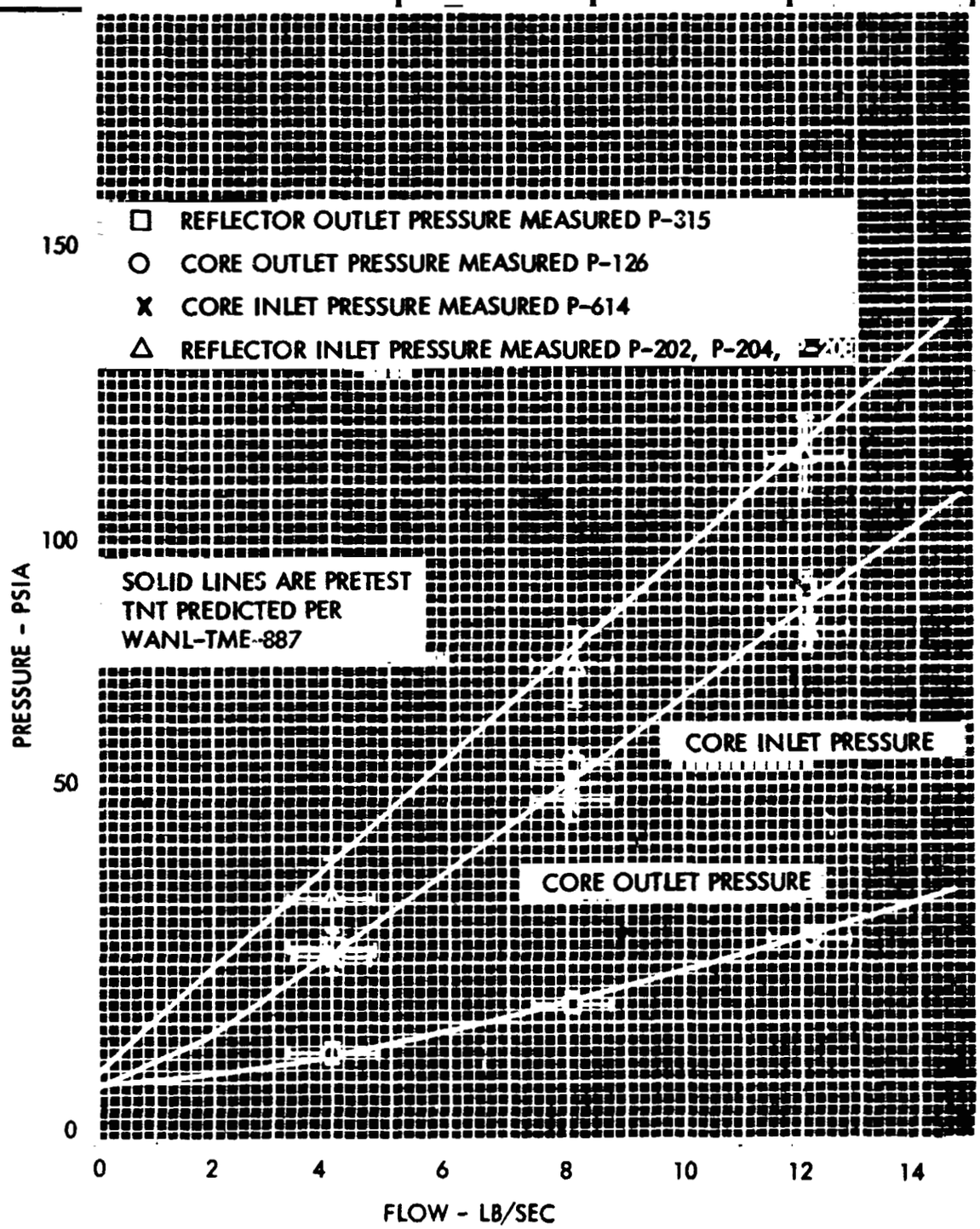

EP IB AMBIENT GH_2 COMPARISON OF PRESSURES	CURVE NO.	FIGURE NO.
		3 - 4

REFERENCE		PREPARED BY	APPROVED BY	Astronuclear

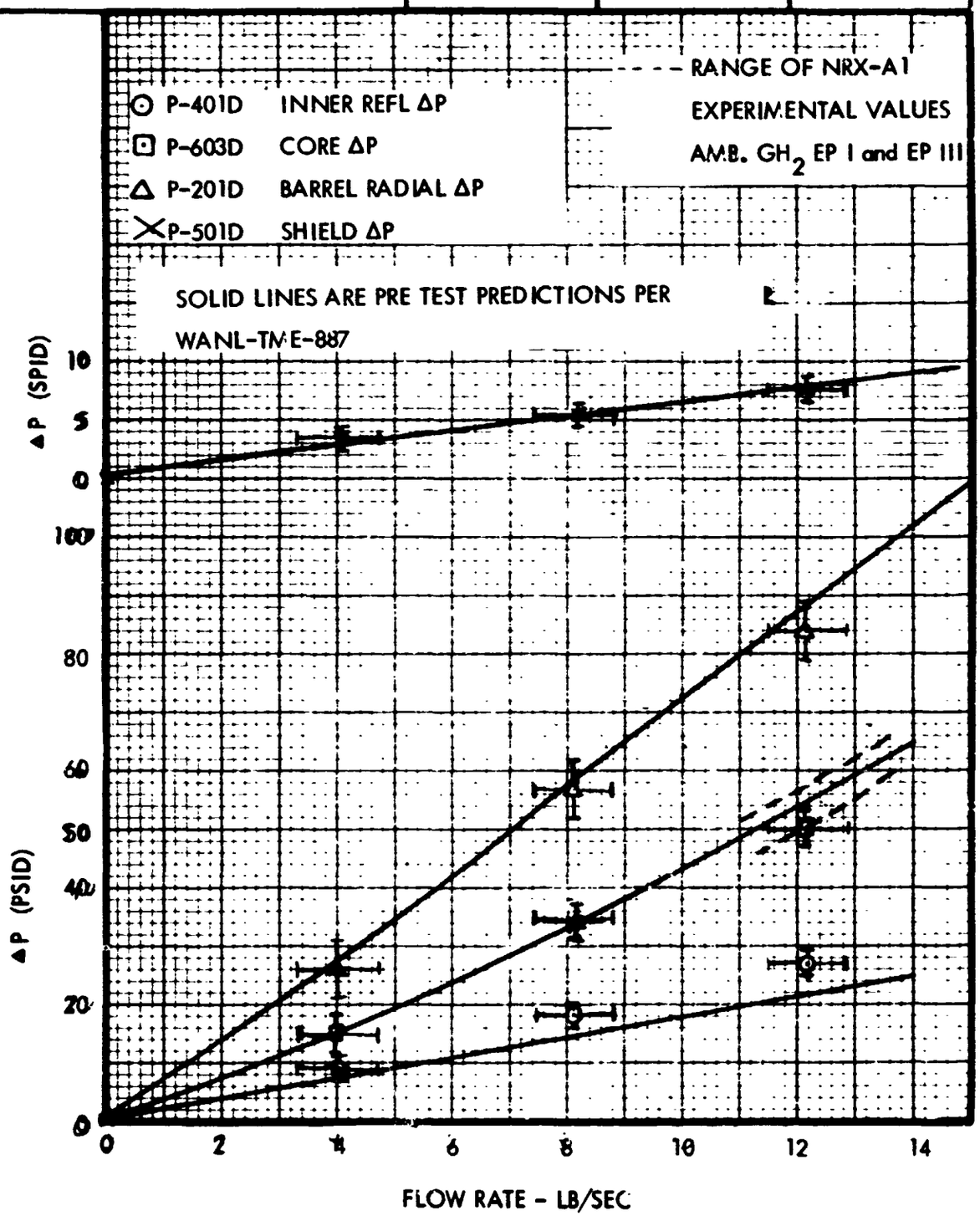

EP IB AMBIENT GH_2 COMPARISON OF COMPONENT PRESSURE DROP	CURVE NO	FIGURE NO.
	IV-4	3 - 5

REFERENCE		PREPARED BY	APPROVED BY	Astronuclear

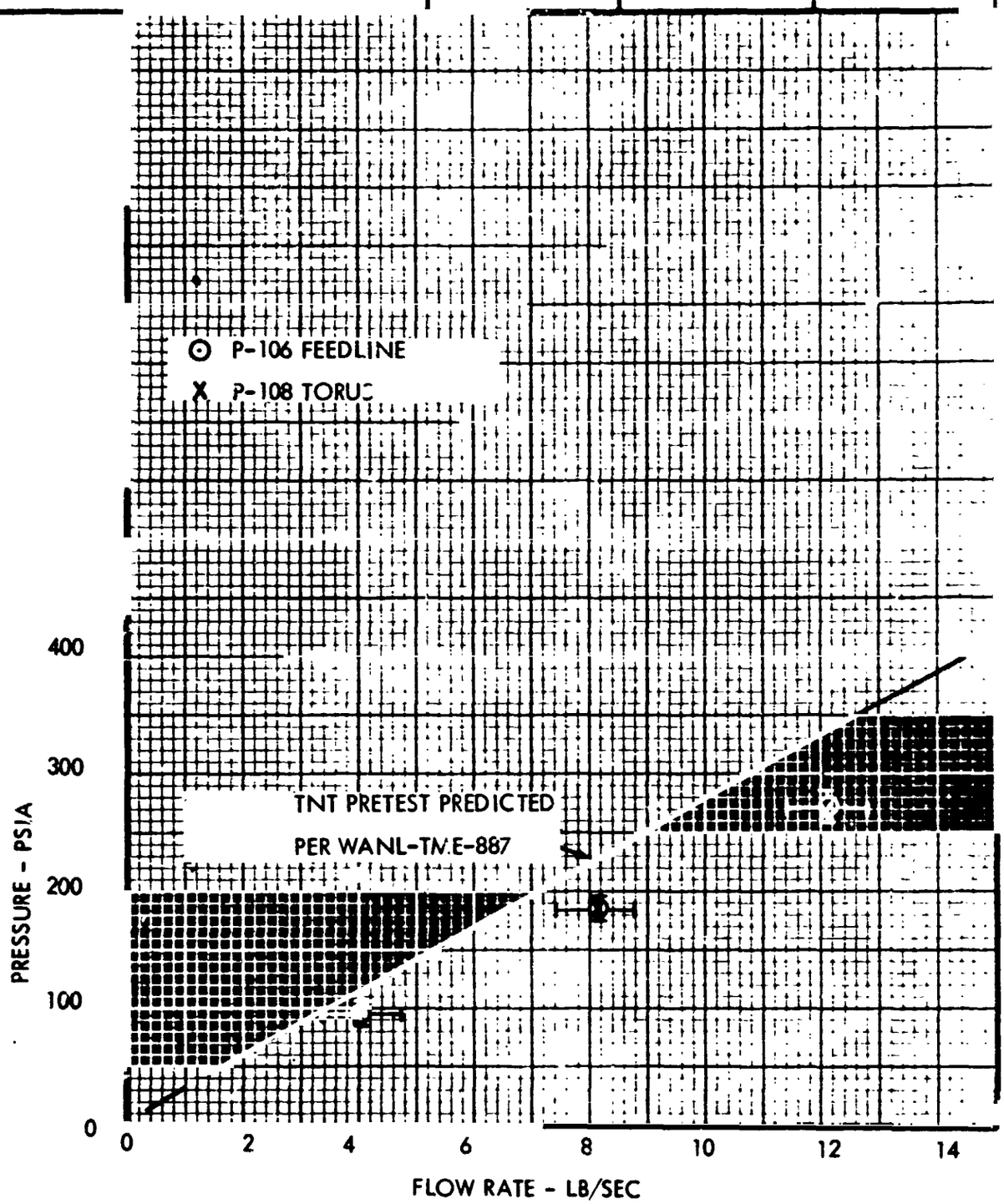

EP IB AMBIENT GH_2 NOZZLE TUBE INLET PRESSURE	CURVE NO	FIGURE NO.
		3 - 6

The nozzle hot side throat area was calculated on the basis of the GH_2 test results and the theoretical flow coefficient. The results of this calculation were as follows:

Design Value	Calculated from GH_2 Test
59.7 in.^{2}	60 ± 3 in.^{2}

These results were obviously of no value in checking the nozzle chamber flow coefficient or area because of the wide error range on the calculated flow area.

LIQUID HYDROGEN TEST

LH_2 FLOW TEST CHRONOLOGY AND DESCRIPTION

A chronology of the two LH_2 flow tests is given in table 3-2. The LH_2 test profile started from initial conditions of 1 KW reactor power (which was maintained for the test by the power control), approximately 2 lb/sec GH_2 flow through the reactor, and a hard chill of the LH_2 feed system to OBV 86. The main propellant valve, OBV 86, just upstream of the reactor was opened and a nominal flow of 2 lb/sec was initiated and held constant until core inlet thermocouple T-781 indicated a temperature decrease of 90°R below ambient. At that time the 1.25 lb/sec^2 programmed flow ramp was initiated and flow increased until the test was terminated by a manual flow shutdown at a nominal flow rate of 16 lb/sec. Based upon quick look data the Data Review Team, with the concurrence of the Test Review Board, recommended a rerun of the LH_2 profile since the observed control drum motion was less than predicted. The second LH_2 flow test was similar to the first except it was terminated at a slightly higher flow rate than the first test. After LH_2 flow had been terminated there was an eight second interval with no measurable reactor flow. At the end of that interval ambient hydrogen flow was introduced and continued until scram.

The majority of the analysis has been confined to the second LH_2 run because a higher flow rate was attained prior to termination of the run. The letters on the chronology are keyed to figure 3-1 and other figures which present data for the LH_2 test as a function of time.

TABLE 3-2

SELECTED CHRONOLOGY EP I-B LH_2

Key	Event	EP IB Control Room Time CKT Seconds
	First LH_2 Test	
	Obtain a hard chill	19607
	Establish 1 kw	19630
	Begin Prechill - Open OBV 86	19661
	Close AVV 11	19664
	Close AVV 2	19699
	Flow ramp begins	19704
	End of LH_2 flow ramp	19713
	No flow through reactor, pressure ambient	19715
	Start GH_2 flow	19720
	Pressure stabilize in reactor	19722
	Scram	19775
	Second LH_2 Test	
	Obtain a hard chill to OBV 86	26397
	Establish 1 kw	26421
A	Begin prechill - Open OBV 86	26544
	Close AVV 11	26547
	Close AVV 2	26579
B	Flow ramp begins	26583.5
C	End of LH_2 Ramp	26595.5
	Pressures peak in reactor	26595.8
	No flow through reactor, pressure ambient	26598
D	Start GH_2 flow, pressures start to rise	26606.4
	pressures stabilize	26608.7
E	Scram	26656.6

REACTOR AND FEED SYSTEM

A simplified schematic of the test cell A facility feed system is given in figure 3-7. In order to maintain the required chill at the turbo-pump inlet it was necessary to leave AVV 2 open during the prechill period. Prechill and flow startup operating procedures and problems are discussed more fully in the 36 day report.[1] The actual reactor prechill flow rate cannot be determined from the venturi meter FE-7, since it gives the total flow through the reactor and through the AVV 2 vent line. However since the prechill time of 40 seconds required to reduce the core inlet temperature 90°F is close to the calculated prechill interval[2] of 48 seconds the flow rate must have been approximately equal to the 2 lb/sec on which the calculation was based.

Prior to the NRX-A2 test it was assumed that the flow lag* which would exist during the flow ramp would be negligible compared to the flow lag observed on NRX-A1 tests with a prechill.[3] One purpose of the LH_2 cold flow tests of the NRX-A2 reactor was to check this assumption.

Flow rates for the second LH_2 test are given in figure 3-8. Planned flow rate, flow rate calculated from venturi data, and flow through the reactor calculated from nozzle chamber temperature and pressure and the nozzle flow equation are given on figure 3-8. This comparison reveals that the reactor flow rate was lagging the venturi flow rate in a manner similar to that which occurred in the NRX-A1 LH_2 tests conducted without a prechill. On the basis of this test the EP IV power test startup power and flow profiles were redesigned to account for the flow lag. The NRX-A1 test results provided the reactor flow profile associated with a 1.25 lb/sec[2] venturi flow ramp for the startup predictions, which were issued in a supplement to WANL-TME-887.[4]

---

1 NTO-R-008, NRX-A2 Site Test Report, 20 November 1964
2 WANL-TME-887, NRX-A2 Test Prediction Report, July 1964
3 WANL-TME-773 and WANL-TME-773, Supplement I, NRX-A1 Thermal Performance
4 WANL-TME-887, Supplement IV, NRX-A2 Prediction Report, Supplement IV
* Flow lag refers to the flow rate through the reactor lagging the flow rate through the venturi during a startup flow ramp. This is caused by an increasing amount of hydrogen storage between the venturi and reactor during the flow ramp.

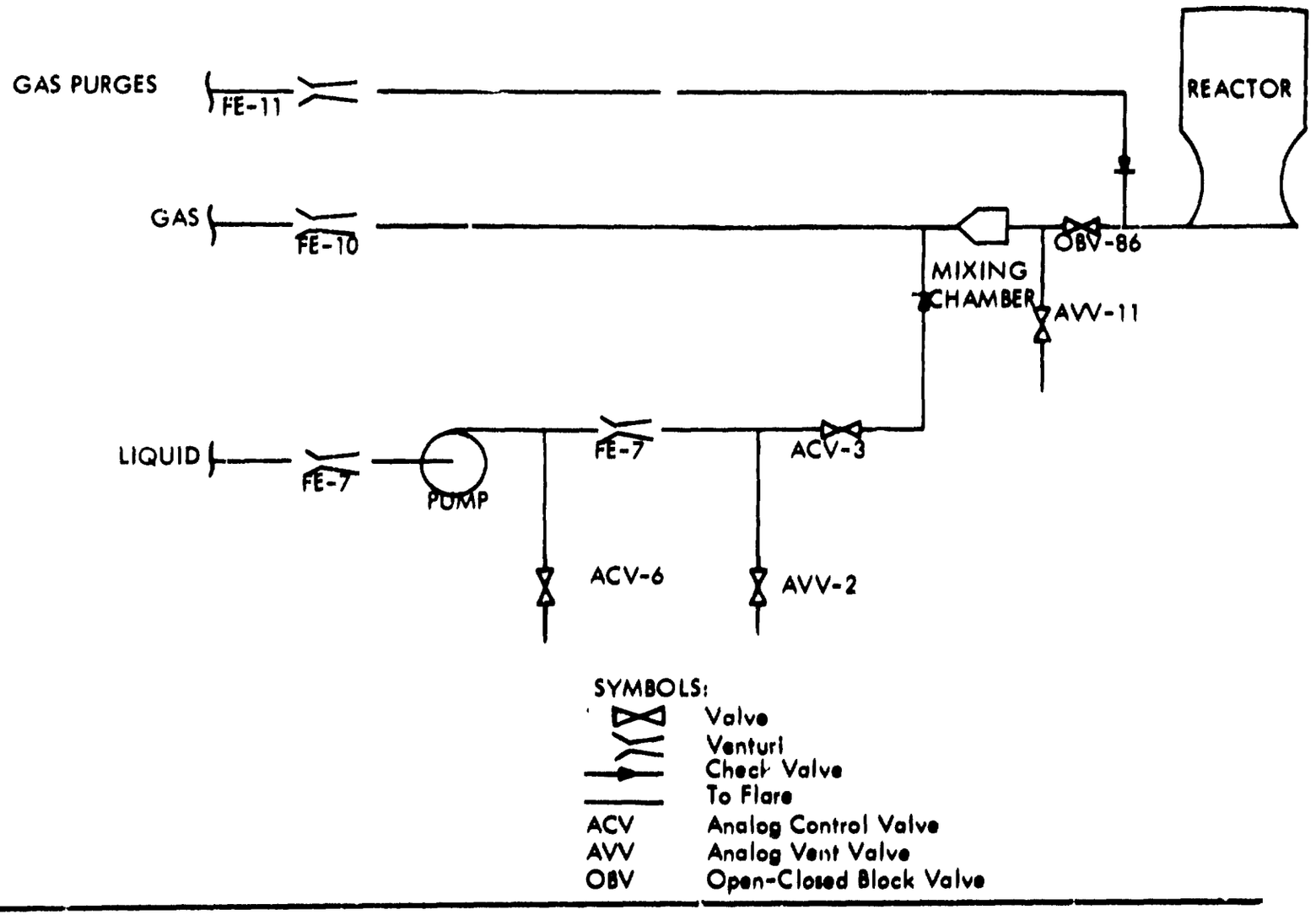

LIQUID H_2 FLOW SCHEMATIC, TEST CELL A	PREPARED BY	APPROVED BY	FIGURE NO
	LKA		3 - 7

REFERENCE		PREPARED BY	APPROVED BY	Astronuclear

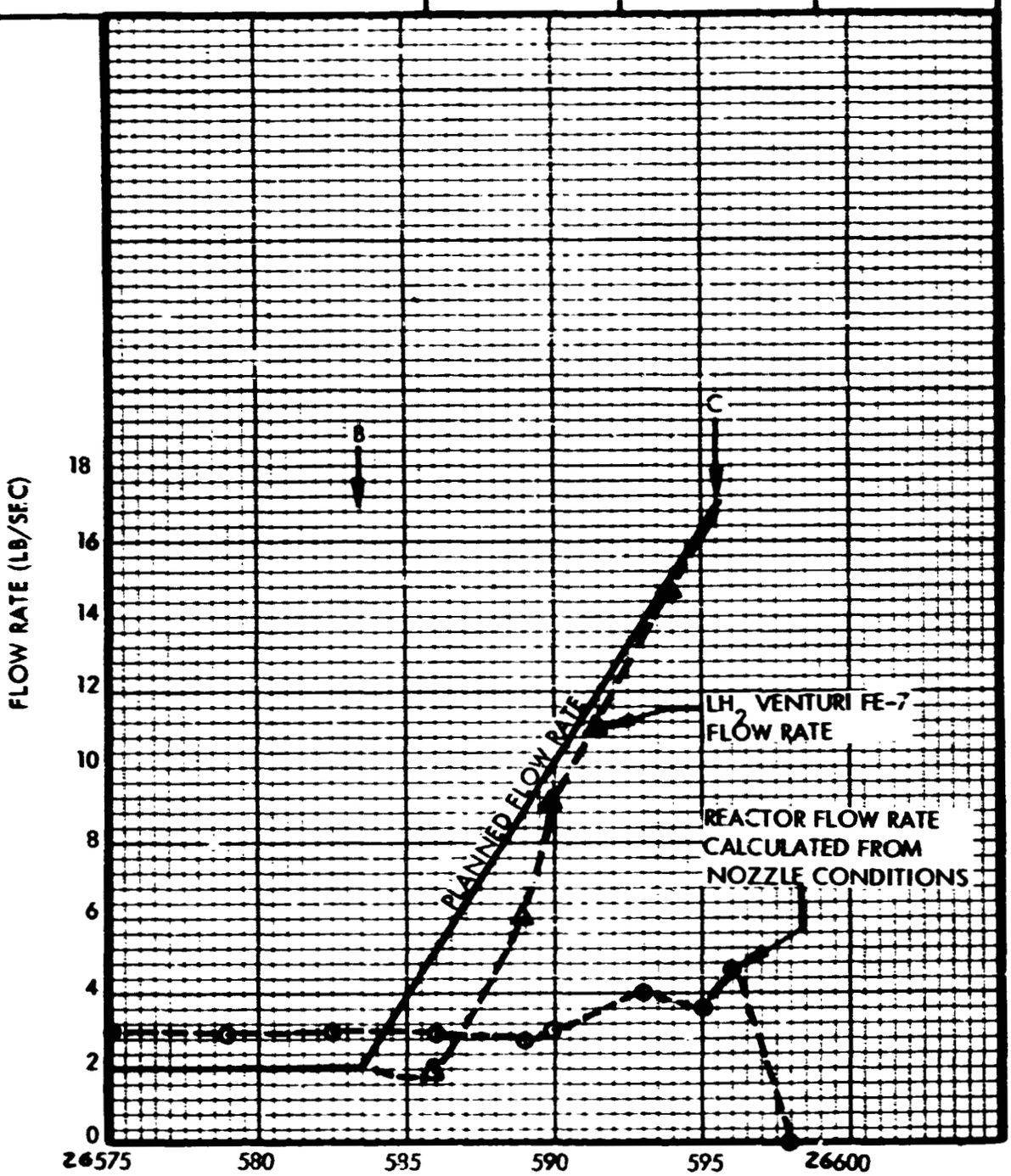

EP I-B 2ND LH_2 TEST FLOW RATE	CURVE NO.	FIGURE NO.
		3 - 8

SYSTEM TEMPERATURES

The highest and lowest reflector inlet and outlet hydrogen temperature traces are on figure 3-9 for the second LH_2 test. In addition the average reflector inlet and outlet temperatures are given at selected times, including the end of the prechill and the end of the flow ramp. These traces reveal a large variation in the individual temperature indications. A similar time trace of the extreme core inlet temperatures and core inlet temperature channel T-781 is given in figure 3-10. It was planned that the flow ramp be initiated when T-781 had been reduced 90°R below the ambient of 540°R. In truth, T-781 was slightly less than 450°R, however the average core inlet temperature was 450°R. The variation in the individual plenum temperature indications has been correlated with angular position in figures 3-11 and 3-12. Core inlet temperatures are given as a function of azimuth position for two times, CR 26583.5 seconds, the end of the prechill; and 26595.5 seconds, the end of the LH_2 ramp while reflector inlet and outlet temperature variations with azimuth are given for the end of the prechill only. These temperature variations which are transmitted from the reflector inlet to the core inlet are probably caused by two phase flow conditions in the nozzle, and were also observed in the NRX-A1 cold flow test.[1] The minimum temperatures appear to occur at the nozzle feed line location (120 degrees) and opposite the feed line (300 degrees). Similar asymmetrical temperatures occurred in the EP IV high power test prechill but were not evident after system pressures had increased during the startup and therefore presented no problem at high power operation. The asymmetrical temperatures during the power test are discussed in chapter 4 under startup (thermal and fluid flow).

SYSTEM PRESSURES

Reflector and core inlet and reflector exit pressure time histories are given in figure 3-13 for the second LH_2 cold flow test. Core, shield, and reflector pressure differential time histories are given for the same LH_2 test in figure 3-14. In all cases, the pressures were low and only rose slightly when the flow ramp was initiated because the reactor flow did not exceed 5 lb/sec.

[1] WANL-TME-773 and WANL-TME-773, Supplement 1, NRX-A1 Thermal Performance, June 1964.

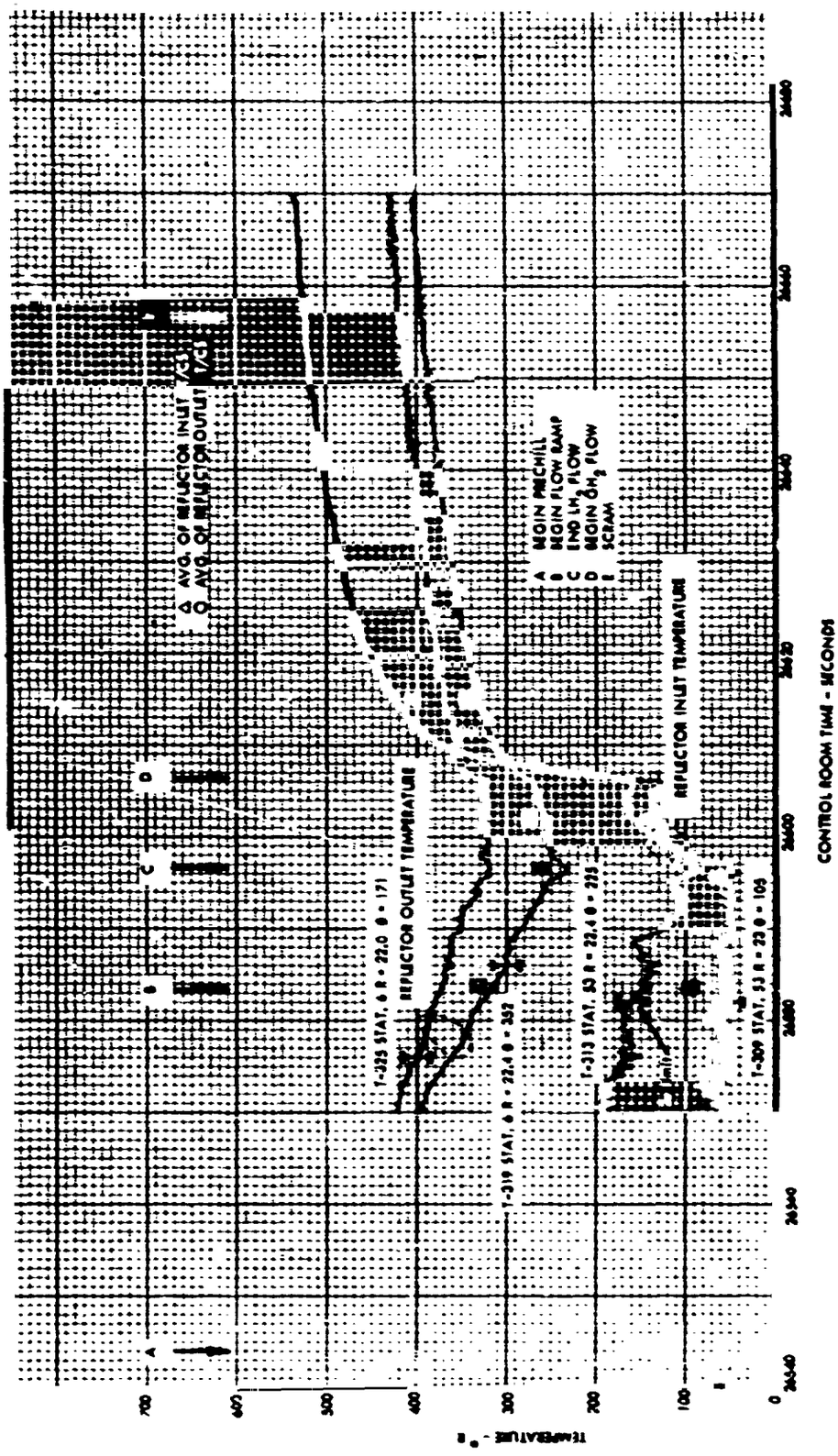

PREPARED BY	APPROVED BY	CURVE NO.
		Fig. III-14

NRX-A2 EP IB LH_2 RUN SPAN OF REFLECTOR INLET AND OUTLET TEMPERATURE: TIME HISTORIES

FIGURE NO. 3-9

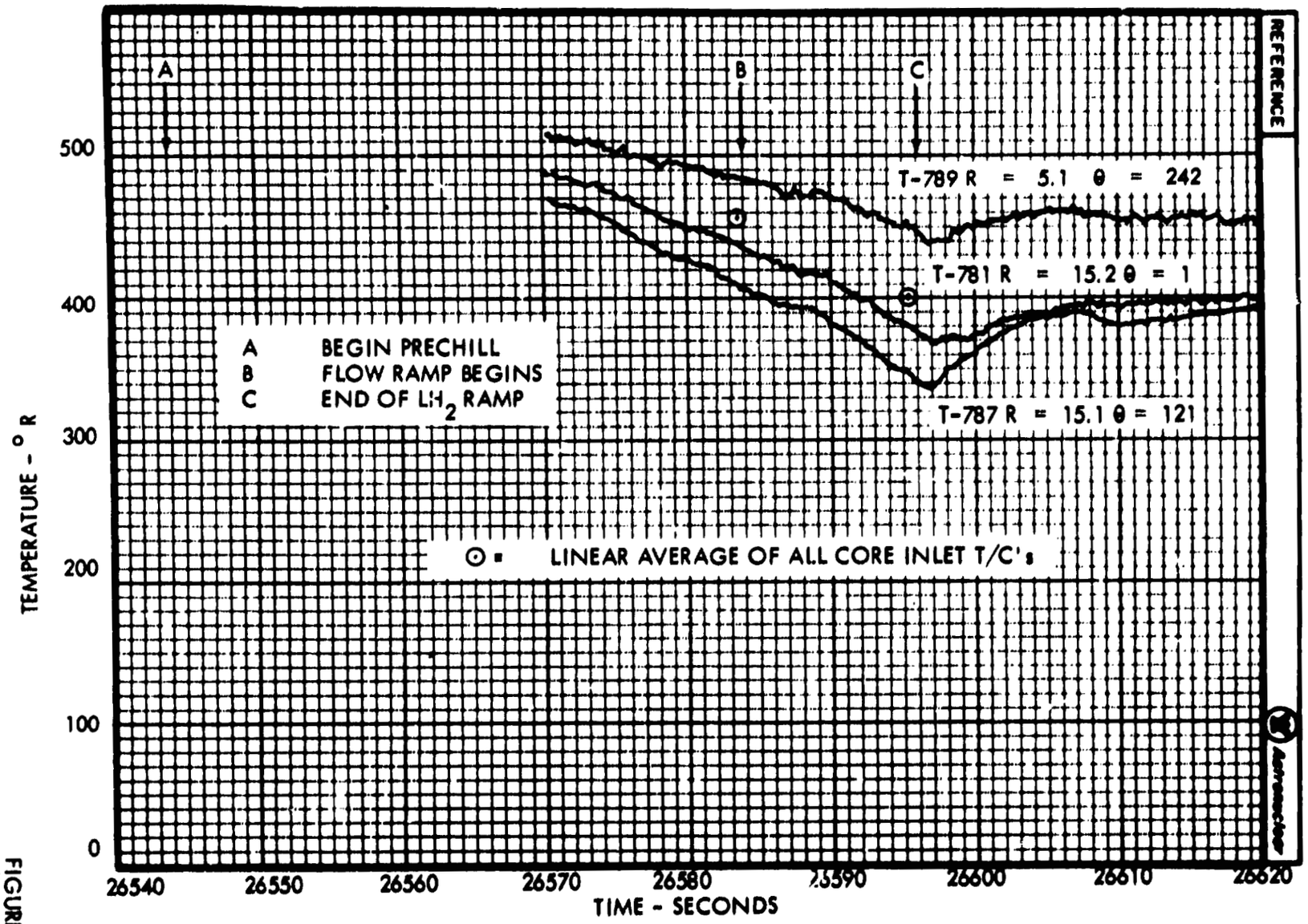

CORE INLET TEMPERATURE VS. TIME, SECOND LH_2 RUN EP I-B	PREPARED BY	APPROVED BY	CURVE NO.

FIGURE NO. 3-19

CONFIDENTIAL RESTRICTED DATA

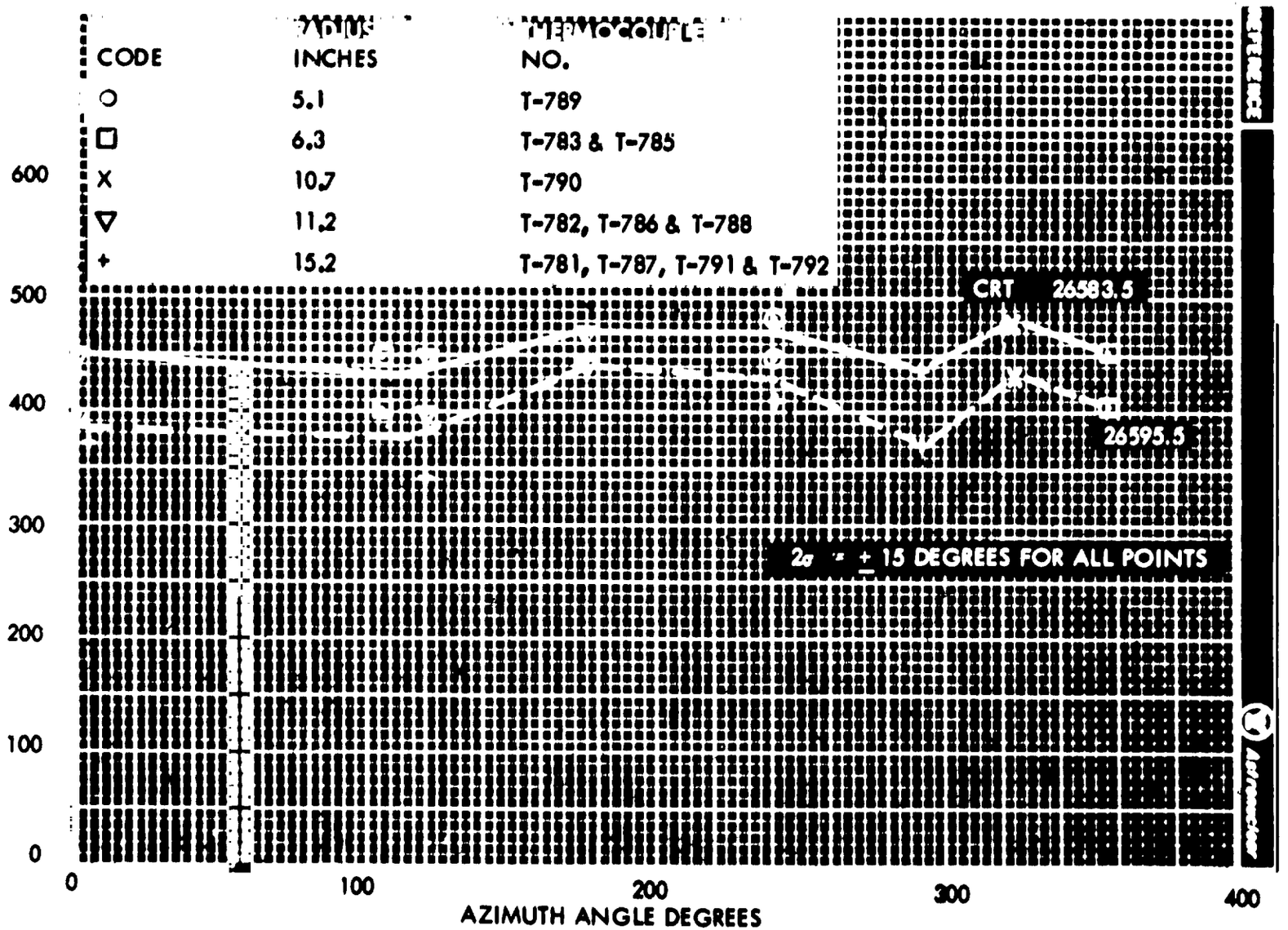

FIGURE NO.	CORE INLET TEMPFRATURE VS. AZIMUTHAL POSITION AT BEGINNING AND END OF FLOW RAMP, SECOND LH_2 RAMP	PREPARED BY	APPROVED BY	CURVE NO.
3 - 11				

CONFIDENTIAL RESTRICTED DATA

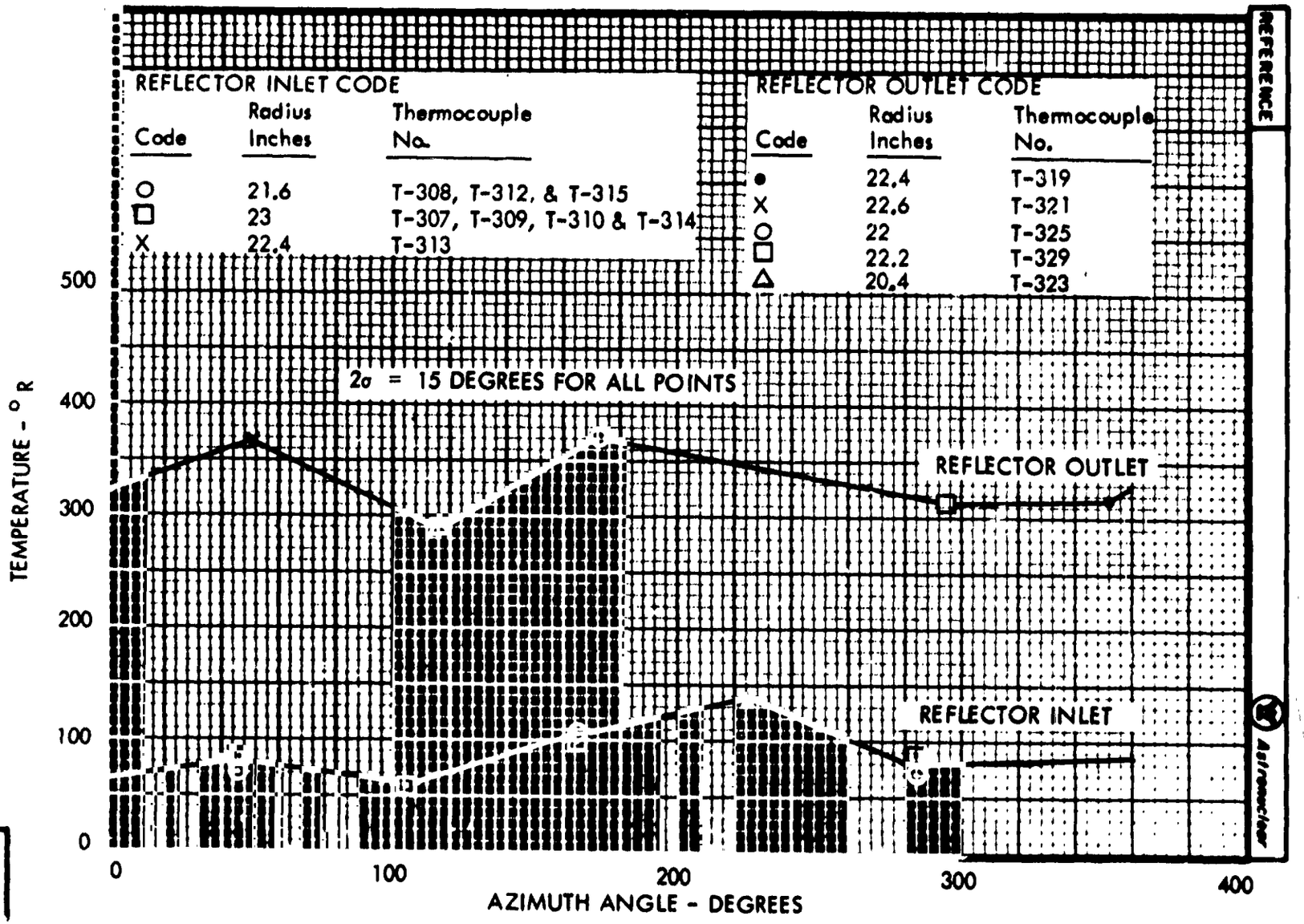

FIGURE NO.	REFLECTOR INLET AND OUTLET TEMPERATURE VS. AZIMUTH AT END OF PRECHILL EP IB (CRT 26583.5)	PREPARED BY	APPROVED BY	CURVE NO.
3-22				

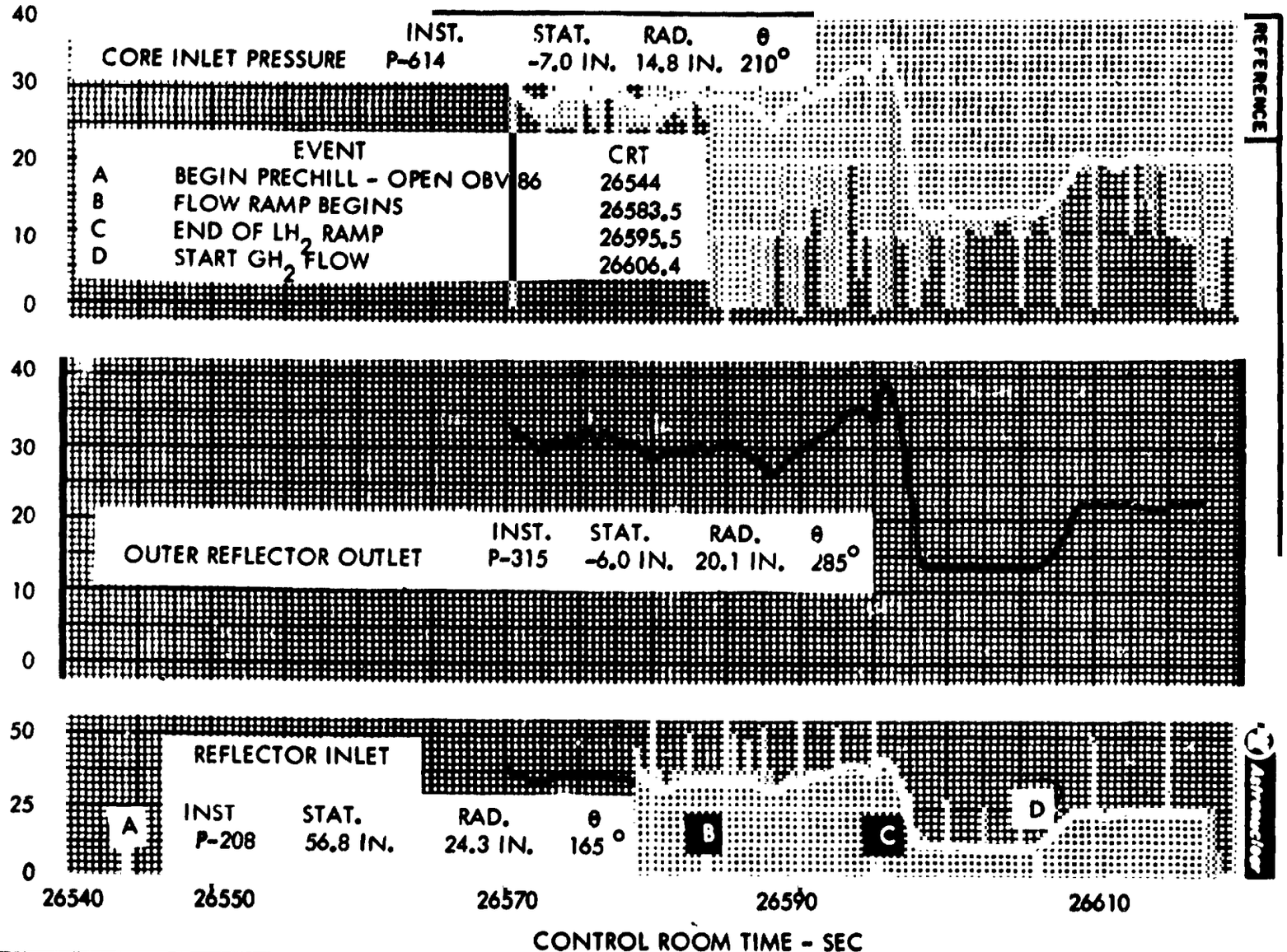

FIGURE NO.	NRX-A2 EP IB 2ND LH_2 RUN: REFLECTOR AND CORE INLET AND EXIT PRESSURE TIME HISTORIES	PREPARED BY	APPROVED BY	CURVE NO.
3 - 13				FIG. III 15b

CONFIDENTIAL - RESTRICTED DATA

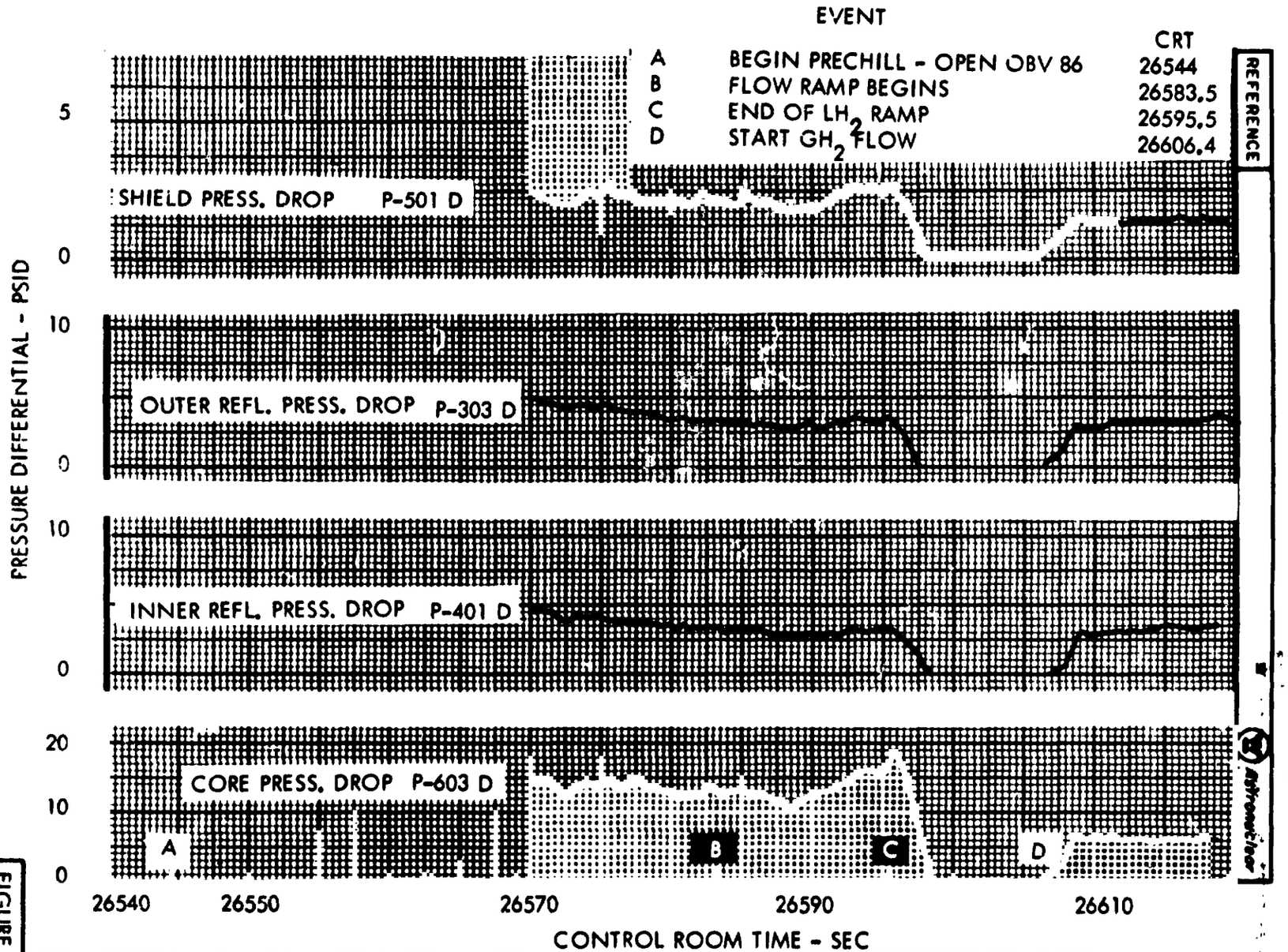

NRX-A2 EP I B 2ND LH_2 RUN: CORE, SHIELD, AND REFLECTOR PRESSURE DROP TIME HISTORIES	PREPARED BY	APPROVED BY	CURVE NO.
			FIG. III 15a

FIGURE NO. 3 - 14

CONFIDENTIAL - RESTRICTED DATA

REFLECTOR MATERIAL TEMPERATURES

Typical reflector sector temperature traces are given in figure 3-15 at station 8, 20, 32 and 45 (axial position in inches measured from core inlet face) for the second LH_2 test. Similar sector temperature traces for the power test prechill and startup are given in figure 4-51. These results show that the maximum thermal gradients in the sector were much larger during the power test. The larger gradients during the power test are due to the fact that these maximum gradients occur after the portion of the startup flow ramp which was reproduced in the EP IB test.

Temperature Coefficient Test - EP II

TEST CHRONOLOGY AND DESCRIPTION

A chronology of the temperature coefficient test is given in table 3-3. This test was performed with only ambient helium coolant. The reactor was operated in power control at a constant power of 1 MW with helium flow as required to maintain station 8 temperature below 700°R. When station 45 core material temperature had reached approximately 1000°R the station 45 feedback control was selected and the temperature controller adjusted the power to maintain the station 45 temperature as helium flow was varied.

Figure 3-2 shows the power, helium feed pressure, and two typical core temperatures during this test. The helium feed pressure is an indication of helium flow rate. As in previous sections, the chronology is keyed to the figures by the capital letters.

TEMPERATURES

The core station 45 material temperature (T-616) and station 32 material temperature (T-642) in figure 3-2 indicate a nearly linear increase with time at constant power until Time CR 28358 when the helium flow rate was increased. When the flow rate was increased, the heat in the central region of the core was carried downstream and station 45 temperatures continued to rise while station 32 temperatures fell. Since the internal generation in the outer reflector was orders of magnitude less than in the fueled region, the rate of temperature increase for T-347 was very small.

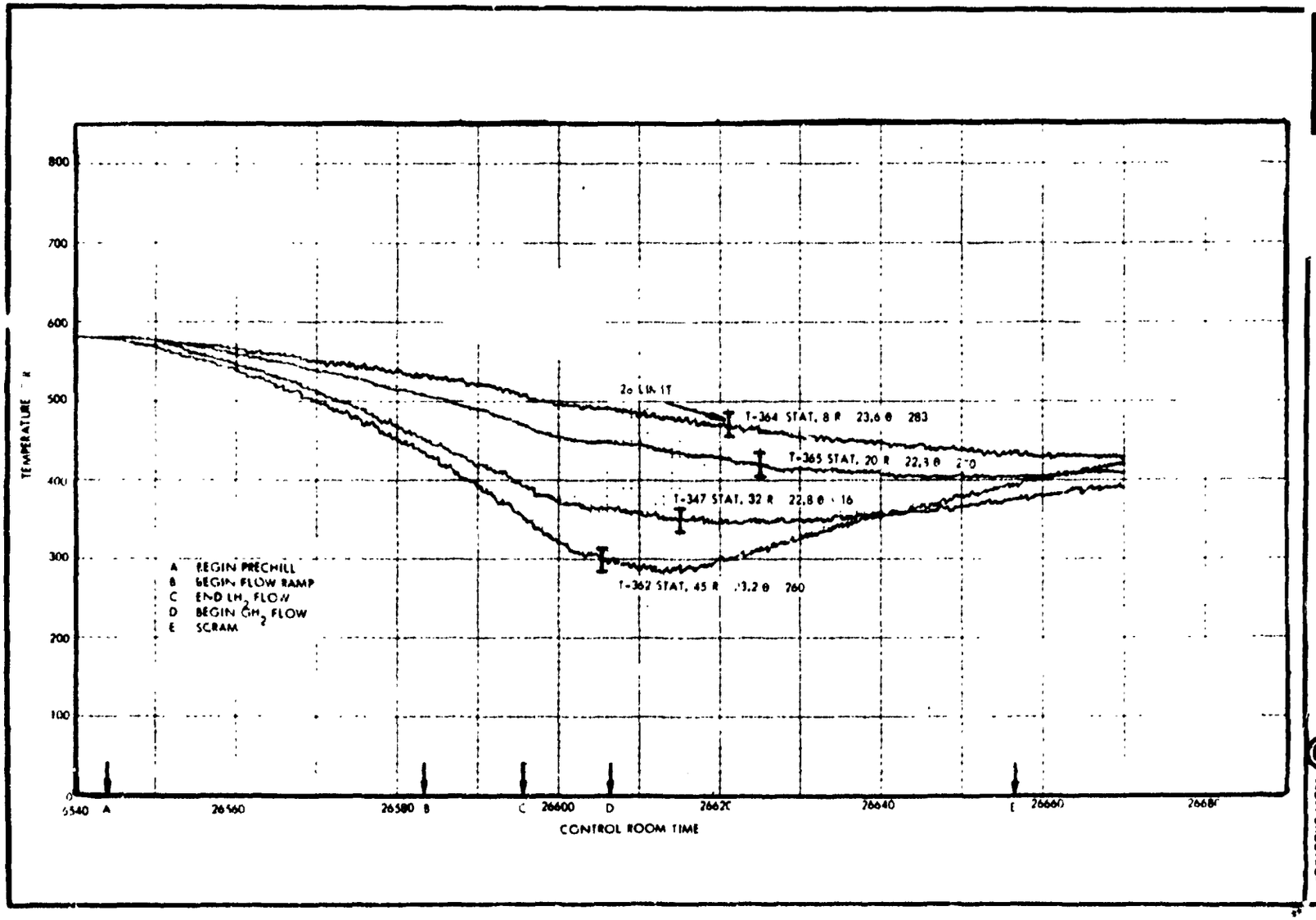

FIGURE NO. 3-15	NRX-A2 EP IB LH_2 RUN TYPICAL OUTER REFLECTOR MATERIAL TEMPERATURE TIME HISTORIES	PREPARED BY	APPROVED BY	CURVE NO

TABLE 3-3

EP II SELECTED CHRONOLOGY TEMPERATURE COEFFICIENT TEST

Key	Event	EP II Control Room Time (Seconds)
A	Establish 1 MW	27766
	Initiated helium flow when T-609 indicated 700°R	27880
	Switched to temperature control	28329
B	Increased helium flow to check temperature loop operation	28358
C	Started lowering power to 100 watts	28536
D	Scram	28589

Radial and axial temperature distribution in the fueled region are given for two times (Time CR 28000 and 28350 second) in figures 3-16, 17 and 18. Maximum temperatures for this test occurred at the latter time. From the temperature distribution for the fueled region it is obvious that a low helium flow rate existed during the entire test. However, the flow rate was so low that the temperature profiles, both radial and axial, were strongly influenced by the shape of the power profiles. A very sharp drop off occurred in the station 32 thermocouple readings at the extreme outer periphery (see figure 3-17 and 3-18). This is probably due to radial in-leakage at this station under the low flow, low power conditions.

NUCLEAR

EP-1A

APPROACH TO CRITICALITY

Peripheral Poison Wire Removal

Peripheral poison wire removal operations were completed prior to experimental plan 1A. Initially the NRX-A2 contained 6990 poison wires, with the loading configuration shown in figure 3-19. With all twelve control drums locked in their zero degree position, poison wires were removed by groups of clusters starting from the core edge. Neutron count rate data was taken after each peripheral removal increment on three BF_3 proportional counters, as shown in figure 3-20, designated safety monitor detectors, and on a fourth, the criticality control detector, which is not shown.

The neutron count rate from each detector was normalized to 1.0 with the full core inventory of 6990 wires, and a plot of inverse count rate against the number of wires removed was developed for each detector.

The peripheral poison wire increments and the raw and normalized count rate data are presented in the NRX-A2 Site Test Report, NTO-R-0008.

REFERENCE	[redacted]	PREPARED BY	APPROVED BY	Astronuclear

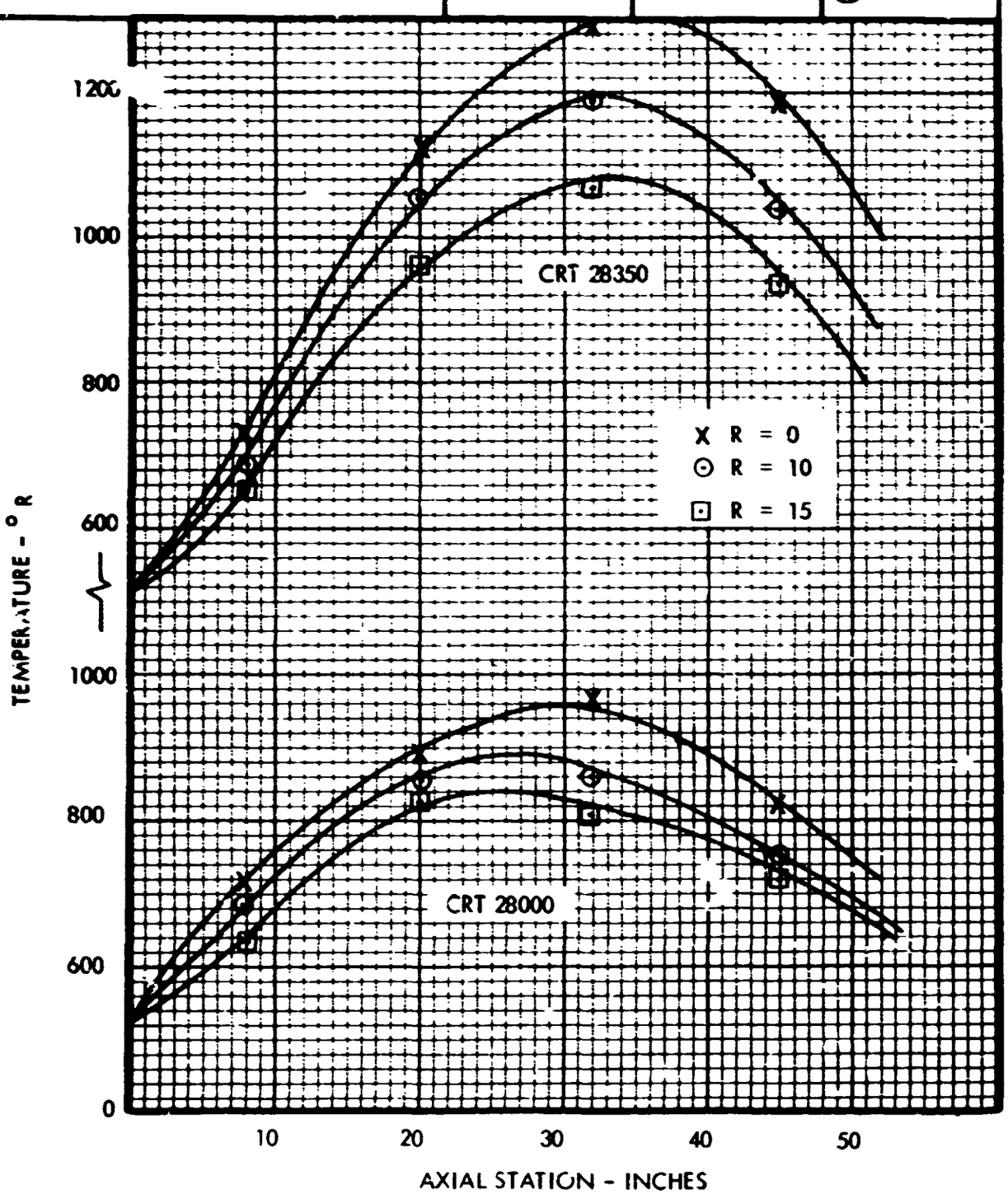

EP II TEMPERATURE COEFFICIENT TEST, AXIAL TEMPERATURE DISTRIBUTION IN CORE

CURVE NO	FIGURE NO.
	3 - 16

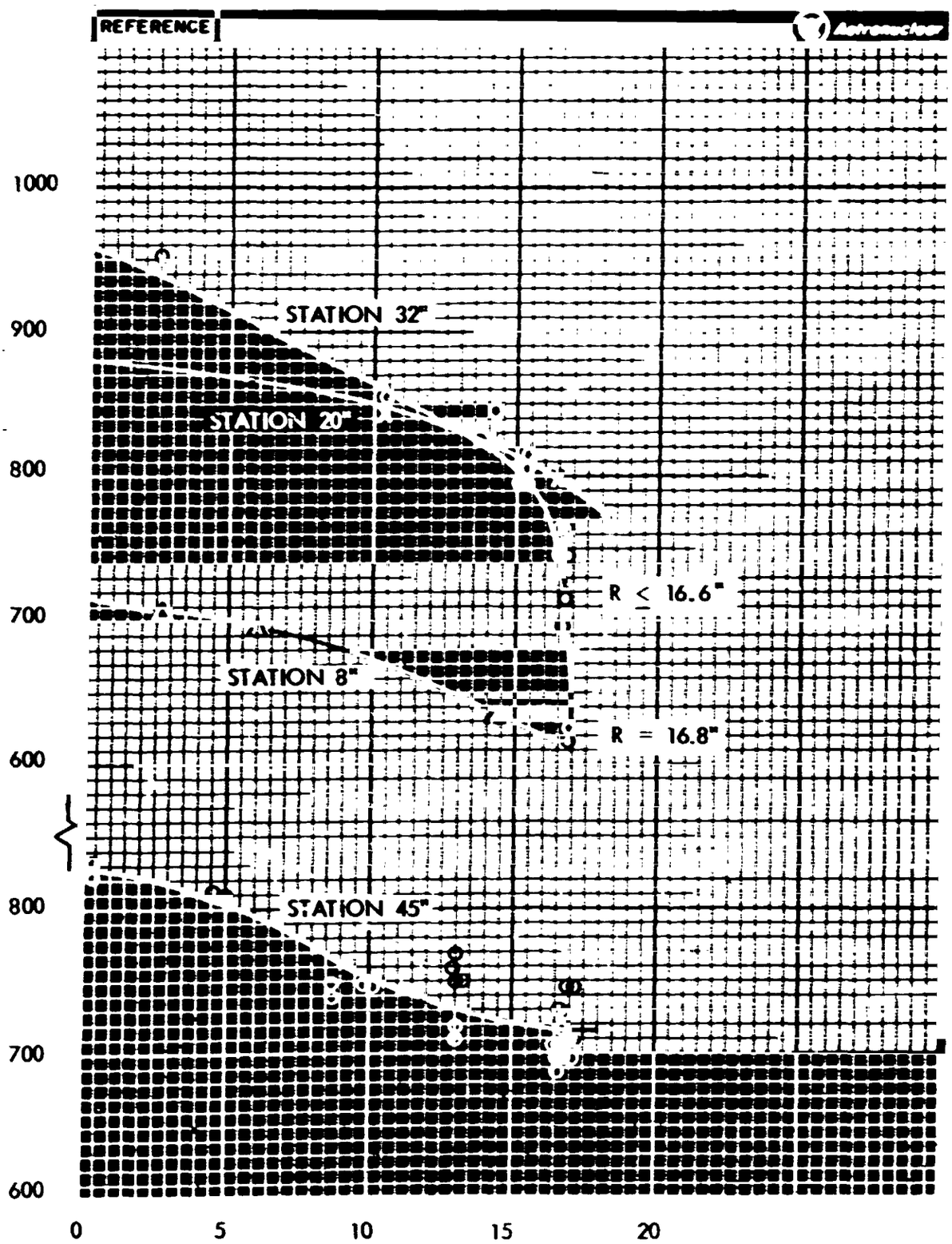

CURVE NO.	
APPROVED BY	
PREPARED BY	

CORE MATERIAL TEMPERATURE EP II CRT 28000

FIGURE NO.

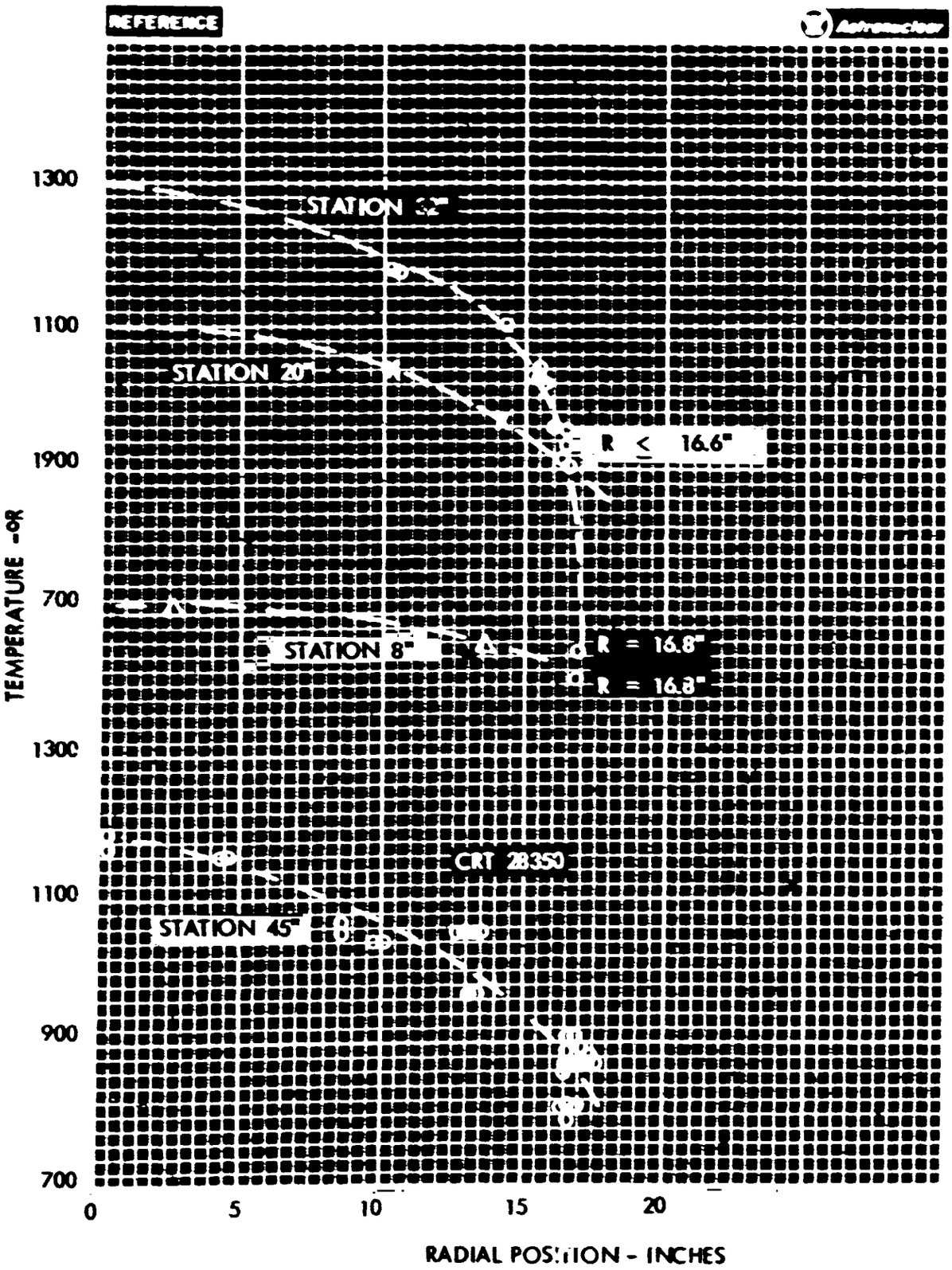

CURVE NO.

APPROVED BY

PREPARED BY

CORE MATERIAL TEMPERATURE FP II CRT 28350

FIGURE NO.

3 - 18

REFERENCE		PREPARED BY	APPROVED BY	Astronuclear
		TFS	[illegible]	

42 POISON WIRES PER CLUSTER

24

36

72

Total Number of Wires for Shipping 6990

Number of Wires to be Present After Nozzle is Installed 798 (Central Region)

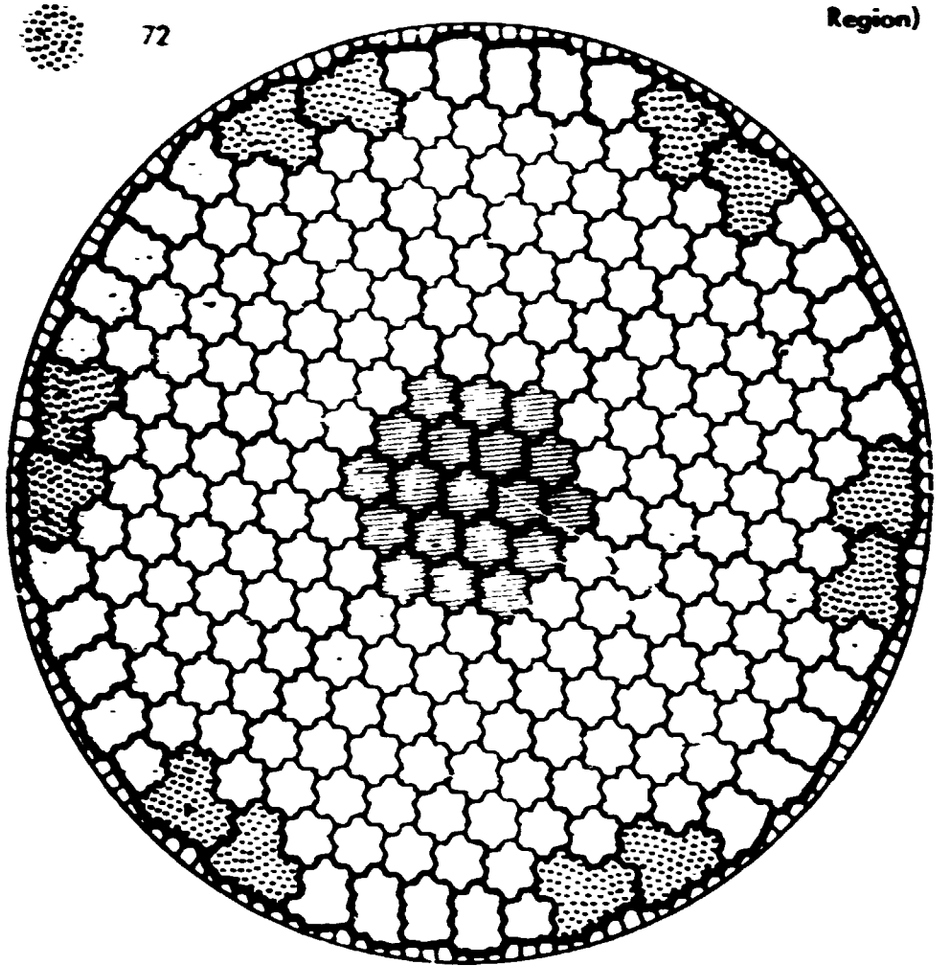

POISON WIRE LOADING PATTERN FOR THE NRX-A2

FIGURE 3 - 19

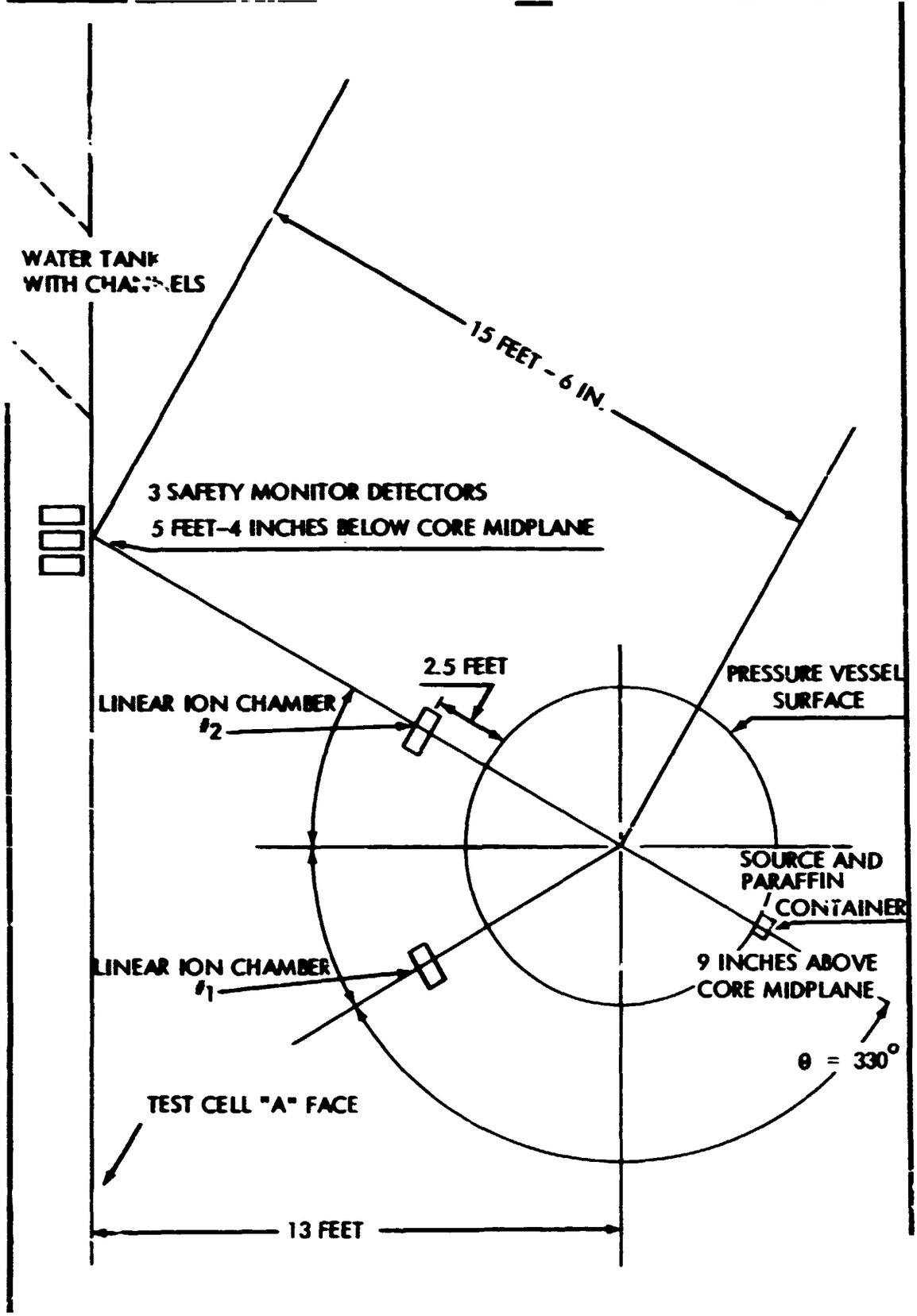

CURVE NO.	APPROVED BY	PREPARED BY

REACTOR-SOURCE-DETECTOR GEOMETRY FOR EP-1A OF NRX-A2

FIGURE NO. 3-20

Because of the slowness in approaching criticality the counting rates on the detectors follow the subcritical multiplication equation; i.e.,

$$\text{Counting rate} = \frac{A}{1-K}$$

In a reactor containing a source, the number of neutrons which exist in this multiplying medium at the end of a sufficiently long interval of time is:

$$n = S\tau\,(1 + K + K^{2} + \ldots\ldots + K^{m-1})$$

In closed form, for long intervals of time this expression becomes

$$n/S\tau = \frac{1}{1-K}$$, This ratio being known as the subcritical multiplication factor.

The constant A is a function of the source and detector geometry, the source strength S , and the neutron lifetime τ. As the multiplication factor K approaches untiy, the counting rate approaches infinity and the reciprocal count rate approaches zero. The inverse count rate data of the three safety monitor detectors was averaged and plotted in figure 3- 21 along with the predicted [1] inverse count rates for three drum bank positions, based on the NRX-A2 PAX experiment.

Extrapolation of this curve to criticality shows that the NRX-A2 is approximately 13.0$ subcritical with all drums positioned at 0 degrees and 19 clusters of 42 poison wires each (total of 798 poison wires) left in the core. (The shutdown of NRX-A2 is further discussed in the following subsection where the 13.0$ value is substantiated).

The difference between the predicted and measured inverse multiplication at the 0 degrees drum bank position is attributed to differences in the source and detector geometry and detector response between the two experiments. Figure 3-22 shows the source and detector locations used in the PAX approach to critical.

1 WANL-TME-887, NRX-A2 Test Prediction Report

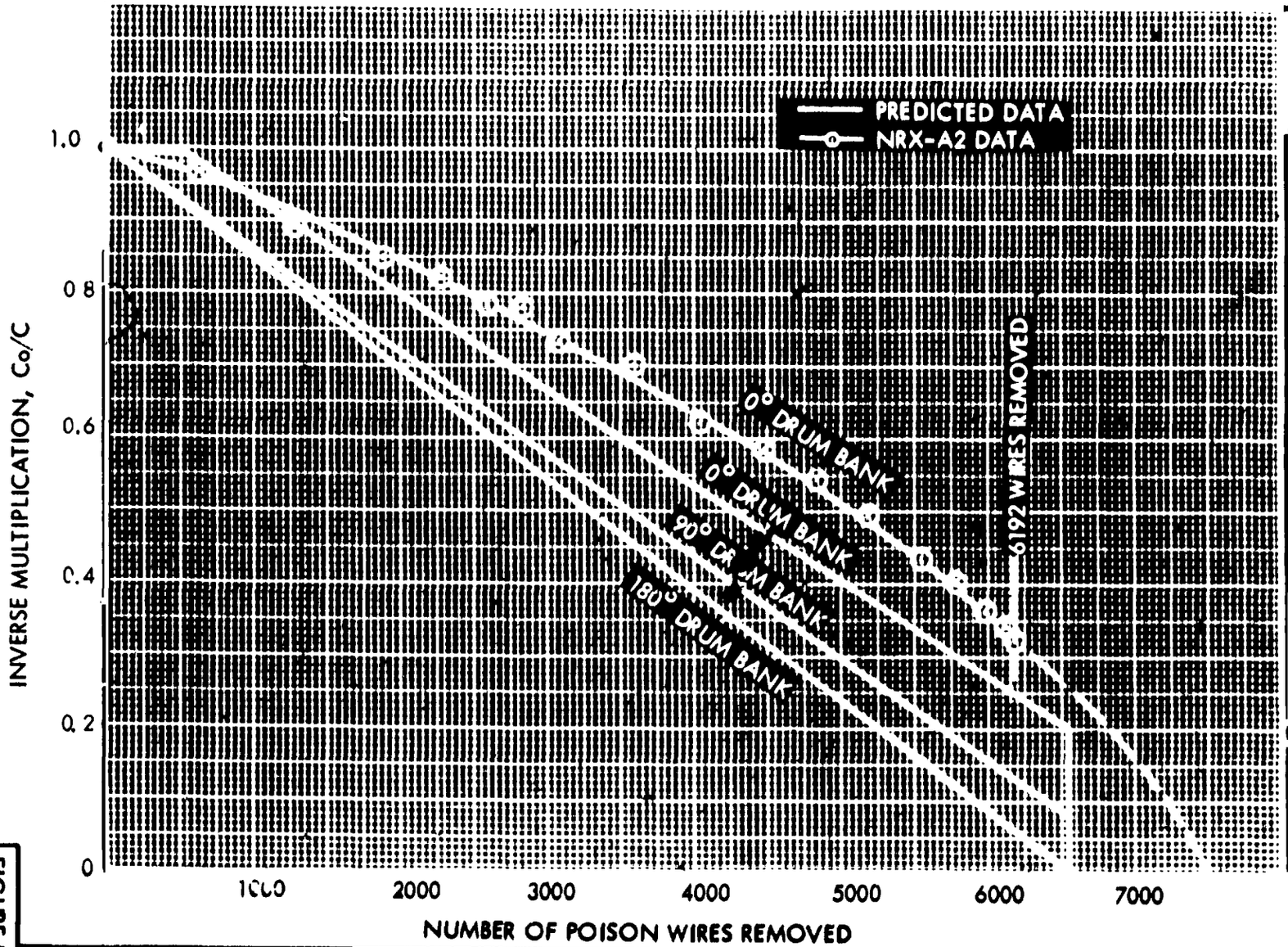

FIGURE NO.	INVERSE MULTIPLICATION VERSUS NUMBER OF PERIPHERAL POISON WIRES REMOVED	PREPARED BY	APPROVED BY	CURVE NO.
3 - 21		TPS Jr.		

REFERENCE

Astronuclear

[redacted]

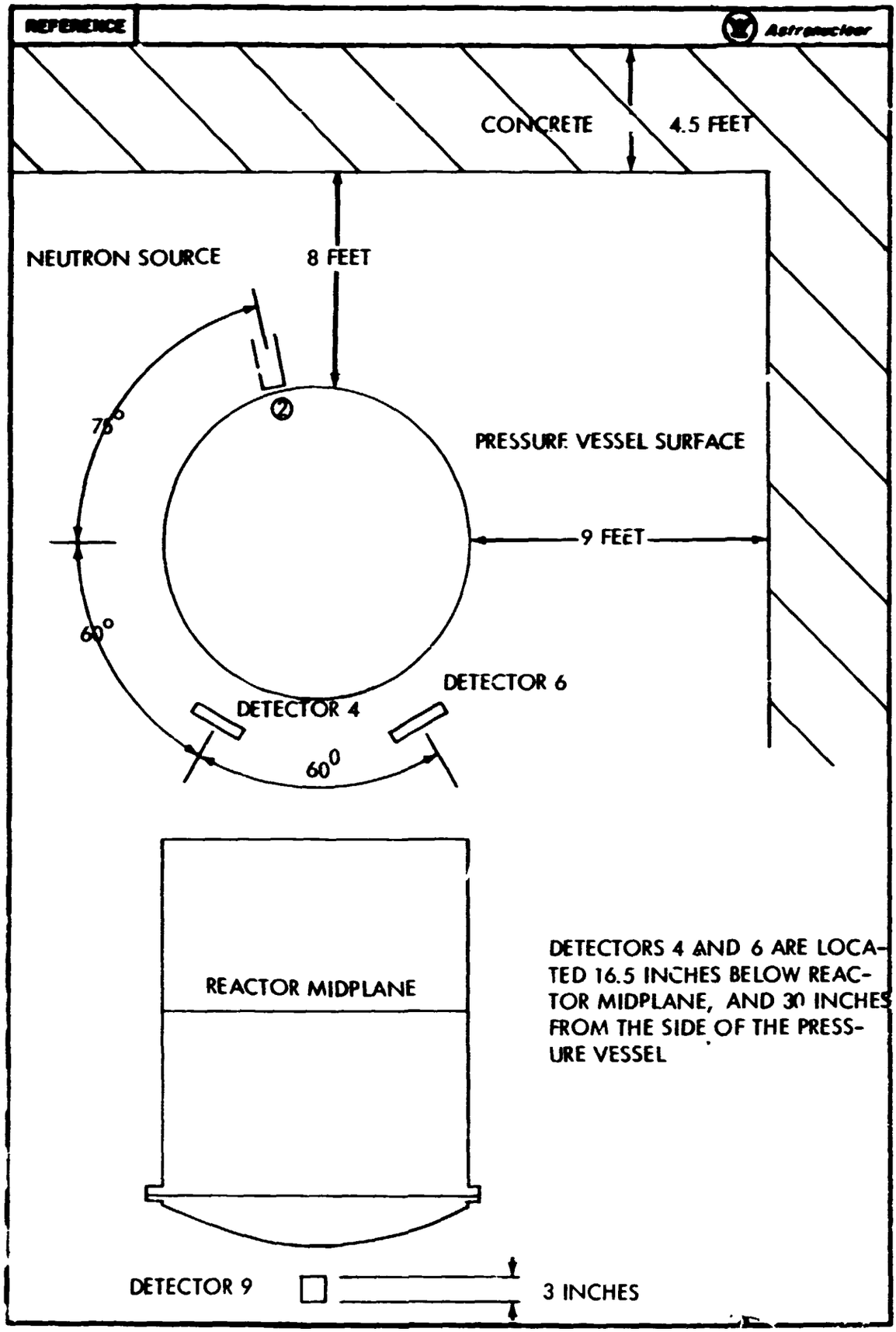

CURVE NO.

APPROVED BY

PREPARED BY

REACTOR-SOURCE-DETECTOR GEOMETRY FOR PAX

FIGURE NO.
3 - 22

Central Poison Wire Removal

Prior to this experimental plan (see subsection 1) all poison wires were removed except those in the central region of the core, 19 clusters of 42 wires each or 798 total. The remaining wires had been calculated to provide sufficient shutdown margin so that inadvertent rotation of the control drums would not cause the reactor to go critical. The approach to initial criticality commenced by the incremental removal of 11 of the 19 poison wire clusters. The removal increments proceeded radially inwards, maintaining approximate symmetry. Table 3-4 shows the sequence in which the poison wire clusters were removed.

During the incremental removal operations, neutron count rate data was obtained at control drum bank positions of 0, 90, and 180 degrees, using the same three safety monitor detectors utilized in the peripheral poison wire removal operations. The neutron count rate data is tabulated in table 3-5. From this data the inverse count rate, or inverse multiplication, was developed and is shown in figure 3-23 for the 0, 90, and 180 degree drum bank positions as a function of poison wires remaining in the core. The zero degree curve has been normalized to 1.0 with the central 798 poison wires remaining in the core.

Initial criticality was achieved with 8 clusters of poison wires remaining in the core. With this poison wire loading, the core was approximately 5.5¢ supercritical with the drums full out, and the critical bank position was 172.9 degrees.

After initial criticality additional count rate data was recorded at the 0 and 90 degree drum bank positions. It should be noted that the data taken following removal increment No. 7 (table 3-5) is affected by power operations after initial criticality. Therefore, it is not used in the inverse multiplication curves of figure 3-23. Also it is seen that early smooth extrapolation of the inverse counting rate at the 180 degree drum bank position could have predicted the initial criticality to within ± 10 poison wires. This verifies the inherent safety of the technique used in the approach to critical. Extrapolating the 90 degree data, it is seen that the inverse count rate reaches zero at about zero wires, which implies criticality with no wires present in the core at a drum bank position of approximately 90 degrees.

TABLE 3-4

EP IA POISON WIRE REMOVAL SEQUENCE

Increment	Clusters
1	1-B1, 3-B1, 5-B1
2	2-B1, 4-B1, 6-B1, 4-B2
3	2-B2, 5-B2
4	3-B2
5	1-B2
6	6-B2, 4-A1
7	6-A1, 3-A1
8	2-A1, 5-A1
9	1-A1, 0-00

TABLE 3-5

EP IA INVERSE MULTIPLICATION DATA

Poison Wire Removal Increment Number	Number of Wires Removed This Step	Number of Wires Remaining in Core	0° DRUM BANK Scaler 1 Counts per 5 minutes	0° DRUM BANK Scaler 2 Counts per 5 minutes	0° DRUM BANK Scaler 3 Counts per 5 minutes	90° DRUM BANK Scaler 1 Counts per 5 minutes	90° DRUM BANK Scaler 2 Counts per 5 minutes	90° DRUM BANK Scaler 3 Counts per 5 minutes	180° DRUM BANK Scaler 1 Counts per 5 minutes	180° DRUM BANK Scaler 2 Counts per 5 minutes	180° DRUM BANK Scaler 3 Counts per 5 minutes
-	---	798	8927	1235	4736	15488	2038	8006	37797	4869	19482
1	126	672	9629	1268	5174	17546	2274	9069	49889	6309	25777
2	168	504	10944	1434	5686	21775	2791	11224	97034	12200	49495
3	84	420	11664	1493	6185	(5094)*	(649)	(2648)	(35714)	(4577)	(18409)
4	42	378	12322	1615	6388	(5555)	(689)	(2820)	(67310)	(8744)	(34788)
5	42	336	12681	1647	.6714	(5718)	(738)	(2973)	Critical	Critical	Critical
6	84	252	14512	1823	.6911	(7531)	(1016)	(3658)	-	-	-
7	84	168	41520	5364	24070	(20381)	(2619)	(10751)	-	-	-
			(7971)	(969)	(4312)				-	-	-
8	84	84	(7302)	(941)	(3845)				-	-	-
			(6972)	(915)	(3785)	(24990)	(3245)	(12873)	-	-	-
			(6251)	(872)	(3447)	(57876)	(7573)	(29961)	-	-	-
9	84	0	(6558)	(828)	(3401)	(126355)	(8512)	(34155)	-	-	-
			(6380)	(838)	(3284)				-	-	-

NOTE * Parentheses indicate one minute count data.

The count rate data for the 0 degree and 90 degree drum positions taken following removal increments 8 and 9 is affected by previous operations at power. In each case several count rates were taken to indicate this effect.

PREPARED BY	APPROVED BY	CURVE NO.

CONFIDENTIAL RESTRICTED DATA

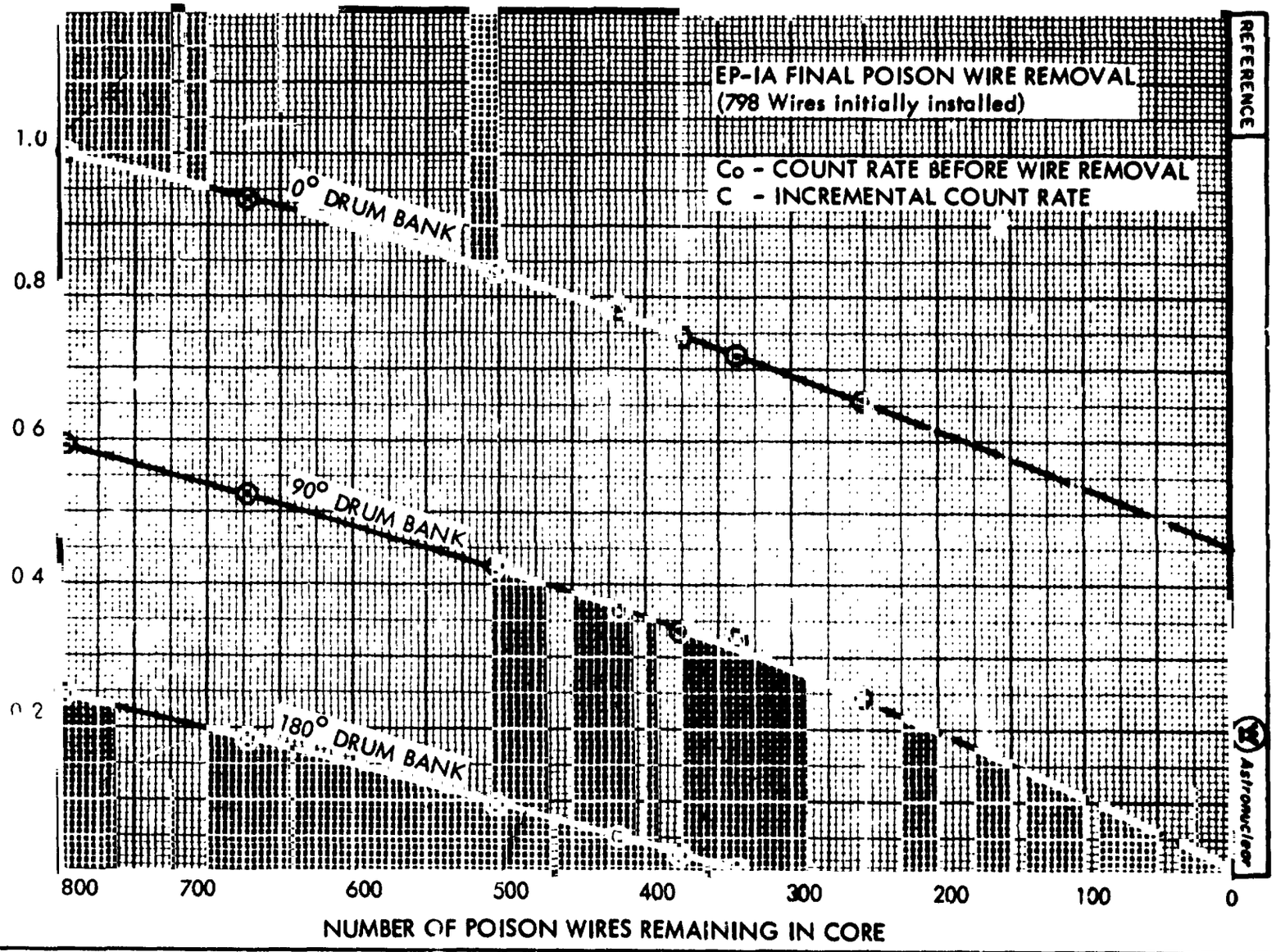

FIGURE NO.	INVERSE MULTIPLICATION VERSUS NUMBER OF POISON WIRES REMAINING	PREPARED BY	APPROVED BY	CURVE NO.
3-23		TPS		

CONFIDENTIAL RESTRICTED DATA

During the final wire removal the control drum bank moved inward, until with no wires present in the core the delayed critical bank position was 98.6 degrees. Before comparison with the predicted 91 degrees ± 10 degrees, corrections must be made to this value for the differences in the reactor configuration between EP 1A and that used in the original prediction. This is discussed in the pages that follow in the section on Delayed Critical Drum Bank Position Without Nozzle where a correction of -1.7 degrees is developed. The comparable delayed critical position then becomes 96.9 degrees indicating the predicted reactivity of NRX-A2 to be too high by the equivalent of 6 degrees drum motion, or 46 cents. The effect of system temperatures on the critical position is also discussed in the same section.

Figure 3-24 shows the measured and predicted delayed critical drum bank positions during the final wire removal, together with a curve of the measured position after adjusting to the configuration used in the predictions. It was predicted that the NRX-A2 would be critical at a control drum bank position of 180 degrees with 425 ± 80 poison wires remaining in the center of the core. The comparable experimental curve shows the NRX-A2 to be critical with all drums at 180 degrees and 360 wires remaining in the core. The discrepancy of 65 poison wires or about 71 cents in reactivity is due to the discrepancy between the predicted critical position of 91 degrees and the measured critical position of 96.9 degrees in both cases with no poison wires present in the core and to differences in poison wire worth between the PAX and NRX-A2 reactors. This difference is shown in figure 3-25.

From the measured worth of the poison wires one is able to calculate the shutdown of the NRX-A2 with 798 poison wires remaining in the center 8 inch circle. Figure 3-26 shows the NRX-A2 shutdown to be 3.75$ at a drum bank position of 180 degrees with the center 8-inch circle containing 798 poison wires. Adding the 9$ drum bank worth, the NRX-A2 shutdown at the 0 degree drum bank position is 3.75$ + 9.00$ = 12.75$, confirming the estimate derived from figure 3-21.

It should be noted that figure 3-26 has been generated by extrapolating the poison wire worth at initial criticality to nearby subcritical regions. The accuracy of the extrapolation has been substantiated by calculations performed for the PAX core (two calculated points

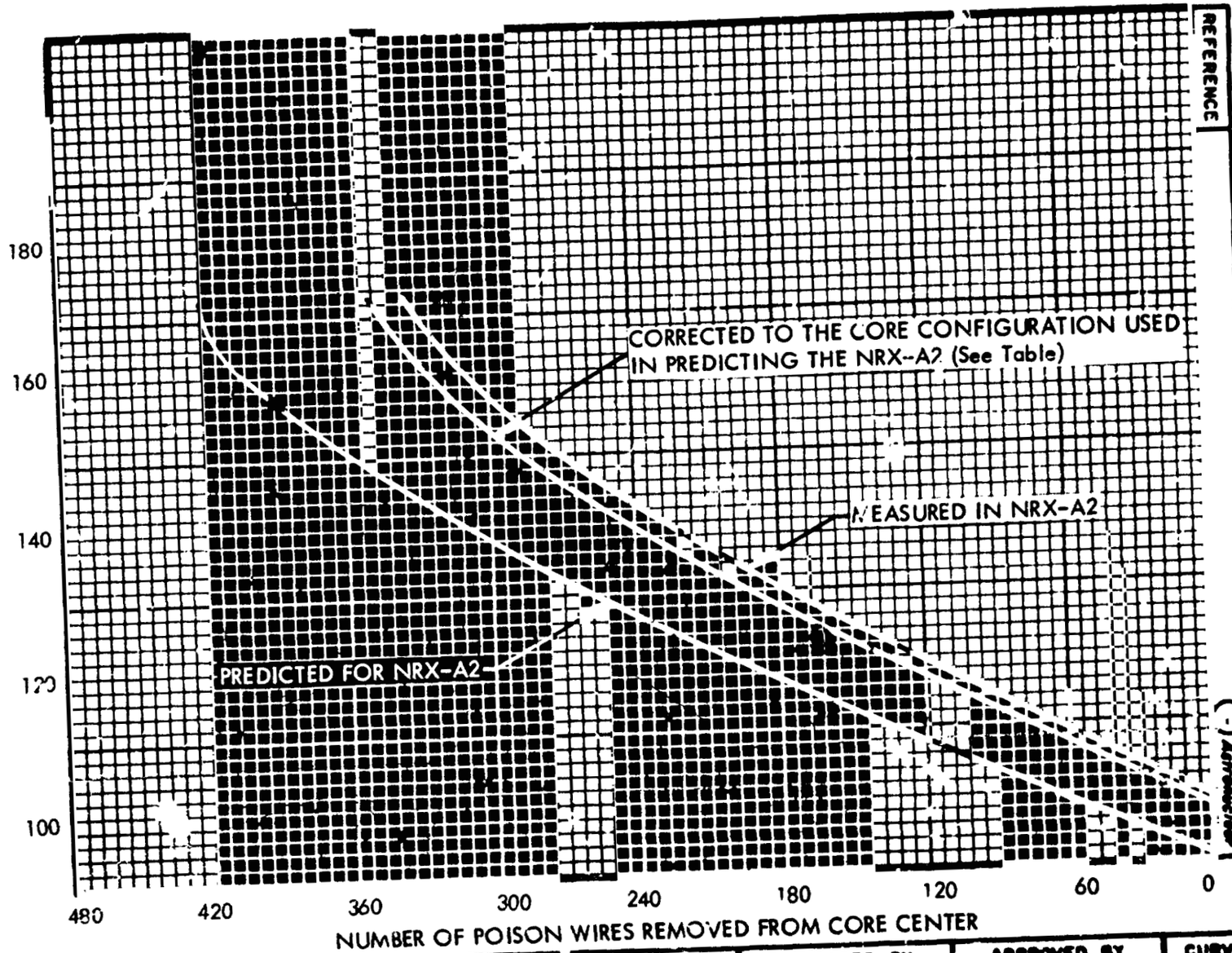

REFERENCE

(-) Astronuclear

FIGURE NO.		PREPARED BY	APPROVED BY	CURVE NO.
3 - 24	CRITICAL DRUM POSITIONS DURING FINAL POISON WIRE REMOVAL			

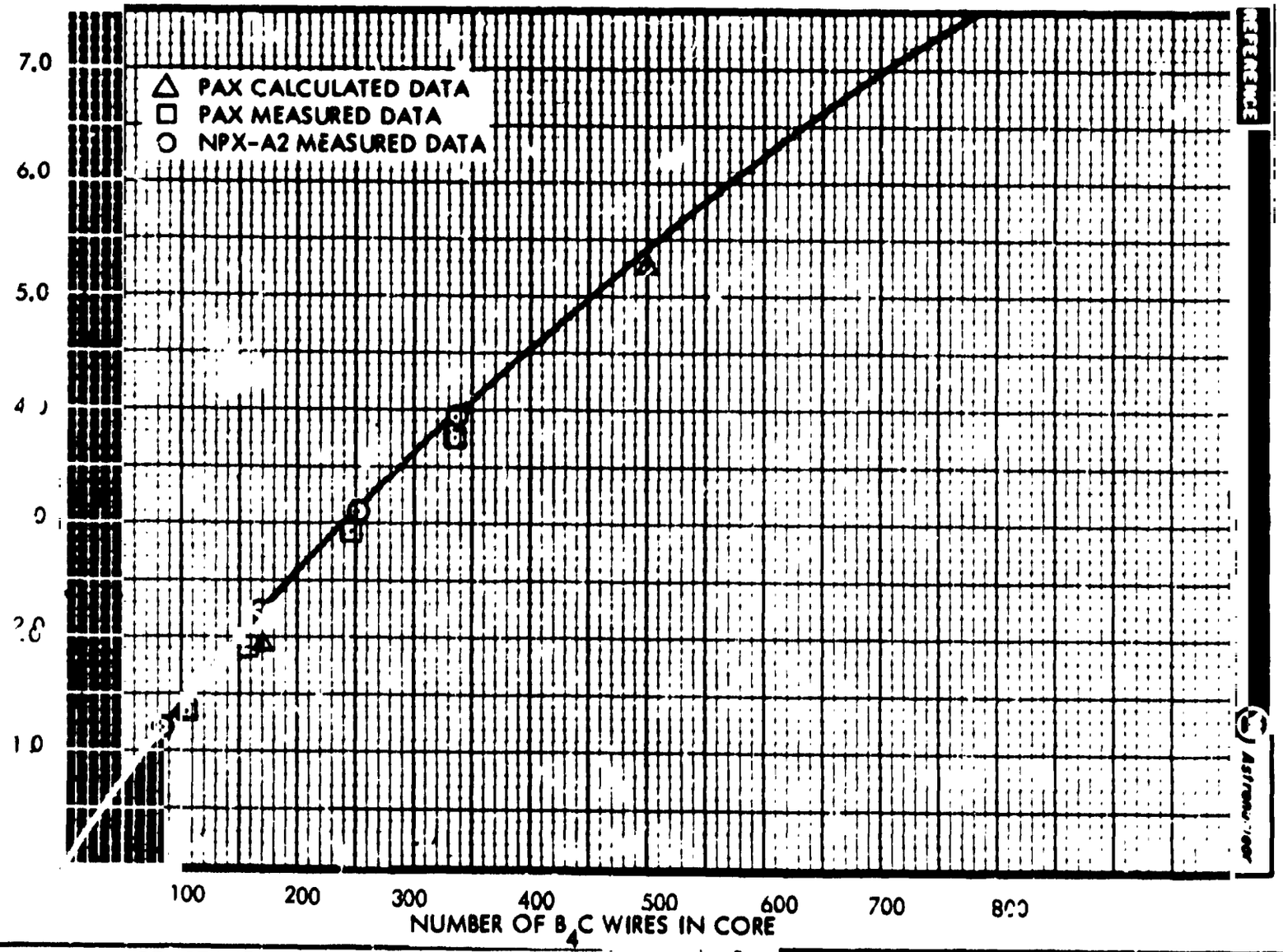

REFERENCE

Astronuclear

REACTIVITY WORTH OF POISON WIRES AT THE CORE CENTER CIRCLE	PREPARED BY	APPROVED BY	CURVE NO.

FIGURE NO. 3-25

CONFIDENTIAL RESTRICTED DATA

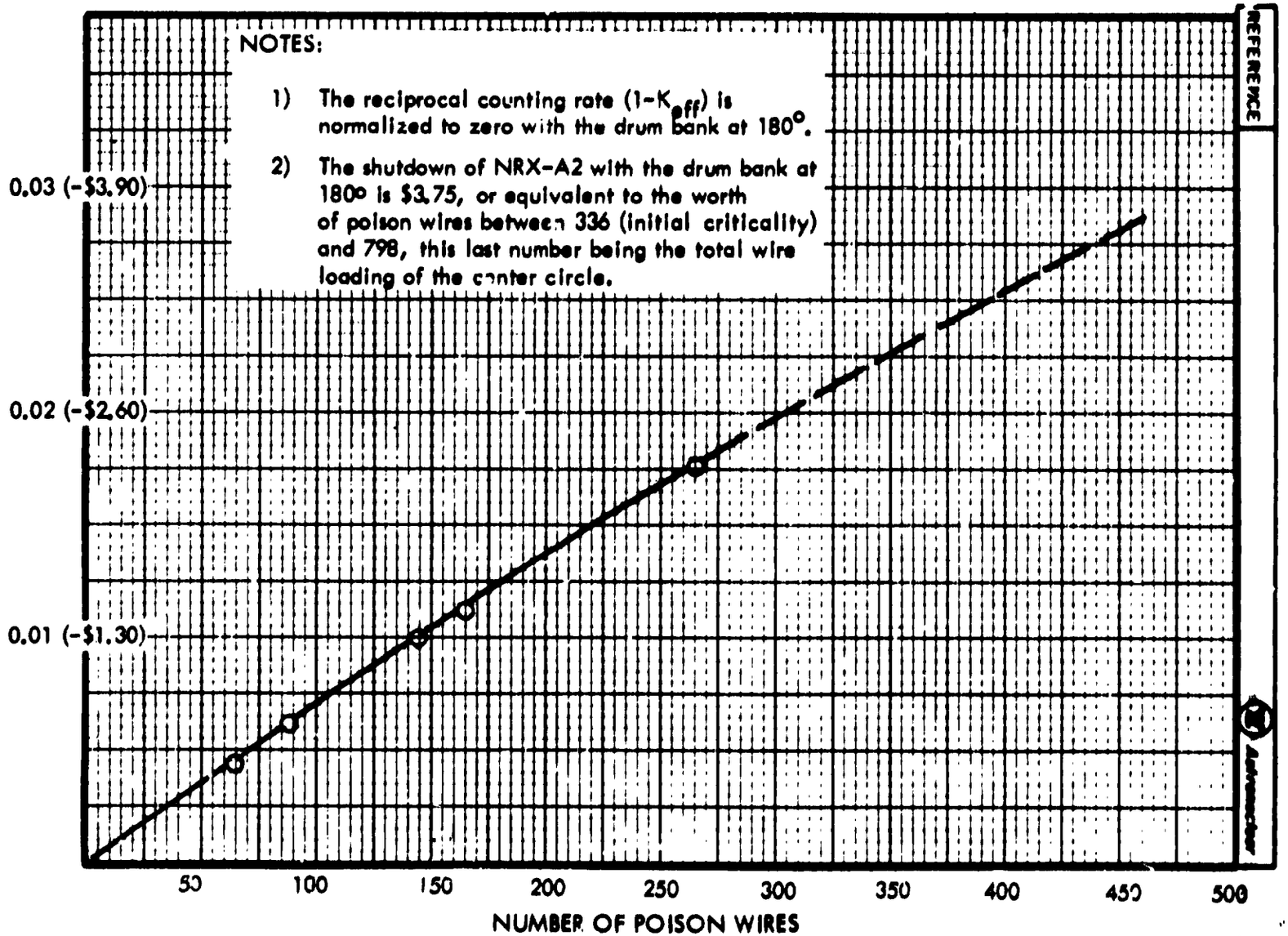

SHUTDOWN OF NRX-A2 VS. NUMBER OF POISON WIRES REMAINING IN CENTER OF CORE WITH DRUM BANK AT 180°	PREPARED BY	APPROVED BY	CURVE NO.

FIGURE NO. 3 - 26

CONFIDENTIAL RESTRICTED DATA
Atomic Energy Act of 1954

are shown in figure 3-25). The shutdown of 3.75$ is associated with NRX-A2 and cannot be applied to reactors such as NRX-A3 which have a different inherent reactivity.

DIFFERENTIAL AND INTEGRAL DRUM BANK WORTH

Following initial criticality the remainder of the poison wires were removed in four steps of two clusters each. After each removal increment, data necessary to determine the differential drum bank worth was obtained. The data points may be classified into three categories depending upon whether the reactor was critical, supercritical on a long period, or supercritical on a short period. All data obtained is tabulated in table 3-6. Figure 3-27 shows the predicted differential control drum bank worth during the final wire removal, together with the experimental points derived from the three conditions described above. The scatter in the data is the result of the operational problems discussed in the NRX-A2 Site Test Report.[1] In each case, the periods were obtained by analysis of the Sanborn Quick Look Data. Since the control drum position measurements were not as accurate as might be desired, the control drum bank worth is more closely represented by the points obtained by comparing the conditions associated with the largest drum movement, i.e., critical to the short period. This data is well represented by the predicted curve, as shown in the figure. The predicted integral drum bank worth shown in figure 3-28 is accordingly verified also, confirming the total control span to be within the predicted 9.0 ± 0.4 dollar estimate, based on PAX. The drum worth measurements in PAX, reported in WANL-TNR-158, Pre-Assembly Experiment in Support of NRX-A2, indicated a total span of 8.57$ for the PAX reactor as it was tested, or 9.73$ if the stainless steel components of the core bundling mechanism were removed. The latter number was further corrected for the estimated 25 kg increase in carbon mass in the NRX-A2 lateral support and inner reflector and for differences in steel, beryllium and boron mass to derive the 9.0$ NRX-A2 prediction.

---

1 NTO-R-0008, NRX-A2 Site Test Report, 30 November 1964

TABLE 3-6

DIFFERENTIAL CONTROL DRUM BANK WORTH DATA AND CRITICAL BANK POSITIONS FOLLOWING POISON WIRE REMOVAL FOR EP IA

Reactor Condition	Banked Drum Position (degrees)	Resulting Period (seconds)	Differential Control Drum Worth - ¢/° at Drum Angle in Degrees: "Called" Crit. to Long Period	"Called" Crit. to Short Period	Short Period to Long Period	Critical Bank Position (degrees)	Shutdown Worth Measurements (dollars)
Initial Criticality	179.22	196	.88				
(8 clusters remaining)	172.93		at 176.08	-	-	172.93	
Following Removal	145.6	152	4.28	4.15	4.14		
Increment No. 6	150.68	20	at 145.13	at 147.67	at 148.14	144.0	9.60
(6 clusters remaining)	144.67	400					
Following Removal	130.45	53.8	6.86	6.23	5.83		
Increment No. 7	133.97	12.2	at 129.34	at 131.1	at 132.21	128.23	8.20
(4 cluster remaining)	128.23						
Following Removal	114.0	500					
Increment No. 8	119.37	8.6		7.11	-	113.7	5.75
(2 clusters remaining)	113.45	-500		at 116.47			
Following Removal	101.32	29.5	8.58	7.81	7.17	98.6	4.80
Increment No. 9	104.47	7.2	at 100.01	at 101.59	at 102.9		
(0 clusters remaining)	98.63						

NOTE: Control drum bank positions are based on the manual average of the individual drum printouts. These values should be rounded off to the nearest tenth.

REFERENCE		PREPARED BY	APPROVED BY	Astronuclear
		TPS		

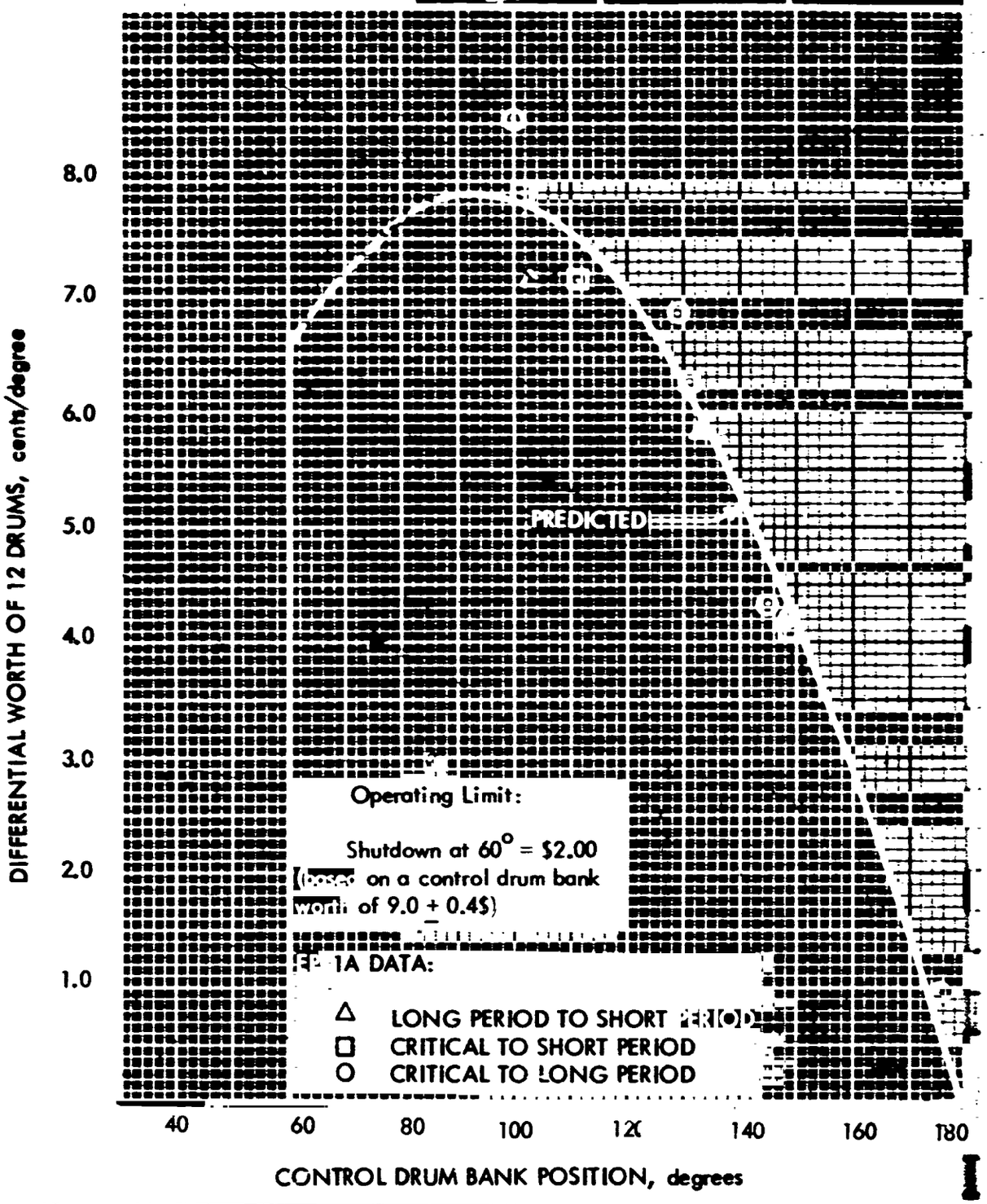

NRX-A2 CONTROL DRUM BANK DIFFERENTIAL WORTH	CURVE NO.	FIGURE NO.
		3-21

REFERENCE

Astronuclear

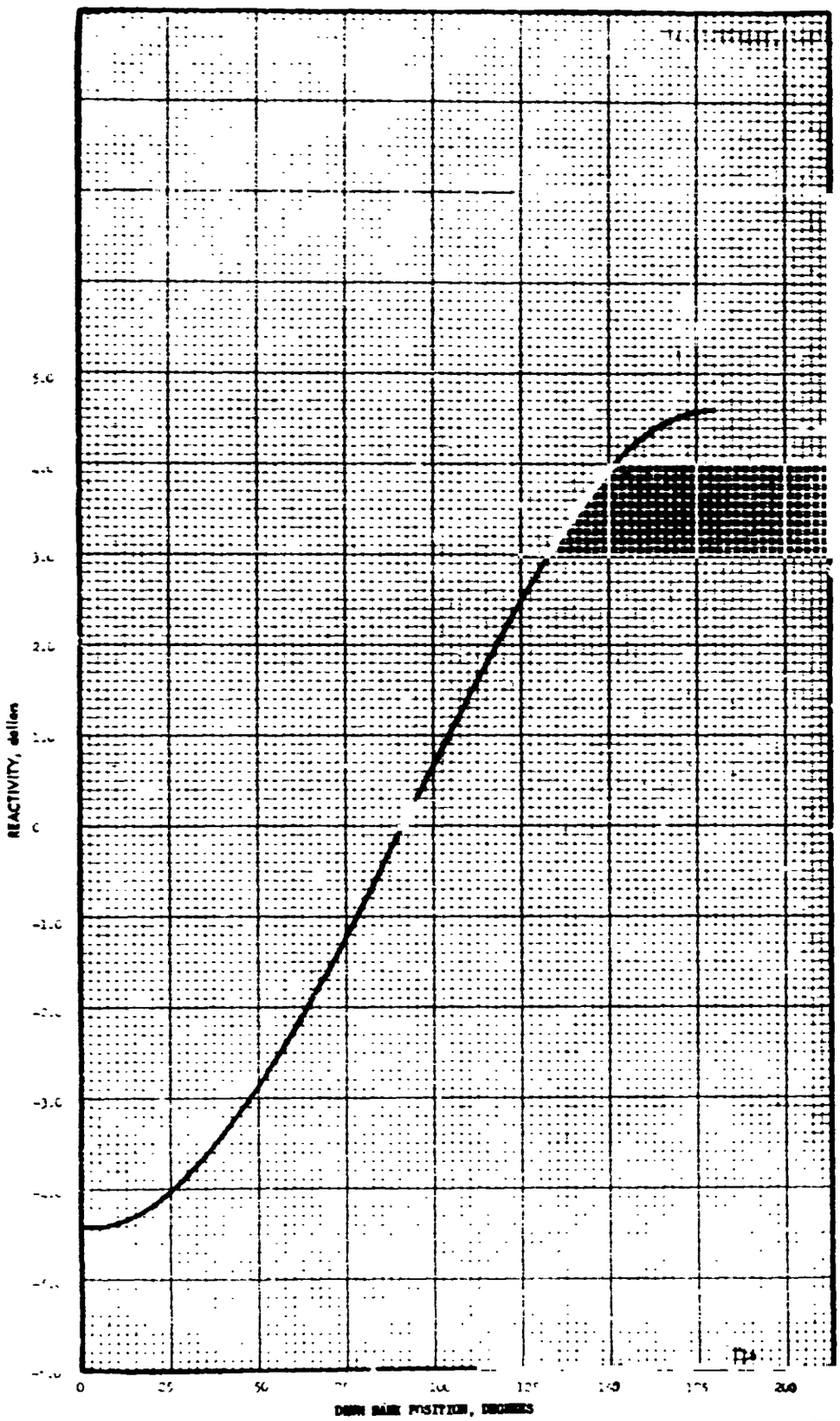

CURVE NO.

APPROVED BY

PREPARED BY

NRX-A2 INTEGRAL CONTROL DRUM BANK WORTH

FIGURE NO.

[redacted] - 28

NRDS regulations demand that all reactor operations maintain a 2$ shutdown capability. From figure 3-28 it can be seen that the drum bank position to provide this shutdown was 60 degrees for NRX-A2. This number includes an uncertainty of ± 0.2$ on the worth of the drums in the interval from 90 degrees to 0 degrees.

The NRX-A2 drum bank measurements during initial criticality substantiated the accuracy of the prediction as can be seen from figure 3-27 and 3-28. After criticality was reached an additional measurement of the differential worths of Control Drums 2 and 8 was made and is discussed in chapter 3 of this report. These measurements also confirm the maximum differential worth of 7.85 cents per degree shown in figure 3-27.

Delayed Critical Drum Bank Position Without Nozzle

Many measurements of the delayed critical control bank position were made during EP 1A. The better of these have been studied in detail and are listed in table 3-7. Of these it appears that the first measurement of 98.6 degrees taken at Time CR 29198 is the best. This conclusion is based on the discussion below.

Early work with the data available in the three day report[1] indicated that the observed variations in the critical bank position (table 3-7) resulted from variations in power. In trying to establish whether the magnitude of this effect would account for the spread in critical positions seen, measurements were made at WANEF of the reactivity error resulting from measurements made at various (low) power levels. The results,[2] shown in figure 3-29, indicate that an error of several degrees in drum bank position can occur during operation in the power range 1 to 2 decades above startup level. However, the linear power indicators (channels 1 and 2, Sanborn 108-A) could not be downranged to give a non-zero reading at this reference level; hence, it was not possible to determine exactly at what decade level the measurements during EP 1A were made. Fortunately, in reviewing the data further, it was seen that the range changes which did occur were sufficient themselves to make corrections for the source

1 NTP-R-0001
2 WANL-TME-1053, "PAX Critical Experiments in Support of NRX-A3.

TABLE 3-7

SELECTED DRUM BANK MEASUREMENTS DURING EP 1A

Control Room Time, seconds	Indicated Power, watts	True Power, watts	Average Drum Position*, degrees	Analysis of Sanborn Data
29198	1200, linear	37, linear	98.6	Very slight upward drift in power, not significant
	50, log	25, log		
34800	10, linear	0.31, linear	98.9	Low Power, signal fairly noisy, but updrift not apparent
35162	62, linear	2 , linear	100.5	Measurement taken after 2 decade increase in power, not enough time for delayed neutrons to come to equilibri
	~100, log	50-60, log		
35703	50, log	25, log	100.2	Drum printout time does not correspond to reasonable time for reading drums, nearest reasonable time shows reactor was supercritical.

*Average of 12 drum digital printout. These are not corrected for calibration errors as noted in tables 5 and 6 of NTO-R-0001. The NRX-A2 36 day report from NTO suggests that this correction not be made.

REFERENCE | PREPARED BY | APPROVED BY | Astronuclear

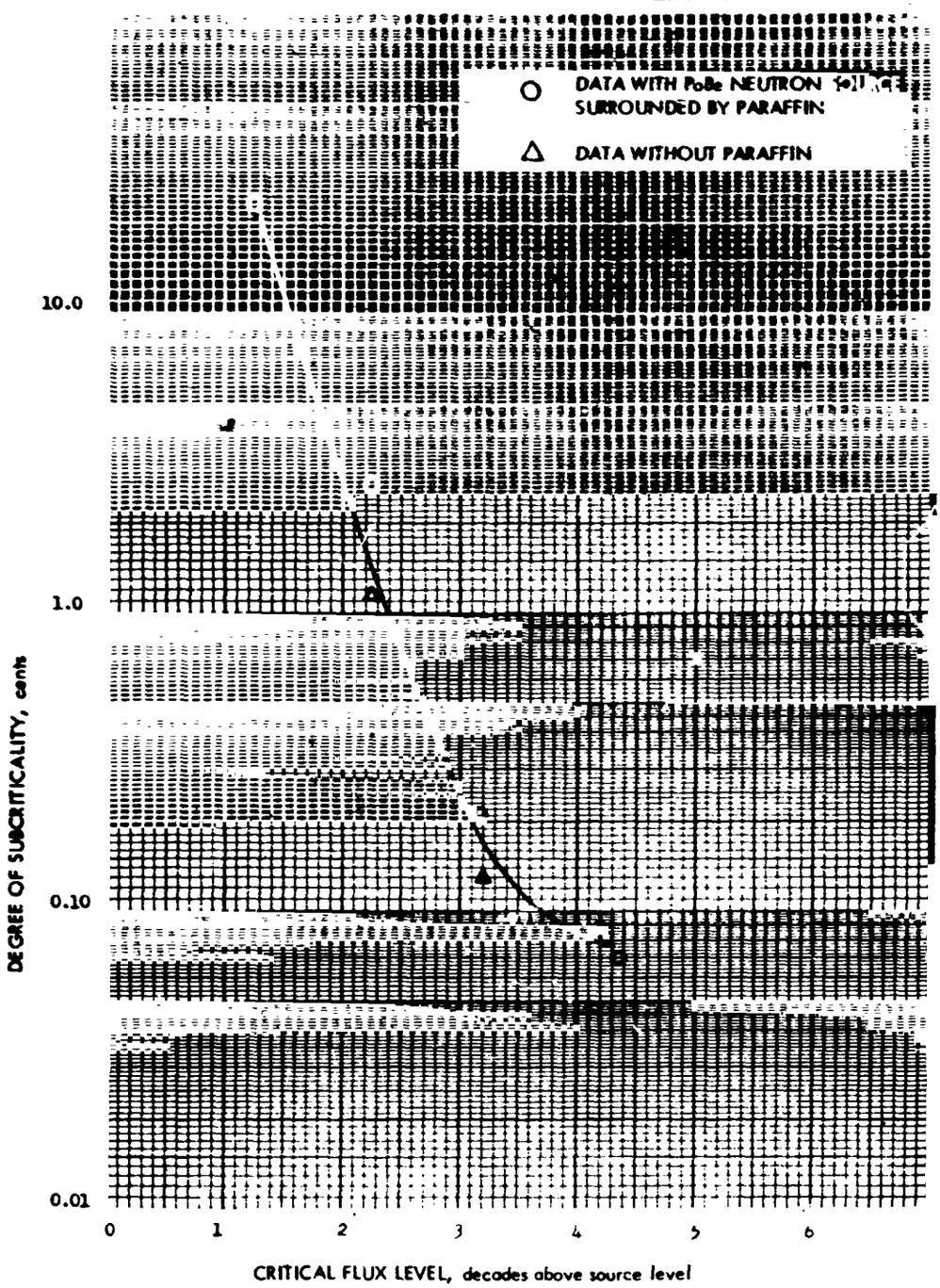

SOURCE EFFECTS ON INDICATED CRITICALITY

FIGURE NO. 3 - 29

effect negligible (per WANEF results). Thus, it was concluded that the reason for the variation in critical positions shown in table 3-7 was not generally a result of the error concomitant with low power measurements. This investigation did, however, reveal the reasons for the apparent discrepancies. These have been listed in table 3-7 for each measurement. The problems that resulted in these discrepancies were generally operational in nature and are well described in the NRX-A2 Site Test Report.[1]

No correction has been made for the deviation of reactor temperature from some (arbitrary) standard. Unless it is clearly evident that core temperatures are significantly above ambient this approach will be followed in the analysis of all critical data in NRX-A2 testing for the following reasons:

1) Generally, during the establishment of a critical condition the data system is not operating and the only channels recording are the Quick Look Channels which provide only limited data. These Sanborn channels, with a quoted accuracy of $\pm$ 2 percent, mask out the small differences that exist in ambient temperature conditions.

2) Review of weather data indicates that these temperature differences were truly small. In addition, the reactor itself should cancel out these differences because of the nearly equal in magnitude but opposite in sign temperature coefficients of the core and beryllium reflector.

Note that all drum positions quoted are as measured in the control room and not necessarily the absolute control drum position. A discussion of the errors inherent in the drum bank measurements appears in chapter 7 of the NRX-A2 Site Test Report.[1]

The configuration of the reactor system was not the same in EP 1A as it was in other testing. The changes that were made to the system after EP 1A are listed in table 3-8 along with their associated reactivity effect measured at WANEF previously reported in WANL-TME-1053. As developed here, the critical bank position expected in EP 1B is 96.9 degrees. Later measurements in EP 1B confirmed this prediction, the measured critical position being 97$\pm$ 0.5 degrees. This additional evidence supports the conclusions reached above concerning the effect of power level on critical position.

1 NTO-R-0008

TABLE 3-8

FACTORS AFFECTING THE CRITICAL BANK POSITION EXPECTED IN OTHER TESTS

Best Critical Bank Position in EP IA		98.6 degrees
Changes Made before EP IA		
Remove Al lid*	-2.2¢	
Remove polyethylene from source*	-4.7¢	
Add Nozzle*	+20.0¢	
Net	+13.1¢	
At 7.7¢/degree this results in 1.7 degrees of drum bank rotation		-1.7
Expected critical bank position in EP IB		96.9 degrees

*These reactivity effects were measured at WANEF.

The WANEF measurement for the nozzle was 18.8¢. This value was rounded to 20¢ to account for additional instrumentation not present in the WANEF measurement.

Worth of Individual Drums

The primary objective of this phase of EP 1A was to assure that the drums were of approximately equal worth rather than to determine the exact worth of each drum. This was to be accomplished by

1) bringing the reactor system to the delayed critical condition
2) establishing equilibrium,
3) rotating each drum (individually) to 180 degrees from the critical bank position,
4) measuring the associated period and
5) inferring the reactivity insertion from this period.

Using the period data in this fashion there appeared to be a significant variation in the worth of the individual drums in the vicinity of the paraffin covered neutron source (see table 3-9 reactivity addition for drums 1, 2, 11, 12).

In an effort to resolve this problem before further testing, several possible sources of error were investigated. These were:

1) a measurement at WANEF of the effect of a polyethylene block on drum worth
2) a reflector system material symmetry verification
3) further study of all measurements.

Effect of Paraffin Block on Drum Worth

To measure the effect of the paraffin neutron shield on drum worth 37.9 kg of paraffin containing the Po-Be startup source were placed against the PAXA reactor in a geometry similar to NRX-A2.[1] Using standard techniques the worth of each drum was then measured over a specific range. Shown in figure 3-30 is a comparison of worths measured with and without the polyethylene block. Note that only the shape of the two worth curves is important, not the absolute level. The reduction in the worth of drum number 1 in both cases results from the presence of a steel clamp used to bundle the core. The difference in the level of the worth curves results from the different ranges selected for drum movement. The variation in the

1 WANL-TME-1053,

CONTROLLED UNCLASSIFIED DATA

TABLE 3-9

DRUM SYMMETRY VERIFICATION, METHOD 2

Drum No.	Stable Period, Seconds	Resulting Reactivity Addition ¢	Core Reactivity Prior to Measurement[1]	Corrected Reactivity Addition[2]	Predicted Reactivity Addition for Actual Drum Motion	Drum No.2 Position Before Measurement Degrees	Measured Minus Predicted Reactivity Change, ¢
1	14.43	33.02	-0.77	33.79	34.3	97.0	-0.5
2	14.86	32.47	-0.024	32.49	33.8	98.2	-1.3
3	12.27	35.62	+2.7	32.92	34.3	97.0	-1.4
4	12.84	34.75	-5.24	40.19	40.8	87.2	-0.6
5	11.98	36.03	-13.94	49.97	49.8	73.0	+0.2
6	11.69	36.46	-13.48	49.94	49.1	74.2	+0.8
7	12.27	35.62	-5.54	41.16	41.4	86.0	-0.2
8	11.27	37.05	-3.70	40.75	39.3	89.4	+1.5
9	10.39	38.47	-3.47	41.94	38.9	89.8	+3.0
10	12.12	35.89	-4.31	40.20	40.3	87.6	-0.1
11	14.57	32.80	-1.39	34.19	33.3	98.8	+0.9
12	14.00	33.48	-8.47	41.95	41.0	86.8	+1.0
							0.3

1 The negative of the numbers in this column is the reactivity addition required to achieve a critical system. It was derived by comparing the bank position in each measurement (average of twelve) with the true critical position of 98.6 degrees and applying a bank worth of 7.7¢/degree to the difference.

2 Column 3 - column 4

REFERENCE		PREPARED BY	APPROVED BY	astronuclear
		Lic		

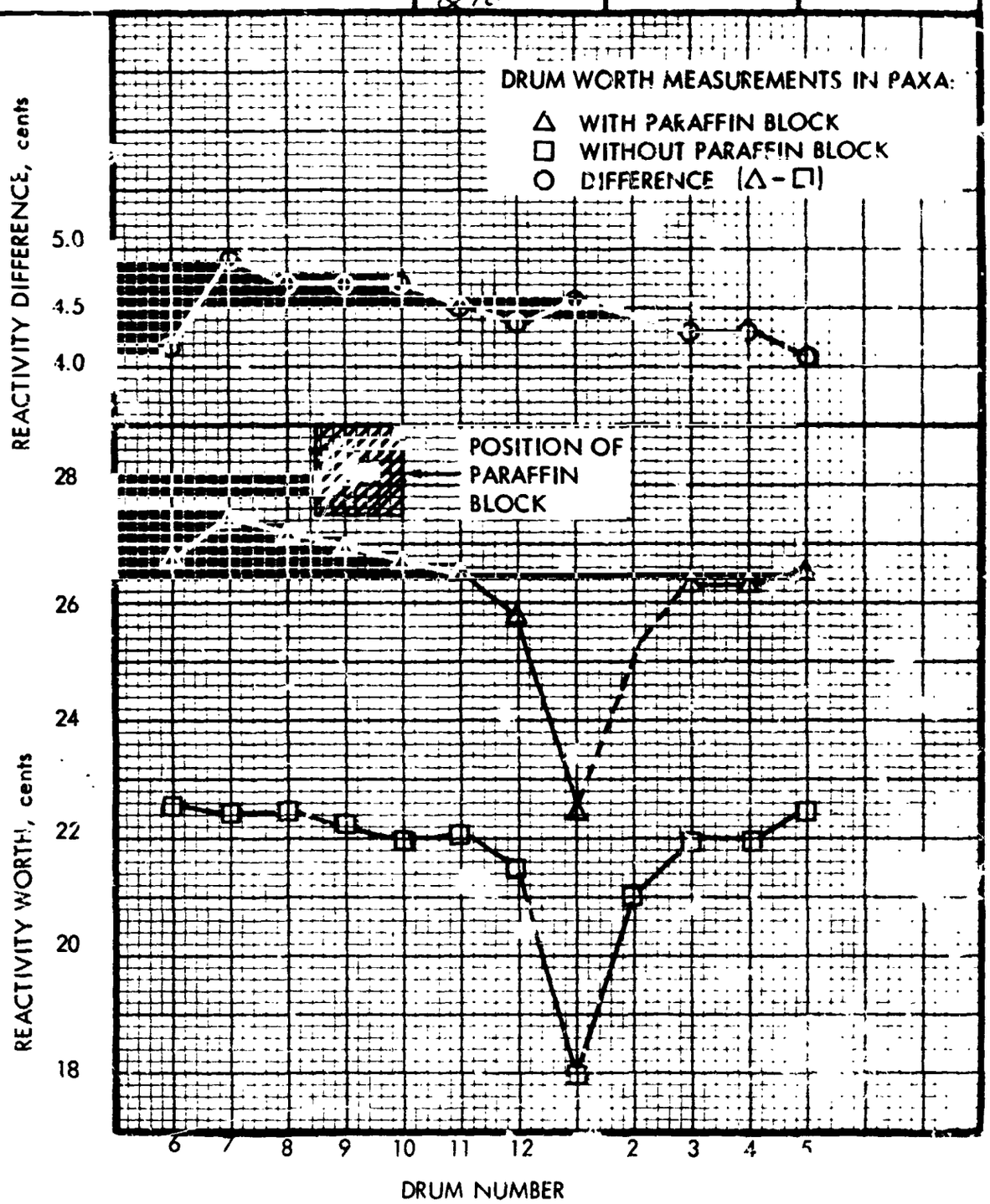

EFFECT OF PARAFFIN BLOCK ON DRUM WORTH	CURVE NO	FIGURE NO.
		3 - 30

difference between the two measurements (uppermost curve) appears to be random and the presence of the polyethylene block (between drums 9 and 10) is clearly not detectable.

Reflector System Material Symmetry

To investigate the possibility that the apparent asymmetry was caused by material differences in the reflector, a detailed study was made of the density, weight and composition of all nuclearly important reflector components. A summary of these parameters appears in table 3-10 for the Control Drum Cylinders, table 3-11 for the Outer Reflector Sectors and table 3-12 for the Control [illegible]. The absence of significant variations indicates that the apparent drum worth asymmetry did not result from composition differences.

Further Study

A closer evaluation of the data revealed that there was a wide variation of conditions under which each control drum was tested. These variations, a result of operational p[illegible]ms during this test,[1] were reflected in steps 2 and 3 of the ideal measurement technique described above. Corrections for the resultant errors have been made by two approaches as discussed below.

Method 1

In this approach, the reactor system is only considered as it existed at the conclusion of each measurement, i.e., one drum at 180 degrees[2] and the other eleven drums at some average bank position. The basis of the correction in this method is the fact that the other eleven drums were not at the same average position in each case. The conditions of each measurement appear in table 3-13. The reactivity correction is developed by converting the bank position difference from 98.6 degrees (arbitrarily used) to reactivity (at 7.7¢/degree) and adding this to the reactivity insertion inferred from the period measurement. The corrected drum worth (98.6 degrees to 180 degrees) appears in the last column of the table along with the deviation from the average

1 See chapter 7 of the NRX-A2 Site Test Report, [illegible]TO-R-0008

2 The digital readout device generally indicated 179 degrees but the change in worth from 179 degrees to 180 degrees is negligible.

TABLE 3-10

CONTROL DRUM CYLINDER

Control Drum	S/N	Identification	Pressing	Bulk density gm	Weight lb	W/o Be	W/o BeO	PPM Ti	PPM Co
1	6027	MQ18	1988	1.858	38.2	98.15	1.97	260	5
2	6025	MQ22	1988	1.858	---	98.15	1.97	260	5
3	6026	MQ14	1265	1.86	38.35	98.00	1.6	200	---
4	6028	MQ24	1988	1.858	38.2	98.15	1.97	260	5
5	6024	MQ28	1988	1.858	38.25	98.15	1.97	260	5
6	6029	MQ26	1472	1.86	38.2	98.50	1.6	---	---
7	6030	MQ16	1988	1.858	38.2	98.15	1.97	260	5
8	6031	MQ27	1988	1.858	38.3	98.15	1.97	260	5
9	6032	MQ10	1212	1.86	38.28	98.4	1.7	240	---
10	6034	MQ17	1988	1.858	38.2	98.15	1.97	260	5
11	6033	MQ20	1988	1.858	38.2	98.15	1.97	260	5
12	6035	MQ23	1988	1.858	38.25	98.15	1.97	260	5

TABLE 3-11

OUTER REFLECTOR SECTORS

Sector	Identification	Pressing	Bulk Density gm/cc	Weight lb	W/o Be	W/o BeO	PPM Ti
1	PH-1	1714	1.85	131.5	99.1	1.4	---
2	PH-11	1759	1.85	131.5	99.1	1.4	220
3	PH-3	1883	1.86	131.0	98.7	1.6	---
4	PH-8	1759	1.85	131.0	98.98	1.56	220
5	PH-5	1759	1.85	131.5	98.98	1.56	220
6	PH-12	1883	1.86	131.0	98.7	1.6	---
7	PH-9	1759	1.85	131.0	98.98	1.56	220
8	PH-15	1883	1.86	131.0	98.7	1.6	---
9	PH-6	1759	1.85	131.5	98.98	1.56	220
10	PH-7	1759	1.85	131.0	98.98	1.56	220
11	PH-2	1714	1.85	131.5	98.98	1.56	---
12	PH-10	1759	1.85	131.5	98.98	1.56	220

TABLE 3-12

CONTROL PLATES

Identification	Density, gm/cc At each end of plate		W/o B-10 At each end of plate		Identification	Density, gm/cc At each end of plate		W/o B-10 At each end of plate	
Al 200	2.55	2.55	20.26	20.41	Al 224	2.55	2.56	20.27	20.19
Al 201	2.55	2.55	20.41	20.27	Al 225	2.56	2.56	20.19	20.19
Al 202	2.55	2.56	20.27	20.14	Al 226	2.56	2.55	19.96	20.22
Al 203	2.53	2.54	20.44	20.47	Al 227	2.55	2.55	20.22	20.25
Al 204	2.55	2.55	20.12	20.94	Al 228	2.55	2.56	20.25	20.02
Al 206	2.54	2.54	20.76	20.56	Al 229	2.55	2.55	20.42	20.44
Al 207	2.54	2.54	20.56	20.80	Al 230	2.55	2.55	20.44	20.36
Al 208	2.54	2.53	20.80	20.71	Al 231	2.55	2.55	20.36	20.66
Al 209	2.55	2.55	19.90	20.14	Al 232	2.56	2.55	20.09	20.48
Al 210	2.55	2.55	20.14	20.62	Al 233	2.55	2.55	20.48	20.44
Al 211	2.55	2.55	20.62	20.02	Al 235	2.56	2.54	20.30	19.76
Al 212	2.55	2.56	19.88	20.18	Al 236	2.54	2.54	19.76	20.17
Al 213	2.56	2.56	20.18	20.27	Al 237	2.56	2.55	20.15	20.10
Al 214	2.56	2.55	20.28	19.97	Al 238	2.55	2.55	20.10	20.44
Al 215	2.54	2.56	20.27	20.24	Al 240	2.56	2.55	20.43	20.27
Al 216	2.56	2.56	20.24	19.97	Al 241	2.55	2.55	20.22	20.15
Al 218	2.54	2.56	20.65	20.24	Al 205	2.55	2.54	20.94	20.32
Al 220	2.54	2.54	21.50	20.08	Al 217	2.54	2.55	20.66	20.24
Al 221	2.54	2.55	20.08	20.23	Al 219	2.56	2.56	20.24	20.31
Al 222	2.55	2.56	20.23	19.90	Al 242	2.55	2.55	20.15	19.98
Al 223	2.56	2.55	20.41	20.27					

TABLE 3-13

DRUM SYMMETRY VERIFICATION, METHOD 1

Drum Number	Position of other 11 drums at end of measurement (θ_1), degrees	Reactivity Correction $(98.6 - \theta_1) \times 7.7$, cents	Reactivity Addition from stable period measurements, cents	Reactivity addition corrected to the same final average drum bank position/deviation from average, cents
1	98.7	-0.8	33.02	32.2 / -1.1
2	98.6	0	32.47	32.5 / -0.8
3	99.2	-4.6	35.62	31.0 / -2.3
4	98.9	-2.3	34.95	32.7 / - 0.6
5	99.0	-3.1	36.03	32.9 / -0.4
6	98.9	-2.3	36.46	34.2 / +0.9
7	99.0	-3.1	35.62	32.5 / -0.8
8	98.9	-2.3	37.05	34.8 / +1.5
9	98.9	-2.3	38.47	36.2 / +2.9
10	99.0	-3.1	35.89	32.8 / -0.5
11	98.5	+0.8	32.80	33.6 / +0.3
12	98.5	+0.8	33.48	34.3 / +1.0
				33.3

of the twelve measurements. These deviations are plotted in figure 3-31. The scatter seen here is a result of the operational problems noted above and a clear correlation of polyethylene position (between drums 12 and 1) with drum worth is not detectable.

Method 2

In this approach, a comparison is made between the measured and expected reactivity insertion for the actual drum motion which occurred. Similar to Method 1 above, the reactivity of the system prior to the measurement is established by comparing the average drum position 98.6 degrees and computing the reactivity based on the difference. These appear in the fifth column of table 3-9. Listed in the sixth column is the actual initial position of drum number 2. The seventh column contains the predicted reactivity addition based on PAX measurements and analytical results for the actual drum motion. The difference between the measured and this predicted reactivity appears in the last column and is plotted in figure 3-31. Again, no correlation with source position (between drums 12 and 1) is evident.

Conclusion

The reactivity worth of the individual drums is approximately uniform and no correlation is detectable between source position and drum worth.

Calibration of Control Drum Number 2

The final phase of EP 1A was the calibration of control drum number 2. The purpose of the calibration was to provide a verification of the predicted differential worth profile so that drum rotations in future testing could be confidently interpreted. The measurements were to be made by the following procedure:

1) Bring the reactor system to the critical condition through use of banked drums 4 to 12
2) Withdraw drums 1 and 3 to 20 degrees and establish equilibrium
3) Withdraw drum 2 to 40 degrees
4) Measure stable period
5) Repeat step 2 through 4, increasing however, in each succeeding measurement, the final position of drum 2 by 20 degrees and the final position of drums 1 and 3 to 10 degrees interval over the drum span.

REFERENCE	PREPARED BY	APPROVED BY	Astronuclear
	L10		

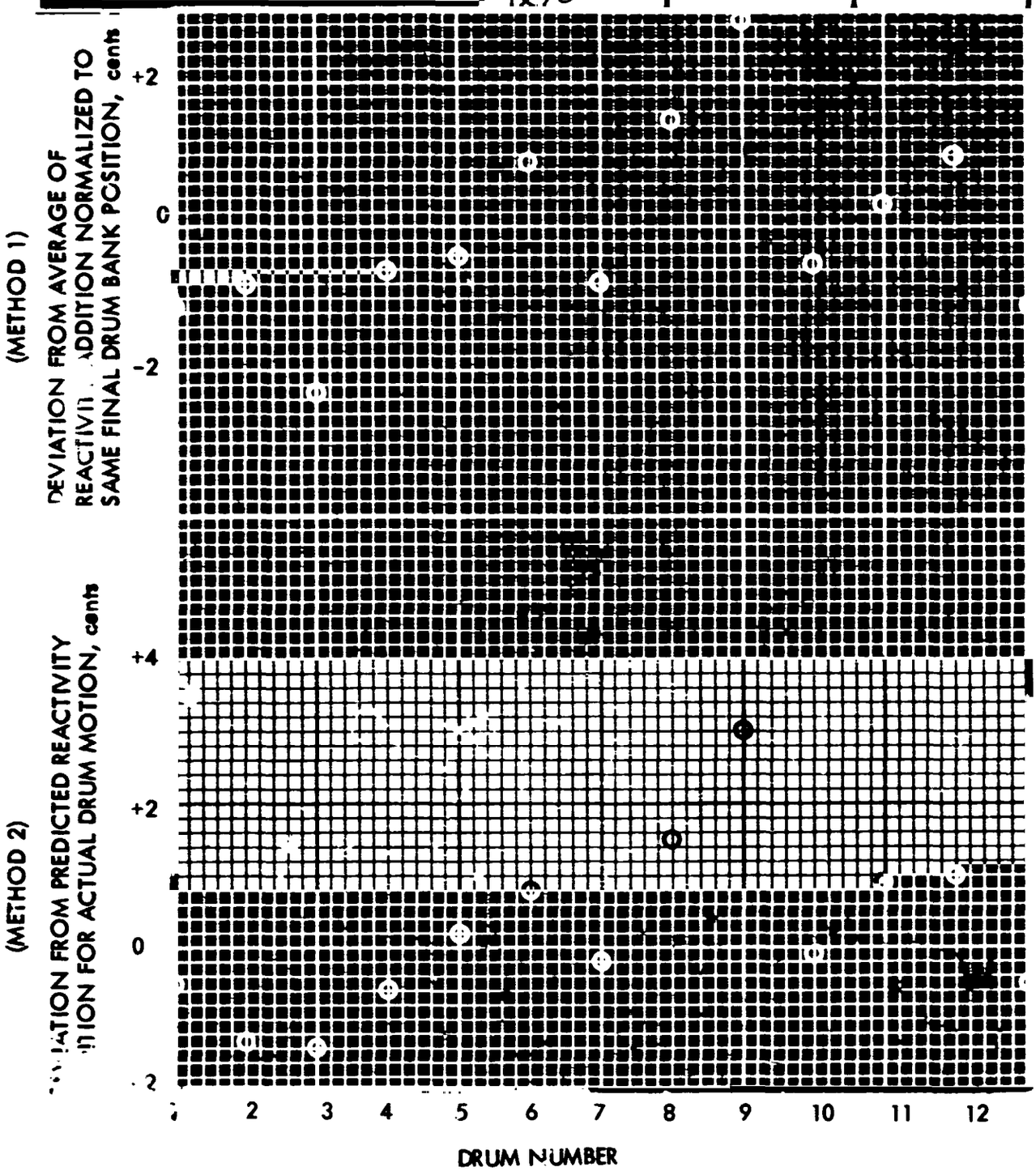

CURVE NO.

FIGURE NO. 3 - 31

EP-1A DRUM WORTH SYMMETRY

Evaluation of the test results indicated that operational problems[1] which hampered interpretation of other measurements in this test prevented to a large extent the acquisition of meaningful results here also. However, several of the measurements that were usable are plotted in figure 3-32 which also shows the predicted[2] differential worth for a single control drum.

The measurement at 90 degrees was repeated in EP II. These results are also plotted in figure 3-32. Error bands for this data are not available but may be inferred qualitatively from the spread between the two data points. The average of the two determinations is 0.665 cents per degree for a single drum (7.9 cents per degree for the 12 drum bank) as compared with the predicted 0.655 cents per degree.

EP 1B TEST

Cold Critical Drum Position

During the Scram Check Phase of this test there were three occasions that permitted an evaluation of the delayed critical drum bank position. These are summarized in table 3-14 along with one more measurement made prior to the first LH_2 run. Only in the first three is the reactor sufficiently close to critical for the results to be usable. Fortunately, these place upper and lower limits on the critical position which may be inferred from these to be 97 ± 0.5 degrees. The effect of system temperatures on these measurements is discussed previously in the section entitled Delayed Critical Drum Bank Position Without Nozzle.

Gaseous Hydrogen Test

The gaseous hydrogen flow test presented an opportunity to measure the reactivity worth of hydrogen in the core under conditions which were readily definable. The test closely followed the planned profile as described in the first section of this chapter. To maintain constant power during the run portion of the test the control drum bank responded in a manner shown in figure 3-33.

---

1 See the NRX-A2 Site Test Report
2 WANL-TME-887, NRX-A2 Test Prediction Report

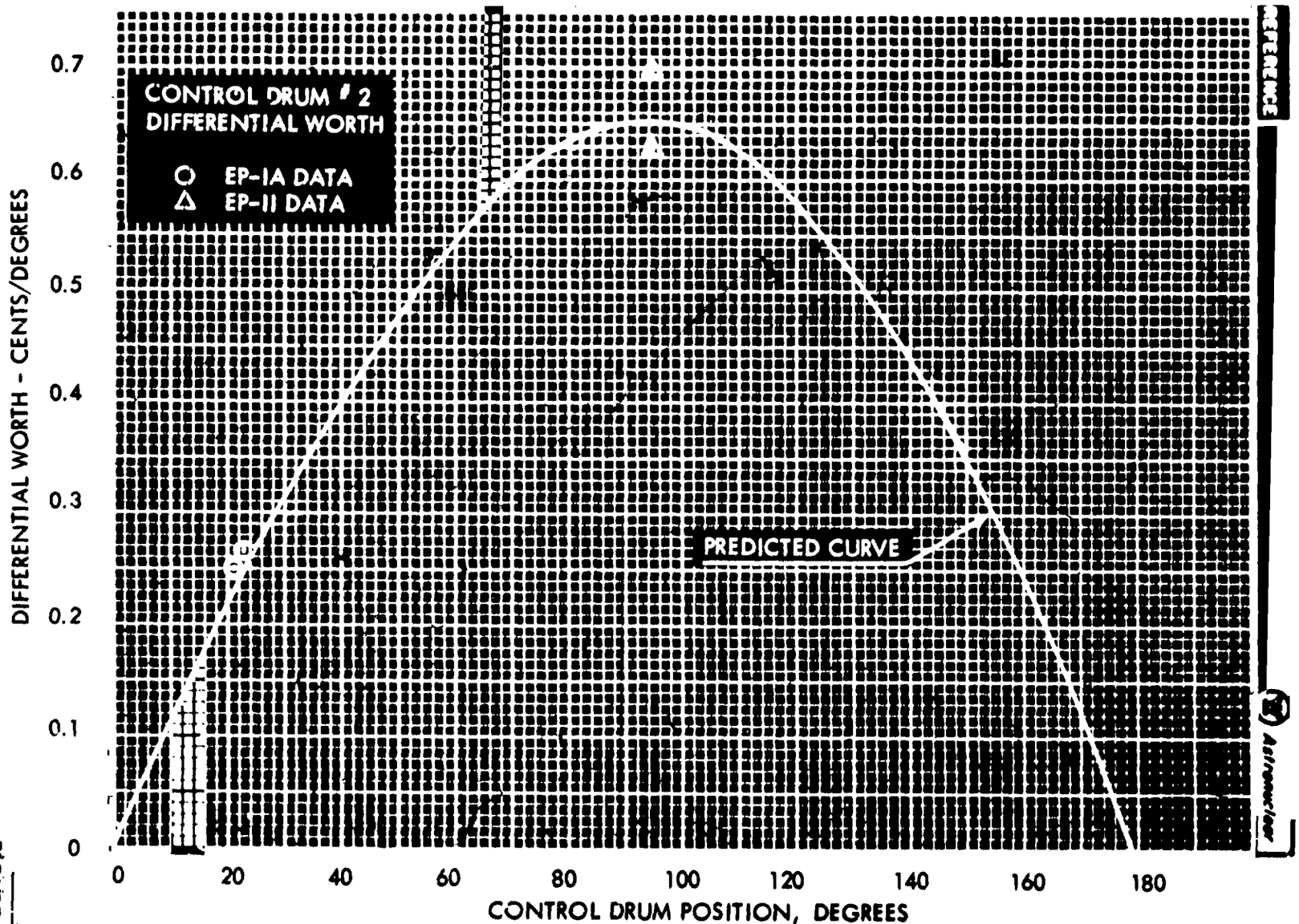

CONTROL DRUM NUMBER 2 DIFFERENTIAL WORTH	PREPARED BY	APPROVED BY	CURVE NO.

FIGURE NO. 3-32

TABLE 3-14

SELECTED DRUM BANK MEASUREMENTS DURING EP IB

Control Room Time, seconds	Indicated Power, watts	True Power, Watts	Average Drum position*-degrees	Analysis of Sanborn Data
10977	50, log	25-50, log	96.5	Immediately following this time drums continued to rotate outward (Sanborn 109-A, Channel 5) indicating sub-critical condition. Appears to rise as much as another 0.9 degrees.
11263	50, log	25-50, log	97.65	Power trace shows reactor to be slightly supercritical.
11436	50, log	25-50, log	97.58	Power trace shows reactor to be slightly supercritical.
15541	1000, log	500-1000 log	100.6	Reactor was not stable. In the seven seconds after 15541 the drums moved to 99.2 degrees and were still not stable.

* Average of 12 drum digital printout. These are not corrected for calibration errors as noted in tables 5 and 6 of NTO-R-0001. The NRX-A2 36 day report from NTO suggests that this correction not be made.

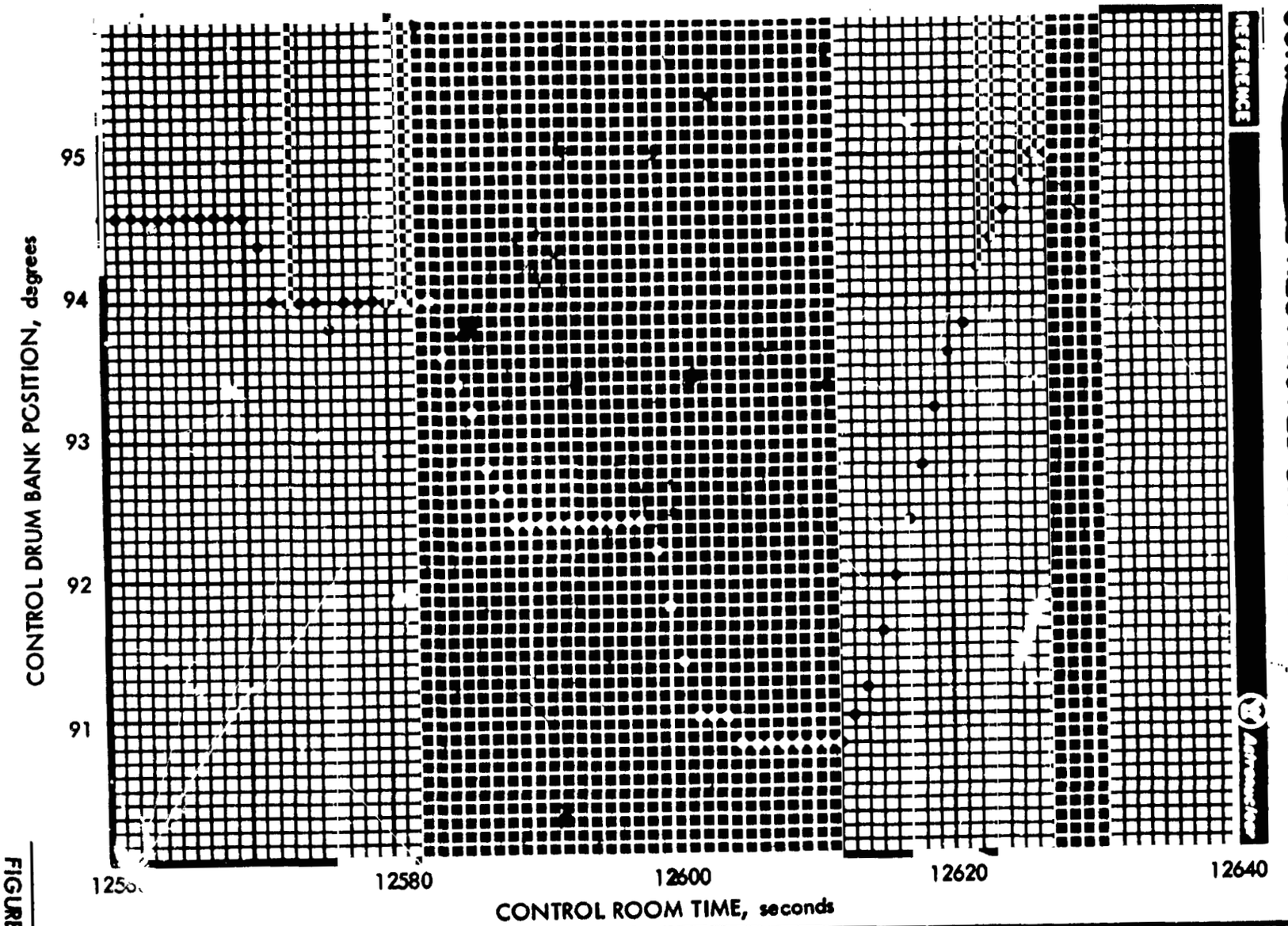

NRX-A2, EP-1B GH_2 PROFILE MEASURED CONTROL DRUM BANK POSITION VERSUS TIME	PREPARED BY	APPROVED BY	CURVE NO.
	L10		

FIGURE NO. 3-33

The critical drum bank position at the start of the profile was 94.6 degrees, deviating about 0.5 to 1 degree from that expected in a reactor at ambient temperatures and with negligible GH_2 flow. Figure 3-34 depicts the measured drum bank position replotted vs. hydrogen mass flow rate along with the calculated position[1] based on the best estimate of the true thermal and fluid flow conditions. The following is evident from inspection of these two graphs: 1) The greater slope of the calculated curve indicates that the product of hydrogen reactivity coefficient and hydrogen mass in the core is greater than the reactivity change actually experienced. 2) The relatively large initial offset from delayed critical (97 degrees) in figure 3-34 indicates a reactivity shift resulting probably from a combination of increased pressurization of the reactor and a higher than expected minimum flow rate. The much larger shift in drum position from 4 to 8 lb/sec than from minimum to 4 lb/sec shown in figure 3-33 is supporting evidence for the second possibility. A more detailed evaluation of analytical results and a discussion of nuclear information gained in this test appears in the sections that follow.

EVALUATION OF HYDROGEN WORTH

The derivation of the hydrogen worth used in this analysis is presented in WANL-TME-936 The core hydrogen worth distribution used for the calculated results in figure 3-34 is typified by the worth of uniform hydrogen, 6.80$/kg derived from axial transport theory calculations. WANEF measurements in support of NRX-A2 yielded a value of 6.30$/kg (± 0.25) for the worth of hydrogen uniformly distributed in the reactor core. For reasons discussed in TME-936 the distribution which led to the 6.80$/kg value was selected for use in predictions of NRX-A2 tests. The total hydrogen reactivity effect in this test may be broken into components resulting from the following:

1) Core coolant channel hydrogen
2) Core fuel porosity diffused hydrogen
3) Lateral support hydrogen
4) Beryllium reflector hydrogen

---

1 Normalized to the measured delayed critical position. See Appendix 1 for a summary of the analytical model.

REFERENCE	PREPARED BY	APPROVED BY	Astronuclear
	L10		

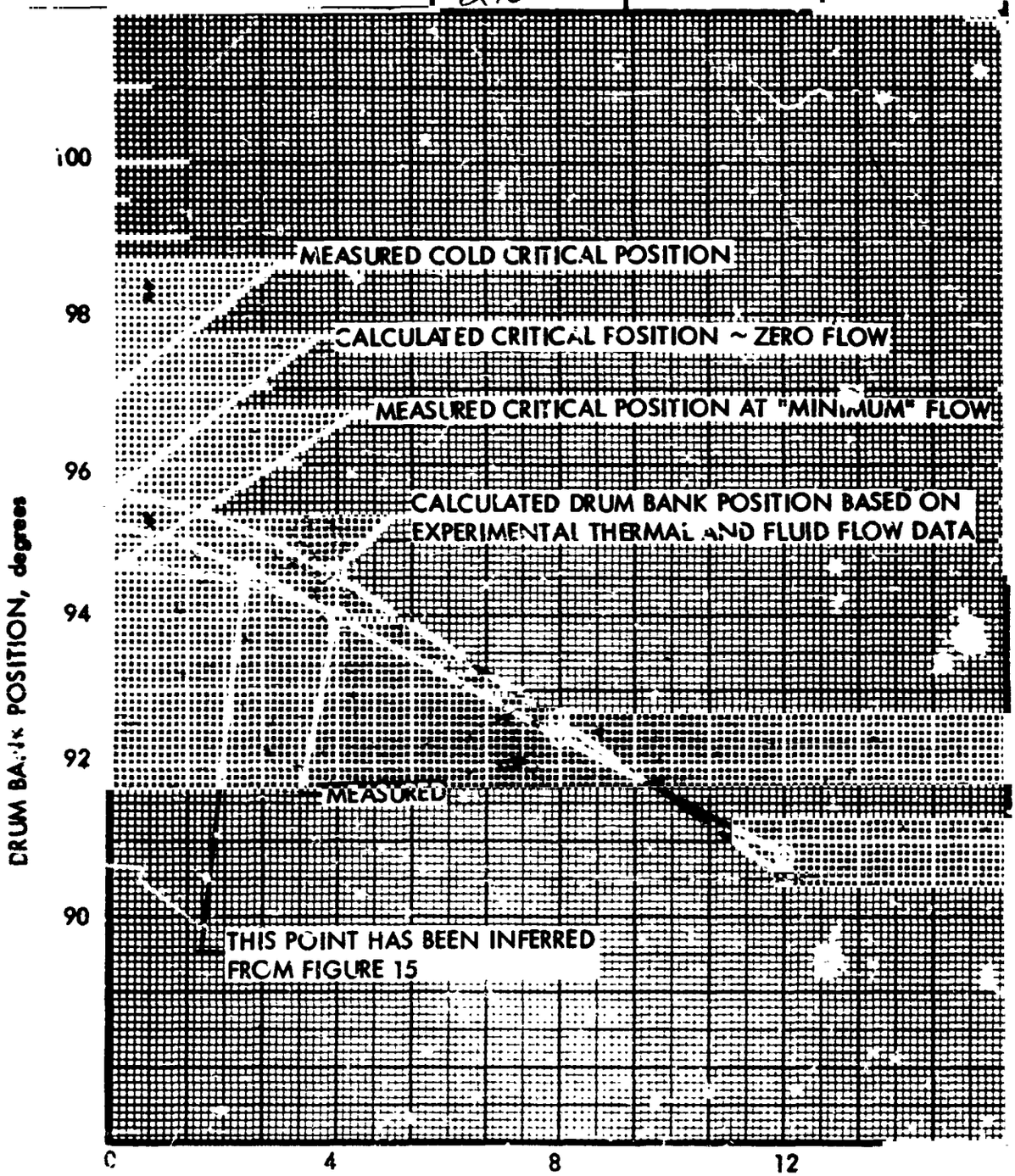

NRX-A2 EP-1B DRUM BANK ROTATION VERSUS GH_2 MASS FLOW RATE	CURVE NO	FIGURE NO.
		3 - 34

The least certain of these is the second effect which results from diffusion of hydrogen into the pores of the fueled and unfueled elements. Because the test was of such short duration (about 1 minute) and at ambient temperatures it will be assumed in evaluating the hydrogen worth that the diffused hydrogen was not gained during the test. Developed in table 3-15 is the error in the calculated values of reactivity change during the test. The diffused hydrogen effect, a factor in the NRX-A2 nuclear model,[1] was automatically included in the reactivity calculation by the COHOT computer program (column 2) and has been subtracted subject to the above assumption from the normalized values in column 4. Appearing in the last column is the ratio of measured to calculated drum bank rotation with its uncertainty to 95 percent confidence. Results from the 8 and the 12 lb/sec holds indicate that the calculated reactivity change is nominally 10 ± 5 percent high. Since 95 percent of the calculated effect results from hydrogen in the core it may be inferred from this that the core hydrogen worth of 6.80¢/kg should be reduced by 10 percent.

EVALUATION OF INITIAL OFFSET

Calculations using the NRX-A2 reactivity model[1] showed that replacement of the air (or helium) in the core by hydrogen at ambient pressure and temperature resulted in a reactivity increase of 10.9¢ or 1.4 degree of drum bank rotation (as shown in figure 3-34). Corrected for diffused hydrogen and reduced by 10 percent as noted above this value becomes 1.1° (and the point in figure 3-34 replotted at 95.9 degrees).

Since the $\Delta\theta$ shown in figure 3-33 was the same from 4 to 8 and 8 to 12 lb/sec it appears reasonable to assume that to a first approximation it will be linear below 4 lb/sec. This means that the initial flow rate at Time CR 12560 was of the order 2.5 lb/sec[2]. This point has been represented by a triangular symbol in figure 3-34 and the extrapolated dash-dot line passing through it intercepts the zero flow axis at a drum position of about 95.2 degree with an uncertainty probably of the order of 0.5 degree.

---

1 See Appendix 1

2 Since 0.6 degree rotation occurred from this initial flow rate to 4 lb/sec and 1.6 resulted from a change in flow rate of 4 lb/sec (4 to 0) the initial flow rate is:

$$4 \times \frac{(1.6 - 0.6)}{1.6} \text{ or } 2.5 \text{ lb/sec.}$$

TABLE 3-15

COMPARISON OF CALCULATED AND MEASURED DRUM ROTATION IN THE EP IB, GH_2 TEST

Flow lb/sec.	Calculated Total Reactivity Change, $	Calculated Diffused H_2 Effect, $	Net Normalized Reactivity Change, $	$\Delta\theta$ Calculated Normalized, degrees[1]	$\Delta\theta$ Measured Normalized, degrees	$\frac{\Delta\theta m}{\Delta\theta c}$
4	0.194	0.021	0.000	0	0	----
8	0.338	0.036	0.129	1.68 ± 0.08[3]	1.6 ± 0.16[2]	0.95 ± 0.12[2]
12	0.506	0.054	0.279	3.62 ± 0.18[3]	3.2 ± 0.16[2]	0.88 ± 0.06[2]

1 Converted at 7.7¢ / degree

2 A 95 percent confidence level

3 A ± 5 percent accuracy assumed, this is probably better than ± 2σ (which is 95 percent confidence).

These factors are summarized in table 3-16 along with a brief note on the uncertainties. As can be seen, there is an overlap in the measured and expected drum bank position at the theoretical condition of no flow. The conclusion to be drawn from this is that the reactivity effect of increased core pressurization was not significant and is probably less than 0.5 degree of drum motion. This analysis does not permit, of course, any conclusion as to the effect of higher pressurization as would be experienced in high power testing.

Liquid Hydrogen Test

The reactivity feedback experienced during both liquid hydrogen runs was significantly less than expected. Drum bank motion during the second LH_2 run is shown in figure 3-35. The predicted drum motion over the profile (to 16 lb/sec flow) was about 17 degrees while the measured motion was only 2 degrees. The anomaly between the predicted and measured control drum motion is attributed to a flow lag between actual reactor flow and FE-7 indicated reactor flow. The flow lag is discussed in the first section of this chapter and in the NRX-A2 Site Test Report. Because of the uncertainty at present in the thermal and fluid flow conditions during this test, further analysis of the nuclear feedback effects has been deferred pending a final thermal analysis.

EP II TEST

Delayed Critical Position

During the Scram Check and Neutronics Calibration I Phases of EP II the reactor was taken critical and in most instances stable conditions were achieved. Drum bank measurements taken during these periods ranged between 96.4 and 96.6 degrees. The critical position has nominally been chosen to be 96.5 degrees.

NEUTRONIC POWER CALIBRATION

Wire Calibration

The power calibration of the NRX-A2 reactor during EP II was performed by exposing 9 wires of 20 w/o 93.5 percent enriched uranium dispersed in aluminum both during a PAX run and at NRDS.

TABLE 3-16

POSSIBLE EFFECT OF PRESSURIZATION

Calculated	
Delayed Critical Measured	97.0 ± 0.5 [1]
Ambient H_2 replacing purge gas	1.1 ± 0.0 [2]
Critical position at no flow	95.9 ± 0.5
Measured	
Inferred from figure 3-34 critical position at no flow	95.2 ± 0.5 [3]

1 See section on EP IB cold critical drum position.

2 No uncertainty has been assigned to this number because hydrogen conditions are well defined (ambient) and hydrogen worth correction has been taken into account.

3 A half degree uncertainty has been assigned to this number to cover the range resulting from:

a. upper limit - linear extrapolation of measured curve (95.6 degrees)

b. lower limit-measured position at a flow noted in the Site Test Report (NTO-R-0008) to be 0.25 lb/sec., but described as "an order of magnitude only" (94.6 degrees).

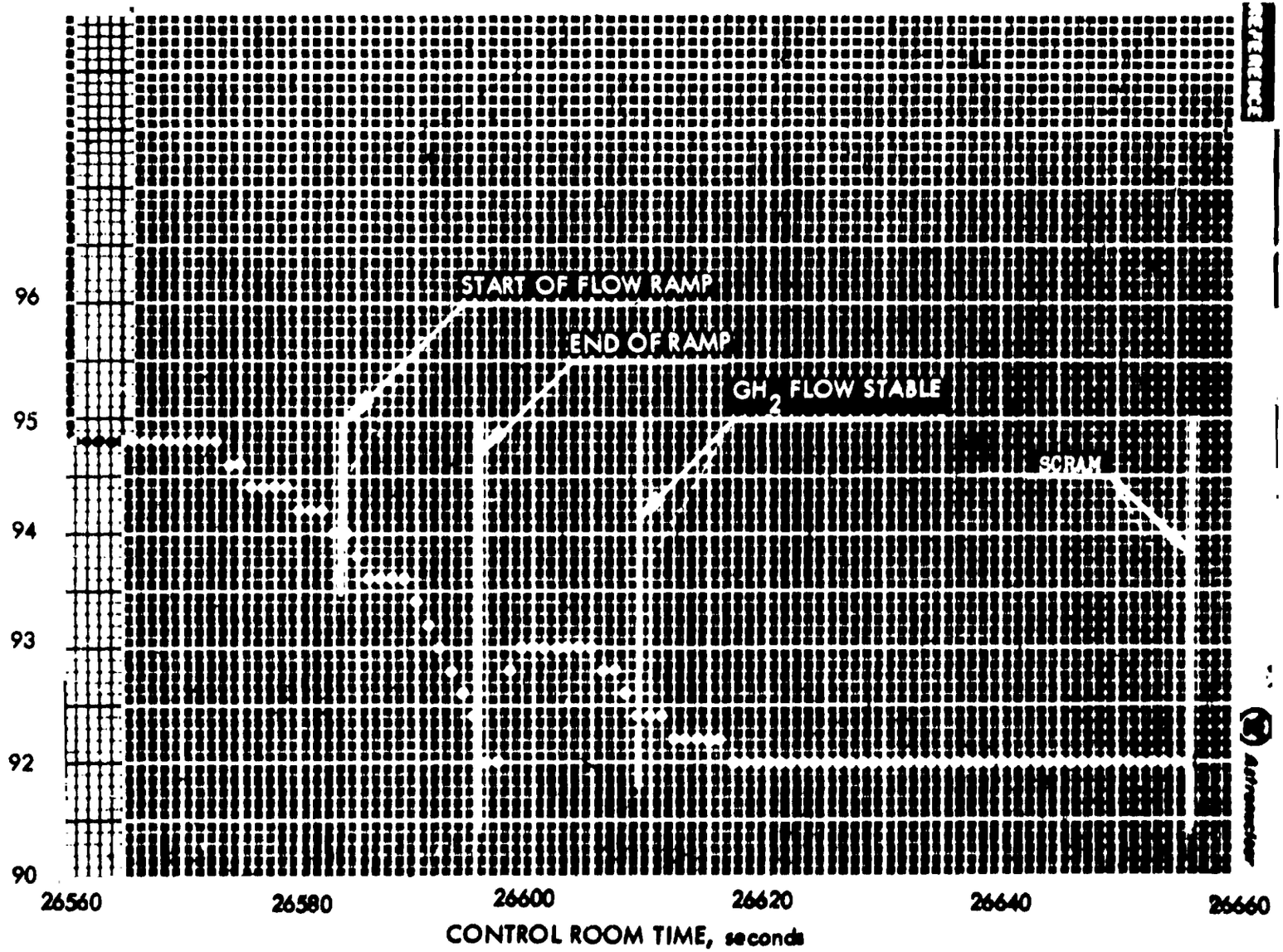

FIGURE NO.			
NRX-A2, EP-1B SECOND LH_2 RUN CONTROL DRUM BANK POSITION VERSUS TIME	PREPARED BY	APPROVED BY	CURVE NO.

These wires, which were 52 inches long and 40 mils in diameter, were inserted in coolant channels 17 and 19 of the central element 000 in PAX during the PAX 120 run and were subsequently radio-chemically analyzed for total fissions by measuring the Mo^{99} isotope. The analyses were performed by three laboratories: LASL, WANL, and APD. The two LASL wire analyses and the six WANL wire analyses were in essential agreement after calibration to some samples generated at LASL, but a single wire analysis by APD was 6 percent lower than the average of the other eight analyses and hence, was discarded.

From extensive fission mapping of the PAX core and radio-chemical analyses of virgin fuel irradiated during the PAX-120 run, a K factor was determined with units of total core fissions per fission/gram of uranium in wire irradiated in channel 17 or 19. The K factor is presumed to be identical in both the PAX and NRX-A2 reactors[1].

In the NRX-A2 core, coolant channels 17 and 19 were not available because of the interlocking support blocks and channels 12 and 13 were used instead. The factors for channels 12 and 13 as given in table 3-17 were obtained from the channel 17 and 19 data and from relative fissions/gram data as reported in table 5-15 of WANL-TNR-158. The average of these values is 1.63×10^5 fissions per fission/gram U in wire (not fission/gram U^{235} as reported in WANL-TNR-158).

The wires irradiated in the NRX-A2 at NRDS were analyzed at three laboratories, WANL, LASL, and NTO. The values resulting from these analyses were reported in NTO-M-0559[2] as shown in table 3-18. The average of all nine analyses gave a value of 3.120×10^{11} fissions per gram of wire with a maximum spread of 2.3 percent using the average K factor given above, adjusted for drum angle. The total fissions in the NRX-A2, EP II run is found to be $\frac{3.120 \times 10^{11}}{0.197} \times 1.63 \times 10^5 \times 1.013 = 2.62 \times 10^{17}$ fissions. The 0.197 in the denominator converts the fission per gram of wire to fissions per gram of uranium in the wire since 0.197 is the measured weight fraction of U in the wire.

---

1 The critical drum angle at WANEF was 90 degrees while at NRDS it was 98.5 degrees. This difference in drum angle has been estimated to increase K by +1.3 percent.

2 NTO-M-0559, NRX-A2 Neutronics Calibration Run - Results of Uranium Aluminum Wire Analyses, J. J. McCown to P. W. Davison, September 22, 1964

TABLE 3-17

K FACTORS FOR CALIBRATION OF NRX-A2[1]
CHANNELS 12 AND 13

PAX Location	K Factor $\frac{\text{total fissions}}{\text{fissions/g-U (wire)}}$
000B13	1.62×10^5
000C13	1.63×10^5
000D13	1.65×10^5
000E13	1.63×10^5
000F13	1.63×10^5
000G13	1.66×10^5
000C12	1.60×10^5
000E12	1.62×10^5
Average	1.63×10^5

1 Taken from WANL-TNR-158, table 5-15

TABLE 3-18

NRX-A2 NEUTRONICS CALIBRATION RUN EP II
URANIUM-ALUMINUM WIRE ANALYSES[1]

Wire No.	Group	Fissions/g-wire
63	WANL	3.103×10^{11}
66	WANL	3.160×10^{11}
69	WANL	3.175×10^{11}
64	NRDS	3.103×10^{11}
67	NRDS	3.109×10^{11}
70	NRDS	3.126×10^{11}
62, 65, 68	LASL[2]	3.10×10^{11}

1 From NTO-M-0559, J. McCown to P. W. Davison

2 Average of three wires. Three analyses agreed within 1 percent

Assuming 190 Mev/fission is the average energy absorbed in the reactor to produce thermal energy[1], the average power during the EP II run of 1200 sec. is determined as

$$\frac{2.62 \times 10^{17} \text{ fissions} \times 190 \ \frac{\text{Mev}}{\text{fission}} \times 1.6 \times 10^{-13} \ \frac{\text{w-sec}}{\text{Mev}}}{1200 \text{ sec} \times 10^{3} \ \frac{\text{w}}{\text{Kw}}}$$

From the data, then the following constants for the EP II run are:

Average Power (based on 190 $\frac{\text{Mev}}{\text{fission}}$ absorbed) = 6.65 kw

Integrated Power = 7.99×10^{6} w-sec

Total Fissions = 2.62×10^{17}

Rabbit Calibration

During the wire calibration on EP II, a sulfur pellet in a pneumatic rabbit gun was positioned approximately at the neck of the nozzle. The rabbit gun pneumatically fires a small, stainless steel capsule (differential rabbit) from a shielded location behind the cell wall to a position 12.5 inches from the axial centerline of the core and 63.8 inches above the core midplane. Transit time of the rabbits between shield and exposure location is 0.9 sec. An integral rabbit can also be positioned at the end of the rabbit gun barrel (near the nozzle neck) and can be removed only during re-entry to the test cell. LASL experience with rabbits containing U^{238} highly depleted in U^{235} and covered with cadmium indicated that the fast neutron leakage at the nozzle position was reasonably linear with thermal power and therefore, provided a valuable method of extrapolating the low power calibration to full power operation. With the NTO acquisition of Test Cell A, it was not immediately apparent that NTO would have the capability of radio-chemical analysis at the test site and since radio-chemistry is necessary for analysis of U^{238} rabbits, a substitute rabbit detection material was sought. Sulfur in the form of compressed anhydrous $(NH_4)_2SO_4$ pellets was used during the NRX-A2 test series. Hence, ammonium sulfate pellets were exposed during EP II in order to calibrate them for further tests.

1 NTO-M-0559, NRX-A2 Neutronics Calibration Run - Results of Uranium Aluminum Wire Analysis, J J McCown to F W Davison, September 22, 1964

Neutronics Tank Calibration

Positioned radially about 20 feet from the reactor in the test cell wall, is a water tank containing boron lined ionization chambers for measuring fast neutron radial leakage. The water tank at test cell A has a 6 inch thick lead shield between the reactor and the front pad of the water tank. The incident radiation impinges upon the lead wall at a 50 degree angle relative to a perpendicular from the wall giving an effective lead thickness of 9.36 inches. The object of the lead is to minimize the ratio of gamma to neutron induced currents in the ion chambers contained within the tank. The desire to reduce the ratio of gamma to neutron induced current is only to reduce the power calibration errors resulting from poor compensation of the ion chambers in high gamma fluxes.

In the forward or low power position where the chambers were calibrated during EP II, the neutron to gamma induced current ratios are very high and any compensation errors in the chambers produce negligible errors in the net signal current from an ion chamber. However, prior to the high power run (EP IV) the chambers are moved back in the water tank to a position where they read 1/1000 of their prior reading. At this location, some 32 percent of the current is induced by gamma rays. At low reactor powers (EP II) this 32 percent is subtracted from the ion chamber signal by the gamma compensated volume of the ion chamber. Above 50 percent of design power, however, the compensating portion of the ion chambers subtracted less and less of the gamma signal until at full power it is estimated that only 10 percent of the gamma signal was subtracted. However, since it has been observed that the compensated chamber (linear no. 2) agreed very closely with differential rabbit determinations of the power, it is believed that the error due to lack of compensation is just canceled by a reduction in the radial leakage with increasing power. The agreement at high powers between axial rabbits and linear No. 2 neutronics is then believed to be a fortuitous cancellation of two opposite effects: lack of compensation and decrease of neutron leakage with increasing reactor power.

Temperature Coefficient Measurements

During the slow temperature rise in EP II a low, constant GHe coolant flow was employed to avoid oxidation. A number of radial temperature measurements were made at four axial stations in the core (Figures 3-16, 17 and 18). Using a J_o Bessel function square radial weighting and a $\sin^2$ axial weighting, an effective nuclear average core temperature has been derived. The progression of this average core temperature with time is shown in figure 3-36. The average beryllium reflector temperature is also included in this figure.

Figure 3-37 displays the comparison of the measured and calculated[1] drum angle changes during the significant portion of EP II. The calculated values were obtained from the nuclear average core temperature rises in figure 3-36, and the A2 temperature coefficient of approximately - 0.11¢/°R. A small correction was made for the increase in Be reflector temperature. This data is replotted against average core temperature in figure 3-38 to show the linearity of the measurements. The error limits on the measured data reflect only the uncertainty in the measurements, not the uncertainty in evaluating the nuclear average core temperature.

Uncertainties in the calculated values are estimated to be 12 percent. Incorporated in this value is the uncertainty in the expansion reactivity coefficient, weighting procedure for average core temperature and the measured temperature.

The data shows substantial agreement with the calculated values. None of the measured values fall outside the error bands which are consistent with those prescribed in WANL-TME-936. This is not to be construed as conclusive confirmation of the A2 operating temperature coefficient since the maximum temperature rise was only 20 percent of the A2 operating temperature. This data will be used to improve the low range analysis consistent with the A2 hot test results.

---

1 The analytical model is summarized in Appendix A.

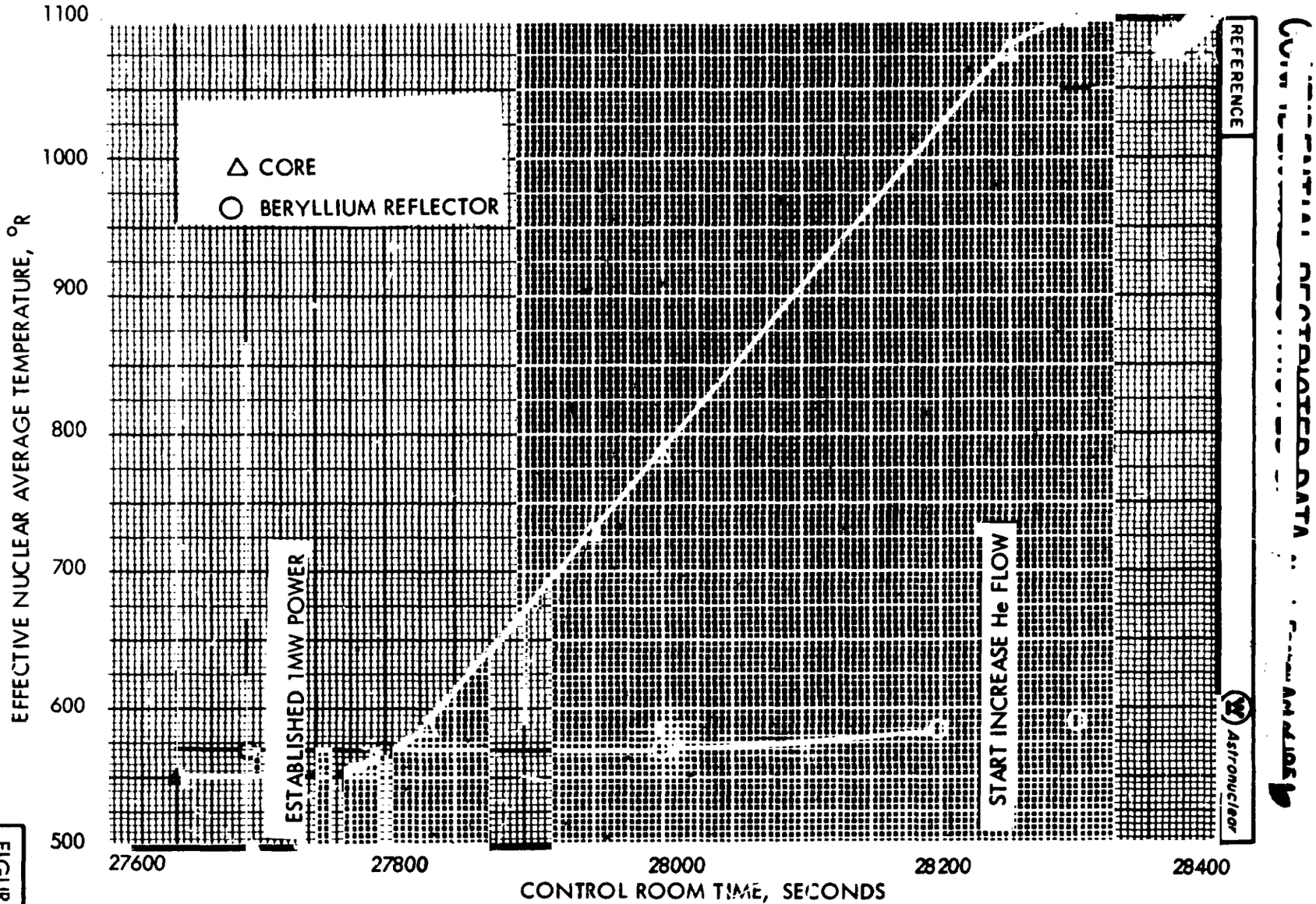

REFERENCE

Astronuclear

FIGURE NO.	NRX-A2, EP-II, MEASURED NUCLEAR AVERAGE TEMPERATURE FOR MAJOR COMPONENTS	PREPARED BY	APPROVED BY	CURVE NO.
3 - 36				

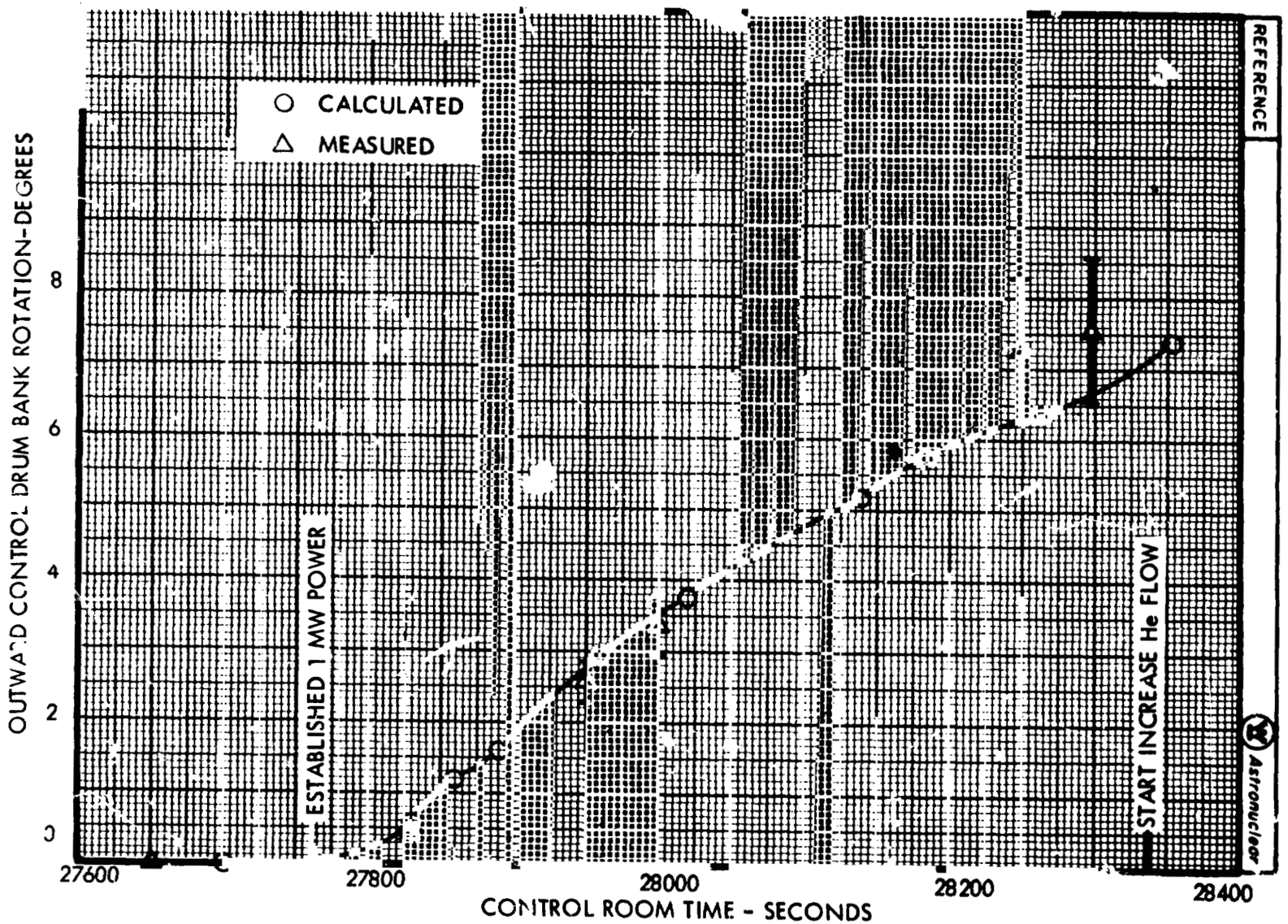

FIGURE NO.	NRX-A2, FP-II CONTROL DRUM BANK ROTATION DURING TEMPERATURE COEFFICIENT TESTS	PREPARED BY	APPROVED BY	CURVE NO.
3 - 37				

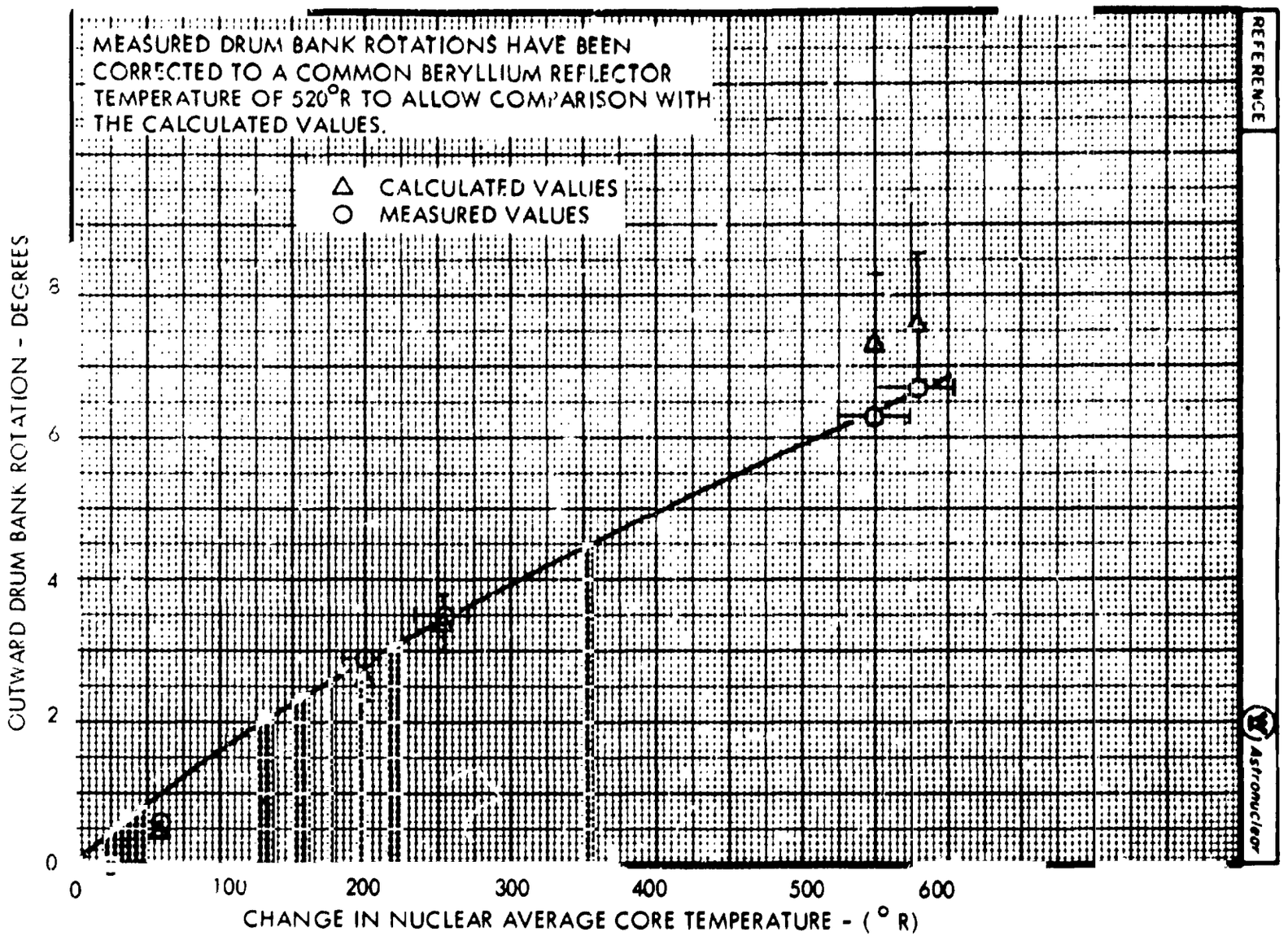

NRX-A2, EP-II	DRUM BANK ROTATION VS CHANGE IN NUCLEAR AVERAGE CORE TEMPERATURE	PREPARED BY	APPROVED BY	CURVE NO
		ALM		

FIGURE NO. 3 - 38

REFERENCE

Astronuclear

Calibration of Control Drum 2

Additional data was acquired in EP II to substantiate the differential drum worth curve. This data is presented and discussed in the previous section in this chapter on the Calibration of Control Drum Number 2.

EP III TEST

Delayed Critical Position

Several excellent critical conditions were attained in the Scram Check Phase of this test. These ranged between 97.4 degrees and 97 degrees with the preponderance at the latter. The delayed critical position has, therefore, been established at 97.0 degrees.

There was some concern that the nozzle cover which was present during this early phase had some effect on the critical position. An effort was made for this reason to remove the cover during a period when the reactor was critical. It was found however that the cover could not be removed remotely because of a mechanical failure in the telescoping arm on the nozzle cover handling boom. The reactor was shut down, and the cover was removed using the reactor shed hoist. Shortly thereafter, a critical condition was again attained, this time with the drum bank at 97.6 degrees (Time CR 23960). The conclusion was that the nozzle cover was worth 0.6 degree drum bank motion. Since this appeared unlikely, it was planned to redo the measurement at the first convenient time.

An opportunity presented itself in EP V to do this and the removal was accomplished while the reactor was critical. There was no detectable drum motion during the removal, indicating that the earlier measurement was in error.

It is concluded that in all critical position analyses the effect of the nozzle cover may be neglected.

Temperature Coefficient

It was not the purpose of this test to acquire nuclearly significant information; however, the reactor did heat up and it is possible to infer a temperature coefficient (admittedly approximate) from the measurements that were taken. These have been summarized in table 3-19.

TABLE 3-19

EP III TEMPERATURE COEFFICIENT

CRT Time seconds	Average Drum Position, degrees	Average Core Temperature °R	Average Beryllium Reflector Temperature, °R
23960	97.6 ± 0.1	520 ± 10	554 ± 10
25542	101.2 ± 0.1	780 ± 40	570 ± 20
Difference	+3.6 ± 0.16*	260 ± 41	16 ± 22
	at	at	at
	7.7¢ / degree	-0.11 ¢/°R**	+0.0943¢ /°R
	is	is	is
	-27.7 ± 1.2¢	-28.6 ± 4.5¢	+1.5 ± 1.9¢

-27.1 ± 4.6¢

* All uncertainties are to the 95 percent confidence level.

** The core temperature coefficient shown in appendix 1 covers the full operational temperature range. The value -0.11¢ /°R applies to the ambient temperature range.

[redacted]

Since the data system recorders were not operating during these times the temperatures shown came from "Quick Look" Sanborn channels and consequently the data is not the best possible. Under this restriction it is gratifying to see the excellent agreement between the measured and calculated reactivity change. Since the calculated reactivity change resulted mainly from the core temperature change, the core temperature coefficient of $-0.11¢/^{\circ}R$ has been reasonably verified.

CHAPTER 4

EXPERIMENTAL PLAN IV - POWER TEST

TEST DESCRIPTION

The high power test was performed on 24 September 1964. The planned profile consisted of a reactor prechill corresponding to a 90°R drop in core inlet temperature followed by a power and flow rise corresponding to a 50°R/sec increase in exit gas temperature to a 50 percent* power hold. Both 76 percent and 83 percent power holds were planned followed by a retreat to a 2200°R chamber temperature and a scram and simultaneous switch to ambient hydrogen coolant. All power and flow changes were planned to be in a manner to correspond to a nozzle chamber temperature change of 50°R/sec, excepting for a 135°R/sec nozzle chamber temperature decrease rate following the scram.

Planned duration of the 50 percent hold was one minute while the 76 percent hold was to be terminated when turbine supply pressure decreased to 1700 psig or after a 5-minute interval. The supply pressure hold termination criteria had been established prior to the test as that turbine pressure which would allow for a reasonable final hold duration. The final hold was to be terminated after a 3-minute interval or at a 1200 psig turbine supply pressure whichever occurred first. A 1200 psig was the minimum tank farm pressure for turbine requirements.[1]

Planned steady state operating conditions were as follows:

Power MW	Power % of 1120 MW	Flow Rate lb/sec	Nozzle Chamber Temperature °R	Duration
560	50	61	2650	1 min.
855	76	71.3	3200	5 min. max.
930	83	71.3	3450	3 min. max.

1 NTO-R-0008, NRX-A2 Site Test Report, 20 November 1964
* Percent of 1120 MW, design power

Operating limits established prior to the test are given in table 4-1.

Figure 4-1 graphically presents the three major parameters - nozzle chamber gas temperature, reactor thermal power, and coolant mass flow rate - as they varied in time during the high power test of the NRX-A2. The calculated nozzle chamber temperatures given at four times during the test are considered to be the best measure of true chamber temperature during the test. A selected chronology of the test is given in table 4-2.

With the reactor in power control at a constant power of about 2 MW and a hard chill of the LH_2 feed system, the main coolant valve OBV 86 was opened at the time designated by A on figure 4-1. A 51 second reactor prechill at a flow rate of approximately 2 lb/sec LH_2 followed, and at time B on the figure the programmed run was initiated. The planned power holds are designated on the figure as the time intervals from C to D, D to E, and E to G with an unprogrammed manual power adjustment at time F.

Power level was higher than planned during the early portion of the startup resulting in nozzle chamber and fuel element temperature increase rates higher than expected. However, when the station 32 material temperature exceeded 1450°R the temperature trim loop became operative and the remaining portion of the power ramp was as planned. The 50 percent power hold was close to planned power and temperature levels, with a duration of approximately one minute. The programmers were switched to run at the end of this hold and power and flow increased to the approximate conditions planned for the 76 percent power hold. During the power rise and the hold, station 32 core material temperature indications began to decrease, due to failure of the thermocouple potting and attendant bypass flow cooling the thermocouple. The temperature control loop trimmed reactor power to the maximum allowable increase of +15 percent during this programmed hold. Thus the power drifted upward during this hold of about 2 minutes. When turbine supply pressure reached 1700 psig the hold was ended and the programmers increased power to the final planned 83 percent power hold. Power during this hold was approximately 1040 MW for about 2 minutes compared to a planned 930 MW. The station 32 core material thermocouples were indicating approximately 1000°R low at the end of this hold. In addition, the nozzle chamber thermocouples were indicating temperatures several hundred

TABLE 4-1

LIMITS ESTABLISHED FOR NRX-A2 OPERATION

Parameter	Limit	Qualification
Nozzle chamber temperature, max.	3620 °R	Set 5 percent above calculated value
(Expected start and retreat rate)	50°R/sec	
(Expected shutdown rate)	135 °R/sec	
Tie Rod temperature, max.	1000 °R	Steady state
	1200 °R	Transient
Fuel Element temperature, max.	800 °R	Air exposed
	1400 °R	Nitrogen exposed
Station 45 fuel element temperature, max.	3910 °R	Set 5 percent above calculated value
Station 32 fuel element temperature, max.	3450 °R	Set 5 percent above calculated value
Core inlet temperature, min.	90 °R	
	250 °R	LH_2 flow test only
Nozzle inlet pressure, max.	1000 psia	
Nozzle chamber pressure, max.	600 psia	
Graphite barrel ΔP, max.	200 psid	
Core ΔP, max.	150 psid	
Reactor period, min.	1 second	
Shutdown reactivity, min.	2 $	
Cooldown limits		
Core orifice	900 °R	
Core support plate temperature, max.	850 °R	
Replacement shield	950 °R	
Inner reflector	750 °R	
Outer reflector	750 °R	
Pressure vessel	850 °R	
Core fuel (with Nitrogen)	1200 °R	200°R low to provide margin for core hot spot

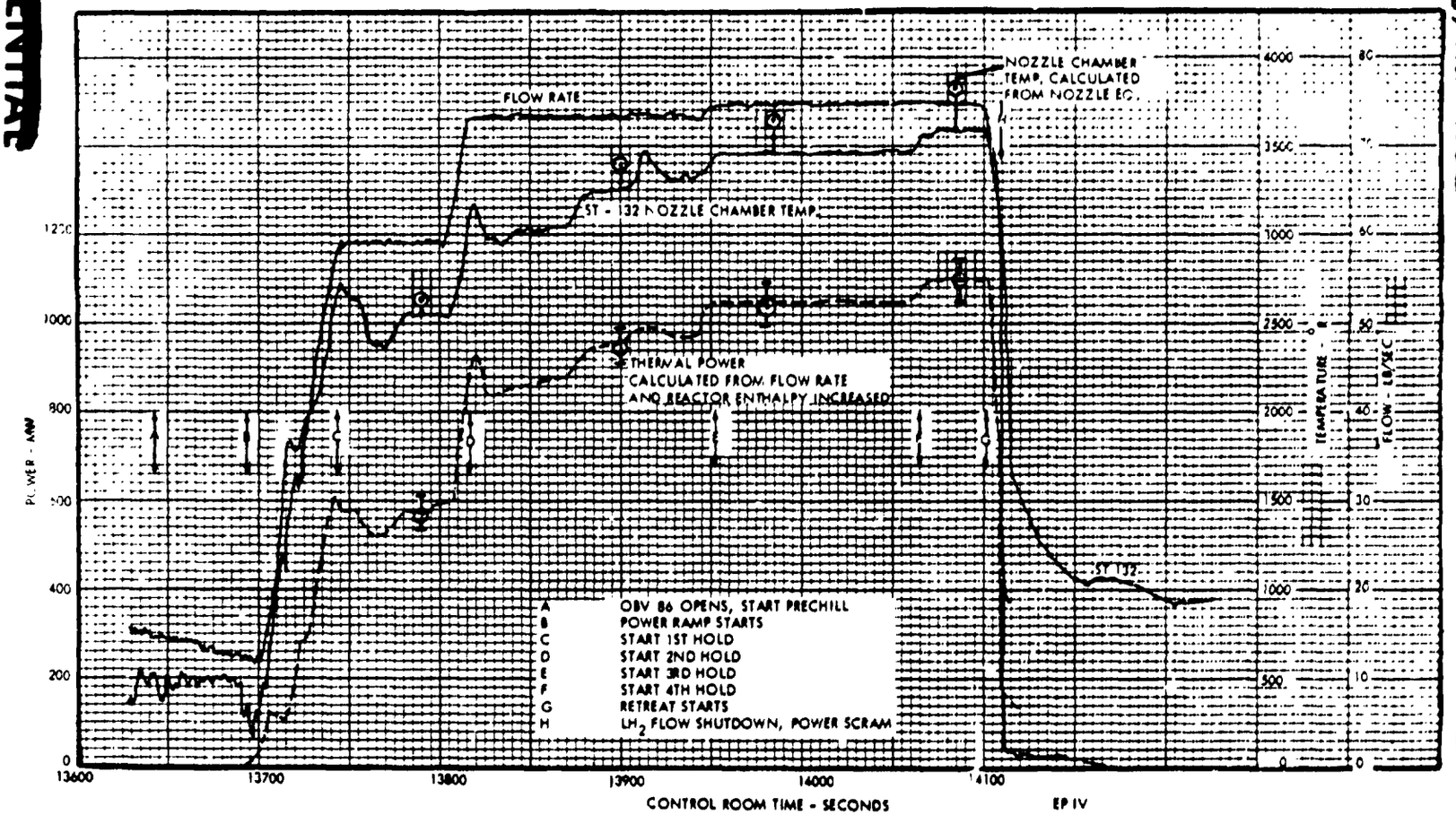

Figure 4-1 POWER, FLOW, AND TEMPERATURE EP-IV

TABLE 4-2

CHRONOLOGY NRX-A2 EP IV

Reference to Figures	Event	Control Room Time
	Automatic power startup	13268
A	Open OBV 86 for prechill	13642
B	Power starts up, end of prechill	13693
	Nozzle pressure exceed critical pressure	13711
	Temperature control trim starts	13713
C	Start of first hold	13743
	Switch to run	13804
D	Start of second hold	13816
	Switch to run	13946
E	Start of third hold	13953
F	Increase power to maximum hold	14065
G	Retreat starts	14101
H	Flow shutdown and power scram	14109
	Nozzle inlet temperature starts to rise as GH_2 flow is established	14113
	Cooldown	

degrees lower than the true mixed mean chamber temperature. No useful information could be obtained from the station 45 core material thermocouples because they saturated at about 3700°R as had been expected. On the basis of these erroneous temperature indications the CTO manually increased the power to the final level of 1096 MW for about 40 seconds.

At the predetermined turbine supply pressure shutdown was initiated with the planned retreat (G on figure 4-1). Eight seconds later a flow shutdown and scram, upon command of the Test Director, terminated the retreat. The shutdown, due to loss of the dewar pressure signal, was from a chamber temperature of 3380°R rather than the planned 2200°R and was consequently more severe.

A restart and post-run critical rod position test was performed approximately 2 hours after shutdown. Following the power test there was a 32 hour cooldown period with ambient hydrogen, ambient nitrogen and cold nitrogen used to remove the decay heat from the reactor.

In summary, EP IV was of 7 minutes duration from the end of the prechill to the scram with an average power of 813 MW and maximum operating conditions of 1096 MW with 75.6 lb/sec LH_2 coolant and 3815°R nozzle chamber temperature.* Operating conditions more severe than planned were successfully sustained by the reactor during the startup, at high power holds and during the reactor shutdown. These extreme operating conditions of power, temperature, pressure and flow are tabulated in table 4-3.

Detailed test data and analysis of the high power test described above follow in this same chapter. The test is considered in the following order.

Contents	Control Room Time Interval
Prechill	13642 to 13693
High Power Holds	13743 to 14101
Startup and Shutdown	13693 to 13743 and 14101 to 14130
Cooldown	14101 on

* Power and nozzle chamber temperatures quoted are determined from a reactor heat balance described in the following section.

TABLE 4-3

NRX-A2 EXTREME OPERATING CONDITIONS

Parameter	Value Observed	When Observed	
Power			
Integrated	6350 MW-Min.	All EP's	
Instantaneous	1096	EP IV	For 40 seconds
Temperatures			
Chamber Rate, Max.	+125°F/sec	EP IV	Startup
Min.	-350°F/sec	EP IV	Shutdown
Unfueled Core Mod., Max.	4350°R	EP IV	Measured thermal capsule
Avg. Min.	200°R	EP IV	Cooldown
Nozzle Chamber, Max.	3815°R	EP IV	Calculated
Tie Rod Exit Gas, Max.	1670°R	EP V	Abort, Transient(negligible core ΔP)
Time above 3250°R	355 sec	EP IV	
Core Orifice Adhesive	1050°R	EP IV	Cooldown prior to first GN_2 pulse (inferred from Station 8)
Inner Reflector, Max.	850°R	EP IV	Cooldown
	1400°R	EP IV	$T_{max.}$
Outer Reflector, Max.	750°R	EP IV	Cooldown
Core Inlet, Min.	47°R	EP V	H_2 Quality estimated between 70 to 90%
Pressures			
Nozzle Chamber Rate, Max.	36 psi/sec	EP IV	Startup
Nozzle Chamber, Max.	581 psia	EP IV	
Feed Line, Max.	855 psia	EP IV	
Core ΔP, Max.	121 psid	EP IV	
Ref. Inlet/Noz. Chamb. ΔP, Max.	172 psid	EP IV	
Nozzle Tube ΔP, Max.	109 psid	EP IV	
Flow			
Rate of change	6 lb/sec^2	EP IV	Startup
LH_2	75.6 lb/sec	EP IV	

PRECHILL

In this section an analysis is made of the prechill interval from time CR 13642 seconds when OBV 86 was opened to time CR 13693 when the programmers were switched to run and power started up.

Thermal and Fluid Flow

REACTOR

Predicted reactor system temperatures at the end of the prechill given in WANL-TME-887 are compared to the measured test temperatures at the end of the prechill period in table 4-4. The pretest calculated values were based on the entire reactor being at an ambient temperature of 540°R when the prechill was initiated. The reactor had been at 2 MW for over 5 minutes prior to the prechill and the reflector and core temperatures were above ambient temperature when OBV 86 was opened. During the prechill interval the core inlet temperature was reduced from 582°R to 455°R, somewhat more than the planned 90°R reduction. Thermocouple T-781 which was used to determine when the 90°R quench had been obtained decreased 114°R during this interval. Although the initial temperatures were considerably higher than those on which the calculations were based, the temperatures at the end of the prechill were very close to expectations as shown in the table.

As in the case of the EP-1 B LH_2 test, actual flow rate could not be obtained from the LH_2 flow meter FE-7 during the prechill, because part of the flow was bypassed through valve AVV2.* However, several things indicate that 2 lb/sec was close to the actual flow rate during the prechill. First, the time for the 90°R temperature reduction at the core inlet, measured and predicted, were in reasonable agreement (48 seconds predicted vs. 44 seconds measured). Also the reflector inlet and exit temperatures (measured and predicted) are in fair agreement as seen on figure 4-2. Since there is reasonable agreement between the predicted and measured values noted above, it is likely that the actual flow rate was close to the planned flow rate of 2 lb/sec.

---

* See figure 3-7 for Test Cell A flow schematic

TABLE 4-4

REACTOR CONDITIONS AT THE END OF PRECHILL
(CRT 13693) PREDICTED AND MEASURED

	Measured	Predicted*
Reflector Inlet (Average of 7 T/C)	43°R	38°R
Reflector outlet (Average of 5 T/C)	331°R	351°R
Core Inlet (Average of 11 T/C)	455°R	443°R
T/C T-781	473°R	---
Nozzle Chamber (Average of 4 T/C)	565°R	606°R
Tie Rod Exit Gas (Average of 4 T/C)	641°R	590°R
Time for 90°R reduction at core inlet	44 sec	48 sec
Actual time of prechill	51 sec	48 sec

*Calculated with pre-run TNT

CORE

Figure 4-3 has four time histories of selected core fluid and material temperatures to illustrate typical conditions in the core region during the prechill and start up. Core inlet thermocouple T-781 decreased during the prechill and continued to decrease at about the same rate after startup was initiated (Time CR 13693) until about Time CR 13710. At this time the flow increased rapidly with a resulting rapid decrease in core inlet temperature, tie rod exit gas temperature, and station 8 core material temperature. During the prechill and startup the core inlet temperature decreased continually to a minimum at the steady state power hold. Conditions during the startup period following the prechill are considered in detail in a later section of this chapter on startup and shutdown.

An azimuth asymmetry which existed at the end of prechill is shown on figure 4-3 and 4-4. This asymmetry is similar to that observed in EP IB with a pronounced minimum at 120°, the location of the nozzle feed line, and an indication or a temperature depression opposite the line at 300°. The variation is somewhat attenuated from an 85°R azimuth variation at reflector inlet to 68°R at the core inlet. However, the maximum variation occurs at the reflector outlet and is 130°R.

The asymmetry shown on figure 4-4 and 4-5 disappears during the power run. This smoothing out of the asymmetry is shown and is discussed more fully in the startup section.

REFLECTOR

The axial distribution of material temperatures at the end of prechill (Time CR 13693) for the reflector, control drum, and control vane are shown on figure 4-6. As may be expected, the nozzle end of the reflector system where the low temperature nozzle exit fluid enters the reflector system is colder than at the dome end. The bulk fluid temperature increases as it passes through the reflector due to the sensible heat pickup from the reflector materials. Also, it is noticed that the control vane which has a low heat capacity is coolest. The control drum and the sectors are less effectively cooled during [illegible] and thus show correspondingly higher material temperatures.

REFERENCE

Astronuclear

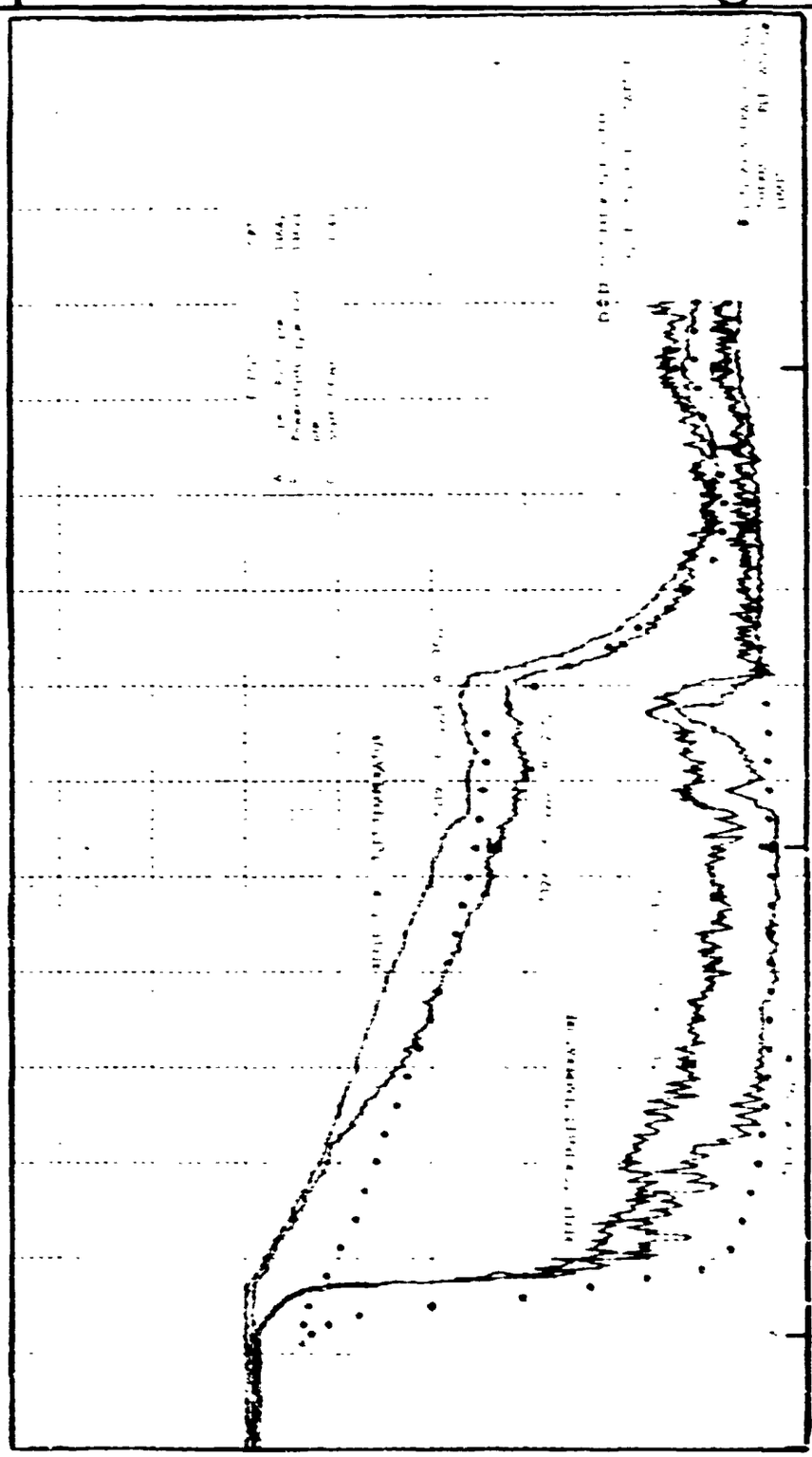

PREPARED BY	APPROVED BY	CURVE NO

NRX-A2 EP IV PRECHILL AND STARTUP TYPICAL REFLECTOR INLET AND OUTLET TEMPERATURE TIME HISTORIES

FIGURE NO.

4 - 2

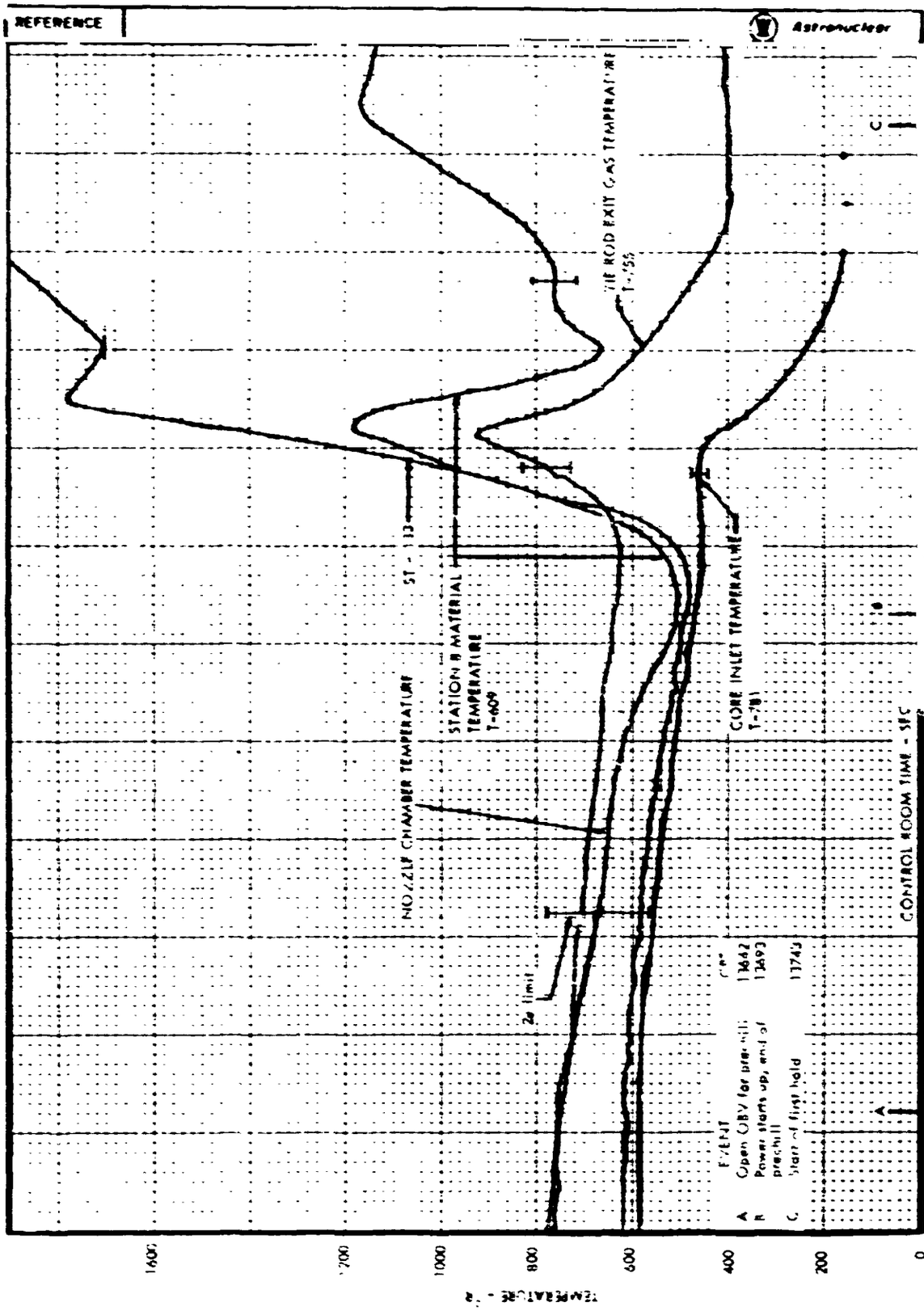

TYPICAL CORE TEMPERATURES VS TIME (PRECHILL)

PREPARED BY

APPROVED BY

FIGURE NO

4 - 3

CONFIDENTIAL RESTRICTED DATA

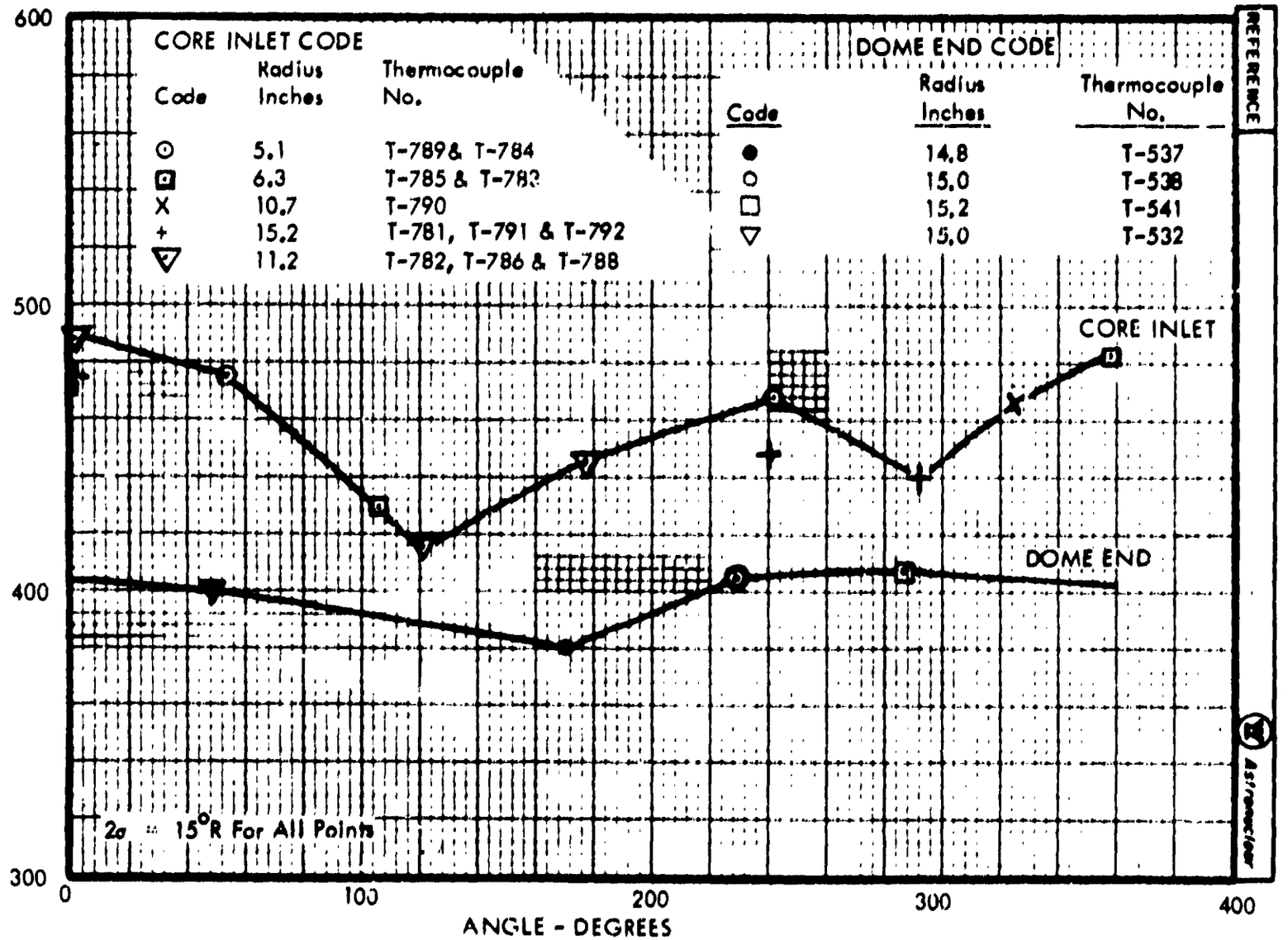

FIGURE NO.	CORE INLET AND DOME END TEMPERATURES VS. AZIMUTHAL POSITION AT END OF PRE CHILL (CRT 13693)	PREPARED BY	APPROVED BY	CURVE NO.
4-4				

CONFIDENTIAL RESTRICTED DATA

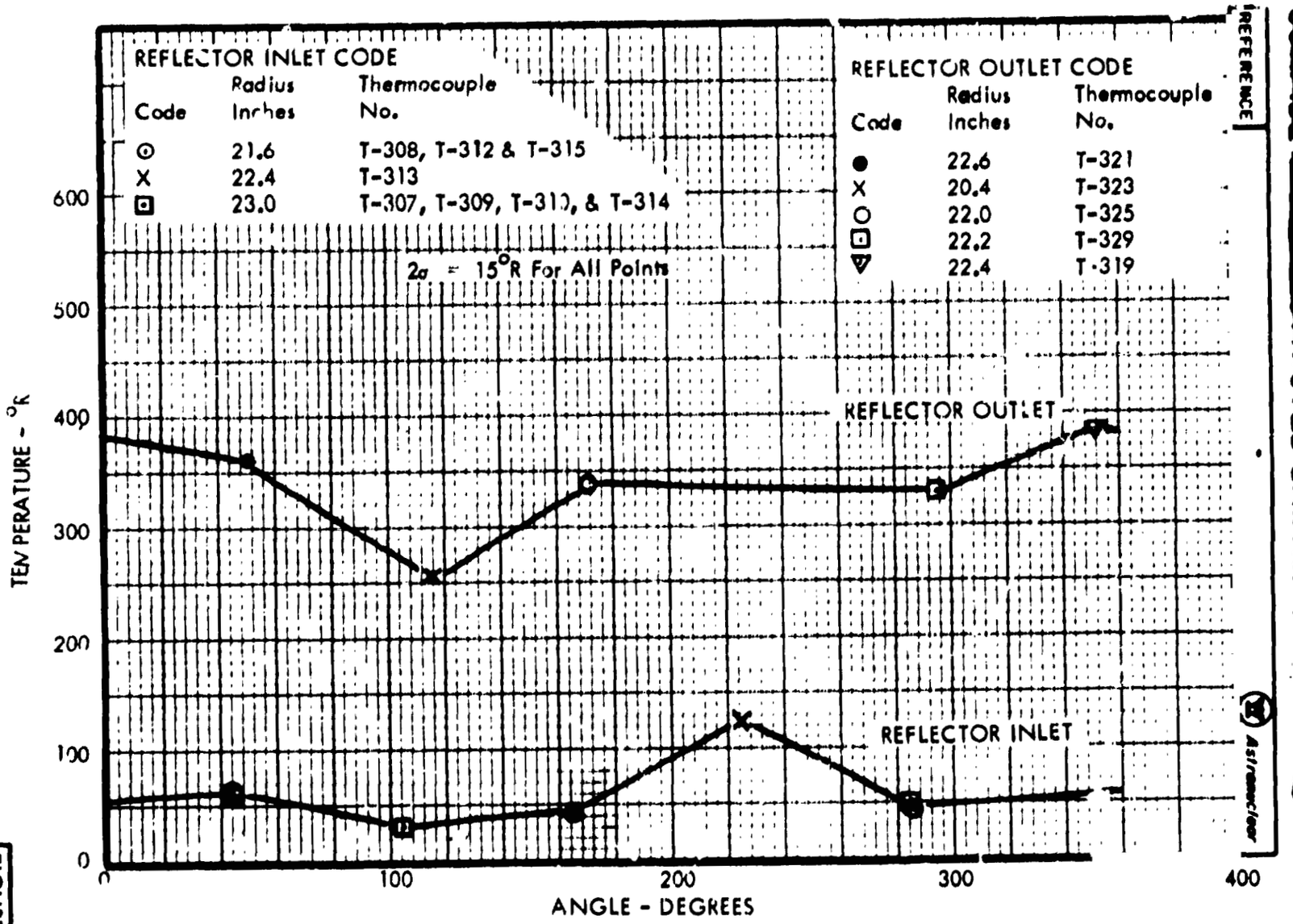

FIGURE NO.		PREPARED BY	APPROVED BY	CURVE NO.
4-5	REFLECTOR INLET AND OUTLET TEMPERATURE VS. AZIMUTH AT END OF PRECHILL (CRT 13693)			

REFERENCE		PREPARED BY	APPROVED BY	Astronuclear

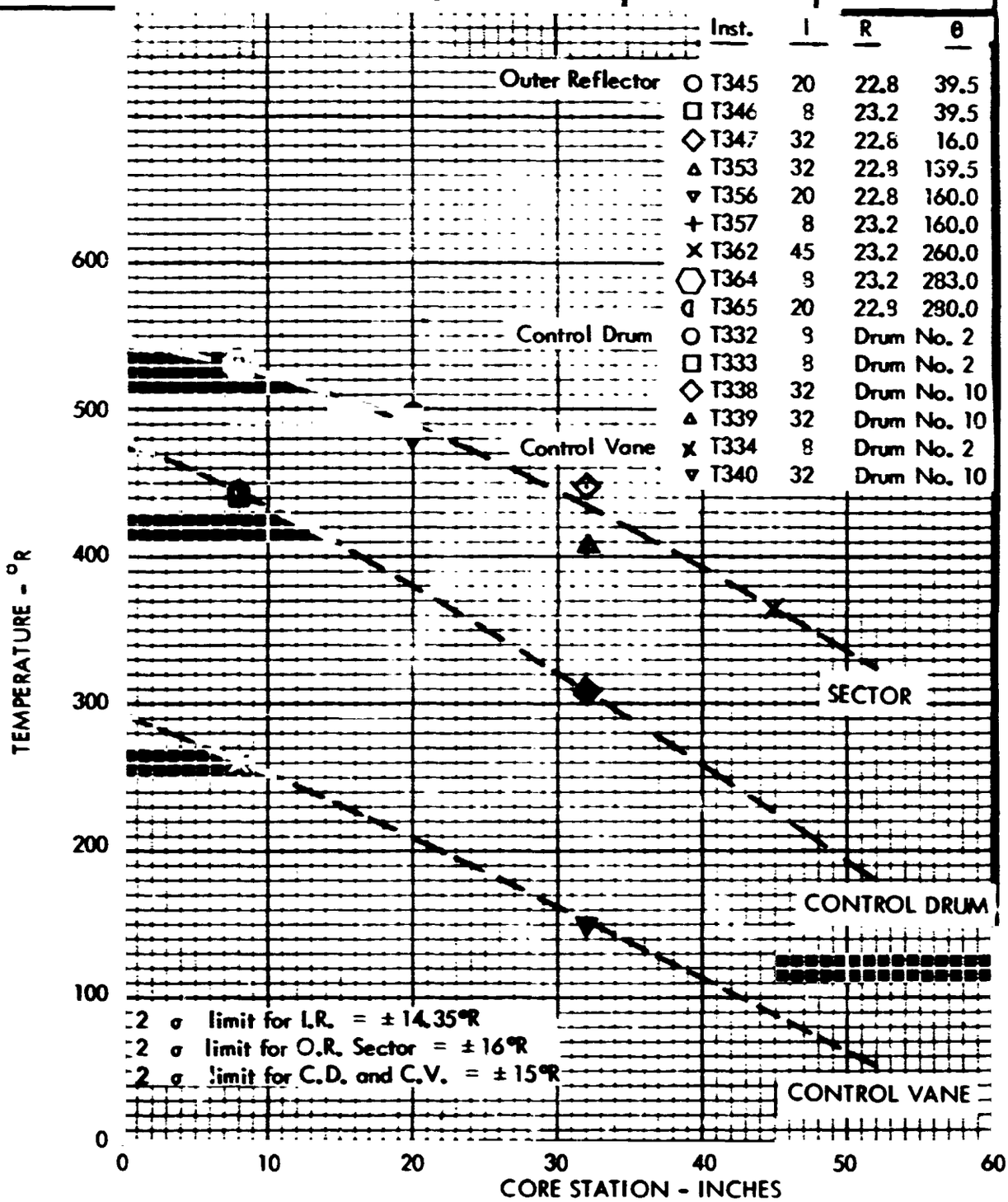

NRX-A2 EP IV CONTROL DRUM, VANE, AND SECTOR TEMPERATURES AT END OF PRECHILL (CRT - 13693)

CURVE NO.	FIGURE NO.
	4 - 6

Inner reflector material and seal chamber fluid temperatures are shown on figure 4-7. The seal chamber temperatures show decreasing temperatures from the dome end to the nozzle end, with the exception of thermocouple T-442 at station 35.3. The cause of this single higher temperature is not known. The other temperature measurements appear to be as might be expected considering the low temperature pin leakage entering the system without high power generation at this time. The axial distribution and temperature level of the inner reflector material temperature as shown in figure 4-7 is similar to the other reflector components shown in figure 4-6. During the transient prechill the inner reflector cylinder cooled more rapidly than did the drum and sector reaching a lower temperature at the end of the prechill. This is as expected.

A comparison of the measured values of reflector inlet and outlet plenum temperatures with those predicted in TME-887 is shown in figure 4-2 for the prechill interval. The calculated values for the prechill interval were from the pretest TNT referenced above, while the values after the prechill (after 13693 seconds) are the results of a postrun calculation. A description of the TNT calculation and comparison to test results for the prechill and startup intervals is in a later section on startup.

Only the traces for the maximum and minimum temperature are shown for both the reflector inlet and outlet on figure 4-2. The linear average of these bulk temperatures is shown by the 2 σ limit error band at the end of the prechill (Time CR 13693) and start of the first power hold (Time CR 13743). The reflector inlet temperature is the average of seven thermocouples and the reflector outlet temperature is an average of five thermocouples. The error band shown is the 2 σ for 95 percent confidence level.

At the start of prechill the temperatures of the reflector inlet plenum dropped rapidly to a steady value of 43°R. The temperature of the outer reflector exit plenum decreased at a slower rate because of the heat pickup in the reflector system. At Time CR 13693 the prechill ends and the startup is initiated. During the startup period the reflector inlet plenum temperature rises, and levels off at 90°R at the start of the first power hold (Time CR 13742).

REFERENCE		PREPARED BY	APPROVED BY	Astronuclear

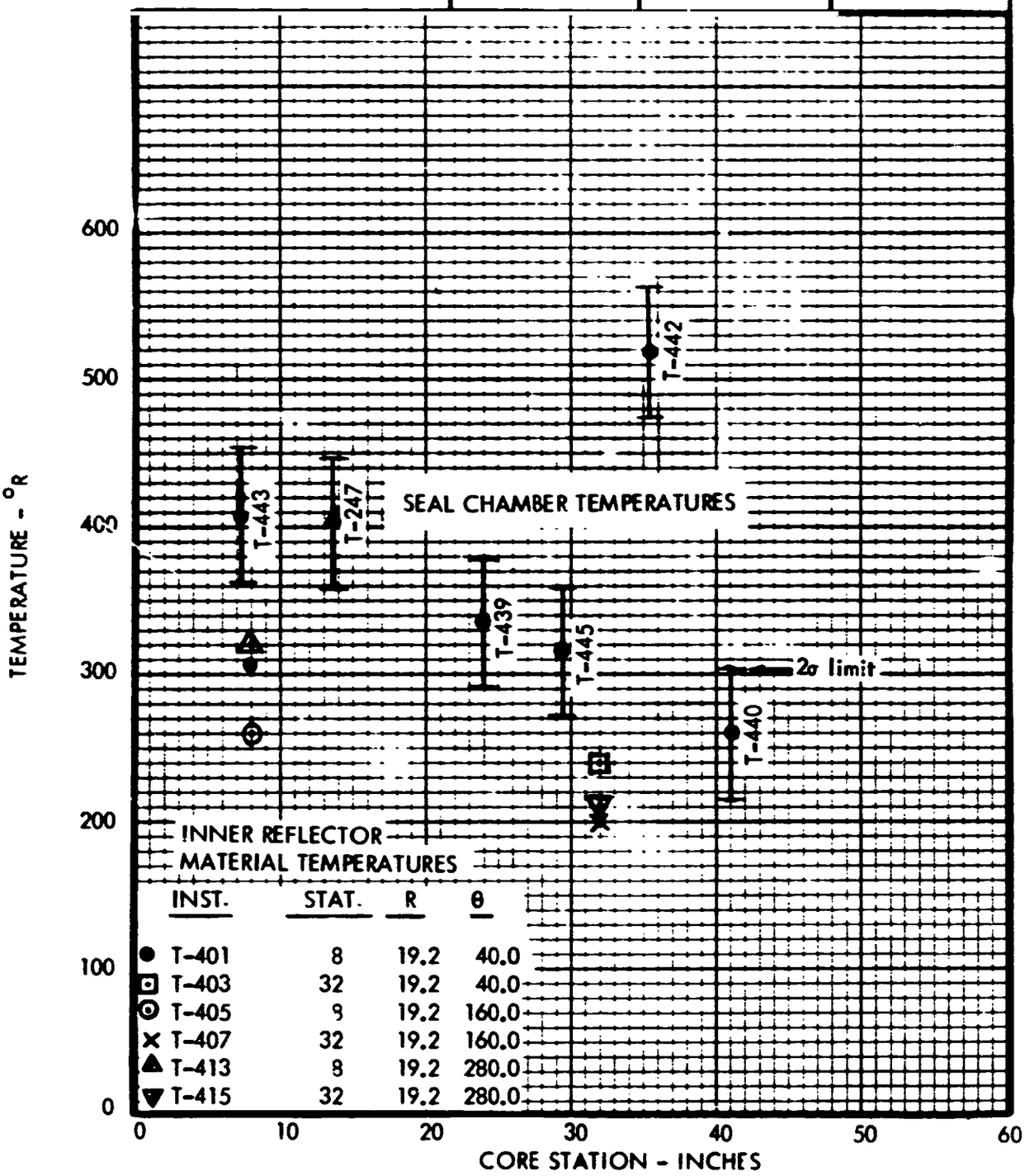

NRX-A2 EP IV INNER REFLECTOR MATERIAL AND SEAL CHAMBER TEMPERATURES AT END OF PRECHILL CRT - 13693	CURVE NO.	FIGURE NO.
		4 - 7

The reflector outlet temperature decreases after the initiation of prechill, and holds steady between Times CR 13695 and CR 13710. After Time CR 13710, when the flow increased rapidly, the reflector outlet temperature decreased rapidly to a minimum value about 100°R and then increased to its steady value of 140°R at the first power hold.

Nuclear

DELAYED CRITICAL BANK POSITION

In only one of the scram checks was the reactor permitted to reach equilibrium. The critical drum bank position in this measurement (at Time CR 9020) was 97.6 degrees with the reactor at slightly elevated temperature. Corrected to ambient conditions this position becomes 97.5 degrees.*

Just prior to the prechill period (Time CR 13642 to 13693) the control bank stablized at 98.6 degrees under influence of low GH_2 flow and elevated reactor temperatures. Following the opening of OBV-86 the control drum bank began rotating inward slowly, reaching ultimately 96.4 degrees at the end of the prechill (Time CR 13693).

HIGH POWER HOLDS

In this section reactor performance and reactor component performance at the steady state high power holds are considered. Transient operation during the startup and shutdown are considered in the section on startup and shutdown. Four operating times were chosen for examination of the experimental data and analyses which were required. These control room times (13790, 13900, 13985 and 14085 seconds), were selected as representative of steady state operations during each of the four high power holds. The run profile on figure 4-1 gives calculated thermal power, measured flow rate and measured nozzle chamber temperature. At the four steady state times, nozzle chamber temperature calculated from the nozzle equation are included.

---

* Analysis of "Quick Look" Sanborn temperature channels indicates a uniform reactor temperature of 570 ± 10°R. The normalization to 528°R results in a drum bank position correction of -0.1 degree.

Thermal and Fluid Flow

POWER DETERMINATION

The liquid hydrogen flow rates were calculated at the selected EP IV hold times. Details of the nozzle - venturi meters and test cell A liquid hydrogen flow calculations are given in the appendix. Results of these calculations for the venturi meter upstream of the pump (FE-4) and the venturi downstream of the pump (FE-7) are given in table 4-5. In addition to these flow rates the 2 σ error is given for the average flow rate, and the tie rod coolant flow and lateral support bypass flow are included.

Calculation of the reactor flow rate and the flow rate accuracy at Time CR 14085 is included as an example at the end of appendix G. The tie rod flow rates given in the table were calculated for the experimental reactor operating conditions using the MCAP program. This calculation is described in more detail in the section on the core later in this chapter of the report. The lateral support system flow rates in the table were obtained by extending Data Book calculations[1] to A2 operating conditions. An experimental verification of these flow rates could not be made, primarily because of the questionable seal chamber temperature indications. Analyses in this report are based on the flow rates in table 4-5, using the average of FE-7 and FE-4 for reactor flow. Nozzle temperature and reactor power is calculated from a heat balance using this average venturi flow rate. The two venturis are in good agreement, however any systematic error in the LH_2 flow rate, which was 6 percent higher than planned, would affect the reactor power levels calculated in this section.

Nozzle chamber temperature measurements were found to be considerably lower than the mixed mean nozzle chamber temperature as determined by other means. The principal cause of this low indication by the chamber thermocouples is believed to be the proximity of the thermocouples to the nozzle wall, as discussed later in this section. The most accurate mixed mean nozzle chamber temperature was calculated from the nozzle flow equation.

---

1 WANL-TME-840, G.2.d.1. Sheet 5. Reactor Analysis Data Book

TABLE 4-5

EP IV HIGH POWER TEST LH_2 FLOW RATES AND NOZZLE CHAMBER TEMPERATURE

Control Room Time (seconds)	13790	13900	13985	14085
Reactor Flow (lb/sec.)				
Inlet venturi (FE-4)	60.1	74.0	75.4	75.4
Discharge venturi (FE-7)	60.2	74.2	75.9	75.8
Average Flow Rate	60.1	74.1	75.6	75.6
2σ Error of Average Flow Rate	$\pm$ 1.6	$\pm$ 1.5	$\pm$ 1.5	$\pm$ 1.5
Tie Rod Channel Flow (lb/sec)	3.64	4.44	4.54	4.57
Lateral Support Flow (lb/sec)	0.28	0.35	0.36	0.36
Nozzle Chamber Temperature	2603°R	3390°R	3644°R	3815°R
2σ Error (°R)	$\pm$ 200	$\pm$ 210	$\pm$ 210	$\pm$ 215
Nozzle Chamber Pressure (psia) Average of p-122 and p-124	382	537.5	568.5	581.5

$$W = KA \quad Pc\sqrt{T_c}$$

where

W = flow rate, lb/sec

P_c = nozzle chamber pressure, psia

T_c = nozzle chamber temperature, ^{o}R

A = nozzle throat area, 59.0 in.^{2} at operating temperature

K = flow coefficient, 0.138 ^{o}R/sec average theoretical value × 0.985

Test values of the chamber pressure and flow rate, a nozzle flow coefficient 1.5 percent less than theoretical, and measured nozzle throat area corrected to operating nozzle temperature were used in the chamber temperature calculation. The resulting nozzle chamber temperatures at the four steady state times and the 2 σ error based on flow and pressure accuracy and a $\pm$ 1 percent 2 σ error on the flow coefficient are given in table 4-5. Chamber pressures used in this calculation which are an average of the two nozzle chamber pressure transducer indications are also included in the table. Computation of the nozzle chamber temperature and its 2 σ error at Time CR 14085 are part of the example at the end of appendix G. On figure 4-1 these calculated values are compared to a typical nozzle chamber thermocouple indication.

A heat balance was performed from the reflector inlet to the nozzle chamber to obtain reactor thermal power. Test pressure and temperature conditions at the reflector inlet gave the inlet enthalpy while nozzle chamber pressure and calculated temperature gave the nozzle chamber enthalpy. Thus, the thermal power MW was calculated from the expression,

$$PWR = W(h_c - h_r)10^{-6}\ 1055 + C$$

where,

PWR = total reactor thermal power in MW

W = reactor flow rate, lb/sec

h_c = nozzle chamber enthalpy, Btu/lb

h_r = reflector inlet enthalpy, Btu/lb

C = nuclear heating in nozzle and radiation from core to nozzle, MW

The regenerative heat transfer between the hot and cold side hydrogen in the nozzle do not appear in the power expression because the hot side heat loss is cancelled by the cold side heat gain, however, nuclear heating in the nozzle and radiation heat transfer from the core to the nozzle are accounted for by C in the above expression. The value of C was calculated and found to be approximately 2 MW at design conditions. At part power operation the C was assumed to be directly proportion to the power. The factors in the power calculation and the calculated power are given in table 4-6. The power calculation and 2 σ error analysis is given for the high power hold at Time CR 14085 in appendix G.

Independent methods of obtaining the reactor power include rabbits which were irradiated for specific time intervals during the test, and neutronics tank detectors. The neutronic power calibration during EP-II was described in the previous chapter while the rabbit and neutronics tank detectors indicating power during the high power test are evaluated in a later section on High Power Holds - Steady State-Nuclear. Reactor thermal power evaluated by the rabbits, the neutronics tank linear number 2, and the heat balance are tabulated in table 4-7 for the four steady state hold times. The agreement of these power measurements is well within the expected accuracy of the measurements.

Also an indirect indication of the adequacy of the power level measurements can be made from another independent source, the total integrated A2 power obtained from post-test radiochemistry. Post-test radiochemistry is described in Chapter 9 of this report. The integrated power from this source and from integrating the linear neutronics power, the rabbit power and the heat balance power are given at the bottom of table 4-7. The total energy obtained from radiochemistry was given[1] with the assigned accuracy indicated in the table. Accuracy of the energies obtained from integrating the power data are not given because of the unknown error associated with the integration. The agreement of the total energy release is very good, with a total variation of less than 6 percent for all four sources. Thus, the radiochemistry results provide an added confirmation of the maximum

1 NTO-M-1671, December 14, 1964, Radiochemistry Measurements on NRX-A2.

TABLE 4-6
DETAILS OF HEAT BALANCE REACTOR POWER CALCULATION, EP IV

Control Room Time	13790	13900	13985	14085
Average Reflector inlet temp. (°R)	92	115	136	136
Reflector inlet pressure (psia)	488	687	731	751
Reflector inlet enthalpy (Btu/lb)	149	217	288	287
Nozzle chamber temperature from table 4-5 (°R)	2603	3390	3644	3815
Nozzle chamber pressure, from table 4-5 (psia)	382	537.5	568.5	581.5
Nozzle chamber enthalpy (Btu/lb)	9183	12259	13280	13991
Enthalpy rise (Btu/lb)	9034	12042	12992	13704
Average flow rate, from table 4-5 (lb/sec)	60.1	74.1	75.6	75.6
C (MW)	1.0	1.7	1.9	2
Reactor thermal power (MW)	574	943	1038	1096

TABLE 4-7

EP IV REACTOR THERMAL POWER AT STEADY STATE HOLDS

Control Room Time, Seconds	Heat Balance, MW	Rabbit MW	Neutronics Tank (Linear No. 2) MW
13790	574 ± 38	537^{+32}_{-72}	527^{+32}_{-72}
13900	943 ± 45	895^{+54}_{-120}	902^{+54}_{-120}
13985	1038 ± 49	979^{+59}_{-131}	983^{+59}_{-131}
14085	1096 ± 50	1059^{+63}_{-142}	1047^{+63}_{-140}

A2 TEST TOTAL REACTOR ENERGY COMPARISON

Detector	Energy release (watt-sec)
Linear neutronics	3.67×10^{11}
Rabbit	3.59×10^{11}
Thermal	3.81×10^{11}
Post Test Radiochemistry	$3.68 \times 10^{11} \pm 0.157 \times 10^{11}$

power level. Heat balance calculated power is used for all calculations described in this report. This power level was selected because the accuracy is better and in order to provide consistency between the various calculations.

A power level could also have been calculated from the measured core temperatures using measured flow rate and core inlet conditions. Rather than make this additional power comparison, core temperatures were calculated from reactor flow rate and reactor power (from heat balance) and then compared to measured core temperatures. These comparisons are made in a later part of this section relative to the core.

REACTOR AND FEED SYSTEM CONDITIONS

For Time CR 14085 at the maximum power hold operating cycle point conditions are given in figure 4-8. All values in the cycle diagram are test data or follow directly from test data unless denoted by an asterisk. These asterisk values were calculated using the best available data and are the best estimate of actual operating conditions. In cases where both a test and calculated value is included, the test data is considered to be unreliable. The calculations methods and the questionable data are described in this section.

The steady operation was at an off-design condition of about 98 percent power and 105 percent flow (1096 MW and 75.6 lb/sec). The notable variations from cycle conditions which would have been expected at this operating condition, all of which are considered in detail in the following portion of this section, were:

a) Reflector inlet temperatures 15°R high due to about 30 percent more heat pickup in nozzle.

b) Core inlet temperatures 35°R high due to 15 percent more heat generation in reflector and high nozzle coolant heat pickup.

c) Core ΔP 5 percent low.

CORE

In this section core thermal and hydraulic test results are presented and compared to calculated results at the steady state hold times. Descriptions of the analyses are also included. The measurements which were available and are considered in detail are the

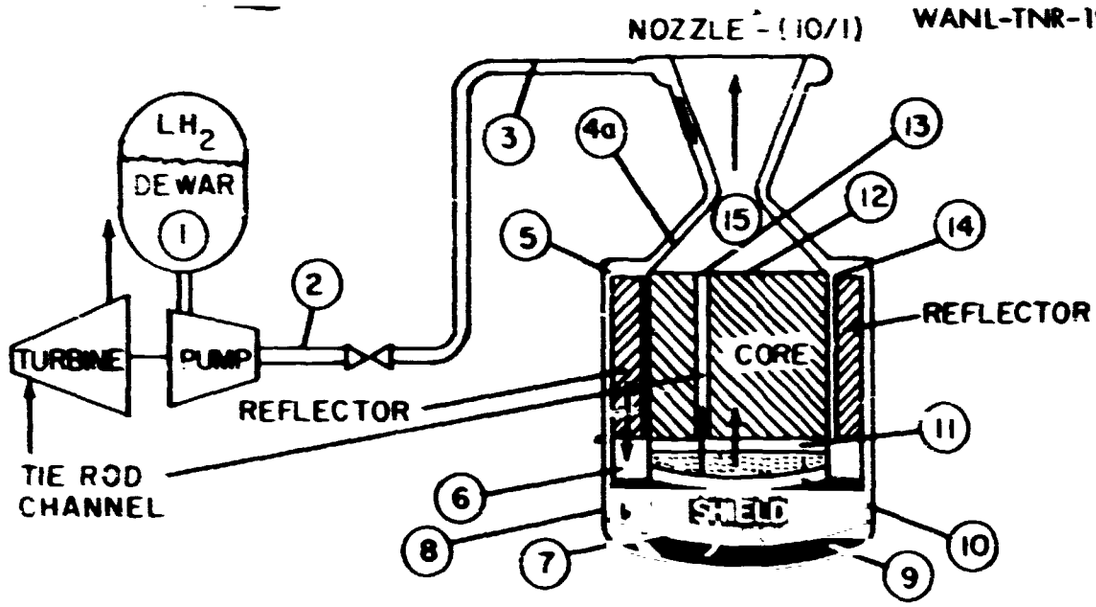

Figure 4-8 NRX-A2 CYCLE CONDITIONS AT TIME CR 14085 SECONDS

STATION	DESCRIPTION	W - lb/sec	P - psia	T - °R	POWER MW
1	Dewar Conditions	75.6	88	38	
2	Pump Outlet	75.6	932	47	
3	Nozzle Inlet	75.6	860	50	
4a	Nozzle Tubes Outlet	75.6	751	136	32.0 (nozzle)
5	Reflector Inlet	75.6	751	136	
6	Reflector Outlet	62.9*	713	232	
7	First Pass Shield Outlet	75.6	707	216	
8	P.V. Annulus Outlet	12.7*	748	155	
9	Second Pass Shield Inlet	75.6	707	216	22.7 (Refl. & 1st Pass Shield)
11	Support Plate Outlet	75.6	702	245 (225)*	0.2* (2nd Pass Shield)
12	Fuel Outlet	70.64*	581	4013*	1066* (Fuel)
13	Tie Rod Outlet	4.60*	581	674 (503)*	5.2* (Tie Rod Channels)
14	Reflector Seal Leakage	0.36*	581	1815*	
15	Nozzle Chamber	75.6	581	3480 (3815)*	1096* (Reactor)

NOTE: All values are test data or follow directly from test data except those values denoted by an asterisk. The asterisk values are calculated as described in the report and considered to be the best values.

core inlet temperature, the core pressure and differential pressure, tie rod exit gas temperatures, and unfueled element material temperatures (time varying thermocouple indications and maximum thermal capsule indications). These detailed core test data and analysis are considered in the following order in this section.

1) Core Inlet Temperatures

Test data and calculation of correction for γ heating in sensor.

2) Core Pressure Measurements

Test data

3) Core Temperature Measurements

A) Thermocouples - Test Data, analysis verifying station 32 thermocouple installation failure, and summary of post-operative thermocouple condition.

B) Thermal Capsules - Description of thermal capsules and their installation, test data obtained, and interpretation of the data.

4) Multiple Regression Fit of Measured Core Temperatures

Analysis of the core material temperature measurements to determine if a true radial temperature profile can be obtained or if different temperature readings are caused by random element-to-element variations.

5) Post-test Calculation of Core Operating Conditions

A) Pressure Drop and Axial Temperature Distribution Calculation - Calculation of the core pressure drop and average axial temperature profile from test data of flow, power, and core inlet conditions and comparison to measurements.

B) Radial Temperature Variations - Calculation of radial temperature distributions and expected random element-to-element temperature variations at station 45 and comparison to measurements.

C) Maximum Calculated Fuel Temperatures - Comparison of maximum calculated core material temperatures to maximum measured core temperatures.

6) Tie Rod Temperatures

Measured and calculated tie rod temperatures and an uncertainty analysis of the calculations.

Core Inlet Temperatures

The core is designed and orificed to run with a perfectly flat radial temperature profile (within a tolerance band due to the use of only 11 orifice sizes). To achieve this profile the core must operate at the design inlet temperature and control drum angle. The inlet temperature is important because the orifice pressure drop depends on the hydrogen properties. With other conditions held constant, a reduction in inlet temperature from the design value will cause a reduction in the impedance across every orifice. The core pressure drop will be reduced as a result, but the more important effect is a redistribution of flow between the fuel element channels. The result is an excess of flow in the low power factor channels and starving of the high power factor channels.

Orificing of the NRX-A2 core took place well in advance of final determination of sufficient information to make a firm prediction of the core inlet temperature. Orificing was based on a 250°R inlet temperature and a 90° hot drum angle. Subsequently, a change in nozzle caused a reduction in pre-run calculated core inlet temperature at full power design conditions to 210°R. This occurred too late to make a change in the orificing but the effects of off-design inlet temperature were included in the calculation of expected core temperatures and hot channel factors. Using the pre-run method based on maximum test conditions of 1096 MW and 75.6 lb/sec flow, the core inlet temperature was calculated to be 190°R. However, the measured average inlet temperature was 245°R at maximum power (Time CR 14085).

There were three reasons for the high measured values of core inlet temperature:

1) The measured nozzle tube exit temperature was 20°R higher than calculated (See the section that follows later in this chapter on the nozzle).

2) The measured heat pickup in the reflector region was high by about 15 percent (See the section that follows later in the chapter on the reflector).

3) There was an unreasonably high measured heat pickup from the dome end plenum to the core inlet.

Item 3 was investigated in detail as discussed below. The thermocouples intended to measure temperatures of the gas at the core inlet were located in the plenum between the

core support plate and the cluster plate region. The thermocouples in this area have a high internal heat generation rate and the coolant flow has a relatively low velocity. An analysis was made to account for the internal heat generation in the thermocouples. Listed below are the assumptions made in correcting the thermocouples for internal heat generation.

1) In determining the heat transfer coefficient it was assumed that the thermocouple saw a hydrogen velocity equal to the average coolant velocity in the area between the support plate and the core. The thermocouples were located between holes in the support plate. The OD of the thermocouple is about 0.065 inch and the typical support plate hole pattern is 0.375 inch holes on a 0.7 inch pitch. Therefore, it is possible that the thermocouple saw a velocity less than the average.

2) The heating rates in the thermocouples were based on those presented in WANL-TME-840, Index Numbers F.3.d.4.21 and F.3.d.4.22. These heating rates are based on 13 minutes at full power and includes the prompt and delayed gamma heating. Since NRX-A2 was not at constant 100 percent power, it was arbitrarily assumed that Time CR 13743 (beginning first hold) was equivalent to 0 time. The delayed gamma heating was adjusted according to the integrated power from Time CR 13743. The prompt gamma heating was adjusted according to the percentage of 1120 MW at the power hold.

Table 4-8 column 2 shows each core inlet thermocouple corrected for internal heat generation at each of the four steady state holds. Temperature corrections of up to 30°R are shown on the average core inlet temperature at Time CR 14085. After making this correction, the core inlet temperatures are from 0 to 3 percent lower than the measured temperatures at the dome end of the shield in column 3. This indicates a systematic error in the correction, probably in heating rates or heat transfer coefficients to the low velocity coolant. It is concluded that internal heating in the core inlet thermocouples effected the temperature indication. However, an accurate correction cannot be calculated. The most accurate value for the core inlet temperatures was found by using the measured temperatures at the dome end of the shield and adding to this the calculated temperature rise of the coolant due to the heat generated in the shield, screen and support plate. This method removes all uncertainties except that due to measured total flow and calculated

TABLE 4-8

AVERAGE CORE INLET TEMPERATURE AS MEASURED, AFTER HEATING CORRECTION, AND CALCULATED BASED ON SHIELD DOME END MEASURED TEMPERATURES

CRT	1 $T_{Core\ Inlet}$ (As Measured)	2 $T_{Core\ Inlet}$ (TC Corrected for Q''')	3 T_s Measured at Dome End of Shield	4 ΔT Across Shield And Support Plate	5 $T_{Core\ Inlet}$ ($T_s + \Delta T$)
13780 (574 MW)	172	148	148	5	153
13900 (943 MW)	219	190	196	8	204
13985 (1038 MW)	233	204	211	8.5	220
14085 (1096 MW)	245	215	216	9*	225

*Based on $0.178^{+0.197}_{-0.080}$ percent of full power heat

Pickup by 75.6 lb/sec coolant flow, WANL-TME-840

total heat generation in the materials. There is no other method of determining the core inlet temperature that is not subject to the same or similar uncertainties, plus others. However, support plate temperature measurements tend to verify the dome end plenum hydrogen temperature measurements.

Based on the information presented in WANL-TME-840, Index Number F.3.b.1, the power generated in the second pass shield, screen, and support plate is $0.178 \begin{smallmatrix}+0.197\\-0.080\end{smallmatrix}$ percent of full power.

At 1096 MW and 75.6 lb/sec flow, the ΔH from dome end to core inlet is:

$$\Delta H = Q/W = \frac{(1096)(.00178)(.948 \times 10^3 \text{ BTU/MW sec})}{75.6}$$

$$\Delta H = 24.6 \begin{smallmatrix}+27.4\\-11.1\end{smallmatrix} \text{ BTU/lb}$$

The resulting ΔT, with uncertainties is:

$$\Delta T = 6.5 \begin{smallmatrix}+7.5\\-3.0\end{smallmatrix} {}^\circ R$$

For analysis, it was decided to split the difference in the uncertainties, and the ΔT at Time CR 14085 was set equal to $9 \pm 5^\circ R$. Other power holds were analyzed in the same manner, and the results are in table 4-8, column 5. Thus, it is concluded that at the maximum power the core inlet temperature was $225^\circ R \pm 9^\circ R$, while it was expected to be $190^\circ R$. This difference is caused by higher than expected heating in the reflector system and higher than expected heat pickup in the nozzle tubes. On the basis of these results the core inlet temperature for the NRX-A reactor at design conditions of 1120 MW and 71.3 lb/sec LH_2 is calculated to be $245^\circ R$.

Core Pressure Measurements

Two sensors, P-122, and P-124, that were located in the nozzle chamber operated reliably during the high power holds. There was one pressure measurement in the core inlet plenum, P-604. The core pressure drop was measured by one instrument, DP-603. The core pressure drop agreement between DP-603 and the difference between absolute pressure measurements at the core inlet and exit was within 1.5 psid or less.

The measured core inlet pressure is on line 4, table 4-9. Line 10 contains measured core exit (nozzle chamber) pressures and line 12 the measured core pressure drop. The maximum measured core pressure drop of 121.2 psid occurs at Time CR 14085 during the highest power hold.

Core Temperature Measurements

THERMOCOUPLES

Thermocouples were located within unfueled elements at four axial stations 8, 20, 32 and 45 inches. (figure 4-9). The number of thermocouples that remained reliably operative during the high power holds were three at station 8, three at station 20 and one at station 32. Twenty five station 45 thermocouples remained operative, but started to degrade as expected during the power hold at 943 MW and were unreliable thereafter.

During disassembly, the instrumentation appeared to be in generally good condition.[1] Only the core thermocouples at station 45 showed signs of extensive environmental effects. The amount of potting compound remaining in the potting slot at station 45 varied. The cement which remained was in poor condition. Surface corrosion and souting around the slot indicated that there was flow through the thermocouple shim hole and out the slot.

The station 32 thermocouples appeared to be in excellent condition except that the potting used to hold the sensing end of the thermocouple to the element was completely missing. In only one case did the potting remain and this case contained the only station 32 thermocouple which did not give a lower than predicted temperature reading. There were two elements found fractured at disassembly which contained station 32 thermocouples. Both fractures were similar and in the vicinity of the cold end of the potting slot.

Only two other major abnormalities were observed during disassembly. The first was the badly damaged sensing ends of the tie rod exit gas thermocouples. These sensing ends were bent and appeared to have been severely rubbed. The second concerned the position

1 WANL-TME-1079, NRX-A2 Instrumentation Disassembly and Post Operative Report, 8 January 1965.

TABLE 4-9

TEST VALUES AND POST TEST CALCULATIONS AT FOUR STEADY STATE HOLDS

Control Room Time Power (thermal)	13790 (574 MW)	13900 (943 MW)	13985 (1038 MW)	14085 (1096 MW)
Core Inlet Temperature, °R				
1. Calculated	153 ± 9	204 ± 9	220 ± 9	225 ± 9
2. Measured*	172	219	233	245
Core Inlet Pressure, Psia				
3. Calculated	462 ± 12.9	652 ± 12.8	691 ± 12.7	707 ± 12.7
4. Measured	460 ± 13	648 ± 13	686 ± 13	701 ± 13
Fuel Element Gas Exit Temp., °R				
5. Calculated	2753 ± 200	3579 ± 210	3839 ± 210	4013 ± 215
Maximum Fuel Temp., °R				
6. Calculated	2937 ± 200	3751 ± 210	4016 ± 210	4327 ± 215
7. Highest Measured	3180 ± 105	4000 ± 105	4050 ± 105	4400 ± 200**
Tie Rod Exit Temperature, °R				
8. Calculated	374	453	485	499
9. Measured	513 ± 26	611 ± 26	657 ± 26	690 ± 26
Core Exit Pressure, Psia				
10. Measured	381 ± 10	536 ± 10	567 ± 10	581 ± 10
Core Pressure Drop, Psid				
11. Calculated	81 ± 8.1	116 ± 8.0	124 ± 7.8	127 ± 7.8
12. Measured	78.7 ± 3.6	111.7 ± 3.6	118.7 ± 3.6	121.2 ± 3.6
Shield Dome End Temperature, °R				
13. Measured	148 ± 7.5	196 ± 7.5	211 ± 7.5	216 ± 7.5
Total Flow, lb/sec				
14. Measured	60.1 ± 1.6	74.1 ± 1.5	75.6 ± 1.5	75.6 ± 1.5
Nozzle Chamber Temp., °R				
15. Calculated from lines 10 and 14.	2603 ± 200	3390 ± 210	3644 ± 210	3815 ± 215

*Core Inlet Temperature Thermocouple Readings Uncorrected for Internal Heat Generation - The Correction is Approximately a 20 - 30°R reduction.

**Highest Thermal Capsule reading at Station 45 Inches.

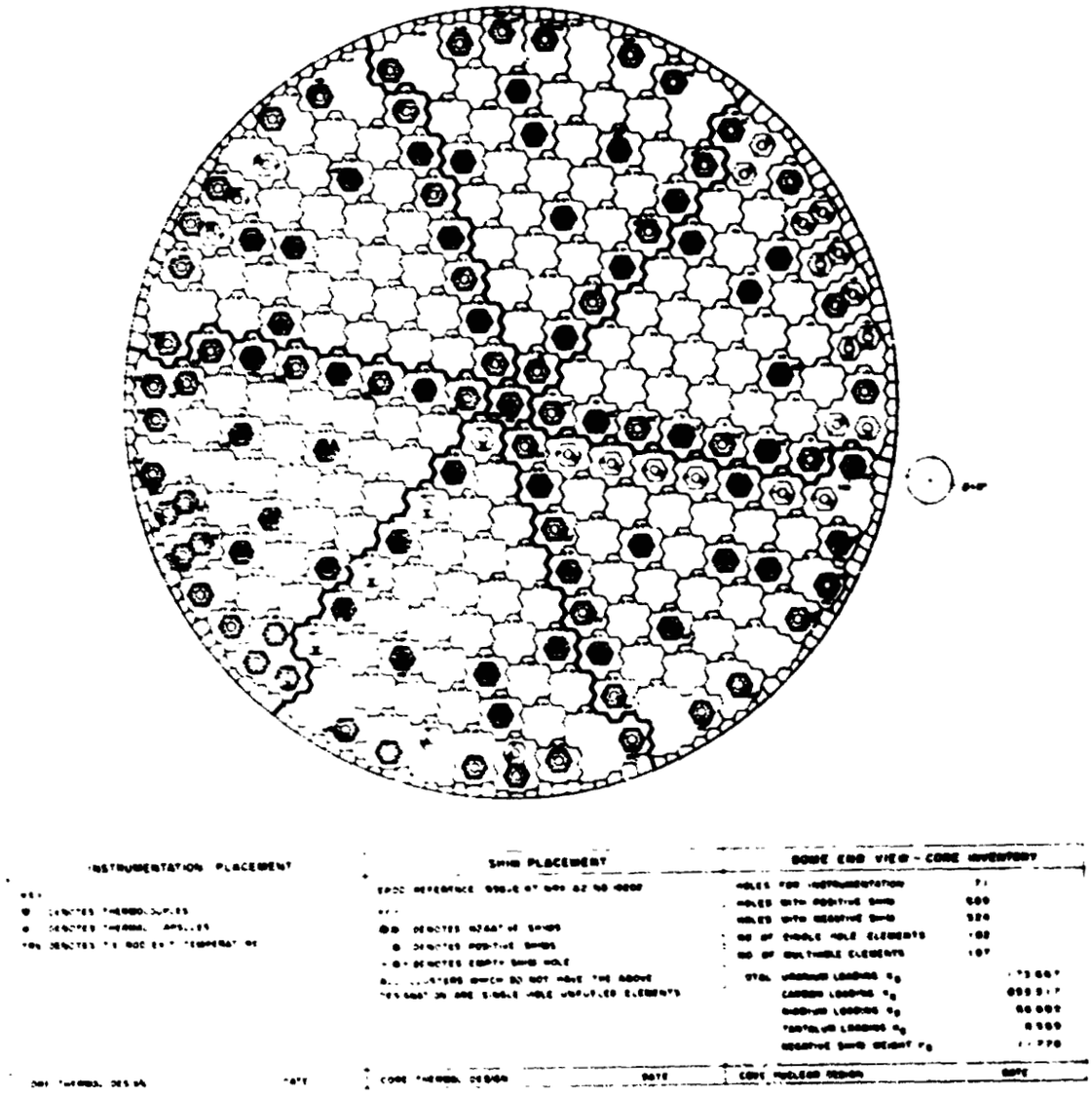

Figure 4 - 9 NRX-A2 Shimming Distribution and Instrumentation Placement

of several seal chamber thermocouples; they appeared to have been installed at other than the specified installation point. These thermocouples were position such that they were unable to sense the true seal chamber gas temperature.

During the four high power holds the thermocouple measurements of core material temperatures showed the expected pre-test trends, except for the station 32 thermocouples. Figure 4-10 contains the time history of one station 45 core material thermocouple and two station 32 core material thermocouples. The trace of the station 45 thermocouple, T-632, was typical of all station 45 thermocouples and was as expected. When the temperature exceeded about 3700°R, the thermocouple degraded and gave an approximately constant indication regardless of temperature. This degradation is the reason station 45 thermocouples were not selected for reactor control. The station 32 thermocouple, T-647, indicated temperatures very close to the expected trend at this location; however, this thermocouple was the only station 32 unit which indicated the expected temperature. Thermocouple T-643 on figure 4-9 is typical of the behavior of the rest of the station 32 thermocouple. They diverged from the expected material temperature during the rise to the second hold and indicated temperatures up to 1200°R low. Post run observations indicated that the potting had failed around the suspect thermocouples allowing flow in the channel through which the thermocouple was inserted. The results of a post test analysis showed that the low temperatures could be attributed solely to this leakage flow. A discussion of this analysis is contained in appendix E.

The 2 σ error in a single thermocouple reading during all high power holds at station 20, 32, or 45 is $\pm$ 105°R. This is based only on the data acquisition system, instrument error, and reading error. The 2 σ error in the calculated temperature at station 45 will be discussed along with the method of post-test calculations.

THERMAL CAPSULE TEMPERATURE MEASUREMENT DESCRIPTION

The utilization of thermal capsule temperature measurement, contrasted to the thermocouple, does not provide a temperature time history. Thermal capsule temperatures are determined during post-operative inspection and define maximum temperatures

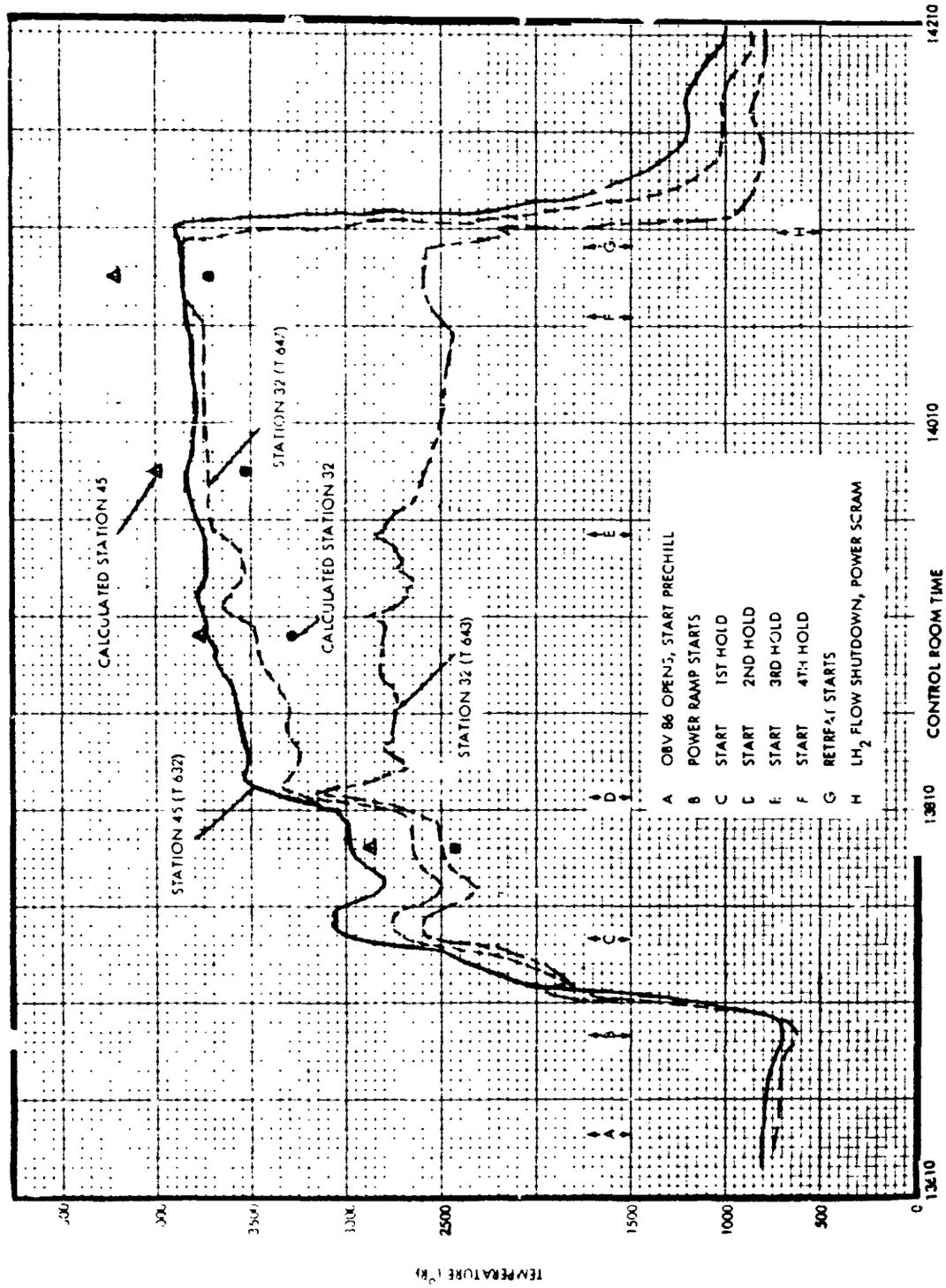

Figure 4-10 NRX-A2 EP-IV CORE MATERIAL TEMPERATURE HISTORIES

experienced for each specific placement. Two inherent advantages of the thermal capsule over the thermocouple are, (1) determination of an axial temperature profile for each thermal capsule placement and (2) no instrumentation leads. When installed these units are potted in permanently and do not perturb the design geometry.

Basically thermal capsule temperature measurement consists of a large number of individual small wire segments that have different calibrated melting temperatures. Each wire segment is selected because of its material composition to provide a given calibrated melting temperature. Table 4-10 identifies the wire segments and their respective composition and melting temperature. In any given thermal capsule placement individual wire segments having different melting temperatures are placed end to end in a groove along the length of an unfueled element and define several arrays of temperature versus position. This arrangement of individual wires provides for a determination of an axial temperature profile and defines a thermal capsule family distribution per placement. In the NRX-A2 one standard family was utilized. Figure 4-11 illustrates the standard thermal capsule family temperature pattern in terms of individual wire melting temperature versus axial position. Also superimposed in figure 4-11 is the axial temperature distribution calculated for the NRX-A2 nominal full power condition. Table 4-11 lists the standard thermal capsule family distribution according to wire code and axial distance from the inlet end. Thermal capsules were also utilized in the unfueled filler strips that form the circumferential boundary of the core periphery. The standard family was employed only in the core region and placements were only in unfueled elements. The thermal capsule family distribution employed in the filler strips was different because of filler strip temperature level and geometry. Each of the three instrumented filler strips were grooved the same; namely, axial positioning of individual units between ledges in the face of the filler strip that is adjacent to the pyrolytic tile. Table 4-12 identifies the filler strip thermal capsule family distribution. Temperature determination is done during post-operative evaluation and consists of reviewing X-ray film which shows whether melting of a placed wire has occurred and if so provides a determination of the material temperature. When a melting condition is questionable then a comparison is made with pre-operative film records of the installed wire that is done prior to cluster assembly.

TABLE 4-10

LIST OF THERMAL CAPSULE METALS AND ALLOYS

WANL Code No.	Wire Composition* Nominal	Indicating Temperature °C ±30°	Indicating Temperature °R ±54°
1	Aluminum	660	1674.9
2	28 copper - 72 silver	780	1895.4
3	20 copper - 80 gold	915	2138.4
4	Silver	970	2237.4
5	82 silver - 18 palladium	1095	2462.4
6	67 silver - 33 palladium	1215	2678.4
7	50 silver - 50 palladium	1310	2849.4
8	25 silver - 75 palladium	1420	3047.4
9	15 silver - 85 palladium	1460	3119.4
10	Palladium	1495	3182.4
27	85 platinum - 50 palladium	1585	3344.4
26	50 platinum - 15	1625	3417.0
12	Rhodium	1675	3506.4
13	12 iridium - 88 platinum	1775	3686.4
14	50 iridium - 50 rhodium	1895	3902.4
15	60 iridium - 40 rhodium	2005	4100.4
16	80 iridium - 20 rhodium	2150	4361.4
17	Molybdenum	2195	4442.4
18	Iridium	2305	4640.4
19	21 tantalum - 79 niobium	2431 - 2507	4868 - 5005
20	Rhenium	2475	4946.4
21	67 tantalum - 33 niobium	2636 - 2763	5237 - 5465
22	78 tantalum - 22 niobium	2631 - 2700	5228 - 5352
23	Tungsten	2705	5360.4
24	90 tantalum - 10 niobium	2830	5585.4
25	Tantalum	2845	5612.4

*These are used in the form of 0.040 Inch wire approximately 0.25 Inch long, and enclosed within graphite cylindrical capsules 0.40 Inches in length.

REFERENCE		PREPARED BY	APPROVED BY	Astronuclear

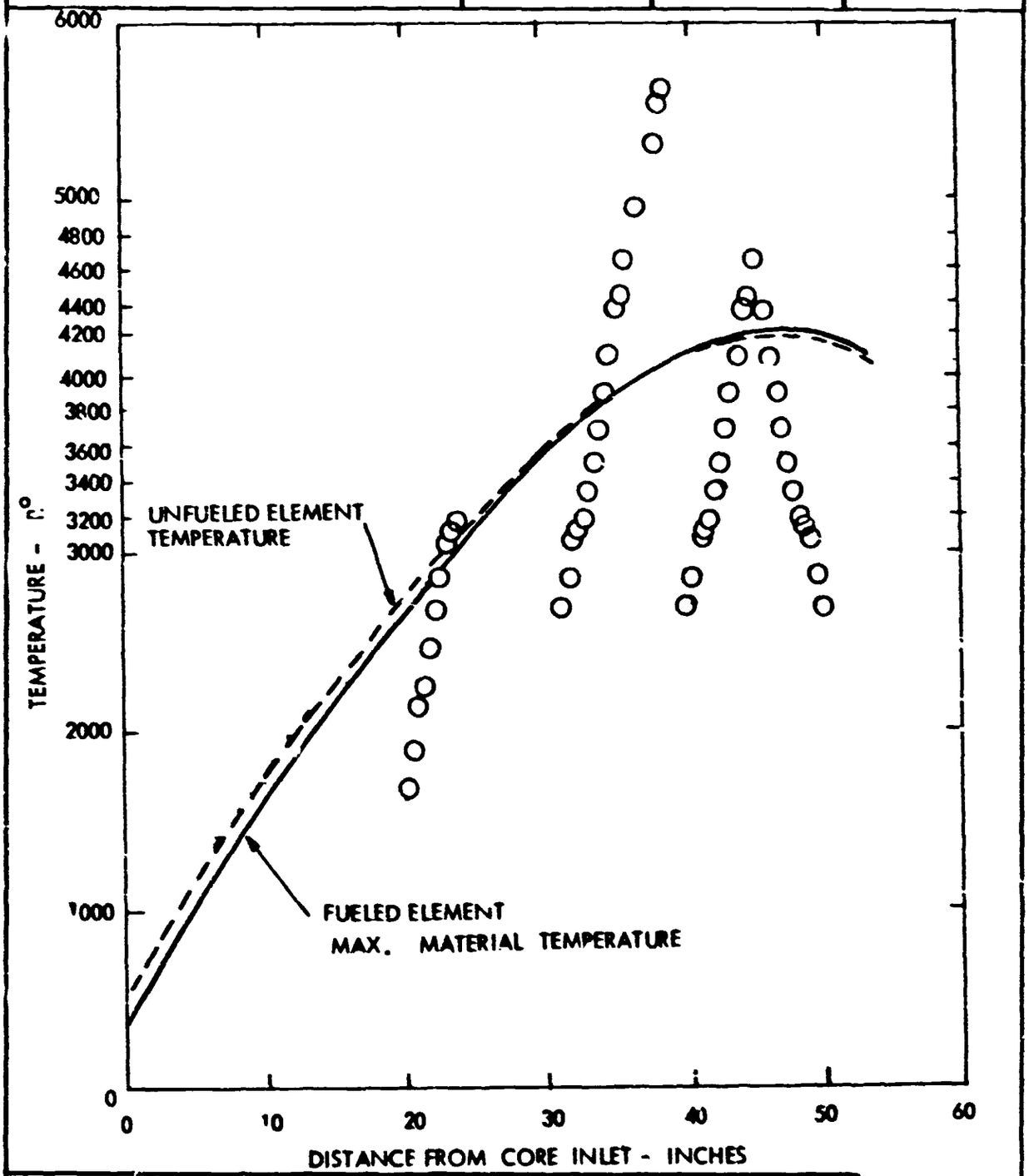

NRX-A2 UNFUELED ELEMENT THERMAL CAPSULE FAMILY WITH AXIAL TEMPERATURE DISTRIBUTION

FIGURE NO. 4 - 11

TABLE 4-11

THERMAL CAPSULE FAMILY DISTRIBUTION

Standard Family		Standard Family	
WANL Code No.	Station - Inches	WANL Code No.	Station - Inches
Inlet of Element			
	•	24	38.6
	20.0	25	39.0
1	20.4	blank	39.4
2	20.8	blank	39.8
3	21.2	blank	40.2
4	21.6	6	40.6
5	22.0	7	41.0
6	22.4	8	41.4
7	22.8	9	41.8
8	23.2	10	42.2
9	23.6	27	42.6
10	24.0	12	43.0
		13	43.4
7 inch Spacer	31.0	14	43.8
		15	44.2
6	31.4	16	44.6
7	31.8	17	45.0
8	32.2	18	45.4
9	32.6	blank	45.8
10	33.0	16	46.2
27	33.4	15	46.6
12	33.8	14	47.0
13	34.2	13	47.4
14	34.6	12	47.8
15	35.0	27	48.2
16	35.4	10	48.6
17	35.8	9	49.0
18	36.2	8	49.4
19	36.6	7	49.8
20	37.0	6	50.2
21	37.4		
22	37.8		
23	38.2	Total wire units per family = 54	

*20 Inch plug when an element with shims is specified otherwise for elements with no shim holes this 20 - Inch section is not grooved.

TABLE 4-12

FILLER STRIP THERMAL CAPSULES

Filler Strips to be Capsuled

Thermal Capsule No.	Filler Strip Sector	Filler Strip No.	Filler Strip θ	General Location On Each Filler Strip
TC 056	2	18	120	Under tile in shelves 5, 7, and 10 (counting from core inlet end) and on "F.S. 19 side" of strip.
TC 057	4	18	240	
TC 058	6	18	360	

Thermal Capsule Family To Be Used in Each of the Above Filler Strips

WANL Code No. See WANL Dwg. 978D074	Axial Location - Inches[1] From Core Inlet End Of Filler Strip	Shelf No. From Core Inlet End of Filler Strip
1	12.75 to 13.15	5
2	13.15 to 13.55	5
3	13.55 to 13.95	5
4	13.95 to 14.35	5
5	14.35 to 14.75	5
6	14.75 to 15.15	5
1	18.93 to 19.33	7
2	19.33 to 19.73	7
3	19.73 to 20.13	7
4	20.13 to 20.53	7
5	20.53 to 20.93	7
6	20.93 to 21.33	7
6	28.20 to 28.60	10
5	28.60 to 29.00	10
4	29.00 to 29.40	10
3	29.40 to 29.80	10
2	29.80 to 30.20	10
1	30.20 to 30.60	10

[1]Must add 4.75 inches to dimensions to get location from core inlet (station 0)

In all there were 53 standard-family thermal capsule core positions that are reported for the NRX-A2. Nineteen of these were positioned in the core central region; i.e., regular clusters, which defined three radial lines of temperature measurements. The other 34 placements were in the core periphery; i.e., irregular clusters and essentially were concentrated in one sector. A description of specific placement and test interpretation is presented in the subsequent section.

TEST DATA INTERPRETATION OF THERMAL CAPSULE PLACEMENTS

The interpretation technique of thermal capsule temperature measurement involves first the determination of a transition boundary in each of the four arrays that are defined in the standard family; i.e., wires that exhibit a fused condition between those which show no change in physical shape. Figure 4-12 is a typical X-ray photograph showing fused and intact thermal capsules. The later condition denotes that the respective local temperature did not exceed the calibrated temperature of the as-placed wire unit. Each established transition point has an axial position by nature of the adjacent coded wire units and their axial position. These points then define a four point axial temperature distribution to which is fitted a characteristic axial temperature profile. The fitting of the profile provides a temperature accuracy that is less than the spread between any two successive wire temperatures. (See lower curve on figure 4-13 for example axial profile fitting) For instance at station 45 the condition of the wire unit in adjacent arrays places the profile in either the upper or lower portion of the spread between two indicator temperatures evaluated. This results in a temperature reading accuracy that is less than $\pm 100^{\circ}R$ $\pm 50^{\circ}R$. The accuracy in individual wire calibration is $\pm 54^{\circ}R$.

Evaluation of NRX-A2 thermal capsule results of in-core temperature distribution are presented for the central region which essentially defines a radial condition whereas the peripheral region reflects radial and small measured azimuth effects. Figure 4-13 shows thermal capsule results of axial temperatures in the central region in which the radial temperature spread at the hot end of the core was within $400^{\circ}R$. Two shaded areas are identified in figure 4-13. Area I bounds 11 axial profiles which indicate temperatures at station 45 in the range of $4300^{\circ}R$ to $4350^{\circ}R$ inclusive. Area II covers 8 profiles with temperature

CONFIDENTIAL RESTRICTED DATA

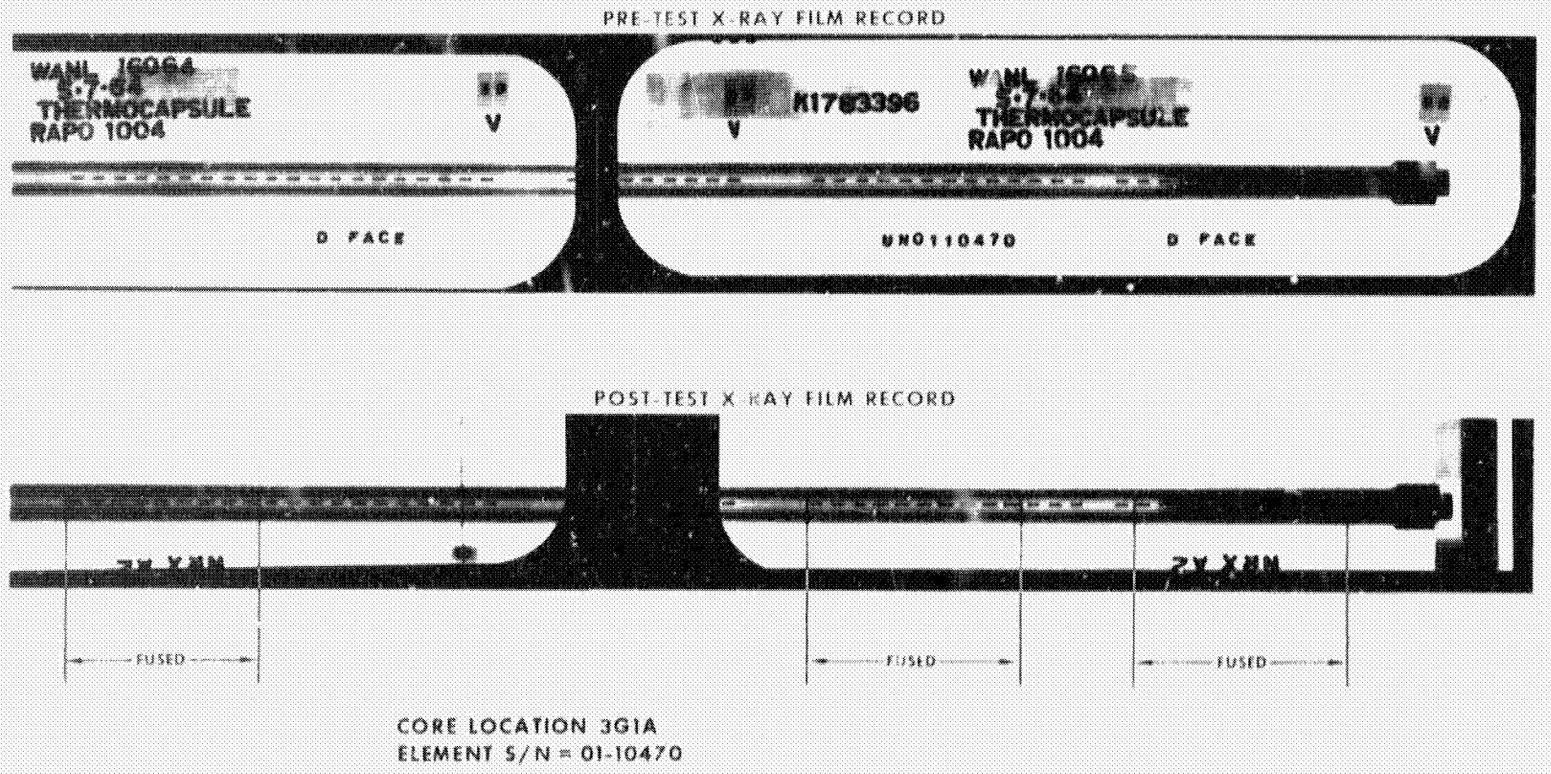

CORE LOCATION 3G1A
ELEMENT S/N = 01-10470

6048798

NRX-A2 THERMAL CAPSULE X-RAY FILM SAMPLE

REFERENCE

ASTRONUCLEONICS

CONFIDENTIAL RESTRICTED DATA

FIGURE NO.	X-RAY OF UNFUELED ELEMENT SHOWING FUSED THERMAL CAPSULES	PREPARED BY	APPROVED BY	CURVE NO
4 - 12				

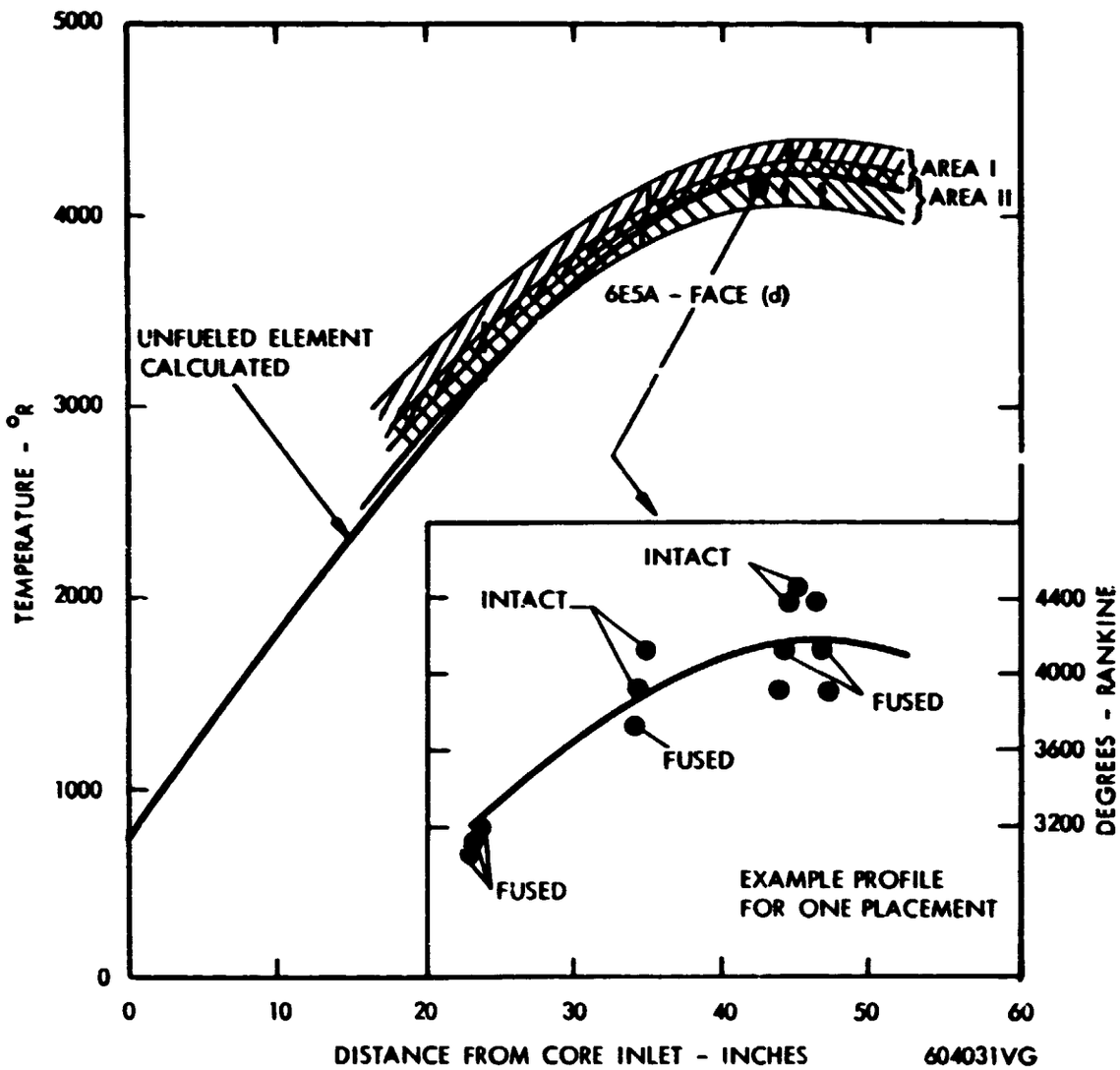

FIGURE 4 - 13

NRX-A2 THERMAL CAPSULE DATE PRELIMINARY 19 RADIAL POSITIONS IN CORE CENTRAL REGION

at station 45 in the range inclusive of 4150°R to 4250°R. Because of control drum effects the temperature distribution in the periphery was wider. Figure 4-14 shows a maximum spread of 500°R in the peripheral region. Area I of figure 4-14 covers 8 profiles in the range of 4350°R - 4400°R; area II has 19 at 4200°R - 4300°R, and area III covers 7 in the range including 4000°R - 4150°R. Figure 4-15 shows the thermal capsule core placement and radial temperature distribution at station 45. Figure 4-16 is an enlargement of Sector-1 at the peripheral region which had a concentration of thermal capsule placements. Figure 4-17 is a radial plot of the station 45 thermal capsule readings.

Thermal capsule temperature measurement in the core filler strips consisted of three placements. The instrumented filler strips are identified in figure 4-15 and are designated as 2-18, see WANL-TME-840. Figure 4-18 shows the thermal capsule family distribution as well as the calculated axial temperature distribution. The test results indicate that the temperatures in these instrumented filler strips were greater than 2678°R at the mid-core plane as well as at station 33. At stations 18-20 however the measured temperatures tend to complement the predicted calculated values.

Temperature levels of these three filler strips when compared circumferentially reflect a similar trend of temperature levels that were measured in the core periphery.

Multiple Regression Fit of Measured Core Temperatures

Due to the off-design inlet temperature and drum angle, the radial temperature profile in EP IV would not be expected to be flat. Figures 4-15 and 4-16 show the core cross section with the station 45 thermal capsule readings and location. The radial variation is quite evident in Sector 1 where eight pairs of thermal capsule readings in eight peripheral elements show an increase in measured temperature with radius. A well-defined radial variation in the core central region cannot be observed on the three radii shown in figure 4-15.

In order to determine if the thermal capsule readings at station 45 show a true dependence on radial location or if the different readings are caused only by random element-to-element temperature variations, a statistical analysis was performed on the temperatures using the

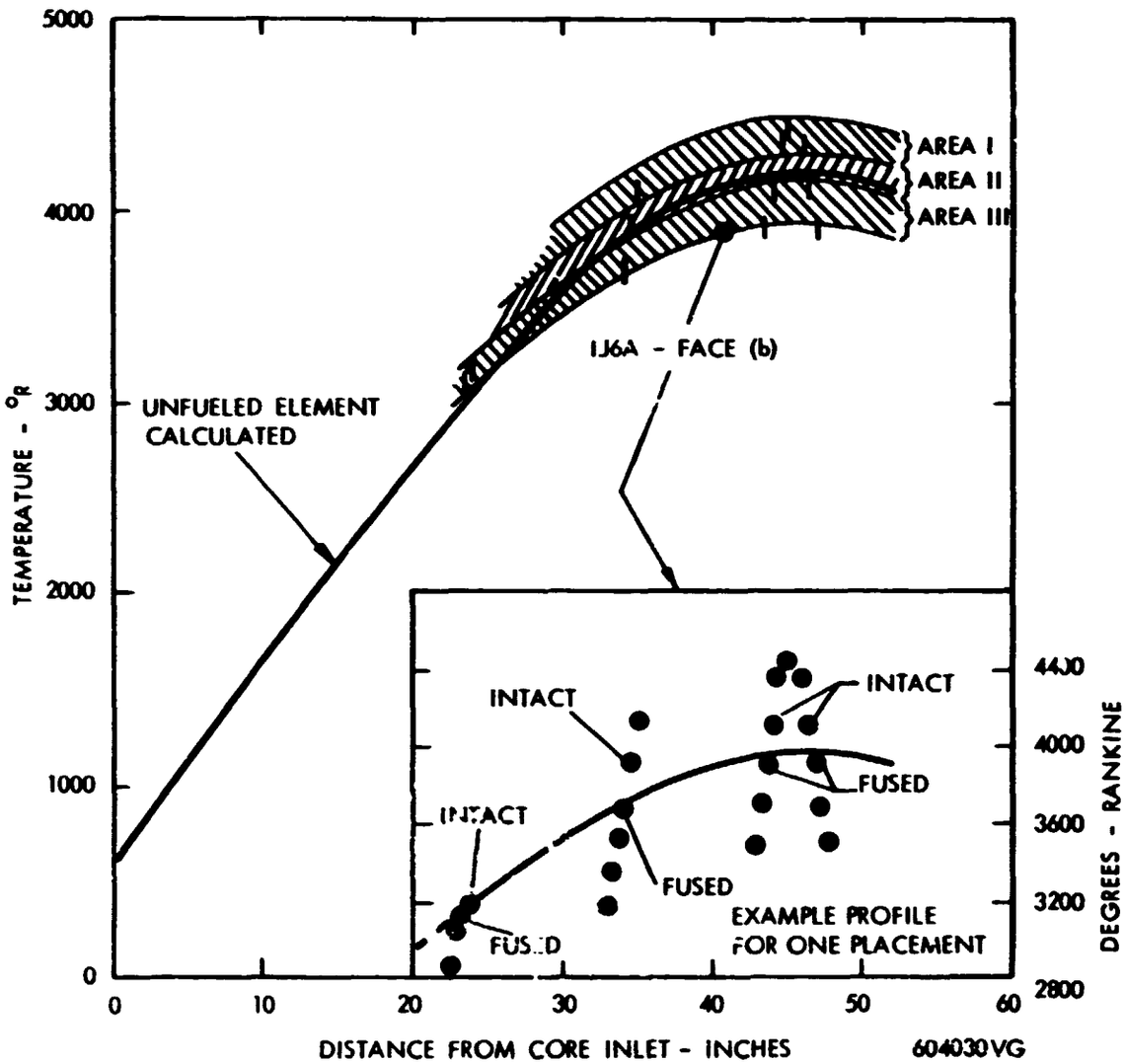

FIGURE 4 - 14

NRX-A2 THERMAL CAPSULE DATA PRELIMINARY 34 RADIAL POSITIONS IN CORE PERIPHERY

REFERENCE		PREPARED BY	APPROVED BY	Astronuclear

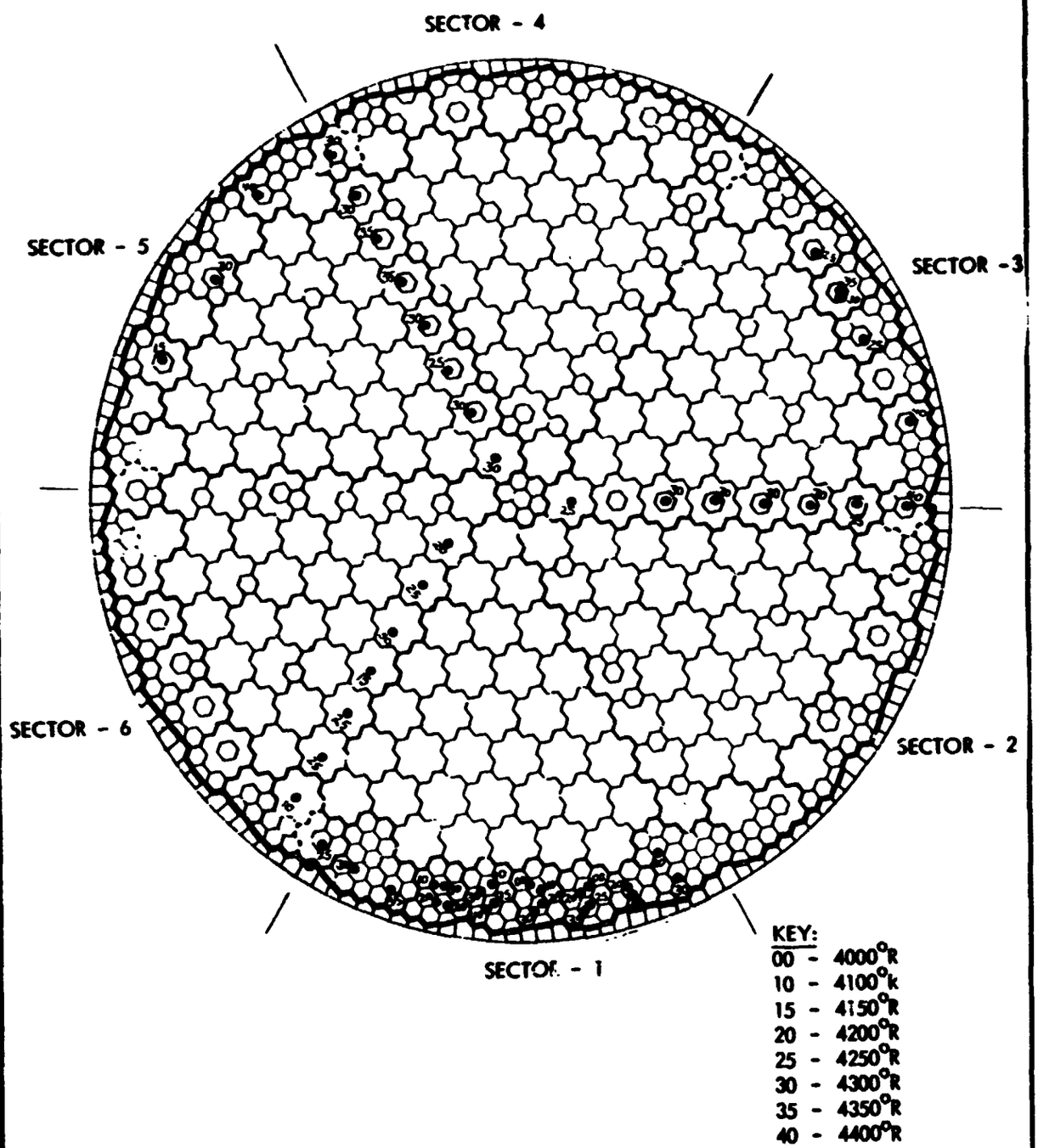

NRX-A2 THERMAL CAPSULE DATA UNFUELED ELEMENT TEMPERATURE AT 45 - INCHES

FIGURE NO. 4 - 15

REFERENCE		PREPARED BY	APPROVED BY	Astronuclear

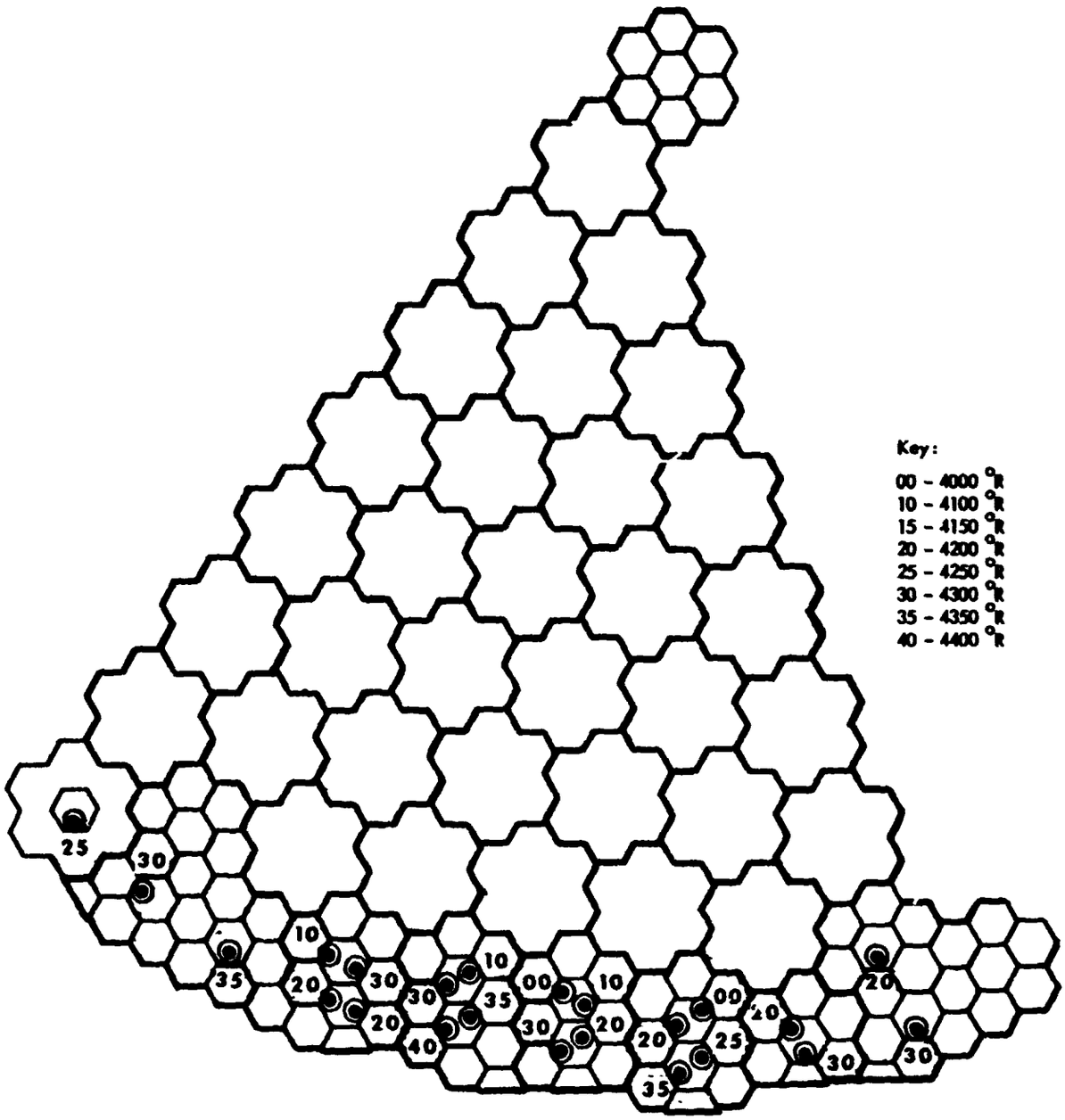

NRX-A2 THERMAL CAPSULE DATA UNFUELED ELEMENT TEMPERATURE AT 45 - INCHES

SECTOR - 1

FIGURE NO. 4 - 16

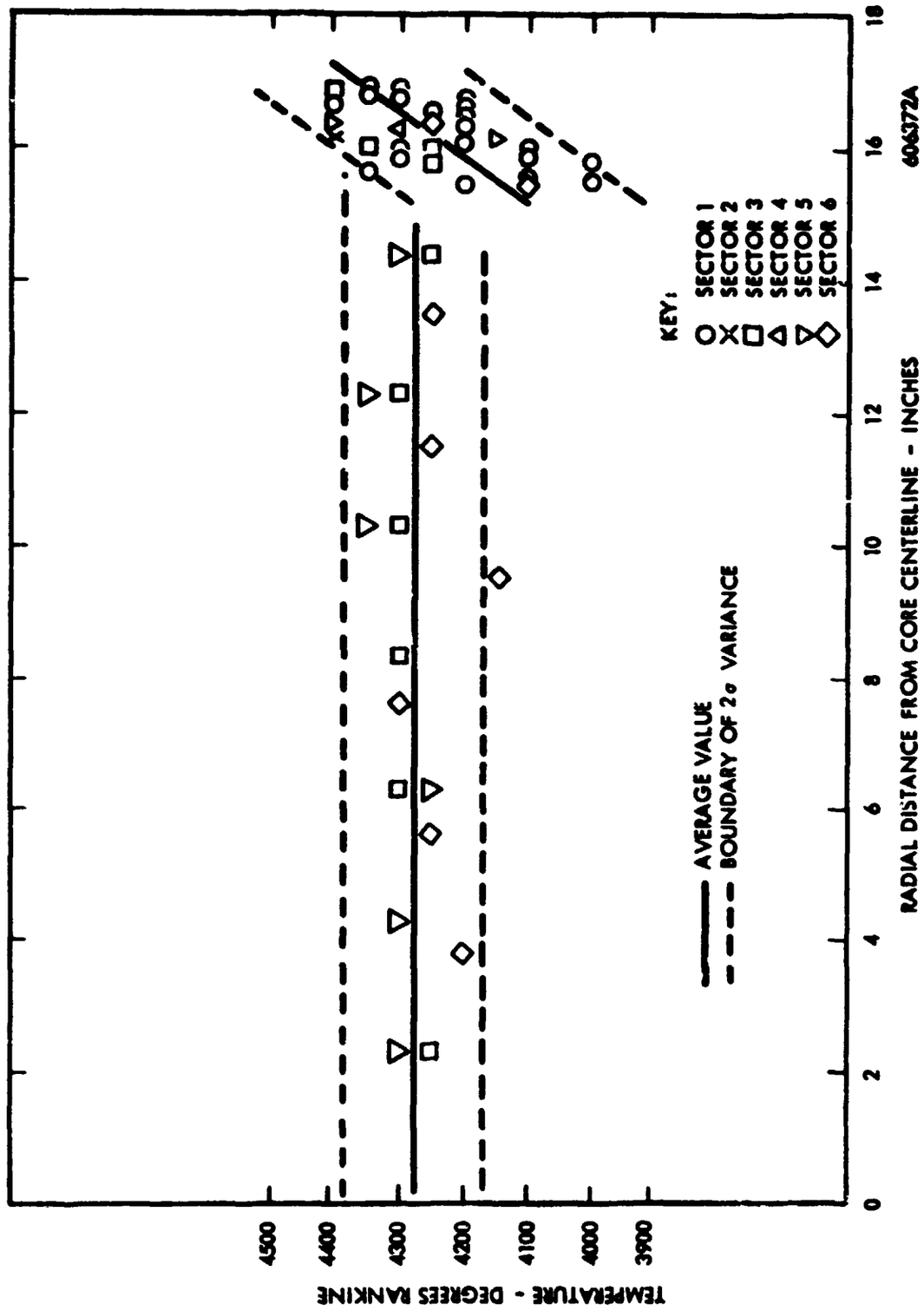

FIGURE 4 - 17, RADIAL PLOT OF STATION 45 THERMAL CAPSULE READINGS

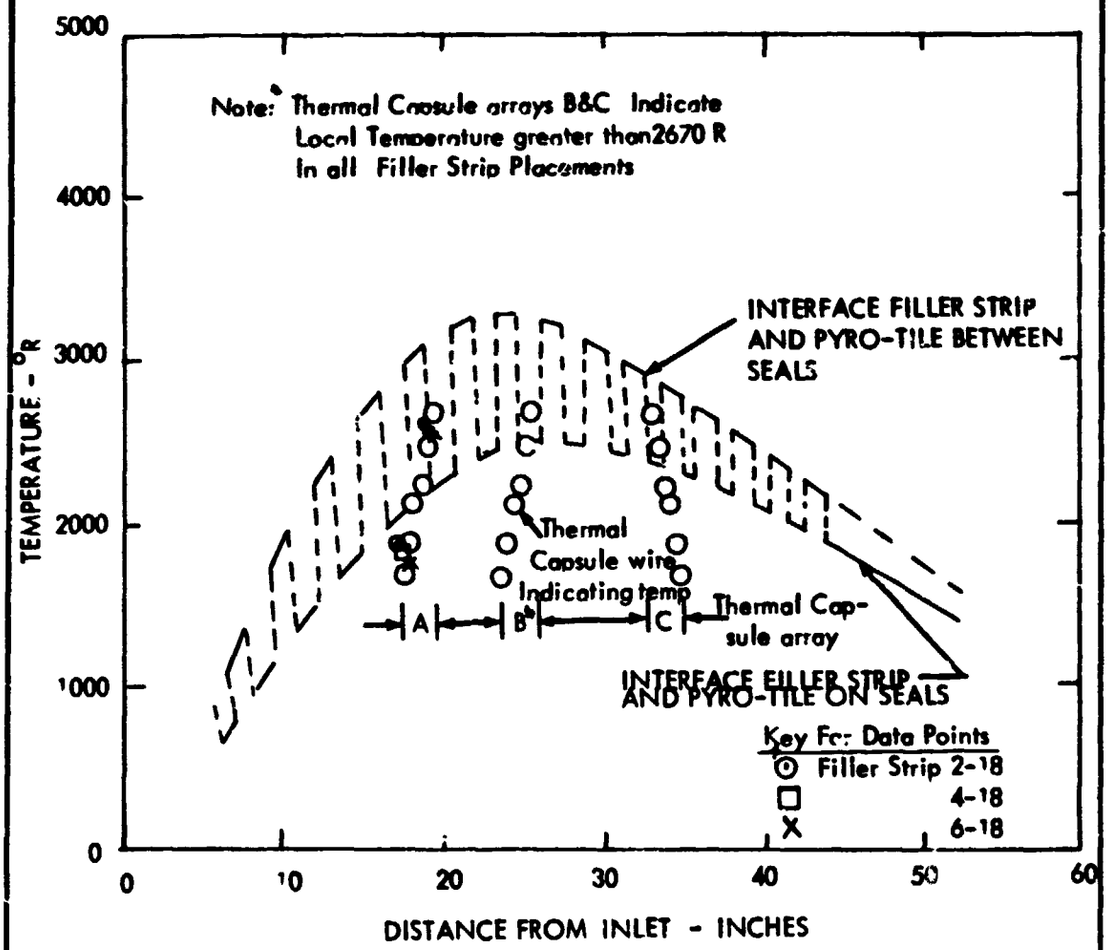

CURVE NO.	APPROVED BY	PREPARED BY

NRX-A2 FILLER STRIP THERMAL CAPSULE FAMILY WITH AXIAL TEMPERATURE DISTRIBUTION

FIGURE NO. 4 - 18

CONFIDENTIAL
RESTRICTED DATA

stepwise multiple regression technique.* The data from 54 thermal capsules, a good size sample for an analysis of this type, were correlated with radius and the random variation of temperature for the correlation was determined. The radial correlation essentially removes systematic variations; and therefore, the deviation of the measured values from the correlation are random variations.

Any polynomial or logarithmic curve fit to the data can be postulated initially. In this case, it was assumed that the equation would have the following form:

$$T = C_o + C_1 r + C_2 r^2 + C_3 r^3 \cdots + C_n r^n$$

where the constants to be determined can have position or negative values. The terms in the assumed equation which have physical significance are determined by the "F level" test,(See appendix F). After the best curve fit to the data is found, the random variation in the data is determined. This variation will include the actual random variation in temperature as well as the accuracy with which an individual temperature can be read. These are combined to make up a total variation by:

$$\sigma^2_{Total} = \sigma^2_{Temp} + \sigma^2_{TC\ Reading}$$

As was discussed previously the melting point of each individual wire was determined to within $\pm 54^oR$. In some cases, the difference in nominal melting points for two adjacent thermal capsules is more than 200^oR. Therefore, the uncertainty in a single measurement is in excess of $\pm 200^oR$. However, when several axial measurements in one element are combined, and the best possible axial temperature profile is drawn through the measured points, the uncertainty in the resulting profile is not more than $\pm 100^oR$. This value is taken to be the 3 standard deviation level for the accuracy of the temperature measurements; i.e. $3\sigma\ TC_{Read} = \pm 100^oR$

The NRX-A2 thermal capsules in the J row and in the central region of the core at station 45 were analyzed separately using the multiple regression code. The central region indicated a constant nominal temperature of 4276^oR with the $3\ \sigma_{total} = 192.3^oR$

---

* SHARE Program CR MPR2 Stepwise multiple linear regression, Esso Research and Engineering Company, 1 July 1958

According to the multiple regression analysis, there was no temperature variation which could be correlated with radius. Subtracting out the random thermal capsule reading error:

$$(3\sigma_{Temp})^2 = (3\sigma_{Total})^2 - (3\sigma\ TC_{Read})^2$$

$$(3\sigma_{Temp})^2 = (192.3)^2 - (100)^2$$

$$(3\sigma_{Temp})^2 = (164)^2$$

Since 2σ errors are used throughout this report, the final result of the thermal capsule multiple regression analysis for the central region of the core at station 45 is:

$$T = 4276 \pm 109^{\circ}R$$

where $109^{\circ}R$ is the 2σ random variation. The same procedure for the periphery indicated the temperature was a linear function of radius:

$$T = (1914 + 143.8\ r)\ ^{\circ}R$$

where r is core radius in inches. The 2σ random temperature variation is $\pm 179^{\circ}R$. The resulting curve fit of the thermal capsule data for the central and peripheral region is given in figure 4-19

The thermal capsule readings used in the above analysis define the maximum temperatures experienced, which would be during the highest power hold at approximately Time CR 14085. For the other power holds, the thermocouple measurements must be used. The NRX-A2 thermocouples are less desirable than the thermal capsules to analyze statistically because of the smaller sample size and also in the periphery there are actually only 2 radii represented. To maintain a sample of sufficient size and distribution the thermocouple data was not broken into separate peripheral and central zones. Only station 45 was analyzed. The only other station with a sufficient number of thermocouples for analysis [illegible] tation 32 but because of leakage around the thermocouple they were not considered dependable.

Table 4-13 summarizes the results of the thermocouple multiple regression analysis at each of the four steady state holds. The table shows the random temperature variation increases with increasing power up to the high power hold. At Time CR 14085 the random variation is smaller than at Time CR 13985. This is attributed to the saturation of the

REFERENCE		PREPARED BY	APPROVED BY	Aerojet

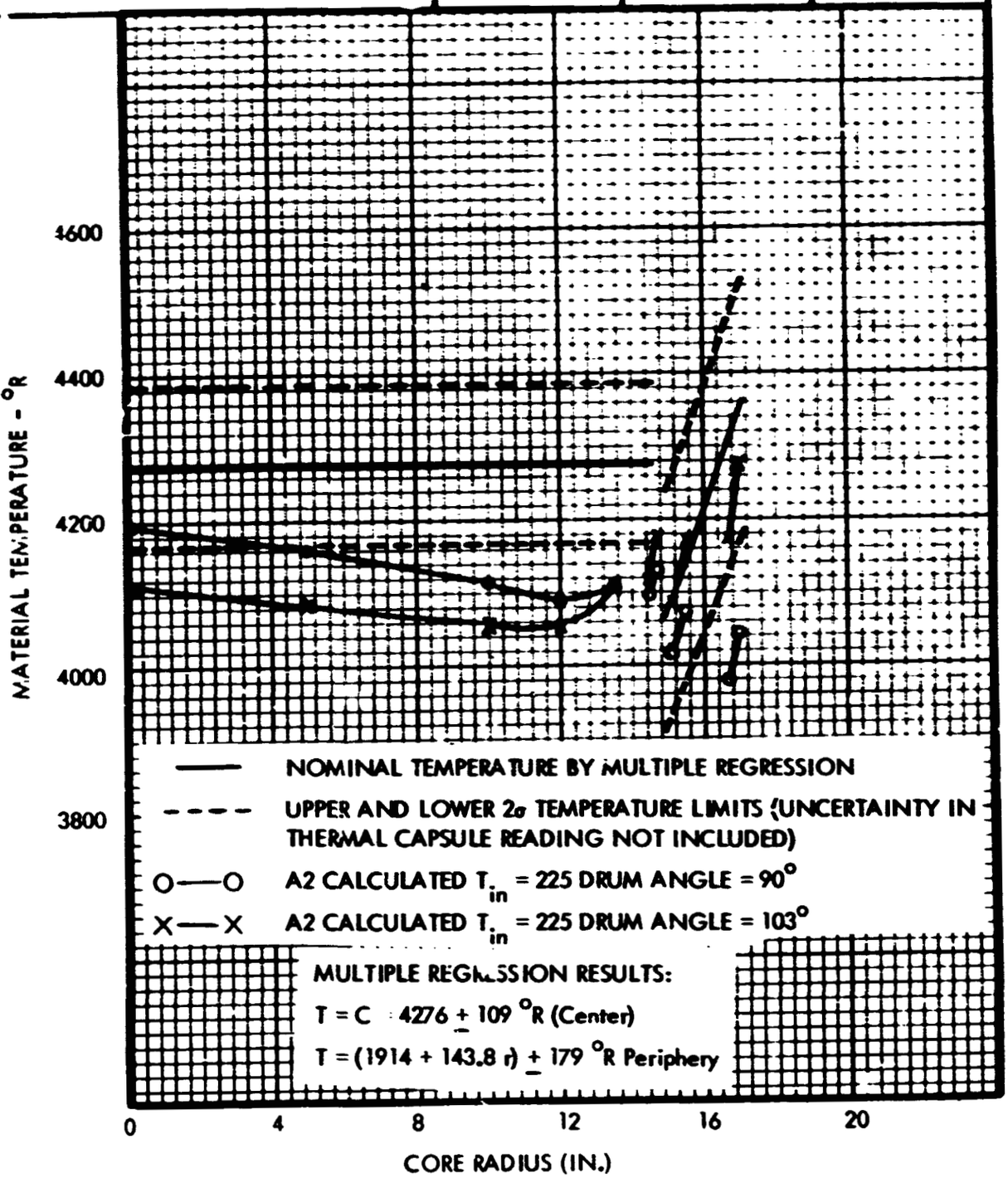

COMPARISON OF NRX-A2 THERMAL CAPSULE RESULTS WITH POST RUN CALCULATIONS AT HIGH POWER

CURVE NO.	FIGURE NO.
[redacted]	4 - 19

TABLE 4-13

MULTIPLE REGRESSION ANALYSIS OF NRX-A2 THERMOCOUPLES, STATION 45

CRT	Average Measured Temperature	Radial Temperature Correlation	2σ Temperature Variation
13790	2983	$T = 3024 - 0.0037\,r$	101°R
13900	3753	$T = 3713 + 0.00026\,r^2$	122°R
13985	3857	$T = 3857$	171°R
14085	3918	$T = 3918$	140°R

where r is radius in inches

thermocouples at Time CR 14085. The temperature variation indicated at Time 13985 may be larger than actually existed due to some of the thermocouples being saturated and others not being saturated. This situation is indicated because the expected radial temperature dependence does not show up in either the Time 13985 or 14085 power holds whereas it does show up in the two lower power holds.

Post Test Calculation of Core Operating Conditions

PRESSURE DROP AND AVERAGE AXIAL TEMPERATURE DISTRIBUTION CALCULATION

Post test calculations with MCAP and the tie rod program were performed utilizing measured input parameters at the four hold times. The purpose of these calculations was to obtain core ΔP and nominal axial temperature distributions. The procedure adopted closely followed the method used for core design.

There was sufficient data redundancy to make possible a choice of alternate procedures, for example, specifying the flow and calculating the pressure drop or vice versa. The measured values having the highest accuracy which were chosen as input for post test calculations are core exit (or nozzle chamber) pressure, shield dome end plenum temperature (described in the first part of this section on the core to calculate core inlet temperature), total reactor flow, and nozzle chamber temperature. The measured values which were used as input at the four high power holds are summarized in table 4-9 lines 10, 13, 14 and 15, respectively.

In the MCAP model, the 30,600 fuel channels were broken into eleven groups of parallel channels according to the power factors* at a drum angle of 90 degrees. These groups, designated as sections are shown in the sample MCAP printout, shown in tables 4-14, 15 and 16. The number of channels in each group varies from a minimum of 70 per group to a maximum of 8850 per group with a power factor range from 0.725 to 1.255. For the average power factor in each group and an 0.095 inch channel diameter, an ideal orifice loss coefficient was selected. (On the average, the mixture of actual orifice sizes in each

* Power factor is the ratio of heat generation rate per channel to average rate

NRX A2 CRT 14085 FLOW 75.6 POWER 1096 MW 1 2/11/65

SECTION	IDENTIFICATION	DIAMETER INCHES	NUMBER OF CHANNELS	POWER FACTOR 1	POWER FACTOR 2	INLET LOSS COEFF	EXIT LOSS COEFF	STABLE USED	
1		0.0950	91.0	1.2550	1.2550	3.35	0.40	1.,	1.
2		0.0950	70.0	1.2440	1.2440	6.01	0.40	1.,	1.
3		0.0950	369.0	1.2150	1.2150	13.99	0.40	1.,	1.
4		0.0950	1673.0	1.1850	1.1850	23.48	0.40	1.,	1.
5		0.0950	3291.0	1.1400	1.1400	40.28	0.40	1.,	1.
6		0.0950	5381.0	1.0900	1.0900	63.48	0.40	1.,	1.
7		0.0950	8850.0	1.0330	1.0330	91.31	0.40	1.,	1.
8		0.0950	8104.0	0.9520	0.9520	135.71	0.40	1.,	1.
9		0.0950	1919.0	0.8570	0.8570	201.24	0.40	1.,	1.
10		0.0950	573.0	0.7920	0.7920	276.25	0.40	1.,	1.
11		0.0950	279.0	0.7250	0.7250	345.98	0.40	1.,	1.

Table 4-14 SAMPLE MCAP PRINTOUT - SHEET 1

PREPARED BY	APPROVED BY	CURVE NO.

SECTION	FLOW/CH. LB/SEC	FLOW/SECT. LB/SEC	MASS FLOW RATE	TS EXIT DEG. R	TF AVG DEG. R	RHO AVG LB/CU FT	POWER 1 MW.	POWER 2 MW.	POWER/SECT. MW.	FLOW RATIO
1	0.2763E-02	0.251	0.389	4084.5	2905.5	0.1145	3.8722	0.	3.87224	-0.
2	0.2748E-02	0.192	0.387	4072.8	2895.9	0.1145	2.9525	0.	2.95254	-0.
3	0.2702E-02	0.997	0.381	4051.2	2876.8	0.1142	15.2013	0.	15.20129	-0.
4	0.2645E-02	4.425	0.373	4037.2	2862.6	0.1138	67.1938	0.	67.19383	-0.
5	0.2549E-02	8.390	0.359	4031.4	2851.9	0.1128	127.1592	0.	127.15921	-0.
6	0.2429E-02	13.070	0.342	4044.0	2853.0	0.1114	198.8652	0.	198.86522	-0.
7	0.2311E-02	20.453	0.326	4030.9	2835.1	0.1103	309.9652	0.	309.96520	-0.
8	0.2161E-02	17.511	0.304	3983.8	2790.2	0.1096	261.5857	0.	261.58569	-0.
9	0.1985E-02	3.808	0.280	3916.7	2728.8	0.1089	55.7257	0.	55.72574	-0.
10	0.1818E-02	1.041	0.256	3945.9	2737.0	0.1071	15.3773	0.	15.37729	-0.
11	0.1707E-02	0.476	0.240	3861.7	2668.3	0.1075	6.8491	0.	6.84910	-0.

TOTAL THERMAL POWER MEGAWATT	TOTAL FLOW RATE LB/SEC	CHAMBER TEMPERATURE DEGREES R	PRESSURE DROP PSI	BASE FLOW RATE -0.
1062.72	70.6162	4014.24	126.571	

02/15/65 TIME= 11.521

Table 4-15 SAMPLE MCAP PRINTOUT SHEET 2

PREPARED BY	APPROVED BY	CURVE NO.

D 7= 9.4999999E-02m 7= 2.3111177E-03

X	P	T	TS	TW	TF	Q	H	RF	V	MACH
0.	707.574	225.00								
0.	670.085	225.00	225.04	364.37	372.32	0.6[illegible]	2366.	0.	3161.07	0.030
2.000	669.582	280.09	280.15	659.78	671.07	1.0388	1419.	69025.	3956.13	0.035
4.000	668.920	359.03	359.13	905.74	923.14	1.3886	1317.	39847.	5062.62	0.039
6.000	668.053	464.08	464.25	1113.33	1137.25	1.6933	1344.	31601.	6579.89	0.044
8.000	666.968	593.88	594.16	1317.41	1348.84	1.7505	1398.	28435.	8393.47	0.050
10.000	665.638	746.35	746.81	1507.61	1547.41	2.1943	1475.	26495.	10526.83	0.056
12.000	664.052	917.63	918.34	1681.01	1729.61	2.4[illegible]	1635.	25190.	12931.46	0.062
14.000	662.203	1103.93	1104.94	1961.87	1920.45	2.5971	1778.	24325.	15560.20	0.069
16.000	660.093	1300.43	1301.82	2042.07	2110.68	2.7349	1915.	23459.	18351.38	0.074
18.000	657.715	1504.65	1506.52	2243.39	2323.14	2.8[illegible]	1998.	22753.	21276.03	0.080
20.000	655.070	1713.69	1716.10	2439.13	2529.74	2.9173	2092.	21931.	24298.62	0.086
22.000	652.163	1923.42	1926.45	2627.35	2727.66	2.9637	2191.	21075.	27365.86	0.091
24.000	648.993	2132.63	2136.33	2810.95	2919.04	2.9681	2280.	20163.	30465.08	0.097
26.000	645.560	2339.83	2344.26	2994.77	3109.59	2.9639	2360.	19355.	33579.32	0.102
28.000	641.868	2543.11	2548.32	3169.88	3298.81	2.9257	2438.	18606.	36685.14	0.108
30.000	637.928	2739.94	2745.96	3333.16	3453.31	2.8515	2515.	17960.	39749.19	0.113
32.000	633.754	2927.47	2934.34	3480.36	3598.63	2.7349	2593.	17415.	42732.06	0.118
34.000	629.362	3103.61	3111.33	3613.46	3727.62	2.5907	2671.	16970.	45603.77	0.122
36.000	624.770	3266.60	3275.18	3730.28	3838.26	2.4169	2748.	16598.	48338.08	0.126
38.000	619.995	3415.41	3424.83	3832.57	3933.05	2.2261	2824.	16298.	50918.21	0.130
40.000	615.054	3549.17	3559.37	3918.40	4010.02	2.0141	2900.	16051.	53328.37	0.134
42.000	609.966	3667.57	3678.55	3989.67	4071.65	1.7915	2975.	15860.	55560.25	0.138
44.000	604.750	3769.91	3781.60	4043.91	4115.03	1.5476	3045.	15712.	57598.45	0.141
46.000	599.428	3855.85	3868.21	4082.44	4142.06	1.2932	3112.	15611.	59431.73	0.144
48.000	594.019	3925.52	3938.48	4106.28	4154.06	1.0346	3172.	15550.	61054.91	0.147
50.000	588.544	3978.86	3992.36	4113.71	4148.97	0.7632	3225.	15524.	62459.32	0.149
52.000	583.020	4016.89	4030.85	4103.38	4124.92	0.4664	3271.	15539.	63652.94	0.152
54.000	577.590	4016.69	4030.93	4029.51	4029.51	0.	0.	15598.	64245.96	0.153
54.000	581.078	4027.06								

Table 4-16 SAMPLE MCAP PRINTOUT SHEET 3

PREPARED BY	APPROVED BY	CURVE NO.

power factor group is equivalent to an ideal orifice). This MCAP model is equivalent to the fuel channels in the as-built core. Each group of channels having a common orifice and power factor is treated as a single channel in the MCAP program to obtain the axial pressure and temperature distributions. The resulting flow per channel is then multiplied by the number of channels in each group to obtain the overall flow and power balance.

The tie rods are represented in the tie rod program by 289 parallel channels broken into 49 groups according to power factor. Each tie rod channel has the same as-built inlet and exit loss coefficient. The lateral support seal bypass flow in the core is assumed constant at 0.36 lb/sec with an exit temperature of 1815°R for all calculations.

A flow schematic for the core model used is shown in figure 4-20 with measured values used as input and calculated results for Time CR 14085. Measured input values are indicated by an asterisk. The overall power balance for the system is written as:

Total core power = (Power from fuel channels) + (Power from tie rods) + (Power from bypass flow)$_{\text{Assumed constant.}}$

$$\text{Total Core Power} = W_{Total}\left[H_{Nozzle\ Chamber} - H_{Core\ Inlet}\right]$$

$$\text{Power from Fuel Channels} = \sum_{i=1}^{11} n_i \; W_i \left[H_{Fuel\ Exit_i} - H_{Core\ Inlet}\right]$$

$$\text{Power from Tie Rods} = \sum_{k=1}^{49} m_k \; W_k \left[H_{Tie\ rod\ Exit_k} - H_{Core\ Inlet}\right]$$

Where

W_{Total} = Total reactor flow.

H = Enthalpy at designated location.

W_i = Flow per fuel channel at power factor i.

n_i = Number of fuel channels in power factor group i.

W_k = Flow per tie rod channel at power factor k.

m_k = Number of tie rod channels in power factor group k.

REFERENCE		PREPARED BY	APPROVED BY	Astronuclear

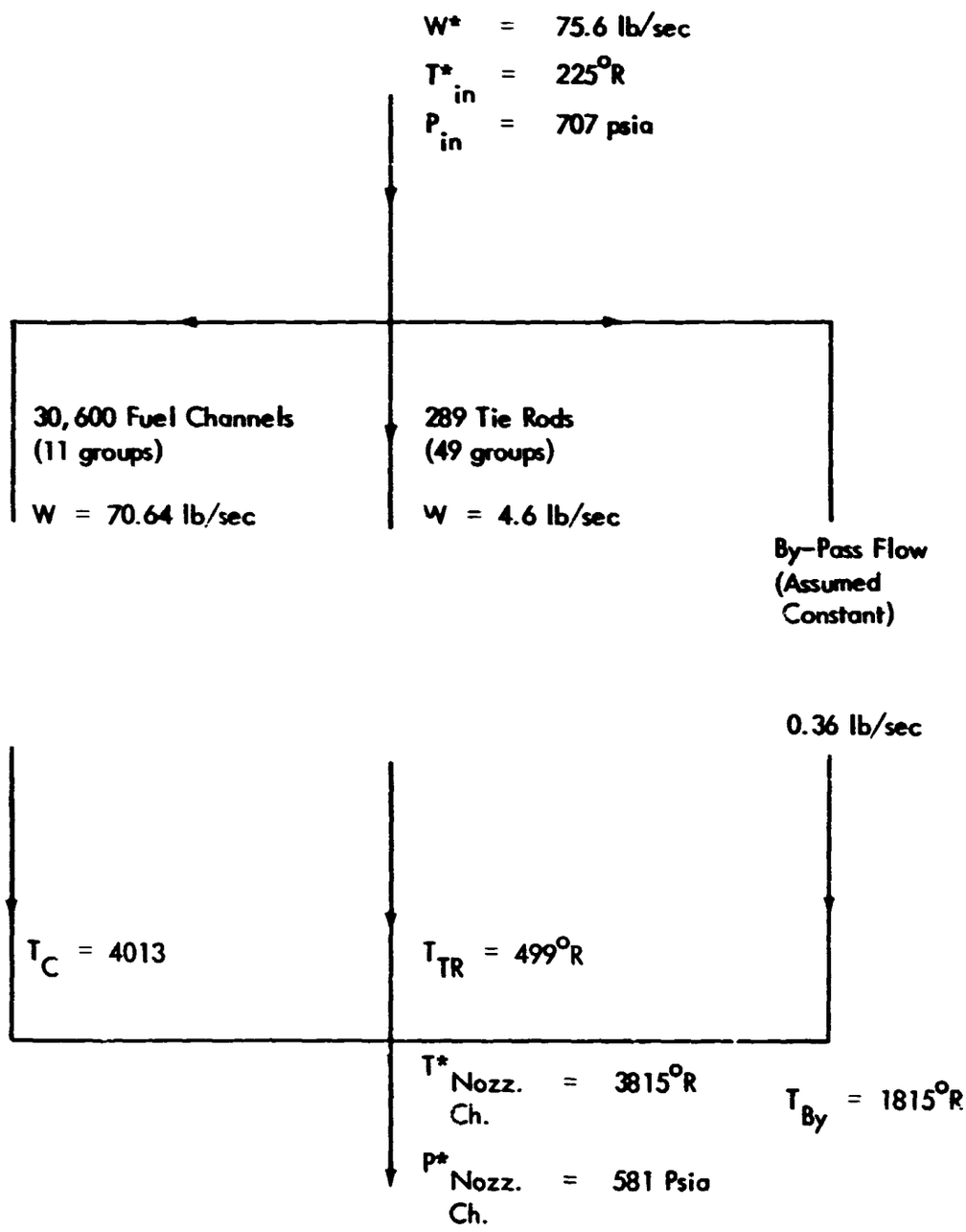

Note: *Measured values used as input, others are calculated. Others are NRX-A2 EP IV Post Test Calculated flow Schematic Time CR 14085 (1096 MW)

NRX-A2 EP IV POST-TEST CALCULATED FLOW SCHEMATIC CRT-14085 (1096 MW)	FIGURE NO.
	4 - 20

The requirement of equal pressure drops in all parallel channels places the additional restriction on the model which enables the calculation of a flow balance between tie rods and fuel channels. The pressure drop and heat transfer correlations used are described in WANL-TNR-128, Vol. III. The mixed mean gas exit temperature from the eleven groups of fuel channels is specified in MCAP, but must be adjusted with each iteration to maintain the constant power as the flow balance between tie rods and fuel channels is adjusted. The final converged solution yields the calculated gas exit temperature and axial temperature distributions for each of the eleven power factor groups. The converged solution also gives a calculated core pressure drop for the measured flow and power.

The same model for the as-built core was used for all power holds. The change in drum angle from 90 degrees at the various holds will not change the calculated overall flow balance, pressure drop, or average gas and material temperature significantly. Individual channel flows and temperatures are affected by the drum angle and a correction was made to obtain the radial temperature profiles which will be discussed. Table 4-9 is a summary of the post test calculated and measured core parameters at each of the four power holds. The calculated values for core pressure drop are within 5 percent of measured and are consistently on the high side. This suggests a possible systematic difference in friction factor, channel roughness, additional leakage, or an error in total reactor flow rate or power.*

Figures 4-21, 22, 23 and 24 show the calculated axial temperature distribution for the average power factor at each of the four high power holds. Also shown is the average and spread of all thermocouple and thermal capsule measurements. There is a 2σ error in each calculated temperature caused by the errors in measured reactor flow, inlet temperature, and nozzle chamber temperature. These are directly applicable to determine the agreement between measured and calculated values to a 95 percent confidence level.

The consistently low calculated temperatures indicate that a systematic error is in the analysis, even though agreement at station 45 inches is within the $2\ \sigma$ limits. There are several possible reasons why measured temperatures could be higher than calculated including an error in measured total reactor flow and/or power.*

*See further analysis in WANL-TNR-199, Supplement I

REFERENCE		PREPARED BY	APPROVED BY	Astronuclear

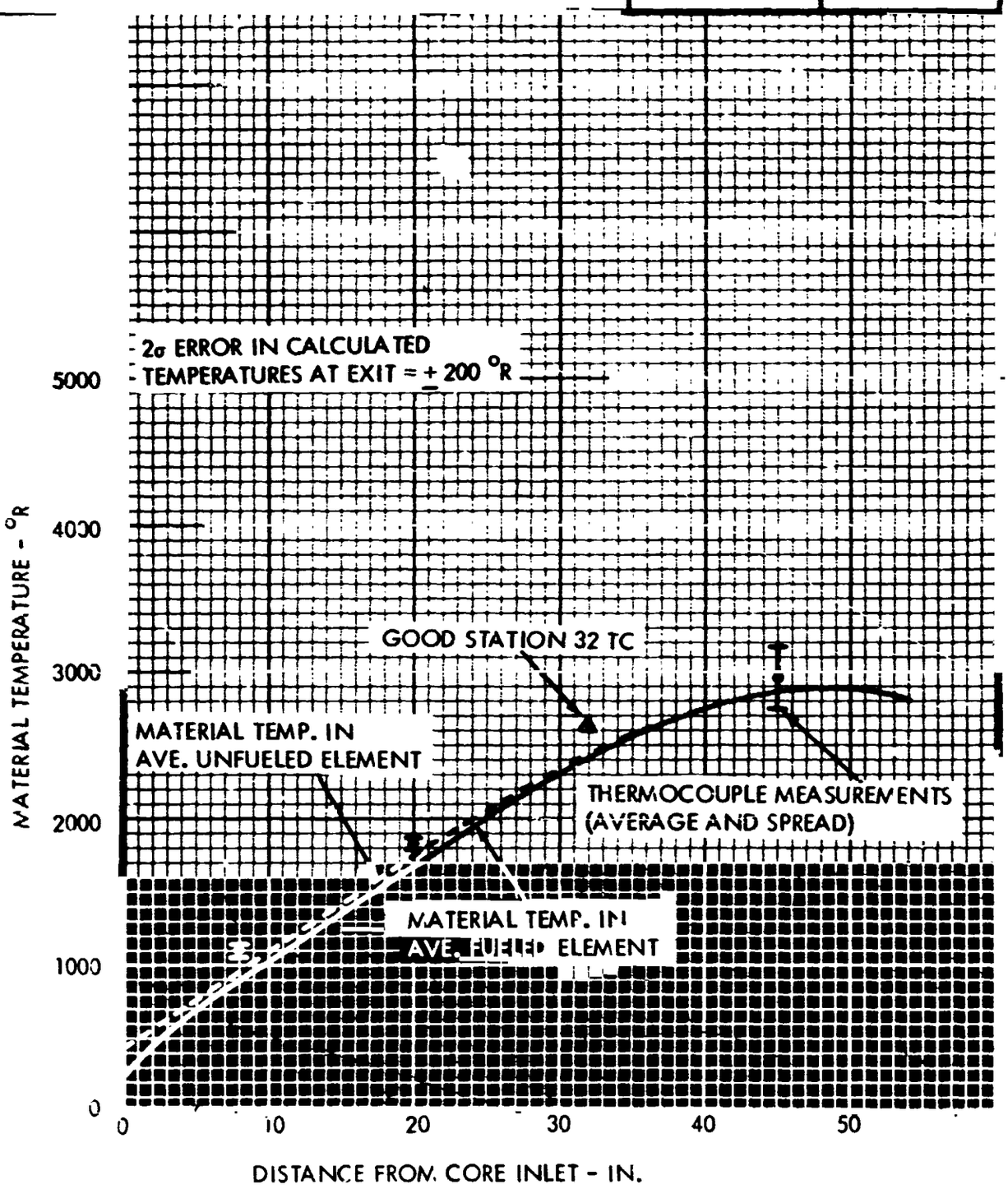

AXIAL TEMPERATURE PROFILE IN AVERAGE FUELED AND UNFUELED ELEMENT CRT-13790 (581 MW)	CURVE NO.	FIGURE NO.
		4 - 21

REFERENCE	PREPARED BY	APPROVED BY	Astronuclear

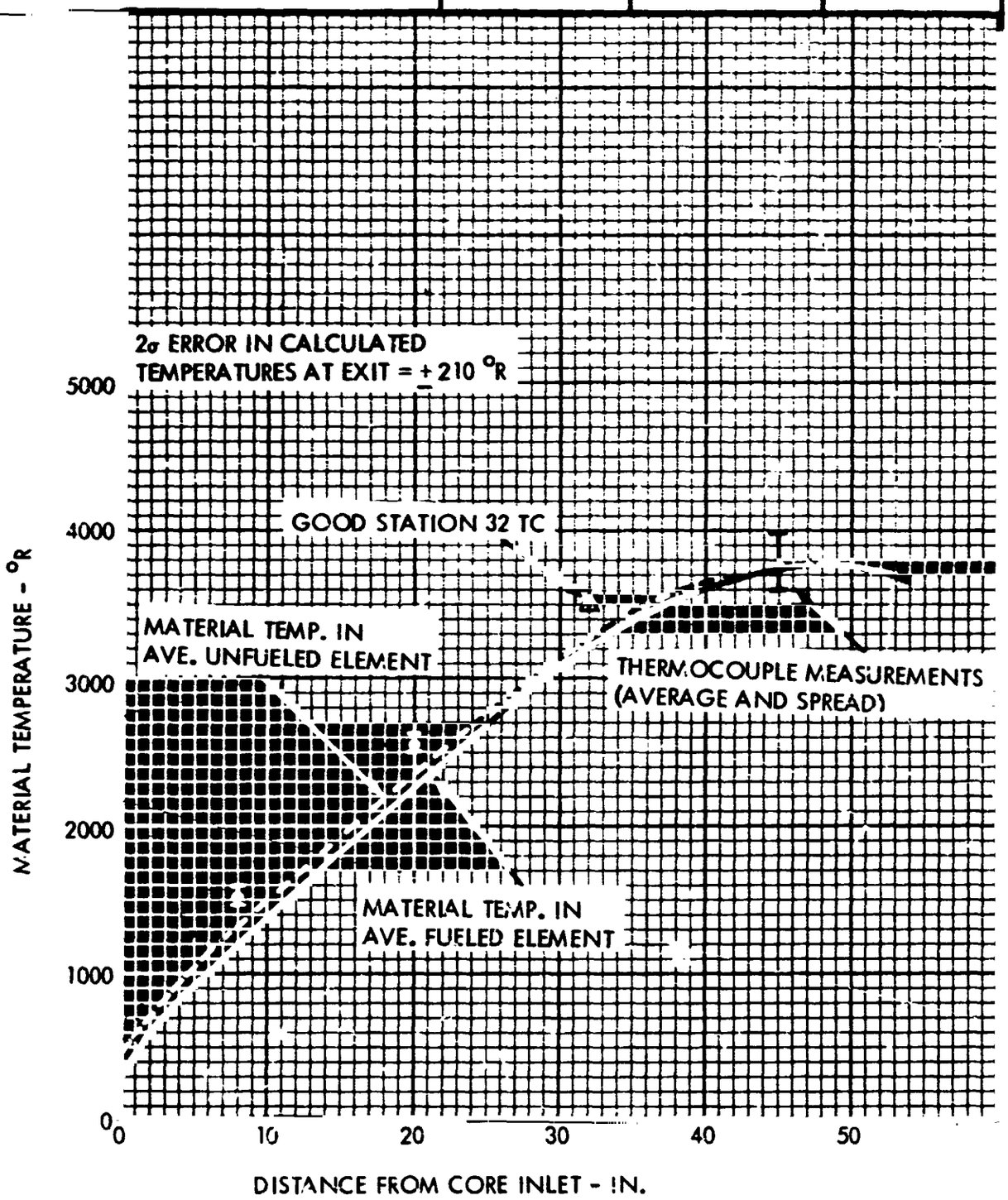

AXIAL TEMPERATURE PROFILE IN AVERAGE FUELED AND UNFUELED ELEMENT CRT-13900 (953 MW)	CURVE NO.	FIGURE NO.
		4 - 22

REFERENCE	PREPARED BY	APPROVED BY	Astronuclear

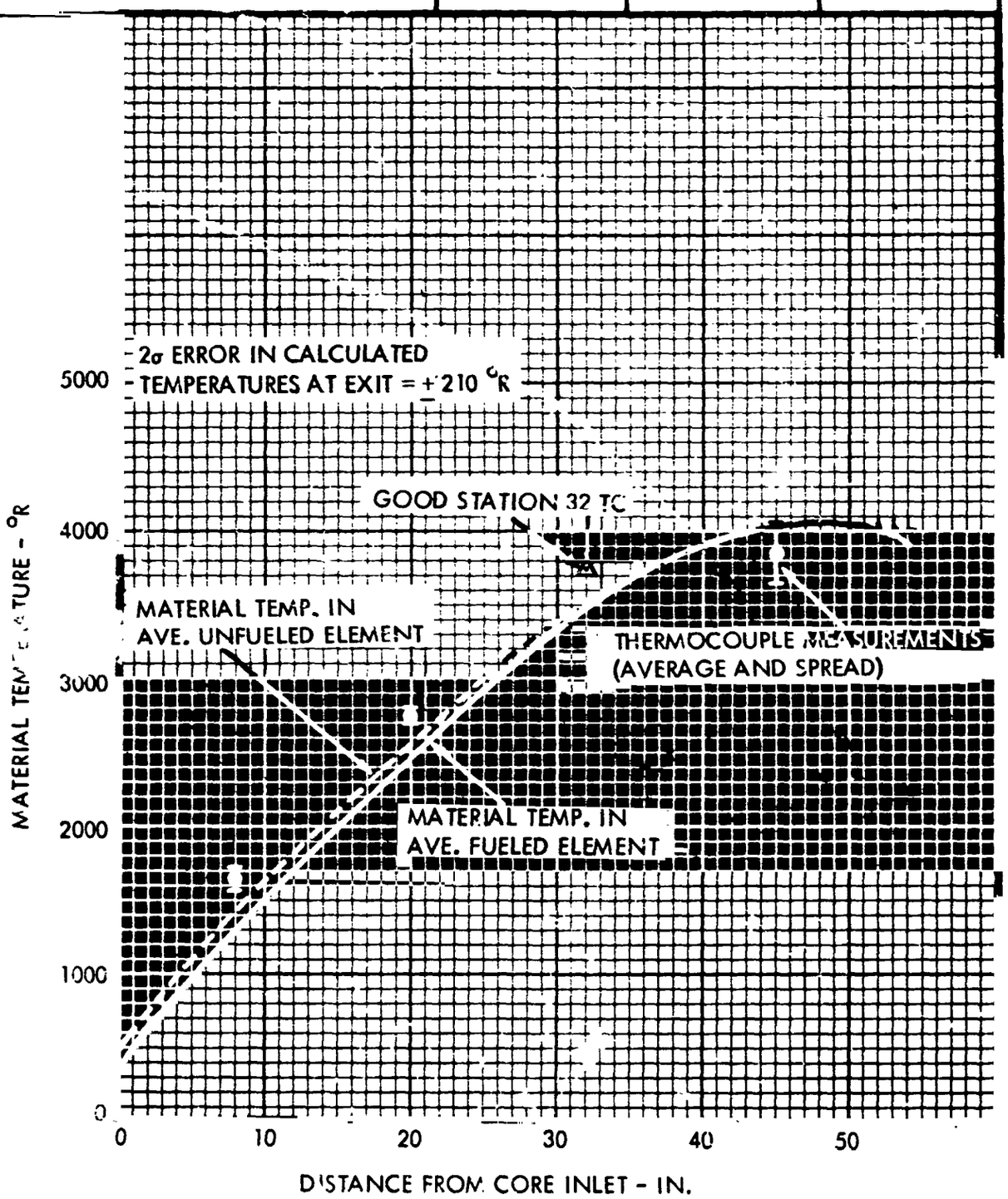

AXIAL TEMPERATURE PROFILE IN AVERAGE FUELED AND UNFUELED ELEMENT CRT - 13985 (1051 MW)	CURVE NO.	FIGURE NO.
		4 - 23

REFERENCE		PREPARED BY	APPROVED BY	Astronuclear

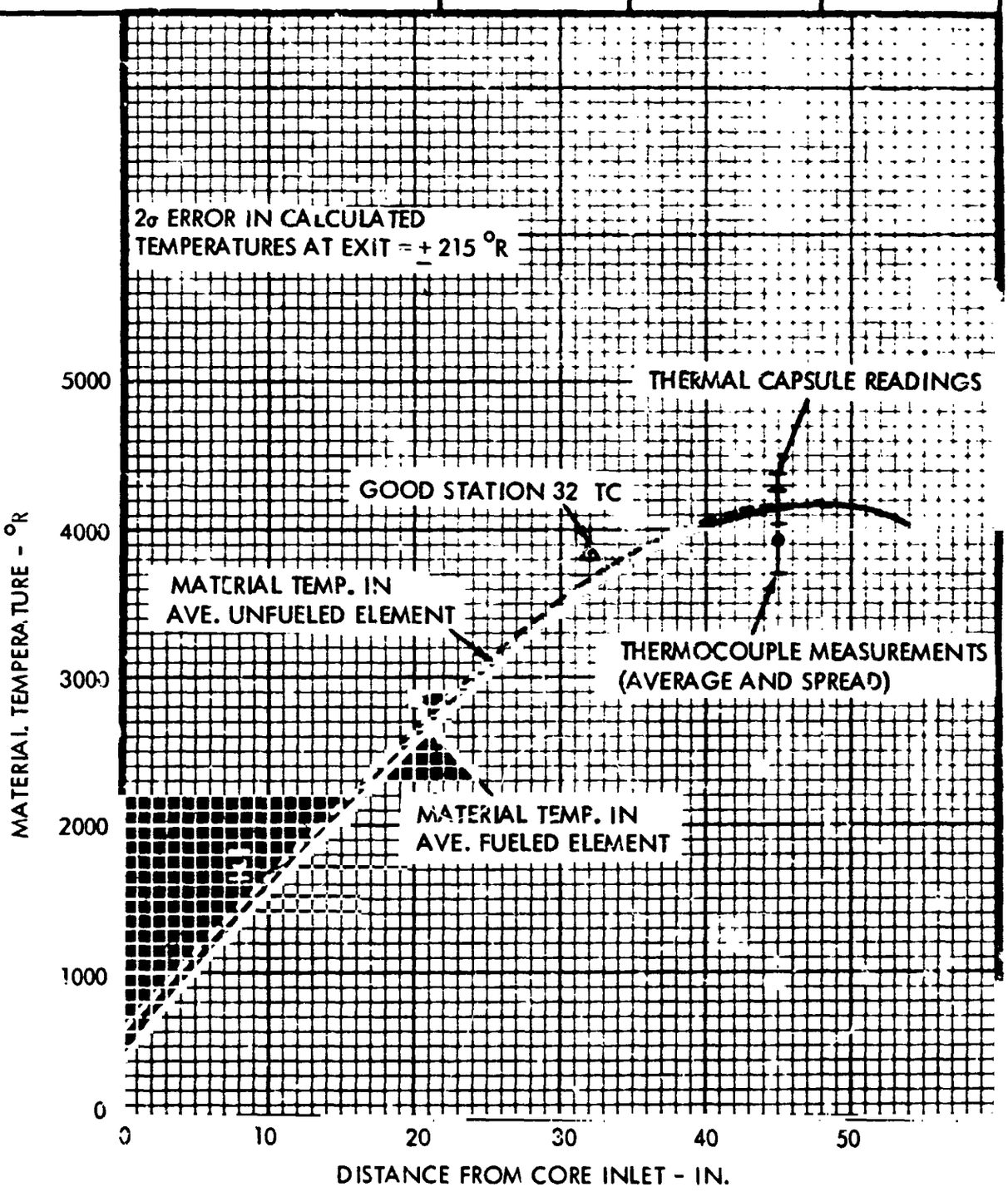

AXIAL TEMPERATURE PROFILE IN AVERAGE FUELED AND UNFUELED ELEMENT CRT - 14085 (1096 MW)	CURVE NO.	FIGURE NO.
		4 - 24

1

An analysis[1] of the effect of gamma heating on a high temperature thermocouple showed that the thermocouple readings operate about 72°R above the shim hole wall temperature. Investigation is underway into the effects of gamma heating on NRX-A2 thermocouples and thermal capsules.[2]

One assumption made in the MCAP-Tie rod iterations previously discussed is worthy of note. The axial fuel temperatures from the average MCAP channel are used as a boundary condition in the tie rod program. The heat generated in the unfueled module is conducted primarily into the fuel channels near the inlet, and primarily into the tie rod channel near the exit. An important assumption made in the analysis is that the heat conducted into the fuel channels is insignificant compared with the heat that is generated in the fuel. This enables the use of the isolated channel MCAP program for the analysis instead of TOSS-MCAP or OPTION which would include conduction effects. If this assumption is valid, then this small amount of heat from the unfueled module is not enough to significantly raise the fuel temperatures which were used as boundary conditions. Since there is evidence of a systematic error in the calculations, investigation of this assumption is being continued.[2]

RADIAL TEMPERATURE VARIATIONS

Since the control drum angle and core inlet temperature during all four high power holds in EP IV were off-design, the radial temperature distribution is not flat. The 90 degree control drum angle was used to calculate the pressure drop and the average fuel temperature, since these are not significantly affected by the drum angle. The effects of the off design inlet temperature can be seen in the radial temperature profile for the 90 degree drum angle in figures 4-19 and 4-25. The high power factor channels, which are starved by a lower than design inlet temperature are located near the core centerline and at the outer edge of each peripheral loading zone (approximate radius 14.6, 15.4 and 17 inches). The highest temperatures are seen to occur in these locations.

---

1 WANL-TME-1076, Effect of Gamma Heating on a High Temperature Thermocouple 8 January 1965

2 WANL-TNR-199 Supplement I, to be published

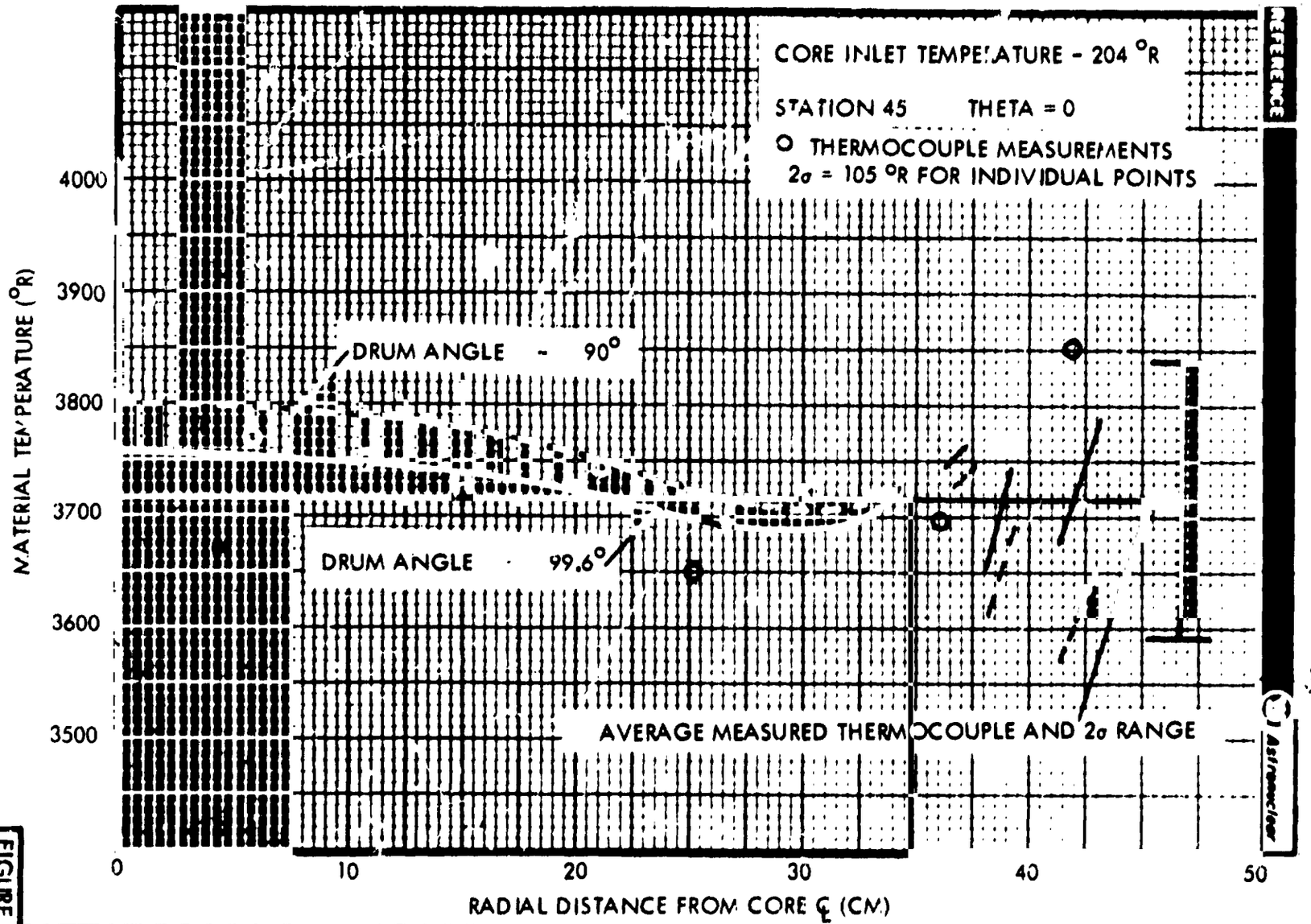

FIGURE NO.		PREPARED BY	APPROVED BY	CURVE NO.
4 - 25	NRX-A2 EP IV CALCULATED AND MEASURED RADIAL TEMP. PROFILE CRT - 13900 (953 MW)			FIG. IV-11

The radial temperature profile at the operating drum angle was obtained by adjusting the MCAP results at a 90 degree angle. The percent change in power factor with drum angle is known at each core location, and the change in gas exit temperature with percent change in power factor is known from parametric data. The gas exit temperatures at the 90 degree drum angle were then adjusted at each radial location according to the drum position.

The off-design drum angles will cause the power to be suppressed near the core centerline and increased near the core periphery. The comparison for drum angle 99.6 degrees vs. 90 degrees in figure 4-25 and 103 degrees vs. 90 degrees in figure 4-19 should be noted. It is seen that the off-design drum angle tends to flatten the radial temperature distribution in the core central region and amplify the temperature increase with radius in the core periphery. These qualitiative results were observed in the statistical treatment of the thermal capsule measurements mentioned in the previous section. The 2 σ random element-to-element variation in temperature in the core central region was $\pm$ 109°R and in the peripheral region it was $\pm$ 179°R. No statistically significant variation in temperature with radius was measured in the core central region.

In the core periphery, the measured temperature was a function of radius according to the multiple regression analysis. The calculated temperature is also a function of radius, although the calculated fine structure was not picked up by the thermal capsule data. In order to accomplish such an analysis more measurements are required.

As an independent check on the measured random variations and also as a check on the statistical method used for hot channel analysis, a calculation was done to determine the random element-to-element temperature variations. This calculation statistically combined all variations due to perturbations which may occur in adjacent fuel elements. The hot channel factors that were used for this analysis were the same ones used for the pre-test hot channel analysis[1] except that those perturbations which are systematic in their effects are excluded. Examples of systematic perturbations which do not affect one element with respect to the adjacent element are inlet temperature, temperature sensing, control drum effects, and

1 WANL-TME-880, Power Capability and Test Profile Analysis for the NRX-A2 Reactor August, 1964

some portions of the nuclear uncertainty. Therefore to determine random fuel element temperature variation these effects are not included. The variables considered and their temperature effects (3σ values) are shown in table 4-17. The resulting temperature variation was calculated by:

$$\Delta T_{Ele} = \left[\Sigma(\Delta T^{*}{}_{Ele}{}^{2}) + \frac{\Sigma(\Delta T^{2}{}_{CH})}{19}\right]^{1/2}$$

Where

ΔT_{Ele} = 3 standard deviation element of element temperature variation

$\Delta T^{*}{}_{Ele}$ = 3 standard deviation element temperature uncertainties

ΔT_{CH} = 3 standard deviation channel temperature uncertainties

Two variations which may cause element to element temperature variation are not included in this analysis, and these are the nuclear hot to cold and control drum effects. These two variations were not included because the net change of power in one element with respect to the six surrounding elements is nearly equal to zero.

The 3σ variations were converted to 2σ variations simply by multiplying the results by 2/3 and the 2σ random variation in the periphery was ± 179°R and in the central region it was ± 155°R. This is very good agreement with the measured 2σ random variations obtained from thermal capsule data. As reported in the previous section, these were ± 179°R in the periphery and ± 109°R in the central region. Due to the tendency toward conservatism in overestimating the size of various perturbations it would be expected that the measured 2σ random variations would be smaller than the calculated variations. This is the case in the central region. In the periphery, the measured 2σ variation is not completely random because of the inclusion of a systematic error due to the variation in fuel loadings in the irregular periphery.

The radial temperature profiles in figure 4-19 show the calculated temperatures to be consistently lower than the measured temperatures but within the 2σ error bands. The consistently lower calculated temperatures are probably due to an inherent systematic error

TABLE 4-17

HOT CHANNEL FACTORS CONSIDERED IN ANALYSIS OF ELEMENT TO ELEMENT TEMPERATURE VARIATION

	Cause	Effect
Gamma Scanning Error*	3σ	3σ
Periphery	± 3%	122°R
Central	± 1%	41°R
PAX Experimental Error*		
Periphery	± 2.13%	85°R
Central	± 1.38%	54°R
Upper Plenum Flow Distribution*	± 4.5%	169°R
Upper Plenum Temperature Distribution*	± 10°R	56°R
Unclad channel diameter	± 0.0005 in.	30°R
Channel orientation	0.018 in.	502°R
Orifice mismatch	± 200°R	± 200°R
Orifice coefficients	± 50°R	± 50°R
Orifice leakage	± 100°R	± 100°R
Fuel concentration	± 4%	± 170°R
Air impedance	±0.0002 in.	± 28°R
Friction multiplier	± 2%	± 26°R

*Denotes element effects, all others are channel effects.

(or errors) as discussed earlier in this section. These possible systematic errors have no bearing on the random element to element variations that have been discussed.

MAXIMUM CALCULATED FUEL TEMPERATURES

The maximum calculated nominal fuel temperature at Time CR 14085 is found at the core periphery in fuel element J5J. This element because of its location is strongly affected by the control drum position. The average power in the element increases by 6.2 percent due to a drum angle change from 90 degrees to 103 degrees. Using the previously described MCAP results for 90 degree control drums and correcting for the average element power due to drum angle effects, the maximum fuel temperature is 4327°R. This temperature carries a ± 215°R tolerance due to errors in the measured input parameters of inlet temperature, flow, and nozzle chamber temperature as indicated in table 4-9. The maximum measured temperature in the core periphery was 4400°R using thermal capsule data.

A statistical hot-channel analysis for the A2 peripheral elements was reported in WANL-TME-880. The 3σ temperature variation due to all effects except drum angle effects and orifice mismatch was 589°R. The temperature sensing, core inlet temperature and data acquisition contributed 12.1 percent to this temperature increase and should be excluded from the post test calculation. The ± 215°R uncertainty due to errors in measured input parameters includes these effects. Removing these uncertainties and converting to a 2σ temperature increase gives ± 345°R for the hot channel considerations shown in table 4-18. The total 2σ temperature increase for a single peripheral channel is found by combining this statistical temperature increase with the increase due to errors in the measured input data used in MCAP.

$$2\sigma_{Total} = \sqrt{\left(\frac{2\sigma_{Start}}{HCF}\right)^2 + (2_{meas})^2}$$

$$= \sqrt{(345)^2 + (215)^2}$$

$$= \pm 420° \text{ R}$$

TABLE 4-16

HOT CHANNEL CONSIDERATIONS

Element Effects	3σ Values
1. Horizontal Power*	± 8.8%
2. Upper Plenum Flow Distribution	± 4.5%
3. Change in Channel Diameter	± 0.0005 in.
4. Heat Transfer Coefficients	± 20%
5. Upper Plenum Temperature Distribution	± 10°R
6. Axial Power Distribution	± 10%
7. Support Block Misalignment	0.0023 in. max.
8. Fuel Conductivity	± 20%
9. Enthalpy - Temperature Conversion	± 2%
Channel Effects	
1. Channel Orientation	0.018 in.
2. Fuel Concentration	± 4°
3. Orifice Leakage	± 100°R
4. Orifice Coefficients	± 50°R
5. Unclad Channel Diameter	± 0.0005 in.
6. Air Impedance Measurement	± 0.0002 in.
7. Friction Factor	± 2%
8. Orifice Mismatch**	± 200°R

*Excluding all drum angle effects

**Not applicable - as orificed model used

The maximum 2σ fuel hot spot temperature is then, 4327 + 407 = 4734°R in element 1J5J. Table 4-19 contains a summary of the results of this section.

Tie Rod Temperatures

Measured tie rod exit gas temperatures are higher than predicted as indicated on figure 4-26. In an attempt to resolve the differences between measured and predicted values, an uncertainty analysis was performed on the variations in the tie rod centering bushing loss coefficient, variations in the heating in the unfueled graphite, variations in core inlet temperature, variations in the thermal conductivity of the pyrographite insulating sleeves, variations in the hydrogen gap thickness between the stainless steel liner and the pyrographite insulating sleeve and variations in thermocouple readout. These variations were considered to be the major contributors to the increase in the tie rod exit gas temperatures. The nominal values used in this analysis appear in table 4-20.

Tie rod exit gas temperatures from four unfueled elements 000 (T-750), 4F1A (T-760), 6J9Q (T-765) and 6J8 (T-755), were measured. The thermocouple in the unfueled element 000 (T-750) operated intermittently during the test series and indicated questionable temperatures and has been neglected in the data reduction analysis.

Experimental tie rod centering bushing loss coefficient data indicated that variations in loss coefficient may result from leakage paths through the centering bushing due to manufacturing tolerances. These leakage paths include leakage flow through the split in the bushing, through the annulus formed by the tie rod and bushing, around the edge where the split bushing insert fits into the centering bushing, and c[illegible] base of the bushing where it is inserted in the unfueled graphite bore. For this analysis, the unsealed condition was considered nominal and a 3σ deviation of ± 50 percent was assumed.

Experimental data from thermal conductivity testing of 12 pyrographite insulating sleeves showed a one standard deviation of ± 30.0 percent over a range of average temperatures from 472°F to 3193°F. Subsequent testing of samples prior to the NRX-A2 test indicated values of thermal conductivity within the range previously tested.

TABLE 4-19

MAXIMUM FUEL TEMPERATURES AT HIGH POWER HOLD CRT 14085 (1096 MW)

Maximum nominal fuel element temperature (calculated station 45)	4327°R ± 215
Calculated 2σ hot spot fuel temperature	4734°R
Calculated 2σ element to element temperature variation	
Central region	155°R
Peripheral region	179°R
Maximum indicated temperature (thermal capsule)	4400°R
Element to element temperature variation based on thermal capsules	
Central region	109°R
Peripheral region	179°R

REFERENCE

Astronuclear

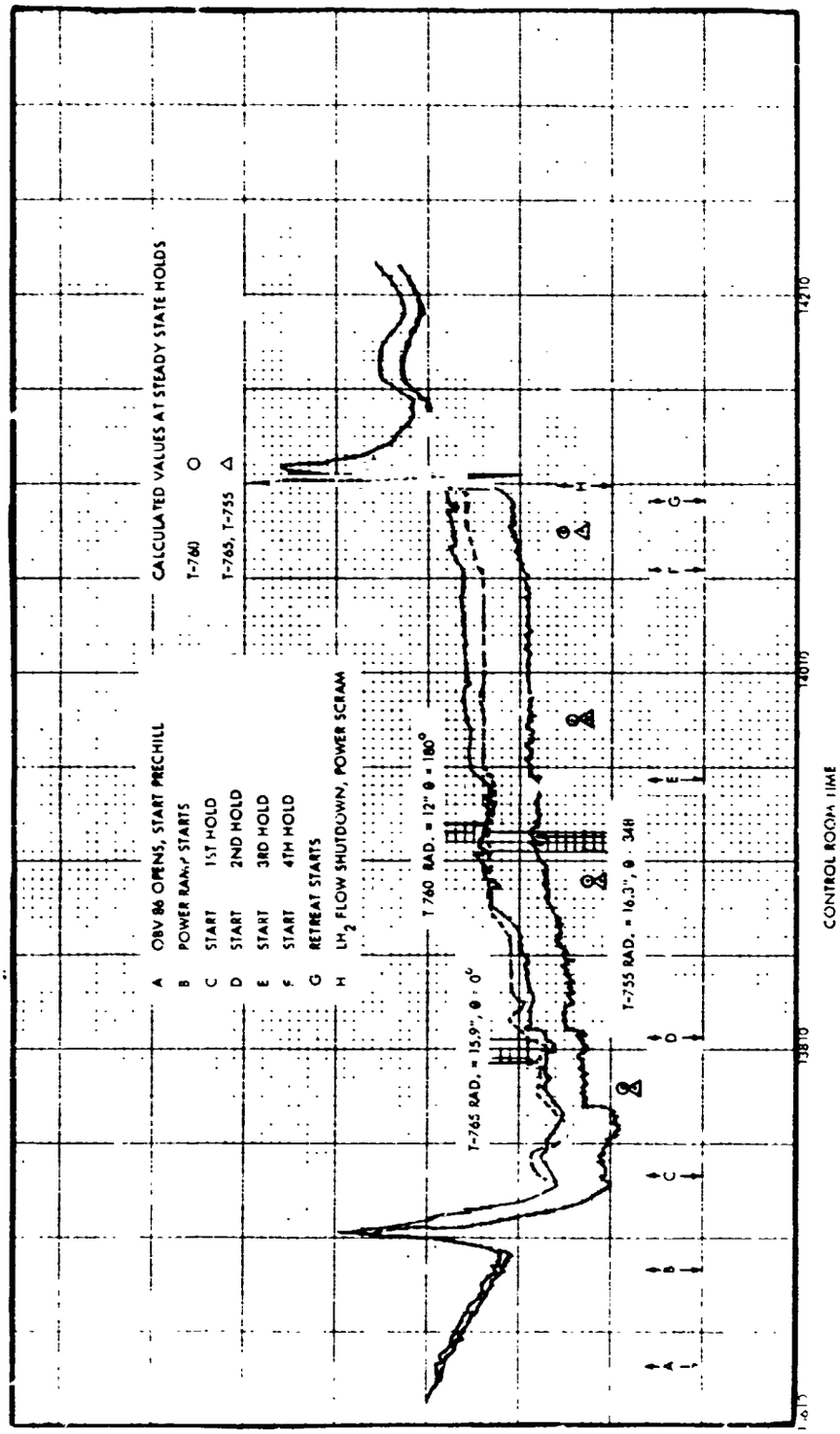

PREPARED BY	APPROVED BY	CURVE NO.

TIE ROD EXIT GAS TEMPERATURE PROFILE EP IV

FIGURE NO. 4 - 26

TABLE 4-20

NOMINAL UNFUELED ELEMENT THERMAL - HYDRAULIC DATA,
EP IV TEST CONDITIONS (14085 CRT)

A. Centering Bushing Inlet Loss Coefficient

Unsealed - 83 (Based on Channel Flow Area)
Sealed - 131 (Based on Channel Flow Area)

B. Pyro Graphite Insulating Sleeve Thermal Conductivity

(Perpendicular to Basal Plane) Btu/hr-ft-°F	(Parallel to Basal Plane) Btu/hr-ft-°F
500°F - 0.33	218
1500°F - 0.27	130
2500°F - 0.22	75

C. Heating In Unfueled Graphite

Core Station	(Btu/sec-in^3)
0.0 in.	0.6457
9.0 in.	1.865
18.0 in.	2.4806
27.0 in.	2.5831
36.0 in.	2.1321
45.0 in.	1.2506
54.0 in.	0.3003

D. Boundary Temperature on Outer Surface of Unfueled Graphite

Core Station	°R
0.0 in.	385
9.0 in.	1468
18.0 in.	2357
27.0 in.	3239
36.0 in.	3881
45.0 in.	4171
54.0 in.	4072

E. Hydrogen Gap Between Stainless Steel Liner and ID of Pyrographite Insulating Sleeve

Nominal Gap Cold	-	0.0065 in.
Minimun Gap Hot	-	0.0070 in.
Nominal Gap Hot	-	0.0080 in.
Maximum Gap Hot	-	0.0090 in.

The nominal hydrogen gap for full power operating conditions is 0.008 inch. The maximum deviation in the hydrogen gap for these conditions is $\pm$ 0.001 inch. This value was assigned a 3σ limit.

The data system error applied to the core inlet plenum and tie rod exit gas thermocouples was factored into the analysis. The data system error for 95 percent confidence (2σ) was estimated to be $\pm$ 2.4 percent of the full scale set up range. For example, the tie rod exit gas temperature set up range for EP IV is 137 - 1990°R. This results in a 2σ error of $\pm$ 45°R in the thermocouple readout. The core inlet temperature set up range for EP IV is 35 - 668°R which results in a 2σ error of $\pm$ 15°R.

Table 4-21 tabulates the uncertainties, deviations, and 3σ temperature increases used for the uncertainty analysis. The temperature variations were combined statistically to determine the 3σ maximum tie rod exit gas temperature for full power and flow EP IV test conditions. The temperature variance is the square of the difference of the deviated temperature minus the same temperature under nominal conditions. These temperature variances were then summed for all considered deviations. Since all deviations considered were input on a 3σ confidence level, the square root of the total variance is the 3σ maximum temperature. At the bottom of table 4-21 is a summary of the measured, calculated, and 3σ maximum tie rod exit gas temperatures for the EP IV full power hold.

Table 4-21 indicates that the 3σ maximum temperatures for T-760 and T-765 are below the measured values. The 3σ maximum temperature in T-755 is above the measured value. The large temperature differences between the measured exit gas temperatures T-765 and T-755 were not expected due to the proximity of each unfueled element to the core periphery. A temperature difference of 32° was calculated between thermocouples T-760 and T-765 which resulted in good agreement with the measured value, 40°R.

Based on a review of EP IV test data, there is reason to believe that the thermocouples located at the exit end of the tie rod element are not sensing the correct exit gas temperature. This could be substantiated by the fact that the 3σ maximum temperatures for T-760 and T-765 are lower than the measured values. The exact position of the thermocouples cannot be verified. Figure 4-27 indicates that the exit gas thermocouples are attached to the

TABLE 4-21

TIE ROD EXIT GAS TEMPERATURE UNCERTAINTY ANALYSIS
EP IV FULL POWER HOLD

UNCERTAINTY	DEVIATION	3σ TEMPERATURE INCREASE
Pyro Sleeve Conductivity	1σ = ± 30%	
T-760		126
T-765		117
T-755		117
Unfueled Graphite Heating	2σ = ± 30%	
T-760		59
T-765		41
T-755		41
Inlet Loss Coefficient	3σ = ± 50%	
T-760		56
T-765		50
T-755		49
Core Inlet Temperature	2σ = ± 15°R	
T-760		38
T-765		35
T-755		36
Hydrogen Gap Between Liner and Pyro	2σ = ± 0.001 in.	
T-760		16
T-765		16
T-755		16
Thermocouple Readout	2σ = ± 45°R	
T-760		68
T-765		68
T-755		68

SUMMARY

	Measured - °R	Calculated - °R	3σ Temp. Increase - °R	3σ Max. Temp. - °R
T-760	733	508	169	677
T-765	693	476	154	630
T-755	597	471	154	625

REFERENCE		PREPARED BY	APPROVED BY	Astronuclear

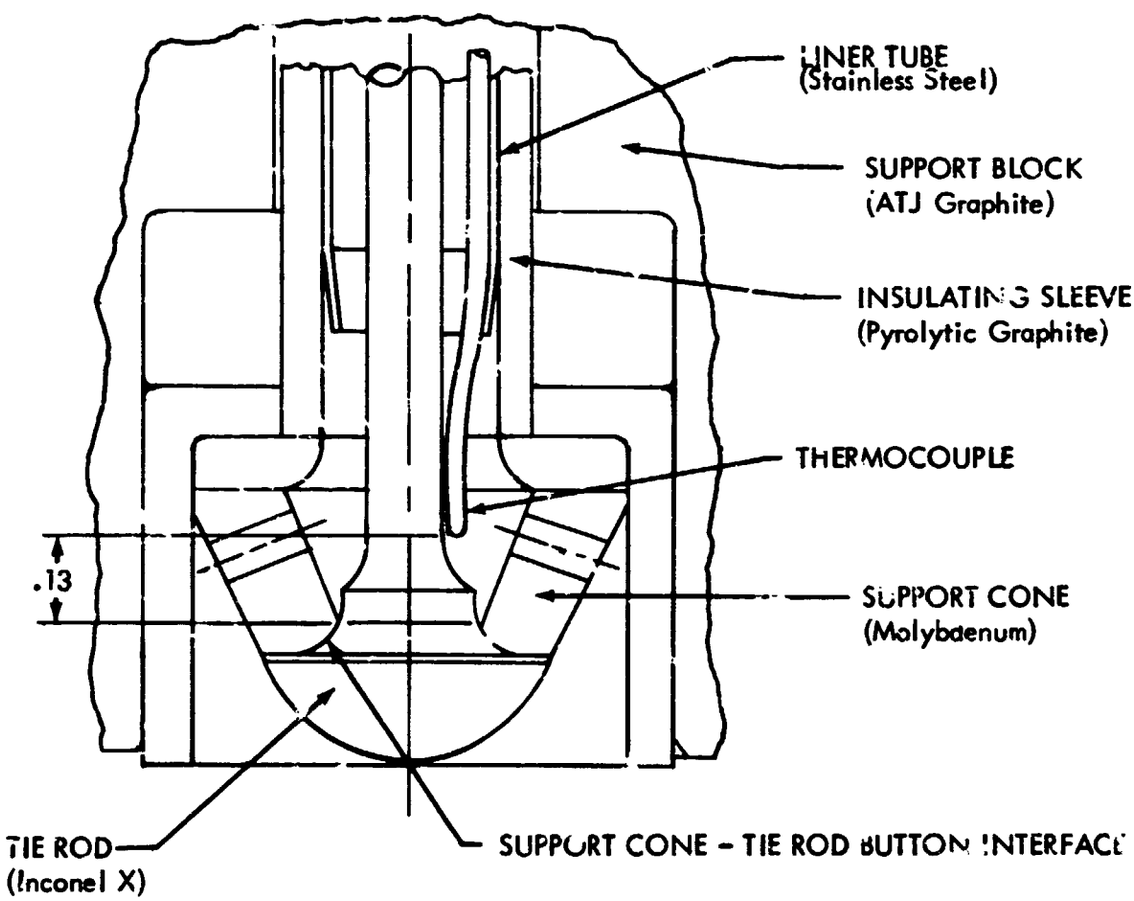

LOCATION OF TIE ROD EXIT GAS THERMOCOUPLE

FIGURE NO. 4 - 27

inside end of the liner tubes. A portion of each thermocouple extends a nominal distance of 0.38 inches beyond the nozzle end of the tube. The nominal clearance between the end of the thermocouple and the forward side of the support - cone - tie rod button interface is 0.13 inch. A slight shift in the thermocouple could result in contact with the molybdenum cone support which is operating 200 - 300°R hotter than the fluid. It has been shown for EP V test conditions where a maximum tie rod exit gas temperature of 1670°R was recorded, that interference resulted, causing the thermocouple extension to buckle. Since restraint is provided for the liner and liner tube at the dome end of the element, these components will expand into the 0.13 inch clearance. Due to the method of restraint, the final axial expansion which could cause thermocouple damage is the difference between the expansion of the tube and expansion of the sleeves. Figure 4-28 is a post-operative photograph of a typical damaged thermocouple.

REFLECTOR

In this section the shield, reflector and lateral support system thermal and hydraulic test results at steady state conditions are presented and compared to calculated values. The pretest predicted values[1] of reflector system temperatures and pressures did not give a meaningful comparison for several reasons; a) operating conditions were not as planned; b) nozzle tube heat pickup was higher than calculated, therefore, reflector inlet conditions were considerably different from those given by the pretest calculations; c) the support ring temperatures were lower than had been expected. These support ring temperatures affect the gap size of the inner-outer reflector annulus under power operating condition. This gap size in turn has a major influence on the reflector system overall pressure drop and flow distribution.

In order to obtain a useful evaluation of the analytical model used for the reflector system analysis and the calculation methods, post test calculations of reflector system temperatures and pressures were performed and compared to test values. Results of these comparisons are given in this section. In particular, comparisons of coolant temperatures

[1] WANL-TME-887, NRX-A2 Test Prediction Report

REFERENCE

Astronuclear

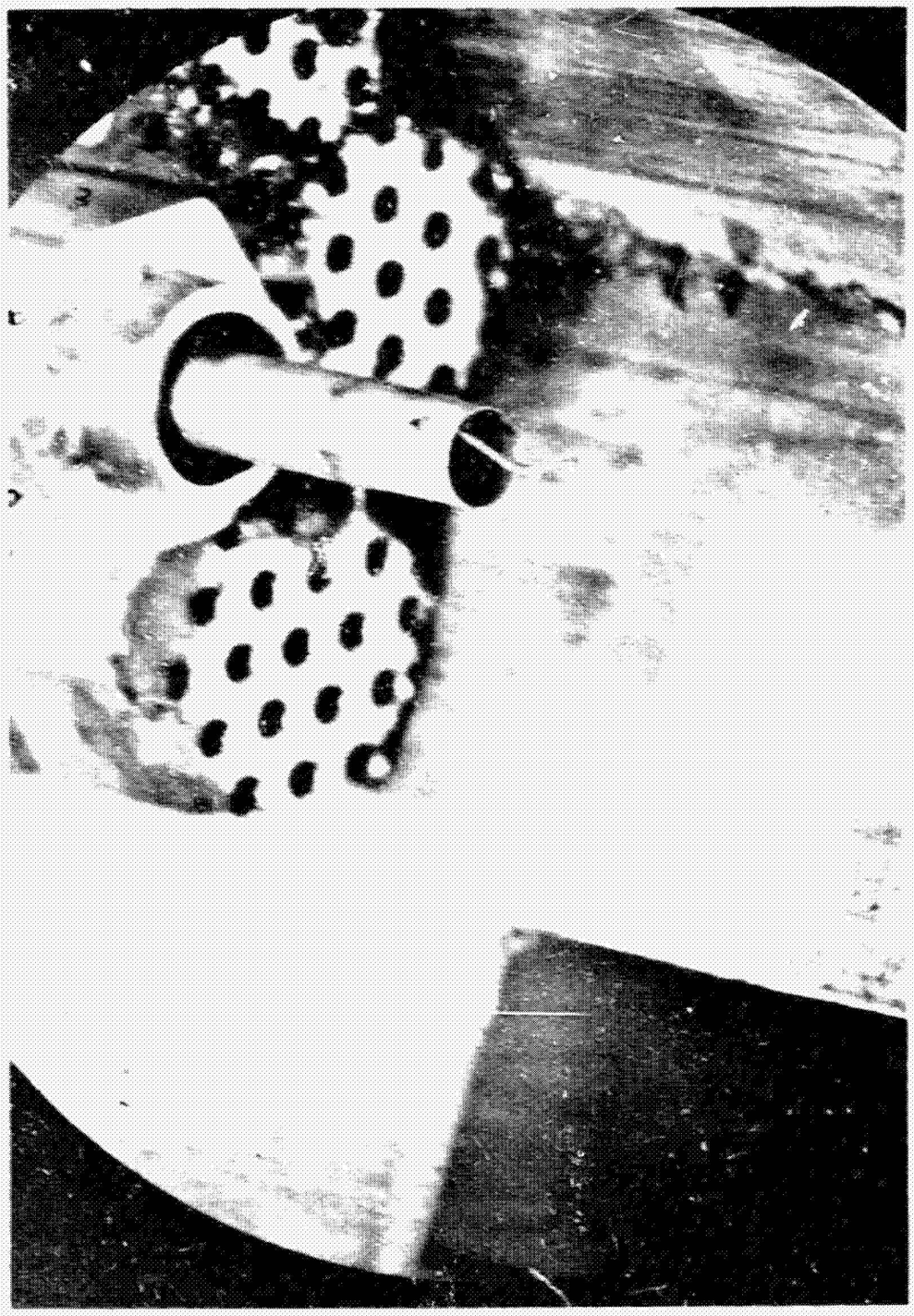

PREPARED BY	APPROVED BY	CURVE NO.

TYPICAL DAMAGED TIE ROD EXIT GAS THERMOCOUPLE

FIGURE NO.

4 - 28

and pressures and material temperatures at the highest power hold at Time CR 14085 seconds (1096 MW thermal power) are presented in more detail. For these calculations at the steady state hold the measured reactor flow rates given in table 4-5 and the measured reflector inlet temperatures and pressures were used. Based on the test measurements of the reflector pressure distribution and temperatures at full power, the inner-outer reflector annulus was recalculated by Reactor Mechanical Design to be 0.092 inch as compared to the pretest value of 0.108 inch. This smaller gap annulus clearance was used in the reflector system analytical model for the post test calculations. In addition, some minor changes in flow impedances of several flow channels in the reflector system were incorporated into the reflector analytical model. These changes were made because additional component test data became available and there were some hardware changes since the pretest calculations were performed. Table 4-22 shows the reflector system analytical model flow characteristics.

In addition to the comparisons of fluid temperatures and pressures the total reflector system heat pickup was calculated from experimental data and is summarized in this section, and the lateral support system performance is compared to calculated performance.

REFLECTOR SYSTEM COOLANT TEMPERATURES AND PRESSURES AT THE HIGHEST POWER HOLD, TIME CR 14085

The parallel flow path in the reflector system is shown in figure 4-29 and 4-30. Included in these figures are the measured and calculated fluid temperatures and pressures at the highest power hold, Time CR 14085. The reflector inlet plenum temperature of 136°R is the average of 7 thermocouple measurements. The reflector exit plenum temperature of 233°R is the average of 5 thermocouple measurements. The inlet and outlet plenum pressures are each an average of 2 pressure measurements. The measured temperature of the coolant exiting from the individual major reflector coolant passage is a single thermocouple reading at a specific location in the outlet plenum. Therefore, these temperatures should be considered only as representative of specific channels exit temperatures and do not represent the average which may be expected from all similar channels.

TABLE 4-22

REFLECTOR SYSTEM HYDRAULIC MODEL - DIMENSIONAL DATA AND LOSS COEFFICIENTS

Channel	Identification	Hydraulic Diameter (in.)	Number of Equivalent Holes	Heat Transfer Area (in^2)	Loss Coefficients, CL[6] Inlet	Intermediate	Outlet
1	Reflector Annulus	0.0184	435.6	13077.4	1.50	1.80[1]	-0.081
2	Pressure Vessel Annulus	0.4120	240.0	16151.2	1.50	0.0	-82.02[2]
3	Sector Cooling Holes	0.1875	384.0	11762.4	4.28[3]	0.0	-1.39[3]
4	Control Drum Cooling Holes	0.1875	228.0	6983.6	2.12[4]	0.0	-6.80[4]
5	Tie Bolt Cooling Holes	0.2500	36.0	1471.6	1.50	0.0	0.20
6	Graphite Reflector Cooling Holes	0.2500	129.0	5881.2	2.00	0.430	-0.061
7	Control Annulus	0.156	646.0	16463.1	18.15	112.0[5]	-13.35
8	Control Vane Inner Annulus, 1st cm	0.2500	12.6	514.8	4.15	0.0	-1.09
9	Control Vane Inner Annulus, 2nd cm	0.2500	12.6	514.8	4.15	0.0	-1.09
10	Control Vane Inner Annulus, 3-5th cm	0.2500	37.8	1544.4	4.15	0.0	-1.09
11	Control Vane Inner Annulus, 6-10th cm	0.2500	63.0	2574.0	4.15	0.0	-1.09
12	Control Vane Outer Annulus, 1st cm	0.1640	18.9	506.5	4.56	0.0	-1.84
13	Control Vane Outer Annulus, 2nd cm	0.1640	18.9	506.5	4.56	0.0	-1.84
14	Control Vane Outer Annulus, 3-5th cm	0.1640	56.7	1518.4	4.56	0.0	-1.84
15	Control Vane Outer Annulus, 6-10th cm	0.1640	94.5	2532.4	4.56	0.0	-1.84

NOTE: The intermediate loss coefficients of channels 1 and 6 are for the pressure loss of coolant discharging from the respective channels into the space under the core support cone. The respective outlet loss coefficients are for the loss of pressure across the core support cone. The intermediate loss coefficient of channel 7 is for the pressure loss of coolant flow through the impedance at the channel outlet. The outlet loss coefficient is for the pressure loss through the drum bearing housing.

1. Calculated based on annulus gap size 0.092 inch

2. Based on test results reported in WANL-TME-832.

3. Based on test results reported in WANL-TME-673.

4. Based on component test.

5. Based on annulus gap size of 0.078 inch.

6. $\Delta P \quad CL \frac{G^2 v}{2g}$ where, ΔP pressure drop, G mass flow rate per unit area (based on flow area of annulus), v specific volume (hydrogen properties based on state points in channel)

PREPARED BY	APPROVED BY	CURVE NO.

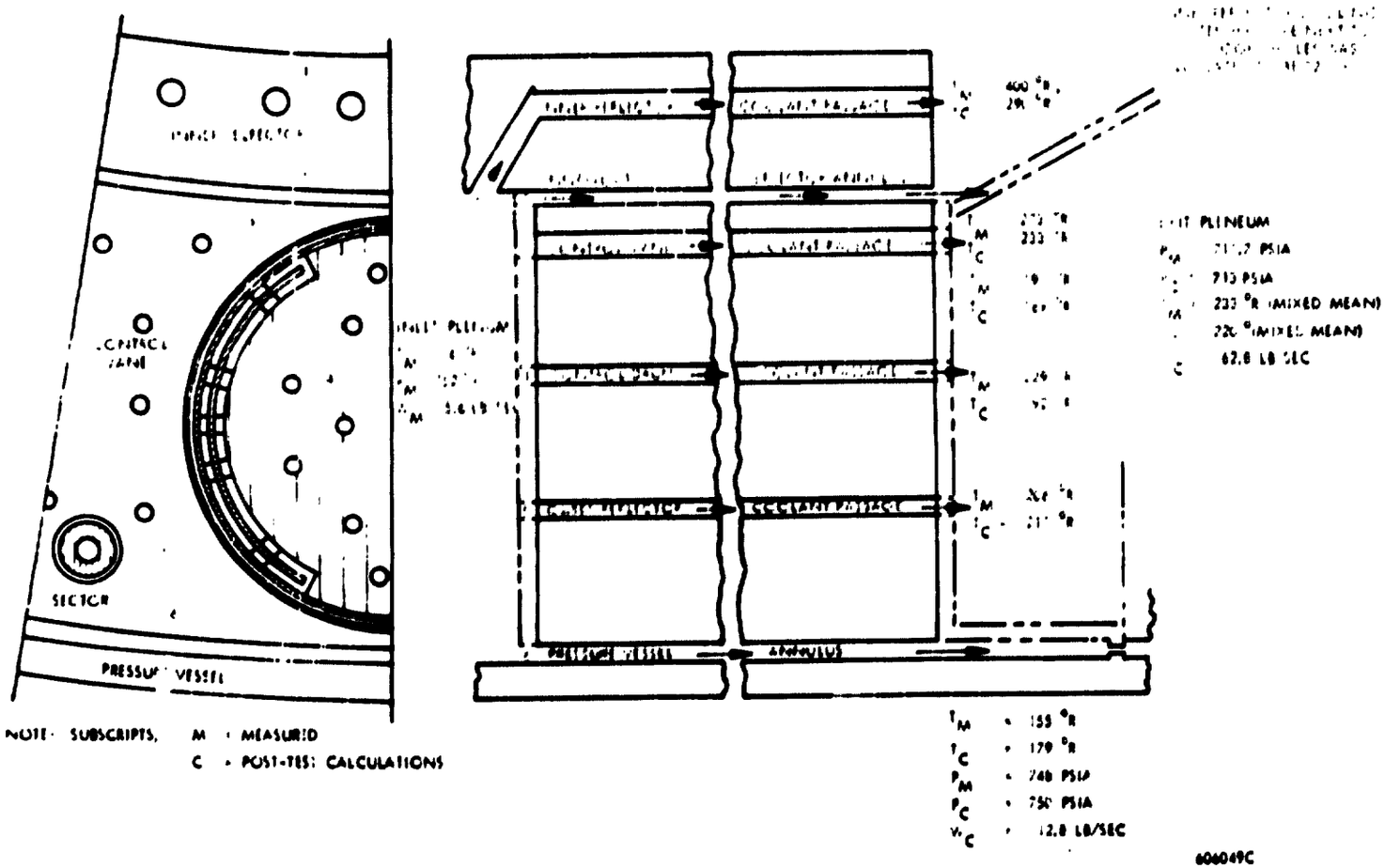

REFLECTOR SYSTEM FLUID TEMPERATURES AND PRESSURES FOR NRX-A2 EP-IV AT CRT 14085	PREPARED BY	APPROVED BY	CURVE NO.

FIGURE NO. 4 - 29

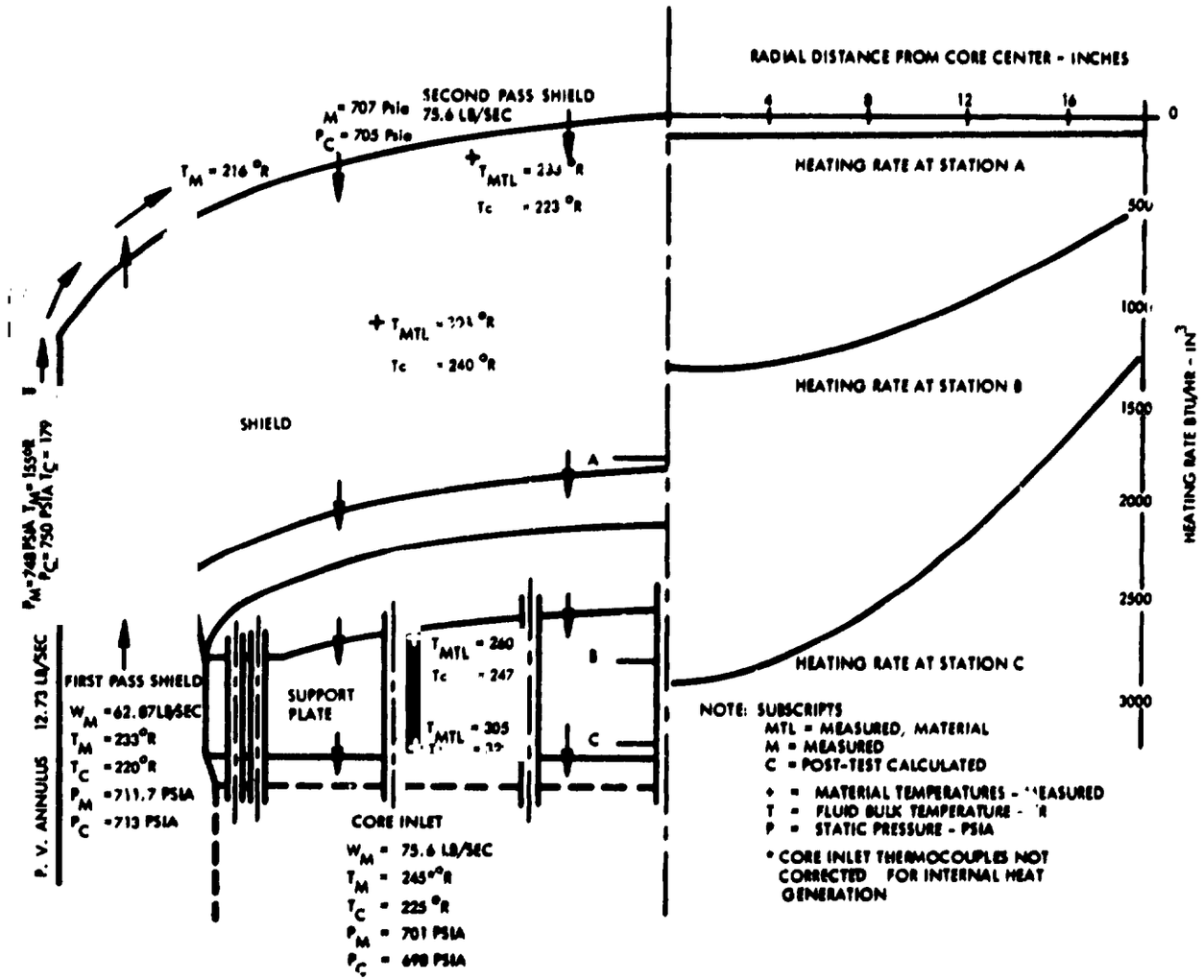

Figure No. 4-30

TEMPERATURES, FLOWS, AND RADIATION HEATING RATES IN SHIELD AND SUPPORT PLATE AT CRT 14085

PREPARED BY	APPROVED BY	CURVE NO.

The post test calculation at the highest power hold was performed by using the computer code MCAP-TOSS.[1] The calculation used the test reflector inlet temperature of 136°R, inlet pressure of 752 psia and flow rate of 75.6 lb/sec. The other parameter specified in the calculation was the total power pickup of the reflector system which was determined by energy balance between reflector inlet and the first shield exit (shield dome end plenum). The power shapes for the various materials are the ones reported in the Reactor Analysis Data Book (WANL-TME-840) in the Radiation and Shielding Section for NRX-A2. The total power pickup in the reflector system will be discussed in the next section.

Figure 4-29 shows the major flow passages in the outer and inner reflectors. The fluid temperatures and pressures at the exit plenum, pressure vessel annulus, sector cooling holes and control drum cooling passages agree reasonably well. In the inner reflector cooling passage, the exit fluid temperature thermocouple was located between two open holes which in turn were between two plugged holes as shown in figure 4-31. The measurement indicated only the local coolant temperature. Fifteen of the 144 inner reflector cooling holes were plugged in the NRX-A2 reactor for pressure measurements of the seal chamber pressure. In the post-test calculation the inner reflector analytical heat conduction model includes some plugged and some open holes. These holes are arranged in the same relative positions as in the NRX-A2 so that the effect of the plugged holes on the coolant exit temperature in the vicinity of the plugged holes can be studied. The calculated coolant exit temperature is 320°R as compared to the measured value of 400°R. This shows that the plugged hole does increase the coolant temperature at the holes near the plugged ones. The calculated nominal inner reflector coolant exit temperature is 290°R as shown in the figure.

Figure 4-30 shows the fluid temperatures and pressures at the shield and core support plate region of the coolant flow. Using the calculated reflector outlet plenum pressure of 713 psia, the pressure drop through the first pass of the shield was calculated to be 8.0 psi, giving a dome plenum pressure of 705 psia. This compares with the measured value of

[1] WANL-TME-967 A Program for Steady State Fluid Flow and Heat Conduction Coupled Calculations of Heat Generating Solids Cooled by Parallel Channels - Using MCAP and TOSS Codes - A. Y. Lee, Oct., 1964

REFERENCE	PREPARED BY	APPROVED BY	

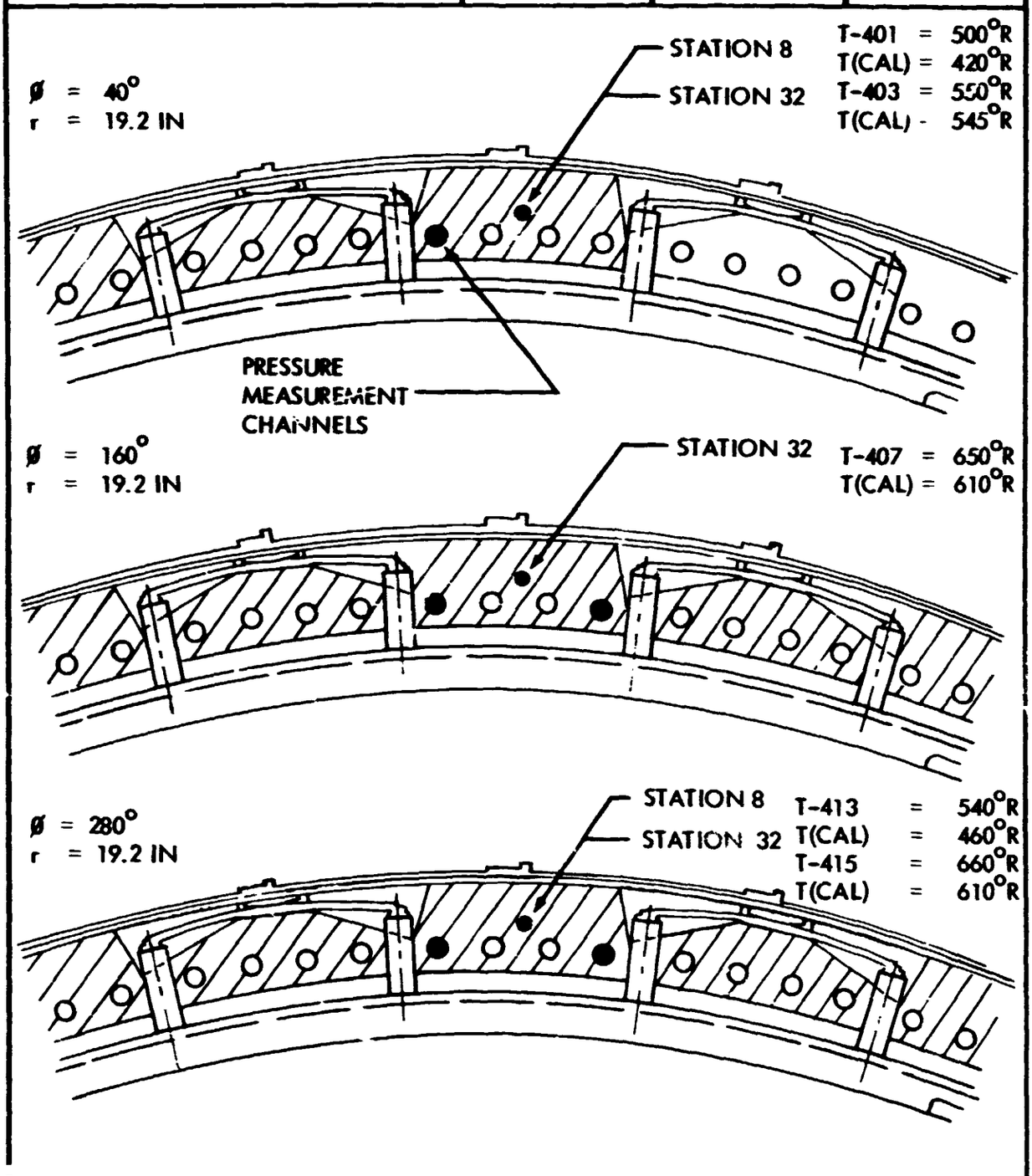

NRX-A2 EP IV INNER REFLECTOR
TEMPERATURES AT CRT 14085

FIGURE NO.
4 - 31

707 psia. The pressure drop across the second pass of the shield and the screen was calculated to be 7 psi and the pressure drop across the support plate was calculated to be about 0.5 psi. These give a calculated core inlet pressure of 698 psia to the nearest psi. This compares with the measured value of 701 psia. Table 4-23 summarizes the pressures and pressure drops throughout the component system.

The comparisons of the calculated and measured shield and core support plate material temperatures are also shown in the figure. The calculated dome end shield material temperature of 223°R was based on the dome plenum temperature of 216°R, this confirms the dome plenum fluid temperature reasonably well. Using this dome plenum temperature at 216°R and the internal heat generation rates of the shield and the support plate as shown in the figure, the calculated core inlet temperature is 225°R as compared to the measured value of 245°R. From the comparison of the support plate calculated and measured temperatures, it is believed that the calculated core inlet temperature of 225°R is consistent with the measured support plate temperature.

REFLECTOR SYSTEM POWER COMPARISON AT VARIOUS POWER HOLDS

Table 4-24 shows a summary of the power picked up in the reflector system calculated from the hydrogen flow rate and the temperature rise across the reflector and first pass of the shield. The power picked up in the reflector system arrived by this method averaged over the four power holds, was 2.15 percent of the total reactor thermal power. Also tabulated on this table is the power which would have been calculated under test flow conditions and inlet temperature using the nuclear heating rates reported in Reactor Analysis Data Book under Radiation and Shielding Section for NRX-A2. (WANL-TME-840). Using the calculated reflected heating rates shows the reflector system absorbs 1.76 percent of the total reactor power at full power conditions. Comparison of these two powers, one reflecting calculated conditions, one reflecting test conditions, it appears that the heating rates as tested are about 15 percent higher than expected from calculation for the high power hold, and about 22 percent if the average of the four power holds is considered.

TABLE 4-23

COMPARISON OF EXPERIMENTAL AND CALCULATED PRESSURES AND DIFFERENTIAL PRESSURES IN THE REFLECTOR SYSTEM

Reflector and Shield System at CRT 14085

	Measured	Calculated
P (Reflector Inlet)*	752 Psia	752 Psia
P (Reflector Exit)	711.3 Psia	713 Psia
P (Dome End Shield)	707 Psia	705 Psia
P (Core Inlet)	701 Psia	698 Psia
P (PV Annulus-Dome End)	748 Psia	750 Psia
ΔP (Outer Reflector)	40.7 Psi	39 Psi
ΔP (Inner Reflector)	38 Psi	35 Psi
ΔP (Shield)		15 Psi

*For post calculation of reflector and shield fluid systems, the measured values of the conditions at the reflector inlet were used.

TABLE 4-24

CALCULATED REFLECTOR HEATING RATES FROM ΔH AND FLOW RATE AND COMPARISON TO NUCLEAR HEATING RATES

	EP IV POWER HOLD CONTROL ROOM TIME				
	13790	13900	13985	14085	Average
Reactor Power	574	941	1038	1096	--
Power of Reflector System plus first pass of shield from test (Calculated by energy balance between reflector inlet and first pass shield exit).	13.6	22.0	20.9	22.7	--
Estimated power deposited in first pass shield	0.3	0.5	0.5	0.5	--
Power of reflector system from test	13.3	21.5	20.4	22.2	--
Power of reflector system using calculated heating rates (Ref: TME-840) (1.76 x Reactor Power)				19.3	--
Reflector system power (test)/reactor power	2.32%	2.29%	1.97%	2.03%	2.15%
Reflector system power (cal)/reactor power	1.76%	1.76%	1.76%	1.76%	1.76%
Reflector system power (test)/reflector system power (cal)	1.32	1.30	1.12	1.15	1.22

REFLECTOR INLET AND OUTLET PLENUM TEMPERATURE AZIMUTH MEASUREMENTS

Figure 4-32 and 4-33 show the average azimuth thermocouple measurements at the reflector inlet and outlet plenums at the various powerholds. The maximum variation in a reading is $\pm 6^{\circ}R$. From the figures, it is seen that there was no detectable azimuth variation in the coolant temperature in the reflector inlet and outlet plenum during these four power holds. However, there was asymmetry during chilldown and the early stage of startup. These are discussed in the startup and the shutdown section of the report.

MATERIAL TEMPERATURES

The measured outer reflector sector material temperatures at the locations of the thermocouples at the 4 power holds are shown in figure 4-34. The calculated material temperature at the vicinity of the thermocouple locations at the highest power hold, Time CR 14085, is also plotted in the figure for comparison. The axial shape of these curves are as expected. The maximum temperature level occurred around the central portion of the reactor where the internal heat generation is maximum. The experimental curve peaks nearer the center of the core than the calculated curve. Maximum deviation of the calculated value from test value at Time CR 14085 is about $50^{\circ}R$. The measured temperatures shown in the figure for the various power holds do not represent the average reflector sector material temperatures. The thermocouples were located in the region where the maximum material temperatures might occur. The maximum calculated sector temperature at Time CR 14085 is $310^{\circ}R$ at core station 20 inches, and at approximately R = 21.8 inches and one inch from the radial edge of the sector. At Time CR 14085 the calculated maximum sector average temperature is $265^{\circ}R$ and the maximum sector average to inner web temperature difference is $50^{\circ}R$.

Figure 4-35 shows the sector material temperatures at core station 8, 20, and 32 plotted as a function of azimuth position. This curve is typical of the steady state operation observed at the other lower power holds. There appears to be little, if any azimuth variation apparent in the sector temperatures. The 2 σ error range of the individual thermocouple readings is $\pm 18^{\circ}R$ and the range of the average values is $\pm 12^{\circ}R$.

REFERENCE

Astronuclear

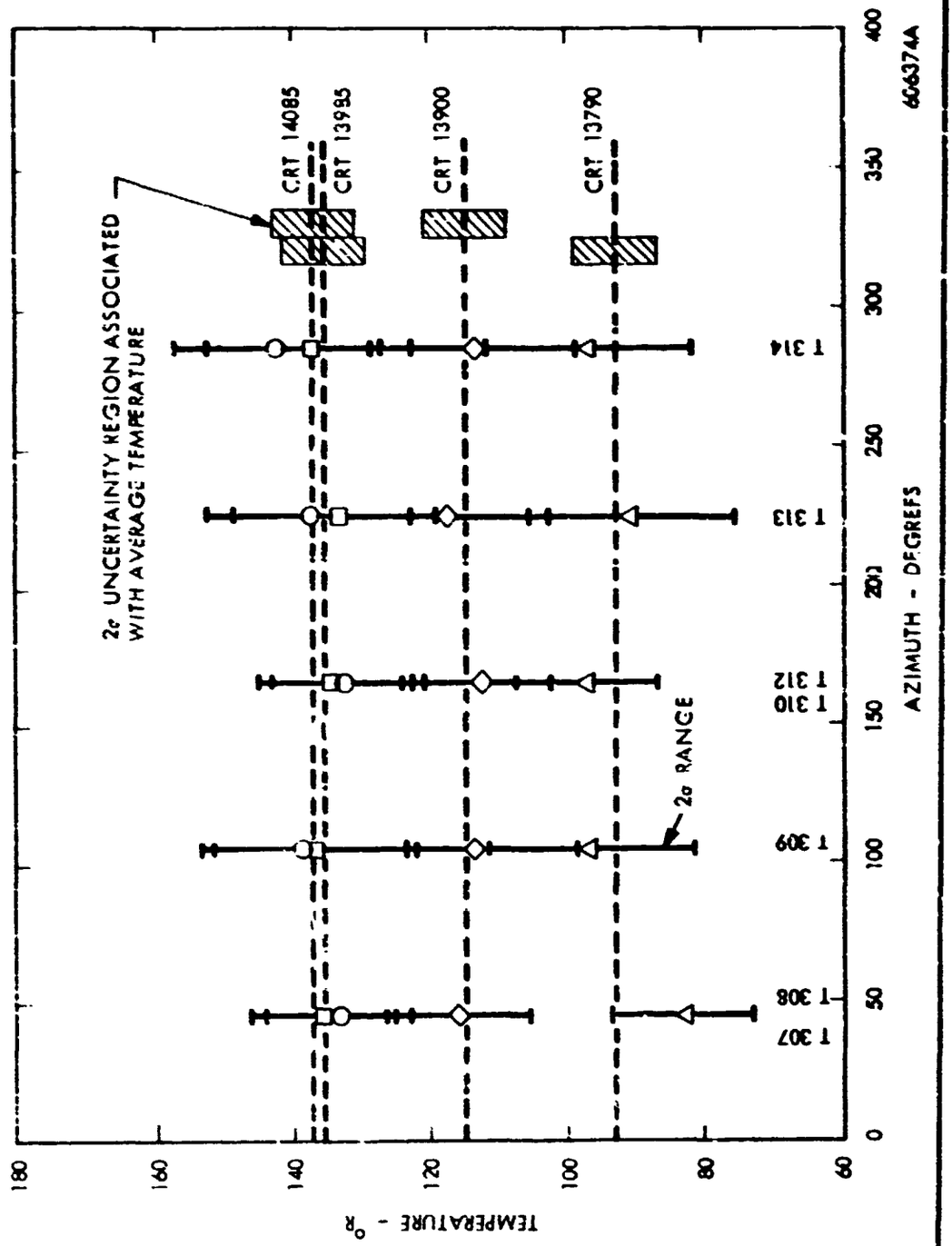

REFLECTOR INLET TEMPERATURE VS AZMUTH FOR THE FOUR POWER HOLDS OF NRX - A2 - EP IV

PREPARED BY	APPROVED BY	CURVE NO.

FIGURE NO.
4 - 32

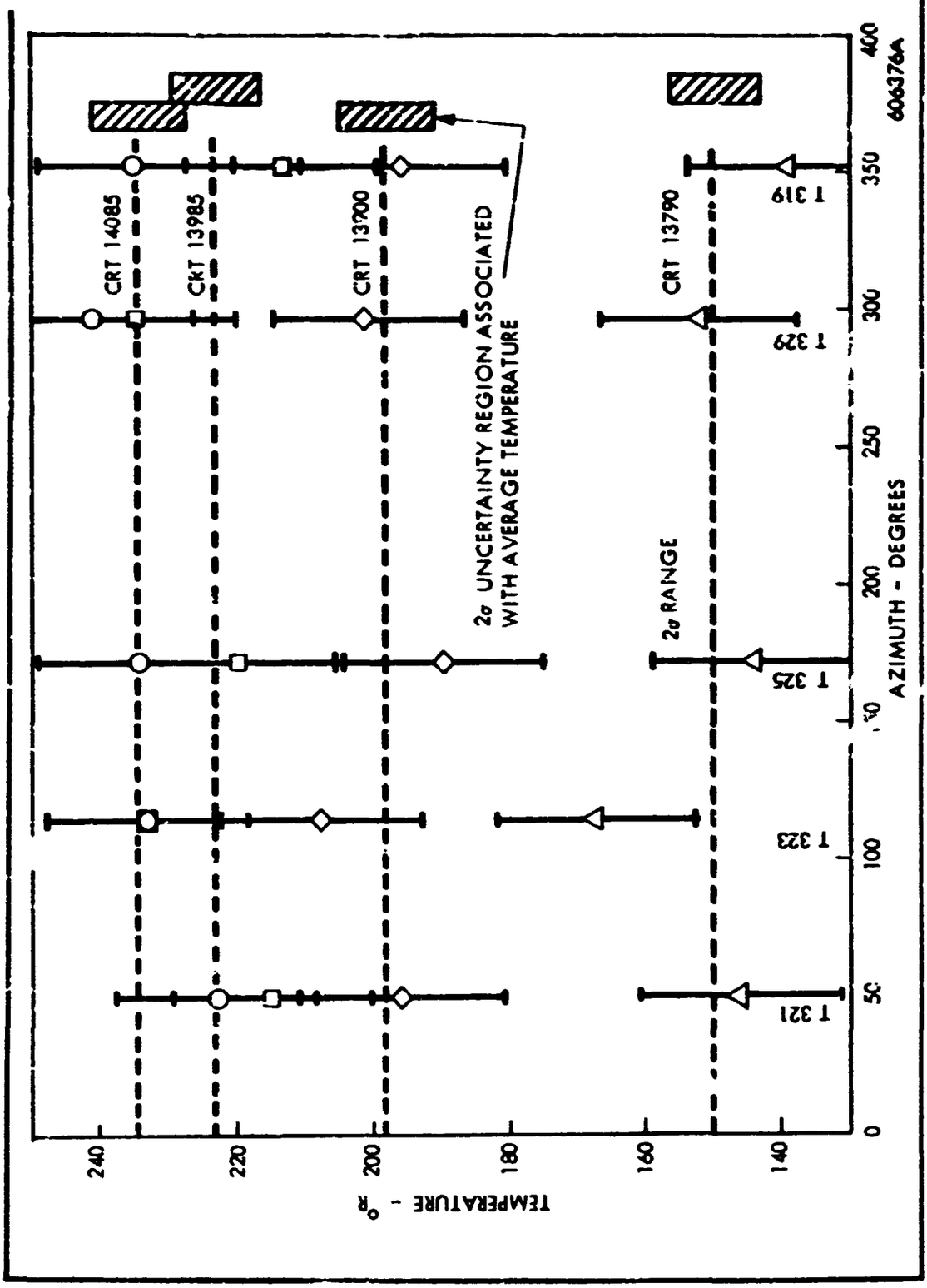

REFLECTOR OUTLET TEMPERATURE VS AZIMUTH FOR THE FOUR POWER HOLDS ON NRX-A2 EP IV

PREPARED BY	APPROVED BY	CURVE NO

FIGURE NO.
4 - 33

REFERENCE		PREPARED BY	APPROVED BY	Astronuclear

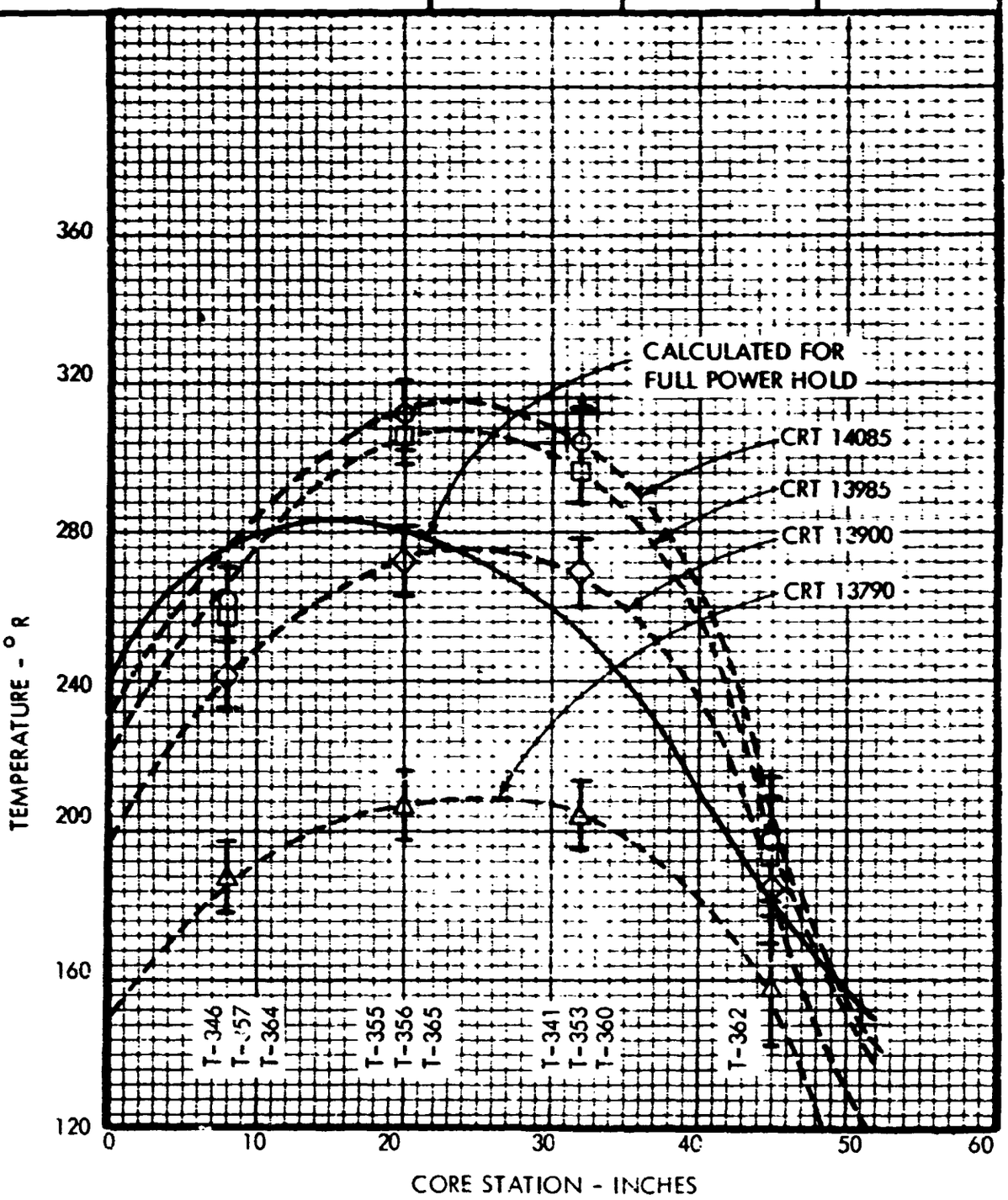

OUTER REFLECTOR SECTOR MATERIAL TEMPERATURE VS. AXIAL POSITION	CURVE NO.	FIGURE NO.
		4 - 34

REFERENCE

Astronuclear

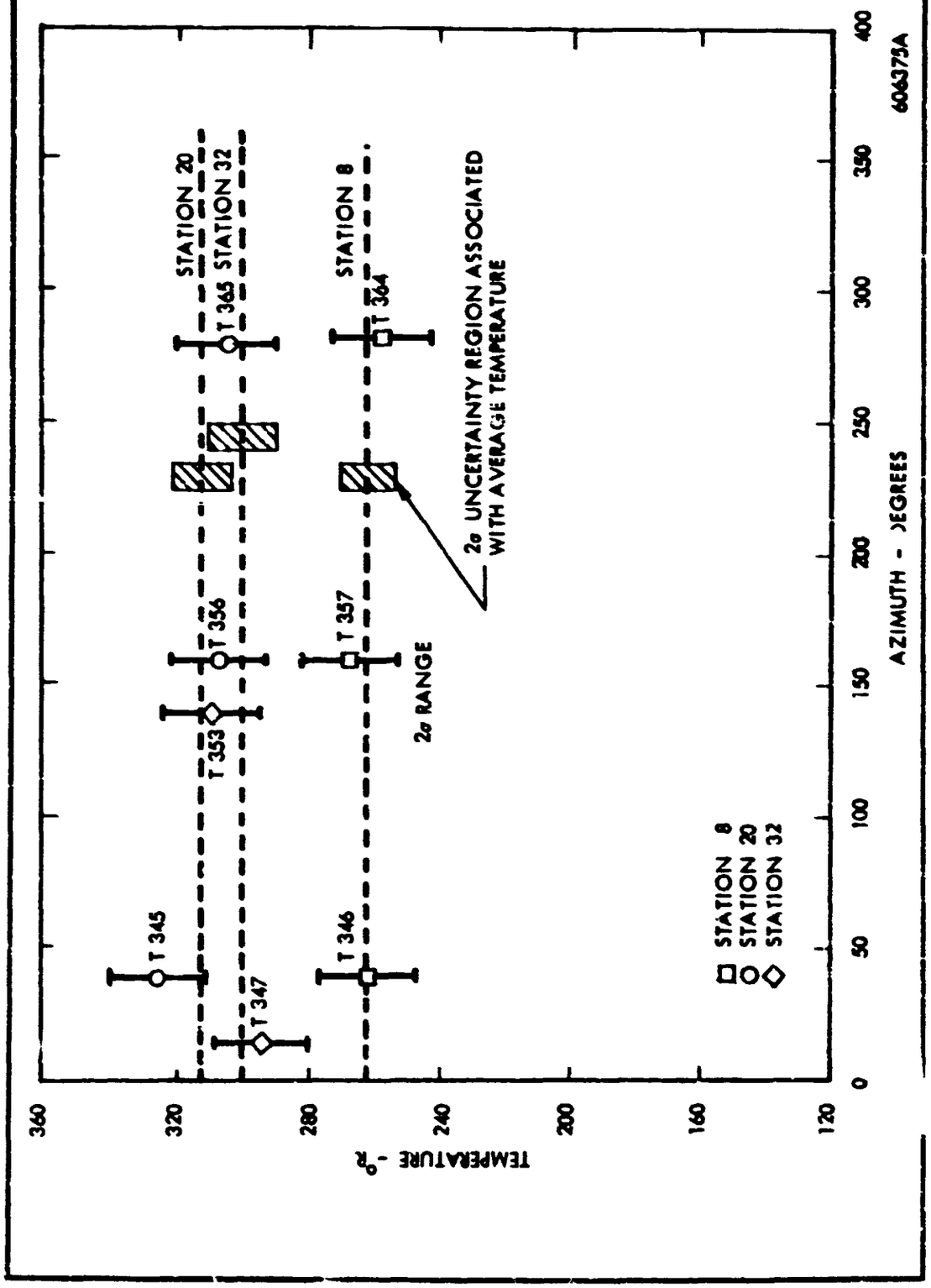

PREPARED BY | APPROVED BY | DATE

AZIMUTH SECTOR TEMPERATURE VARIATION IN NRX-A2 EP I V

FIGURE NO.
4 - 35

Figure 4-36 shows the measured control drum and control vane temperatures at the highest power hold Time CR 14085. Included in this figure are the calculated local nodal temperatures at the vicinity of the thermocouples. The calculated values agree very well with the measured values. The temperature difference across the control drum at station 8 with the drum operating at an average temperature slightly above 226°R was measured to be 42°R, the comparable value was calculated to be 37°R.

Table 4-25 tabulates the measured control drum and control vane temperatures at the four power holds and the calculated values at the highest power hold.

The experimental temperatures of the inner reflector material at the three power holds, Time CR 13790, 13900, and 14085, are shown in figure 4-37. A sketch of the inner reflector and the thermocouple locations is shown in figure 4-31. The thermocouples T 413, T 407, T 415 are located between two open and plugged holes whereas T 401 and T 403 are near one plugged hole. With the effect of the plugged holes taken into consideration in the post-test analysis, the calculated material temperature at the vicinity of the thermocouples at the highest power hold, Time 14085, are shown in the figures. The upper curve in figure 4-37 is the calculated temperature at the location between two plugged holes and the lower curve near one plugged hole. It is seen in figure 4-31 that the maximum deviation between the calculated and measured values is 80°R. At core station 32 and at the same radial location, but away from any plugged hole, the average material temperature was calculated to be 110°R lower than the temperature measured between two plugged holes.

Figure 4-38 shows the time trace of the inner reflector material temperature as measured by the thermocouple T 415. It is seen that the material temperature continued to rise during the power holds. A similar result was also observed in KIWI B4E tests. This temperature increase is believed to be caused by a decrease in material thermal conductivity due to irradiation damage. The values of thermal conductivity used in these calculations are those on unirradiated graphite, not impregnated H4LM. Experimental data on thermal conductivity, are not available at this time. Preliminary investigation shows that a 7 percent decrease (linear) in the inner reflector material thermal conductivity over the same period of time as the third power hold (110 seconds) would result in

REFERENCE		PREPARED BY	APPROVED BY	Astronuclear

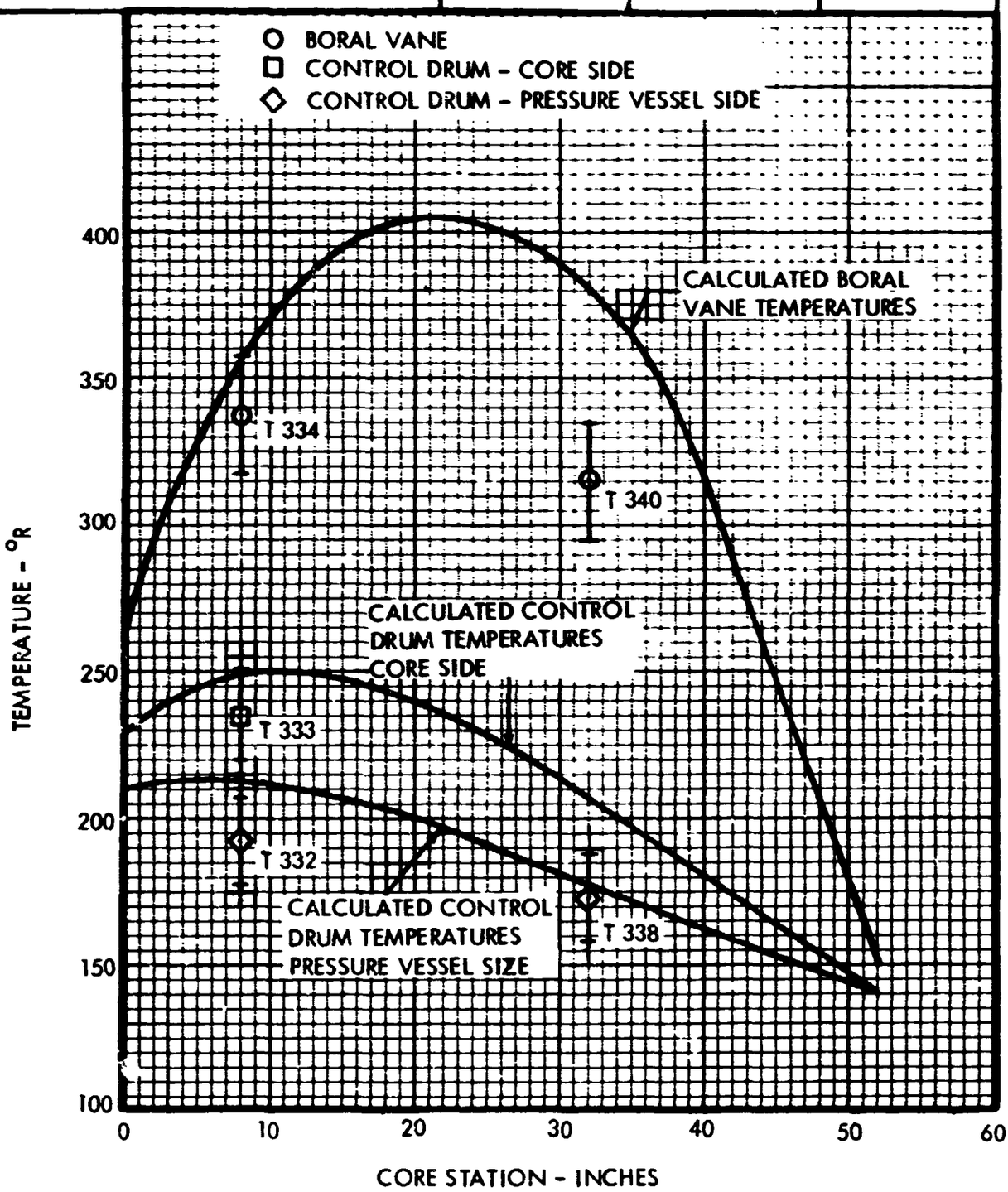

CONTROL DRUM AND BORAL VANE TEMPERATURES FOR NRX-A2 EP IV	CURVE NO.	FIGURE NO.
		4 - 36

TABLE 4-25

NRX-A2 EP IV

CONTROL DRUM AND CONTROL VANE TEMPERATURES

CONTROL DRUM TEMPERATURES

Drum No.	Station	Temperatures at Specified Control Room Time				
		13790	13900	13985	14085	Calculated High Power
2	8.0	120	159	178	188	213
2	8.0	151	206	223	235	248
10	32.0	103	150	168	173	178
10	32.0		INOPERATIVE			

CONTROL VANE TEMPERATURES

Drum No.	Station	Temperatures at Specified Control Room Time				
		13790	13900	13985	14085	Calculated High Power
2	8	240	315	320	338	356
10	32	230	282	305	315	380

REFERENCE		PREPARED BY	APPROVED BY	Astronuclear

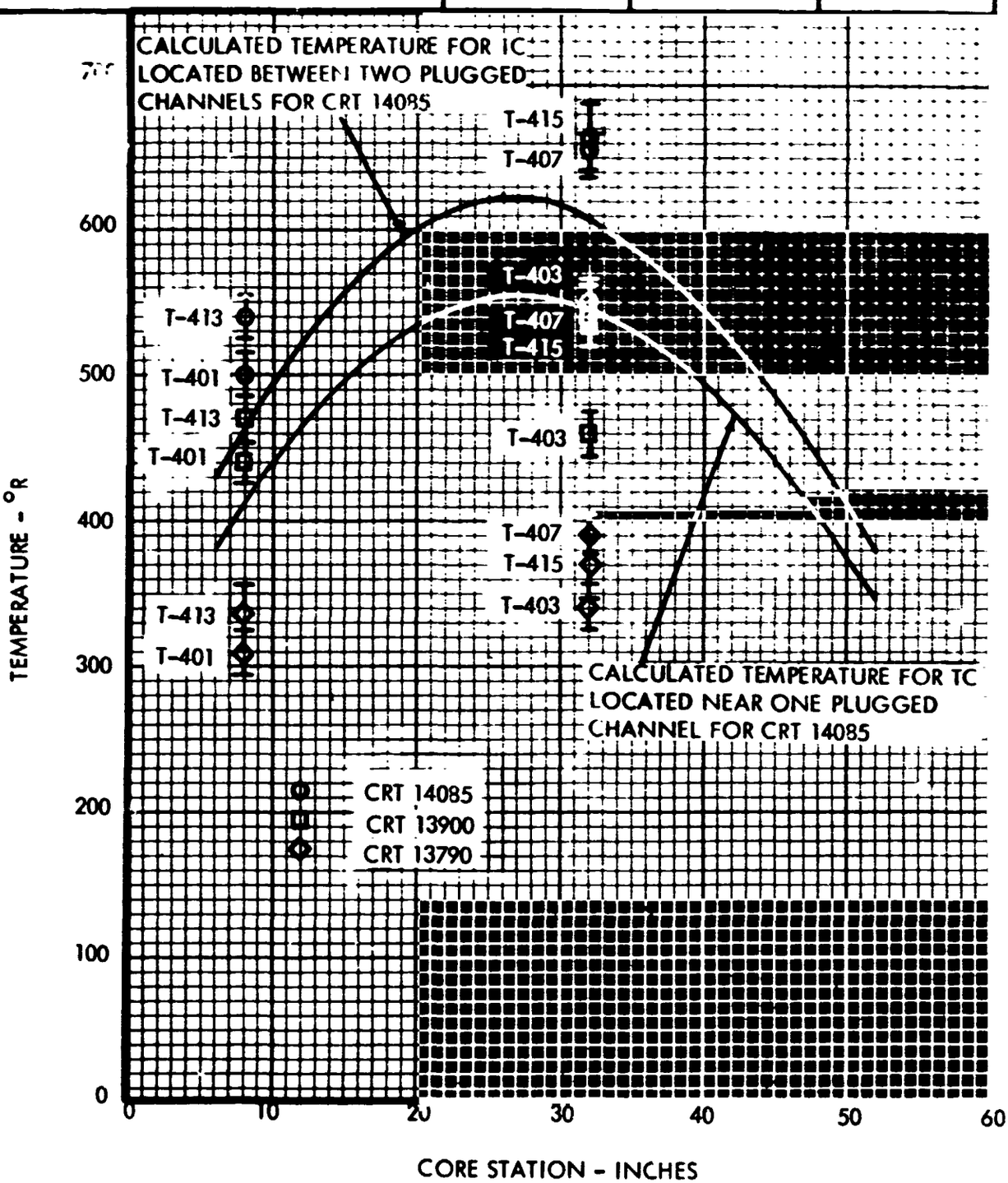

NRX-A2 EP IV INNER REFLECTOR AXIAL TEMPERATURE VARIATION	CURVE NO.	FIGURE NO.
	[redacted]	4 - 97

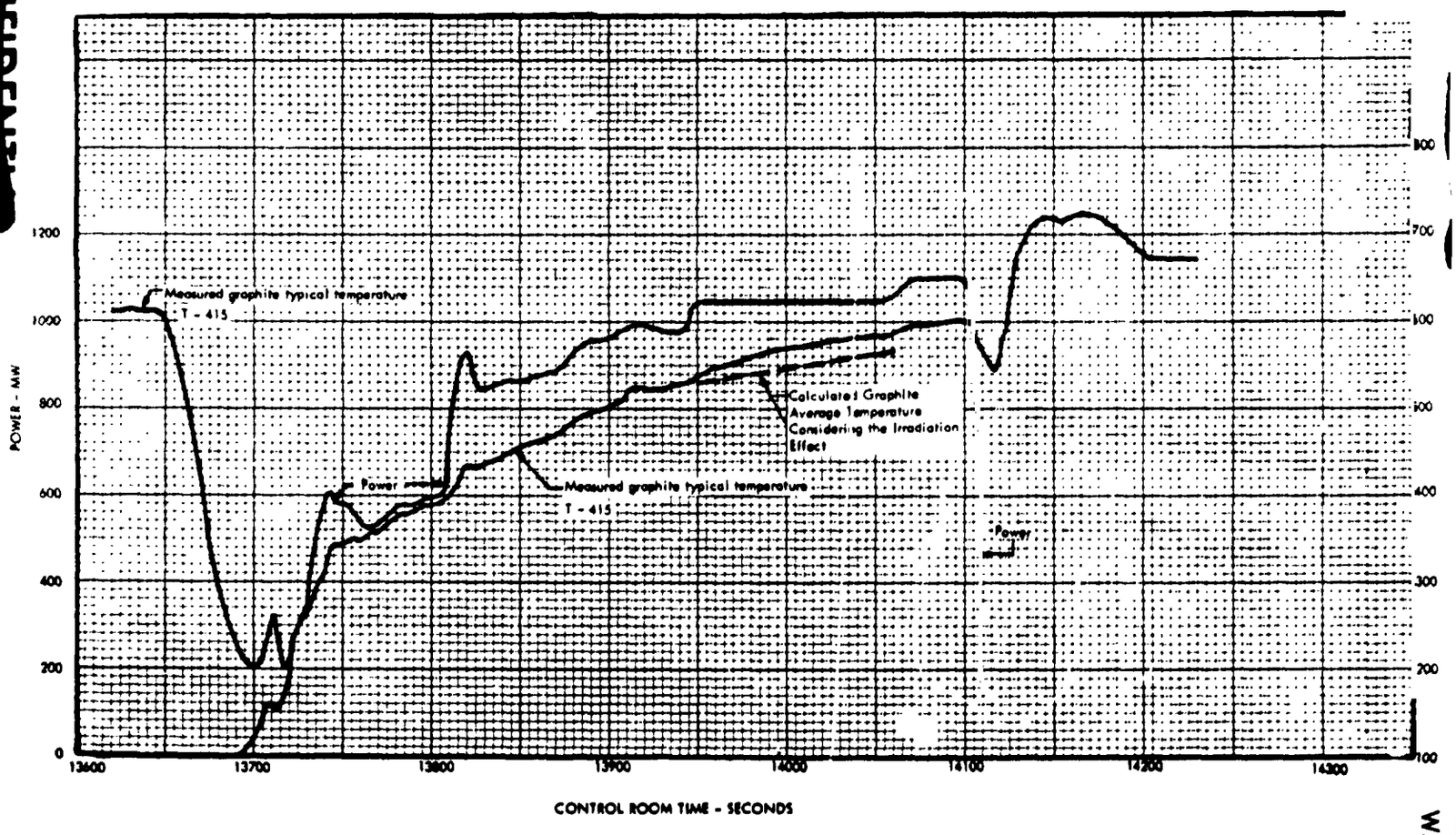

FIGURE 4-38, COMPARISON OF MEASURED AND CALCULATED INNER REFLECTOR TEMPERATURE

an increase in the material temperature with similar slope as shown by the trace of T 415. The dash-line in figure indicates the calculated inner reflector average temperature at core station 32 considering the 7 percent decrease in thermal conductivity during the 110 seconds due to irradiation effect.

Table 4-26 tabulated the measured support rings, shield, reflector tie bolt, and support plate temperatures at the four power holds. The comparison of the shield and support plate material temperatures with calculated values have been previously discussed.

LATERAL SUPPORT SYSTEM

The lateral support system fluid flow path, fluid temperature and pressure and material temperatures during the high power hold, Time CR 14085, are shown in figure 4-39 and 4-40. In figure 4-39 Curve A is the predicted filler strip temperature at the filler strip-pyro-tile interface at points between seals at full power and Curve B is the predicted filler strip temperature at the filler strip-pyro-tile interface at points on seals at full power.[3] The axial average filler strip temperature along this interface is between these two curves. The thermal capsule measurements at the 3 filler strip pyro-tile interface locations are shown on the figure for comparison. At core station 19.2 inches (on seal) the thermal capsule indicated a temperature of 2450°R as compared to the predicted value of 2300°R. At the other two core stations the thermal capsules fused, indicating a temperature of the material above 2678°R which was the highest melting temperature of the capsule wires installed in the NRX-A2 filler strips. The coolant temperature in the seal system was measured by thermocouples at locations between seals. A typical thermocouple installation is shown at D and the detail of the installation is also shown in the figure. The measured fluid temperature is much lower than the predicted temperature (Curve C). If one compares the fluid temperature measurements with the predicted inner reflector material temperature at the surface of the seal chamber between seals (Curve E), it is evident that the thermocouples were measuring much closer to the inner reflector wall temperature than to the fluid bulk temperature.

[3] WANL-TME-840, Reactor Analysis Data Book

TABLE 4-26

MISCELLANEOUS COMPONENT TEMPERATURES

		Station	Radius	Theta	CONTROL ROOM TIME			
					13790	13900	13985	14085
SUPPORT RINGS								
2σ Error ± 15°R	T374	52.3	23.1	190	117	147	159	166
	T382	-0.3	23.2	190	154	198	212	217
SHIELD MATERIAL								
2σ Error ± 15°R	T523	-25.9	8.1	163	164	209	226	233
	T525	-19.9	11.6	163	205	267	289	301
OUTER REFLECTOR BOLTS								
2σ Error ± 15°R	T370	20.0	23.7	134	154	198	215	223
	T372	32.0	23.7	284	162	208	219	230
SUPPORT PLATE								
2σ Error ± 15°R	T772	-7.5	10.2	165	188	235	250	260
2σ Error ± 23°R	T773	-1.5	10.1	169	210	--	290	305

REFERENCE

Astronuclear

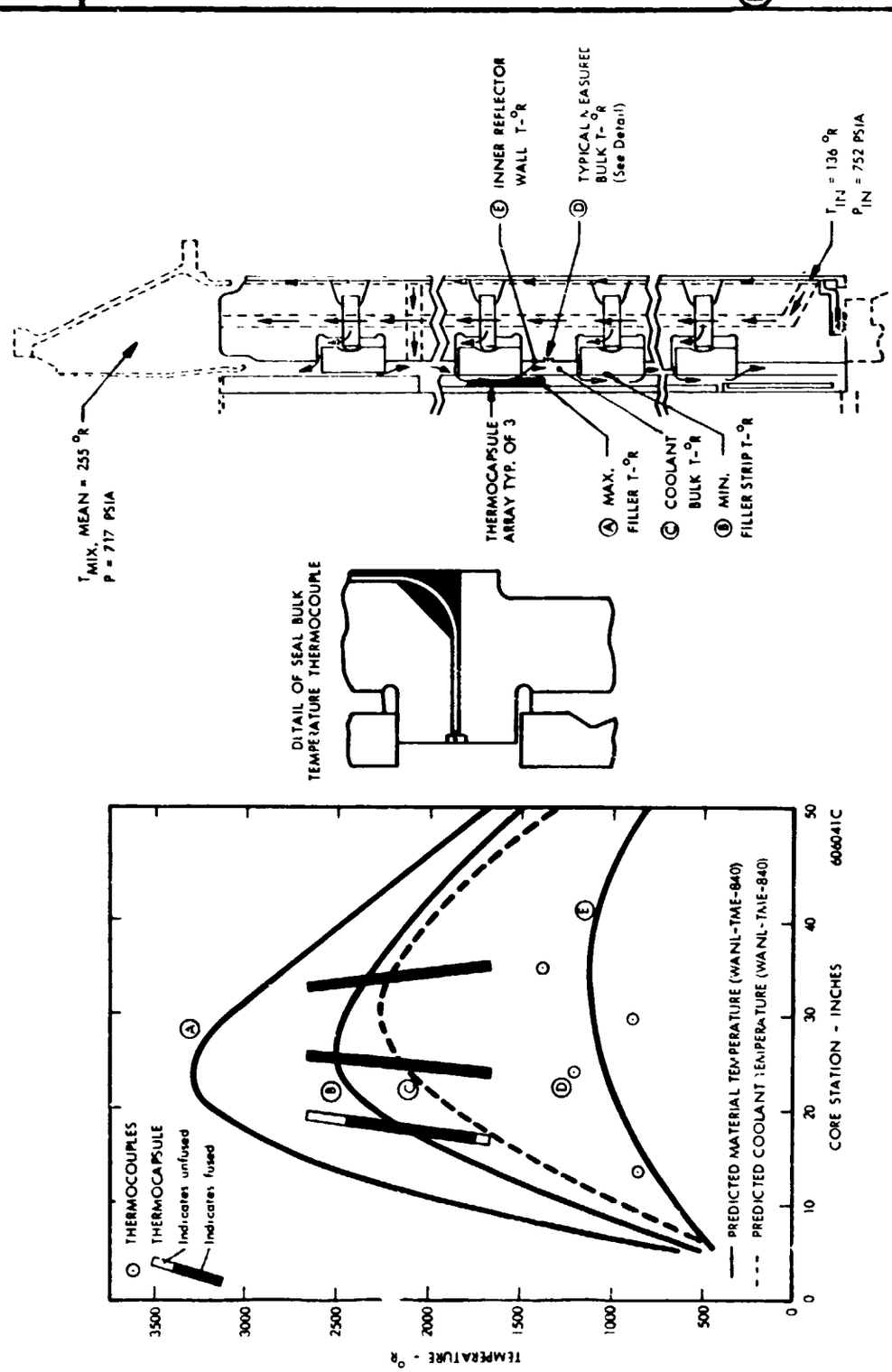

PREPARED BY	APPROVED BY	CURVE NO.

NRX-A2 EP LATERAL SUPPORT HYDROGEN AND MATERIAL TEMPERATURE AT HIGH POWER HOLD CRT 14085 (MEASURED AND CALCULATED)

FIGURE NO. 4 - 39

REFERENCE		PREPARED BY	APPROVED BY	Astronuclear

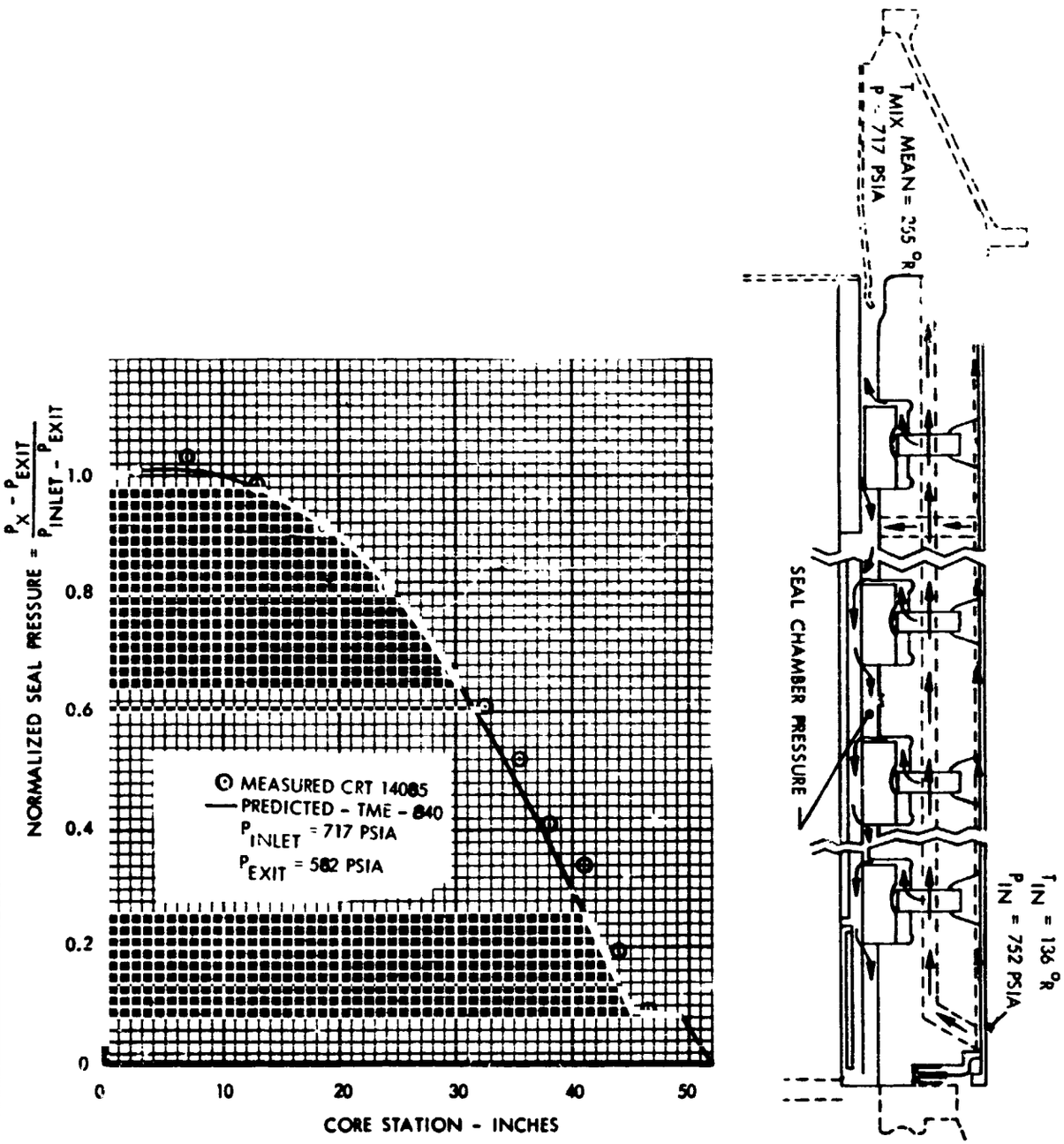

NRX-A2 EP IV NORMALIZED SEAL CHAMBER PRESSURE DISTRIBUTION AT HIGH POWER HOLD CRT 14085

FIGURE NO. 4 - 40

Reviewing the thermocouple installation, th[illegible] is entirely possib'e. The thermocouple is recessed back into the inner reflector and could be reasonably expected to measure the boundary temperature of the flow in that chamber. This type of installation was necessary to prevent damage to the filler strips, if the core should bottom out on the inner reflector either during shipping or during operation. The thermal growth of the core and the uncertainty in the relative inward movement of the inner reflector made it inadvisable to place a thermocouple inside the envelope of the ID of the inner reflector. An analysis of the effect of increased lateral support flow on the chamber temperatures is in progress. In addition a detailed analysis to determine the temperature the recessed thermocouples would indicate is planned. These results will be published.[2]

Figure 4-40 shows the comparison of the measured and the predicted normalized pressure distribution in the seal chamber at the high power hold, Time CR 14085. The reason for comparing the normalized values is that the prediction did not have the same inlet and exit pressure as in the test. From this figure it is seen that the predicted pressure distribution shape agrees very well with the measured one. The normalized pressure distributions measured during the other three steady state hold periods also agree well with calculated values shown for the high power hold at Time CR 14085 in figure 4-40.

NOZZLE

Information on nozzle geometry and heat transfer coefficients which were based on the results of Aerojet chemical firing tests, were furnished by AGC in July of 1964. This information which is given in the appendix was used in conjunction with the TNT code to calculate nozzle operating characteristics prior to the NRX-A2 test[1]. It was necessary to repeat the TNT calculation after the test in order to obtain results comparable to actual test conditions rather than planned conditions. More details of the rerun TNT are given in the following subsection. Nozzle tube conditions at the four steady state times from the TNT calculation are compared to the test values in table 4-27.

---

[1] WANL-TME-887, NRX-A2 Test Prediction Report

[2] WANL-TNR-199, Supplement 1, to be published

TABLE 4-27

COMPARISON OF TEST AND POST TEST CALCULATED
NOZZLE TUBE PRESSURES AND TEMPERATURES AT HOLDS

Control Room Time (seconds)	13790		13900		13985		14085	
	TNT	TEST	TNT	TEST	TNT	TEST	TNT	TEST
Nozzle tube inlet pressure (psia)	539	547	783	788	835	833	858	855
Nozzle tube exit pressure (psia)	481	490	636	687	729	731	748	752
Nozzle tube ΔP (psid)	58	57	97	101	106	102	110	103
Nozzle tube inlet temperature (°R)	46	45 ± 5	49	45 ± 5	49	45 ± 5	50	45 ± 5
Nozzle tube exit temperature (°R)	81	90	104	113	111	129	116	128
Nozzle tube inlet enthalpy (Btu/lb)	-72	(-72)*	-57	(-57)*	-55	(-55)*	-54	(-54)*
Nozzle tube exit enthalpy (Btu/lb)	98	149	172	217	197	288	216	287
Nozzle tube Δh (Btu/lb)	170	221	229	274	252	343	270	342
Nozzle tube Δh test/ Δh_{TNT}	1.30		1.20		1.36		1.27	

*Assumed to be the same as for the TNT calculation because nozzle inlet enthalpy could not be accurately determined from test data.

Nozzle tube inlet pressure and differential pressure agree reasonably well with calculated values. Nozzle tube exit temperatures and enthalpy increase did not agree with the calculated values, the actual nozzle heat pickup being about 30 percent more than calculated. These nozzle heat transfer test results are quite useful and will lead to improved heat transfer correlations for use in the TNT U-tube nozzle model. The ability to properly calculate nozzle coolant heating is of importance because of its effect on downstream fluid conditions. The core inlet temperature higher than calculated was partially due to the higher than expected heat pickup in the nozzle and partially due to reflector heating rates higher than predicted (although within the assigned accuracy).

Nozzle chamber thermocouples indicated temperatures which were several hundred degrees Rankine less than the actual mixed mean nozzle chamber temperatures during EP IV high power operation. These low temperatures have been primarily attributed to gas temperature at the thermocouple location lower than the average nozzle chamber gas temperature. The nozzle chamber thermocouples extend approximately 1.3 inches from the nozzle tubes into the gas stream at a location approximately 15 inches downstream of the core. The gas at the thermocouple location could be at a reduced temperature for two reasons, 1) lower temperature hydrogen exiting from the lateral support system would mix with the core flow, and 2) heat would be transferred to the 15 inch length of nozzle wall which the peripheral flow follows. Calculations have been performed which show that these effects plus thermal radiation from the thermocouple to the nozzle could account for the depressed temperatures observed.

Nuclear

FEEDBACK REACTIVITY

Feedback reactivity resulting from the presence of hydrogen coolant and temperature variation in the reactor system has been calculated by the methods developed in WANL-TME-936 and summarized in appendix A. Table 4-28 shows a comparison of measured and calculated control drum bank positions at the four steady state comparison points during EP IV. The table also includes a listing of the nuclearly significantly parameters at these four times.

TABLE 4-28

COMPARISON OF MEASURED AND CALCULATED CONTROL BANK POSITION

CR Time seconds	Average Core Temperature °R	Average Be Temperature, °R	Average Core H_2 Density lb/ft^3	Calculated Feedback Reactivity, ¢	Calculated Drum Bank Rotation[1] and Position[2], degrees	Measured Drum Bank Position degrees,	Difference (M-C), degrees
13790	1949	106	0.104	89.0	-11.6/85.9	95.5	9.6
13900	2621	151	0.128	27.2	- 3.5/94.0	99.6	5.6
13985	2780	163	0.116	10.5	- 1.4/96.1	101.2	5.1
14085	2921	173	0.119	-13.8	+ 1.8/99.3	103.2	3.9

1 Converted at 7.7¢/°R

2 Normalized to the measured cold critical position of 97.5 degrees.

The data presented is the result of post-test TNT calculations (See the startup section that follows) for the actual test profile and represents a measure of the entire prediction accuracy - both nuclear and thermal. Efforts are continuing to separate these two effects by analysis of data that is considered to be the best estimate of the true thermal and fluid flow conditions.

IMPLICATIONS OF DIFFERENCES BETWEEN MEASURED AND CALCULATED DRUM BANK POSITION

Before a comparison can be made between the measured and calculated drum bank positions one additional effect must be taken into account. This effect is the corrosion that was measured by the pre- and post test criticality checks to be worth 2.6 degrees of bank rotation. It has been added to the predicted drum bank position during the entire profile by assuming that it is proportional to the time integral of power. The resultant corrected drum bank position shown in figure 4-41 indicates that at end of life (4th hold, Time CR 14085) the error is 1.3 degrees, only 10 ¢ in reactivity. This is well within the quoted 2σ uncertainty band of ± 30¢. Comparison of the measured and calculated drum position at earlier times during the test indicates the presence of a time dependent, approximately linear error which may be associated with the diffused hydrogen effect discussed in the section on Gaseous Hydrogen Test under EP1B of Chapter 3. Efforts to understand this discrepancy are continuing.

REACTOR POWER

Reactor power was continuously measured by neutronic tank detectors and integrated power over selected time intervals was measured by rabbits. These detectors were described in a previous section. Analysis of this data is presented in this section.

Correction Factors

There are three possible correction factors which could be applied to the neutronics and rabbit calibration to convert the data to instantaneous thermal power. These are:

REFERENCE

Astronuclear

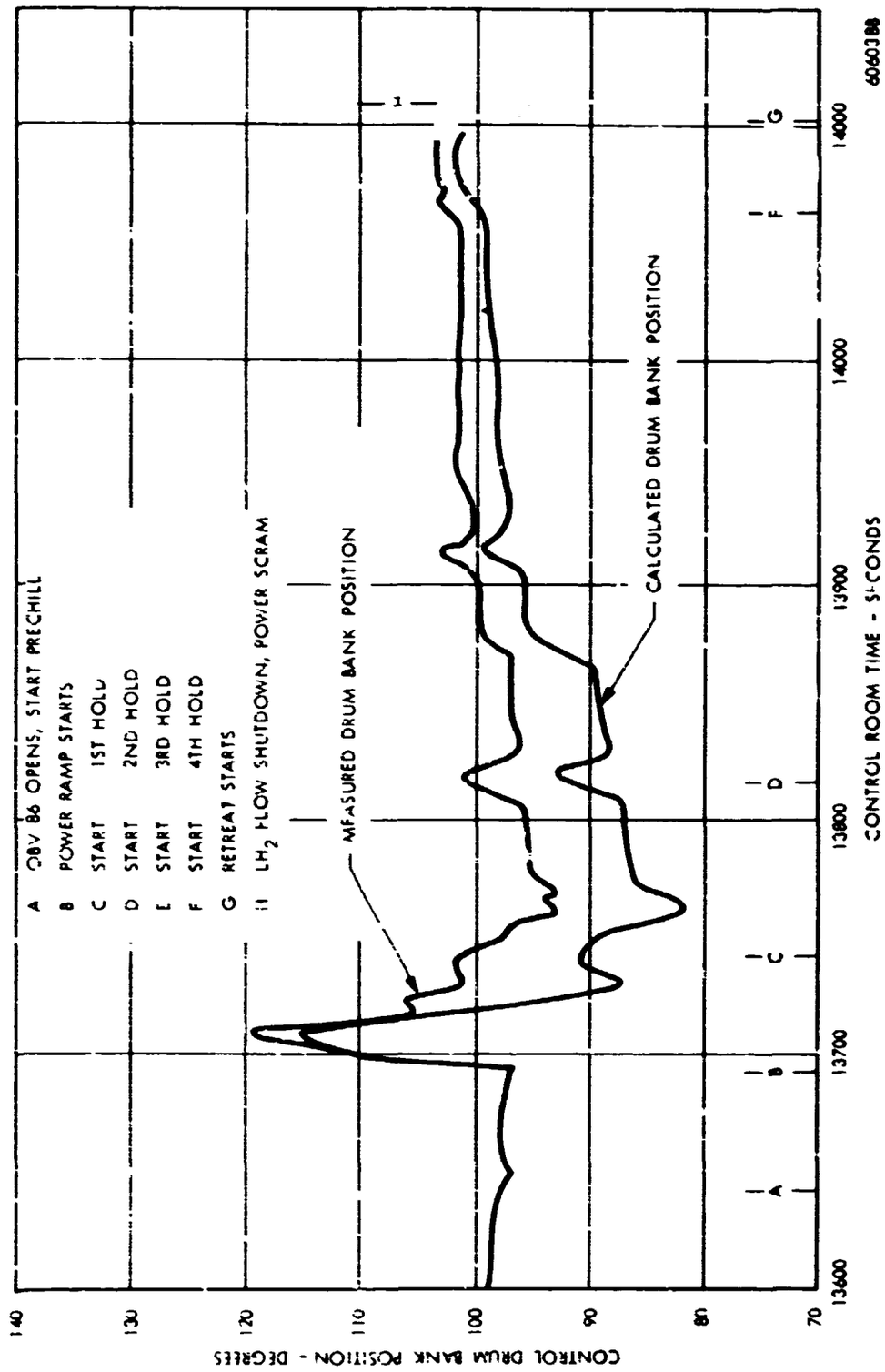

PREPARED BY	APPROVED BY	CURVE NO.

NRX-A2 EP IV CONTROL DRUM BANK POSITION BURING THE HIGH POWER TEST, MEASURED CALCULATED

FIGURE NO. 4 - 41

1) A correction for fission product buildup
2) A correction for changes in leakage flux per watt with power
3) A correction for operating drum angle.

The first correction can be obtained by running a code such as the WANL S4 code for the actual fission profile to obtain the Mev/fission of betas and gammas as a function of time through the run, adding this to the prompt (instantaneous) energy absorption rate, and then ratioing this total $\frac{\text{Mev}}{\text{Fission}}$ absorbed to the 190 Mev/fission previously assumed for the calibration. Correction factors at selected times during the EP IVA and EP V runs are given in tables 4-29 and 4-30.

The second correction, a correction for changes in leakage flux per watt with changes in power, flow rate, and external detector position has also been considered for correcting EP IVA data. In order to estimate the effects of temperature and flow rate on the changes in radial and axial leakage per watt of thermal power, two dimensional transport calculations were run by using an 8 group (3 fast and 5 thermal) TDC code mockup of the hot, full flow and cold, no flow conditions. Based on these calculations, the axial leakage fluxes were calculated as a function of position on the external radial and axial surfaces. Assuming that the radiation is emitted, isotropically at the surface of the reactor, the change in flux at the radial or axial point would be proportional to the area weighted integral of the radial or axial leakage currents, respectively. It was further assumed that the detector response both of the axially located rabbit and the radially located neutronics tank, was proportional to fast neutrons of energies greater than 0.82 MEV. Based on these assumptions the decrease in radial leakage was 7.7 percent and in axial leakage 5.8 percent. Neither of these assumptions is strictly correct. For example, the difference in radial leakage at the core midplane where the leakage would be more important if the radiation were peaked in a direction perpendicular to the reactor surface is 4 percent rather than 7.7 percent. The change in leakage over the nozzle end surface varies from 1 percent at the centerline to 7 percent at the outer reflector surface as compared with 5.8 percent for the assumed isotropic emission. The axial leakage would be further reduced by the fact that the sulfur rabbit sees neutrons of energy > 2.9 Mev. rather than 0.82 Mev and the

TABLE 4-29

CORRECTION FACTORS FOR EP IVA FOR BUILDUP OF DECAY GAMMAS AND BETAS

Control Room Time (seconds)	Correction Factor
13790	1.000
13900	1.004
13985	1.007
14085	1.008

TABLE 4-30

CORRECTION FACTORS FOR EP V FOR BUILDUP OF DECAY GAMMAS AND BETAS

Control Room Time (seconds)	Correction Factor
18600	1.000
18750	1.003
18900	1.001
19400	1.014
19600	1.011

higher the neutron energy, the less sensitive the correction is to the cold to hot variations. The radial leakage correction is further complicated by the lack of a detector to compensate for gamma rays at high power levels. That is, the detector reads current induced by both gamma ionization and neutron absorption, but due to its construction, it subtracts out the gamma contribution unless the absolute gamma levels are too high. However, beyond a certain gamma level the chamber fails to subtract out all of the gamma ionization and hence, the detector reads high. Beyond this point, the lack of compensation increases and the divergence between the detector response and the leakage rate should increase. This error has been estimated to be as much as 20 percent in the high power range (1). This error, however, must be at least partially offset by the decrease in radial leakage with increase in power previously mentioned since the compensated ion chamber follows the rabbit determination fairly closely. (table 4-31). Thus, due to the fortuitous cancellation of the lack of gamma compensation by the relatively larger decrease in leakage in the radial direction, it appears that the linear channel No. 2 data follows the nozzle rabbit data fairly closely.

Also shown in table 4-31 is a comparison of linear channel No. 1 with linear channel No. 2 data. The linear channel No. 1 detector was operated in an uncompensated mode while the channel No. 2 detector was operated in a compensated mode. The differences between the two detectors are large even at low power. These large differences are unexplainable.

Log power signals, although quite accurate for control purposes, are difficult to read on Sanborn charts. A 2 percent Sanborn error is equivalent to 38 percent error in power and since Sanborn data frequently exhibits one to two percent error in span and offset, a $\pm$ 30 percent deviation between log indications is not unusual.

All multiplexed power indication data was found to be erroneous and hence was not used. Therefore, only the rabbit data and the linear No. 2 data as read from Sanborn charts and corrected for span and zero offset, was used in the power analysis.

---

[1] NTO-M-0671, Reactor and Neutronics Summary Report NRX-A2 Test Series, Part 1, H. Mortenson, October 29, 1964

TABLE 4-31

NEUTRONIC POWER INDICATIONS DURING EP IVA*

Instantaneous Time	Irradiation Interval From	Irradiation Interval To	Linear No. 2 (Percent Design Power)	Linear No. 1 (Percent Design Power)	Rabbit (Percent Design Power)	Percentage Difference Lin. No. 1 vs. Lin. No. 2	Percentage Difference Rabbit vs. Lin. No. 2
13416	13408	13606	0.160	0.116	(0.162)+ 0.156	-27	+1.7
13790	13745	13804	46.4	36.6	(47.3) 46.8	-21	+1.9
13900	13819	13946	78.2	72.4	(78.6) 75.5	-20	+0.5
13985	13960	14001	84.9	69.1	(85.7) 85.8	-19	+0.9
14085	14004	14090	90.5	72.8	(92.6) 88.7	-20	+2.3

*Taken from NTO-M-0671, Reactor and Nuetronics Summary Report, NRX-A2 Test Series, Part I, H. Mortenson, October, 1964

+ ( ) indicates corrected to instantaneous value

without brackets indicates experimental result for rabbit irradiation interval

Based on the previous discussion, it appears that the behavior of the linear neutronics in the detector tank is too complicated to understand. However, since it agrees fairly well with the nozzle rabbit which theoretically should be easier to understand, then an effort should be made to obtain leakage correction factors for the nozzle rabbit which could be also applied to the neutronics data. Based on the calculations to date, it appears that the correction factor for the nozzle rabbit should be in the direction of increase of the indicated thermal power with increase in power. To calculate the exact correction factor would require modification of one of the two existing two dimensional transport codes to obtain a printout of the angular leakage currents and then an integration over angle and surface area to obtain the flux arriving at the external detector point. Since this correction is believed to be less than 5 percent and since calculations of this type are not believed to be any more accurate than this uncertainty, this correction has presently been omitted. Third, a correction to account for differences in drum angle between operating and calibration must be made. A correction for the operating vs calibration drum angle of + 1.3 percent has been included as well as the corrections for fission product buildup as listed in tables 4-29 and 4-30 for the stated hold points. Thus, both the measured neutronics and rabbit power determinations during EP IVA have been corrected to the values shown in table 4-7. The total energy release for the thermal and neutronics data, which were obtained by integrating under the respective power vs. time curves, are also given in table 4-32.

Estimated Accuracy of the Data

Based on a calibration to LASL standards, the relative precision of radiochemical wire analysis has been found to be $\pm$ 3 percent which is also consistent with the accuracy of analyzing different isotopes in the same solution. However, differences of 9 percent exist among various laboratories analyzing the same standard solution and WANL and USNRDL using their own respective calibrations determined the LASL solution to contain 12 and 9 percent less fissions, respectively, than quoted by LASL. Thus, it appears that the LASL value is biased toward the higher values. Assuming other uncertainties as quoted in

TABLE 4-32

COMPARISON OF INTEGRATED ENERGY RELEASE DURING NRX-A2 TESTS

Experimental Plan	Detector	Total Fissions	Energy Release + w - sec
EP II	U-Al wire calibration	2.62×10^{17}	7.99×10^{6}
EP IV	Linear Neutronics	1.07×10^{22}	3.26×10^{11} (3.25×10^{11})*
	Rabbit	-----	-----**
	Thermal	1.12×10^{22}	3.41×10^{11}
EP V	Linear Neutronics	1.35×10^{21}	4.08×10^{10} (4.26×10^{10})*
	Rabbit	1.40×10^{21}	4.24×10^{10}
EP IV and EP V	Linear Neutronics	1.21×10^{22}	3.67×10^{11}
	Rabbit	1.19×10^{22}	3.59×10^{11}
	Thermal	1.25×10^{22}	3.81×10^{11}
	Post Test Radiochemistry	1.21×10^{22}***	3.68×10^{11}

* From NTO-M-0671 - Part IV, 14 December 1964

** Integral rabbit data lost by melting of pellet

*** From NTO-02-006

\+ Based on assuming 190 Mev/fission thermal energy absorbed averaged over the run.

WANL-TNR-158[1], the accuracy of the PAX power calibration on which the EP II calibration is based, is estimated to be −13 percent to + 5 percent. To this inaccuracy estimate must be added the inaccuracies of the rabbit sulfur activity determination which is quoted to be ± 3 percent. Hence, the overall inaccuracy of the rabbit power determination is estimated to be −13.4 to + 6.0 percent. A comparison of the neutronics and rabbit power determinations for EP IVA together with their uncertainty margins are presented in table 4-7.

[1]WANL-TNR-158, Preassembly Experiment (PAX) in Support of NRX-A2

STARTUP AND SHUTDOWN

Thermal and Fluid Flow - Startup

REACTOR

Based on the results of the EP IB liquid hydrogen test described in Chapter 3 the reactor flow was expected to lag the venturi flow during the first 15 seconds of the startup. Reactor flow during this interval was obtained from NRX-A1 cold flow test results[1], and the power demand had been reprogrammed prior to EP IV to give the desired 50°R/sec nozzle chamber temperature startup. Given on figure 4-42 are the NRX-A2 EP IV flow demand profile, the LH_2 flow profile measured at the venturi meter downstream of the pump, FE-7, and the reactor flow rate which was calculated from measured nozzle chamber conditions. Super-imposed on the same figure in the proper relation to the demand flow profile are the NRX-A1 and NRX-A2 EP IB second LH_2 test reactor flow rates. These results show that the actual reactor flow rate during the startup was very similar to that which was expected. The flow lag was analyzed in some detail for NRX-A2[2].

The power, flow, and station 32 core material temperature control demands as they were cut on the program drums, are given in figure 4-43, except that power demand was on a log scale rather than a linear scale. After the prechill the controller was switched to run and the program drums rotated simultaneously and were stopped at the planned hold points.

The dotted curves on figure 4-44 are the power demand and the planned nozzle chamber temperature while the actual power and chamber temperature are given by the solid curves. It can be seen that the power was higher than programmed during the early stage of the startup (Time CR 13700 to 13720) and the nozzle chamber temperature increased at about 125°R/sec, while 50°R/sec was the expected rate. At Time CR 13712 designated on the figure, station 32 temperature control loop became effective in the control system and began to trim the power thereby controlling the startup temperature ramp. The effect of the high power on core material temperatures for this same time interval are given on figure 4-45. This higher power (than programmed during startup) was due to an error in setting up the programmer[3].

1 WANL-TME-773 and Supplement 1, NRX-A1 Performance
2 WANL-TME-1017, NRX-A2 Flow Lag, October 26, 1964
3 NTO-R0008, NRX-A2 Test Prediction Report, July 1964

REFERENCE		PREPARED BY	APPROVED BY	Astronuclear

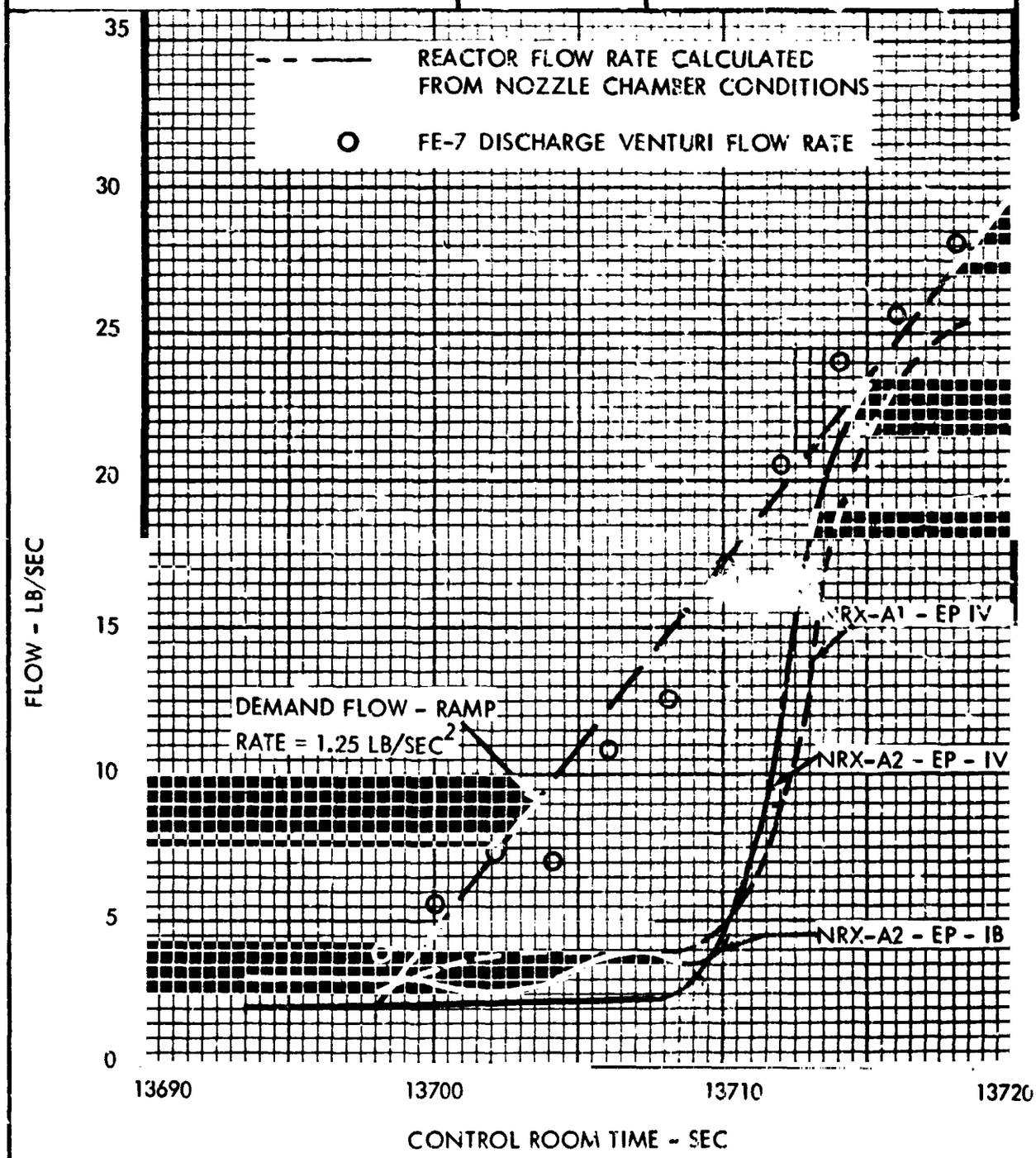

STARTUP LH_2 FLOW LAG

FIGURE NO. 4-42

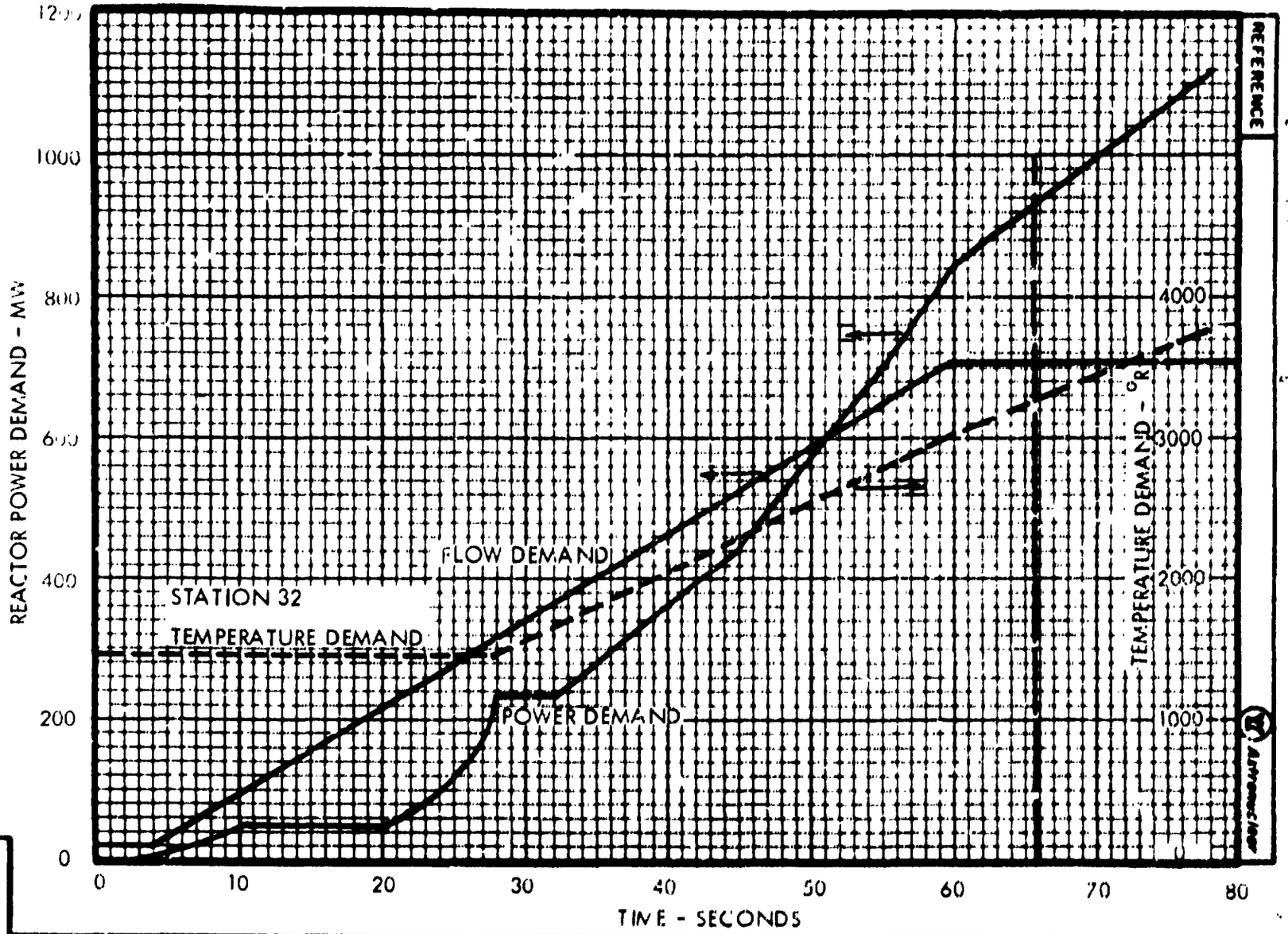

FIGURE NO.	POWER, FLOW AND TEMPERATURE DEMANDS	PREPARED BY	APPROVED BY	CURVE NO.
4 - 43				IV-36

REFERENCE		PREPARED BY	APPROVED BY	Astronuclear

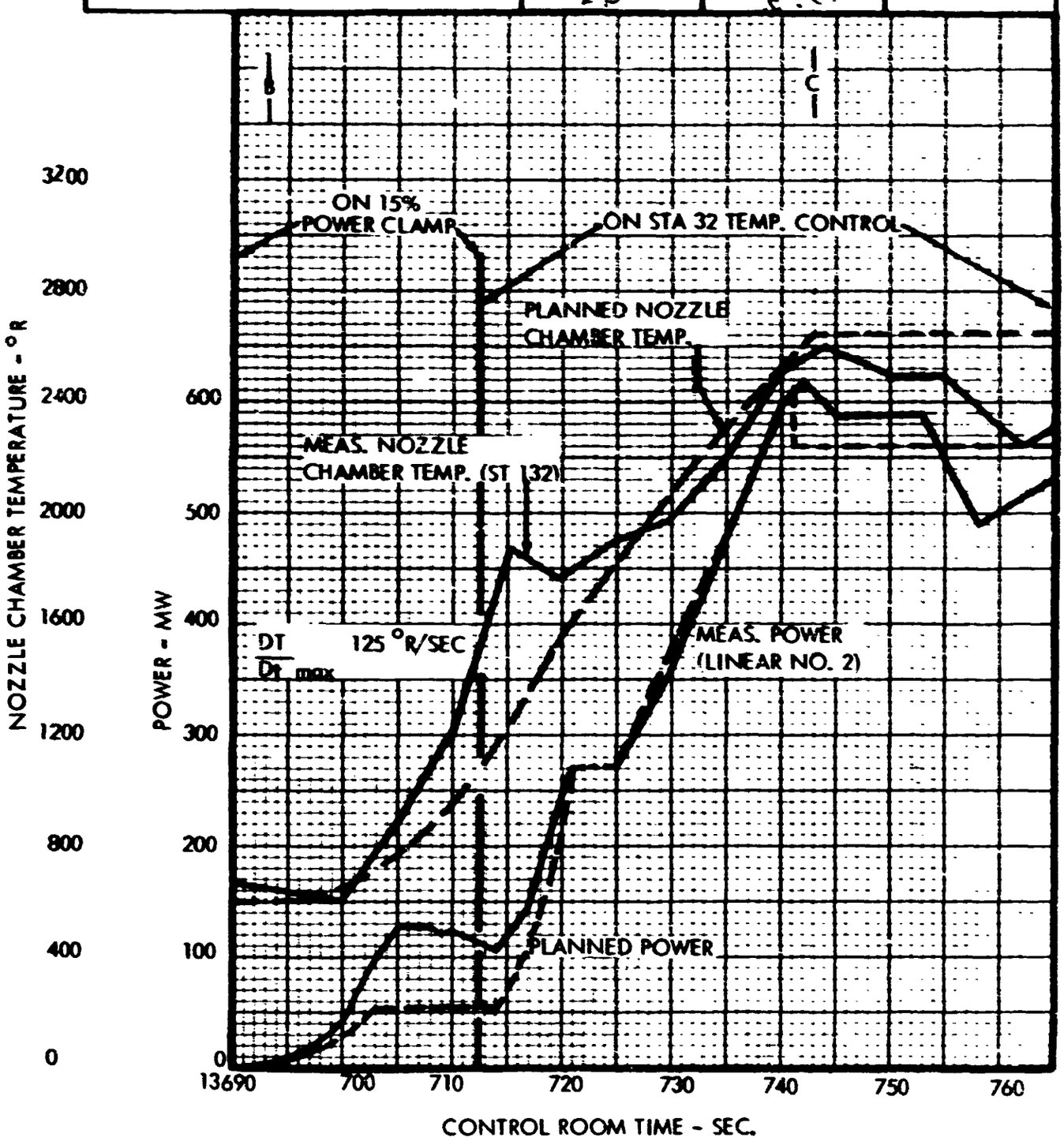

NRX-A2 EP IV STARTUP POWER AND NOZZLE CHAMBER TEMPERATURE	CURVE NO	FIGURE NO.
		4 - 44

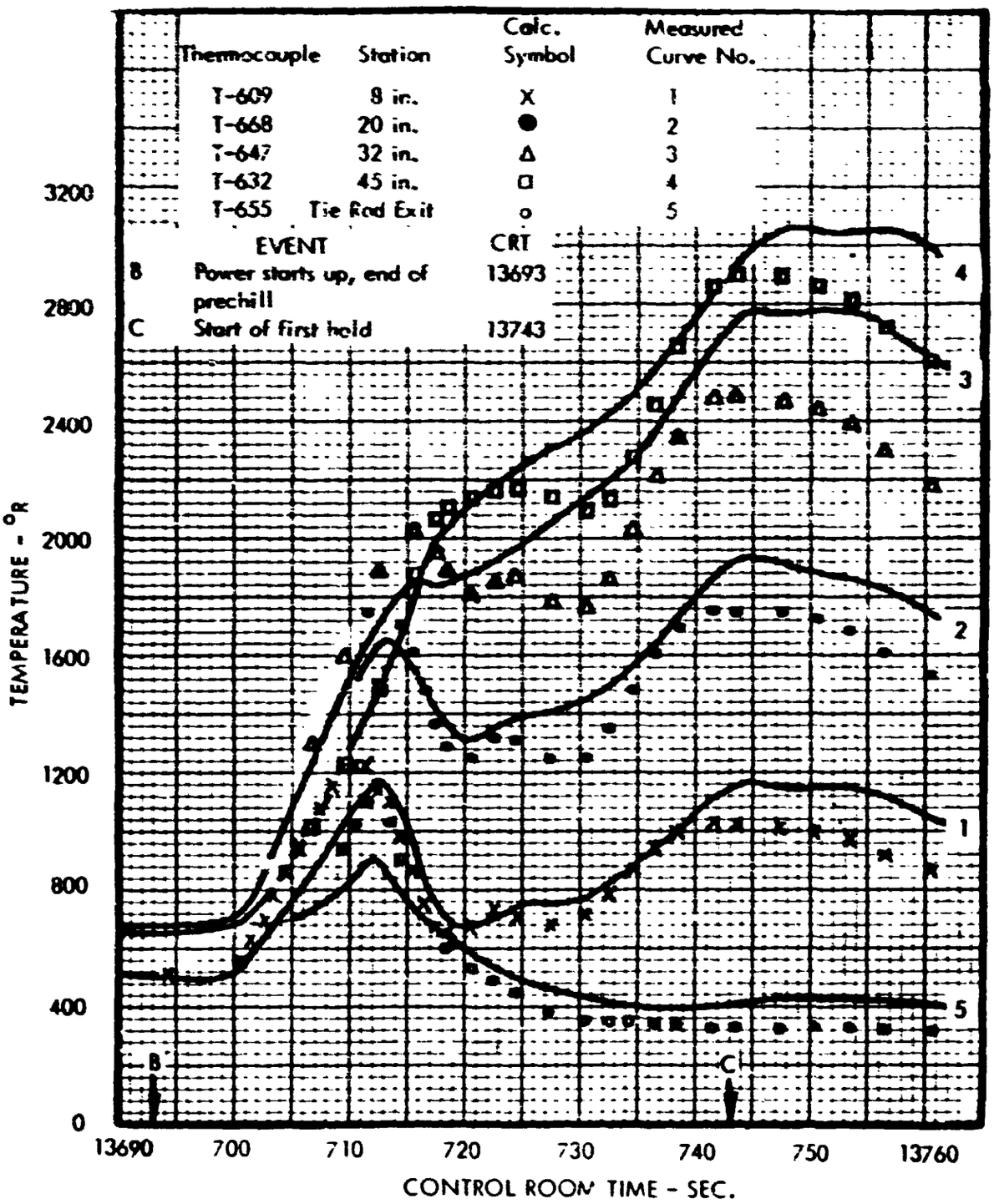

FIGURE 4-45, CORE MATERIAL TEMPERATURES AND TIE ROD EXIT TEMPERATURES DURING STARTUP

TNT CALCULATED AND MEASURED STARTUP CONDITIONS

Pre-test predicted operating conditions for the NRX-A2 test were calculated with the TNT reactor model and given in WANL-TME-887[1]. Because the operating power and flow profiles during the test were considerably different from planned, the pre-test calculations were no longer applicable. In order to provide a better comparison of test data and calculations, operating conditions were recalculated using the TNT code and the test power and flow. There were no changes in the reactor model from that used in the pre-test calculations.

Flow rate used was that calculated from nozzle chamber conditions shown in figure 4-42 while power was obtained from linear number 2 neutronic power channel, increased by the appropriate ratio to coincide with thermal calculated power at the steady state hold times. The calculation was performed from the beginning of startup through the entire test profile. Steady state high power operation comparisons were in very poor agreement because of the higher than expected nozzle heat pickup and reflector heating rate. A comparison of TNT and measures nozzle operating conditions was given in table 4-27. On the basis of these comparisons the TNT reactor model is being adjusted. Because these variations in heat pickup have a small effect on startup calculations, a comparison of measured and calculated temperatures and pressures during prechill* and startup are included in this section as a measure of the ability of the TNT calculation to reproduce transient reactor conditions.

These comparisons of TNT calculated and test results during prechill and startup show that the TNT model closely reproduced the reactor condition during this transient. In particular, the transient core temperature distribution agreement was remarkably good.

The TNT comparisons are given on the figures listed below, and a discussion is included in the following pages.

TNT AND TEST STARTUP COMPARISONS

Figure No.	Comparisons Of
4-45	Core Material Temperatures and Tie Rod Exit Temperature

*As noted above, the TNT was rerun from the beginning of startup. All TNT results for the prechill period (to Time CR 13693) are from the pretest TNT.

1 WANL-TME-887, NRX-A2 Test Prediction Report, July 1964

4-2	Reflector Inlet and Outlet Temperatures
4-46	Core Inlet Pressure and Core ΔP
4-47	Reflector Inlet and Outlet Pressure and Reflector ΔP

CORE-STARTUP PERIOD

Figure 4-45 shows a comparison of measured and TNT post test calculated selected material temperatures in the core region during the startup period (Time CR 13693 to CR 13743).

This comparison shows that the core temperature distribution during the transient is very closely reproduced by the TNT code. However, the calculated temperatures are slightly low as steady state is approached. This discrepancy is presently being investigated with an improved model.

Figure 4-46 is a comparison of measured and TNT post test calculated values of core inlet pressure and core pressure drop. The measured values of core pressure drop and core inlet pressure agree very well with those calculated during this startup period.

REFLECTOR - STARTUP

The azimuth temperature variation at the reflector inlet, reflector outlet, dome end plenum, and core inlet at the end of prechill (Time CR 13693) were given in figure 4-4 and 4-5. This figure shows a similarity of geometric temperature variation in all plenums with a minimum in the vicinity of the nozzle feed line (θ = 120 degree location), and in some cases an indication of a lesser temperature depression opposite the feed line (θ = 300 degrees). The flow rate and system pressures began to increase rapidly at Time CR 13709 and shortly thereafter the temperature asymmetry was gone. No adverse effect of this temperature asymmetry during the early stages of startup is evident.

In figure 4-48 the two extreme fluid thermocouple indications at the reflector inlet plenum are shown with the pressure at the same location. In the upper part of the figure is the azimuth temperature variations when the reflector inlet pressure is less than critical pressure and when it exceeds critical pressure. It is noted that the azimuth temperature variation has been drastically reduced. At the core inlet the asymmetry persisted for a longer time, however it disappeared on the ramp to the first power hold. Figure 4-49

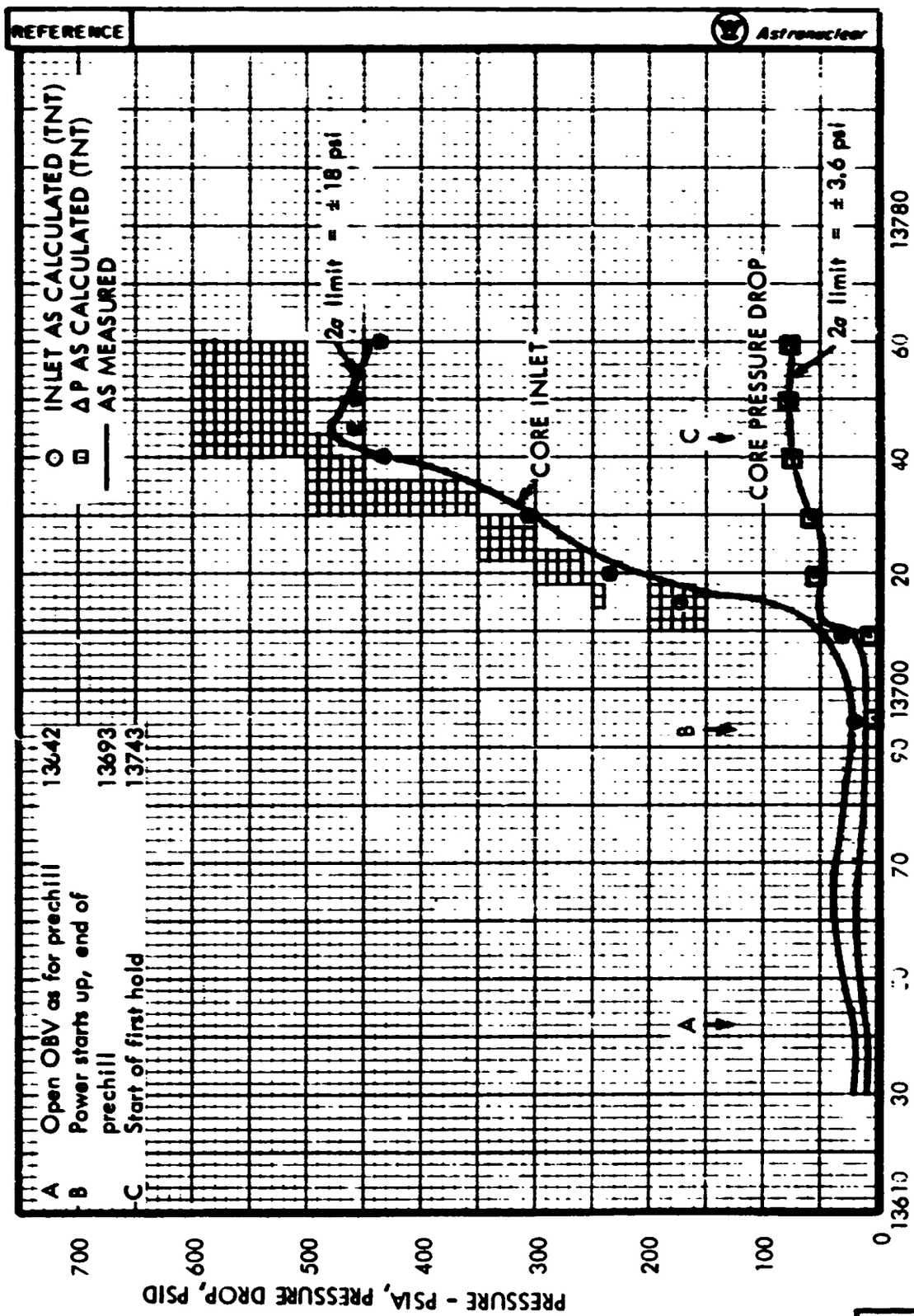

CORE INLET PRESSURE AND CORE ΔP VS. TIME

PREPARED BY	APPROVED BY	CURVE NO

FIGURE NO.
4 - 46

REFERENCE

Astronuclear

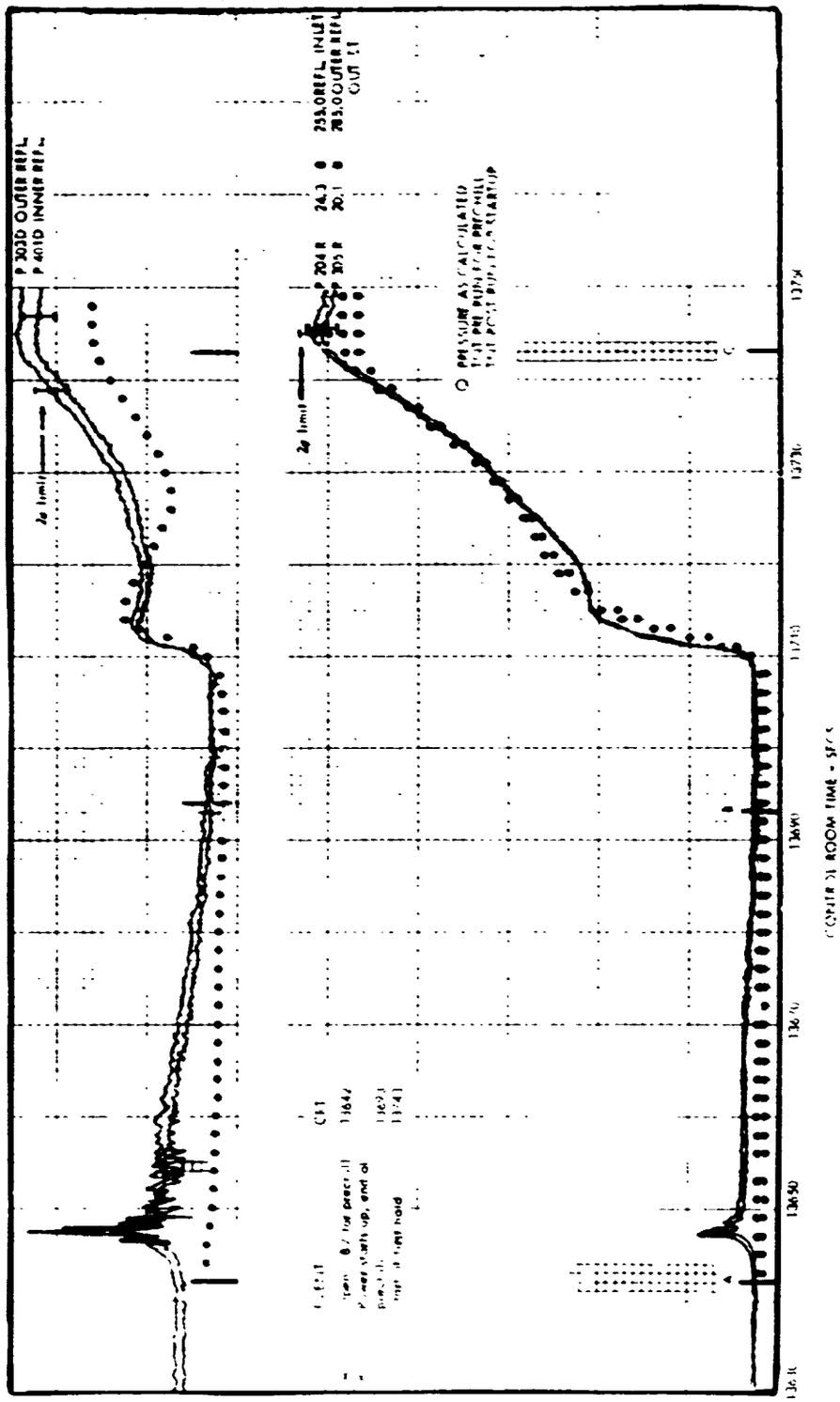

PREPARED BY	APPROVED BY	CURVE NO.

NRX-A2 EP IV PRECHILL AND STARTUP REFLECTOR INLET, OUTLET AND DIFFERENTIAL PRESSURE TIME HISTORIES

FIGURE NO.
4 - 47

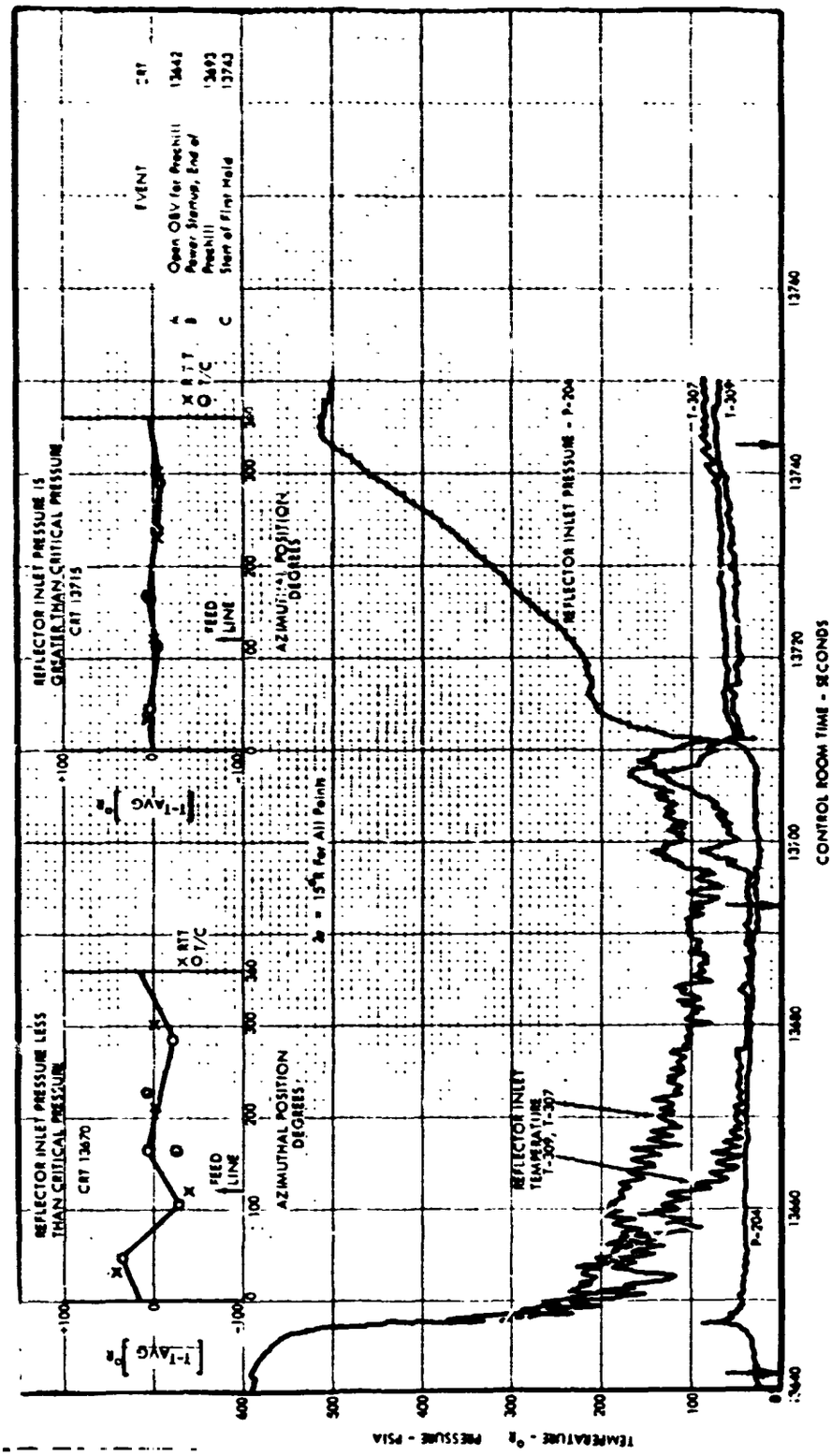

FIGURE 4 - 48

PRESSURE AND TEMPERATURE TO ILLUSTRATE ASSEMBLY AT REFLECTOR INLET

shows that the asymmetry was still in evidence at Time CR 13720 but not at 13790, during the power hold. At this time the measured values are all within the 2σ error limit. The azimuth temperature variation is probably associated with two phase flow in the nozzle, but the times at which it reduces drastically cannot be directly correlated with exceeding hydrogen critical pressure, and as noted above, the asymmetry persists at the core inlet for 10 to 15 seconds longer than at the reflector inlet. As far as the EP IV high power reactor operation is concerned it is concluded that the thermal asymmetries cause no adverse effect during the startup and are not evident during the steady holds.

The TNT calculated and test values of reflector inlet and reflector outlet fluid temperatures during the prechill and startup were given in figure 4-7 and show excellent agreement.

The lower curve of figure 4-47 is a comparison of calculated (TNT post run with test power and flow schedules input) and measured values of the reflector inlet and exit pressure. During the prechill and startup the calculated values are within the 2σ limit of the measured values. At the start of the first power hold (Time CR 13743) the calculated values are about 10 psi below this 2σ limit.

The upper curve in figure 4-47 is a comparison of the calculated and measured pressure drops. As seen on the figure the calculated values are below the measured by about 8 psid. There are several reasons for this; first, the flow annulus between the inner and outer reflector has been calculated using measured temperature and pressure conditions in the reactor during the power run. This reevaluation showed the annulus width to be an average of 0.092 inch, compared with the value of 0.108 inch used for the TNT model. This change in annulus width in conjunction with the associated impedance ring change represents an increase in the total flow impedance of the reflector system. Secondly, the percent of total reactor power measured in the reflector region was 15 percent higher than that used for post test TNT calculations. This increase in reflector power results in increased pressure drop across the reflector system. These two items and the measured reflector inlet temperature have been incorporated into the post test MCAP-TOSS reflector steady state model, and the post-test values calculated at the high power hold (Time CR 14085) give an outer

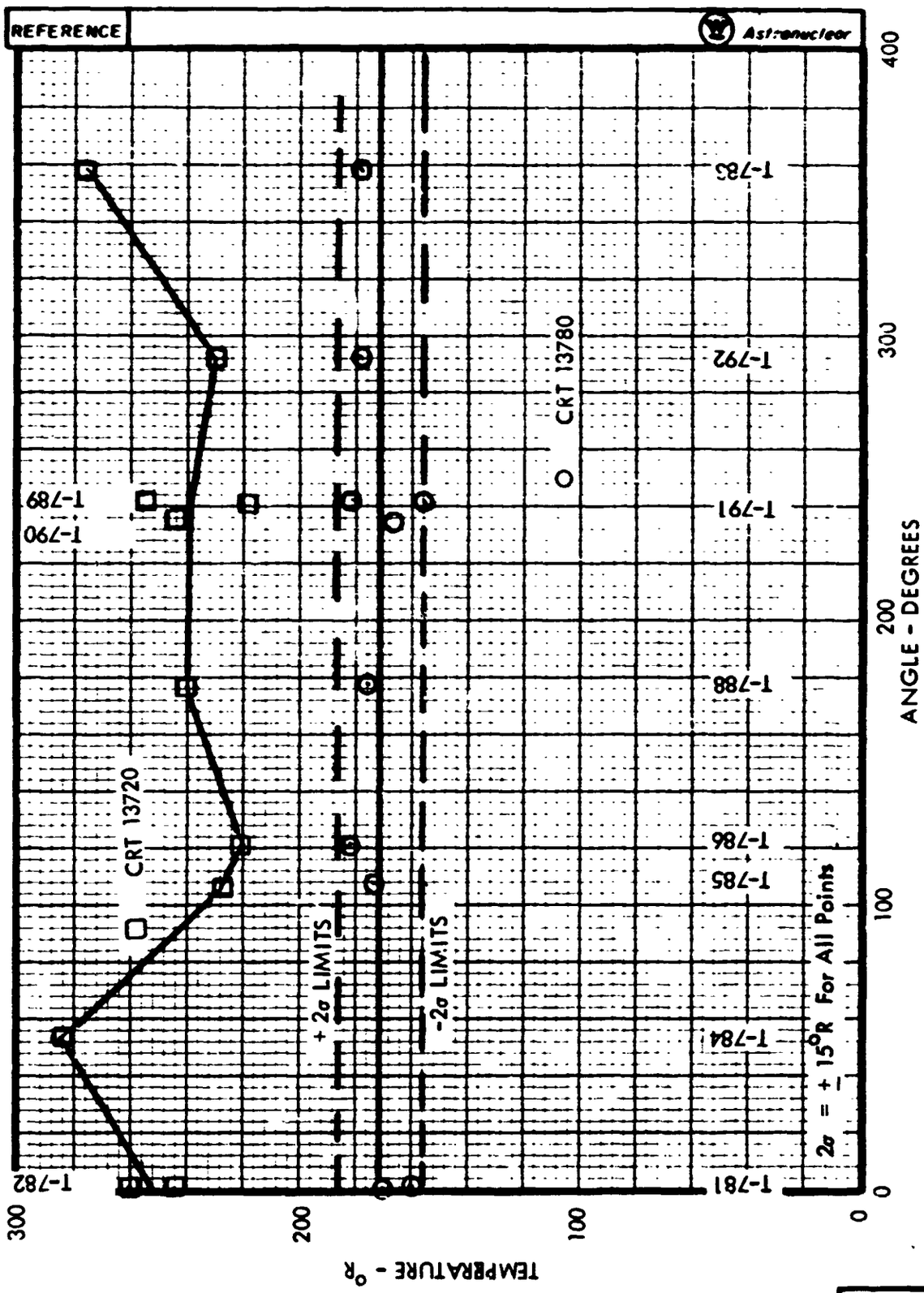

CURVE NO.	APPROVED BY	PREPARED BY

CORE INLET AZIMUTHAL TEMPERATURE VARIATION AT CRT - 13720 AND CRT 13780

FIGURE NO.
4 - 49

reflector pressure drop which is 0.3 psid lower than the measured value and is well within the 2σ limit of 1.8 psid for this measurements.

The small spikes in reflector pressure and pressure drop, shown on figure 4-47 occurring at about Time CR 13648 is most likely due to the closing of bypass valve AVV-11, resulting in a small surge and increase in flow at this time.

The upper and lower material temperature traces for both the inner reflector and the control drum are shown in figure 4-50. The inner reflector chills at a faster rate than the control drum, however during a power run these temperatures run higher than the control drum and therefore during the startup these temperatures cross and rise above the control drum temperatures.

Figure 4-51 shows selected material temperatures of the outer reflector during the prechill and startup. The temperatures continue to drop even after the startup has been initiated. The station 45 thermocouple reaches its minimum value at Time CR 13716 and then begins to rise. Station 32 and 8 being further downstream reach their minimum values at the later times of Time CR 13725 and 13729 respectively.

Thermal and Fluid Flow - Shutdown

At the completion of the run the programmers were switched to retreat, i.e. the demand profiles on figure 4-43 moved in the reverse direction from the hold point indicated by the vertical dotted line. Power and flow began to decrease and nine seconds later a manual flow shutdown and power scram were initiated due to apparent loss of Dewar pressure. The planned shutdown was to retreat with the nozzle chamber temperature decreasing at 50°F/sec until nozzle chamber temperature had been reduced to 2200°R, then to initiate a flow shutdown and power scram. Calculations[1] indicated that the scram at the end of this retreat would result in a maximum nozzle chamber temperature decrease of 135°F/sec. The scram at shutdown of the EP IV test occurred when nozzle chamber temperature had only decreased about 350°R from the maximum of 3815°R on the retreat, and was consequently more severe than the planned shutdown.

[1]WANL-TME-887, Supplement IV, NRX-A2 Test Prediction Report

REFERENCE

Astronuclear

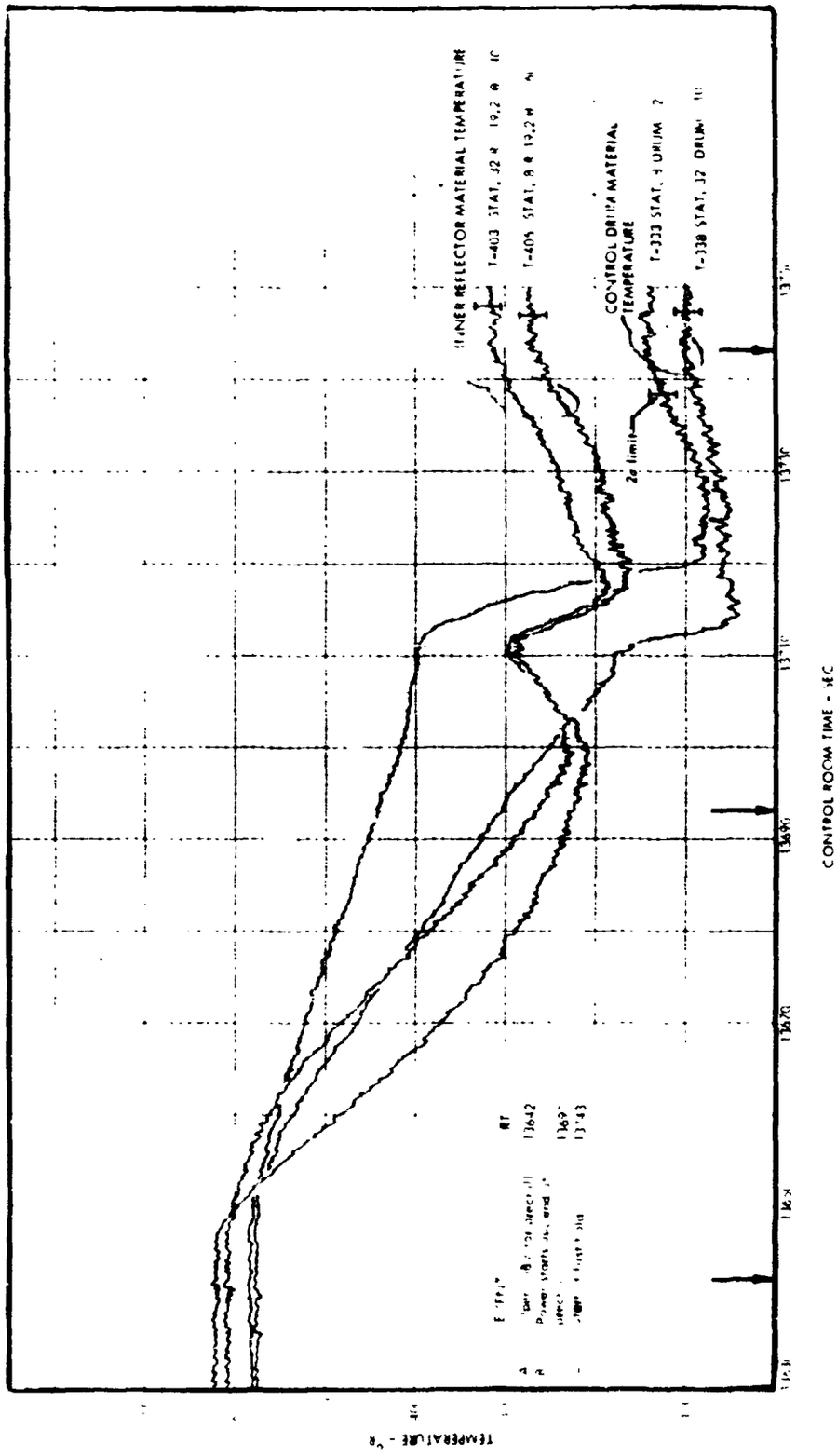

PREPARED BY	APPROVED BY	SURVE NO

NRX-A2 EPIV PRECHILL AND STARTUP SELECTED INNER REFLECTOR AND CONTROL DRUM MATERIAL TEMPERATURE TIME HISTORIES

FIGURE NO.
4 - 50

REFERENCE

Astronuclear

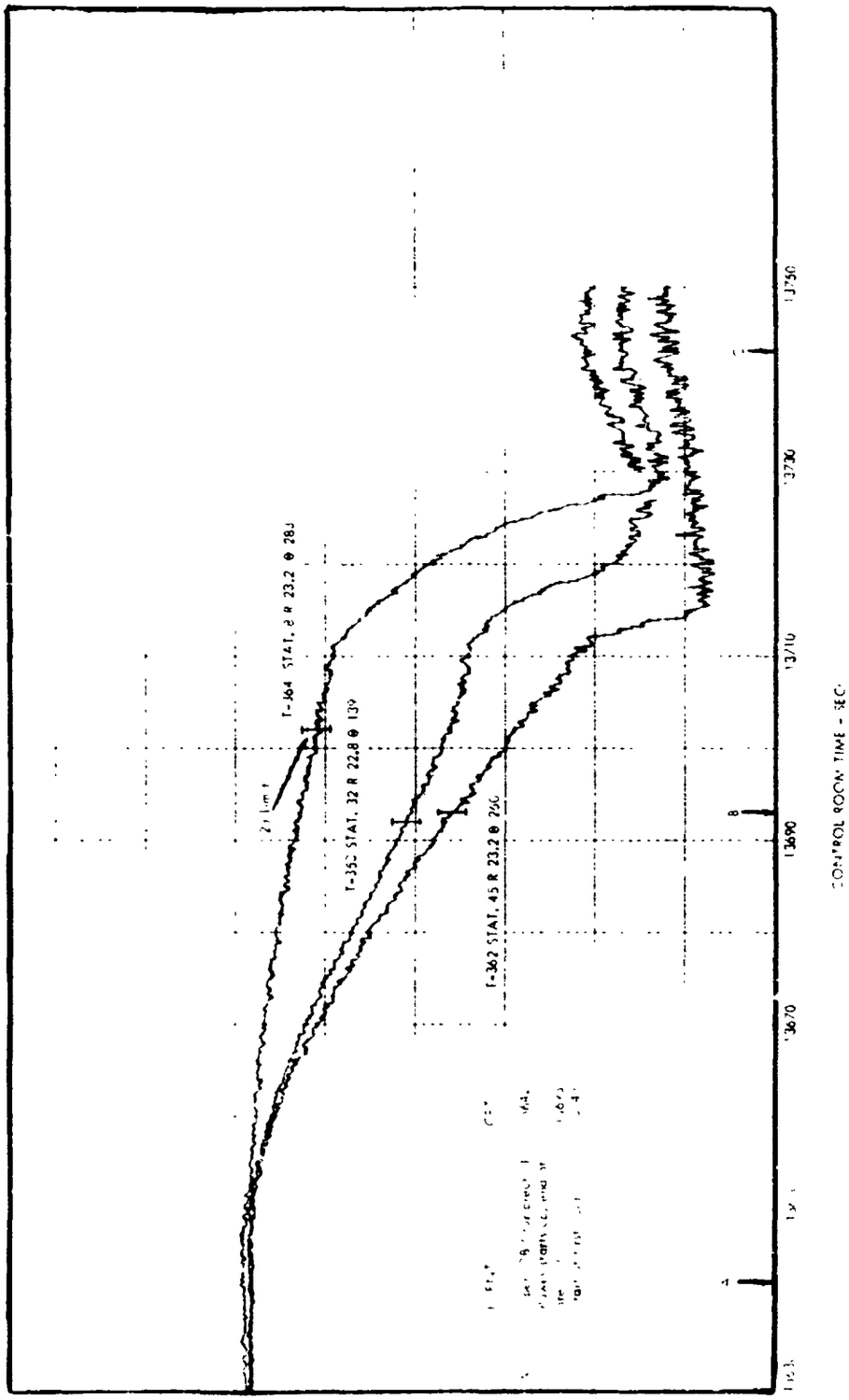

PREPARED BY	APPROVED BY	CURVE NO.

NRX-A2 EP IV PRECHILL AND STARTUP SELECTED OUTER REFLECTOR MATERIAL TEMPERATURE TIME HISTORIES

FIGURE NO. 4 - 51

A comparison of the planned and test nozzle chamber temperatures for the shutdown interval is made in figure 4-52. The maximum nozzle chamber temperature decrease rate was 350°R/sec versus the 135°F/sec planned. Although the nozzle chamber thermocouple was not giving the mixed mean nozzle chamber temperature, its rate of change is probably a good indication of the decrease rate of chamber temperature. Initial chamber temperature decrease rates were greater than 50°R/sec preceding the scram because there was a lag in the response of the reactor power to the demanded downward ramp and then a sudden decrease in reactor power of over 100 MW. This is illustrated by comparison of the shutdown demands to the measured variables in figure 4-53. The bottom curve of this figure shows that flow responded well to demand flow. The middle curve shows that temperature demand had resulted in the maximum +15 percent power trim and had no control effect for the shutdown. The top curve of this figure indicates that there was a six-second delay in response of the power to the power demand. When the power did respond to the demand, there was a sudden decrease of over 100 MW just as the flow had begun to decrease resulting in a cooldown rate in excess of 50°R/sec. If the flow shutdown and scram had not occurred, the nozzle chamber temperature decrease rate would have approached 50°R/sec as the retreat continued. The delay in power response to the demand is attributed to saturation of the power demand signal amplifier which has been replaced.

Tie rod exit gas temperatures peak at 1200°R, the exact limit for a transient during EP IV. Tie rod time-temperature traces were given in figure 4-26. Core inlet temperature for the shutdown interval is given in figure 4-54. The minimum core inlet temperature during the shutdown was 150°R.

At the time the reactor was scrammed, ambient GH_2 was introduced into the feedline upstream of the mixing chamber. The PCV-41 pressure control loop was activated to introduced gaseous hydrogen at 50 percent of the nozzle inlet pressure which existed just prior to the scram. As indicated by the reactor flow rate in figure 4-52, there were some oscillations caused by the control loop as the GH_2 forced the 200 pounds of LH_2 out of the system piping and mixing chamber. These oscillations were evident in the nozzle inlet pressure also, as shown in the figure.

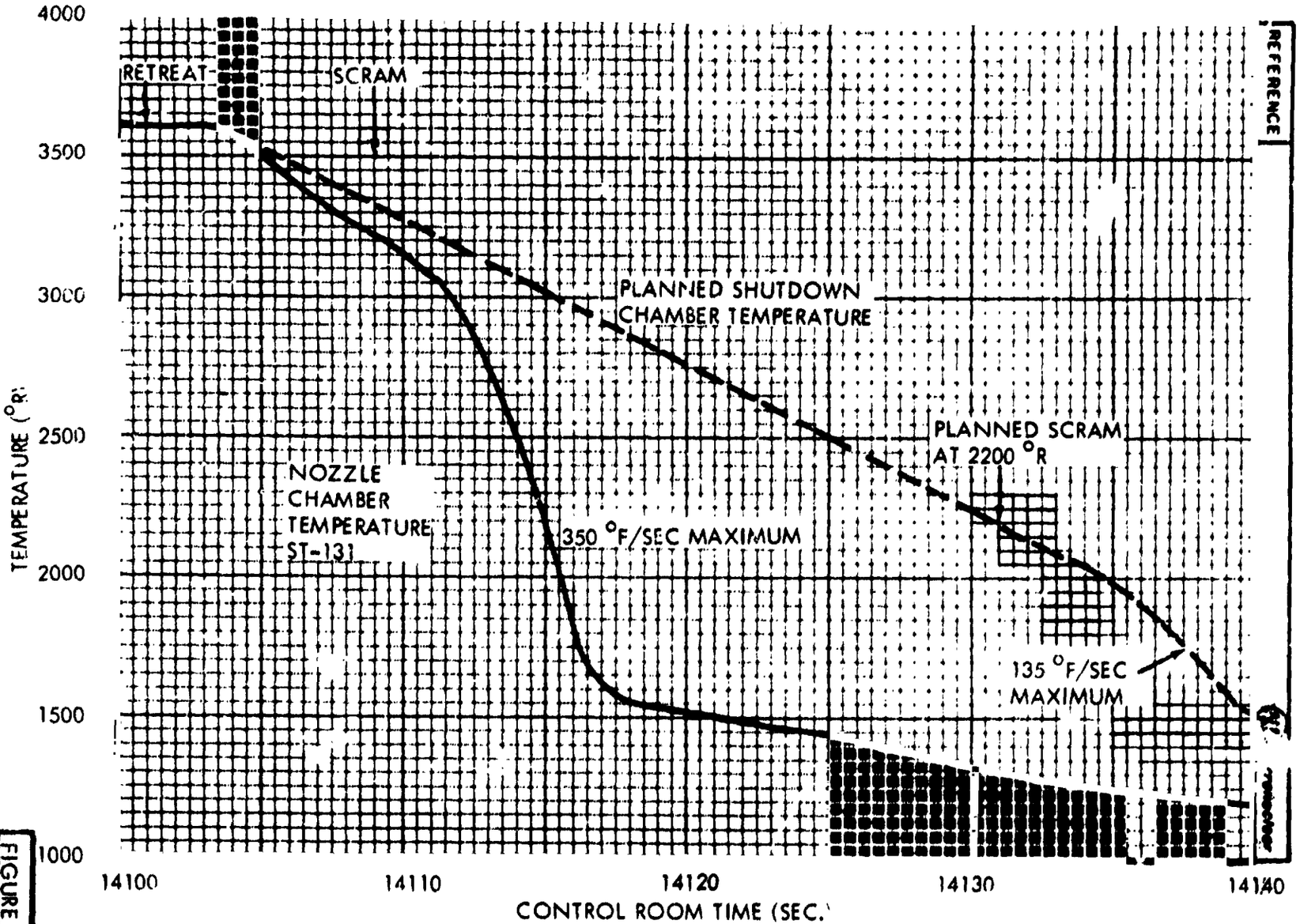

FIGURE NO.	NRX-A2 SHUTDOWN NOZZLE CHAMBER TEMPERATURE	PREPARED BY	APPROVED BY	CURVE NO.
4 - 52		LB		

REFERENCE	PREPARED BY	APPROVED BY	Aerojet

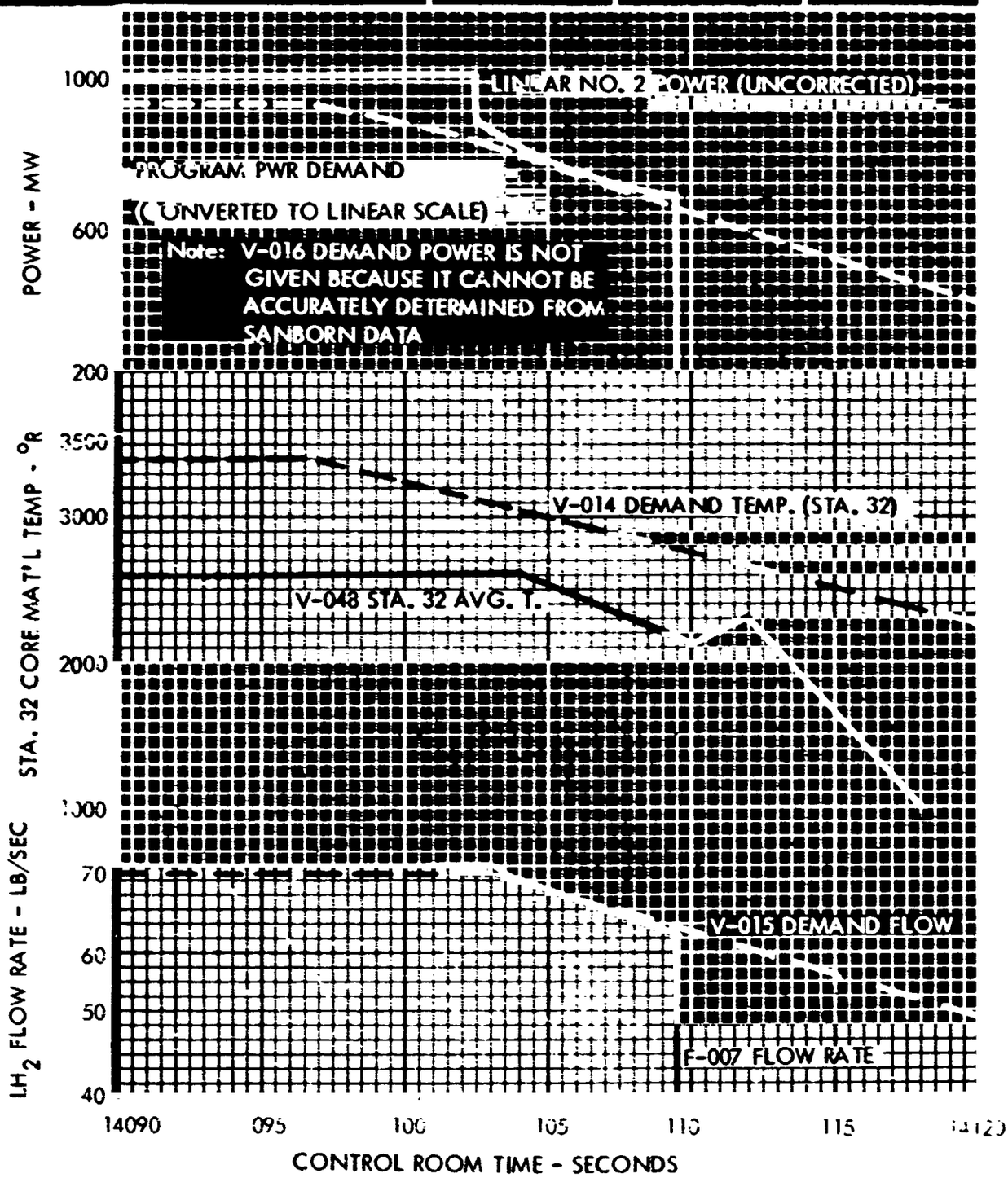

SHUTDOWN VARIABLES AND DEMANDS	CURVE NO.	FIGURE NO.
		4 - 53

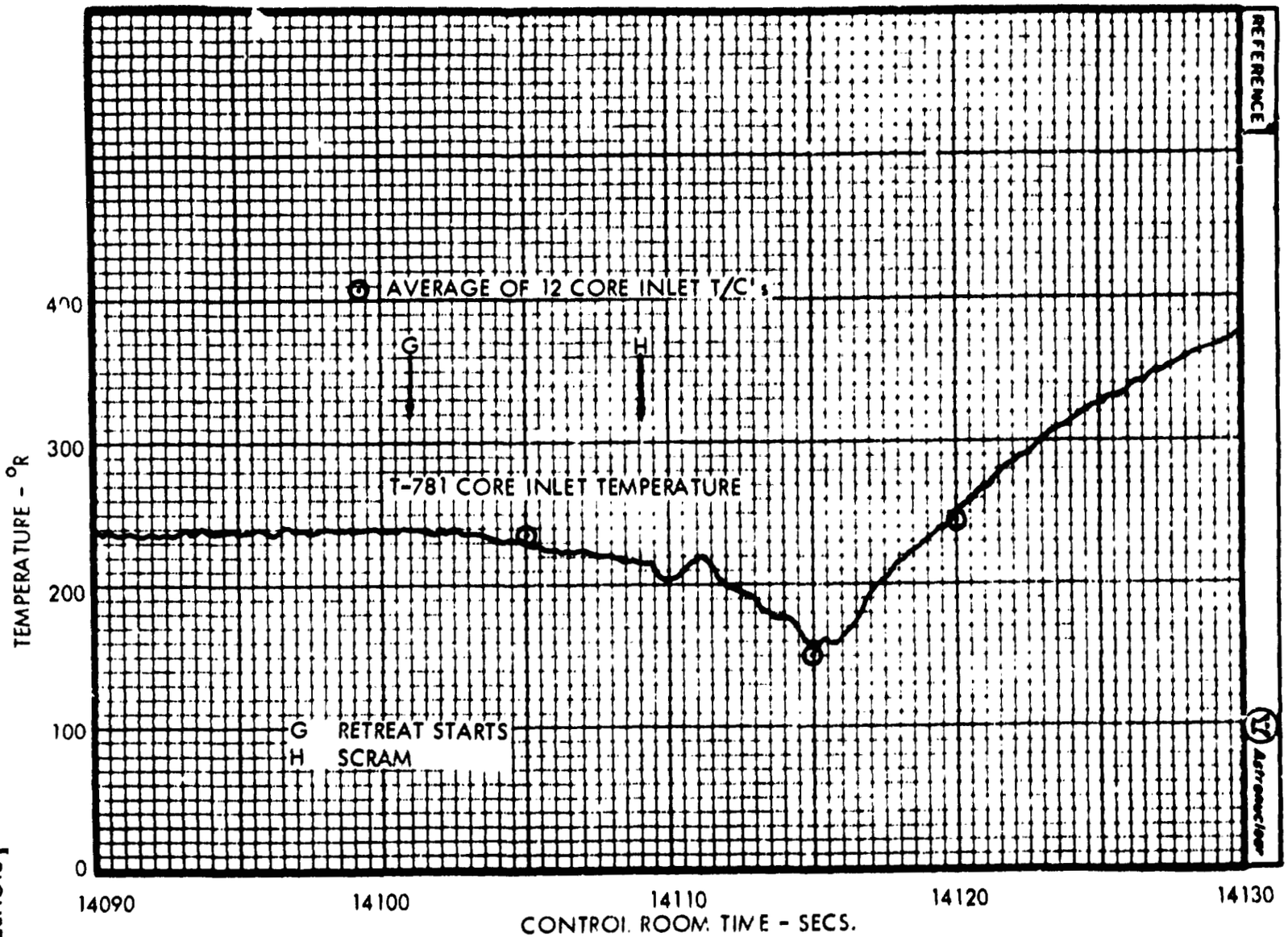

CORE INLET TEMPERATURE VERSUS TIME	PREPARED BY	APPROVED BY	CURVE NO.

FIGURE NO. 4-34

REFERENCE		PREPARED BY	APPROVED BY	Astronuclear

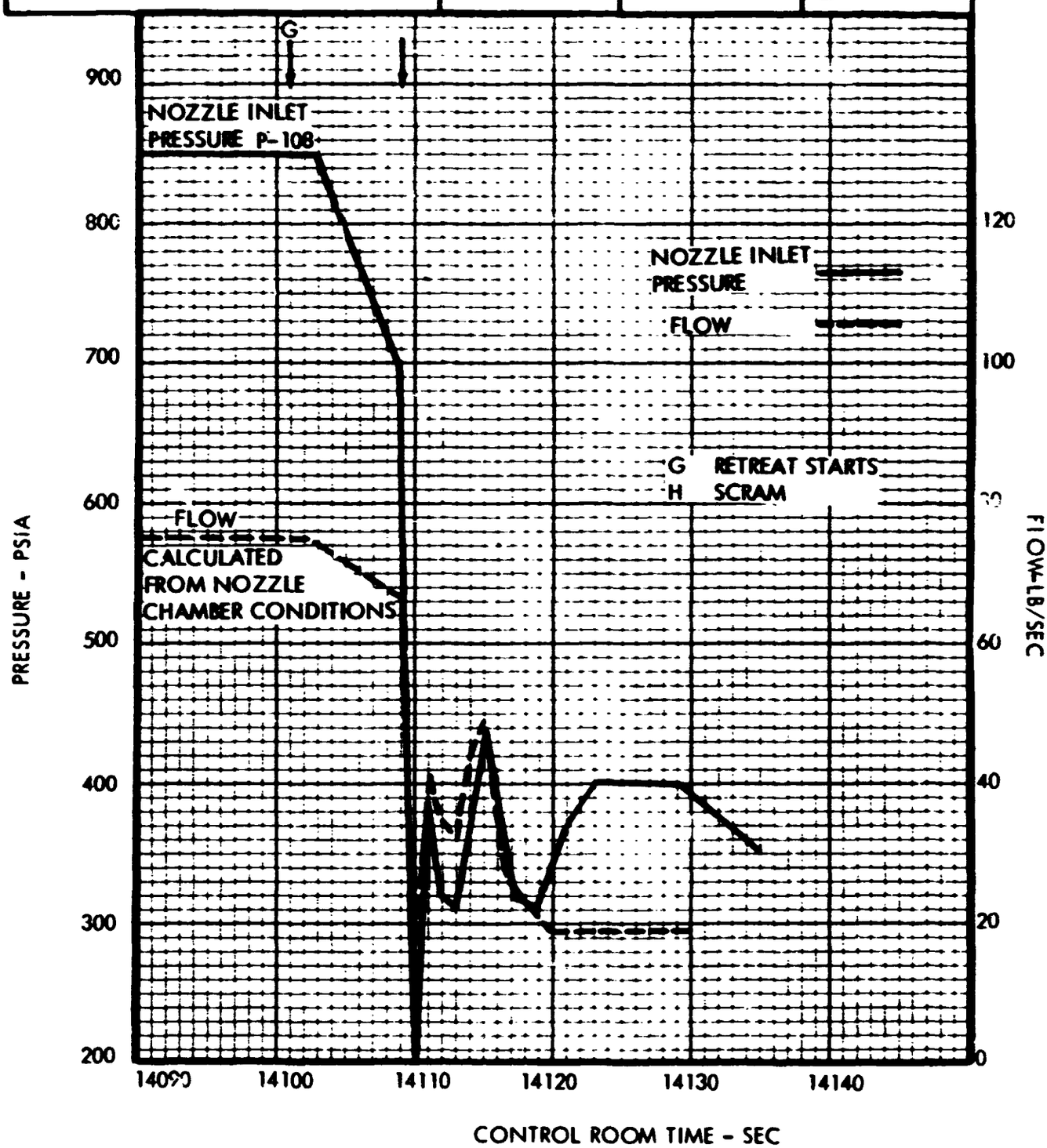

REACTOR SHUTDOWN HISTORY	CURVE NO.	FIGURE NO.
		4 - 56

REFERENCE		PREPARED BY	APPROVED BY	Astronuclear

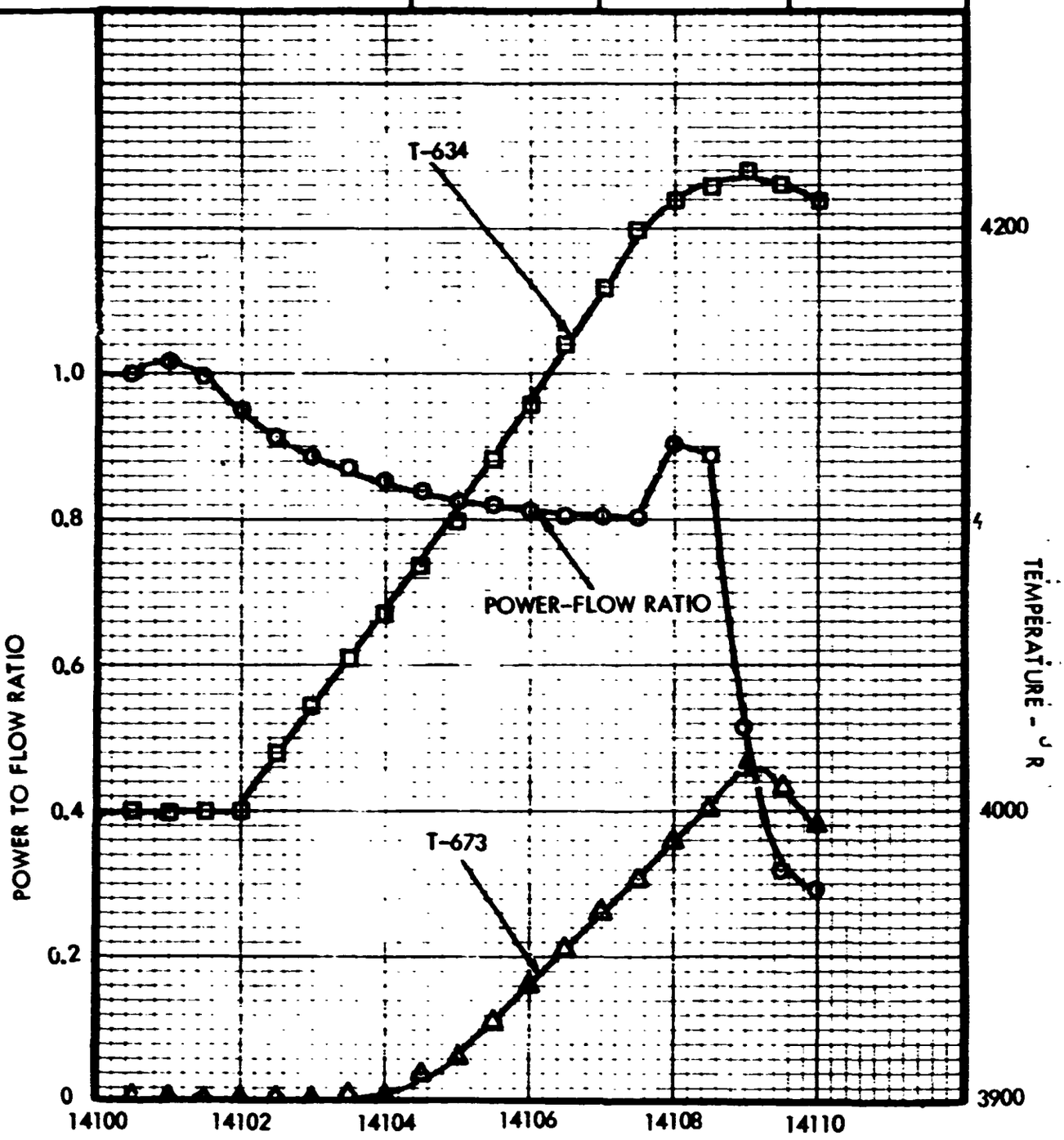

NRX-A2 EP IV SHUTDOWN STATION 45 TEMPERATURE SPIKE ANOMALY	CURVE NO	FIGURE NO.
		4 - 56

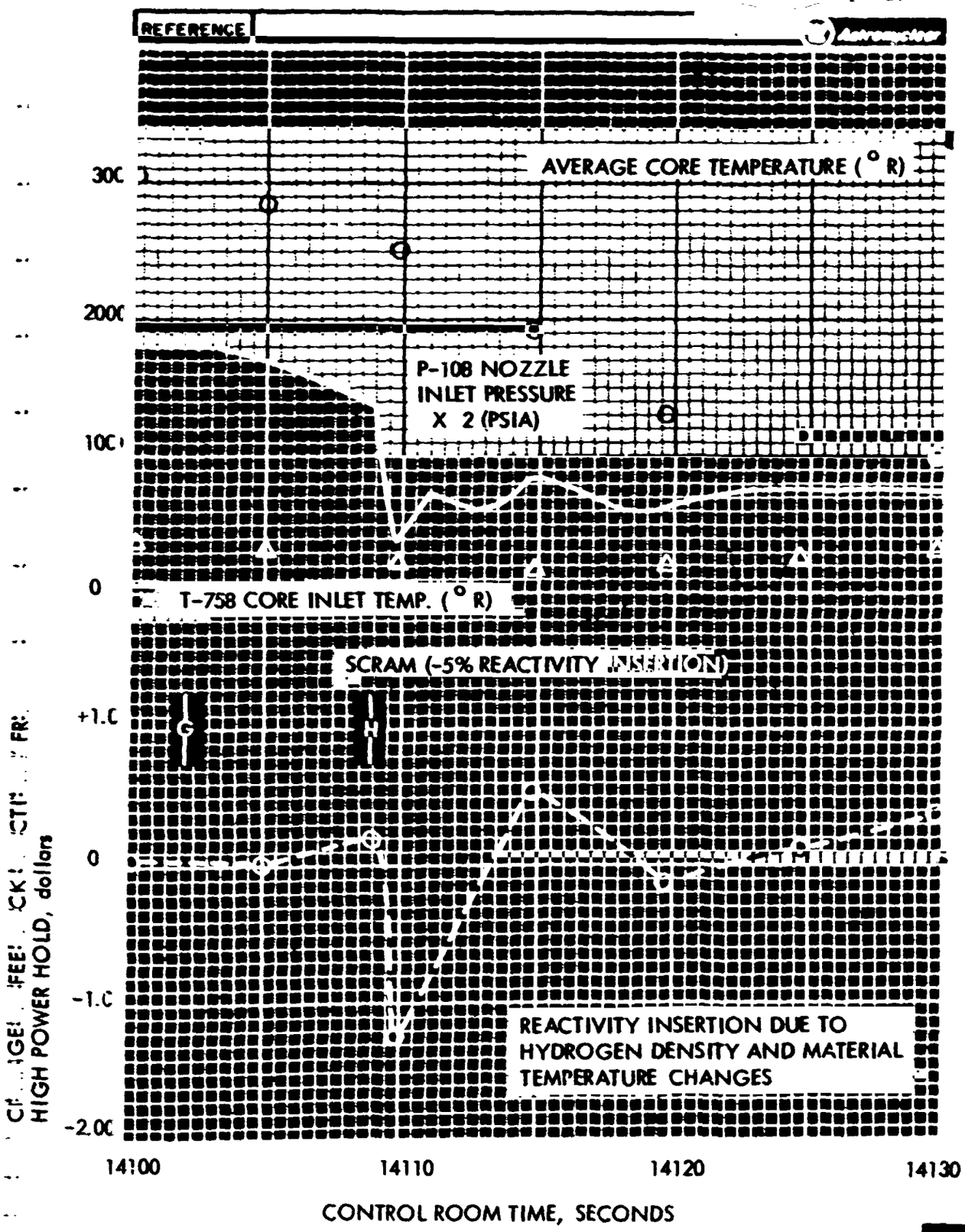

CURVE NO.	APPROVED BY	PREPARED BY

NRX-A2 EP-IV SHUTDOWN REACTIVITY

FIGURE NO. 4 - 57

Immediately following the reactor shutdown 16 of the station 45 material temperatures indicated a rise in temperature and four of these thermocouples failed.

Two of the temperatures which peaked (T-676 and T-634) are given on figure 4-56 as a function of time. The power-flow ratio for this shutdown interval is also given on this figure. If the temperature had actually increased, the power-flow ratio should have shown a similar increase, which it did not. Therefore, a temperature rise at shutdown is considered most unlikely. The temperature peaks and thermocouple failures at shutdown occurred only in station 45 instruments and these were saturated prior to shutdown; i.e., indicating several hundred degrees less than true temperature because of the high temperature environment of the thermocouple and the thermocouple lead. The fact that the thermocouple signal is degraded because of the high temperature of the lead, suggests the possibility of an increased output occurring when the lead temperature drops. This may have been the cause of the apparent temperature peaks, differential thermal conditions between the lead and central element. The exact cause of these failures could not be determined during post-operative inspections.[1]

Nuclear

SHUTDOWN

The reactivity effect due to the sudden changes in reactor temperatures and coolant hydrogen densities has been calculated for the shutdown interval. The result of this calculation, based on experimental temperature and pressure measurements, is given in figure 4-57. The lower curve on this figure shows that during the shutdown period the maximum positive reactivity insertion is only 60 cents due to the changes in system temperatures and coolant flow conditions from those of the full power hold. The points shown were calculated with the simplified techniques discussed in the appendix. They indicate the inherent safety from nuclear excursion during the shutdown period. The 60 cents positive reactivity insertion occurs after the drum bank has been scrammed. This scram inserts -4 to -5 dollars of reactivity into the system. The net reactivity of the system is thus about -3 dollars, well within the 2 dollar shutdown margin required at the site.

[1]WANL-TME-1079, NRX-A2 Instrumentation Disassembly and Post Operative Report

COOLDOWN

Figure 4-58 summarizes the flow rates during cooldown. This figure and figure 4-59 are taken directly from the NRX-A2 Site Test Report[1] since this report presents the best available information on flow rates and coolant usage during cooldown. Time zero for the cooldown analysis is designated as Time CR 14109 seconds and corresponds to the time of reactor scram. The PCV-41 pressure control loop was activated simultaneously with reactor scram. About 11 seconds were required to exhaust the approximate 200 lb of LH_2 that is stored in the piping system and mixing chamber during operation. Continuous ambient GH_2 cooling between 20 and 6 lb/sec was maintained until 125 seconds after scram. At his time the maximum core temperature was well below 1400°R and therefore ambient nitrogen cooling was initiated at approximately 30 lb/sec. The continuous ambient nitrogen flow was manually controlled between approximately 30 and 5 lb/sec. Pulse cooling with approximately 5 lb/sec of ambient nitrogen was initiated at about 1 hour after scram. Pulses were initiated by one of the following temperature limitations: 900°R core station 8, 850°R inner reflector, and 850°R support plate. The core station 8 temperature exceeded the 900°R limit by 150°R before the first ambient nitrogen pulse was initiated. The purpose of the core station 8 temperature limit was to limit the orifice adhesive temperature. The orifice adhesive has been successfuly tested at 1200°R, however without gamma radiation effects. In addition, the orifice was undoubtedly at a lower temperature than core station 8. Thus, the orifice adhesive was probably not damaged during cooldown. After approximately 13000 seconds (3.6 hours) 200°R GN_2 at about 5 lb/sec was used for pulse cooling. During this period an excessive amount of coolant was used because a faulty core support plate thermocouple gave readings higher than the operating limit. As a result, the core was cooled inefficiently to approximately 200°R. Pulse cooling was ended at 32 hours after scram.

[1]NTO-R-0008, NRX-A2 Site Test Report, November 20, 1964

REFERENCE

Astronuclear

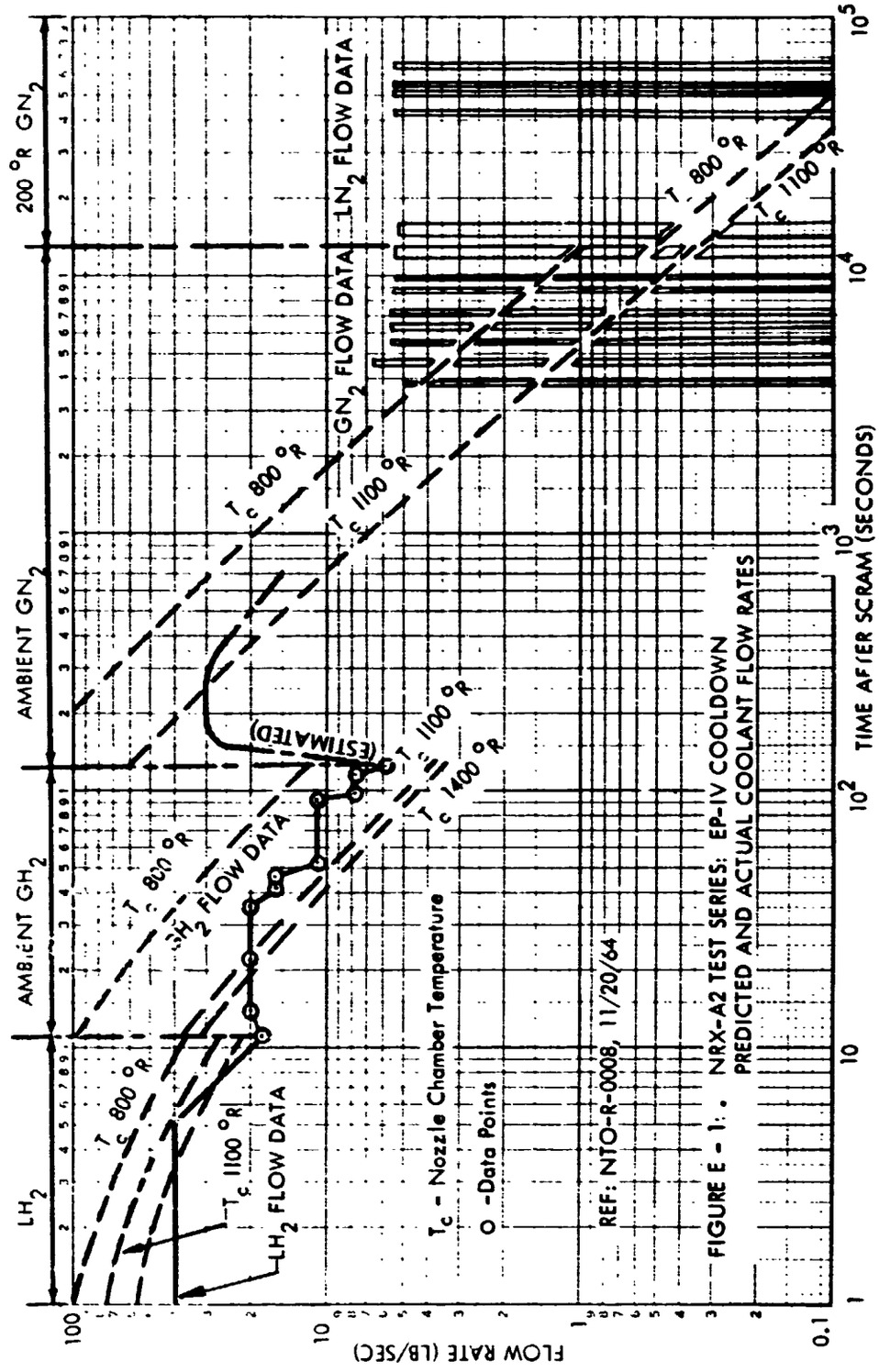

PREPARED BY	APPROVED BY	CURVE NO.

NRX-A2 EP IV COOLDOWN PREDICTED AND ACTUAL COOLANT FLOW RATES

FIGURE NO. 4 - 58

The total quantities of all fluids used during cooldown are shown on figure 4-59. Figure 4-58 and 4-59 also show calculated coolant flow rates and coolant usage for constant chamber temperatures between 800°R and 1400°R. The following description from the NRX-A2 Site Test Report applies to the calculated data on these two figures: The predicted (calculated) values shown are for an integrated power 3×10^5 MW-sec and a peak power of 102 percent. The reactor decay power was computed by the Way-Wigner fission product decay model and a summation of six delayed neutron groups to obtain the delayed neutron power decay. This model has been verified by using data obtained following the completion of KIWI B-4D and B-4E tests. Calculated flow rates and coolant usage are only shown to indicate the approximate coolant exit conditions that existed during cooldown. More detailed analysis was not deemed necessary in view of the uncertainties of the available cooldown data. A comparison of KIWI B-4E and NRX-A2 cooldown gas requirements is given in table. In order to evaluate the efficiency of cooldown the average exit gas temperature for all gases used during the cooldown has been calculated and is given in the table. These absolute temperatures on a relative basis are a good indication of the efficiency of the cooldowns.

The cooldown was not compared directly with the pre-test predictions primarily because the power profile was different than the one used for the predictions and the coolant usage and control was considerably different than assumed. Figure 4-60 shows a comparison between the predicted decay power during cooldown, and two experimental power values. The calculated power is based on the EP IV power profile and was calculated with the latest decay power calculation method[2]. The experimental power values are based on heat storage in the core during intervals between ambient nitrogen coolant pulses. Since only relative changes in core temperature were required for this calculation, the results

[1]NTO-R-0008, NRX-A2 Site Test Report, November 20, 1964
[2]WANL-TME-840, Reactor Analysis Data Book, February 1965 Revision

REFERENCE

Astronuclear

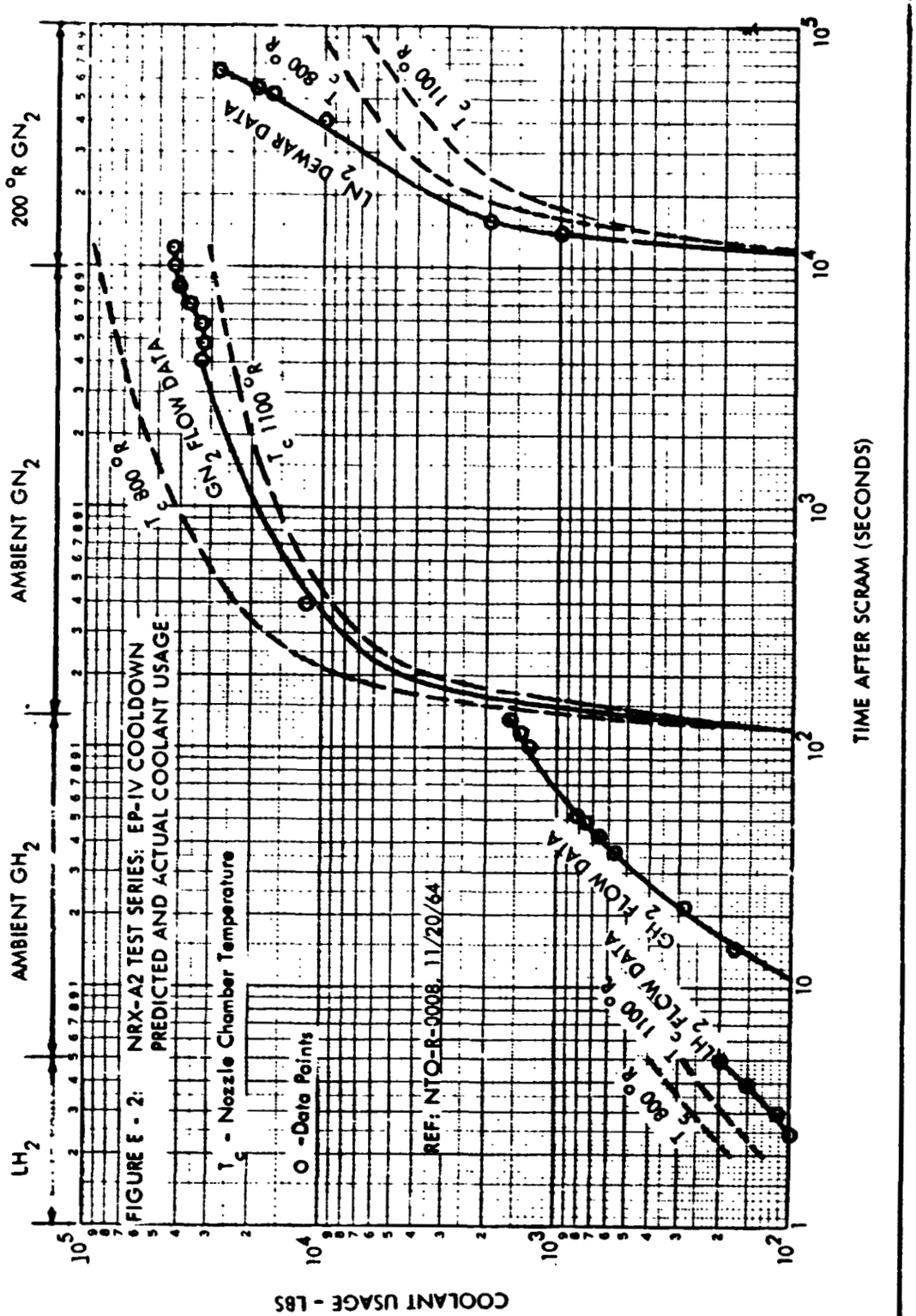

PREPARED BY	APPROVED BY	CURVE NO

NRX-A2 EP IV COOLDOWN - PREDICTED AND ACTUAL COOLANT USAGE

FIGURE NO.
4 - 59

are not influenced by the considerable inaccuracies of the measured core temperatures at low absolute temperatures. The experimental values were increased by 7 percent to convert core power to total reactor power. The agreement between the two experimental values and the predicted power is exceptionally good. Due to the limited cooldown data only two experimental power values at approximately one and two hours after scram could be calculated. However, these tv. points are sufficient to check the absolute value of the predicted decay power curve. As expected, the experimental values are below the calculated power since the heat loss from the core was neglected in the experimental power determination.

REFERENCE		PREPARED BY	APPROVED BY	Astronuclear

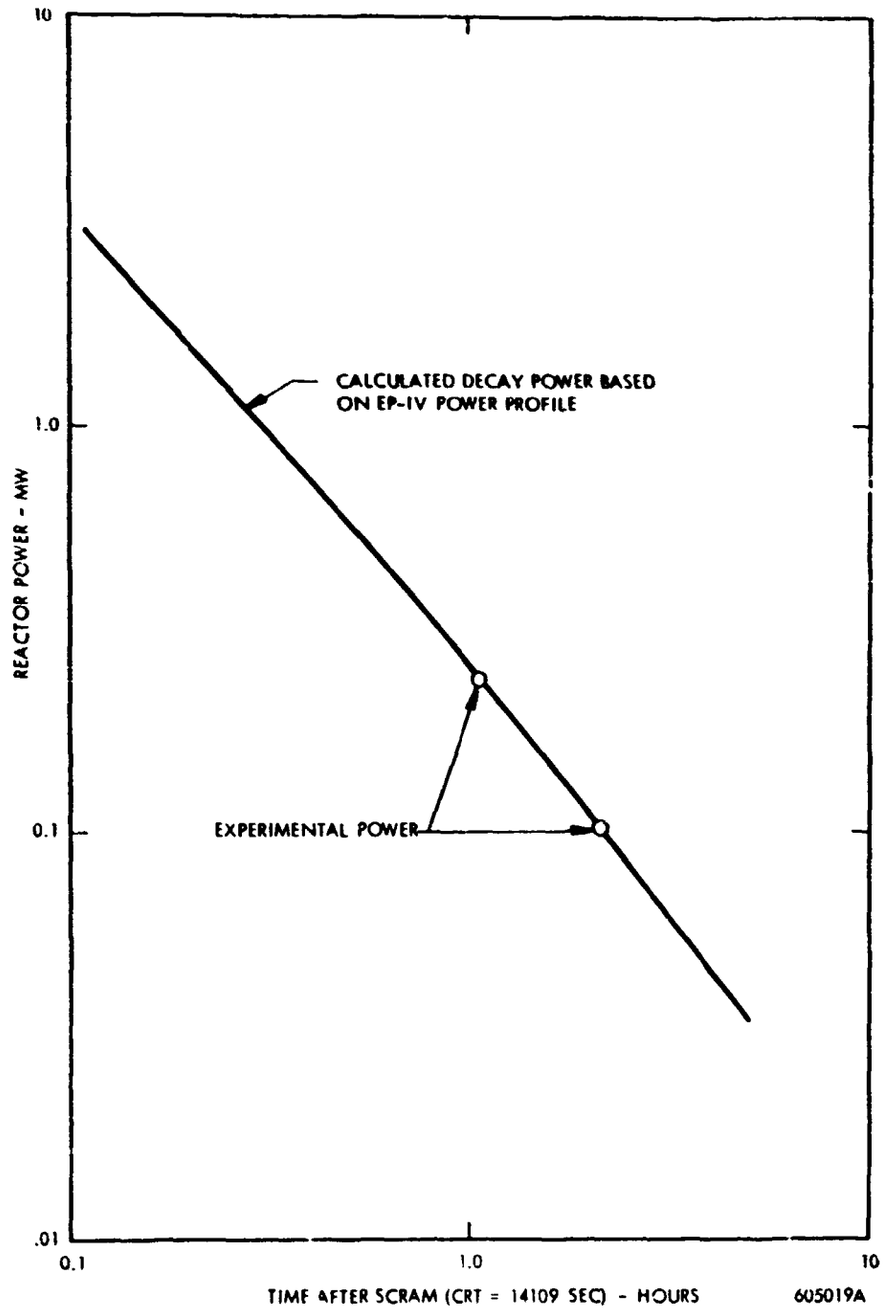

COMPARISON BETWEEN EXPERIMENTAL AND CALCULATED DECAY POWER DURING COOLDOWN FOLLOWING EP-IV

FIGURE NO. 4 - 60

CHAPTER 5

EXPERIMENTAL PLAN V LOW POWER MAPPING TEST

TEST OBJECTIVES, DESCRIPTION, AND CHRONOLOGY

The low power mapping test, EP V, was designed to achieve the following major objectives:

1. To demonstrate stable reactor operation and to gain performance data in the low power reactor operating region which is achievable with Dewar pressure feed.

2. To demonstrate stable reactor operation with two phase hydrogen core inlet conditions, and thus eliminate the minimum 90°R core inlet limitation.

3. To demonstrate stable reactor operation with fixed control drums and flow control.

On 15 October 1964 the lower power test was performed. These objectives were achieved during the EP V test. The reactor was operated stably at seven distinct steady state holds covering a range of 21.3 - 52.6 MW in thermal power and 5.2 - 13.5 lb/sec in liquid hydrogen flow rate. A considerable portion of the test was performed with two phase conditions in the reflector region and at the core inlet. During fixed control drum operation a power variation between 21.3 and 52.6 MW was accomplished by controlling the flow between 5.2 and 13.4 lb/sec. Power response as a result of variations in flow was completely stable.

Two figures, the low power performance map and the time variation of power, flow, and control drum bank position, describe the EP V test chronology. Figure 5-1 illustrates the steady state low power performance map with pre-test (TNT calculation) curves representing 1000°R average tie rod exit temperature, zero reactivity feedback, and +1.0$ reactivity feedback. These reactivity feedback lines were calculated with our simplified equations which are based on the detailed nuclear design reactivity calculation method[1].

[1] WANL-TME-936, Development of a Method for Computing the Cold-to-Hot Reactivity Change in the NRX-A Assembly, 30 September 1964

REFERENCE	PREPARED BY	APPROVED BY	Astronuclear
	W. A. K.		

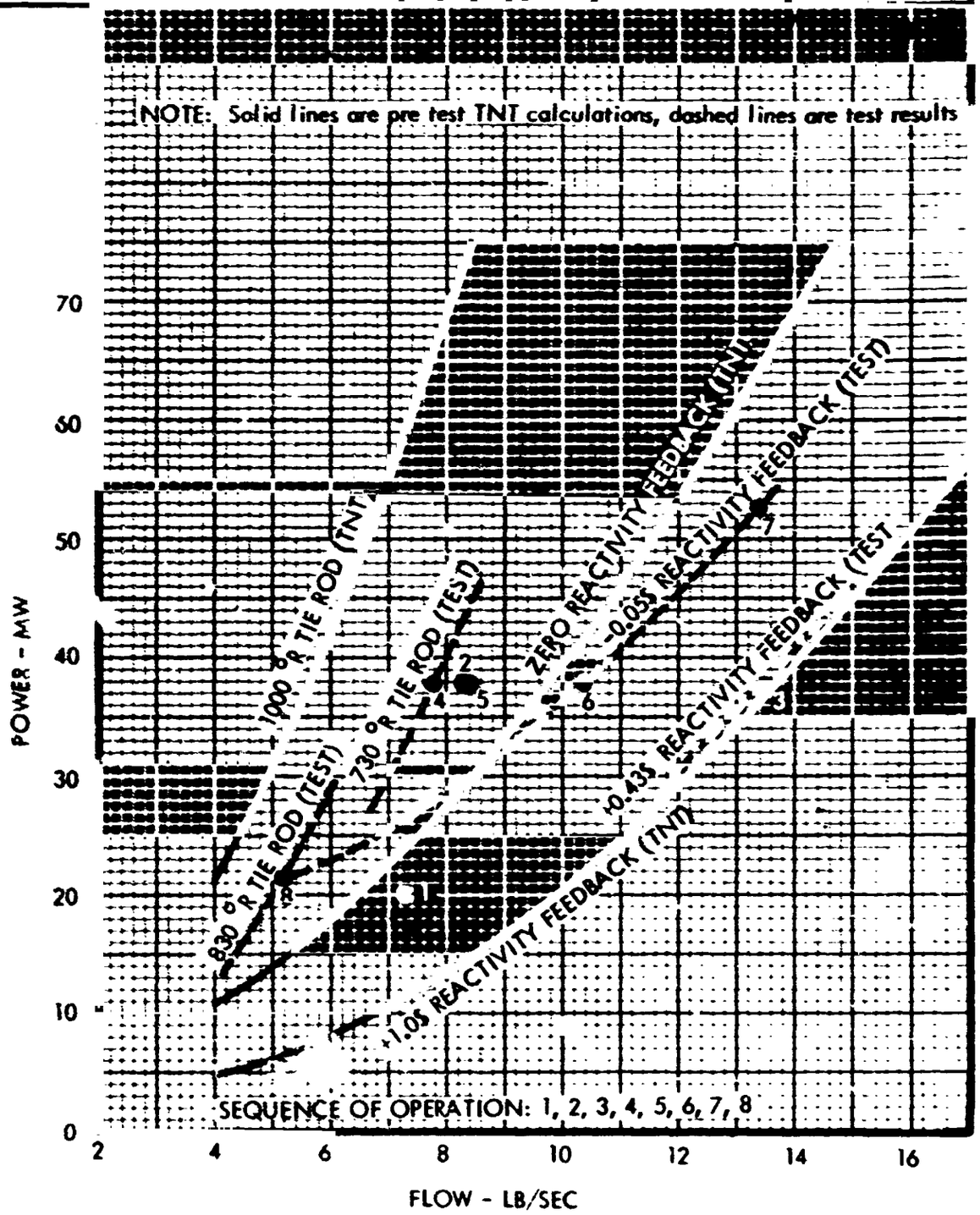

EP-V LOW POWER MAPPING TEST LOW POWER PERFORMANCE MAP	CURVE NO	FIGURE NO.
		5-1

The four simplified equations calculate reactivity feedback as a function of average core hydrogen density, average core material temperature, average inner reflector density, and average outer reflector temperature. These simplified equations lose accuracy in the low power operating region. Conservative reactor operation is possible at any flow – power points that fall between the 1000°R tie rod coolant exit temperature and the +1.0$ feedback reactivity curves. These limits are extremely conservative since the EP V test was the first attempt to operate in the low power region. For example, the tie rod exit temperature limitation for normal transients is 1200°R, while the total available shutdown reactivity from a 90 degree control drum position is approximately 4$. The constant power and flow points that were achieved during the EP V test are superimposed on the performance map. In addition, test results are used to show the approximate location of lines that represent 730°R tie rod temperature, -0.05$ reactivity feedback, and +0.43$ reactivity feedback. The time variation of power, flow and control drum bank position starting from the conclusion of the prechill is shown on figure 5-2. The constant power and flow points that were achieved during the test are indicated on figure 5-2. In general the transients during the EP V test were very slow compared to normal startup and shutdown operation. The entire test from start of prechill to reactor scram required approximately 20 minutes.

The EP V test consisted of two parts; one, constant power with flow control, and two, fixed control drum with flow control. On figure 5-1 the constant power part consists of points 2, 3, 4, 5, and 6, and the fixed control drum part consisted of points 6, 7, and 8. The initial part of the test consisted of a prechill with approximately 2 lb/sec flow and 1 MW power until the core inlet temperature had decreased to 300°R. At this time the power was increased to 19.8 MW* with a 2.5 second period, and the flow was increased to 7.3 lb/sec*. These conditions of flow and power (point 1) were maintained for approximately 120 seconds, which was not sufficient to establish steady state reactor conditions. Point 1 was required to circumvent the system flow lag which forced the

* The best estimate of thermal power, and average venturi flow are specified. These values should correspond exactly with figure 5-1. Figure 5-2 shows Linear No. 2 (measured) power which is about 9 percent greater than calculated thermal power.

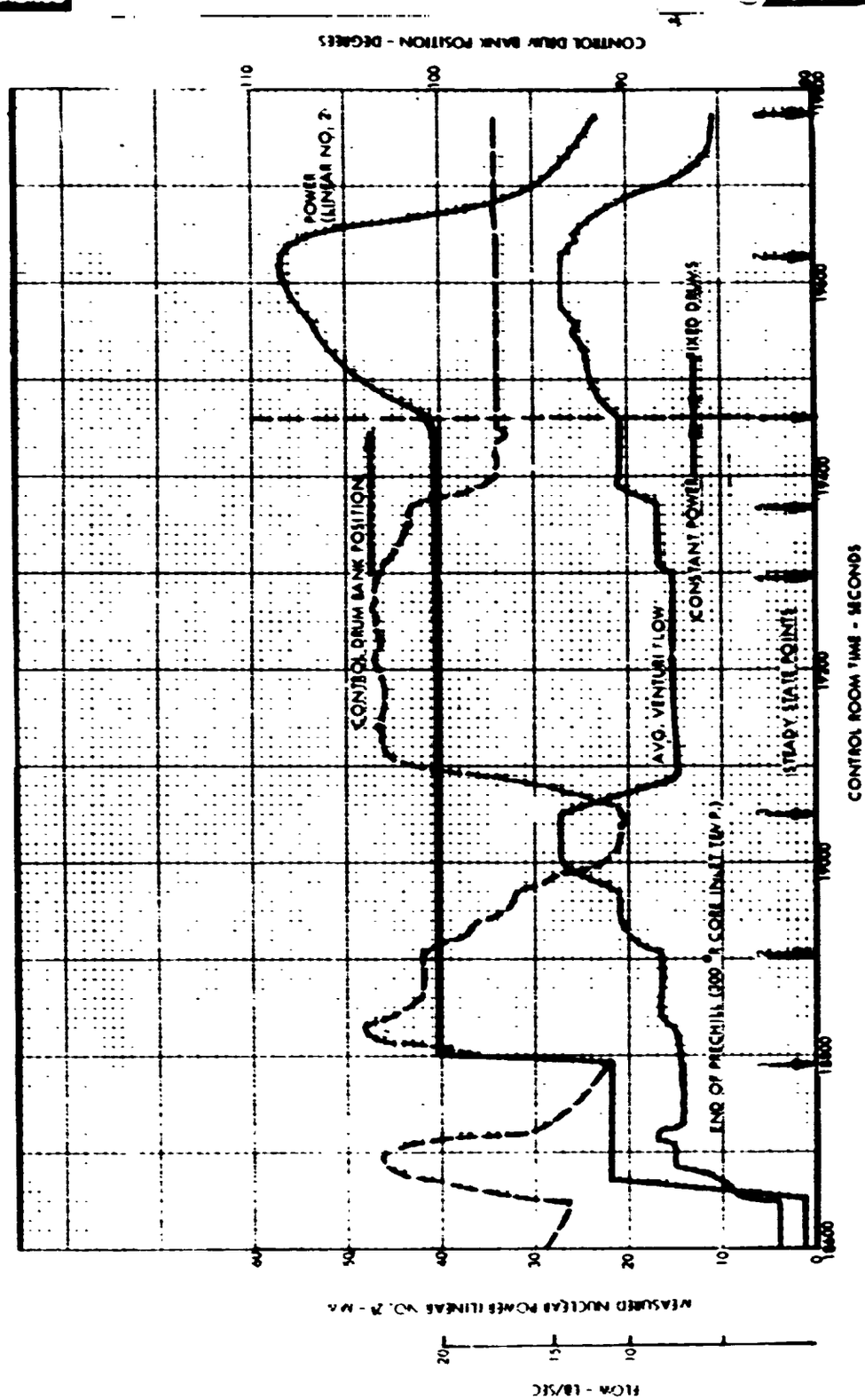

PREPARED BY	APPROVED BY	CURVE NO.

ΔP-V LOW POWER MAPPING TEST:
POWER FLOW AND CONTROL DRUM POSITION VS. TIME

Fig. No.
5 - 2

discontinuation of the first attempt to perform the test. At this time the power was increased to 37.7 MW*, and the flow to 8.3 lb/sec*. The resulting steady state condition (point 2) is the base point for the constant power test. Starting from point 2 steady state reactor operation at constant power with variations in flow was achieved at points 3, 4, and 5. The maximum reactivity feedback equal to +0.43$ occurred at point 3 with 13.5 lb/sec* flow. Point 4 with 7.8 lb/sec* flow produced the highest tie rod temperature that was observed during the test. Analysis of the test results indicates that this observed tie rod thermocouple was in error, and that the actual tie rod temperature was only approximately 730°R at point 4. The fixed control drum test was initiated from point 4 with 10.5 lb/sec* flow, 37.7 MW* power, and -0.05$ experimental reactivity feedback. Starting from point 4 the flow was gradually increased to 13.4 lb/sec* (maximum flow with 100 psia Test Cell A Dewar pressure) and maintained until stable reactor operation at 56.7 MW* (point 7) was achieved. From point 7 the flow was slowly decreased to 5.2 lb/sec*, with a corresponding power decrease to 22.9 MW* (point 8). From point 8 an automatic shutdown (reactor scram, discontinuation of liquid hydrogen flow, and initiation of approximately 5 lb/sec of ambient hydrogen) was used to complete the test.

The analysis of the EP V test will be divided into two parts; one, the low power steady state operating conditions and two, reactor operation with fixed control drums. The most significant reactor conditions will be compared with TNT calculations using the pre-test reactor model and calculation procedure.

STEADY STATE OPERATING CONDITIONS - THERMAL

Thermal and Fluid Flow - Analysis of Data

A major objective of the EP V test was to obtain steady state data in the low power-low flow operating region. Such data is required to determine the low power operating map. Seven steady state points were achieved during the EP V test. These steady state points are indicated on figure 5-1; the low power performance map, and on figure 5-2, the

*The best estimate of thermal power, and average venturi flow are specified. These values should correspond exactly with figure 5-1. Figure 5-2 shows Linear No. 2 (measured) power which is about 9 percent greater than calculated thermal power.

time variation of power, flow, and control drum position. Thermal performance data for these seven steady state points and one intermediate hold during the startup is tabulated in table 5-1. This section will cover the determination of thermal power and the significant reactor performance conditions at these seven low power holds.

The thermal power calculation was based on points 2-6. These points are characterized by constant nuclear power (Linear No. 2 measurement). Calculated nozzle chamber temperature and average venturi flow were used to determine the thermal power. The choked nozzle flow equation using measured nozzle chamber pressure and average venturi flow was used to calculate the nozzle chamber temperature. The calculated nozzle chamber temperature was used in place of the measured temperature due to the inaccuracy of these thermocouples at the relatively low temperatures that occurred during EP V. Thermal power for the EP IV test was determined by multiplying the flow rate times the coolant enthalpy difference between nozzle chamber and reflector inlet plenum. This method was not used for EP V since the reflector inlet enthalpy could not be accurately determined due to two-phase conditions and the inaccuracies of plenum temperature measurements at near liquid hydrogen temperatures. Therefore, a curve based on TNT prediction calculations which gives chamber temperature as a function of the power-to-flow ratio was used. This curve which is approximately linear was calculated for flow rates between 7 and 14 lb/sec, and chamber temperatures between 800 and 2000°R. With this curve the flow-to-power ratio was found as a function of chamber temperature for points 2-6. The thermal power was then calculated by multiplying the power to flow ratio times the average venturi flow rate. The accuracy of this method is only affected by the accuracy with which the TNT code predicts the nozzle heat pickup. The predicted nozzle heat pickup at these operating conditions is less than 3 percent of the total reactor coolant enthalpy rise (nozzle torus to nozzle chamber). Therefore with this method a 50 percent error in calculating the nozzle heat pickup results in only a 1.5 percent error in determining total reactor power. For points 2 - 6, the average calculated thermal power equal to 37.7 MW is approximately 8 percent lower than the measured nuclear power (Linear No. 2) of 40.6 MW. The thermal power for points 7 and 8 was determined by multiplying the measured nuclear power times

TABLE 5-1

EP-V LOW POWER MAPPING: STEADY STATE TEST DATA

Point Designation	Intermediate Hold	Constant Power				Fixed Drums		
Map Point	1	2	3	4	5	6	7	8
CRT Time	18790	18905	19050	19295	19365	19460	19625	19775
Linear No. 2 (test) power - MW	21.4	40.6	40.6	40.6	40.5	41.0	56.7	22.9
Thermal power - MW	19.8	37.7	37.7	37.7	37.7	37.7	52.6	21.3
Flow - lb/sec	7.30	8.32	13.47	7.82	8.40	10.47	13.42	5.21
Feed line: T	40	41	38	40	40	39	38	40
P	37	60	64	58	59	61	83	34
Reflector Inlet: T	40	58	47 (TP)	93	52	46 (TP)	49 (TP)	42 (TP)
P	32	52	60	49	52	55	76	30
Core Inlet: T	49	125	47 (TP)	152	140	46 (TP)	59	91
P	31	49	58	46	49	53	73	28
Core Exit: T mixed measured	550	1070	670	1210	1150	880	960	810
T mixed calculated	665	1220	800	1270	1250	1000	1230	980
T Tie rod	—	765	345	730	710	460	560	830
P	23.1	35.7	46.7	34.2	36.5	40.8	58	21.6
Pressure Drops: Nozzle	4.5	7.5	4	9	7.3	6	7.3	4.3
Reflector	12.	3	1.5	3	3	2	2.5	1.5
Shield	nil	nil	nil	nil	nil	nil	nil	nil
Core	7	13	11	12	12	12	15	6
Core Temperatures: Station 8	243	406	339	443	414	363	411	326
Station 20	530	824	577	1022	900	695	743	656
Station 32	646	1140	768	1430	1290	1007	993	834
Station 45	692	1512	915	1627	1543	1218	1428	1213
Reactivity Feedback - $	-0.54	-0.37	+0.43	-0.59	-0.42	-0.05	-0.05	-0.06

Notes: 1. Temperatures - °R, Pressures - psia, pressure drops - psi
2. (TP) designates two phase hydrogen conditions, temperatures shown correspond to pressures.
3. Plenum pressures were changed slightly from test data to correspond to pressure drops.

0.92 which is the ratio of calculated thermal to measured nuclear power for points 2 - 6. Based on thermal power and average venturi flow the reactor operated in the range of 21.3 to 52.6 MW power and 5.2 to 13.5 lb/sec flow during the EP V test.

A conservative reactor operating limitation before the NRX-A2 test was a minimum core inlet temperature equal to 90°R. The purpose of this limitation was to assure completely gaseous hydrogen at the core inlet. It was felt that the high densities associated with liquid or two phase hydrogen could produce excessive and/or unstable positive reactivity feedback which in turn, could produce power oscillations or an uncontrollable power increase. The EP V test proved these considerations to be unfounded. During the test, the reactor operated stably at two distinct steady state holds (points 3 and 6), with two-phase hydrogen conditions at the core inlet. The plenum temperature measurements were inaccurate at two phase hydrogen temperatures, and only the existence of two phase conditions could be established. The two phase temperatures that are shown in table 5-1 are based on the measured pressures. Stable reactor operation with two phase hydrogen at the core inlet may be inferred since no power oscillations or other signs of instability were observed. Change in reactivity feedback during constant power operation were accompanied by nearly proportional changes in control drum position. Figure 5-2 shows that a smooth inward rotation of the control drums occurred during the transition from point 2 (single phase at core inlet) to point 3 (two phase core inlet conditions). This proves that for the test conditions the transition from single phase to two phase does not cause a sudden or abrupt change in reactivity feedback. Therefore, on the basis of EP V results, the core inlet temperature limitation of 90°R can be eliminated and replaced by a more general positive reactivity limitation which is measured by a change in control drum position from the cold critical position. This will simplify and increase the area of the reactor operating region since only one lower limitation (reactivity feedback) is required.

The tie rod exit gas temperature limitation forms the upper boundary of the low power operating map. For this reason it is important to accurately locate the tie rod limitation line. Table 5-1 shows that tie rod exit gas temperatures (average of T-755 and T-765 measurements) ranged between 345 and 830°R. Tie rod thermocouple T-760 gave unexplainably higher

readings than the other two during part of the test. Tie rod thermocouples T-755 and T-765 gave consistent readings during the test with a difference between readings of less than 50°R. On the other hand, at Time CRT 13900 seconds T-760 read 470°R higher then T-765, while at 19775 seconds T-760 read higher by only 20°R. This unexplained and abnormal behavior may have been caused by the T-760 thermocouple contacting the hotter molybdenum cone during part of the test. For this reason T-760 readings were neglected, and the average of T-755 and T-765 is shown in table 5-1. Point 4 was the planned point on the 1000°R tie rod exit gas temperature line (See the low power performance map, figure 5-1); however, by neglecting the T-760 measurement the tie rod temperature at point 4 was only 730°R. The maximum tie rod exit gas temperature of 830°R occurred at point 8. The 55°R difference in tie rod temperatures between points 2 and 5 which have nearly identical power and flow may be due to transient effects (either point may not be completely steady state). To summarize, the test results indicate that the predicted 1000°R tie rod curve of figure 5-1 is approximately correct and thus a considerable operating region exists between conservative tie rod (1000°R) and conservative but arbitrary reactivity feedback (+1.0$) limitations.

The calculated steady state nozzle chamber temperatures using the nozzle compatibility equation ranged between 800 and 1270°R. These are considerably higher than the average of three nozzle chamber temperature measurements. This effect is identical to EPIV results. Some of the core station temperatures appear higher than would be expected with the corresponding nozzle chamber temperatures. This effect may be due to the inaccuracies of these thermocouples at relatively low temperatures. The pressure drops are relatively low and show no unexpected behavior. The question of temperature asymmetries in the plenums is still under investigation, and any asymmetries will be reported in a supplement to this report. In general, most pressure and temperature instruments were operating at the low end of their scale, and therefore, are subject to substantial inaccuracies in measuring absolute values.

Thermal and Fluid Flow - Comparison with TNT Calculations

This section covers the comparison between test results and TNT prediction calculations. The tabulated comparison of thermal performance at three steady state points is shown on table 5-2, and a graphical comparison of selected performance conditions is illustrated on the low power performance map, figure 5-1. The pre-test reactor model and calculation procedure was used for all TNT comparison calculations. During the EP V test, most transducers and thermocouples were operating near the low end of their scale. Two exceptions are the chamber pressure and tie rod temperature measurements. This reason is probably the major cause for inaccuracies in the test results, and the major reason for any discrepancies in the comparison with calculated results.

The three steady state points that were selected for comparison are the maximum and minimum flow conditions during constant 37.7 MW (thermal) power operation (points 3 and 4) and the maximum power point which occurred during the fixed control drum operation (point 7). Good comparison between plenum temperatures (reflector and core inlets) exist for points 3 and 7 where two phase or near two phase hydrogen conditions existed during the test. At point 3 the predicted core inlet quality is 0.47. (approximately, 53 percent liquid by weight). This is the maximum calculated liquid percentage at the core inlet during the EP V test. The TNT results for point 4 show considerably lower plenum temperatures, although the calculation correctly predicts single phase conditions at the core inlet. The TNT calculations show considerably lower tie rod temperatures. This is identical to the TNT comparison with the high power test results. Good comparison exists for unfueled element station 8 temperatures. For the other stations the comparison is only good at a few points. The comparison between pressures is relatively good considering that these transducers were operating at the low end of the scale.

The low power performance map, figure 5-1, shows a comparison of predicted tie rod temperature and reactivity feedback with test results. Two experimental points with 730°R and 830°R tie rod temperatures are compared with the predicted 1000°R tie rod line. The comparison is good, and shows that the 1000°R tie rod line is approximately correct. The predicted zero and one dollar reactivity feedback lines are steeper and also closer together

TABLE 5-2

EP-V LOW POWER MAPPING TEST COMPARISON BETWEEN TNT PREDICTIONS AND TEST DATA

Point Designation	3		4		7	
CRT Test Time	19050		19295		19625	
	TNT	Test	TNT	Test	TNT	Test
Power, % of 1120 MW	3.37		3.37		4.7	
Flow, lb/sec	13.47		7.82		13.42	
Nozzle Torus:						
Pressure, psia	63	64	53	58	76	83
Temperature, °R	40	38	40	40	41	38
Reflector Inlet:						
Pressure, psia	58	60	46	49	70	76
Temperature, °R	47	47	45	93	49	49
Quality	0.17	--	0.61	1.	0.31	--
Core Inlet:						
Pressure, psia	55	58	44	46	66	73
Temperature, °R	46.5	47	51	152	48	59
Quality	0.47	--	1.00	1	0.75	1
Nozzle Chamber:						
Pressure, psia	46	46.7	35	34.2	54	58
Mixed Temperature, °R	770	800	1345	1270	1086	1230
Tie Rod Exit Temperature	255	345	607	730	349	560
Pressure Drops. (psi)						
Nozzle tube	4.7	4	6.6	9	6.1	7.3
Reflector	2.3	1.5	1.6	3.0	2.6	2.5
Core	9.4	11.0	8.8	12.0	11.5	15.0
Core Material Temperatures:						
Station 8 in.	360	339	463	443	442	411
Station 20 in.	468	577	745	1022	640	743
Station 32 in.	674	768	1124	1430	940	993
Station 45 in.	808	915	1374	1627	1130	1428
Reactivity Feedback - $	+0.88	+0.43	-0.37	-0.59	+0.37	-0.05

than the experimental data would indicate. These TNT reactivity calculations are based on four simplified equations which lack accuracy at these low power and flow operating conditions. The test point with maximum reactivity feedback of 0.43 percent falls approximatel, on the 1.0$ TNT predicted reactivity feedback curve. This implies that the 1.0$ reactivity feedback curve should be further to the right on figure 5-1. To summarize, the conservative and somewhat arbitrary low power operating region based on test results is considerably larger than the pre-test TNT calculated map. The primary reason is that the test 1.0$ reactivity feedback line is less restrictive than indicated by the pre-test predictions.

FIXED DRUM TEST TRANSIENT REACTOR OPERATION - THERMAL

Thermal and Fluid Flow - Comparison of Data With TNT Calculations

The fixed control drum test proved that reactor operation with flow control is feasible. Pre-test calculations showed that with fixed control drums an increase in hydrogen flow adds positive reactivity which increases power until the negative effect of temperature again cancels the positive hydrogen effect. By the same reasoning, a decrease in flow causes a decrease in power. The fixed control drum test proved that this effect happens smoothly for the relatively slow variations in flow that occurred.

The fixed control drum test results were compared with TNT calculations. The pre-test reactor model and calculation procedure was used; however, the detailed nuclear design reactivity feedback calculation method was used in place of the four simplified equations used to predict the low power performance map (See figure 5-1). Figure 5-3 shows the averaged venturi flow, measured Linear No. 2 power, and TNT calculated power. A comparison between test power and flow shows that every change in flow results in a nearly simultaneous power change in the same direction. In addition, the power curve shows no oscillations or other unexpected results. Using only the average venturi flow as input and the condition of fixed control drum position, the entire fixed control drum test was calculated with the TNT code. The TNT calculated power is shown by the dashed line on figure 5-3. The calculated power shows a greater relative variation than the measured power; however, the response is also stable. The difference between test and calculated power appears to

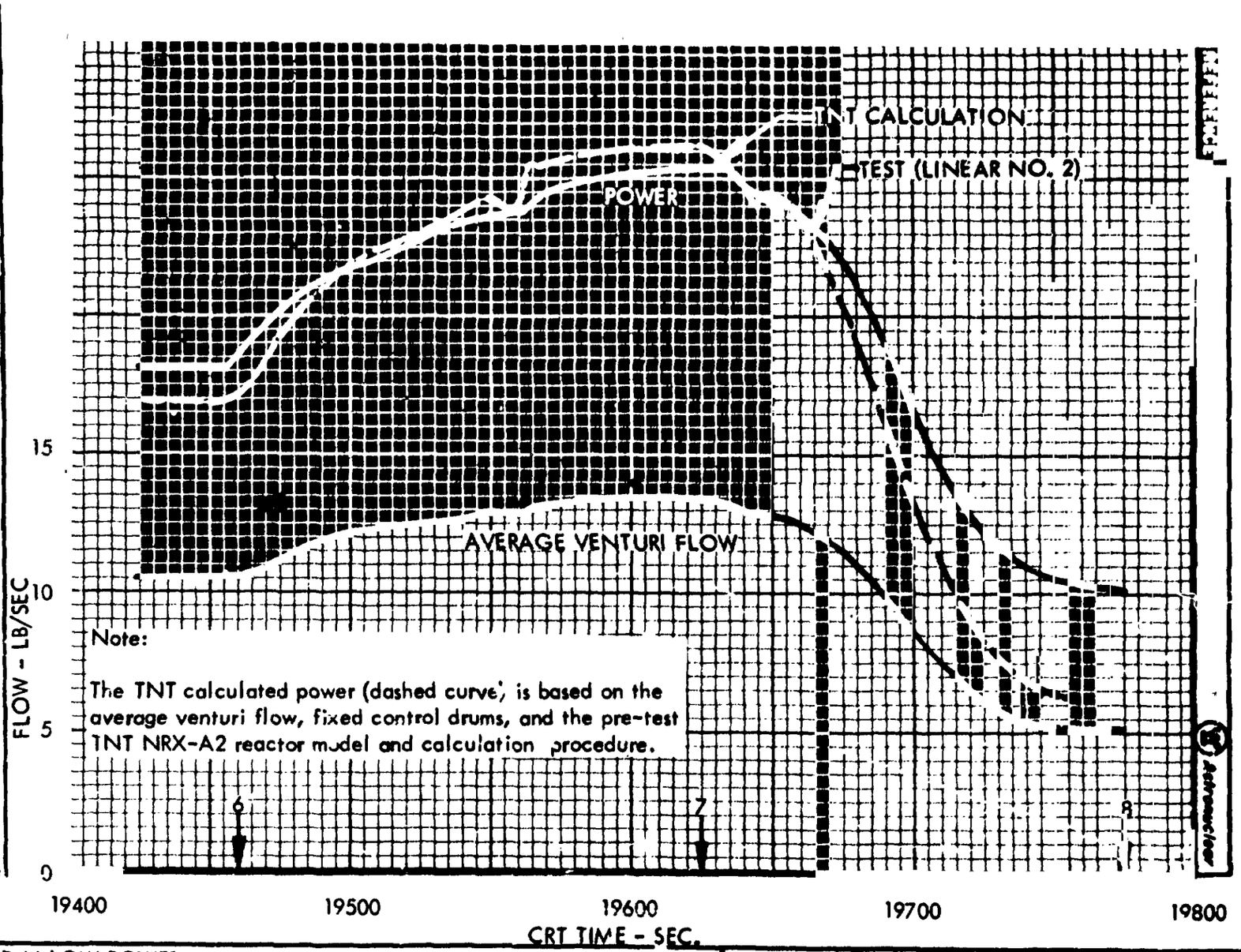

FIGURE NO.	EP-V LOW POWER MAPPING TEST: FIXED CONTROL DRUMS POWER AND FLOW	PREPARED BY	APPROVED BY	CURVE NO.
5-3		WEK		

be due to a combination of reactor model, calculation procedure, and uncertainty of test data. Figure 5-4 shows tie rod and nozzle chamber temperatures and figure 5-5 shows reactor plenum pressures during the fixed control drum test. On both figures the corresponding test results at the three steady state holds (points 6, 7 and 8) are indicated. As a result of the difference between test and calculated power, the calculated curves only approximately duplicate the test results. Additional analysis is presently in progress to improve the accuracy with which the TNT code duplicates these test results for both steady state and transient fixed control drum operation.

NUCLEAR CONSIDERATIONS

Delayed Critical Bank Position

Measurements during EP V of the critical bank position ranged between 96.0 degree and 96.2 degrees. The latter value, measured at a higher power level is the accepted delayed critical position in EP V.

During the early phases of EP V the worth of the nozzle cover was remeasured and found to be negligible. The removal of the cover was performed while the reactor was critical (between Time CR 6208 and 6320) so that the measurement is clearly better than the one performed in EP III (resulted in a 0.6° effect) which took nearly 2 hours during which time the reactor could easily have undergone some heating by the sun.

Feedback Reactivity

A comparison of the calculated* and measured drum bank position during three holds in EP V is presented in table 5-3. Shown also are the nuclearly significant parameters upon which the reactivity calculation is based. These points are plotted in figure 5-6 which also shows the power, flow and measured drum position throughout the test profile.

The agreement between the measured and calculated drum motion is excellent, providing additional evidence of the validity of the temperature coefficients and the hydrogen worth coefficients in the low power range. A correction of 10 percent in the

*The analytical model is summarized in appendix 1.

CONFIDENTIAL RESTRICTED DATA

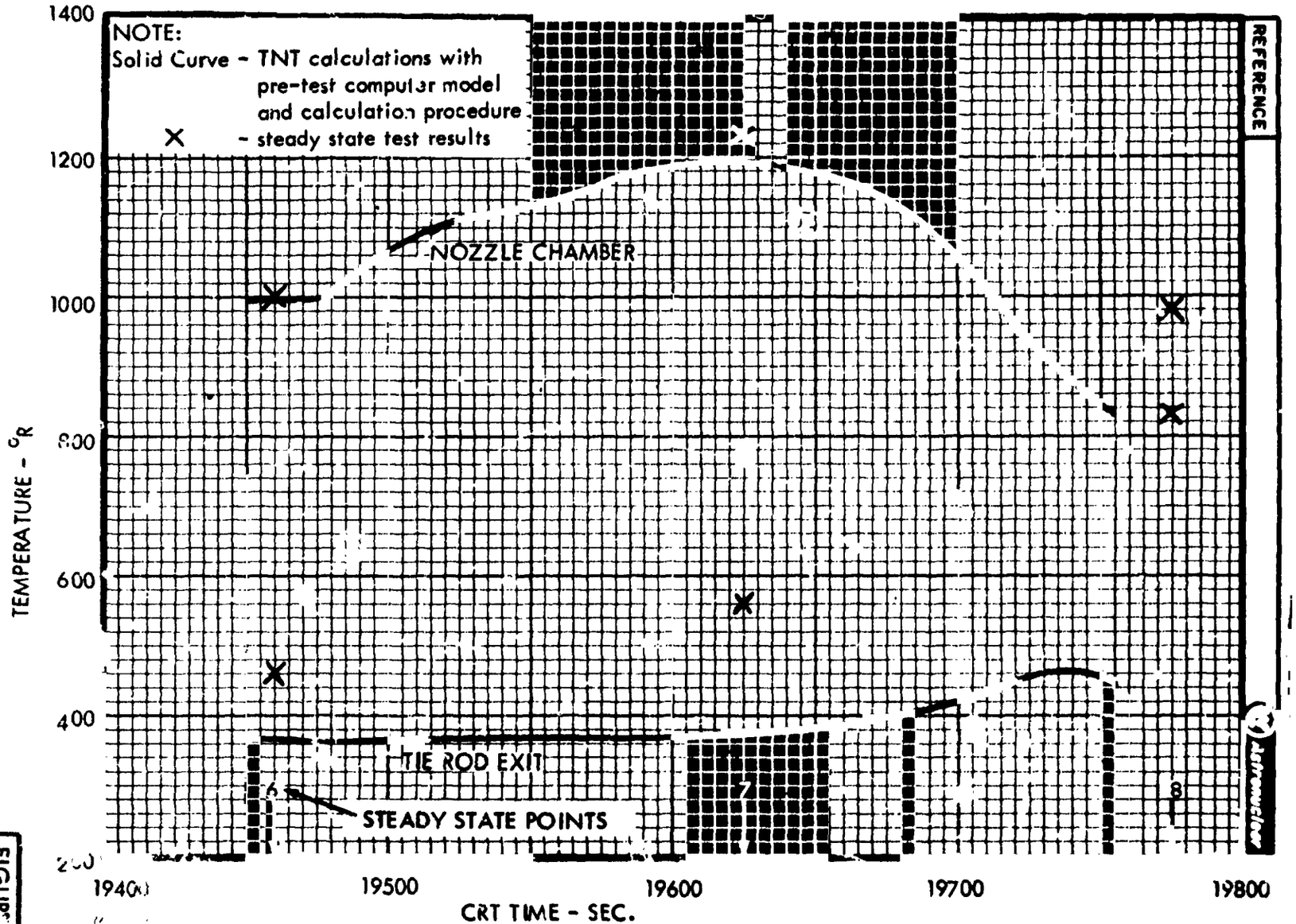

FIGURE NO.	EP-V LOW POWER MAPPING TEST: FIXED CONTROL DRUMS NOZZLE CHAMBER AND TIE ROD TEMPERATURES	PREPARED BY	APPROVED BY	CURVE NO.
5.4		WJK		

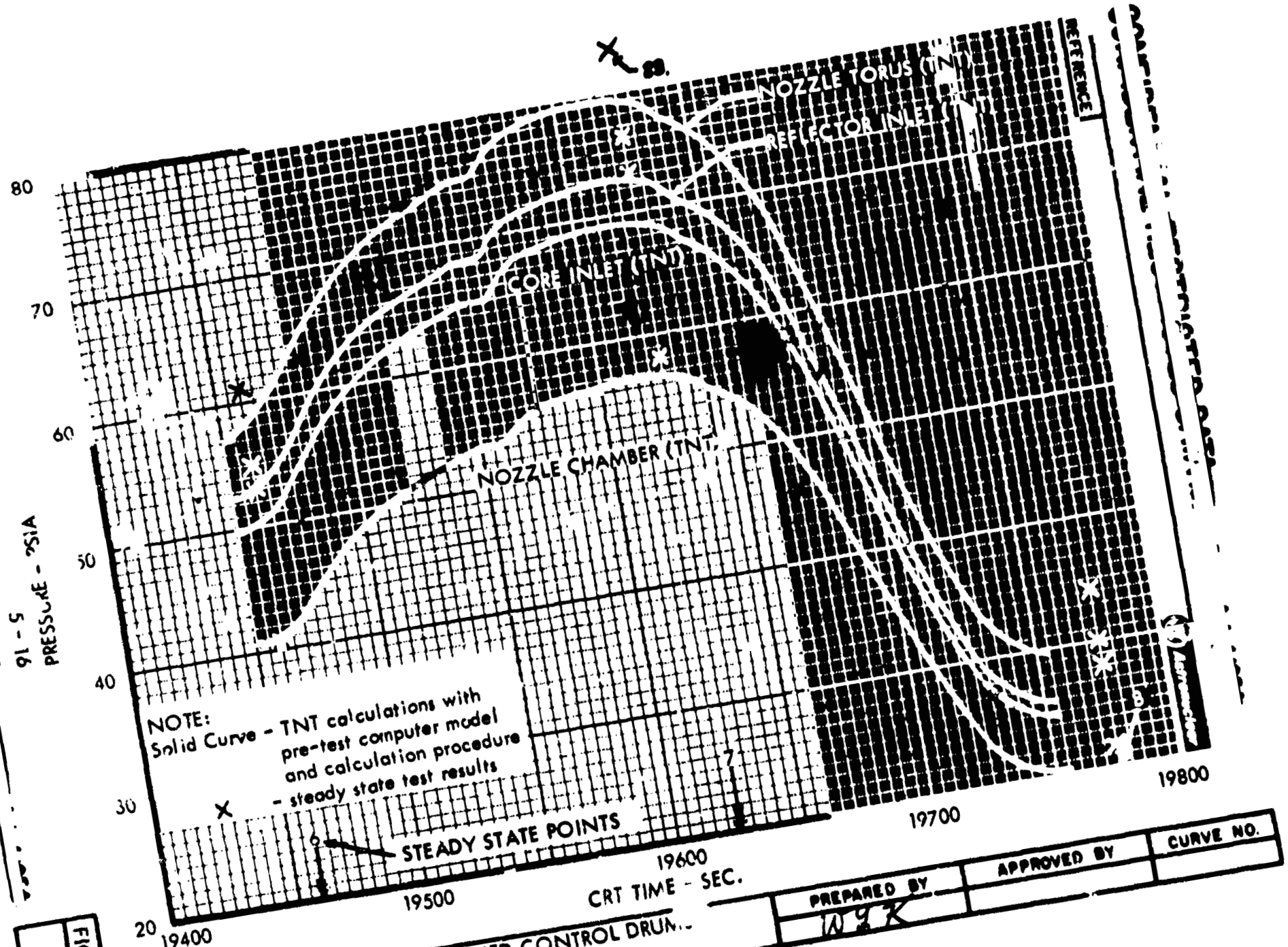

PREPARED BY	APPROVED BY	CURVE NO.
WGK		

FIGURE NO. 5-5

EP-V LOW POWER MAPPING TEST: FIXED CONTROL DRUM
REACTOR PLENUM PRESSURES

TABLE 5-3

COMPARISON OF CALCULATED AND MEASURED CONTROL DRUM BANK POSITION

Time CR (seconds)	Average Core Temperature, °R	Average Be Temperature, °R	Average Core H_2 Density, lb/ft^3	Calculated Feedback Reactivity, ¢	Calculated Drum Bank Rotation[1] and Position[2], degrees	Measured Drum Bank Position, degrees	Difference (M-C), degrees
19050	644	58	0.0424	34.9	-7.1/89.1	90.6	1.5
19295	1052	57	0.0187	-57.4	+7.5/103.7	103.8	0.1
19625	882	58	0.0330	7.4	-1.0/95.2	96.8	1.6

1 Converted at 7.7¢/°R

2 Normalized to the measured cold critical position of 96.2°.

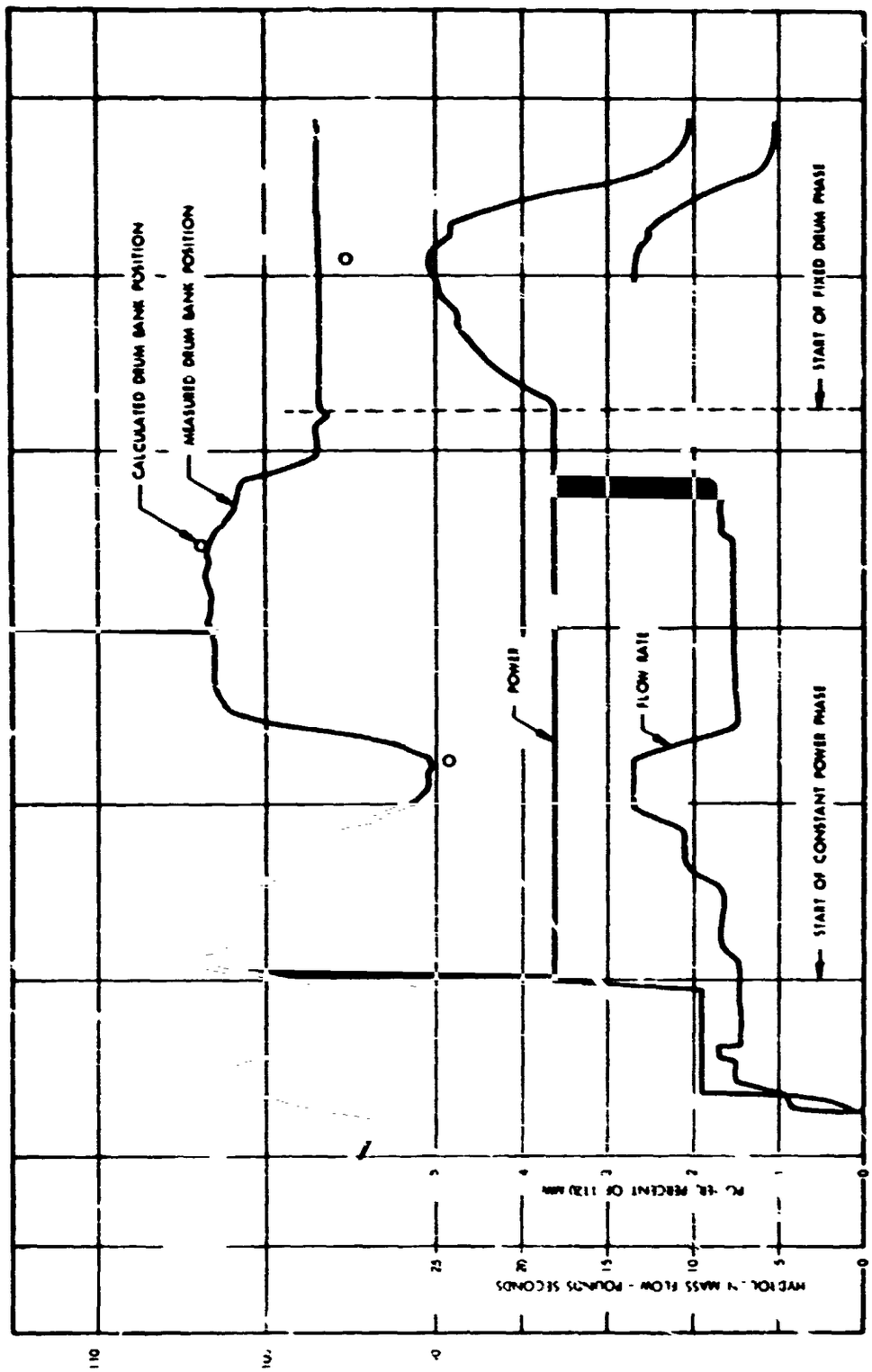

PREPARED BY	APPROVED BY	CURVE NO.

CONTROL ROOM TIME - SECONDS
NRX-A2 EP-V LOW POWER MAPPING TEST

Fig. No. 5-6

hydrogen worth as discussed in an earlier section results in an outward shift in all three calculated points. The shifts and new difference between measured and calculated results are tabulated below.

Time CR	Core H_2 Feedback Reactivity, ¢	Correction ¢, degrees	New Difference (M-C), degrees
19050	109	-10.9, +1.4	+0.1
19295	43	- 4.3, +0.6	-0.5
19625	89	- 8.9, +1.2	+0.4

Note that the 10 percent reduction in hydrogen worth generally aids the agreement and adds supporting evidence to the 10 percent reduction.

CHAPTER 6

REVIEW OF NUCLEAR DATA

ANTICRITICALITY SYSTEM

A central poison wire array with seven wires per fuel element in 19 clusters was provided to allow final wire withdrawal through the nozzle.[1] This array had been calculated to provide at least 2.0$ shutdown even if the control drums were inadvertently moved outward to 180 degrees.[2] Since criticality was attained at 180 degrees with 336 wires remaining, the worth of the additional (798 - 336 =) 462 wires represents the shutdown margin available in NRX-A2, approximately 3.7$. If the NRX-A2 reactivity had not been overpredicted by 0.5$ this margin would have been 3.2$.

CONTROL WORTH

The observed critical drum bank position during the approach to criticality and the subsequent differential worth measurements on control drum No. 2 both confirm the control span of the NRX-A2 reactor to be within the predicted 9.0$ ± 0.4$ span. The NRX-A2 approach to criticality yields a third confirmation. The NRX-A2 drum worth from 98.6 to 172.9 degrees was measured to be equivalent to 336 poison wires. In order to relate this to a reactivity, this 336 wire configuration was reproduced in the PAX-B reactor at WANEF and was found to be worth 3.85$. The NRX-A2 predicted drum worth of 4.00$, for the 98.6 degrees/172.9 degrees interval was in excellent agreement.

CRITICALITY MEASUREMENTS

Pretest Conditions

Summarized in table 6-1 are the delayed critical control drum bank positions measured

1 WANL-TME-840, Reactor Analysis Data Book, p. E-29.
2 WANL-TME-761, NRX-A2 Safety Evaluation Report, Supplement 1, Addendum 1 of 22 July 1964

in all the EP's and discussed in other sections of this report. As can be seen, all of the pretest critical positions show excellent consistency. As a best value a critical angle of 97.0 ± 0.5 degrees may be selected for the reactor in the operating configuration. The predicted position[1] of 91 degrees implies an overestimate in reactivity of 0.5$. The reason for this error is not known; an error of this magnitude could arise from reasonable differences in the non-destructive data for the PAX and NRX-A2 fuel*, as for example 2 percent in uranium.

An uncertainty has not been attached to these measurements because generally the positions tabulated were reproduced in several successive measurements and are consequently well substantiated.** The small differences that occurred from test to test (excluding EP V) are apparently not the result of random measurement error but represent small changes in the reactor. Changes in the data acquisition system or in the moisture content of the core are two possibilities.

Weather conditions during the test series have been studied in detail and appear to have been fairly uniform. Moreover as mentioned previously, the reactor itself is rather insensitive to small differences in temperature, if the core and reflector are at the same temperature. The drum bank differences are small enough however to have resulted from minor nonuniformities, such as warming of the beryllium reflector by the sun, which would not necessarily be seen on the Quick Look thermocouple channels

Material Loss in EP IV

Shown in table 6-1 are two conflicting measurements of the critical position following EP IV. The shift in the critical bank position is between 1 degree and 2.6 degrees of drum motion depending upon the value taken.

---

1 WANL-TME-887, NRX-A2 Test Prediction Report
* This data was the basis for the shimming of the NRX-A2.
** An exception is the value for EP IB.

TABLE 6-1

SUMMARY OF CRITICAL CONTROL DRUM BANK POSITIONS

	Critical Bank Position-degrees	
EP	Pre-test	Post-test
IA	96.9[1]	------
IB	97.0	------
II	96.5	------
III	97.0	------
IV	97.5[2]	100.1, 98.0[3]
V	96.2	97.0[4]

1. This value results from corrections to the measured 98.6 degrees in order to take account of differences between the physical reactor configuration in EP IA and the other tests.
2. The measured value was 97.6 degrees. Temperature correction reduced this by 0.1 degrees.
3. The measured values here were 101.8 and 99.6 degrees at 500 kw and 100 kw power, respectively. Temperature corrections produce the values listed.
4. The measured value was 97.6 degrees. Correction for elevated temperature reduced this to 97.0 degrees.

Careful weighing of about 200 fuel elements indicated an average loss of about one gram. Assuming this to be carbon loss from the bores, the reactivity loss is equivalent to about 1 degree of drum motion. Although this data tends to confirm the 99.6 degrees measurement (corrected to 98.6 degrees at ambient conditions) the higher value was obtained c. 500 kw versus 100 kw for the 99.6 degrees measurement, and may be more accurate as it should be less affected by the photoneutron source in the outer reflector. Although the reported temperatures for the two measurements are essentially the same, it is possible that the actual conditions were different.

Depending upon which of the EP IV post test measurements is adopted, an apparent reactivity gain equivalent to 2 to 4 degrees occurred from EP IV to EP V. Aside from error in the data system the most likely hypothesis is that the reactivity gain resulted from moisture pickup either from the purge gas passing through the reactor between these two tests or atmospheric humidity.* The mechanism might be adsorption of water onto the graphite surfaces or hydrolysis - the reaction of water vapor with uranium. The latter process is possible if fuel temperatures during EP IV were high enough to have caused migration of the uranium through the pyrolytic carbon fuel bead coating.** Whether, or to what extent, migration occurred in NRX-A2 will be determined by presently metallographic work being conducted.

Apparent Reactivity Loss in EP V

A small change in the pre-test and post-test critical positions was experienced in EP V. The magnitude of the difference (0.8 degree after temperature correction) is small and may have resulted from one of several causes (for example):

---

* Due to gas shortages, the purge system did not operate for a period of several days after EP IV. The relative humidity during this time varied daily (typically) between 25 and 39 percent with an average at about 30 percent.

** This effect has been discussed in WANL-TME-761, Supplement 4. In this pre-test document, an estimate of 30¢ reactivity pickup is made for operation at extreme conditions.

1) the method by which the temperature correction was made
2) uncertainty in the temperature
3) a small amount of adsorbed hydrogen driven off during the test

This effect is related to some of the problems discussed above and resolution may come when more is learned about these other problems.

Accuracy of Critical Bank Measurements

The absolute accuracy of the digital printout device is quoted at ± 0.5 degree.[1] Data on the true position of the control drum plates presented in the 3 day report on EP IA (NTO-R-0001) and later refuted in NTO-R-0008 indicates the uncertainty in the absolute position of the vanes. It is not known but most probably is in the range of 0.5 to 1 degree. Knowledge of the true position of the control plate is important to an understanding of fission measurements and accurate shimming of future reactors. It is not as important to the analysis presented in this report because drum position differences are generally used. The dominant factor under these conditions is the resolution of the measuring device. Since the digital drum printout machine prints only angular positions to even tenths, the resolution is ± 0.1 degree. In any difference between drum positions the uncertainty will be ± 0.16 degree to 95 percent confidence.

Operating Reactivity Changes

The predicted reactivity swing from ambient to 100 percent power and flow conditions was -0.52$ or 6.6 degrees drum withdrawal. The observed difference was (103 - 97 =) 6 degrees, of which 1 to 2.6 degrees represents the reactivity related to material loss. A number of uncertainties particularly in the quantity and worth of hydrogen adsorbed in the fuel have been identified, so that the agreement is in part believed to be fortuitous.

---

1 NTO-R-0008

HYDROGEN WORTH

Considerable data relating to hydrogen worth has been acquired during the NRX-A2 test program. While a better understanding in certain areas has resulted, there remain some unresolved problems. From the standpoint of hydrogen worth measurement, the EP IB GH_2 test was the most valuable. This test indicated that the analytically determined core hydrogen worth, typified by 6.80$/kg for a uniform distribution, overestimated the true worth by about 10 percent. This conclusion confirmed earlier PAX measurements on the worth of hydrogen contained in polyethylene that showed a 5 to 10 percent difference compared to calculations. Additional evidence supporting this result was obtained in EP V. The hydrogen worth inferred from EP IV is not conclusive, but is not in clear disagreement. The time dependent error in the calculated EP IV feedback reactivity seems to be related to a hydrogen effect, possibly the so called diffused hydrogen.

EP IB also established that the apparent core pressurization effect is probably small. Noted in the initial portion of the EP IB GH_2 run, the magnitude of the effect was suspected to be worth 2.5 degrees of drum motion. Analysis showed that the effect is probably less than 0.5 degree.

TEMPERATURE COEFFICIENT

The temperature coefficients were substantiated in EP II, EP III, EP V and at end of life in EP IV. No clear disagreement was demonstrated by any of the analyzed data. However, the excellent agreement in the low power testing contrasted to the errors in calculations in the early portions of EP IV high power testing, indicate that while the total reactivity feedback effect has been well predicted, the analytical model may need added sophistication. The effect, for example, of the radial and axial temperature distribution, not specifically a parameter in the reactivity feedback calculations, may ultimately explain some of the unresolved problems.

NUCLEAR PROBLEM AREAS

Analysis of NRX-A2 test data has resulted in identification of certain key analytical problem areas. Recognizing that the success of future testing will be contingent in part on a better understanding of these problems, efforts have been made to isolate them and initiate work toward their solution. The listing below contains both priority items (P) and those of secondary importance.

(P) 1) Magnitude and Time Dependence of the Diffused Hydrogen Effect

2) Effect of Pressure Surges on Reactivity

(P) 3) Reactivity Effect of Various Radial and Axial Temperature Distributions

4) Mode of Core Expansion

5) Purge Gas Moisture Retention in the Reactor Core Before and After Power Testing

6) Meaning of Post Test Criticality Measurements (Effects of Photoneutron Source)

7) Beryllium Reflector Temperature Effect on Reactivity

CHAPTER 7

REVIEW OF THERMAL DATA

PERFORMANCE

EP IV Test

The reactor successfully was subjected to severe operating conditions during the startup, shutdown, and at steady state operation during EP IV. Maximum nozzle chamber temperature rate of change was +125°R/sec during startup and -350°R/sec during shutdown. Extreme operating conditions during the test series were listed in table 4-3. Nozzle chamber thermocouples did not indicate average chamber temperature, therefore it was calculated from flow and chamber pressure using the choked nozzle relation. Reactor thermal power was calculated from an energy balance using these nozzle chamber temperatures. At the 40 second maximum reactor power hold these values were 75.6 ± 1.5* lb/sec LH_2 flow, 3815° ±215°R nozzle chamber temperature and 1096 ±50 mw total thermal power.

The reactor power given above was confirmed within the calculated accuracy by rabbit-measured power, and linear neutronic channel number 2 power. The peak power level was also indirectly confirmed by comparable quantities of total energy release during the test series obtained from integrated thermal power and from post-operative radiochemistry. Maximum reactor power implied from core thermal capsule material temperature measurements agrees within the accuracy of the measurements, however, this comparison is not completely satisfying because core temperatures imply a power level 5 percent higher than 1096 MW.** Total energy release during EP IV was 3.41×10^{11} watt-seconds, or an average of 813 MW over the 7 minute test, while total energy release was 3.81×10^{11} watt-seconds for the test series.

---

* All accuracies given in this section are 2σ (95 percent confidence) range.

** A refinement in the temperature calculation model at the sensor location leads to better agreement between calculated and measured core temperatures. This will be published in TNR-199, Supplement I.

Best values of steady state system operating conditions were given in the cycle diagram of figure 4-8.

A post test calculation of the reactor operating conditions using measured power and flow profiles was performed with the TNT code and the reactor model used for pretest predictions given in WANL-TME-887. Comparison of this calculation to test data demonstrated the adequacy of the TNT transient startup representation and the necessity for adjustments to the model in several regions to more closely represent operation conditions at steady state.

Preliminary cold flow tests performed in EP 1B demonstrated that it was necessary to take the LH_2 storage between LH_2 venturi meter and the reactor into account for the power test startup.

EP V Test

The reactor was operated for approximately 20 minutes with 5 to 13 lb/sec LH_2 flow, 21 to 53 MW reactor power, and a nozzle chamber temperature of up to 1300°R. The objectives of the test were achieved. A considerable portion of the test was performed with two phase conditions in the reflector region and at the core inlet. Comparison of the measured data with TNT calculated conditions was reasonable considering the inaccuracy of the test results caused by the fact that most transducers were operating near the low end of their scales.

CORE

Core Material Temperatures

Station 32 thermocouples indicated temperatures up to 1200°R less than core material temperatures because of lost putting compound and bypass flow through the thermocouple lead channel. The best indication of maximum core temperatures were obtained from the thermal capsules located in the central elements which indicated temperatures from 4000°R to 4400°R at station 45. A multiple regression fit of the thermal capsule data was performed in order to correlate the temperatures with core radius. This data fit shows that the average temperature

of the entire central region* of the core was 4276° ± 109°R and there was no significant radial variation. At the core periphery the data fit reveals a linear radial variation rising to a maximum of 4360° ± 179°R at the core periphery. Families of thermal capsules in four clusters indicated the maximum temperature of 4400°R in the J row.

Core fuel element temperatures at maximum power were calculated for the test conditions of core inlet temperature, operating control drum angle and measured reactor flow rate and power (1096 MW). Correlating the results of this calculation as a function of radius gives a reasonably flat radial profile in the central region of the core at a nominal level of 4080° ± 215°R and an increasing temperature toward the core periphery to a maximum of 4327°R ± 215°R at the core periphery. The maximum calculated temperature occurs in element J-5-J which was also one of the 4 highest thermal capsule indications. The reason for the high peripheral temperatures is the fact that the core was orificed for an operating drum angle of 90 degrees and an inlet hydrogen temperature of 250°R while the maximum operating condition was 103 degrees drum angle and 225°R core inlet temperature.

The calculated values are almost 200°R lower in the central region. Possible reasons for this variation which are being investigated include: temperature sensors over indicating due to internal heating, calculational model used to facilitate central element and fuel element heat interchange, core bypass flow in excess of 0.36 lb/sec, higher reactor power, or lower reactor flow. The results of this investigation will be included in a supplement to this report to be published at a later date.

Core Pressure Drop

Calculated core pressure drop was about 5 percent lower than measured core pressure drop. This may be due to a change in flow impedance during the test. Core pressure drop calculated using the results of post-operative fuel elements is to be compared with measured core ΔP.

---

* Central region of the core is defined as all clusters except the J row.

[1] WANL-TNR-199 Supplement 1, to be published

Tie Rod Exit Gas Temperatures

Measured tie rod temperatures were 130° to 260°R higher than calculated during EP IV and EP V tests. Also the indicated temperatures were erratic, T-755 was about 100°R lower than T-760 and T-765 during EP IV, while T-760 was up to 465°R higher than the other two operative thermocouples during EP V. The erratic behavior and high indications have been attributed to the thermocouple contacting the hotter molybdenum core during the test, as evidenced by the bent thermocouples observed during disassembly.

REFLECTOR, SHIELD AND LATERAL SUPPORT

The power picked up in the reflector system was calculated from measured LH_2 flow rate and measured temperatures at the four power holds. A linear average of this calculated power at the four holds was (2.15 ± 0.18) percent of total reactor thermal power, while calculated nuclear heating rates give a reflector power equal to $1.76 \begin{smallmatrix}+0.6\\-0.5\end{smallmatrix}$ percent of reactor power. A comparison of these values indicates that the measured reflector heating rate was about 20 percent higher than the calculated heating rate but was within the error range of the calculated rate. This measurement provides more accurate reflector heating than was previously available.

Comparisons of measured conditions and pretest calculated conditions were not meaningful because (a) the test was considerably different than planned; (b) nozzle tube exit temperature (reflector inlet) was higher than pretest calculations indicated; (c) the support ring temperatures, which affect the inner-outer reflector gap size and thereby overall reflector impedance, were lower than had been expected; and (d) reflector heating rate was high, as mentioned above. On the basis of the measured test power and flow rate, measured reflector inlet temperature, measured reflector heating rate (at the maximum power hold) and measured support ring temperature, the reflector, shield and lateral support system conditions were calculated at the highest power hold. The calculated pressures, fluid temperatures and material temperatures were compared to measured values in order to confirm the calculational method and to discover any anomalies in operation of these components

during the test. Generally there was reasonable agreement between the measured and calculated values. Items of interest obtained from this comparison are listed below.

1) All calculated pressures including the lateral support pressure distribution were in good agreement with measurements.

2) All calculated plenum fluid temperatures concurred well with measured temperatures. Single thermocouple temperature indications for the hydrogen exiting from individual major reflector coolant passages were in reasonable agreement with calculations, considering that the measurements do not represent the average of all similar channels.

3) Lateral support seal chamber fluid temperature measurements were about 800°R lower than calculated. Reviewing both other temperature measurements in the lateral support region and the thermocouple installation leads to the conclusion that these thermocouples were most likely indicating inner reflector material temperature, rather than the average seal fluid temperature.

4) Material temperature measurements in the shield, support plate, filler strips, inner reflector, outer reflector, control drums, and boral vane were all adequately close to calculated values. However, the graphite inner reflector material temperatures increased with time throughout the test, even at the steady state holds. This increase is believed to be due to a decrease in graphite thermal conductivity with irradiation, although experimental data on the effect of irradiation on H4LM graphite conductivity is not presently available.

5) Temperature symmetry was evident at steady state operation during EP IV in reflector inlet, reflector outlet, dome end, and core inlet plenums. During EP V azimuth temperature asymmetries are evident. These asymmetries and their cause are being studied in detail.

NOZZLE

The nozzle tube inlet pressure and pressure drop calculated with the TNT Reactor Model agreed well with test measurements. However, heat pickup of the nozzle coolant was about 30 percent greater than calculated.

Temperature distribution at the nozzle tube exit was symmetrical throughout the high power test after hydrogen pressure exceeded critical pressure during the startup. An azimuth temperature asymmetry during prechill and the first portion of startup was apparently oriented with the nozzle feedline, but had no significant effect on operation.

THERMAL PROBLEM AREAS

Analysis of the NRX-A2 test data has resulted in the identification of certain problem areas or potential problem areas. In some cases it has not been ascertained whether the problem is associated with the analysis or with the reactor or reactor instrumentation. These items are listed below:

1) Effect of irradiation on thermal conductivity of graphite (rising inner reflector temperatures).
2) Internal heat generation effect on core instrumentation
3) Low power operation azimuth temperature asymmetries
4) Calculation of central element temperature at instrument location
5) Reactor and nozzle model for computation of system conditions
6) Corrosion analysis
7) Tie rod temperatures

CHAPTER 8

DOSIMETRY

EXPERIMENTAL PROGRAM

An experimental radiation measurement program was carried out in conjunction with the NRX-A2 reactor tests. Radiation measurements were made during the calibration run (EP II), and high power run (EP IV), and the restart run (EP V). Many dosimeters were exposed during both the EP IV and EP V runs. Measurements are necessary to evaluate properly such aspects of the radiation environment as the distribution of the leakage radiation from the reactor, the variation of the radiation with distance, and the environmental perturbations such as the test cell wall, privy roof, and instrumentation ladder. The chief importance of the experimental program is to verify the analytical techniques used to predict the radiation environment during the reactor tests, to provide confidence in their application to nuclear rocket flight testing, and to delineate areas wherein the analytical techniques are inadequate. In these latter areas, the measurements may provide a basis for future predictions.

Approximately 1000 radiation measurements were made during the NRX-A2 tests. This number includes the fission foils, gold foils, sulfur pellets, and gamma dosimeters provided by the Los Alamos Scientific Laboratory and referred to in this report as LASL data.

It is not the purpose of this section to tabulate, interpret, or ascertain the validity of all the NRX-A2 radiation measurements, nor to describe experimental techniques. Rather, the intent is to compare available measurements with the analytical data. A separate report[1], published by WANEF, is being issued which describes the experiments in detail. The validity

[1]WANL-TME-1081, NRX-A2 Dosimetry Measurements, Westinghouse Electric Corporation, Astronuclear Experimental Facility, March, 1965

of measurements will be discussed only to the extent necessary to establish agreement or disagreement with calculated data.

Dosimetry Method

Dosimetry employed in the NRX-A2 tests was of the passive or integral type from which was obtained total exposure doses and fluxes for the various reactor runs. Independent determination of the total power generated in these runs was necessary in order to provide a basis for direct comparison of the radiation measurements made in one run with those made in another. The integrated power levels[1] (refer to chapter III of this report) used to normalize the radiation data to a one watt power level are as follows:

Reactor Run	Watt-Seconds
EP II	7.85×10^{6}
EP IV	3.46×10^{11}
EP V	4.54×10^{10}

Five types of gamma dosimeters were used. Major emphasis was placed on silver metaphospate glass rods, cobalt borosilicate glass plates, and film dosimeters. Bismuth glass and lithium fluoride thermoluminescent detectors were used at several locations. The combination of these detectors covered a gamma dose range of 0.01 to 10^{6} roentgens.

A threshold and resonance neutron detector system was used to make neutron flux measurements in the fast and resonance energy range. Copper, cobalt, and gold were exposed with and without cadmium covers to obtain neutron fluxes in the thermal and resonance energy ranges. A fission foil neutron detection system used extensively by Los Alamos Scientific Laboratory in the KIWI series of reactor tests provided a means of measuring the fast neutron flux in three broad energy bands, i.e., 0.004 Mev to 0.75 Mev, 0.75 Mev to 1.5 Mev, and 1.5 Mev to 2.9 Mev. Sulfur pellets and nickel foils were used to measure the neutron flux with energies greater than 2.9 Mev*. Fast neutron rad doses were determined

[1] WANL-TME-1081, NRX-A2 Dosimetry Measurements, Westinghouse Electric Corporation, Astronuclear Experimental Facility, March, 1965

*LASL reports the sulfur threshold as 2.5 Mev, whereas WANL uses a 2.9 Mev threshold

by LASL by applying conversion factors obtained by first collision theory to the measured neutron spectra for energies greater than 0.004 Mev.

Dosimetry Placement

Dosimeter positions and implementation which yielded useful data are identified in table 8-1. The NRX-A2 dosimetry program included a somewhat more extensive implementation than is presented in table 8-1. However, not all of the instrumented locations yielded adequate data for reduction and analysis for several reasons:

1) All aluminum, magnesium, and nickel dosimeters on EP II received insufficient irradiation for counting purposes because of the unexpected low EP II power level, and hence, low radiation leakage.

2) All dosimetry on the pressure vessel bands on the high power run were lost because of band failure.

3) Gamma dosimeters on the meridian and equatorial ring were physically damaged due to flare heating on the high power run.

4) Some of the gamma dosimeters on the trolley line were lost because the coloration used for analysis was annealed out due to flare heating during the EP IV run.

5) Some cadmium covers and ammonium sulfate pellets melted on the meridian ring at locations within the area of the fire on the pressure vessel forward flange.

The first criticality test, EP II, was a reactor calibration run in which the reactor power level was held for 20 minutes at a low level (6.66 kw). Because of this low power level, dosimeters could be placed close to the reactor. Dosimetry placement on the vessel surface, and on the meridian and equatorial rings is shown in the photograph in figure 8-1. By means of the axial and circumferential dosimeter placement on the vessel surface, and the meridian and equatorial ring dosimetry, it is possible to study the polar, azimuthal, and axial distribution of radiation leaking from the vessel.

Circumferential placement on the vessel surface consisted of eleven positions at station 26 between Reactor θ = 42 degrees and Reactor θ = 72 degrees as is shown in figure 8-2. Reactor stations are distances in inches from the dome end of the core. Station 26 is at the

TABLE 8 - 1

DOSIMETER PLACEMENT* DURING LOW AND HIGH POWER NRX-A2 RUNS

	Gamma Dosimetry					Neutron Dosimetry							
	WANL				LASL	WANL					LASL		
Location	Film	Glass Rod	Cobalt Glass	TLD**	Glass	Au	Co	Cu	Ni	S	Au	S	Fission Foils
Propellant Feed Line	II	II	IV										
Pressure Vessel	II	II				II	II	II		II			
Equatorial Ring	II	II		II	II		IV	II	IV	II IV	II	II	II
Meridian Ring	II	II		II	II		IV	II	IV	II IV	II	II	II
Trolley Line	II	II	IV V	II IV	II IV,V		IV	II	IV V	II IV	II IV,V	II IV,V	II IV,V
Instrumentation Ladder	II	II	IV		II					II	II	II	II
Test Cell Wall	II	II			II					II IV	II	II	II
Privy Roof Top	II	II	IV		II			II	IV		II	II	II
Test Car Locations	II	II	IV				IV		IV	II IV	II	II	

* Dosimeters were placed at additional locations not listed here. These additional locations have been omitted either because the experimental results are not yet available or because the dosimeters failed to yield useful data for reasons described in Chapter 8.

** Thermoluminescent dosimetry

REFERENCE | Astronuclear

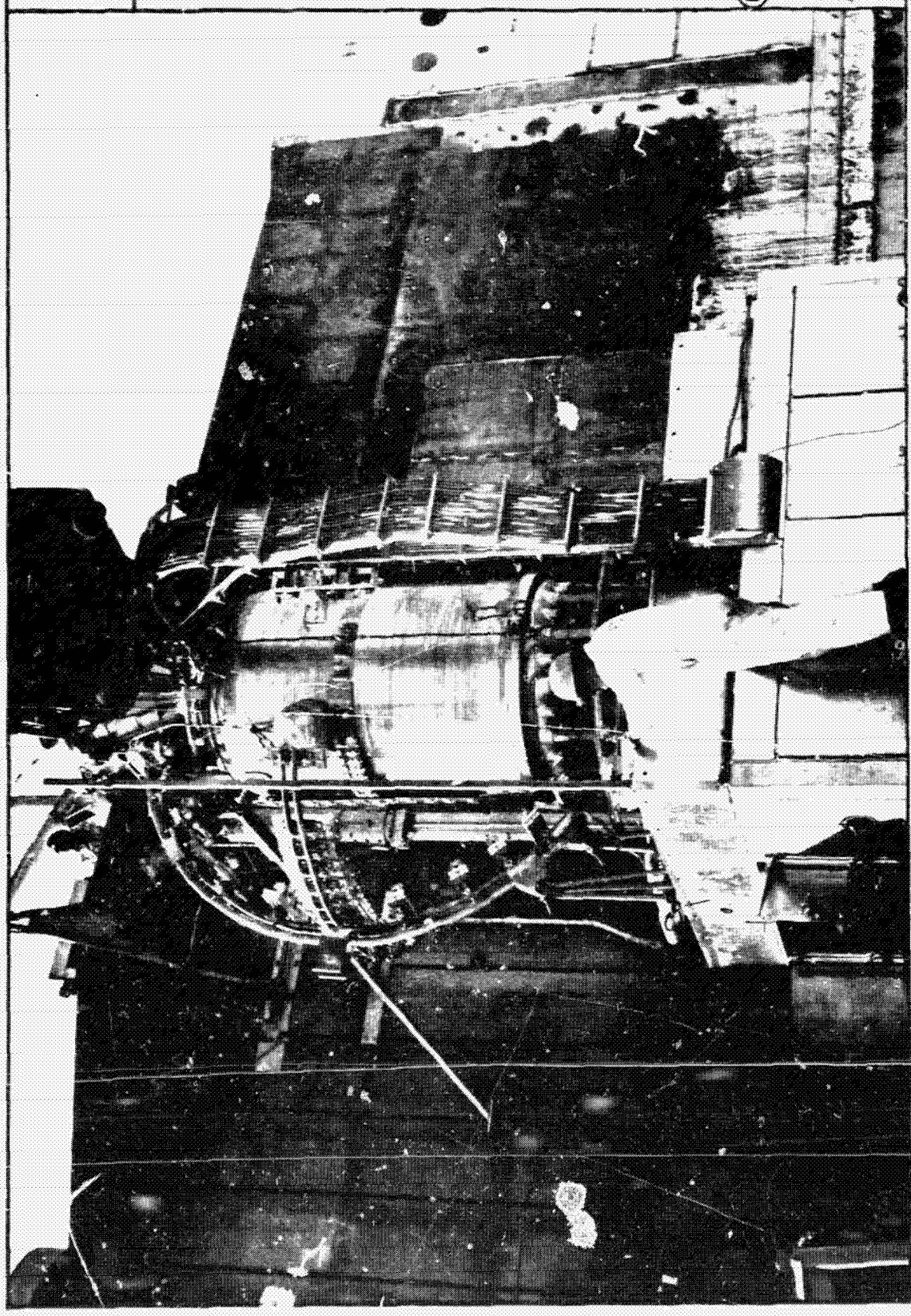

Fig. No. 8-1 NRX-A2 Reactor Showing Meridian and Equatorial Ring and Dosimeter Placement on Vessel

PREPARED BY	APPROVED BY	CURVE NO

Fig. 8-1

REFERENCE		PREPARED BY	APPROVED BY	Astronuclear

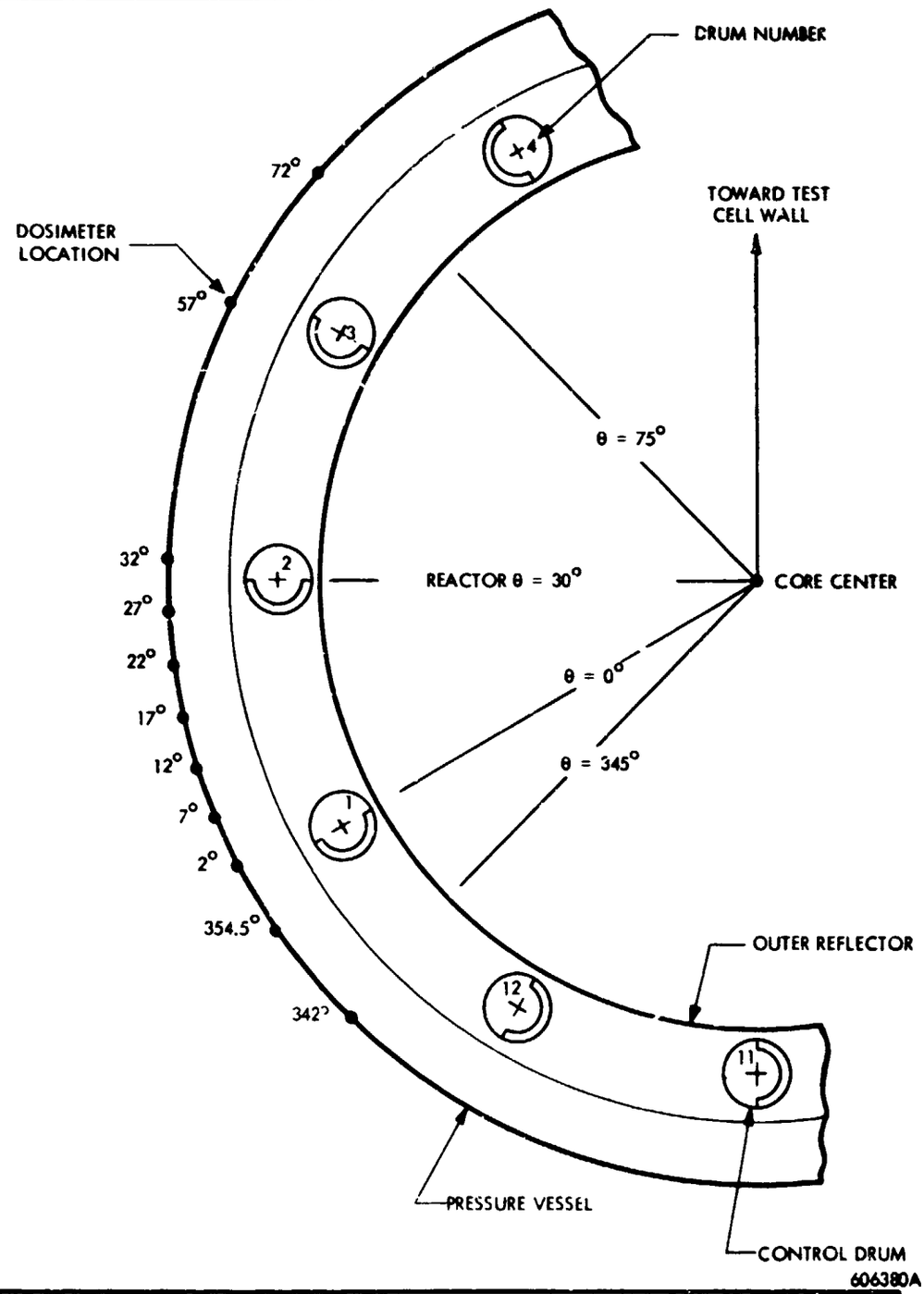

Cross Sectional View, at Horizontal Midplane (Station 26) Looking Toward Dome.

Figure No. 8-2

core midplane, and station 52 at the nozzle end of the core. Reactor θ is the core azimuthal angle, defined such that Reactor θ = 0 degrees is located 120 degrees from the normal to the test cell wall (counter clockwise, looking toward dome). Axial placement on the vessel surface consisted of eleven positions at Reactor θ = 48.5 degrees between station 0 and station 52 as is shown in figure 8-3.

Also, gold, copper and cobalt wires were used on the vessel surface.

The meridian ring held a total of twelve dosimeter stations on a 5 foot arc centered on the geometrical center of the reactor core as is shown in figure 8-3. The meridian ring was located at Reactor θ = 30 degrees.

The equatorial ring was affixed at right angles to the meridian ring at station 26. This ring held thirteen dosimeter stations. The first or farthest from the test cell wall, was located at a Reactor θ = 345 degrees. Stations were then implemented from 0 degrees to 50 degrees in 5 degree intervals. Stations were implemented at 60 and 75 degrees also. All stations on this ring were located 5 feet from the core center. Equatorial ring dosimeter placement is shown in figure 8-4.

Other locations instrumented for EP II were the propellant feedline, instrumentation ladder, test cell wall, test car, privy roof top, and trolley line.

Measurements during the high power run EP IV were obtained, in general, at greater distances from the reactor than during the calibration run. The radial distribution of the radiation field was studied with dosimeters located at 12, 27.5, and 35 feet from the reactor (on poles) and from 62 to 2700 feet from the reactor on the trolley line. These dosimeters, together with the EP II dosimeter on the surface of the reactor and the equatorial ring dosimeters, provided a means for determining the radial distribution from the vessel surface to 2700 feet from the reactor. The trolley line was positioned at Reactor θ = 345 degrees.

There are no data from EP IV for the vessel surface due to the loss of the bands. However, some measurements were obtained at most of the other locations during the high power run (See table 8-1). Many dosimeters were left in place during both the EP IV and EP V runs.

During EP V, the restart run, several locations on the trolley line were instrumented.

REFERENCE		PREPARED BY	APPROVED BY	Astronuclear

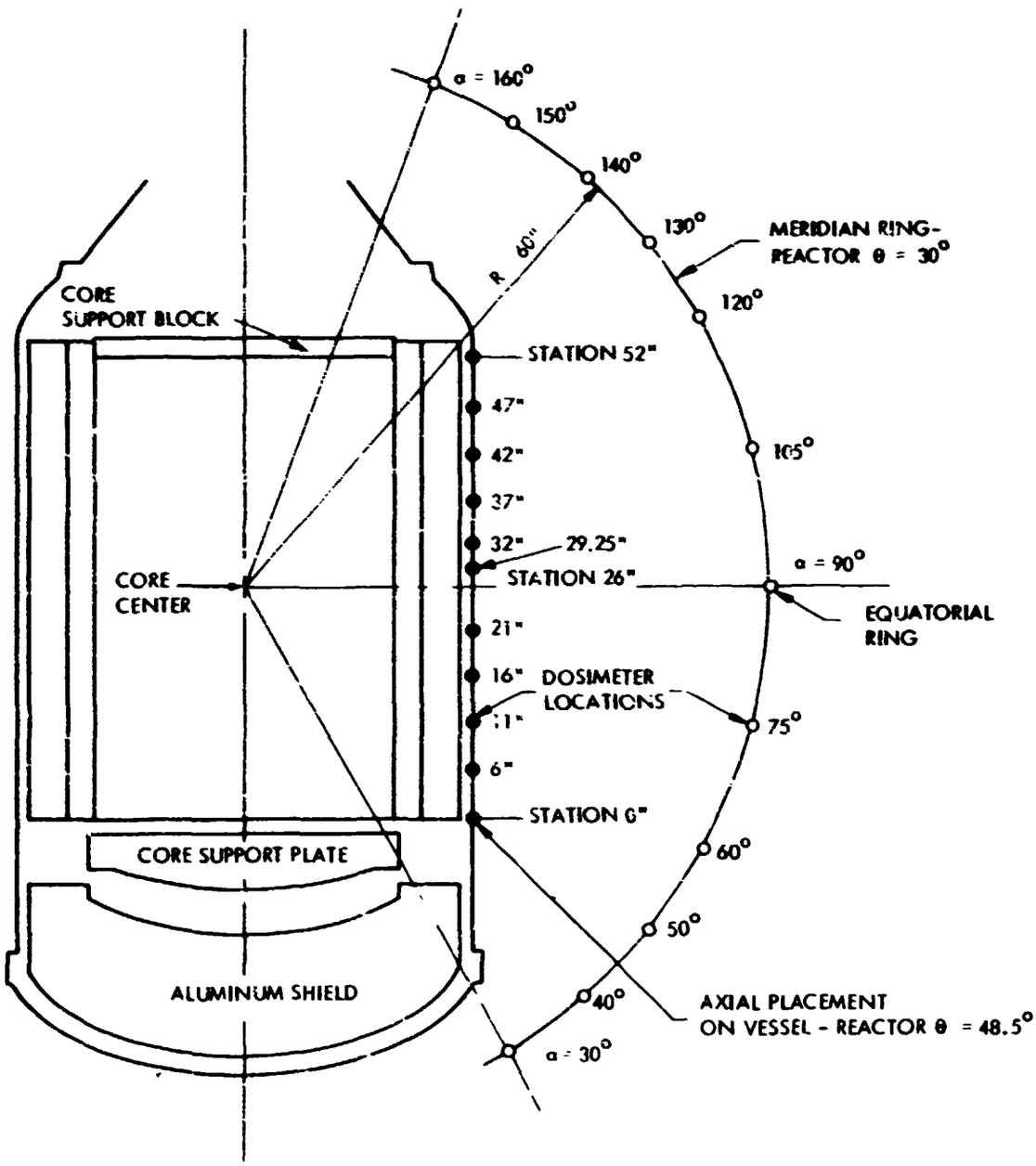

NRX-A2 Cross Sectional View Locating Dosimeter Positions on the Meridian Ring and on the Vessel Surface (Axial Placement)

Figure No. 8-3

REFERENCE		PREPARED BY	APPROVED BY	Astronuclear

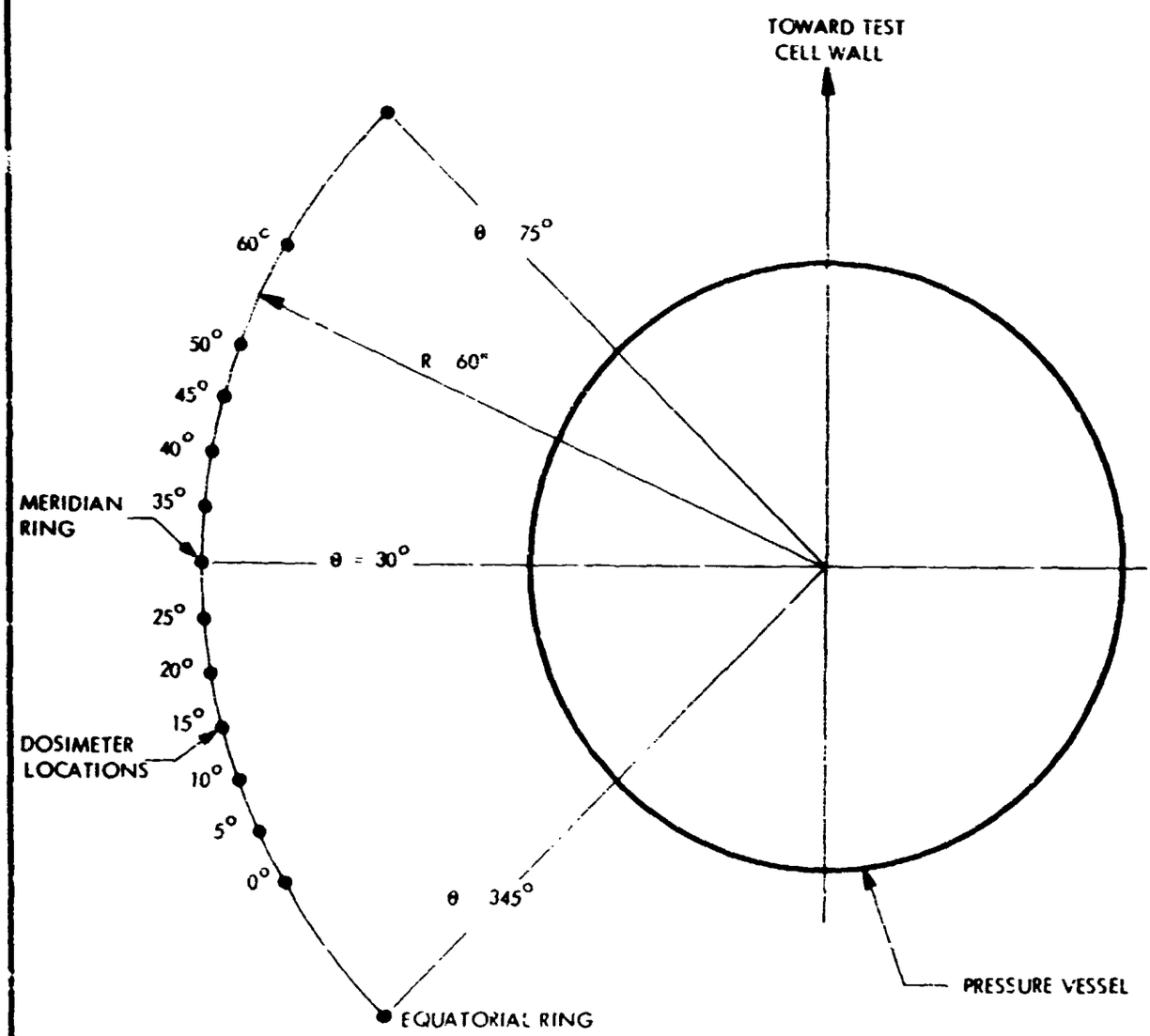

CROSS SECTIONAL VIEW AT HORIZONTAL MIDPLANE (STATION 26) LOOKING TOWARD DOME

Cross Sectional View At Horizontal Midplane (Station 26) Looking Toward Dome	Figure No. 8-4

ANALYTICAL METHODS

The Standard Design Methods employed in predicting the NRX-A2 radiation environment (except at locations under the privy roof) have been reported in detail[1,2,3]. Therefore, the methods, per se, will not be discussed in this report in detail. However, their application to the various NRX-A2 dosimeter locations will be described.

Gamma Ray Dose Rates

SURFACE OF THE PRESSURE VESSEL

Gamma ray dose rates at the pressure vessel surface were predicted by combining data from Monte Carlo Program 18-0 and point kernel Program 14-0[5]. Monte Carlo Program 18-0 calculated the energy deposited in regions describing the pressure vessel in the axial direction. Point kernel Program 14-0 was used to obtain the radial distribution of the gamma rays. The Monte Carlo energy deposition data were converted from watts per gram-carbon to rads-carbon per hour by the exact relationship: 3.6×10^3 rads per hour = one watt per gram. Since the pressure vessel does not contain carbon, the calculated value of watts per gram-carbon was adjusted by applying the ratio of gamma ray heating in carbon to that for aluminum.

The technique described above was time consuming and somewhat involved, and of course, required many assumptions. To improve calculation of gamma ray surface dose

---

[1] WANL-TNR-128, Vol. II, Reactor Analysis of NRX-A, Radiation Analysis, Westinghouse Electric Corporation, Astronuclear Laboratory, Radiation and Shielding Group, September, 1963

[2] WANL-TMF-941, Progress on an Automated Radiation Analysis Program, Westinghouse Electric Corporation, Astronuclear Laboratory, H. C. Woodsum, August, 1964

[3] WANL-TNR-165, Radiation Analysis of NRX-A2 by Various Methods, Westinghouse Electric Corporation, Astronuclear Laboratory, M. A. Capo, December, 1964

[4] GEMP-102, Specialized Reactor Shield Monte Carlo Program 18-0, General Electric Co., NMPO, J. E. MacDonald, et al., October, 1961

[5] XDC-59-2-16, Shielding Computer Program 14-0 and 14-1 Reactor Shield Analysis, General Electric Co., ANPD, W. E. Edwards, et al., January, 1959

rates, the ETA (Escape Tape Analyzer) code[1] was written in Fortran. This code analyzes the Monte Carol Program 18-0 escape tapes and calculates the energy escaping the surface of the reactor system, as well as the dose, flux, or heating rate on the surface of the reactor assembly. Results of the initial application of the ETA code indicate that this technique is more accurate and reliable in predicting surface dose rates than the previously used method.

MERIDIAN RING AND RADIAL TRAVERSE

Point kernel program 14-0 was used exclusively to predict gamma ray dose rates at dosimeter locations on the meridian ring as a function of radial distance from the reactor. Thirteen gamma ray source energy groups were employed in this analysis. Source strengths of gamma rays due to neutron capture and inelastic scattering in materials inside the pressure vessel were obtained from the HIC-I and NORMALIZER codes.[1,2,3] These two codes employed 50 group neutron fluxes from the one-dimensional diffusion code PIMG[4] to calculate appropriate gamma ray reaction rates which were normalized to the two-dimensional, four group diffusion code, CURE,[5] data. The predicted gamma ray dose rates in this report include, therefore, not only primary gamma rays from the reactor, but all known sources of secondary gamma rays born outside the core, within the pressure vessel. Throughout this analysis, infinite media water buildup factors were employed in the point kernel code.

---

[1]WANL-TME-941, Progress on an Automated Radiation Analysis Program, Westinghouse Electric Corporation, Astronuclear Laboratory, H. C. Woodsum, August, 1964

[2]WANL-TNR-128, Vol. II, Reactor Analysis of NRX-A, Radiation Analysis, Westinghouse Electric Corporation, Astronuclear Laboratory, Radiation and Shielding Group, Sept., 1963

[3]WANL-TNR-165, Radiation Analysis of NRX-A2 by Various Methods, Westinghouse Electric Corporation, Astronuclear Laboratory, M. A. Capo, December, 1964

[4]WAPD-TM-135, PIMG-4. One-Dimensional Multigroup P_1 Code for the IBM 704, Westinghouse Electric Corporation, BAPD, H. Bohl, Jr., et al., July, 1959

[5]APEX-452, CURE - A Two-Space Dimension, Multigroup Code for the IBM-704, General Electric Corporation, ANPD, F. M. Trantham, Jr., August, 1963

The technique employed to calculate the contribution due to air scattering of gamma rays has been documented.[1]

BELOW THE PRIVY ROOF

Analysis of the radiation environment is extremely difficult in physical surroundings such as exist under the privy roof, because of the additional sources of radiation which must be considered, such as wall capture gamma rays, privy roof capture gamma rays, and gamma radiation scattered from the wall. The methods employed to calculate the gamma ray radiation at locations under the privy roof are not part of the Standard Design Methods[1, 2, 3] (except for the direct beam dose contributions). Hence, these methods will be described here in some detail.

Privy Roof Capture Gamma Rays

An axial, one dimensional, eighteen group transport code, DTK,[4] was run to calculate neutron fluxes as a function of centerline position in the privy roof. In the DTK calculations the roof was placed adjacent to the pressure vessel to avoid the problem of accounting for the radial leakage in the void region which exists between the vessel surface and the top of the roof. Core geometrical buckling was used for all regions in the DTK to account for radial leakage. The capture rates at selected axial positions, Z', in the roof were calculated in the usual manner as follows:

$$C_{mZ'} \text{ (absorption/cm}^3\text{-sec)} = \sum_{i=1}^{18} \phi_i \sigma_{a_{im}} N_m \qquad (8\text{-}1)$$

---

[1] WANL-TNR-128, Vol II, Reactor Analysis of NRX-A, Radiation Analysis, Westinghouse Electric Corporation, Astronuclear Laboratory, Radiation and Shielding Group, Sept., 1963

[2] WANL-TME-941, Progress on an Automated Radiation Analysis Program, Westinghouse Electric Corporation, Astronuclear Laboratory, H. C. Woodsum, August, 1964

[3] WANL-TNR-167, Radiation Analysis of NRX-A2 by Various Methods, Westinghouse Electric Corporation, Astronuclear Laboratory, M. A. Capo, December, 1964

[4] Unpublished, Los Alamos Scientific Laboratory

where

ϕ_i = DTK neutron flux for i_{th} neutron energy group

σa_{im} = Microscopic absorption cross section for i^{th} enegry group for material m (DTK cross sections)

N_m = Atom density for material, m

$C_{mZ'}$ = Absorption/cm^3-sec for material, m, at axial DTK location Z'

Since the roof was located adjacent to the pressure vessel in the DTK code, a further adjustment of the absorption rates was necessary as follows:

$$C_{mZ} = C_{mZ'} \left(\frac{Z'}{Z}\right)^2 \qquad (8\text{-}2)$$

where

Z' = Axial distance from the DTK mesh point to the center of the core, cm

Z = Actual distance from the point in question to the center of the core, cm

$\left(\frac{Z'}{Z}\right)^2$ = Distance correction (usual "inverse R^2" correction)

C_{mZ} = Absorption rate at locations, Z, for each material, m

The values of $C_{mZ'}$, the absorption rates, were used as the axial distribution of the gamma ray sources in point kernel program 14-0 to calculate the dose rate from the roof. The radial distribution of the gamma ray sources was assumed to follow the shape of the fast neutron flux incident on the roof. Source energy spectra for each material, m, were obtained.[1,2] Since Program 14-0 applies only to cylindrical source geometries, the roof was considered to be a right circular cylindrical source with a radius of 160.5 cm. This radius was selected to preserve the surface area of the roof. All material layers in the roof

---

[1]ORNL-2904, A Compilation of Information on Gamma Ray Spectra Resulting from Thermal Neutron Capture, E. Troubetzkoy and H. Goldstein, Oak Ridge National Laboratory, 1961

[2]APEX-407, Gamma Ray Energy Spectra from Thermal Neutron Capture, F. E. DeLoume, General Electric Co., ANPD, August, 1958

(such as the aluminum and water) were described in the point kernel code geometry in an effort to preserve as closely as possible the attenuation characteristics of the roof.

Wall Capture Gamma Rays

Calculation of the gamma dose rate at the detector resulting from neutron capture in the test cell wall was based on the following assumptions:

1) Removal of a fast neutron results in the immediate generation and capture of a thermal neutron[1].

2) Thermal neutrons incident on the wall are captured at the concrete surface.

3) Each capture results in the generation of a 6 Mev photon emitted isotropically.

4) The effect of distance attenuation within the wall may be neglected in the case of the incident beam.

5) The photons are generated a distance of $1/\mu$ in the wall for purposes of computing the inverse R^2 effect of distance between source and detector point.

The derivation of the equations used in this calculational model is shown below:

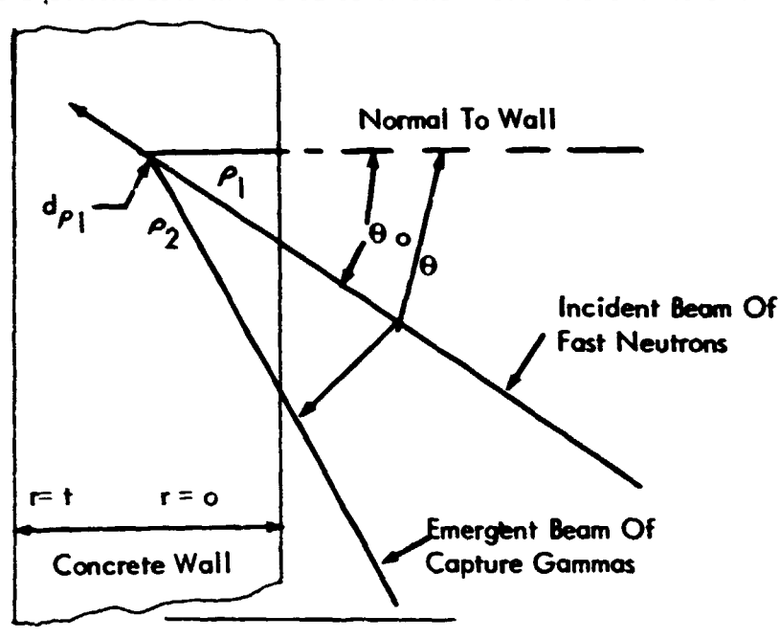

[1] N-2-3062, Estimation of Total Dose Rate Below the Privy Roof Shield, Los Alamos Scientific Laboratory, R. E. Malenfaut, February, 1961

The incident fast neutron beam is attenuated in the test cell wall as a function of the slant penetration distance ρ_1, i.e.:

$$S(\rho_1) = S_0 e^{-\Sigma r \rho_1} \tag{8-3}$$

where

$S(\rho_1)$ = fast neutron flux at ρ_1

S_0 = fast neutron flux at the surface

Σ_r = Removal cross section

The number of neutrons removed in the element of path length $d\rho_1$ is:

$$S_0 \Sigma_r e^{-\Sigma r \rho_1} d\rho_1$$

From assumption (1) and (3), the isotropic emission rate at ρ_1 in the interval $d\rho_1$ is:

$$6 S_0 \Sigma_r e^{-\Sigma r \rho_1} d\rho_1 \quad \text{mev/cm}^3\text{-sec.}$$

The photon beam directed toward the receiver point is attenuated as a function of the slant penetration of the emergent beam. The photon flux, I_o, at the wall surface is therefore:

$$dI_o = 6 S_0 \Sigma_r e^{-\Sigma r \rho_1} \frac{e^{-\mu \rho_2}}{4\pi \rho_2^{\,2}} d\rho_1 \tag{8-4}$$

The above expression may be written in terms of a normal penetration, r, the incident angle θ_o, and the emergent angle θ because:

$$\rho_1 = r \sec \theta_o$$

$$d\rho_1 = \sec \theta_o \, dr$$

hence:

$$dI_o = \frac{6 S_0 \Sigma_r \; e^{-r(\Sigma r \sec \theta_0 + \mu \sec \theta)} \sec \theta_0 dr}{4 \pi \rho_2^{\,2}} \tag{8-5}$$

In order to simplify the integration, it is assumed for distance attenuation purposes that all of the gammas are generated one relaxation length from the surface along the slant path ρ_2; then the photon beam directed toward the receiver point due to photons generated through the wall (r = o to r = t) is:

$$I_0 = \int_0^t \frac{6S_0\Sigma_r e^{-r(\Sigma r \sec\theta_0 + \mu \sec\theta)}}{4\pi(\frac{1}{\mu})^2} \sec\theta_0 \, dr \qquad (8\text{-}6)$$

$$I_0 = \frac{6S_0\Sigma_r \sec\theta_0}{4\pi(\frac{1}{\mu})^2(\Sigma_r \sec\theta_0 + \mu\sec\theta)} \left[1 - e^{-t(\Sigma r \sec\theta_0 + \mu\sec\theta)}\right] \qquad (8\text{-}7)$$

The total beam directed toward the receiver point is equal to the area, A, of a surface of assumed uniform incident flux times the above expression. The total arriving at the receiver point, a distance R away from the source area is:

$$I_0 = \frac{6S_0\Sigma_r \sec\theta_0 \, (A\cos\theta_0)}{4\pi(R+\frac{1}{\mu})^2 \, (\Sigma_r \sec\theta_0 + \mu\sec\theta)} \left[1 - e^{-t\,(\Sigma_r \sec\theta_0 + \mu\sec\theta)}\right] \qquad (8\text{-}8)$$

The total gamma intensity at the receiver point, including the photons resulting from captures of thermal neutrons from the reactor at the surface of the test cell wall, is therefore:

$$I\,(\text{Total}) = I_0 + \frac{6\phi_{th}\,(A\cos\theta)}{4\pi R^2} \qquad (8\text{-}9)$$

The test cell wall was divided into 43 areas for purposes of computing the capture gamma dose rate under the privy roof and at test car locations. Thermal neutron fluxes for E<1.86 ev, and fast neutron fluxes for 1.86 ev > E > 10 Mev were obtained.[1]

Gamma Rays Scattered From the Test Cell Wall and Pad

Calculation of radiation levels resulting from gamma ray scattering from the wall and pad were made using a multiple scatter albedo model suggested by Dr. A. Foderaro.[2]

---

[1] WANL-TME-840, Reactor Analysis Data Book, Westinghouse Electric Corporation, Astronuclear Laboratory

[2] Memo from Dr. A. Foderaro, Procedure for NRX-A Scatter Shield Analysis

The gamma ray albedo formula is:

$$D(E) = D_0(E) A \beta(E) \cos\theta \left(\frac{1}{r^2}\right) \tag{8-10}$$

where $D(E)$ = Scattered gamma ray flux at detector for 13 energy groups, E

$D_0(E)$ = Gamma ray flux at scattering area for 13 energy groups, E, calculated by Point Kernel Program 14-0

A = Scattering area

$\beta(E)$ = Gamma ray energy albedo [1] at normal incidence on concrete for 13 energy groups, E

θ = Angle between the reflected ray and the normal to the scattering area

r = Distance between the center of the scattering area and the detector point

The gamma ray dose rate was computed by applying appropriate flux to dose conversion factors to values of D(E). The wall and pad were divided into 43 and 38 scattering areas, respectively, for purposes of computing the scattered radiation levels under the roof and on the test car.

Direct Beam Dose Rates

Direct beam gamma dose rates under the roof were calculated in the same manner described above for the meridian ring and radial traverse except that attenuation in the privy roof was accounted for.

[1] "Monte Carlo Calculations of Gamma Ray Back Scattering", M. J. Berger, D. J. Raso, Radiation Research, 12, 20-37, 1960

Fast Neutron Fluxes and Dose Rates

SURFACE OF THE VESSEL, MERIDIAN RING, AND RADIAL TRAVERSE

The fast neutron flux levels presented in this section are based on Program 14-0 differential neutron number fluxes. In Program 14-0, moments method data for water were employed in computing the differential neutron number flux. In order for the flux levels outside the vessel to be consistent with those inside, the Program 14-0 fluxes were normalized at the vessel surface to Program CURE results as follows:

$$\left[N_{E>1\,Mev}\right]_{\alpha,R} = \frac{\left[\phi(E>1\,Mev)\right]_{\alpha,R=Rs}}{\left[\int_{E=1\,Mev}^{E=10\,Mev} I(E)\,dE\right]_{\alpha,R=Rs}} \left[\int_{E=1\,Mev}^{E=10\,Mev} I(E)\,dE\right]_{\alpha,R} \qquad (8\text{-}11)$$

where:

$N_{E>1\,Mev}$	=	flux for neutrons with energy greater than 1 Mev, neutrons per square centimeter per second
α	=	polar angle in degrees measured about the center of the core from the axial centerline with $\alpha = 0^{\circ}$ located at the dome end
R	=	separation distance from the center of the core to the detector
$\phi(E>1\,Mev)$	=	flux of neutrons with energies greater than 1 Mev from CURE Program
R_s	=	separation distance from center of the core to the surface of the reactor.
$I(E)$	=	differential neutron number spectra computed by Program 14-0, neutrons per square centimeter per second per Mev interval.

The fast neutron dose rates are based on Albert-Welton kernel dose rates computed by Program 14-0 and normalized as follows:

$$[D]_{a,R} = \frac{[\phi(E > 1\ \text{Mev})]_{a,R=Rs}}{\left[\int_{E=1\ \text{Mev}}^{E=10\ \text{Mev}} I(E)\,dE\right]_{a,R=Rs}} [D_N]_{a,R} \qquad (8\text{-}12)$$

D = Normalized fast neutron dose rate, rads per hour

D_N = fast neutron dose rate computed by Program 14-0

All other terms were defined above.

Monte Carlo Program 18-0 data were also analyzed to obtain the neutron flux (E>2.5 Mev) at the surface of the pressure vessel. The Monte Carlo method is,of course, inherently more accurate than the method described above, and hence was employed to define more accurately the surface flux levels. The Program 18-0 neutron escape tapes were analyzed using data reduction code 20-8[1]. This code places the escaping neutrons into energy and angle bins at specified areas on the surface of the reactor assembly. In converting the 20-8 output to a flux, an "average" energy was applied to the energy bin data. Also, an average sec θ was applied to the angle bin data to account for the absorption in a "theoretical" detector located at the surface. This calculation is similar to, but not as exact, as that performed by the new ETA code described in the previous section on Gamma Ray Dose Rates. The ETA code was not available when this analysis was performed.

UNDER THE PRIVY ROOF

To determine the neutron fluxes under the privy roof, it is necessary to consider other sources of neutrons in addition to the direct beam neutron radiation. These sources are

[1]GEMP-123, Program 20-8, A Program for Interpreting Program 18-0 Source and Escape Particle Tapes, J. P. Yalch, J. E. MacDonald, General Electric Co., NMPO, January, 1964

scattering from the wall and pad, and air scattering. The methods used to compute the latter two radiation components are described below.

Neutron Scattering From the Wall and Pad

Calculations of radiation levels resulting from wall and pad scattering were made using a multiple scatter albedo model suggested by Dr. A. Foderaro[1].

The neutron albedo formula used is:

$$D = (D_0 \; A \beta \cos^{2/3} \theta_0 \cos \theta)/r^2 \qquad (8\text{-}13)$$

where:

D	=	Scattered neutron flux at detector
D_0	=	Neutron flux incident on a scattering area[2]
A	=	Scattering area
β	=	Neutron dose albedo for normal incidence and reflection on concrete ($\sim$0.111 for neutron energies greater than 1 Mev)
θ_0	=	Angle between the incident ray and the normal to the scattering area
θ	=	Angle between the reflected ray and the normal to the scattering area
r	=	Distance between the center of the scattering area and the detector point

The same scattering areas employed in the gamma ray analysis were also used in the neutron calculation.

Air Scattered Neutrons

An "upper limit" estimate of the neutron flux under the privy roof resulting from air

[1]Memo from Dr. A. Foderaro, Procedure for NRX-A Scatter Shield Analysis.

[2]WANL-TME-840, Reactor Analysis Data Book, Westinghouse Electric Corporation, Astronuclear Laboratory

scattered neutrons was obtained from data.[1] The referenced data are presented as a curve of air scattered neutron dose rates as a function of the angle of emission of a 1.1 Mev point, monodirectional source for a source-detector separatic distance of 10 feet. The data, presented in Rem hr^{-1} per source neutron-sec^{-1}, were converted to Rads (tissue) by dividing by an RBE of 8[2], and to a flux greater than 1 Mev basis by multiplying by a flux-to-dose factor of 4.85×10^4 obtained from the Data Book[3]. Hence:

$$F(\theta)\frac{\text{neutrons } (E > 1 \text{ Mev})/\text{cm}^2\ \text{sec}}{\text{source neutron/sec}} = f(\theta)\frac{\text{rem/hr}}{\text{source neutron/sec}} \times \frac{4.85 \times 10^4}{8} \qquad (8\text{-}14)$$

These data were subsequently applied to the flux emitted in the unit solid angle $d\Omega$ centered about the polar angle θ.

The point source of neutrons emitted into solid angle $d\Omega$ about θ was obtained from data tabulated as a function of polar angle at 10 feet from the reactor in reference 3.

$$S(\theta)\,d\Omega = \frac{\left[S(\theta)\right]_{10\,\text{ft.}} \times 4\pi\,(10\text{ ft} \times 30.5\text{ cm/ft})^2}{4\pi\ \text{solid angle}}\ \frac{\text{source neutron/sec}}{\text{unit solid angle}} \qquad (8\text{-}15)$$

Unit solid angle is

$$d\Omega = \sin\theta\, d\theta\, d\phi,$$

there θ and ϕ are polar and azimuth angles, respectively. The air scatter neutron flux 10 feet from the anisotropic point source is therefore:

$$N = \int_\theta \int_\phi F(\theta) S(\theta) \sin\theta\, d\theta\, d\phi \qquad (8\text{-}16)$$

---

[1] Reactor Handbook, Vol. III, Part B, Shielding, E. . Blizard, Editor, 1962

[2] XDC-59-8-179, Conversion of Neutron or Gamma Ray Flux to Absorbed Dose Rate, General Electric Co., ANPD, B. J. Henderson, August, 1959

[3] WANL-TME-840, Reactor Analysis Data Book, Westinghouse Electric Corporation, Astronuclear Laboratory

Because of the azimuth symmetry of the functions, ϕ is integrated from 0 to 2π, and because the privy roof subtends an angle of about 45 degrees with respect to core center, θ is integrated from $\pi/4$ to π. Put in incremental form for purposes of numerical integration, N becomes:

$$N = 2\pi \sum_{45^\circ}^{180^\circ} F(\theta) S(\theta) \sin\theta \Delta\theta \qquad (8\text{-}17)$$

Trapezoidal integration was performed to obtain a value of

$$1.6 \times 10^{-10} \frac{\text{neutrons/cm}^2\text{-sec}}{\text{fission second}}$$

for the air scattered neutron flux with energies greater than 1 Mev.

The value for the air scattered neutron flux is a conservative upper limit for the following reasons:

1) The presence of the test cell wall and pad limits the volume of air in which the scattering occurs. This was not taken into account in the calculation.

2) Some of the scattered neutrons resulting from source neutrons emitted at polar angles between 45° and 180° must pass through the privy roof to arrive at the detector point. This was not accounted for in the calcaultions.

Thermal and Epithermal Neutron Data

Thermal and epithermal reaction rates, i.e., flux times macroscopic activation cross section, were calculated for comparison with measured reaction rates as follows:

The epithermal reaction rate (RR epithermal) for flux levels constant with time is defined as,

$$\text{RR epithermal} = \int_{0.4\ \text{ev}}^{\infty} \phi(E)\, \Sigma_{act}(E)\, dE \qquad (8\text{-}18)$$

$\phi(E)$ neutron flux about

$\Sigma(E)_{act}$ = macroscopic a[illegible] [illegible]ction about energy E

With similar terminology, the thermal reaction rate (RR thermal) is defined as:

$$\text{RR thermal} = \int_0^{0.4\ ev} \phi(E)\ \Sigma_{th}(E)_{act}\ dE \qquad (8\text{-}19)$$

The limit of 0.4 ev was selected as the cadmium cut-off[1], i.e., at energies below 0.4 ev it is assumed that cadmium essentially stops all neutrons and at energies above 0.4 ev it is assumed that cadmium is transparent to neutrons.

The epithermal reaction rate as measured by experiment is:

$$\text{RR epithermal} = A^c_\infty \qquad (8\text{-}20)$$

where,

A^c_∞ is the saturated activity of a wire completely covered with cadmium

The thermal reaction rate is then:

$$\text{RR thermal} = A^b_\infty - A^c_\infty \qquad (8\text{-}21)$$

where,

A^b_∞ is the saturated activity of a bare wire exposed to the same flux as the covered wire.

By replacing the integrals by summations over energy, reaction rates were calculated and compared to those experimentally determined.

Calculated and measured reaction rates were compared instead of fluxes since the fundamental measured quantity is the reaction rate. To obtain the "thermal" or epithermal" flux, an average activation cross section must be defined to permit its removal from the integral.

The calculated neutron fluxes employed in this analysis were obtained from a sixteen group

---

[1]Nuclear Reactor Experiments, Hoag, J. B., D. Van Nostrand Company, Inc., Princeton, New Jersey

(11 fast and 5 thermal groups) r-z, transport code, TDC[1,2]. Specifically, TDC fluxes at the outer lateral surface of the beryllium reflector were utilized. Cross sections applied in the equations above were obtained from a sixteen group GAM-TNS-II[3,4] calculation and were weighted over the beryllium reflector spectrum.

Use of the TDC code in this analysis is a departure from the method used in calculation of the fast flux data described in the preceding section of this report.

There are several reasons for this. The fast neutron external environment had already been predicted employing Standard Design Method I[5]. Subsequent work was performed in an effort to improve upon Standard Design Method I,[1,6] which resulted in Standard Design Method II.[1,6] Standard Design Method II does in fact employ a 16 group TDC calculation for all neutron radiation analysis. The effect of various facets of the Standard Design Method II on external neutron environment will be evaluated in the near future. In WANL-TNR-165 the effect of the Standard Design Method II on internal environment was evaluated and reported.

---

[1]WANL-TME-941, Progress on an Automated Radiation Analysis Program, Westinghouse Electric Corporation, Astronuclear Laboratory

[2]LAMS-2346, The DSN and TDC Neutron Transport Code, Los Alamos Scientific Laboratory B. G. Carlson, et. al

[3]GA-1850, GAM-I - A Consistent P_1 Multigroup Code for the Calculation of Fast Neutron Spectra and Multigroup Constants, work done by J. S. Dudek, G. J. Jounou, E. J. Leshan. Report written by G. J. Jounou, J. S. Dudek, June, 1961

[4]WANL-TME-263, TNS, An IBM 7090 Program for Computing Thermal Neutron Spectra and Multithermal Group Cross Sections, C. A. Stevens, S. Young, Westinghouse Electric Corporation, Astronuclear Laboratory

[5]WANL-TNR-128, Vol. II, Reactor Analysis of NRX-A, Radiation Analysis, Westinghouse Electric Corporation, Astronuclear Laboratory, Radiation and Shielding Group, September 1963

[6]WANL-TNR-165, Radiation Analysis of NRX-A2 by Various Methods, Westinghouse Electric Corporation, Astronuclear Laboratory, M. A. Capo, December, 1964

COMPARISONS OF EXPERIMENTAL AND CALCULATED GAMMA RAY DATA

Pressure Vessel Surface

Experimental gamma ray dose rates (R/hr-watt) obtained on an axial traverse at the surface of the pressure vessel during EP II are plotted in figure 8-5 as a function of reactor station. (Station 0 is located at the dome end of the core. Positive stations are measured in inches from this reference toward the nozzle end of the reactor.) Both film and glass rod data for the EP II low power run are presented. The film data are significantly lower than the glass rod data at most axial positions because the film had been saturated. The film data are considered reliable only up to about 400 r. The calculated data from WANL-TME-840[1] are shown as a solid curve in figure 8-5. Near the core midplane (station 21) the calculated gamma ray dose rate is only 20 percent higher than the glass rod measurement. In fact, the shape and magnitude of the WANL-TME-840 data are in excellent agreement except at the dome end of the core (station 0). This discrepancy at the dome end can be explained on the basis of the experimental conditions. The WANL-TME-840 calculations were performed for the hot reactor with 100 percent hydrogen flow rate. This, of course, implies high density hydrogen at the dome end of the core. Calculations of thermal fluxes at the dome end of the core show that an increase of a factor of five can be noted when hydrogen at 100 percent flow and power conditions is employed. Thus, the secondary gamma ray capture rate in the suppressor plate, titanium support structure, and other regions would be significantly higher for the hot case. The dose rate due to secondary gamma rays at station 0 is about equal to half of the primary gamma ray dose rate. Thus, for a cold case the dose rate at station 0 should be decreased by approximately 30 percent, yielding a value of about 0.4 R/hr-watt. This value is in better agreement with the measured data.

Some more recently calculated data is also presented in figure 8-5 (also for the hot condition). These data shown by the dashed lines in histogram form were obtained from the

---

[1]WANL-TME-840, Reactor Analysis Data Book, Westinghouse Electric Corporation, Astronuclear Laboratory

REFERENCE		PREPARED BY	APPROVED BY	Astronuclear

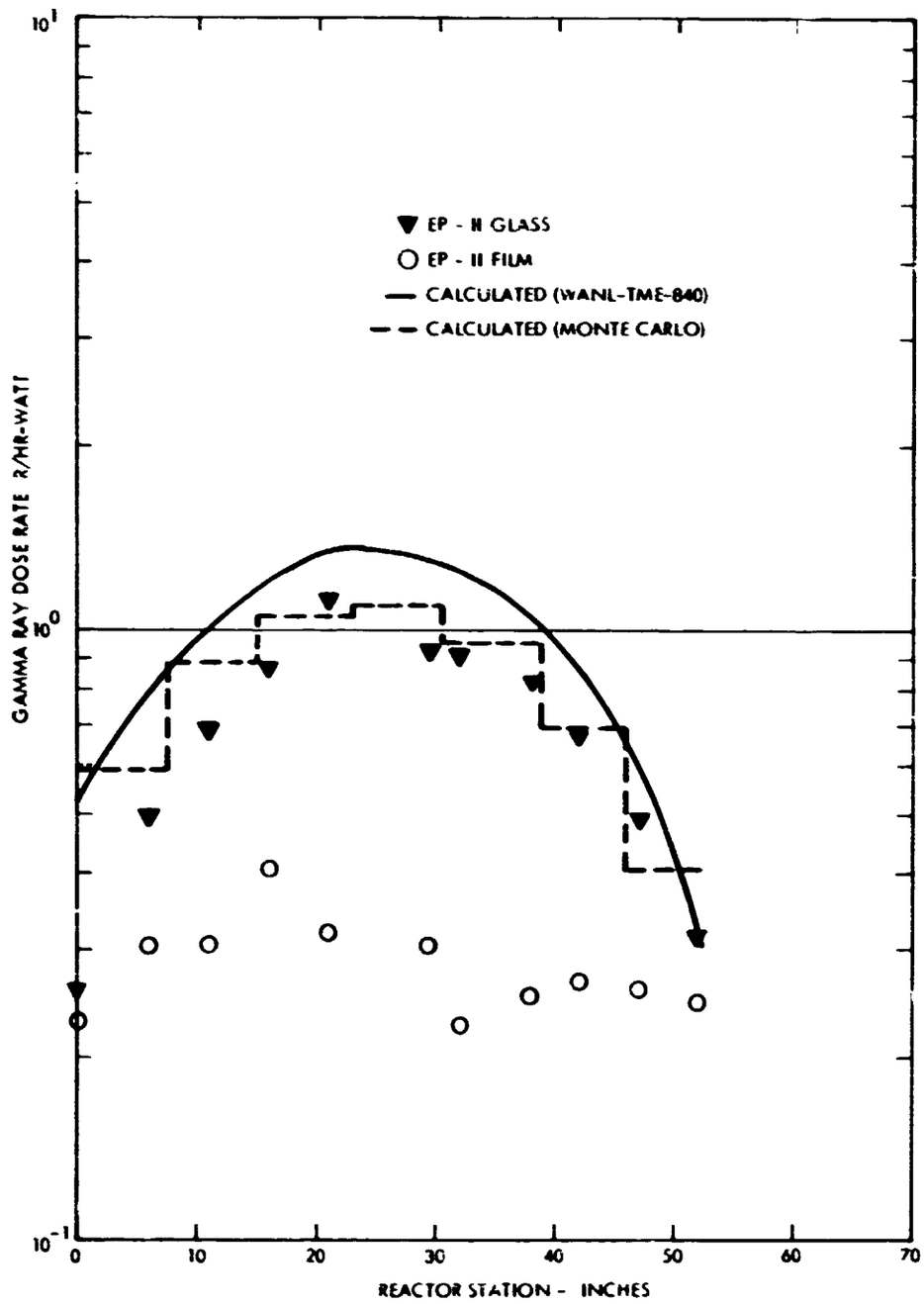

EXPERIMENTAL AND CALCULATED GAMMA RAY DOSE RATE ON THE SURFACE OF THE PRESSURE VESSEL (AXIAL TRAVERSE)

Figure No. 8-5

new ETA[1,2] (Escape Tape Analyzer) code. This code analyzes the Monte Carlo Program 18-0[3] escape tape data and calculates, among other quantities, the gamma ray dose at the surface of the pressure vessel along prescribed surface areas. These data appear to be in somewhat better agreement with the experimental data than are the WANL-TME-840 calculations.

Experimental gamma ray dose rates (R/hr-watt) obtained on a circumferential traverse at the pressure vessel surface are plotted in figure 8-6 as a function of reactor azimuth angle, θ. (Refer to figure 8-2 for schematic diagram showing location of dosimeters.) This circumferential traverse was obtained at the core midplane, station 26. Both the film and glass rod data for the EP II run are presented. Again it should be noted that the film data are saturated, and hence, are not reliable. The arrows shown in figure 8-6 locate, as closely as possible, the position of the control drums (Refer to figure 8-2). It appears that little or no scalloping effect can be noted in the vicinity of the drums. The calculated values are presented in figure 8-6 for comparison purposes. These calculations are identical to those for station 26, shown in figure 8-5. The computer codes used to calculate gamma ray dose rates are not capable of employing any azimuth variation in power distribution or reactor geometry. Hence, no azimuth calculated traverse of gamma rays dose rates is given.

Equatorial Ring

Due to a slight misalignment[4] of the equatorial ring assembly, all dosimeters are not equidistant from the center of the reactor core. Reference to figure 8-4 can clarify the

---

[1]WANL-TME-941, Progress on an Automated Radiation Analysis Program, Westinghouse Electric Corporation, Astronuclear Laboratory, H. C. Woodsum, August, 1964

[2]WANL-TNR-165, Radiation Analysis of NRX-A2 by Various Methods, Westinghouse Electric Corporation, Astronuclear Laboratory, M. A. Capo, December, 1964

[3]GEMP-102, Specialized Reactor Shield Monte Carlo Program 18-0, General Electric Co., NMPO, J. E. MacDonald, et al. October, 1961

[4]WANL-TME-1081, NRX-A2 Dosimetry Measurements, Westinghouse Electric Corporation, Astronuclear Experimental Facility, March, 1965

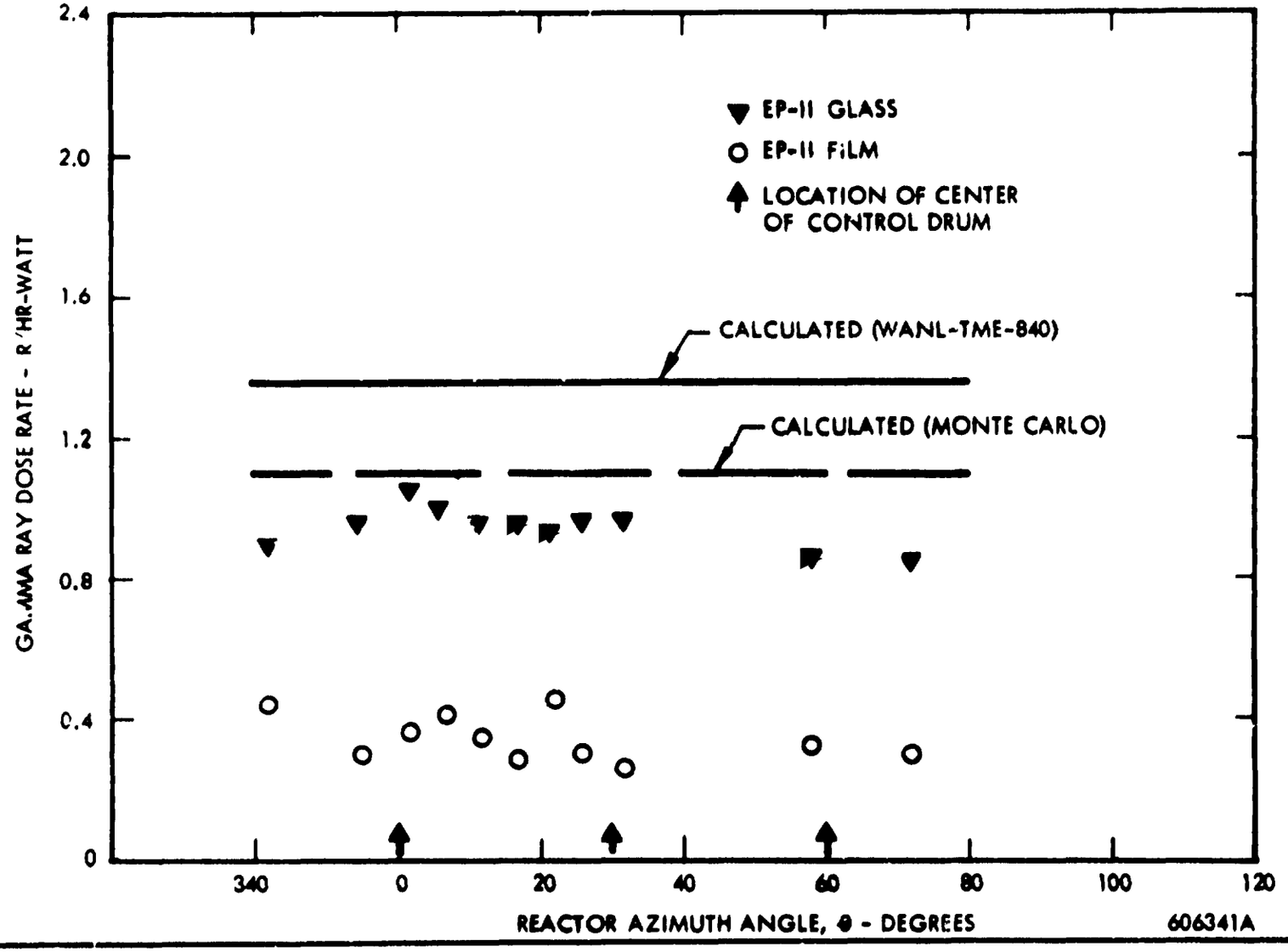

FIGURE NO. 8-6

EXPERIMENTAL AND CALCULATED GAMMA RAY DOSE RATE ON THE SURFACE OF THE PRESSURE VESSEL (CIRCUMFERENTIAL TRAVERSE)

PREPARED BY	APPROVED BY	CURVE NO.

definition of the misalignment. The dosimeters at θ = 345 degrees, 0 degrees, 5 degrees, etc., are actually a few inches closer to the core than are those at θ = 75 degrees, 60 degrees, 50 degrees, etc.

Experimental gamma ray dose rates (R/hr-watt) at locations on the equatorial ring are presented in figure 8-7 as a function of reactor azimuth angle, θ. (Refer to figure 8-4 for dosimeter locations on the equatorial ring.) The equatorial ring was located five feet from the center of the core on the midplane. The following dosimeter data obtained during the EP II run are shown: film and glass rod data, glass data obtained by LASL, and one measurement (θ = 20 degrees) obtained with a thermoluminescent detector (TLD). The LASL glass data are about a factor of 1.5 higher than the WANL glass data due probably to a difference in calibration.[1] The film data are slightly lower than the WANL glass data. The TLD data point is in reasonable agreement with the WANL glass data and with the calculated data. As a function of azimuth angle all measured data appear to be reasonably flat and no scalloping effect is noted. The misalignment of the ring is evidenced in figure 8-7 since the experimental data have a tendency to increase from 75 degrees to 345 degrees which is away from the test cell wall. Any existing scalloping effect would, of course, be less pronounced as the distance from the reactor increases. The calculated data point (from α = 90 degrees on meridian ring, figure 8-8) shown in figure 8-7 is in good agreement with the WANL glass or TLD data. The TLD data is reported to be more reliable than either glass or film.[1]

Meridian Ring

Experimental gamma ray dose rates (R/hr-watt) at locations on the meridian ring are plotted in figure 8-8 as a function of reactor polar angle, α. The position, α = 0 degrees, is located at the dome end centerline of the core, and α = 180 degrees is located at the nozzle end centerline. The meridian ring was located five feet from the center of the core. (Refer to figure 8-3 for dosimeter location on the meridian ring.) The following dosimetry

[1] WANL-TME-1081, NRX-A2 Dosimetry Measurements, Westinghouse Electric Corporation, Astronuclear Experimental Facility, March, 1965

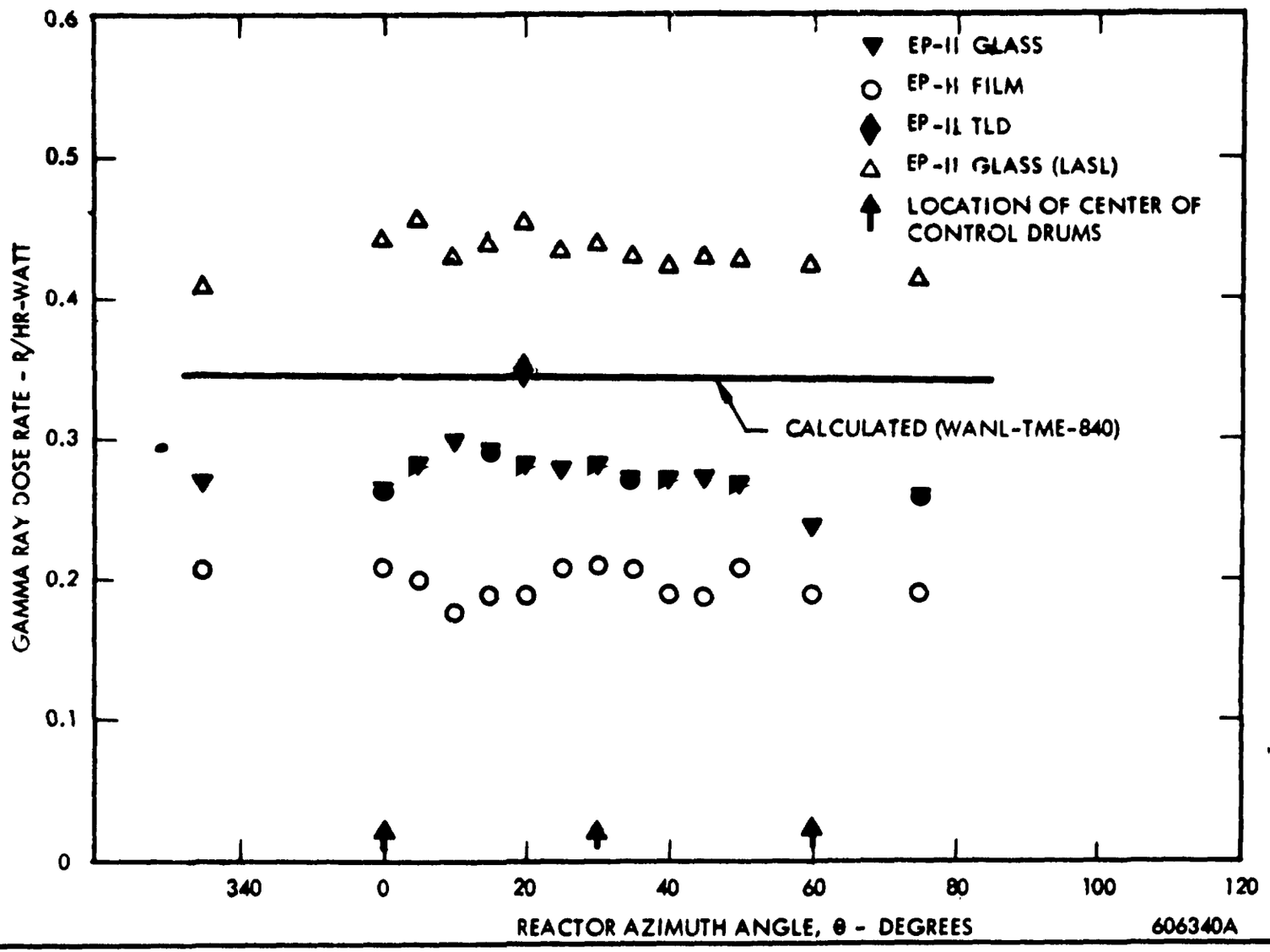

Figure No. 8-7

EXPERIMENTAL AND CALCULATED GAMMA RAY DOSE ON THE EQUATORIAL RING

PREPARED BY	APPROVED BY	CURVE NO.

REFERENCE

Astronuclear

data obtained during the EP II run are shown: film and glass rod data, glass data obtained by LASL, and two measurements obtained with a TLD detector. As was the case on the equatorial ring, it is noted that the LASL glass data is about a factor of 1.5 higher than the WANL glass data. The TLD measurement at $\alpha = 30$ degrees is in reasonable agreement with both the WANL glass and film data. At the nozzle end ($\alpha = 160$ degrees), however, the TLD data is about a factor of 2 higher than the WANL glass data. This is probably because the TLD has a fast neutron response, and since the fast neutron flux is quite high at this location, the TLD is also reading some fast neutrons.[1]

The calculated data from WANL-TME-840 are shown as the solid curve in figure 8-8. The calculated data is in good agreement, both in shape and magnitude, with the average of the measurements. At $\alpha = 90$ degrees the ratio of calculated to measured (WANL-glass) data is about 1.2.

Also shown in figure 8-8 is a best fit to KIWI B-4A gamma dose measurements (dashed curve) normalized at $\alpha = 90$ degrees to the TME-840 calculated data. The A2 and B4 data are not comparable on an "absolute" basis since the A2 and B4 meridian rings were not located at the same distance from the center of the core. This curve clearly illustrates the effect of the aluminum mockup shield employed in the NRX-A2 reactor. The KIWI B4A, of course, did not have such a shield. At $\alpha = 45$ degrees, it is noted that the KIWI data is beginning to increase as a function of α, whereas both the A2 measured and calculated data are beginning to decrease. (The aluminum mockup shield, located at the dome end of the core, is employed to simulate the effect of a "flight" shield that may be used in a future application of NRX flight-type systems). From $\alpha = 45$ degrees to $\alpha = 30$ degrees the calculated gamma ray dose has decreased by a factor of 4 due to shield attenuation. The calculated attenuation effect of the shield at $\alpha = 0$ degrees on the centerline is a factor of 20. The shield is about 14 inches in thickness on the centerline.

---

[1] WANL-TME-1081, NRX-A2 Dosimetry Measurements, Westinghouse Electric Corporation, Astronuclear Experimental Facility, March, 1965

REFERENCE	PREPARED BY	APPROVED BY	Astronuclear

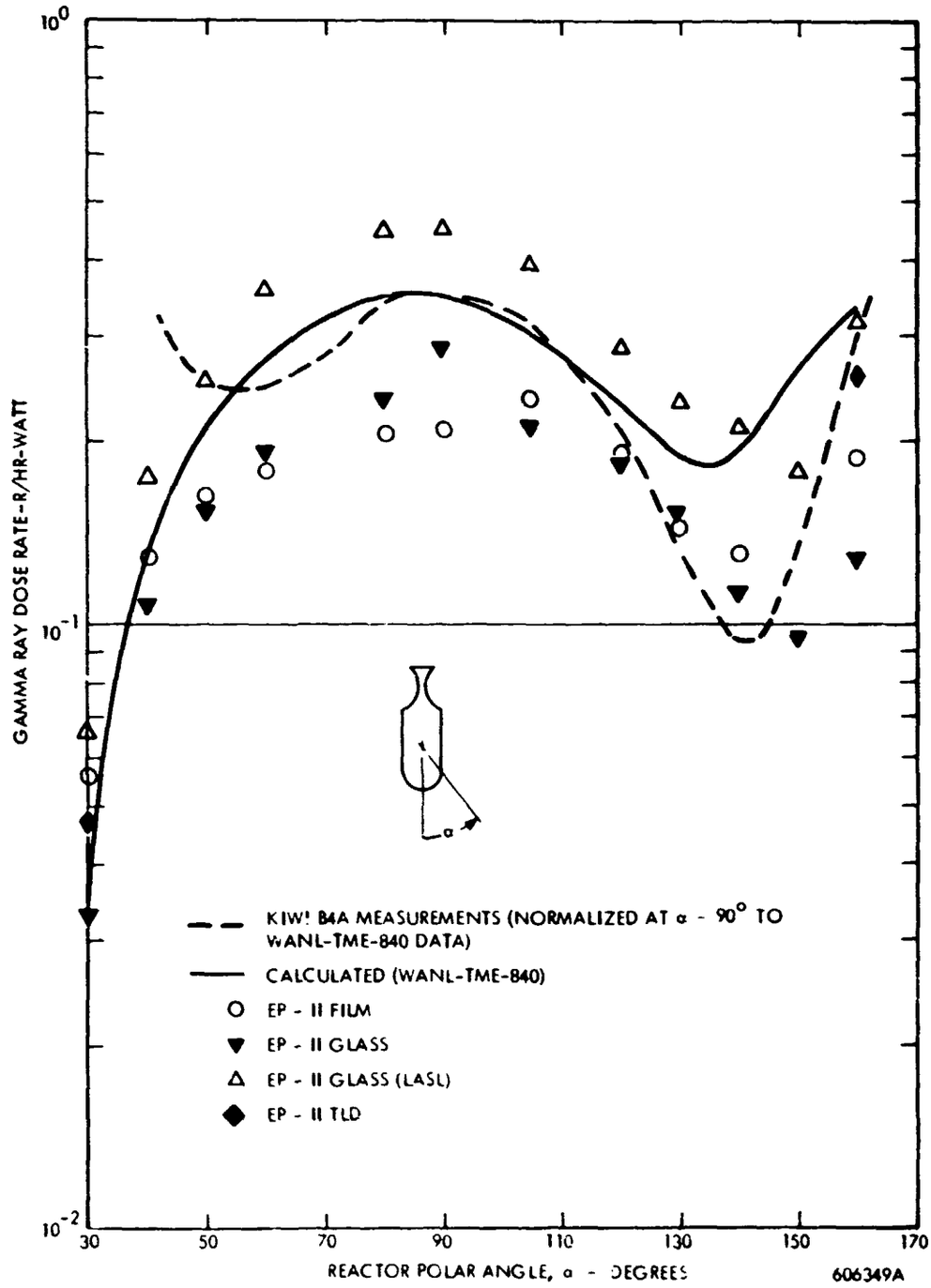

EXPERIMENTAL AND CALCULATED GAMMA RAY DOSE RATE ON THE MERIDIAN RING

Figure No. 8-8

Radial Midplane

A comparison of experimental and calculated gamma ray dose rates is shown as a function of radial distance from the reactor in figure 8-9. These data were taken during the low and high power runs at the vessel surface, five feet from the reactor on the equatorial ring, and on the trolley line and trolley line extension. (Several KIWI B4A measurements are included for comparison). The calculated curve includes core gamma rays and secondary gamma rays from neutron interactions in reactor components outside the core, but within the pressure vessel. The calculated data also include the effect of air scattering.

The calculated curve is within a factor of 1.3 higher than a "best fit" of the experimental data out to about twenty feet from the reactor. At greater distances, the "best fit" of the experimental data is greater than the calculated curve by a factor of two at 100 feet and a factor of three at 1000 feet.

The uncertainty in the calculation of the NRX-A2 gamma dose has been set at a factor of 1.5 in reference 1. Agreement to within a factor of 1.3 to 1.5 between experimental and calculated gamma dose has been observed previously in an analysis of KIWI dosimetry[2] The agreement between calculation and experiment observed in this analysis within 20 feet of the reactor on the midplane is within the presently set uncertainty of the calculations.

Disagreement between the experimental and calculated data at distances greater than 50 feet has been observed in an anlysis of KIWI dosimetry[2] where it was attributed to neglecting the effects of air scattering in the calculations. The NRX-A2 analysis includes the effects of air scattering; therefore, it appears that the disagreement may be due to ground scattering effects not included, or overestimation of the attenuation properties of air for the condition at the test site.

The glass rod dosimeters (WANL) exposed during the EP IV run were annealed out at

---

[1]WANL-TME-840, Reactor Analysis Data Book, Westinghouse Electric Corporation, Astronuclear Laboratory

[2]WANL-TME-767, Analysis of KIWI-B4A Radiation Measurements, Westinghouse Electric Corporation, Astronuclear Laboratory, L. D. Stephenson, May, 1964

REFERENCE		PREPARED BY	APPROVED BY	Astronuclear

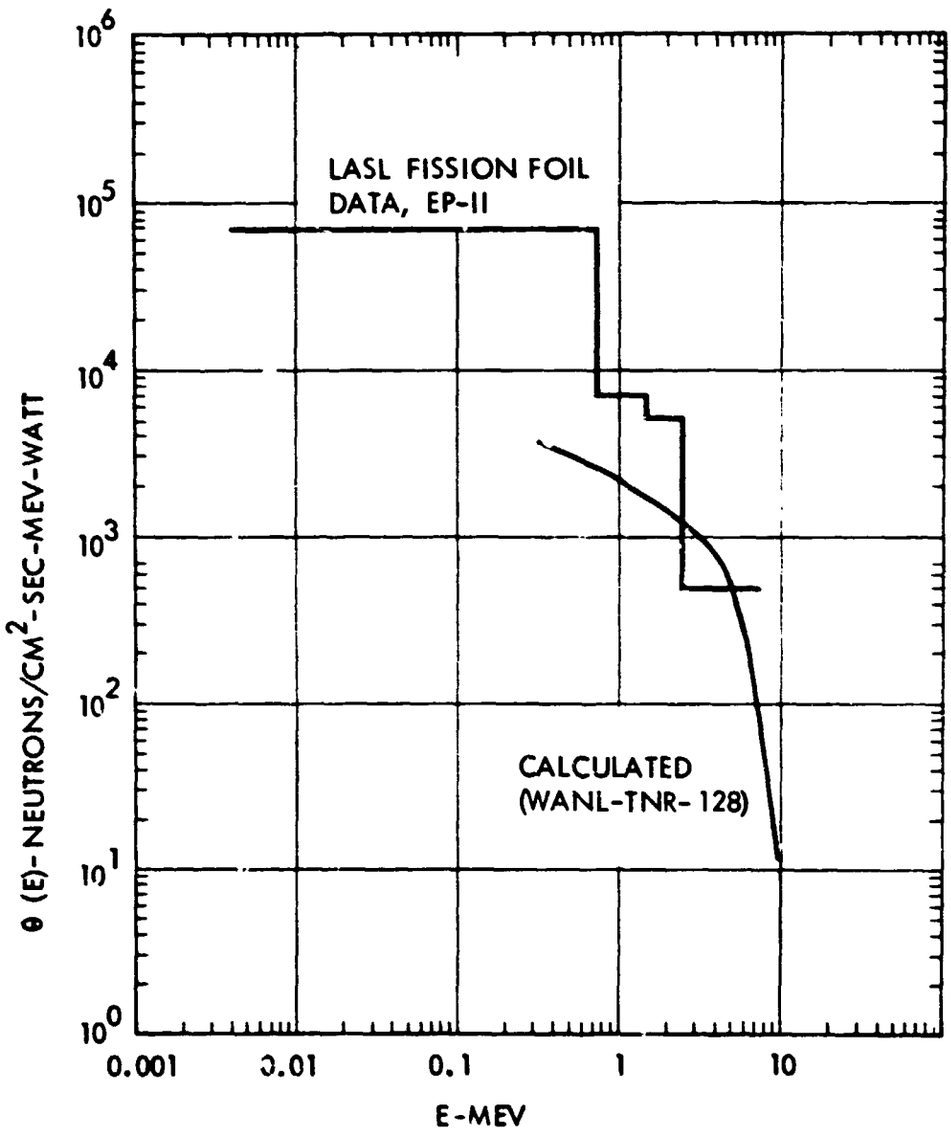

EXPERIMENTAL AND CALCULATED GAMMA RAY DOSE RATE AS A FUNCTION OF DISTANCE FROM THE REACTOR

FIGURE NO 8-9

distances less than 62 feet due to the high temperatures caused by the hydrogen flare.[1] This is evidenced in figure 8-9 by the different slope exhibited by the data points referred to by the diamond-shaped symbol.

Below the Privy Roof

Experimental gamma ray dose rates were obtained at five locations in the vicinity of the test car and test cell wall. The data are plotted in figure 8-10 as a function of radial distance from the reactor center. The dosimeter positions are designated as locations 1, 2, 3, 4, and 5. These dosimeters are located at different distances below the core midplane. Location No. 1 is 17 feet below the center of the core; No. 2 is about 15 feet, No. 3 is about 14 feet, and locations No. 4 and 5 are about 12 feet below the center of the core. Locations 1, 2, and 5 are completely within the shadow of the roof, whereas locations 3 and 4 are not. The calculated data presented in figure 8-10 are for a radial traverse located 12 feet below the core center.

Figure 8-10 shows that the EP II film data are consistently higher than the EP II glass data, and that the EP II glass data are higher than the EP IV glass data, at locations 2, 3, and 4. The EP II and EP IV glass data are, however, in good agreement at location No. 1. At locations 2, 3, and 4, it is believed that the film is higher than the EP II glass because the film has a high response at low energies. At locations under the roof, the gamma ray spectra is softer than that on the radial traverse or meridian ring because of the large number of low energy photons under the roof resulting from scattering from the test cell wall and pad.

The calculated gamma ray dose rate shown in figure 8-10 includes the following contributions:

1) Wall capture gamma rays
2) Gamma rays scattered from the wall and pad
3) Privy roof capture gamma rays
4) Direct beam gamma rays

---

[1]WANL-TME-1081, NRX-A2 Dosimetry Measurements, Westinghouse Electric Corporation, Astronuclear Experimental Facility, March, 1965

REFERENCE	PREPARED BY	APPROVED BY	Astronuclear

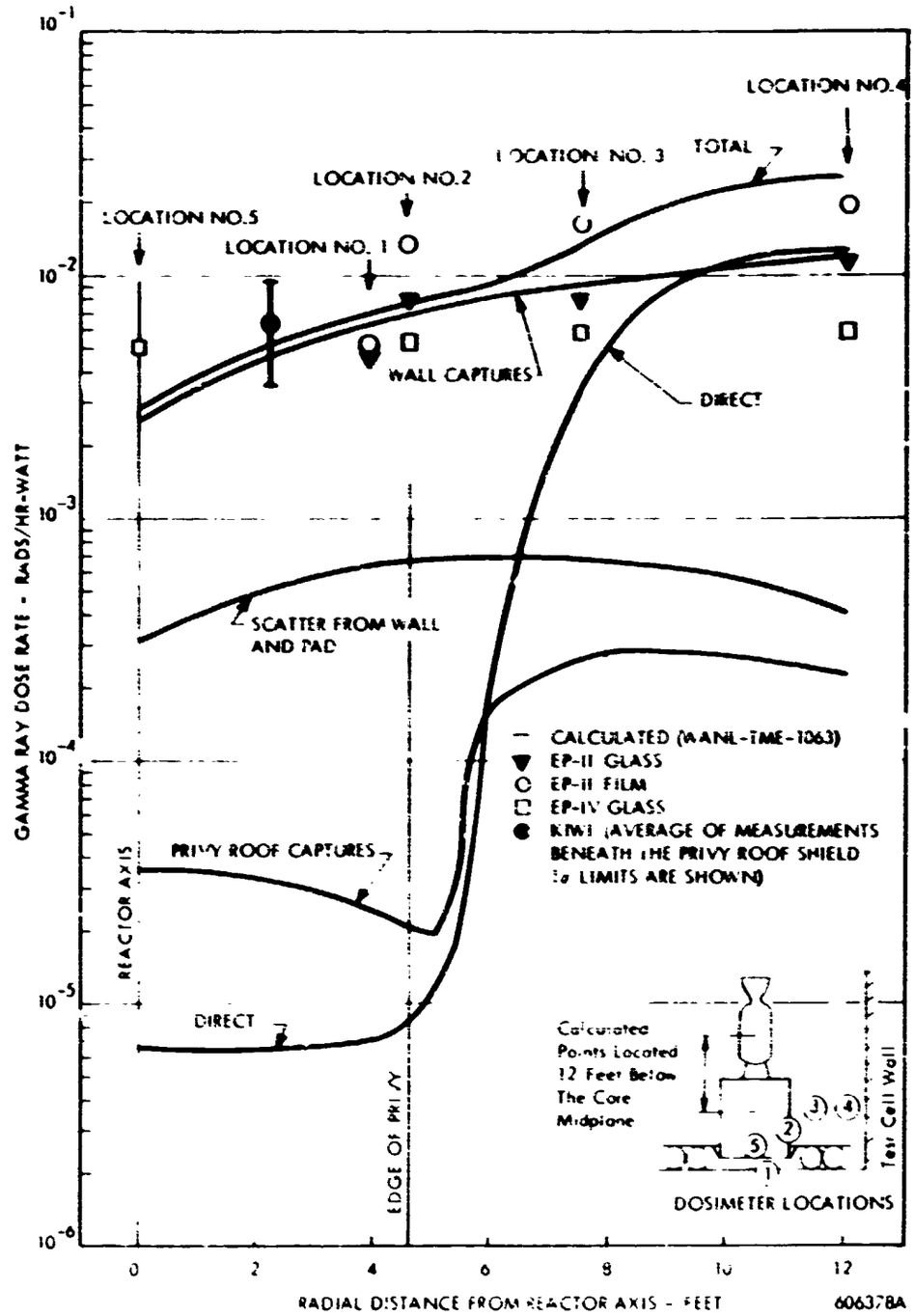

EXPERIMENTAL AND CALCULATED GAMMA RAY DOSE RATES UNDER THE PRIVY ROOF SHIELD AND AT TEST CAR LOCATION

Figure No. 8-10

The total gamma ray dose rate is within a factor of two or less of the average value of the experimental data at all locations. However, the effect of the difference in distance between calculated and experimental data points has not been evaluated.

Additional Locations

Experimental gamma ray dose rate data were also obtained at two locations on top of the privy roof, one location on the instrumentation ladder, and one location at the propellant feed line. These measured data are summarized in table 8-2 and are compared with calculations.

Table 8-2 shows that the WANL film data are higher than the glass data on top of the roof, a trend which was previously noted under the roof. The LASL glass data is higher than the WANL glass data, a trend previously noted on the meridian ring. The calculated data are within a factor of two of the experimental data. These calculations account for the dose rate from the reactor core and secondary gamma rays within the vessel, but do not include roof or wall capture gamma rays.

The calculated data at the instrumentation ladder is in reasonable agreement with the average of the measurements. Here again one notes that the measurements are not in good agreement with each other.

The WANL film and glass data are in better agreement at the propellant feed line. The calculation is low probably due to the attenuation effect of the nozzle which was not included in this analysis. A similar effect was noted on the meridian ring at polar angles, α = 140 degrees to 160 degrees.

COMPARISON OF EXPERIMENTAL AND CALCULATED FAST NEUTRON FLUX AND DOSE RATE

Pressure Vessel Surface

Experimental fast neutron fluxes (neutron/cm^2-sec-watt) obtained during the EP II run on an axial traverse at the surface of the pressure vessel are plotted in figure 8-11 as a function of reactor station. These measurements were made with 3/4 inch, ammonium sulphate pellets having a 2.9 Mev threshold. The scatter of the measured data points is

TABLE 8 - 2

EXPERIMENTAL AND CALCULATED GAMMA RAY DOSE RATE AT ADDITIONAL LOCATIONS

Description	Location: Reactor θ	Location: Station Inches	Location: Radius Inches	Measured* Gamma Dose Rate (R/HR-watt): WANL Film	Measured* Gamma Dose Rate (R/HR-watt): WANL Glass	Measured* Gamma Dose Rate (R/HR-watt): LASL Glass	Calculated Dose Rate (R/HR - watt)
Top of Privy Roof	345°	-51.2	49.2	0.042	0.022	0.045	0.023
Top of Privy Roof	345°	-51.2	66.7	0.051	0.033	0.061	0.046
Instrumentation Ladder	300°	20.0	60.0	0.207	0.319	0.495	~0.350
Propellant Feed Line	120°	100.9	25.5	0.105	0.097	----	0.074

* Measured during EP-II

REFERENCE		PREPARED BY	APPROVED BY	Astronuclear

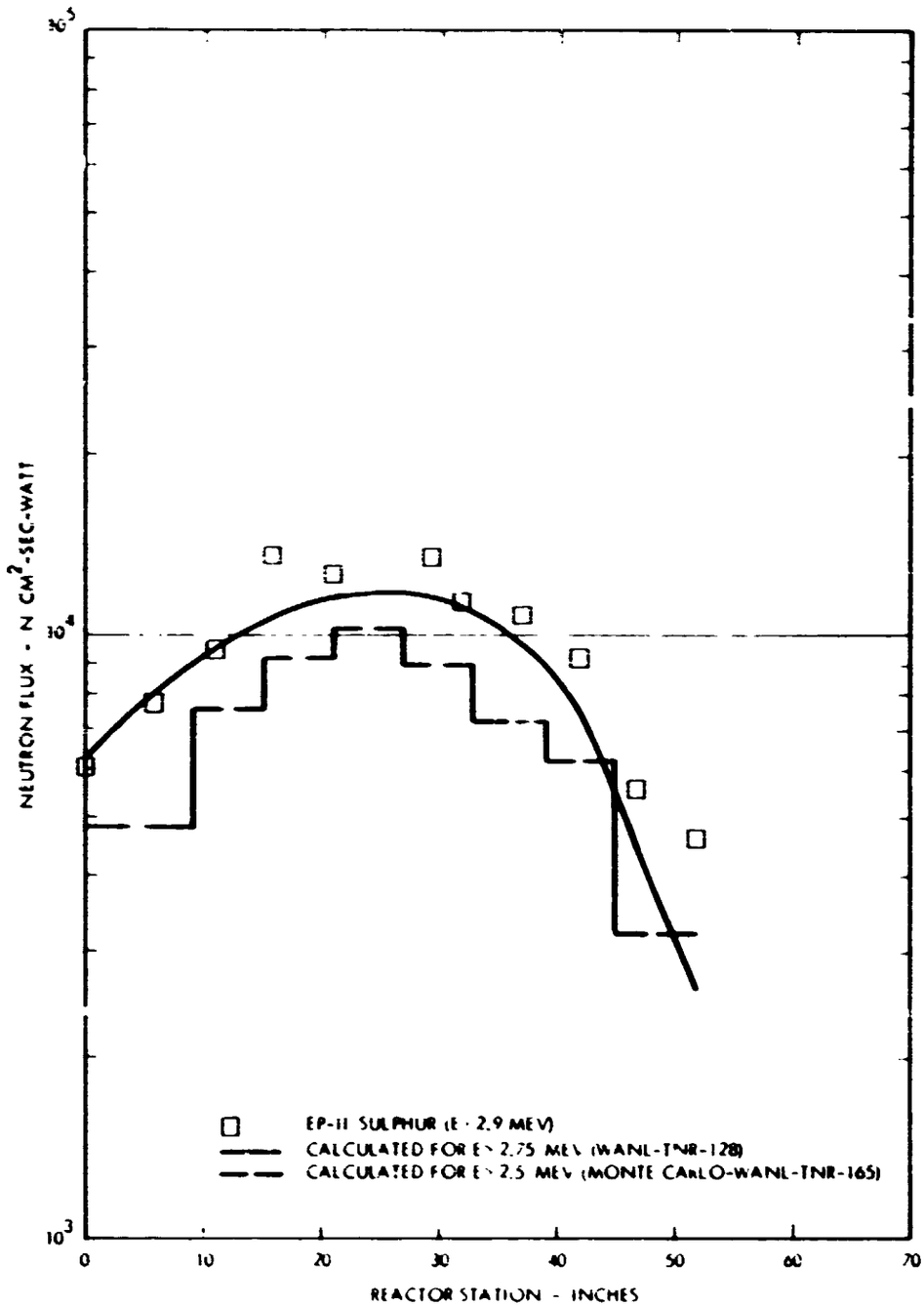

EXPERIMENTAL AND CALCULATED FAST NEUTRON FLUX ON THE SURFACE OF THE PRESSURE VESSEL (AXIAL TRAVERSE)

Figure No. 8-11

due to the low exposure levels and type of pellet used as described in WANL-TME-1081.

It is most important to note that all WANL experimental sulfur data obtained during the NRX-A2 reactor runs were normalized to the WANL nickel data at a point (α = 90 degrees, figure 8-17) on the meridian ring. This normalization was necessary because of uncertainties in the sulfur data calibration which is explained in detail in the previously mentioned dosimetry report.

The calculated flux for E>2.75 Mev from WANL-TNR-128 are presented as the solid curve on figure 8-11. Both the shape and magnitude of the calculated fast flux are in reasonable agreement with the measurements. The calculated data from WANL-TNR-128 are based on point kernel neutron spectra calculations in which water moments data were employed. The point kernel data were normalized to diffusion program CURE data as previously explained in this chapter.

Also shown in figure 8-11 (dashed line histogram) are some recent calculations[1] of fast flux (E>2.5 Mev) obtained from Monte Carlo Program 18-0. The Monte Carlo data were reduced to a flux at the surface of the vessel using Program 20-8. In using this program, an average neutron energy must be applied to the energy bin output data. An average value of secant θ must be applied to the angle bin data to account for absorption in the theoretical detector. These two assumptions place uncertainties on the accuracy of the histogram plotted in figure 8-11 of about 30 percent. The Monte Carlo geometry[1] on which these data are based was terminated at the dome end of the core; the geometry did not include any material located above the dome end. Hence, the histogram would tend to be too low between station 0 and 10 since some of the neutrons would backscatter toward the core if the entire geometry had been described.

The experimental sulfur data are plotted in figure 8-12 at the pressure vessel surface as a function of reactor azimuth angle, θ. (Refer to figure 8-2 for schematic diagram showing the location of dosimeters) The control drum positions are shown by the arrows on figure 8-12. The sulfur pellets used on this circumferential traverse are of the same type as used on the

[1]WANL-TNR-165, Radiation Analysis of NRX-A2 by Various Methods, Westinghouse Electric Corporation, Astronuclear Laboratory, M. A. Capo, December, 1964

REFERENCE		PREPARED BY	APPROVED BY	Astronuclear

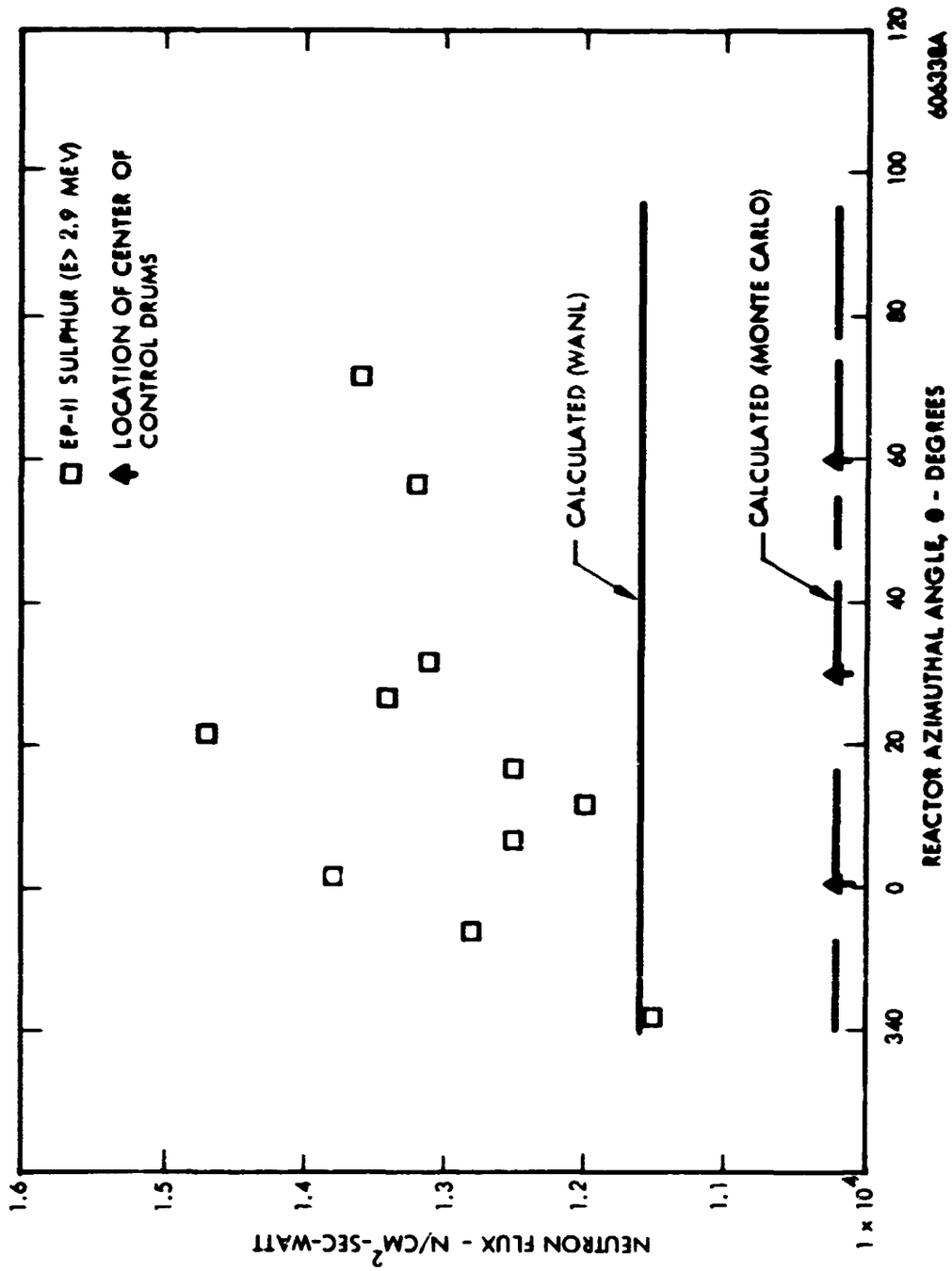

EXPERIMENTAL AND CALCULATED FAST NEUTRON FLUX ON THE SURFACE OF THE PRESSURE VESSEL (CIRCUMFERENTIAL TRAVERSE)

Figure No 8-12

axial traverse. A slight (10 to 15 percent) increase in fast flux is observed in the vicinity of 357 degrees and 22 degrees near the control drums. Sufficient data are not available in the vicinity of $\theta = 60$ degrees to conclude if scalloping is also present at that location. Recent PAX, preassembly experiment, measurements indicate that about a 20 percent increase in fast flux can be observed in the vicinity of the drums. It is believed that this increase in fast flux is due to a decrease in attenuation in the vicinity of the vanes. Further analysis and comparison of PAX data should clarify this problem.

The calculated data given in figure 8-12 are identical to those for station 26 on figure 8-11. The analytical techniques employed in WANL-TNR-128 for calculating the neutron flux at the surface could not account for any azimuth variation of power or geometry. Hence, no azimuth variation of calculated data is shown here. The calculated data are in reasonable agreement with these measurements.

Equatorial Ring

Experimental fast neutron fluxes at locations on the equatorial ring are plotted as a function of reactor azimuth angle in figure 8-13. The equatorial ring was located five feet from the centerline of the core on the midplane. (Refer to figure 8-4 for dosimeter locations on the equatorial ring). Due to a misalignment[1] of the equatorial ring assembly, all dosimeters are not exactly equidistant from the center of the core. The dosimeters at $\theta = 345$ degrees and thereabouts (figure 8-4) are actually a few inches closer to the core than are those at the locations near $\theta = 75$ degrees. This misalignment effect is evidenced in figure 8-13 since the experimental data shows a significant trend of being higher at 345 degrees than at 75 degrees.

Both the WANL and LASL sulfur data obtained during the EP II run are plotted in figure 8-13. The WANL sulfur measurements were made with 1.5 inch ammonium sulfate pellets. The WANL EP II sulfur data are higher than the LASL sulfur data by 30 to 40 percent.

The EP IV nickel data shown in figure 8-13 are believed to be the most reliable of the three sets of WANL data.[1] The EP II WANL sulfur data (due to a lower flux during EP II)

[1]WANL-TME-1081, NRX-A2 Dosimetry Measurements, Westinghouse Electric Corporation, Astronuclear Experimental Facility, March, 1965

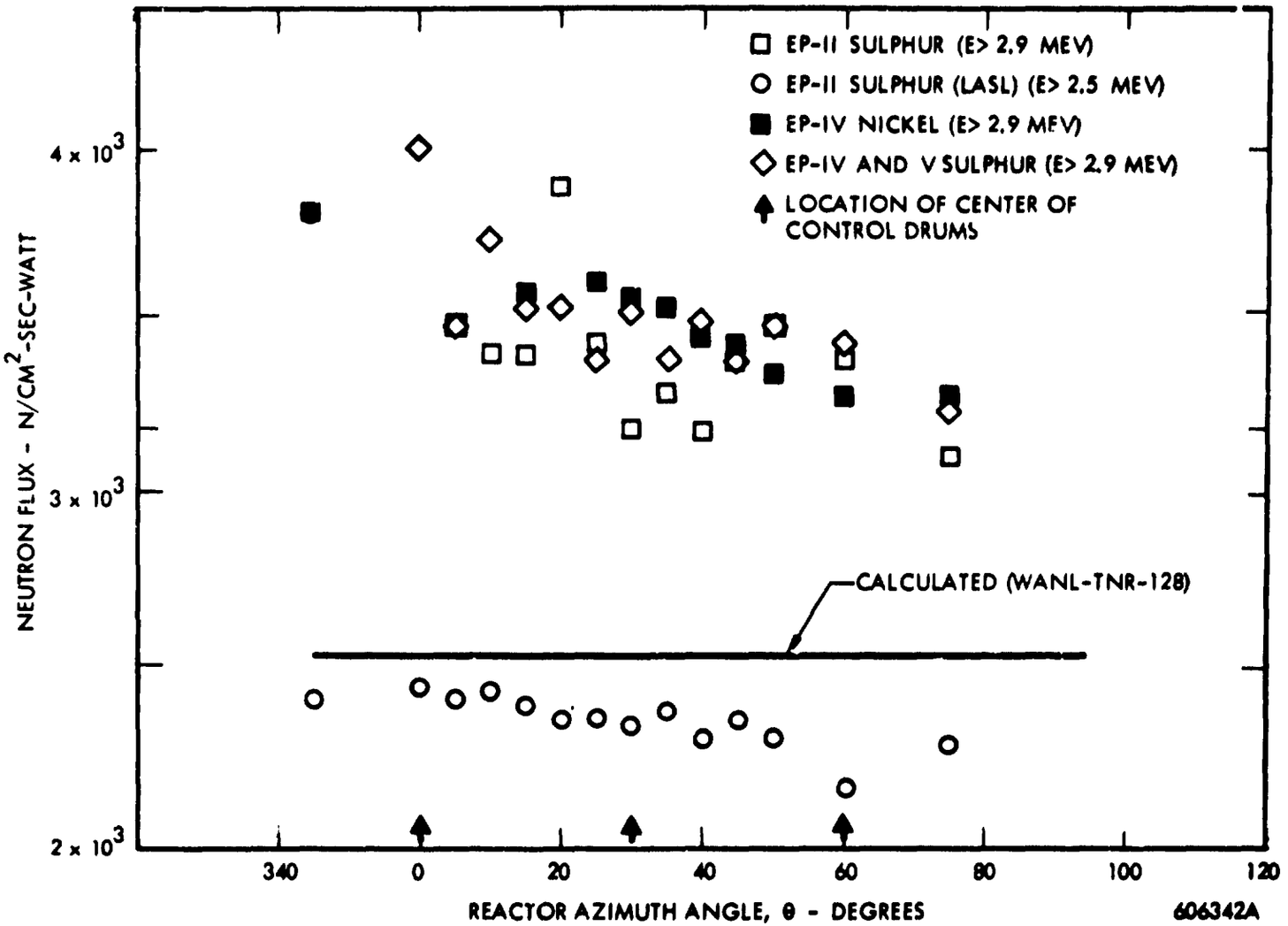

Figure No.	EXPERIMENTAL AND CALCULATED FAST NEUTRON FLUX ON THE EQUATORIAL RING	PREPARED BY	APPROVED BY	CURVE NO.
8-13				

exhibits the most severe spread as a function of position. No noticeable scalloping effect can be observed from these measurements.

Calculation of azimuth variations in fast neutron flux was not possible with the analytical techniques employed here. The calculated data indicated on figure 8-13 is identical to that given in figure 8-17 for a = 90 degrees on the meridian ring. The calculation agrees well with the LASL sulfur data, but is 40 percent lower than the nickel measurements.

Experimental data based on LASL fission foil measurements on the equatorial ring are shown in figure 8-14. (The LASL sulfur data are repeated here for comparison purposes). The fission foil measurements yield fast neutron fluxes within the following energy ranges: 0.004> E>0.75 Mev, 0.75> E>1.5 Mev, and 1.5>E>2.5 Mev. The data in energy range 0.004 > E > 0.75 Mev appear to be relatively flat as a function of angle, and have about the same shape as the sulfur data. More spread of data is indicated by the energy groups 0.75 > E > 1.5, or 1.5 > E > 2.5 Mev. The narrower the energy band of spectral measurements, the more statistical fluctuation occurs in the measured data. It is not believed that the fission foil data presented here shows any real evidence of scalloping.

No calculated values of these energy ranges are shown for comparison in figure 8-14. The reason for this omission is more easily explained by reference to figure 8-15. Figure 8-15 presents the experimental fission foil spectra at a location 5 feet from the core center on the midplane. The calculated spectra data from WANL-TNR-128 are also presented. It is readily noted that the calculated data are considerably lower than measurements at any energies below 2.5 Mev. The calculated data are based on moments method data for water. Even though these results were normalized to the CURE data the use of water moments data under-predicts the spectra in this range. It is more accurate to employ beryllium or carbon moments data as was illustrated in analysis of the KIWI B4A reactor.[1] (At the time of the analysis given in WANL-TNR-128, the carbon data were not available in a form compatible with required point kernel code input format.) Hence, no further attempts will be made in this report to compare the fission foil data at any locations with WANL-TNR-128 calculations.

---

[1]WANL-TME-767, Analysis of KIWI-B4A Radiation Measurements, Westinghouse Electric Corporation, Astronuclear Laboratory, L. D. Stephenson, May, 1964

REFERENCE	PREPARED BY	APPROVED BY	Astronuclear
	[redacted]	[redacted]	

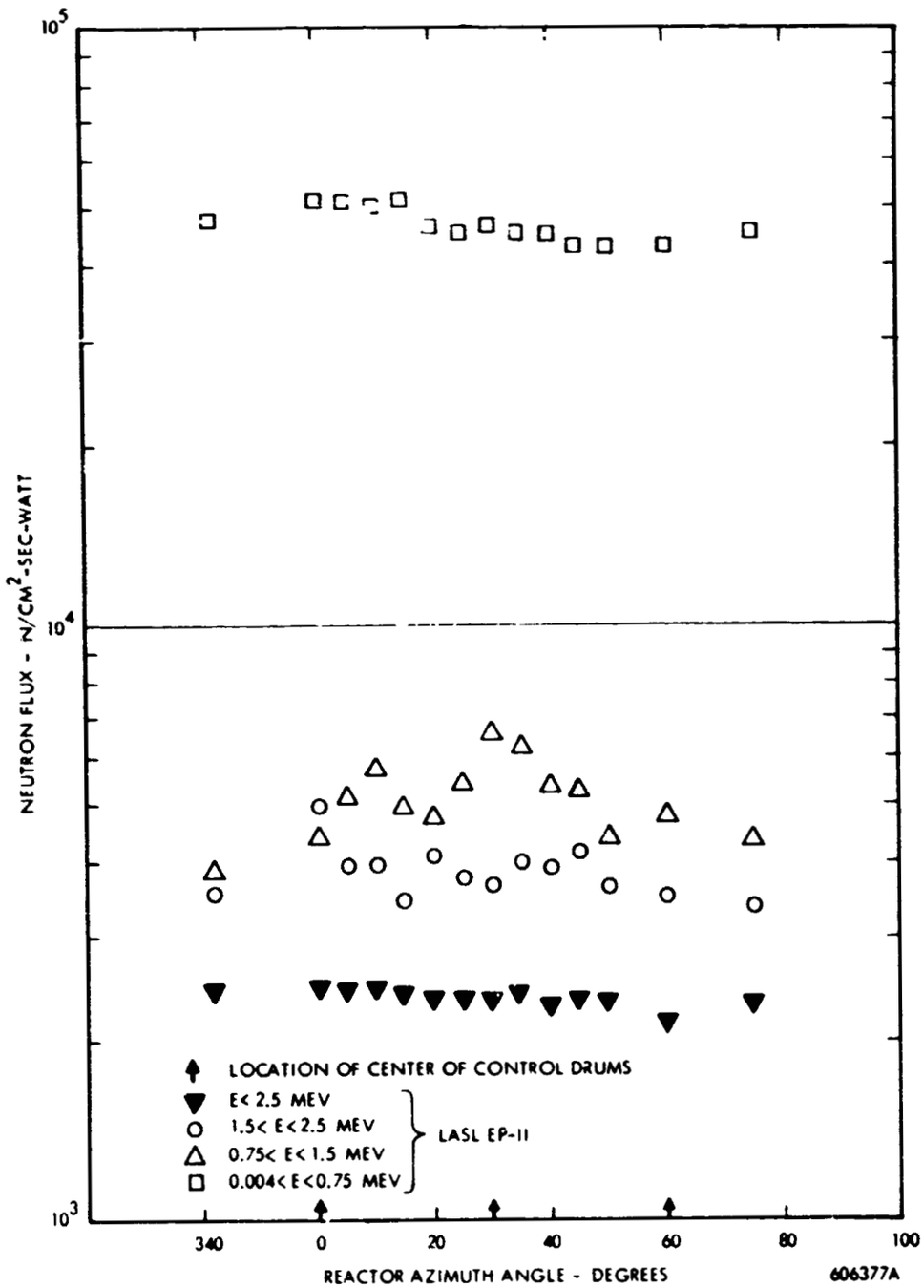

EXPERIMENTAL FISSION FOIL DATA ON THE EQUATORIAL RING

Figure No. 8-14

The LASL fast neutron dose rate on the equatorial ring is plotted in figure 8-16 as a function of reactor azimuth angle, θ. This fast neutron dose rate is computed from the fission foil data by applying appropriate flux to dose conversion factors. The calculated azimuth variation of fast neutron dose rate is not available with present analytical techniques. The calculated data indicated in figure 8-16 is identical to the neutron dose value on the meridian ring, α = 90 degrees, from figure 8-17. The calculation is obviously low by a factor of 2 to 3. This is due to a combination of uncertainties associated with the analytical methods employed. Previous analysis of KIWI data[1] indicated that it is more accurate to compute a fast dose from the point kernel neutron spectra data resulting from application of beryllium or carbon moments data for this purpose.

Meridian Ring

Experimental fast neutron flux data at locations on the meridian ring are plotted in figure 8-17 as a function of reactor polar angle. (Refer to figure 8-3 for dosimeter locations on the meridian ring.) The meridian ring is located five feet from the center of the core. Experimental data on the meridian ring includes WANL and LASL sulfur data obtained during the EP II run, and WANL nickel and sulfur data obtained during the EP IV run. The solid curve in figure 8-17 refers to the calculated data from WANL-TNR-128. As was the case on the equatorial ring, the LASL sulfur data is consistently lower by 30 percent than the WANL sulfur data. Both EP II and EP IV WANL sulfur data were normalized to the WANL nickel data at α = 90 degrees. The WANL sulfur measurements were made with pellets similar to those used on the equatorial ring. The WANL EP II sulfur, and EP IV nickel and sulfur show about the same "shape" as a function of angle. Calculated data agree well both in shape and magnitude with the experimental data. At α = 90 degrees, on the core midplane, the calculated data is 35 percent lower than the WANL measurements. Also shown as a dash curve in figure 8-17 is a best fit to KIWI B4A fast neutron flux measurements (E > 2.5 Mev), normalized at α = 90 degrees to the TNR-128 calculated data. The A2 and B4 measured data

[1]WANL-TME-767, Analysis of KIWI-B4A Radiation Measurements, Westinghouse Electric Corporation, Astronuclear Laboratory, L. D. Stephenson, May, 1964

REFERENCE	PREPARED BY	APPROVED BY	Astronuclear

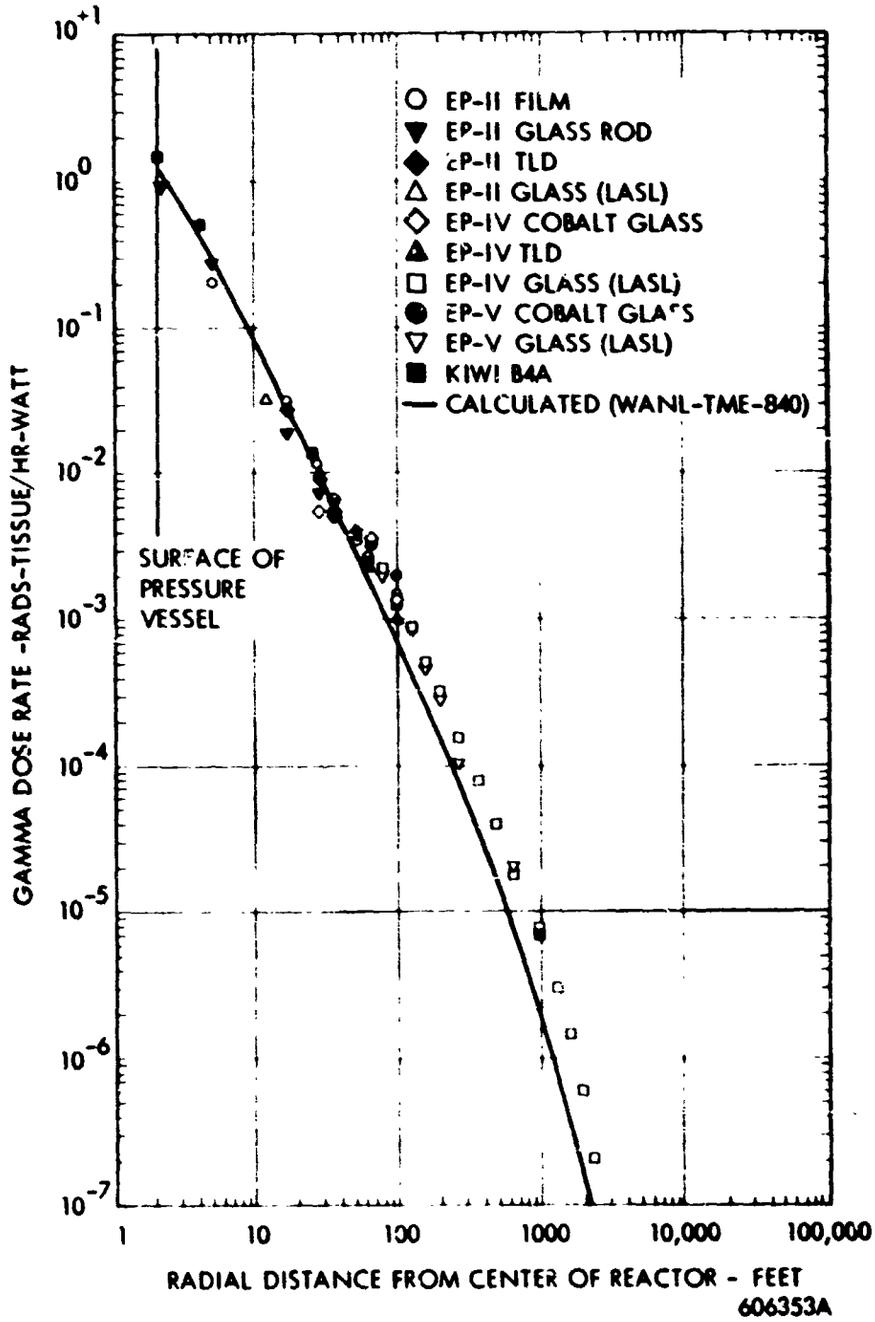

EXPERIMENTAL AND CALCULATED NEUTRON SECTOR 5 FEET FROM THE CENTER OF THE CORE ON THE MIDPLANE, REACTOR $\Theta = 345^{\circ}$

Figure No. 8-15

REFERENCE

Astronuclear

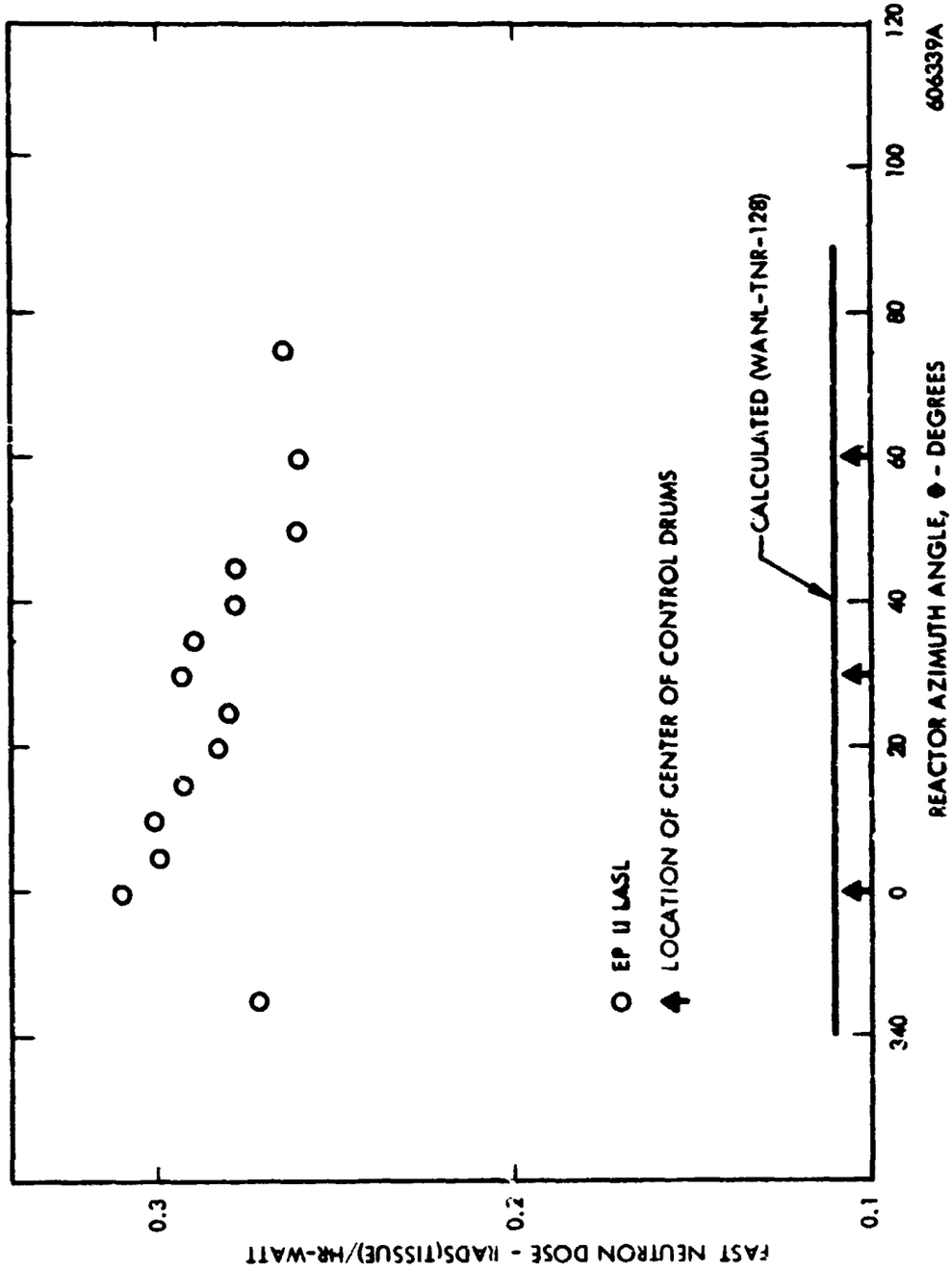

PREPARED BY	APPROVED BY	CURVE NO.

EXPERIMENTAL AND CALCULATED FAST NEUTRON DOSE RATE ON THE EQUATORIAL RING

Figure No. 8-16

REFERENCE	PREPARED BY	APPROVED BY	Astronuclear

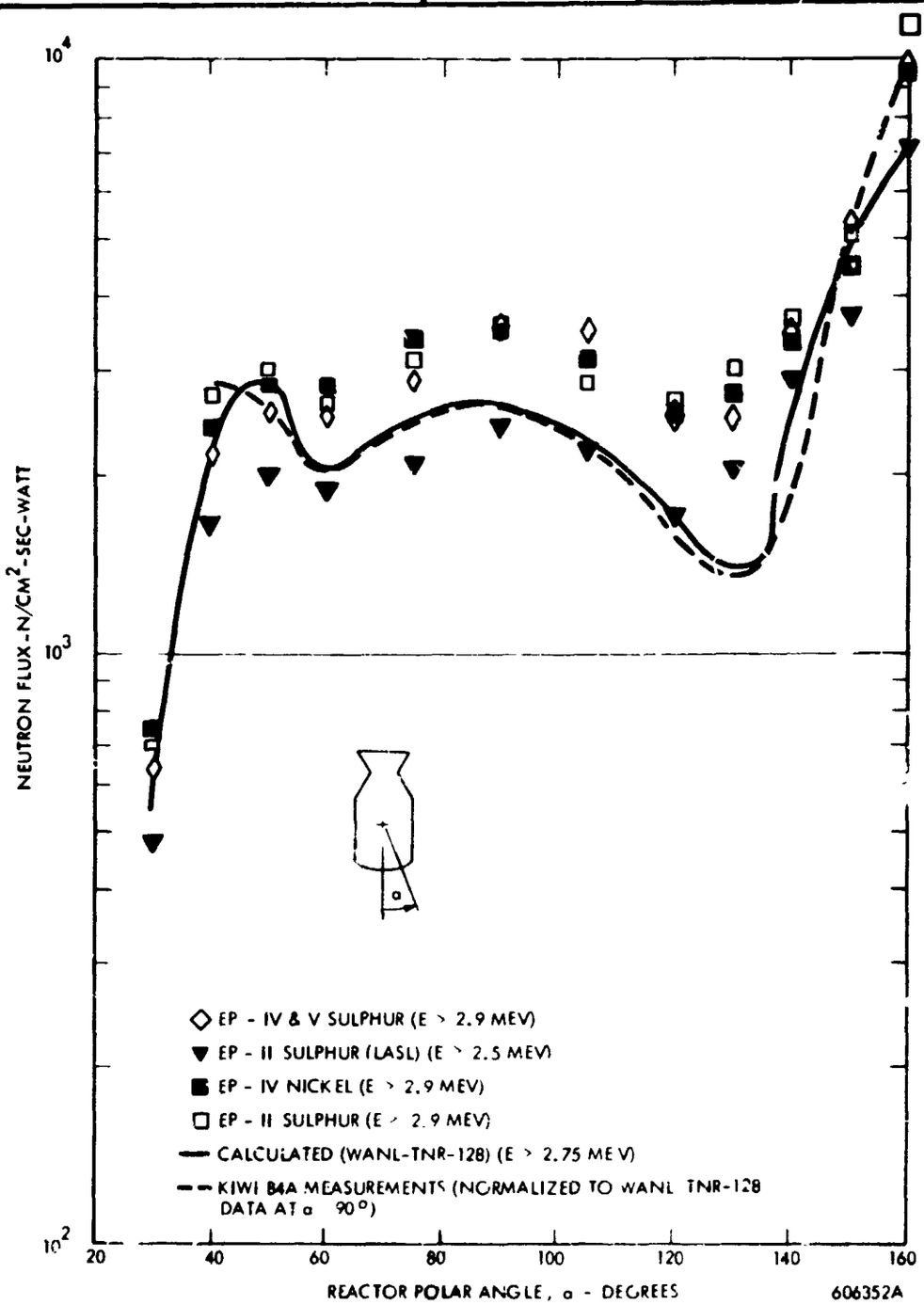

EXPERIMENTAL AND CALCULATED FAST NEUTRON FLUX ON THE MERIDIAN RING

Figure No. 8-17

REFERENCE		PREPARED BY	APPROVED BY	Astronuclear

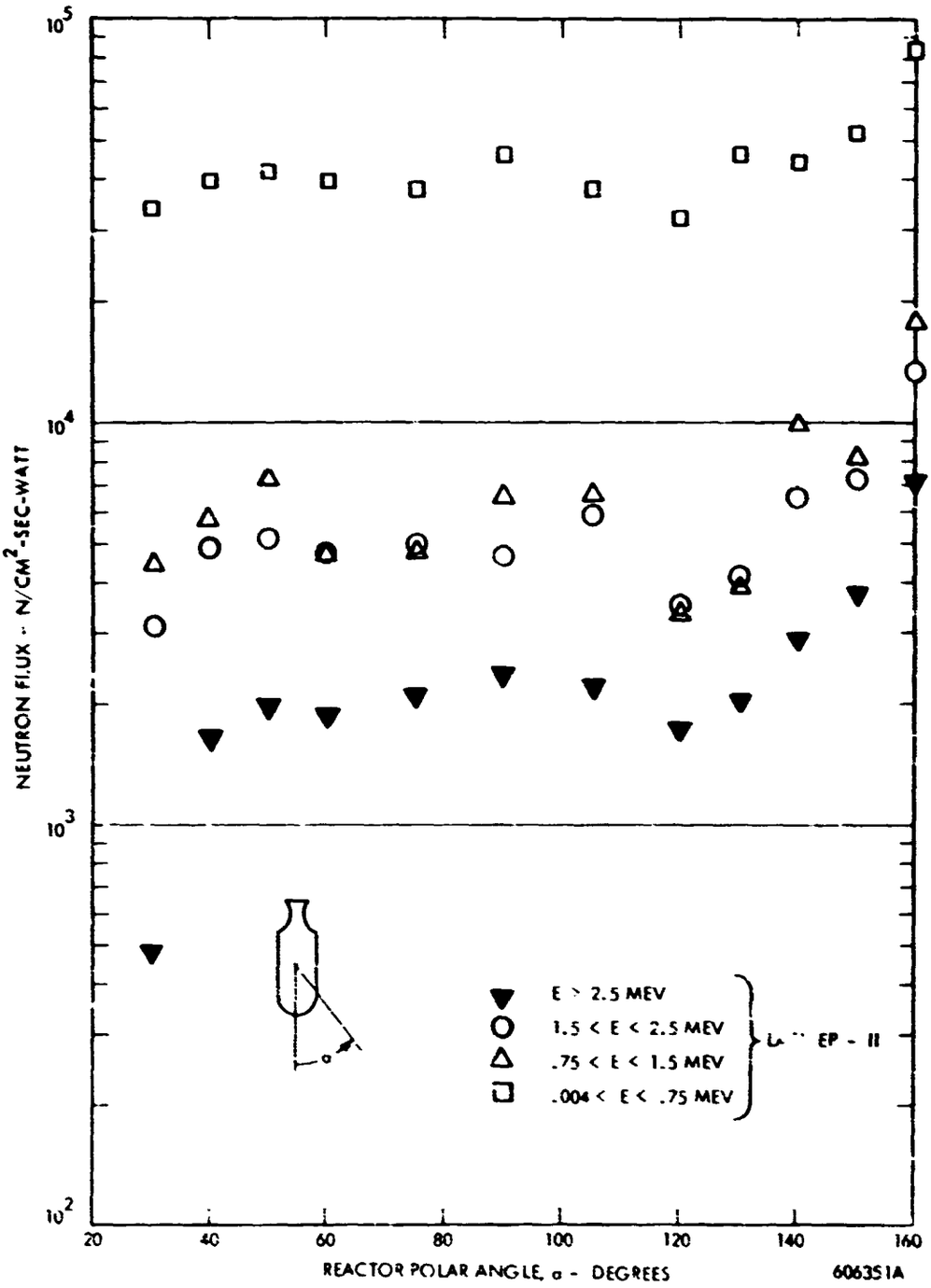

EXPERIMENTAL FISSION FOIL DATA ON THE MERIDIAN RING

Figure No 8-18

REFERENCE		PREPARED BY	APPROVED BY	Astronuclear

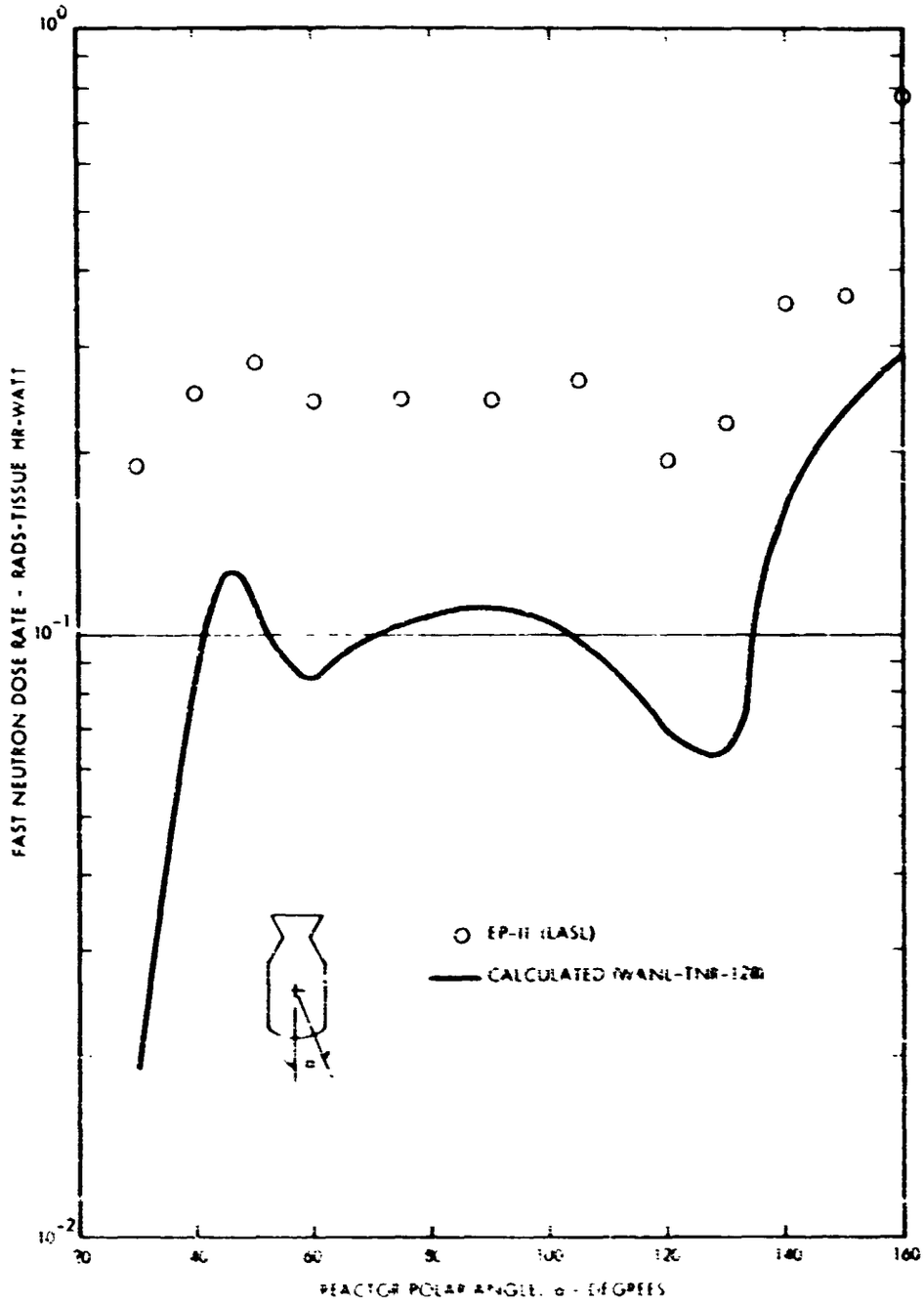

EXPERIMENTAL AND CALCULATED FAST NEUTRON DOSE RATE ON THE MERIDIAN RING

Figure No. 8-19

are not comparable on an "absolute" basis since the A2 and B4 meridian rings were not located at the same distance from the center of the core. The KIWI B4A data are shown here for comparison purposes to illustrate the effect of the aluminum mockup shield on the A2 neutron flux. The B4A, of course, did not have a shield. The KIWI data is beginning to increase as a function of α, at α = 40 degrees. The A2 measured data show a significant factor of 3 decrease from α = 40 degrees to α = 30 degrees due to the shield attenuation.

Experimental LASL fission foil data are presented at locations on the meridian ring as a function of reactor polar angle in figure 8-18. (The sulfur data are repeated in figure 8-18 for purposes of comparison.) No calculated data for these energies are given for the reasons stated in the previous section. It is readily observed that the shape of the lowest energy neutrons, $0.004 < E < 0.75$ Mev is relatively flat as a function of polar angle, whereas the shape of the neutrons with the highest $E > 2.5$ Mev changes more severely as a function of angle. The reason is as follows: The fast neutron energies ($E > 2.5$) are more severely influenced by attenuation of materials surrounding the reactor. The lower energy neutrons are caused by down scatter of the higher energy neutrons as well as those born in the core. Hence, their shape would be influenced less by the material attenuation.

The fast neutron dose rate on the meridian ring as a function of polar angle is plotted in figure 8-19. The calculated dose rate is again low by more than a factor of 2. However, the shape of the calculated neutron dose is in good agreement with the measurements. The experimental fast neutron dose was calculated by LASL by applying appropriate flux to dose conversion factors to the measured fission foil data.

Radial Midplane

Comparison of experimental and calculated fast neutron fluxes as a function of radial distance from the reactor is shown in figure 8-20. These data were obtained during the low and high power runs at the vessel surface, five feet from the reactor on the equatorial ring, and on the trolley line and trolley line extension. (Several KIWI B4A measurements are included for comparison.) The calculated fast neutron flux ($E > 2.75$ Mev) out to a distance of 20 feet from the center of the core were obtained from WANL-TNR-128. At

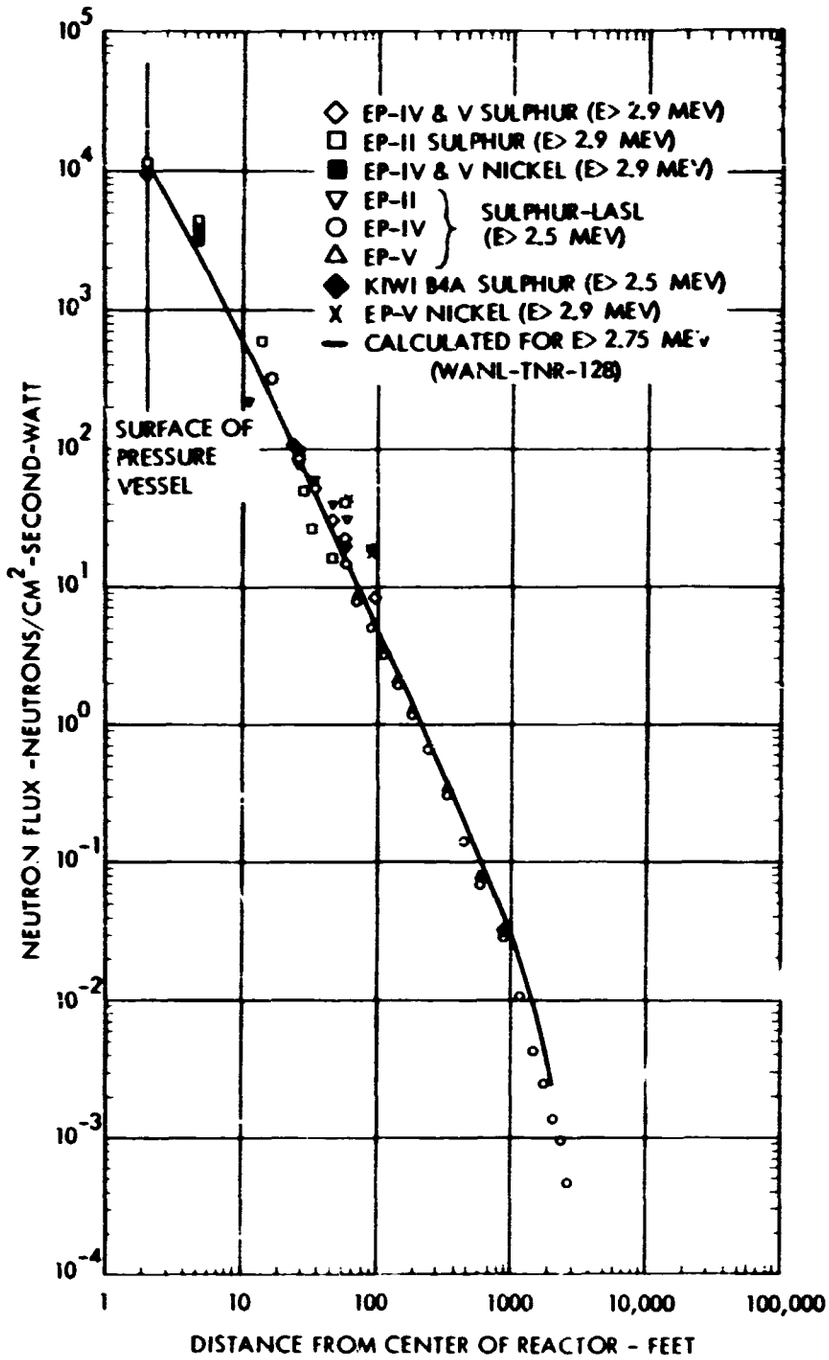

EXPERIMENTAL AND CALCULATED FAST NEUTRON FLUX AS A FUNCTION OF DISTANCE FROM THE REACTOR

Figure No. 8-20

20 feet, the fast flux was normalized to the fast dose to obtain the fall-off as a function of cistance beyond 20 feet. This normalization may, however, over emphasize the effect of fast neutron air scattering.

The calculated fast flux agrees to within a factor of 1.5 with a "best fit" to the experimental data. The agreement between the measurements and calculations presented here are well within the uncertainty factor of 2 quoted in WANL-TNR-128.

The WANL sulfur data shown in figure 8-20 again shows evidence of being higher than the LASL sulfur data. These WANL measurements were obtained with 1.5 inch pure sulfur pellets. The WANL nickel data discrepancy at 62 and 100 feet is still not presently understood.

Figures 8-21, 22 and 23 present experimental neutron fluxes vs. radial distances for the following energy ranges, respectively: $0.004 < E < 0.75$ Mev, $0.75 < E < 1.5$ Mev, and $1.5 < E < 2.5$ Mev. The radial fall-off of these fluxes appear to be in reasonably good agreement with the fall-off shown in figure 8-20 for the fast flux data thus indicating little spectral change. No calculated values within these energy ranges are presented for the reasons explained in the section above relative to the equatorial ring fluxes.

The experimental fast neutron dose rate as a function of radial distance from the reactor is presented in figure 8-24. The calculated neutron dose rate is about a factor of 2 lower than the measurements. The reason for this discrepancy is also discussed in the section above relative to the equatorial ring dose rates. The shape of the calculated curve is in good agreement with a best fit to the experimental data.

Below Privy Roof

Experimental fast neutron flux data were obtained at four locations in the vicinity of the test car and test cell wall. The data are presented in figure 8-25 as a function of radial distance from the reactor center. The dosimeter positions are identified as locations 1, 2, 3, and 4. These dosimeter positions are located at different distances below the core midplane. Location No. 1 is 17 feet below the core center; location No. 2 is 14 feet below the core center; and locations 3 and 4 are about 12 feet below the core center. Locations 1 and 2 are completely in the shadow of the privy roof whereas locations 3 and 4 are not. The

REFERENCE		PREPARED BY	APPROVED BY
		[redacted]	[redacted]

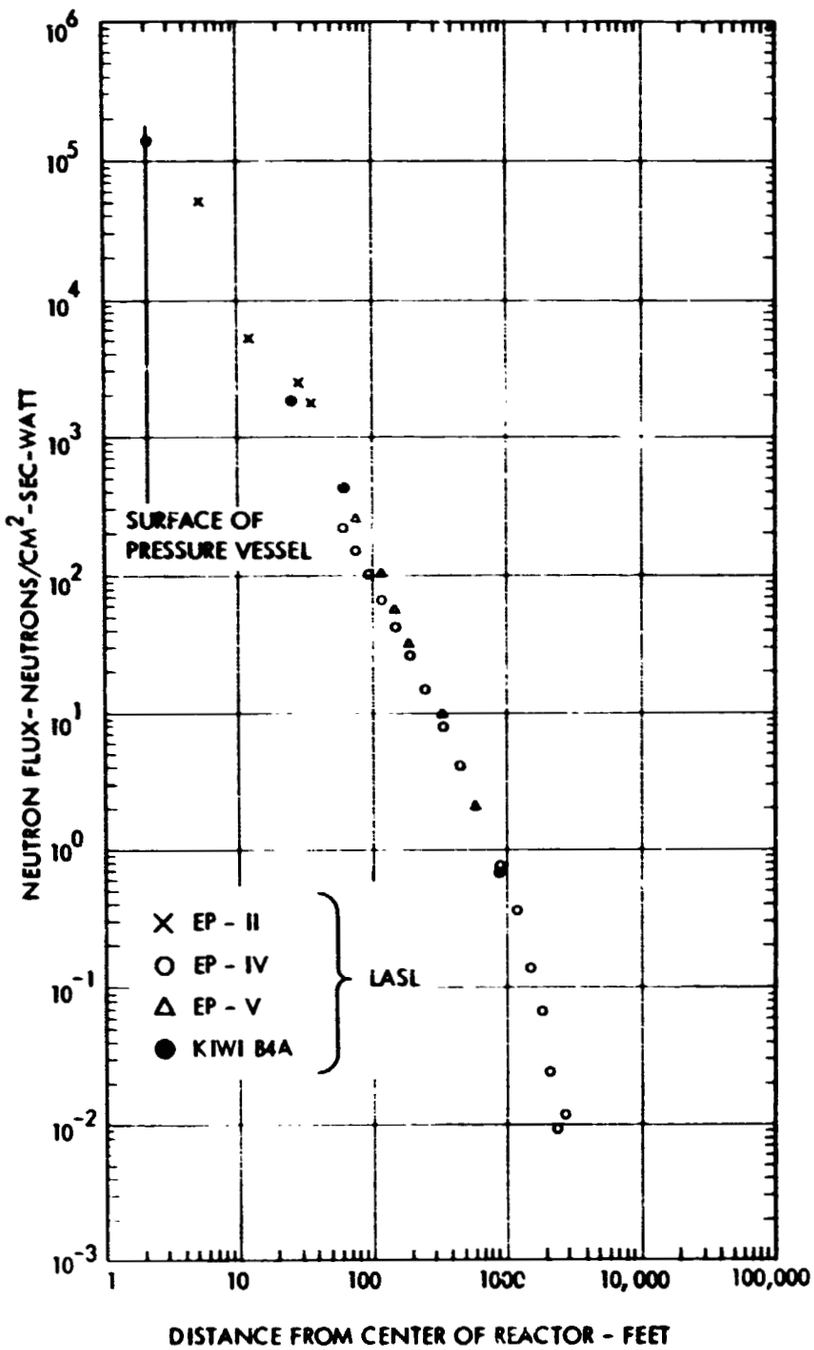

EXPERIMENTAL FISSION-FOIL DATA (0.004<E < 0.75 Mev) AS A FUNCTION OF DISTANCE FROM THE REACTOR

Figure No. 8-21

REFERENCE | PREPARED BY | APPROVED BY | Astronuclear

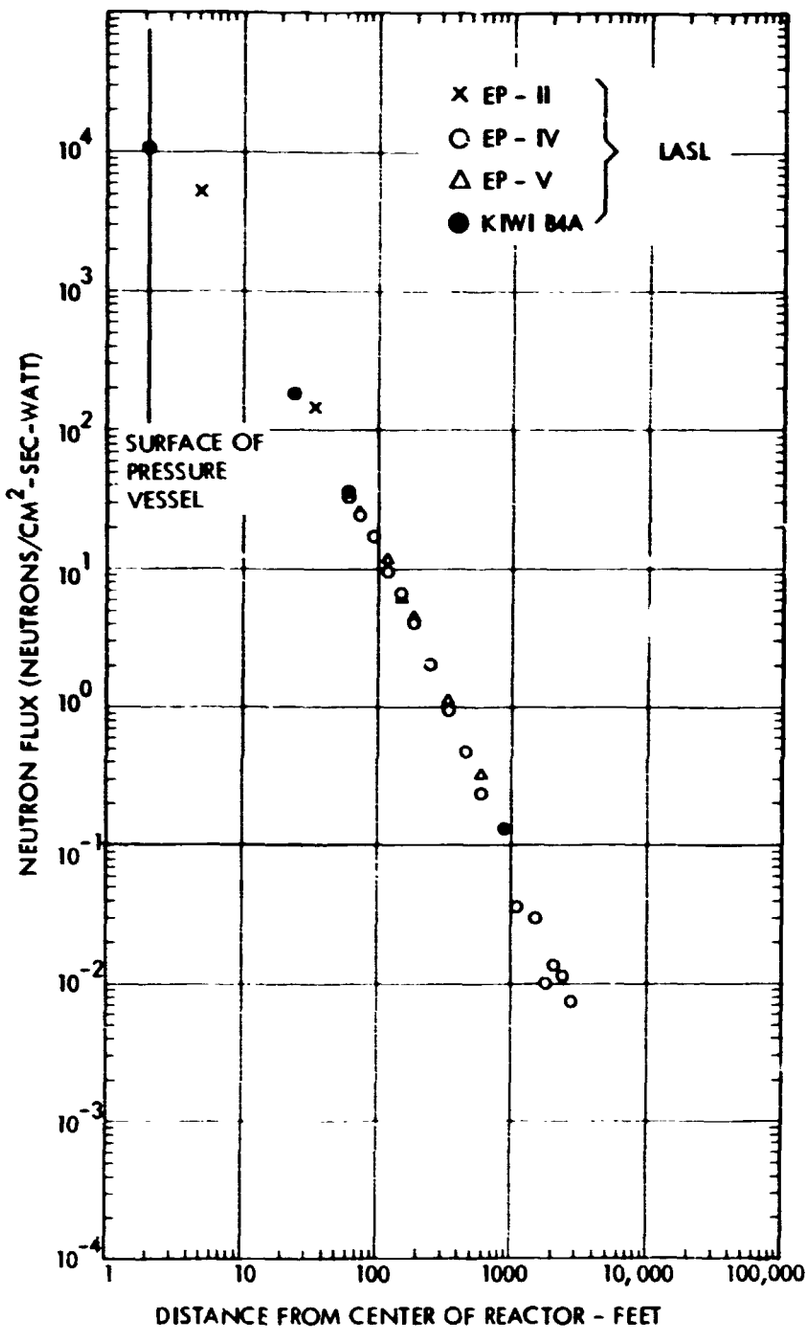

EXPERIMENTAL FISSION FOIL DATA (0.75 < E < 1.5 Mev) AS A FUNCTION OF DISTANCE FROM THE REACTOR

Figure No 8-22

REFERENCE		PREPARED BY	APPROVED BY	Astronuclear

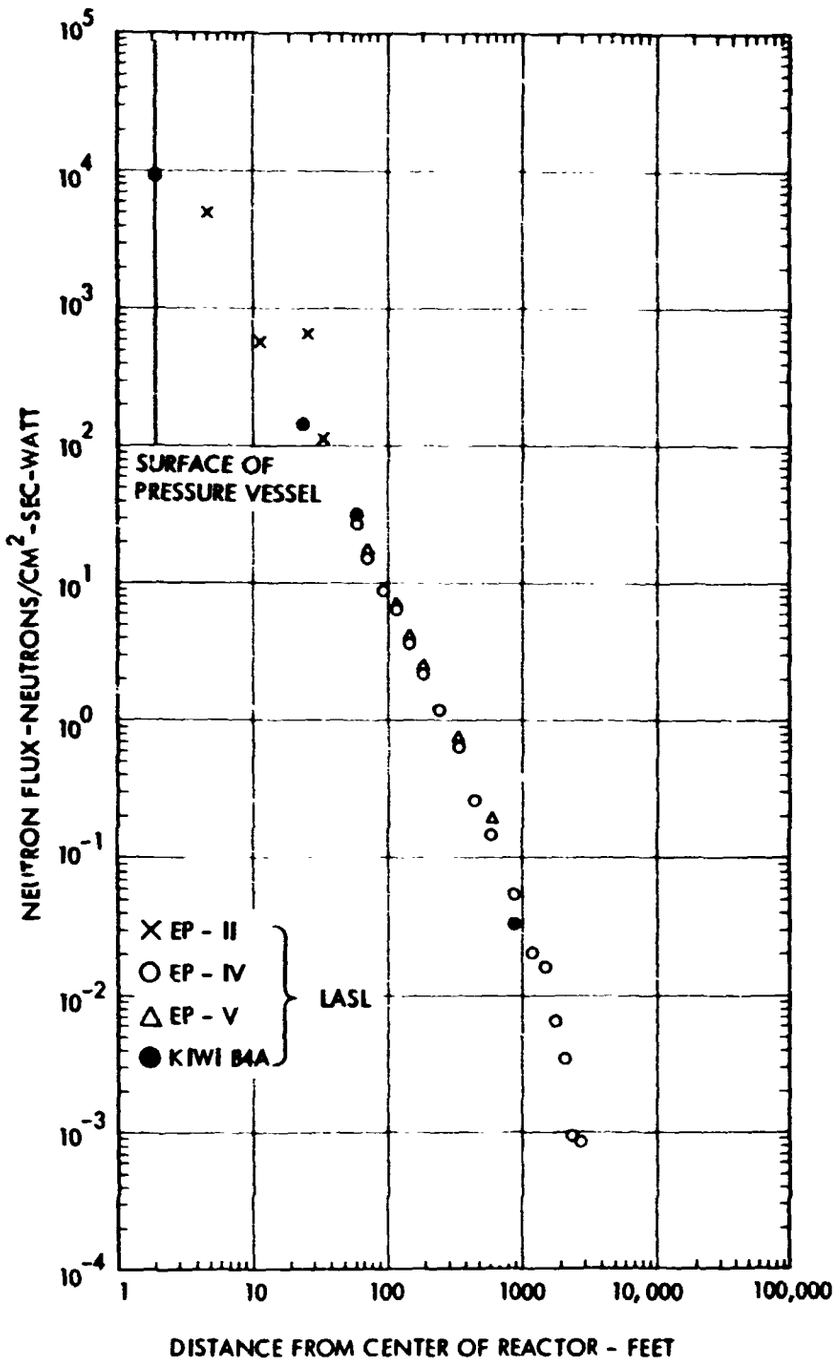

EXPERIMENTAL FISSION FOIL DATA (1.5 < E < 2.5 Mev) AS A FUNCTION OF DISTANCE FROM THE REACTOR

Figure No. 8-23

REFERENCE		PREPARED BY	APPROVED BY	Astronuclear

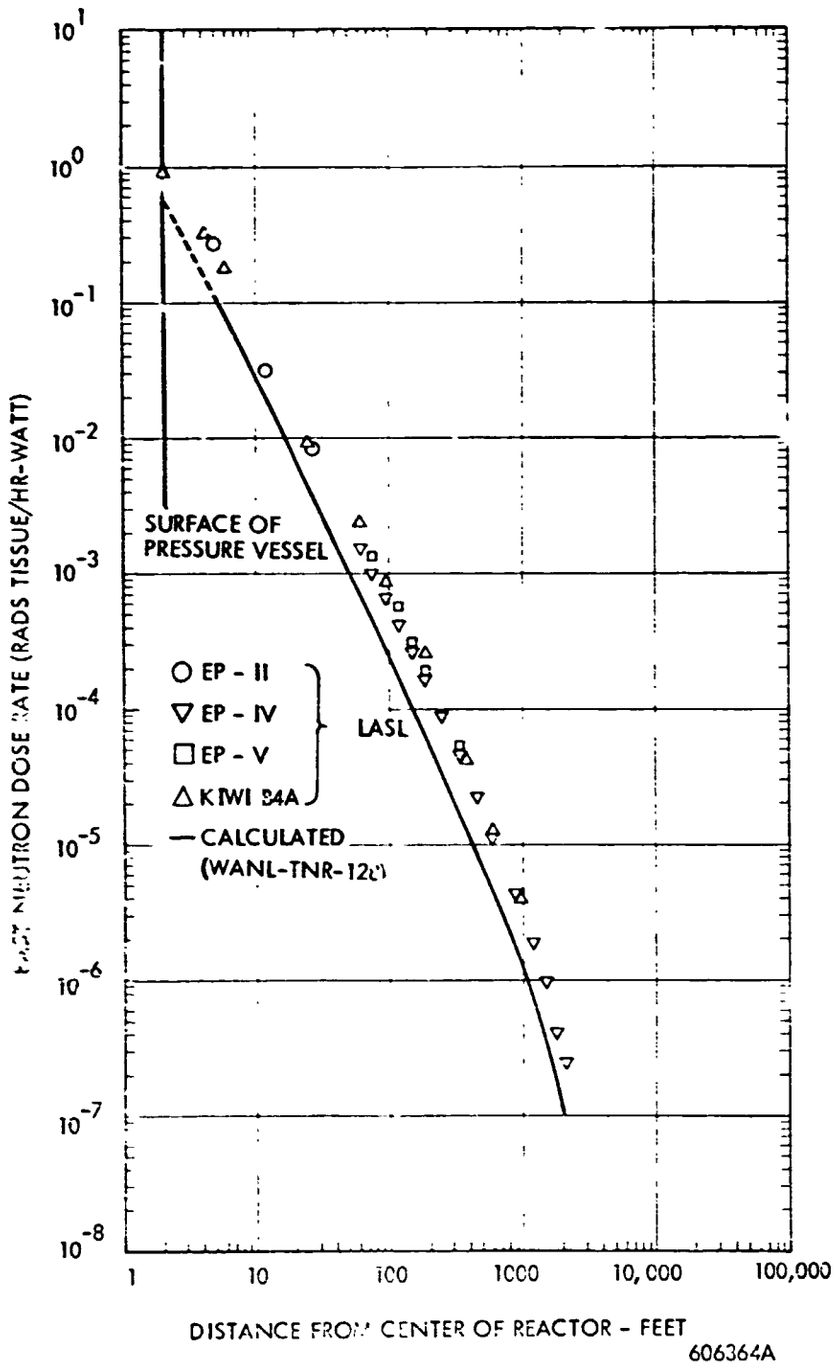

EXPERIMENTAL AND CALCULATED FAST NEUTRON DOSE AS A FUNCTION OF DISTANCE FROM THE REACTOR

Figure No. 8-24

REFERENCE		PREPARED BY	APPROVED BY	Astronuclear

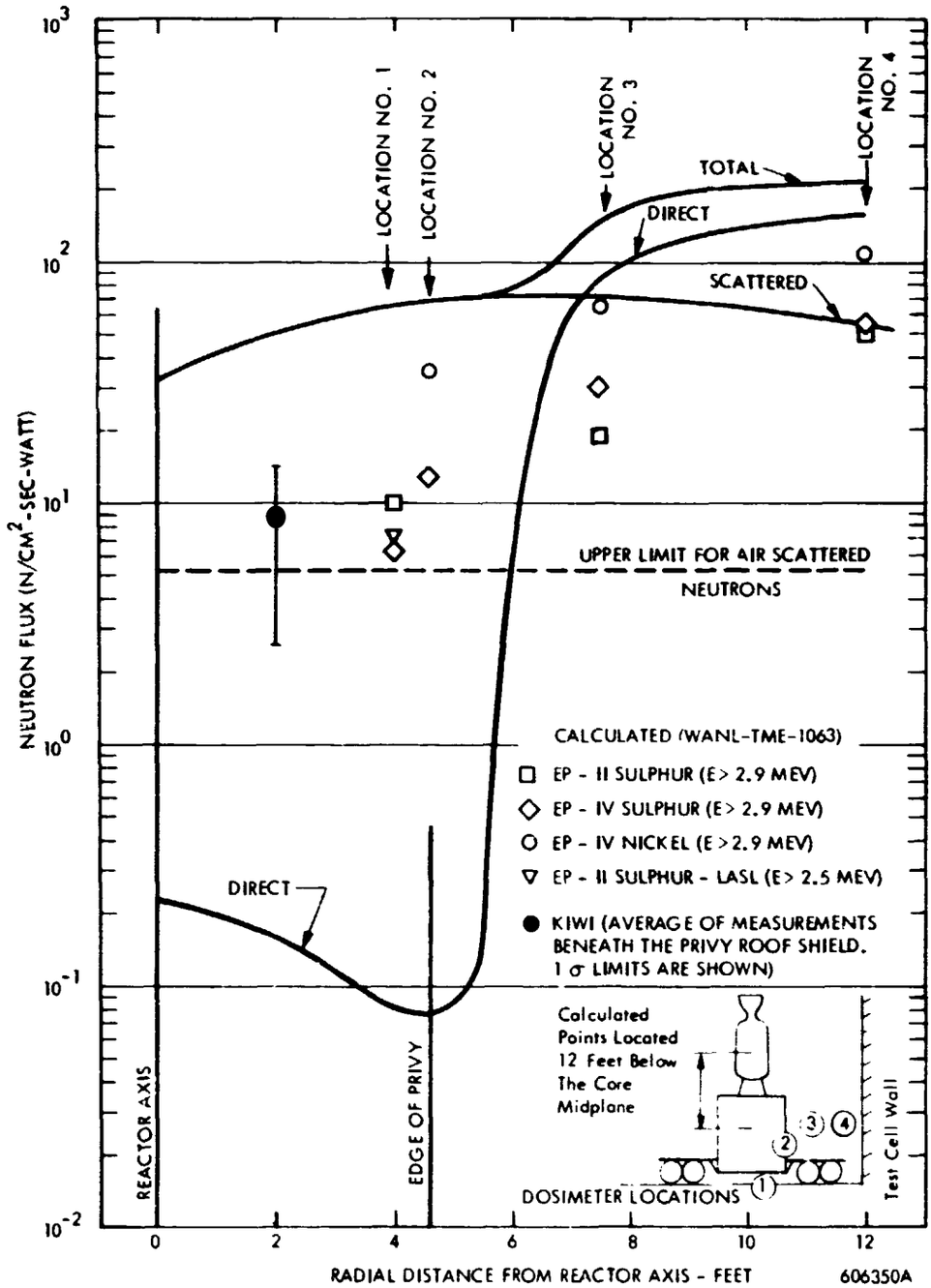

EXPERIMENTAL AND CALCULATED FAST NEUTRON FLUX UNDER THE PRIVY ROOF SHIELD AND AT TEST CAR LOCATION

Figure No. 8-25

calculated data are presented for a radial traverse located 12 feet below the core center. The effect of the difference in distance between calculated and experimental data points has not been evaluated.

Figure 8-25 shows that the nickel EP IV measurements are consistently higher than the EP II or EP IV sulfur data. This phenomena, which was not observed on the meridian ring, is being investigated by WANEF. The EP II and EP IV sulfur data are in reasonable agreement. The LASL EP II sulfur data at location No. 1 is 40 percent lower than the WANL EP II sulfur; a similar difference was noted at the meridian ring. For purposes of comparison the average value of KIWI measurements beneath the roof is indicated.

The calculated fast neutron flux data include:

1) The direct beam contribution from the core
2) Neutrons scattered from the wall and pad
3) An estimate of the upper limit of air scattered neutron radiation.

The total, as well as the components, are plotted in figure 8-25. The scattered component predominates out to a radius of about 7 feet. Outside the shadow of the roof the direct beam component becomes increasingly important as a function of radius. At a radius of 13 feet the total calculated flux is a factor of 4 higher than the sulfur measurements and a factor of 2 higher than the nickel measurements.

It should be noted that this type of geometry is a most difficult one to analyze. Disagreements between measurements and calculations, at locations such as described here, are not uncommon.

Additional Locations

Experimental fast neutron flux data were also obtained at three locations on top of the privy roof, and one location on the instrumentation ladder. These measured data are summarized in table 8-3 and are compared with calculations.

LASL sulfur measurements were made at two locations on top of the roof during the EP II run, and a WANL nickel measurement was made at one additional location during the EP IV run. No overlap of measured data between reactor runs is available on top of the roof. The calculated data are higher than the LASL sulfur data as expected since the same trend existed

TABLE 8-3

EXPERIMENTAL AND CALCULATED FAST NEUTRON FLUX AT ADDITIONAL LOCATIONS

Description	Location: Reactor θ	Location: Station Inches	Location: Radius Inches	Measured Fast Neutron Flux (N/cm^2-sec-watt): WANL Sulfur (EP II)(1)	WANL Nickel (EP IV)(1)	LASL Sulfur (EP II)(2)	Calculated(3) N/cm^2-sec-watt
Top of Privy roof	345°	-51.2	49.2	--------	--------	2.24×10^2	3.75×10^2
Top of Privy Roof	345°	-51.2	66.7	--------	--------	4.15×10^2	5.46×10^2
Top of Privy Roof	345°	-55.2	0	--------	4.66×10^2(1)	--------	3.22×10^2
Instrumentation Ladder	300°	20	60	4.16×10^3(1)	--------	2.59×10^3	2.65×10^3

(1) E > 2.9 mev

(2) E > 2.5 mev

(3) E > 2.75 mev

on the meridian ring. The calculated data is lower than the measured nickel data and greater than the LASL sulfur data on top of the roof; this was also observed in the case of the meridian ring comparisons. The calculated data presented in table 8-3 are direct beam fluxes and do not include any contributions from scattering from the roof or wall.

Both LASL and WANL sulfur measurements during the EP II run are given for a location on the instrumentation ladder. This location is five feet from the core center near the core midplane. The difference between the two measurements is noted to be more severe than on the meridian ring. The calculation is in good agreement with the LASL sulfur measurement.

COMPARISON OF EXPERIMENTAL AND CALCULATED THERMAL AND EPITHERMAL NEUTRON FLUXES

Calculated thermal and epithermal reaction rates, i.e., flux times macroscopic activation cross section, were compared with measured reaction rates determined from cadmium covered and bare gold, copper, and cobalt wires placed axially along the outside lateral surface of the pressure vessel.

No test data on the lateral surface of the pressure vessel exists for EP IV because the bands used to support the various detectors were destroyed during the test. For this reason, the comparisons given here are for EP II only. The multigroup TDC problem used in the analysis closely matched the NRX-A2 under EP II test conditions with the exception of the following:

1) The privy roof was not included
2) The pressure vessel was not included
3) The design conditions were 1120 MW thermal power and 100 percent hydrogen flow
4) The nozzle was not considered

The TDC problem employed here had been run for another analysis. The differences in the TDC problem described above are not expected to markedly change the spectrum, and hence, the results of this analysis. The discussions which follow point out any of these effects where it is felt that they enter into disagreement of calculated and measured reaction rates. Calculated and measured reaction rates were compared instead of fluxes since the fundamental measured quantity is the reaction rate. (Refer to the sections in this same chapter on Thermal

and Epithermal Neutron Data under Analytical Methods for detailed discussion.)

A comparison of calculated and measured thermal reaction rates is given in table 8-4. Agreement for copper and cobalt is fairly good. The gold data agreement is not quite as good, but the experimental data is within a factor of two of the calculated reaction rate with the latter being the higher.

Figures 8-26, 27 and 28 show comparisons of the calculated and measured epithermal reaction rates versus axial position for cobalt, copper, and gold, respectively. The calculated reaction rates were normalized to the experimental values at the midplane. With the exception of gold, the calculated and measured shapes agree well.

Since nearly all of the epithermal reactions in gold come from the 30,000 barn (peak) absorption resonance at 4.9 ev, it is hypothesized that a localized source of neutrons near 5 ev in energy exists in or near the dome end of the reactor which was not evident in the transport analysis. One possibility is that the source comes from the flange of the pressure vessel or from the water in the test stand roof.

A significant spectral change near 5 ev along the pressure vessel surface in the axial direction is evidenced by the change in the measured cadmium ratio for gold. As shown in table 8-5, the cadmium ratios near the dome end of the core (reactor stations 0.0 to 15.5) are approximately a factor of two lower than those toward the nozzle end of the core (reactor stations 20.5 to 51.5). The low values of cadmium ratio (bare/covered) correspond to a hardened spectrum above 0.4 ev, i.e., the epithermal absorption is large compared with the thermal absorption.

Figures 8-29, 30 and 31 show comparisons of the calculated and measured thermal reaction rates for cobalt, copper, and gold, respectively on the surface of the vessel as a function of reactor station. Again, the gold shows poor agreement while the agreement for cobalt and copper is good.

The calculated cadmium ratios for gold presented in table 8-5 appear low by a factor of three compared with the measured cadmium ratios near the nozzle end of the core. It is probable that this disparity comes from neglecting self-shielding at the 4.9 ev gold resonance in the calculated epithermal reaction rate. The diameter of the gold wire used in the experiment was approximately 5 absorption mean free paths (20 mils) at the peak of

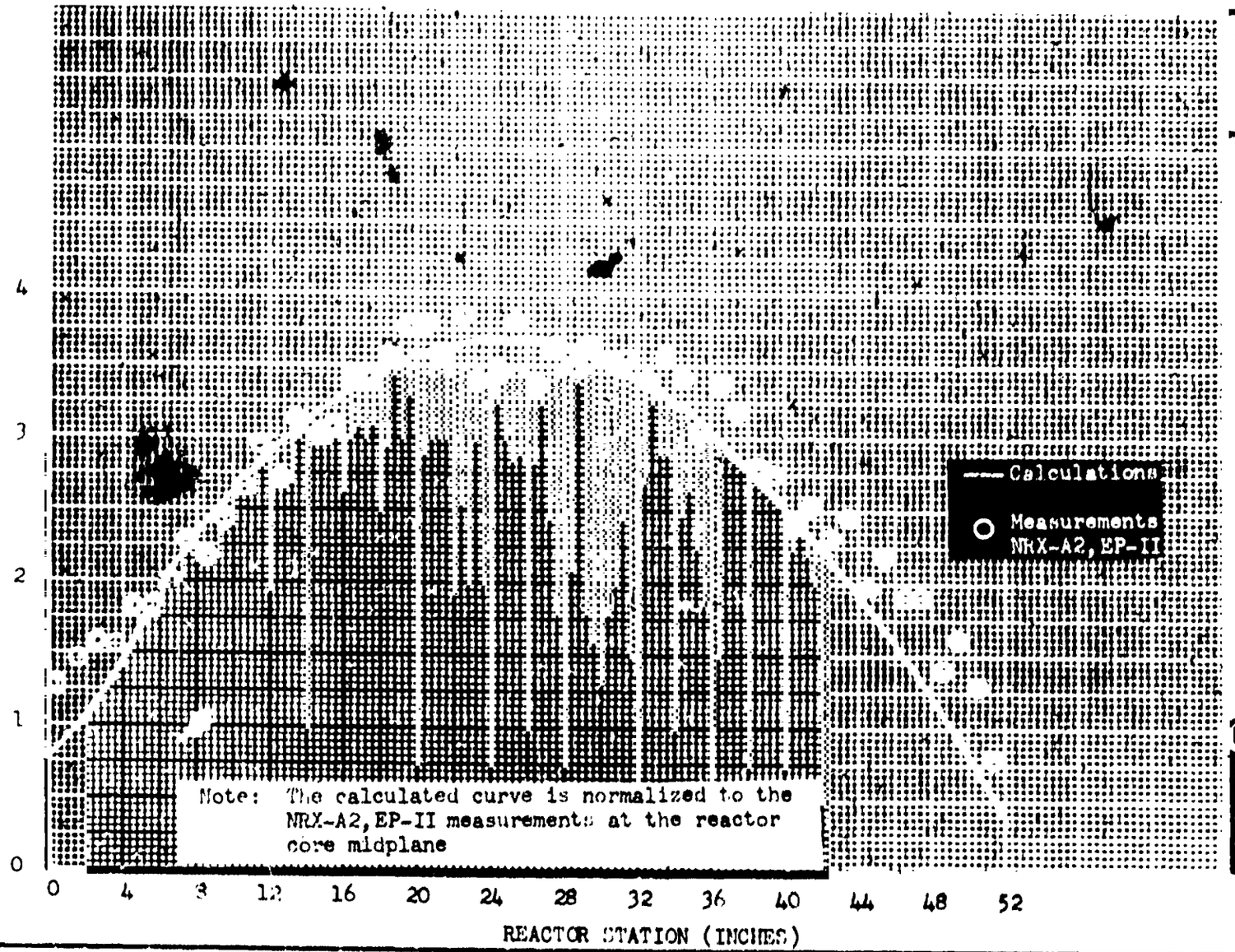

Figure No.	COMPARISON OF CALCULATED AND MEASURED REACTION RATES FOR COBALT AT THE SURFACE OF THE PRESSURE VESSEL (E > 0.4 EV)	PREPARED BY	APPROVED BY	CURVE NO.
C-26				

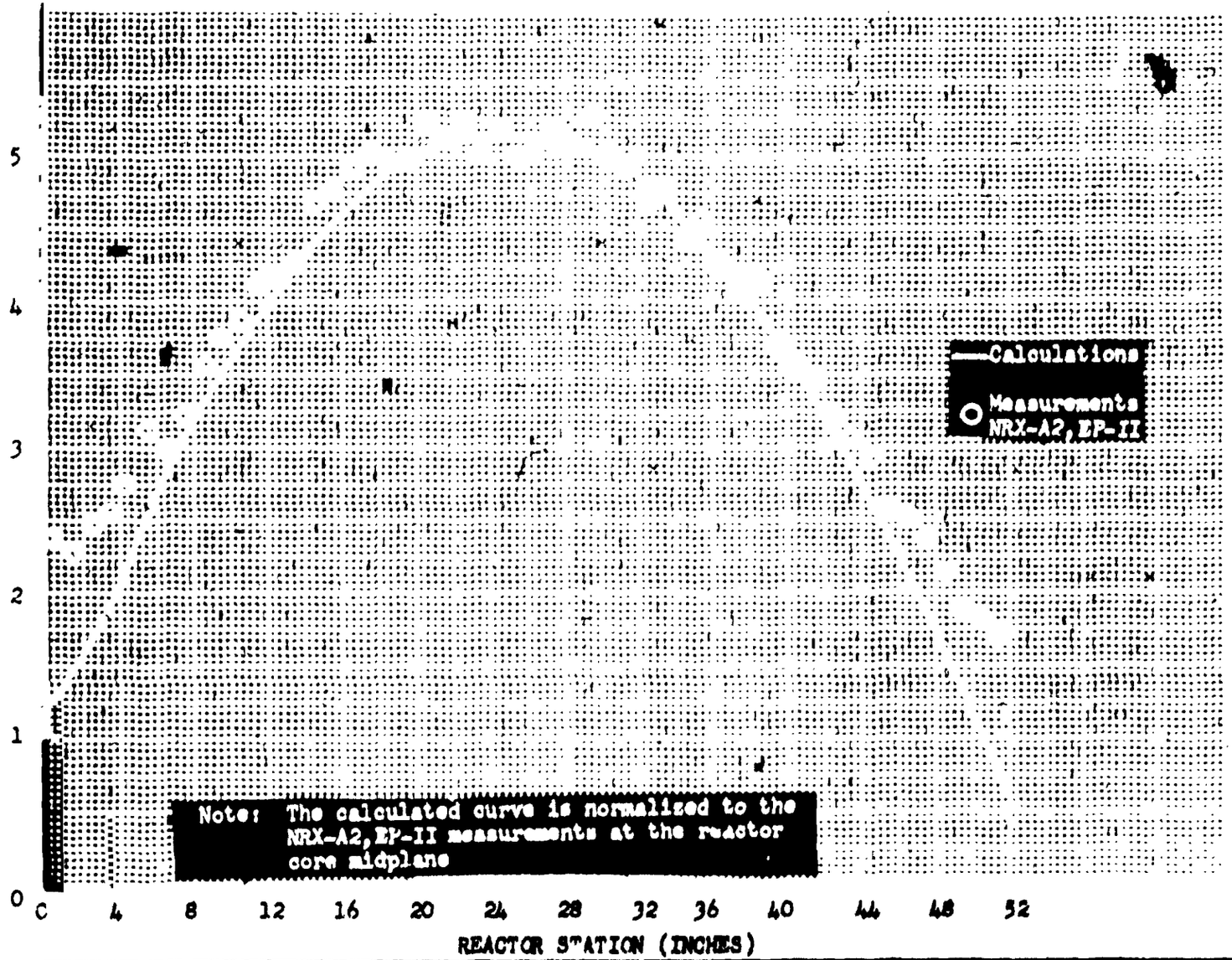

Figure No.	COMPARISON OF CALCULATED AND MEASURED REACTION RATES FOR COPPER AT THE SURFACE OF THE PRESSURE VESSEL (E > 0.4 EV)	PREPARED BY	APPROVED BY	CURVE NO.
8-27				

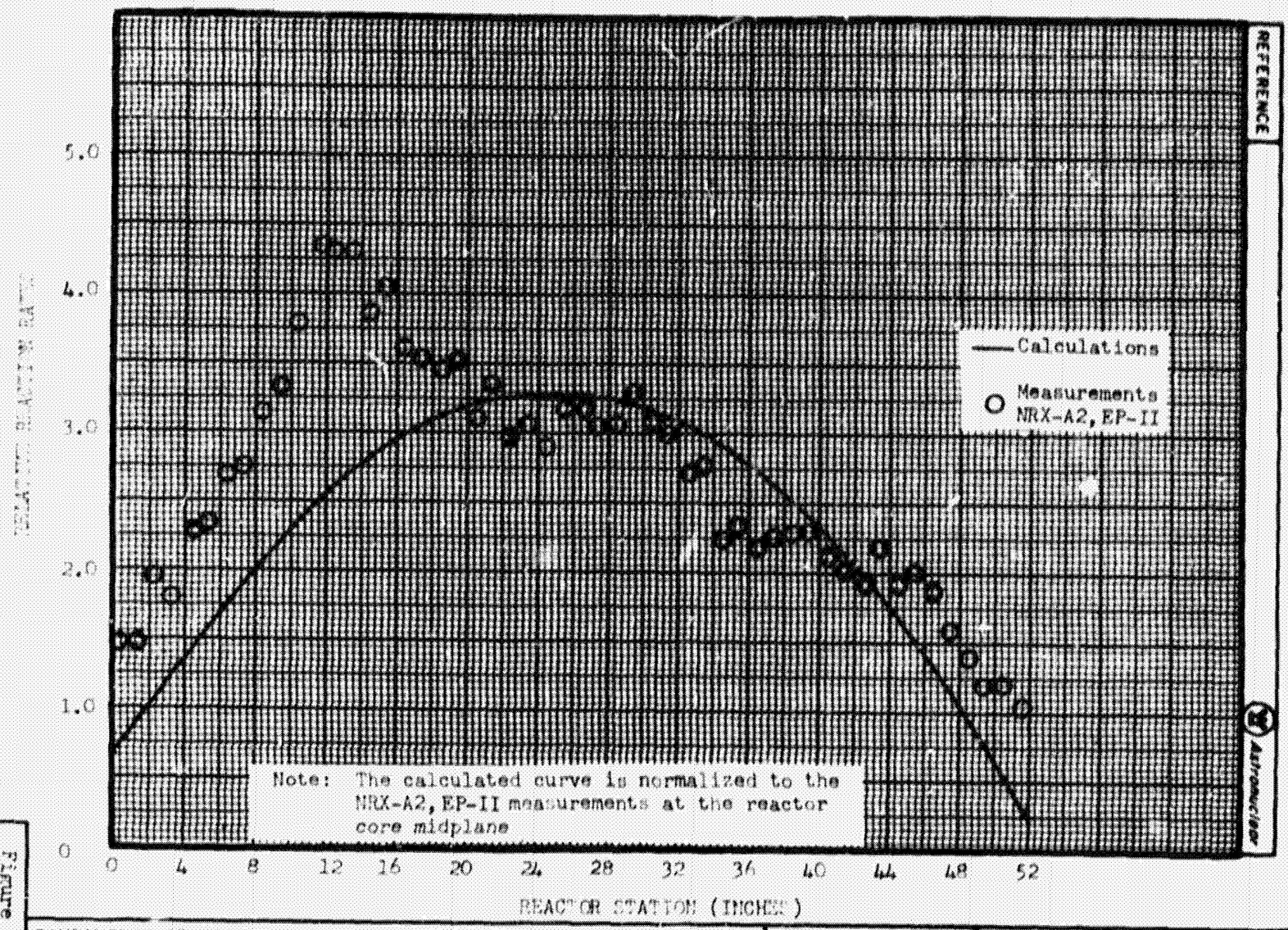

Figure 8-38

COMPARISON OF CALCULATED AND MEASURED REACTION RATES FOR GOLD AT THE SURFACE OF THE PRESSURE VESSEL (E > 0.4 EV)

PREPARED BY	APPROVED BY	CURVE NO

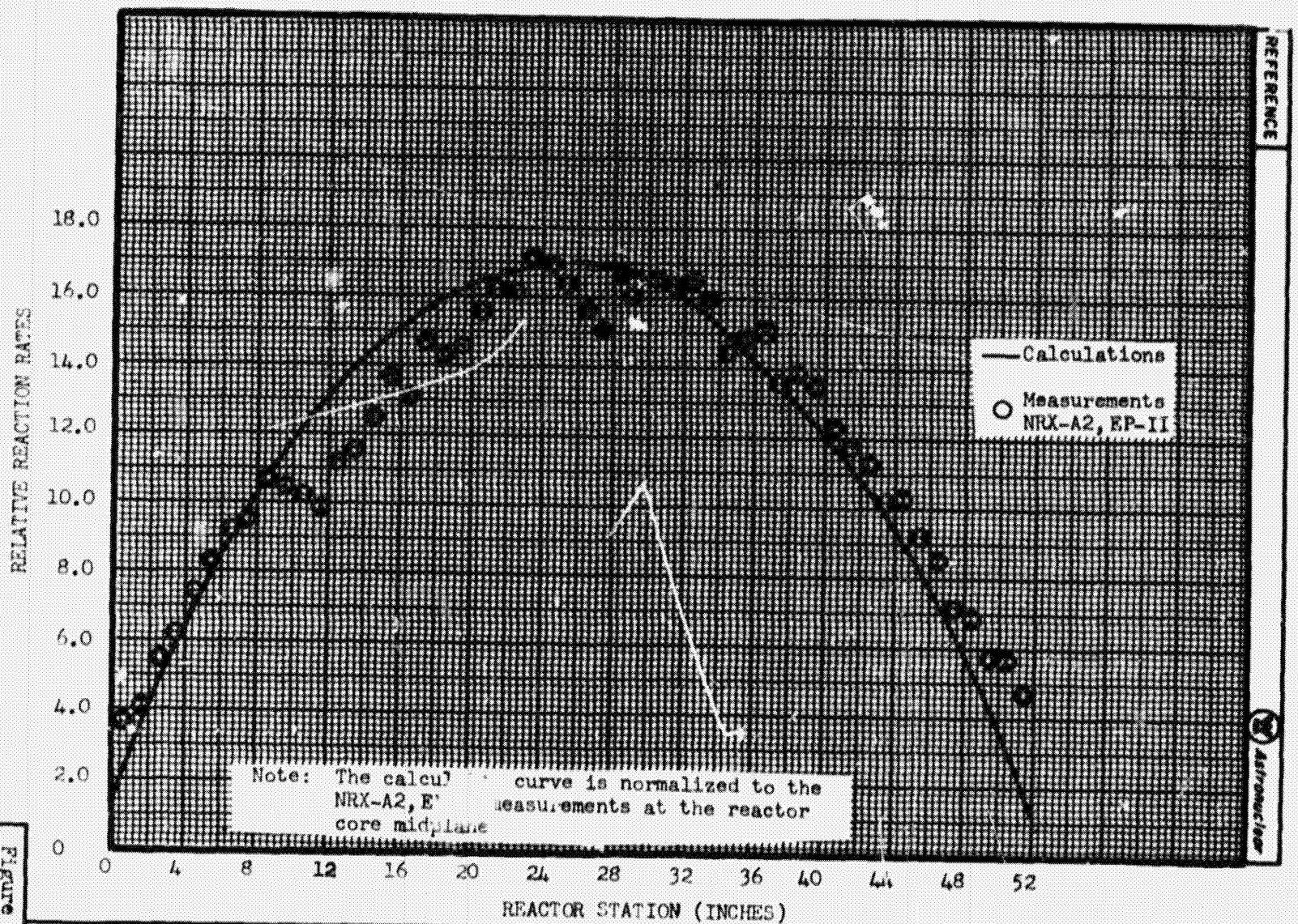

Figure No.	COMPARISON OF CALCULATED AND MEASURED REACTION RATES FOR COBALT AT THE SURFACE OF THE PRESSURE VESSEL (E < 0.4 EV)	PREPARED BY	APPROVED BY	CURVE NO.
8-29				

[redacted]

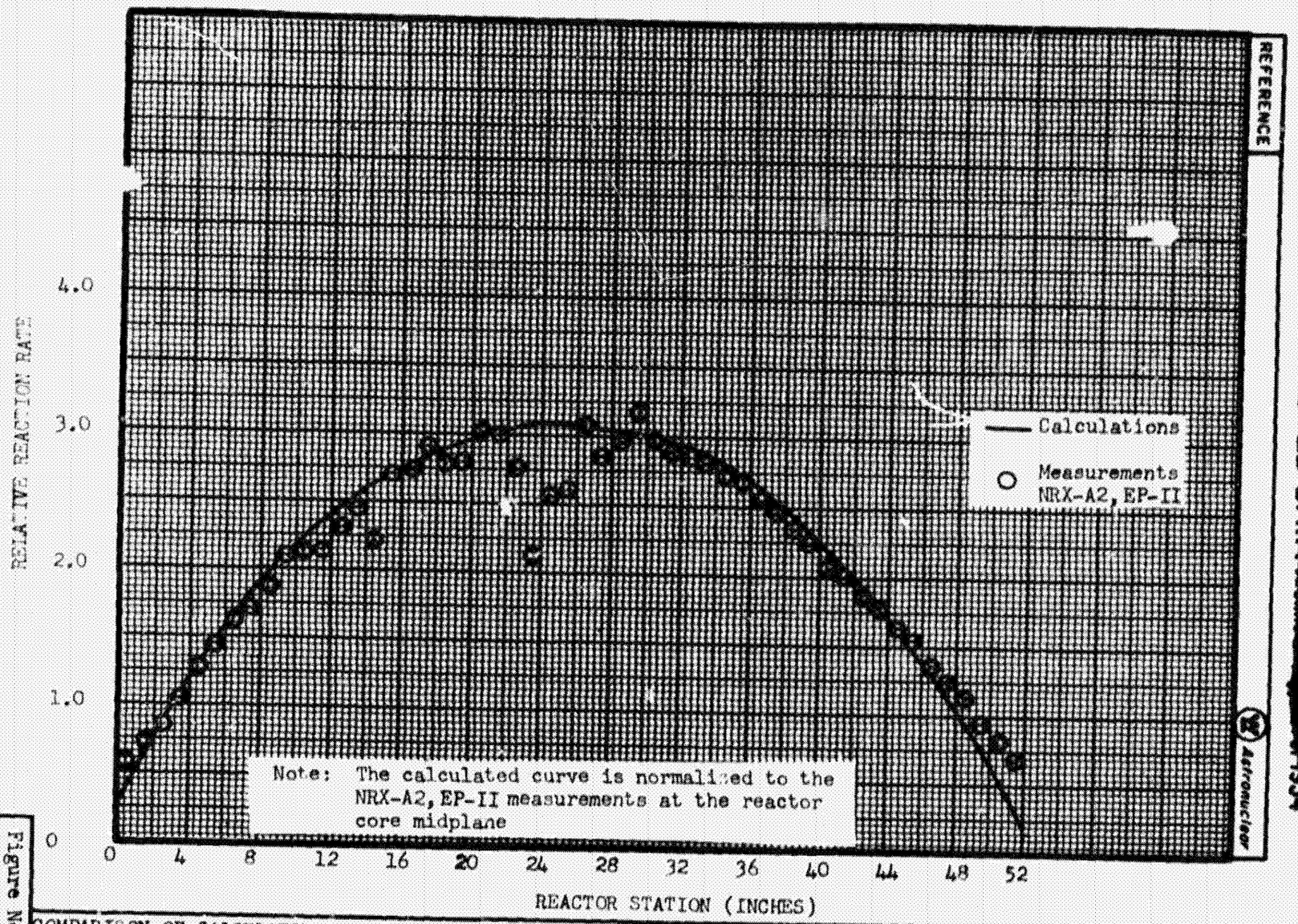

Figure No.	COMPARISON OF CALCULATED AND MEASURED REACTION RATES FOR COPPER AT THE SURFACE OF THE PRESSURE VESSEL (E < 0.4 EV)	PREPARED BY	APPROVED BY	CURVE NO.
8-30				

[redacted]

[redacted]

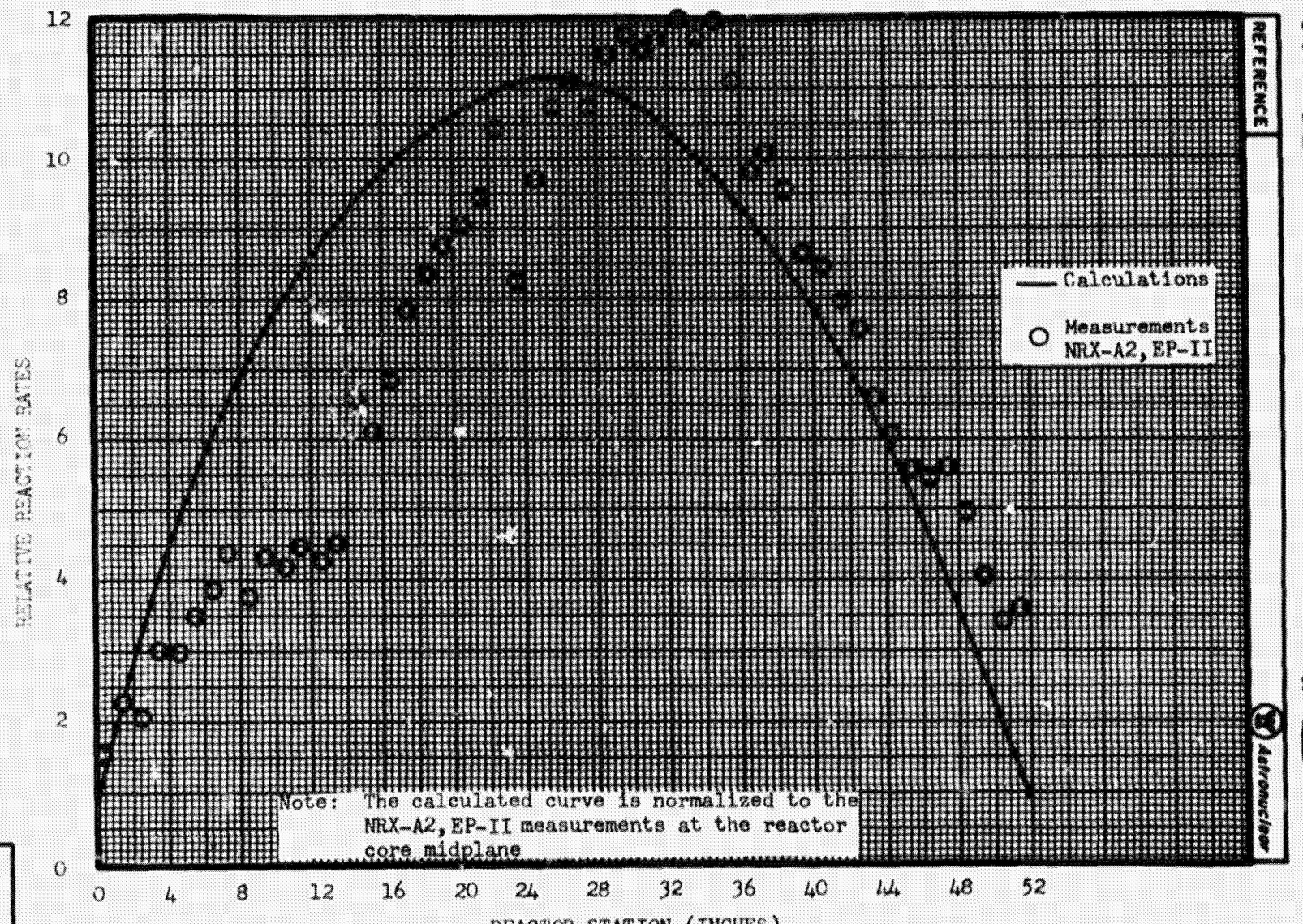

Figure No.	COMPARISON OF CALCULATED AND MEASURED REACTION RATES FOR GOLD AT THE SURFACE OF THE PRESSURE VESSEL (E < 0.4 EV)	PREPARED BY	APPROVED BY	CURVE NO.
8-31				

[redacted]

TABLE 8-4

CALCULATED AND MEASURED REACTION RATES ON THE LATERAL SURFACE OF THE PRESSURE VESSEL AT THE CORE MIDPLANE

	REACTIONS (CM^3-sec-watt		
	Gold	Copper	Cobalt
Measured	3.62×10^4	3.24×10^3	3.13×10^4
Calculated	7.24×10^4	4.84×10^3	4.3×10^4

• Measured during EP II

TABLE 8-5

CALCULATED AND MEASURED CADMIUM RATIOS ALONG LATERAL SURFACE OF THE PRESSURE VESSEL

Reactor Station (Inches)	Cobalt		Copper		Gold	
	Calculated	Measured*	Calculated	Measured*	Calculated	Measured*
49.46	5.33	4.51	6.26	6.03	1.45	4.38
39.27	5.46	5.91	6.45	7.09	1.47	4.74
26.75	5.43	5.65	6.38	7.09	1.64	4.53
15.02	5.44	5.29	6.41	6.69	1.46	2.54
3.87	5.21	4.99	5.10	5.13	1.44	2.69

* Measured during EP II

Measured in inches from the dome end of the core

the 4.9 ev absorption resonance indicating that self-shielding corrections should be applied. Inclusion of self-shielding correction factors for the 4.9 ev gold resonance would decrease the epithermal reaction rates, thereby raising the cadmium ratio.

It is interesting to note that the calculated epithermal and thermal reaction rates for cobalt, copper, and gold exhibit greater fall-off near the dome end and nozzle end of the core than is measured. It is likely that this effect comes from neglecting the test stand roof and nozzle in the TDC analysis. The amount of reflection these components cause at the core ends has not yet been investigated.

The bands used to support the various detectors during exposure contained a significant mass of material and these, together with the various wires and cadmium tubes used to cover some of the wires, produced some serious perturbations. As a result, much of the EP II data exhibits spurious scatter -- more than can be accounted for by counting statistics alone. The cadmium covered wire data exhibits considerable spread due to counting statistics resulting from the lower activation rates.

The circumferential wire data have not been analyzed at present as no satisfactory R-θ multi-group transport problem is available for the comparison.

CONCLUSIONS AND RECOMMENDATIONS

Gamma Ray Environment

It is evident from the preceding comparisons that no severe disagreement was noted between calculated and measured gamma ray dose rates. The poorest agreement was noted in three areas: 1) at locations on the meridian ring toward the nozzle end of the core, 2) at locations on the radial traverse greater than 200 feet from the reactor and, 3) at locations under the privy roof and on the test car.

To improve the agreement between calculated and measured data in these three areas, it is suggested that: 1) the attenuation due to the nozzle be included in the analysis of calculations on the meridian ring at the nozzle end of the core; 2) the gamma ray air scattering, and/or ground scattering contributions be reevaluated analytically at locations greater than 200 feet on the radial traverse; and, 3) the capture gamma ray contribution be reevaluated at locations under the roof and on the test car. In regard to the wall capture

gamma rays, it is believed that application of recent measurements of thermal and fast fluxes (both at the surface and as a function of distance in the wall) made at the PAX reactor at WANEF in calculating the gamma ray source terms in the wall will improve this part of the analysis.

In general it was noted that the techniques employed in the Standard Design Methods have predicted the gamma ray environment to within about 30 percent accuracy. Of special interest is the improvement in the calculated data at the vessel surface effected by using the ETA code to reduce the Monte Carlo data. It is suggested that this code be used in future NRX analysis to replace the point kernel calculations on the vessel surface.

On the basis of the experimental data, little or no gamma ray scalloping effect was observed. This observation is quite important since, if a source scalloping effect did exist, it could drastically effect a change in calculational techniques which quite possibly could result in an increase in cost for such an analysis.

In regard to measurements during future NRX reactor tests two suggestions are presented: 1) employ additional thermoluminescent dosimeters on all traverses such as meridian ring, trolley lines, etc. to obtain a better correlation between the response of the detectors and the glass detectors, and 2) employ dosimeters at many more locations under the privy roof and at test car locations to enable a better understanding of the environment in these locations.

Fast Neutron Environment

From comparisons of the measured and calculated fast neutron data previously presented, it is evident that the disagreement is more severe in some areas than was noted in the gamma ray comparisons. This phenomena was to be expected since analysis of KIWI[1] data indicated a similar trend.

The poorest agreement between measured and calculated fast neutron data occurs: 1) in comparisons of the fast neutron dose rate at all locations, and 2) in comparisons of fast neutron fluxes in the energy range $0.004 < E < 2.5$ Mev. The calculated fast neutron

[1]WANL-TME-767, Analysis of KIWI-B4A Radiation Measurements, Westinghouse Electric Corporation, Astronuclear Laboratory, L. D. Stephenson, May, 1964

dose rate is consistently low by a factor of about 2 due to the uncertainties associated with applying the Albert-Welton kernel and removal cross sections to the NRX-A2 system. In the NRX-A2 reactor system little or no hydrogeneous material is encountered. Neither the Albert-Welton theory nor removal cross section theory apply in such a system. It is recommended that, for calculation of fast neutron dose rates, the Albert-Welton kernel and removal cross sections should no longer be employed. Instead it is suggested that the dose rate be computed from the neutron spectra output data obtained from the point kernel program. This neutron spectra should be generated by employing either beryllium or carbon moments data. The use of water moments data should be abandoned in generating neutron spectra since comparisons in this report of measured and calculated spectra over the energy range, $0.004 < E < 2.5$ Mev, clearly showed that water data underpredicts the spectra for neutron energies less than 3 Mev.

It was generally noted that the predicted fast neutron flux data ($E > 2.9$ Mev) agreed to within a factor of 1.3 to 1.4 of the measurements on the vessel surface, equatorial ring, meridian ring, and radial traverse. In all fairness to the predicted fast neutron fluxes, it should be noted that much uncertainty appears to be associated with the measured data. Every effort should be made during the next NRX test series to eliminate as far as possible such uncertainties. For example, additional nickel detectors could be positioned on the radial traverse between 10 and 62.5 feet from the core. The three nickel points acquired during the A2 test on this traverse are not in good agreement with similar sulfur data.

From measurements of fast flux on the pressure vessel during the EP II run, and subsequent measurements made at PAX, a slight scalloping effect is observed. This effect must be studied more closely to determine its relationship to the internal and external neutron environment and/or heating rates.

The calculated environment under the privy roof and at test car locations must be reevaluated in the light of the NRX-A2 measurements. The discrepancy between the measurements in this area also requires further investigation

Thermal and Epithermal Neutron Data

In the previous comparison of calculated and measured reation rates in gold along the pressure vessel axial surface it was stated that the probable cause of the poor agreement is a source of 5 ev neutrons not accounted for in the analytical treatment. It is most likely that the source is in the pressure vessel flange and/or the test cell roof.

It is suggested that an effort be made during future NRX reactor tests to understand the nature of this problem. Specifically, this could be accomplished by the placement of gold foils on the test cell roof and flange shielded from the reactor with gold and cadmium.

It is also recommended that refinements be incorporated in future analytical calculations so that test conditions are better represented. The changes suggested are as follows:

1) Inclusion of the pressure vessel on TDC and r-θ DDK problems

2) Inclusion of the pressure vessel flange on TDC problems

3) Use of a fine mesh space next to the pressure vessel surface to effectively calculate the flux at the surface. Transport codes such as TDC and DDK inherently calculate the average flux in the mesh interval. The flux at the reactor surface must be obtained by extrapolating from the last mesh interval outwards.

4) The running of a multi-group r-θ DDK problem which gives reasonable neutron scalloping. No satisfactory problem exists at present.

5) Modification of DDK to give the directional neutron fluxes at the reactor surface. The equatorial ring data could then be analyzed using the angular leakage fluxes from an r-θ DDK problem.

6) Resonance self-shielding correction factors should be developed for gold and cobalt.

Correlation of High Power vs. Low Power Data

One of the objectives of the NRX-A2 dosimetry program was to provide data showing differences in the external radiation environment for the high power vs low power conditions. Unfortunately most of the overlap test data was lost due to the hydrogen fires which occurred around the pressure vessel periphery during EP IV, due to annealing out of the gamma dose response on the gamma dosimeters, melting of dosimeters, loss due to low exposure levels, and

loss due to decay of dosimeters while the reactor was sitting on the pad. Nevertheless some overlap points were obtained between EP II and EP IV and between EP V and EP IV.

The following observations of this data are made:

1) The gamma doses from EP IV glass data are lower than doses from EP II glass data. This may be due to annealing or fading effects on the EP IV glass. Correlation of gamma data at other locations shows no clear trend of difference between low and high power runs.

2) The sulfur data on the meridian ring from EP IV and V appears to be below similar data from EP II at most locations but there is too much scatter in the data to assign a quantitiative value.

3) However, the EP IV and V sulfur data on the radial traverse given in figure 8-20 appears to be above the similar EP II sulfur data.

4) EP IV data from fission foil measurements (Figures 8-21, 22, and 23) generally seem to be slightly above the EP V and EP II data for the radial traverses.

5) No clear trend is exhibited in the sulfur data on the test car, under the privy roof, or on the equatorial rings. In the former two locations, at least, there was insufficient exposure during EP-II to provide good counting statistics and hence the data show much scatter.

In conclusion, it can be said that it appears that there is a slight decrease in radial fast neutron leakage at high vs low power level but the magnitude of this effect does not appear to exceed 10 to 20 percent.

No difference in gamma leakage can be noted due to the scatter of the data.

CHAPTER 9

POST - OPERATIVE EXAMINATION

RADIOCHEMISTRY

Radial Power Distributions From Post-Run Calculations, Measurements and Radiochemistry

Following the NRX-A2 power test at NRDS the radial fission product distribution was established by gross ion measurements and radio-chemical analysis. An effective control drum angle was obtained for the entire test profile enabling a calculated power distribution to be compared directly with the observed power measurements. This was necessary since the control drum angle and power level both influence the rate of fission product deposition in a particular element. The effective control drum angle of 99.7 degrees was obtained by weighting the control drum angle during the test with the appropriate power levels. The calculated power distribution used in the comparison was derived from the pre-test predictions adjusted to the 99.7 degrees control drum angle. The pre-test power distribution used to orifice NRX-A2 was calculated for the 90 degree control drum angle. This was based on the test profile originally contemplated for NRX-A2 which indicated that the reactor would operate at the 90 degree drum position for the high power hold.

The NRX-A2 pre-test power predictions were obtained from hot calculations which were adjusted with corrections from an ambient experiment.[1] The ambient experimental power measurements were performed on the NRX-A2 PAX reactor at the WANL Waltz Mill Site Critical Facility. Ambient power calculations[2] were compared with these experimental results; the differences noted were assumed to be in error in the analytical model.

Using the same model, operating power distributions were calculated for different control drum angles. These power distributions were adjusted by means of the above experimental

1 WANL-TNR-158, Preassembly Experiment (PAX) in Support of NRX-A2.
2 WANL-TME-879, NRX-A2 Power Distribution Analysis

corrections. The power distribution corresponding to a 99.7 degree control drum angle was interpolated from the 90 and 105 degree pre-test power predictions. The power produced in an element was adjusted to account for the individual element loadings being different than nominal; the element loadings used in this comparison were obtained by averaging the actual loadings for a given element location from each core sector. This approach was taken in order that a comparison could be made with an observed power distribution constructed by averaging the individual element measurements from each core sector.

The measured hot radial power distribution was constructed from gross gamma radiation intensity measurements[1] made on all the core elements except eighteen which were either broken in disassembly or in the R-MAD hot test cell where the measurements were performed. The individual element gamma intensity readings are a measure of the power produced by an element relative to another during the entire hot test; this is based on the assumption of negligible fission product loss during the test. The gamma intensity readings of the individual fuel elements were divided by their respective uranium loading to obtain the relative fissions per gram distribution. Average values for the relative fissions per cc and fissions per gram were derived for each element location by averaging the gamma intensity readings from each core sector. These average element intensities were compared with the calculated power distribution corresponding to the 99.7 degree control drum angle.

Radiochemical fission product analysis was performed on thirteen fueled elements. These elements were ground to a powder and 50 gram samples of each were dissolved and analyzed for fission products. Using "K" factors previously determined on LASL calibration samples, fissions per gram values were obtained for each element. These individual fission per gram values were normalized to the radiochemistry value obtained for the element in the 000 position; this was done to make the calculated power distribution, gross ion measurements and radiochemistry all directly comparable.

---

1 NTO-62-006, Radiochemical Measurements on NRX-A2, 28 December 1964

Comparisons of the calculated and observed power distributions were made along four radial traverses. Figures 9-1 through 9-4 present a comparison of the measured and calculated fissions per gram flux shapes; the same comparison was made for the relative fissions per cc distributions, Figures 9-5 through 9-8. The radiochemistry values are shown on the fissions per gram traverse nearest their azimuthal position. Radio-chemical results were examined these elements to obtain corrections which could be applied to the gross ion measurements to account for any differences in the self-attenuation of the gamma rays in the different loaded elements. The random differences between the gross ion chamber measurements and radiochemistry made it impossible to obtain the correction for self-attenuation in the different loaded elements. This will be explored in more detail after the hot NRX-A3 test when about 50 elements will be analyzed by radiochemistry.

Agreement between the calculations and the gross ion measurements are within 1 to 2 percent in the central core region; a difference of 11 percent was observed in the peripheral region of the J4M radial traverse. To obtain an understanding of the larger differences in the peripheral elements a comparison was made of the calculated and measured power distribution is consistently low, the average difference was approximately 7.2 percent. This difference is explained later in this section.

Calculated and Measured Cold to Hot Power Change

Figure 9-10 shows a comparison between the calculated cold-to-hot power change and that derived from the cold PAX wire measurements and the hot NRX-A2 gross ion measurements. The PAX experimental power distribution was constructed by measurement of the fission product activity induced in uranium-aluminum detector wires irradiated in the core's coolant channels. These cold power measurements were made for a 90 degree control drum angle; adjustment to the 99.7 degree angle was necessary for comparison with the gross ion measurements. The importance of this adjustment is shown in figure 9-16 which shows the calculated power distribution at drum bank positions of 90 degree and 103.2 degrees (position in 4th hold of high power test). The percent power change in a given fuel element per degree of drum rotation used to adjust the PAX measurements has been confirmed experimentally for control drum bank rotations from 90 to 130 degrees.

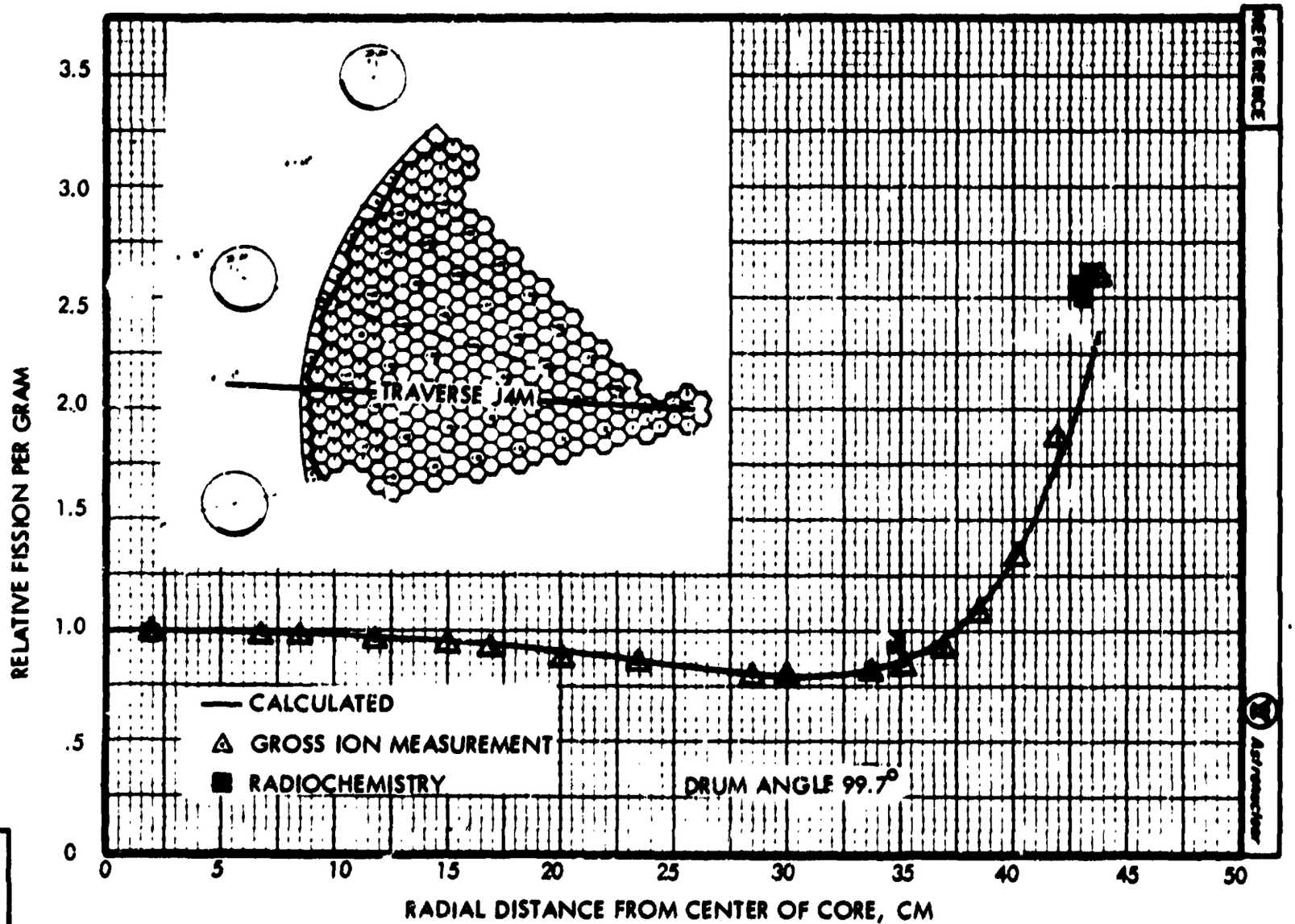

COMPARISON OF THE MEASURED AND PREDICTED POWER DISTRIBUTIONS THROUGH TRAVERSE 00B TO J4M, FISSIONS PER GRAM	PREPARED BY	APPROVED BY	CURVE NO.
	R.V.R.		

FIGURE NO. 9-1

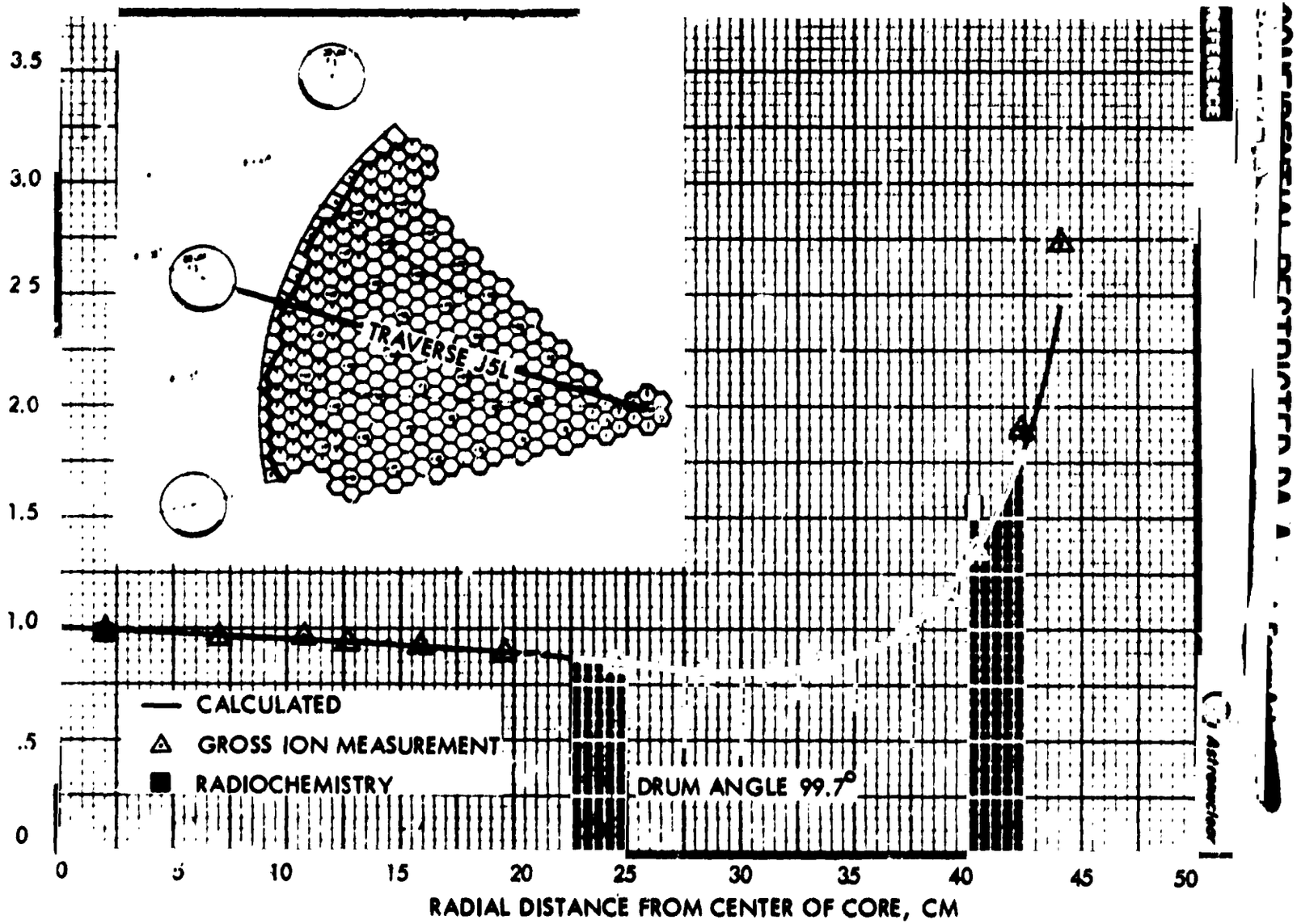

FIGURE NO.	COMPARISON OF THE MEASURED AND PREDICTED POWER DISTRIBUTIONS THROUGH TRAVERSE 00B TO J5L, FISSIONS PER GRAM	PREPARED BY	APPROVED BY	CURVE NO.
9-2		R. V. R.		

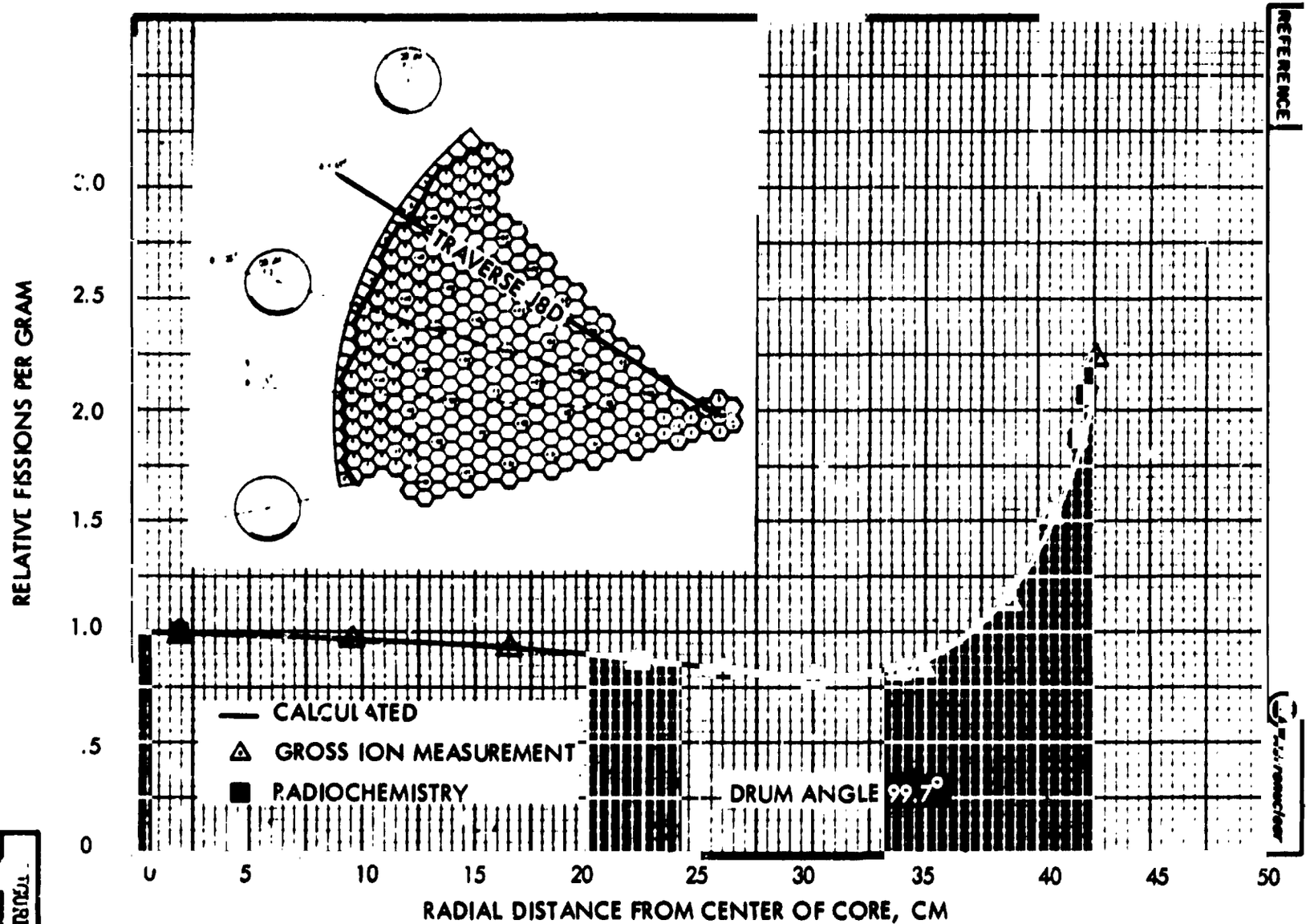

FIGURE NO.	COMPARISON OF THE MEASURED AND PREDICTED POWER DISTRIBUTIONS THROUGH TRAVERSE 00B TO J8D, FISSIONS PER GRAM	PREPARED BY	APPROVED BY	CURVE NO.
9-3		R.V.R.		

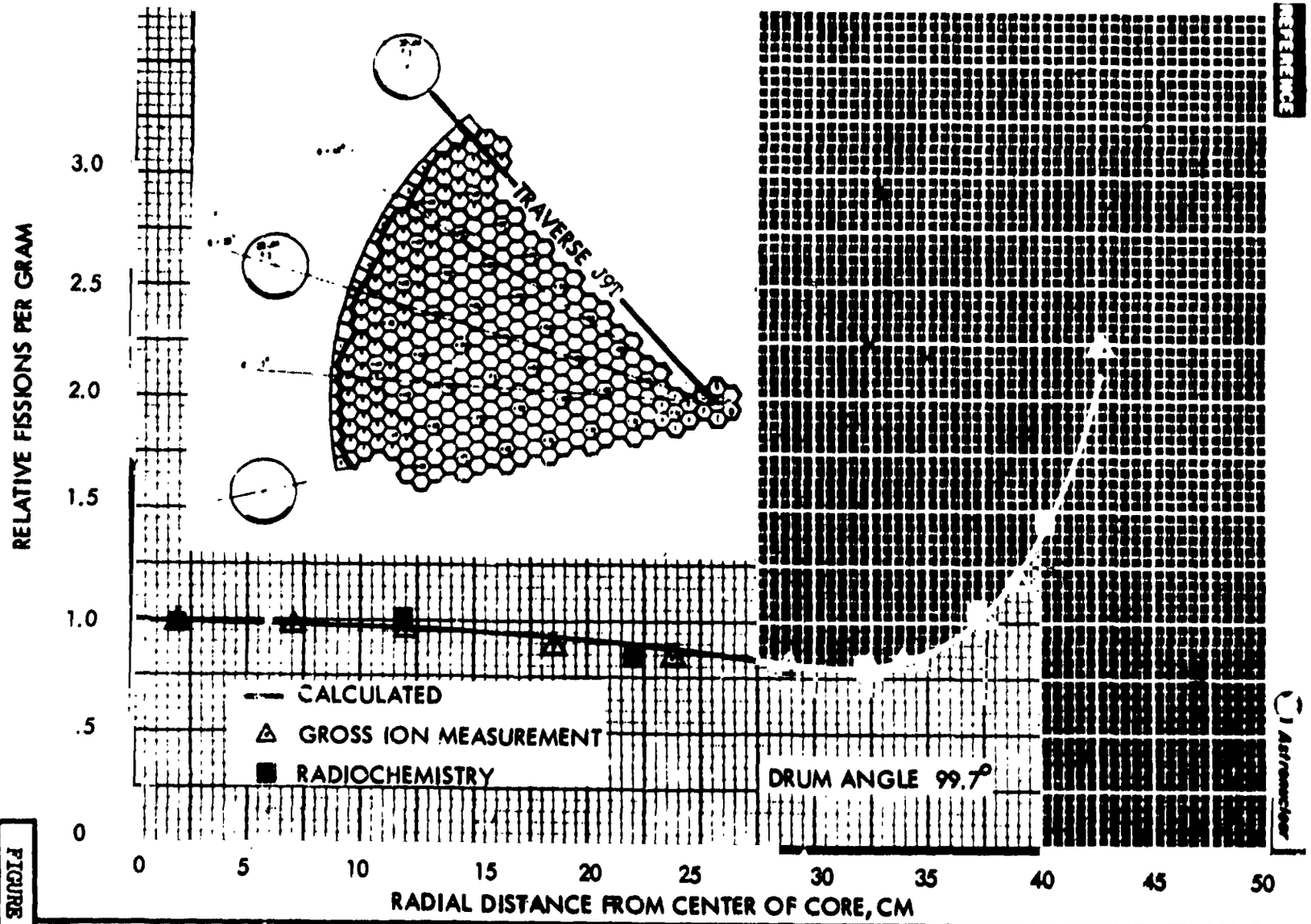

FIGURE NO.	COMPARISON OF THE MEASURED AND PREDICTED POWER DISTRIBUTIONS THROUGH TRAVERSE 00B to J9T, FISSIONS PER GRAM	PREPARED BY	APPROVED BY	CURVE NO.
9-4		R. V. R.		

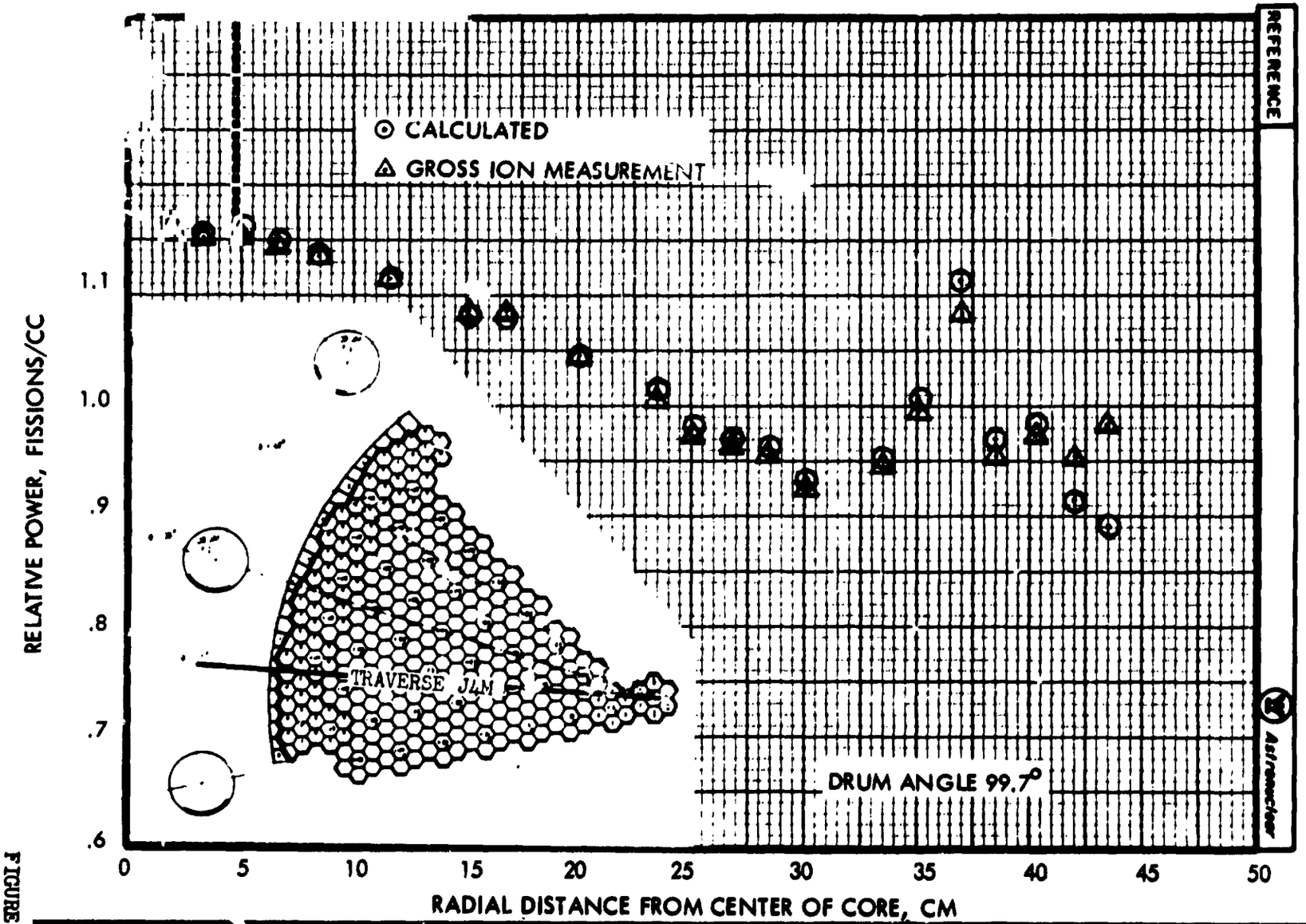

COMPARISON OF THE MEASURED AND PREDICTED POWER DISTRIBUTIONS THROUGH TRAVERSE 00B to J4M, FISSIONS PER CC	PREPARED BY	APPROVED BY	CURVE NO.
	R.V.R.		

REFERENCE

Astronuclear

FIGURE NO. 9-5

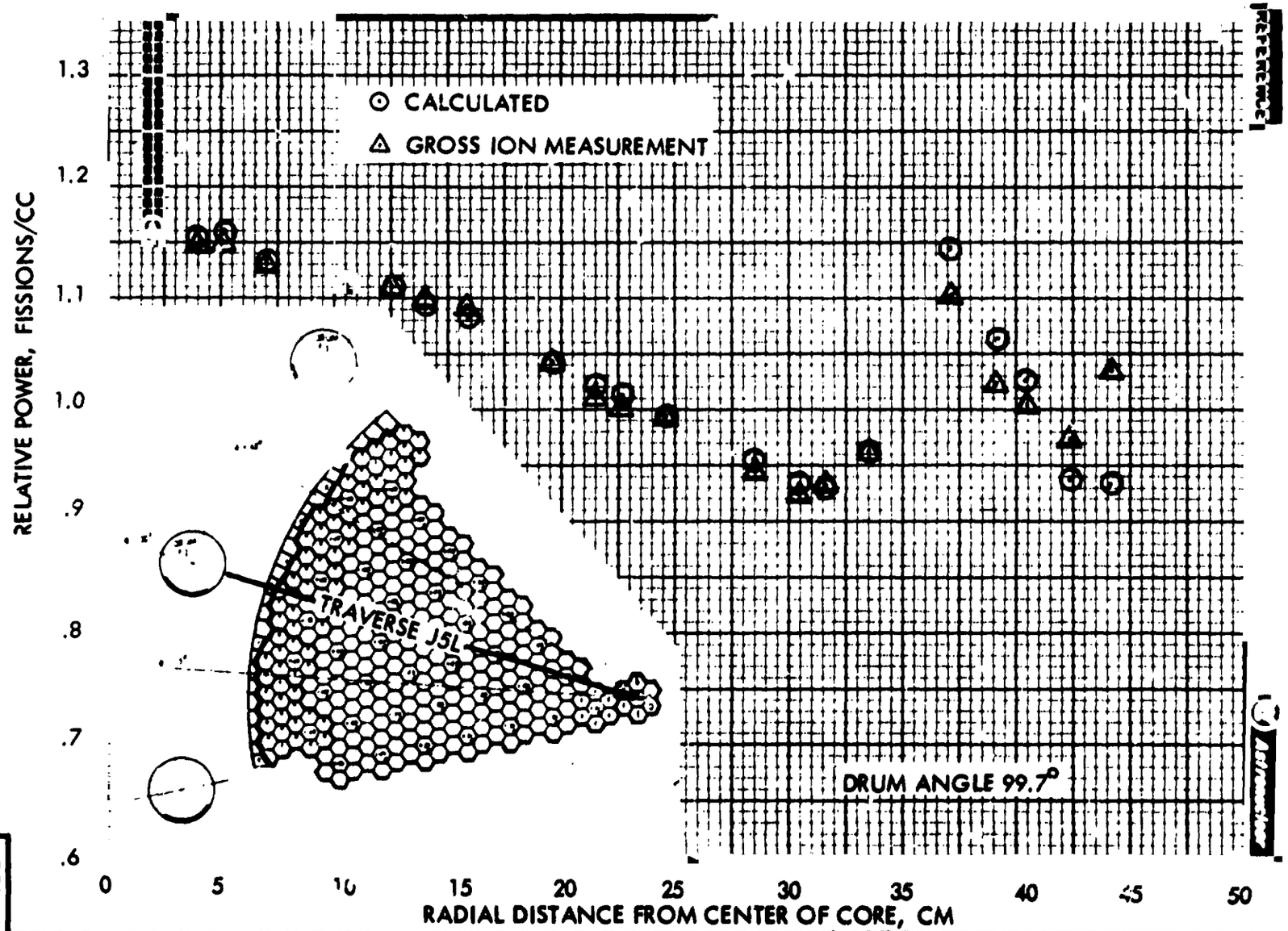

FIGURE NO.	COMPARISON OF THE MEASURED AND PREDICTED POWER DISTRIBUTIONS THROUGH TRAVERSE 008 to J5L, FISSIONS PER CC	PREPARED BY	APPROVED BY	CURVE NO.
9-9		R.V.R.		

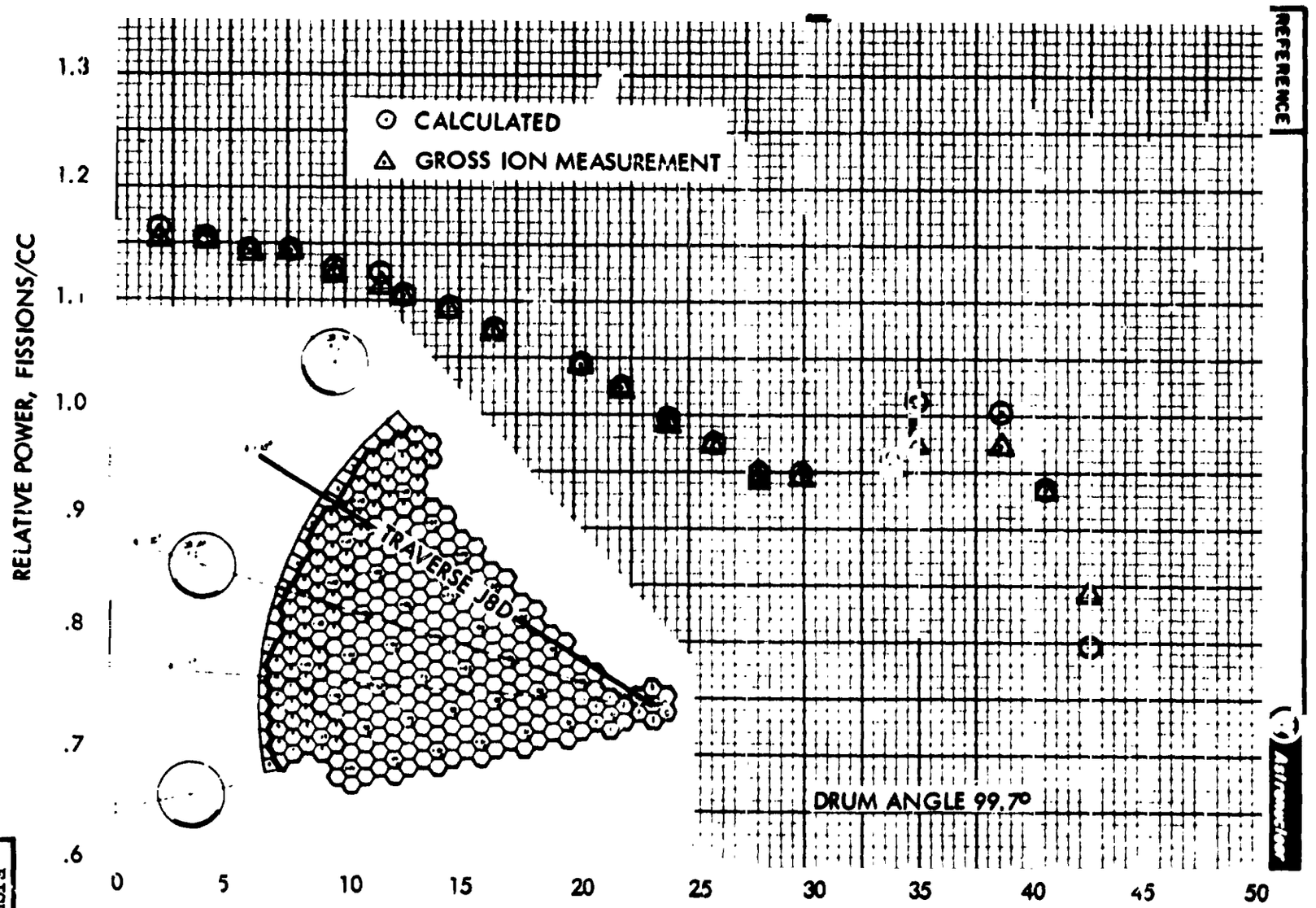

FIGURE NO.	COMPARISON OF THE MEASURED AND PREDICTED POWER DISTRIBUTIONS THROUGH TRAVERSE 00B TO J8D, FISSIONS PER CC	PREPARED BY	APPROVED BY	CURVE NO.
9-7		R.V.R.		

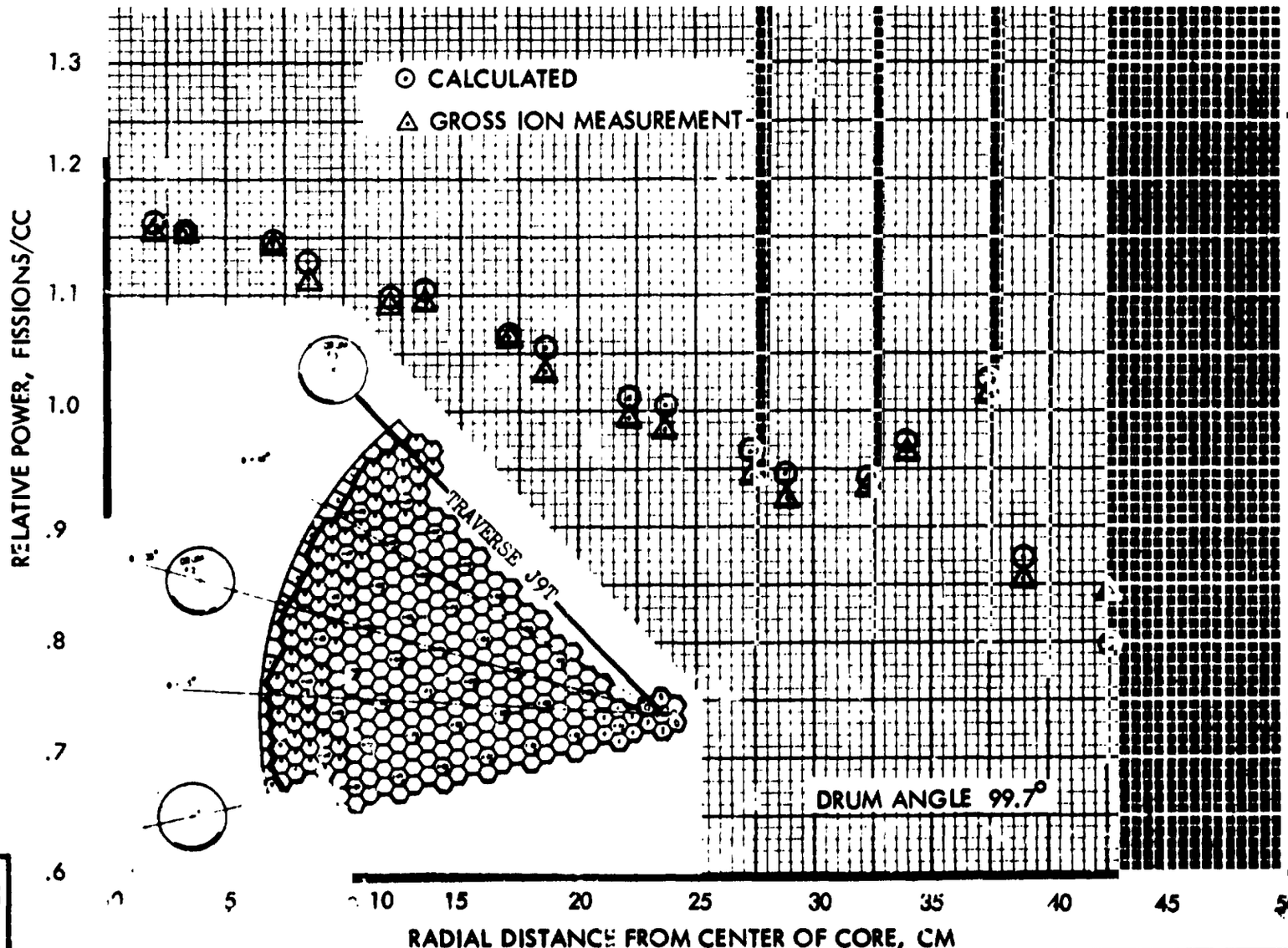

FIGURE NO.	COMPARISON OF THE MEASURED AND PREDICTED POWER DISTRIBUTIONS THROUGH TRAVERSE 00B to J9T, FISSIONS PER CC	PREPARED BY	APPROVED BY	CURVE NO.
9-8		R.V.R.		

REFERENCE

Astronuclear

CONFIDENTIAL RESTRICTED DATA

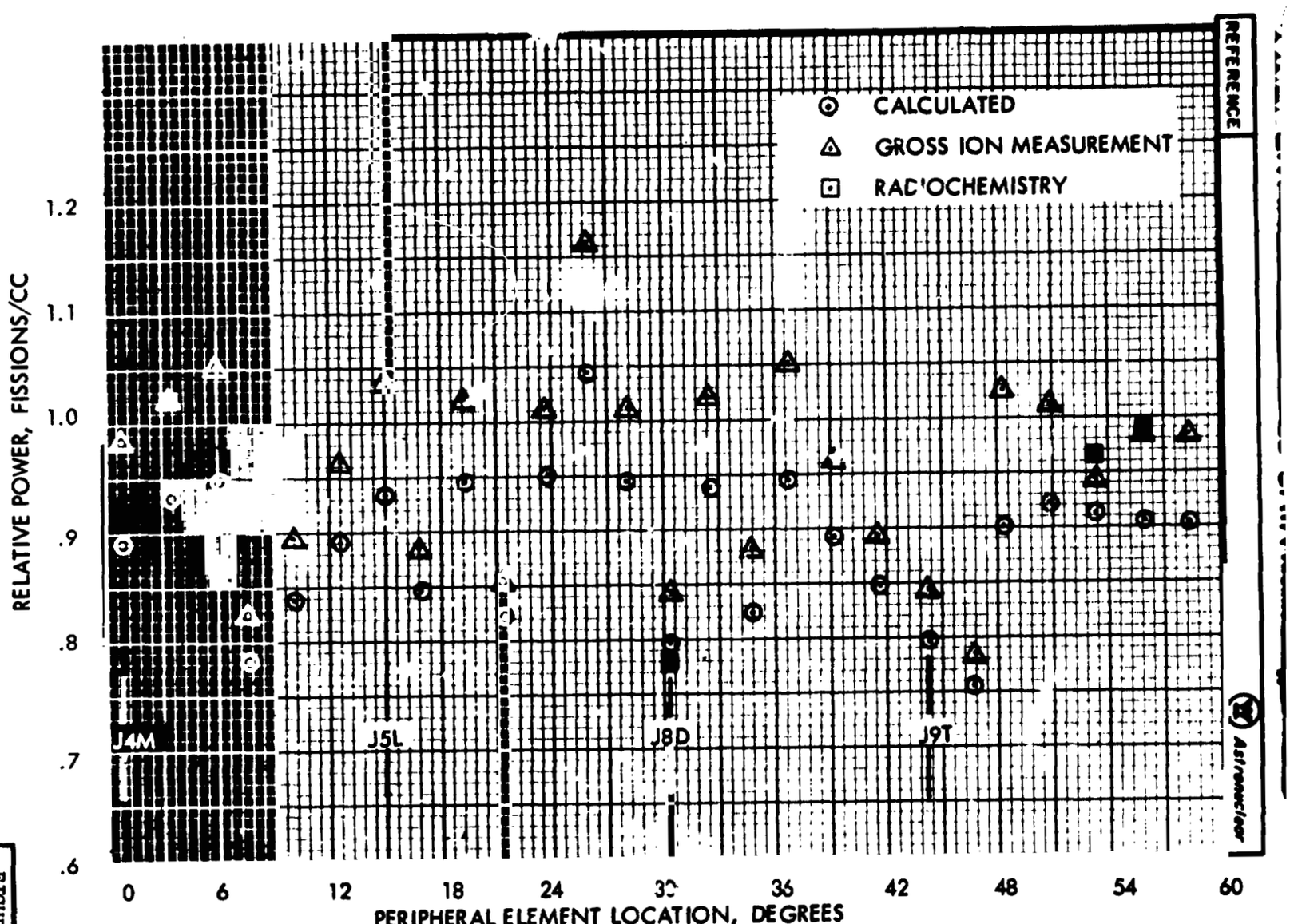

REFERENCE

Astronuclear

FIGURE NO.	AZIMUTHA POWER VARIATIONS IN THE PERIPHERAL FUEL ELEMENTS, MEASUREMENTS AND PREDICTIONS	PREPARED BY	APPROVED BY	CURVE NO.
9-9		R.V.R.		

CONFIDENTIAL DESTRICTED DATA

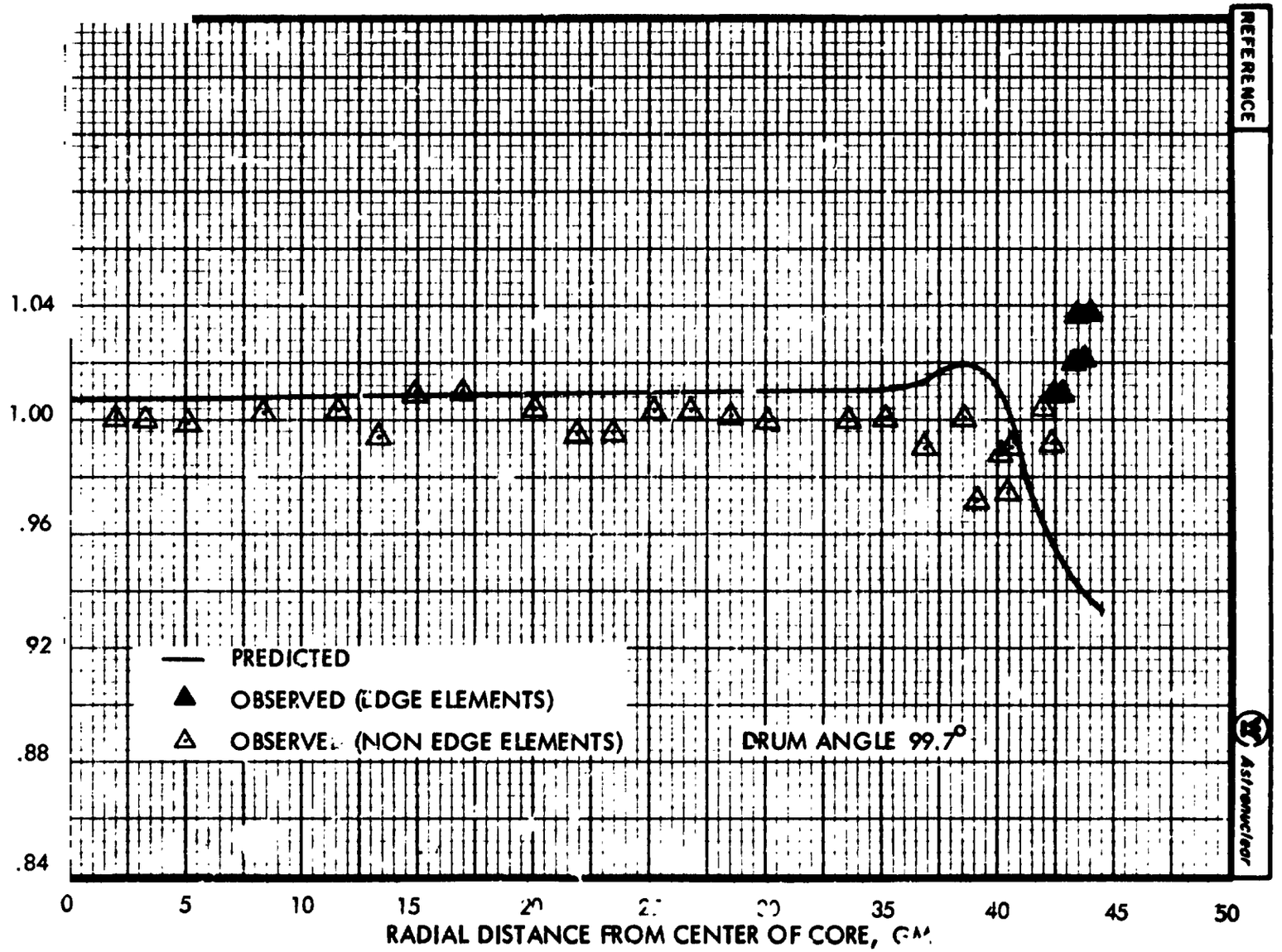

FIGURE NO.	COMPARISON OF THE PREDICTED AND OBSERVED (COLD PAX-HOT NRX-A2) RATIO OF THE COLD TO HOT POWER DISTRIBUTIONS	PREPARED BY	APPROVED BY	CURVE NO.
6-10		R. V. R.		

The calculations indicated less than a 1 percent increase in power in the central core region, and a sharp reduction of 7 percent at the periphery (from 39 cm to the core edge) in going to the operating conditions. The comparison of the adjusted cold PAX power distribution and the hot NRX-A2 gross ion measurements indicates little or no difference in the cold and hot power distribution except in the edge fuel elements where the observed cold to hot power change shows an increase of 2 to 4 percent. The differences in the calculated and gross ion measurements noted in the previous section of this chapter at the core periphery can be explained in terms of this complete reversal between the predicted and measured cold-to-hot power change. This conclusion is based on the assumption that the gross ion measurements need no correction for self-attenuation in the different loaded elements. This is somewhat substantiated by the results shown in figure 9-9 which shows agreement between three radiochemistry and gross ion measurements while one radiochemistry sample differs by 7.7 percent.

Power Gradients Across Peripheral Fuel Elements Derived from Predictions, Radiochemistry and NRX-A2 PAX Measurements

The power distributions across the flats of four peripheral fuel elements were determined by radiochemistry. One inch longitudinal sections were cut from each fuel element at the core midplane. These individual sections were in turn sliced axially into six wafers by making cuts through the coolant channels parallel to the "a" and "d" faces of the element. Radiochemical analysis was performed on these individual wafers. The fissions per gram values derived from these radiochemistry samples represent an average for the entire wafer. A distribution corresponding to an average power of unity in the element was derived by weighting the radiochemistry results with their respective volumes in the one inch longitudinal sections.

The power distributions in the same four fuel elements were derived from the NRX-A2 PAX wire measurements and the pre-test predictions. Both the PAX measurements and the predicted fissions per gram values in the 19 coolant channels were normalized to an average of unity in the individual fuel elements. These normalized values were in turn averaged for each row of coolant channels parallel to the radiochemistry wafers. This normalization scheme was necessary to make the radiochemistry results comparable to the predictions and PAX

measurements.

Figures 9-11 through 9-14 show a comparison of the power gradients across the four fuel elements as derived from these radiochemical wafers, NRX-A2 PAX measurements, and predictions. The comparisons are made on the basis of an average power of unity in the individual fuel elements. Although the absolute level of power in the peripheral elements was underestimated, the calculated gradients are in agreement with radiochemistry and the cold PAX results. The gradients across the four fuel elements differ slightly due to their particular orientation and location in the core.

MEASURED AND PREDICTED AXIAL POWER DISTRIBUTIONS

Axial gamma scan measurements were made on selected fuel elements. Figure 9-15 shows a comparison of the power distributions derived from these gamma scans for elements 1J3U and 1B1E and the corresponding analytical predictions. These two elements were chosen for the comparison since detailed measurements had been taken at the core inlet end. The comparisons of the different power shapes were made by normalizing the axial peak value to unity for each distribution.

The analytical predictions were calculated by means of the two dimensional transport Code TDC. The entire reactor was represented in R, Z geometry and the control vanes by an annular ring. The TDC axial power distributions corresponding to the approximate radial positions of elements 1J3U and 1B1E were used in the comparison.

Figure 9-15 shows good overall agreement between the gamma scan measurements and the analytical predictions. It is of particular interest to note the excellent agreement between the gamma scan measurements and the analytical prediction at the inlet end of the reactor.

RADIATION EXPOSURE FOR MAJOR REACTOR COMPONENTS

As reported in table 3-7 the total fissions experienced by the NRX-A2 reactor during the test series was 1.3×10^{22}. Based on this value and the radiation levels on a per fission

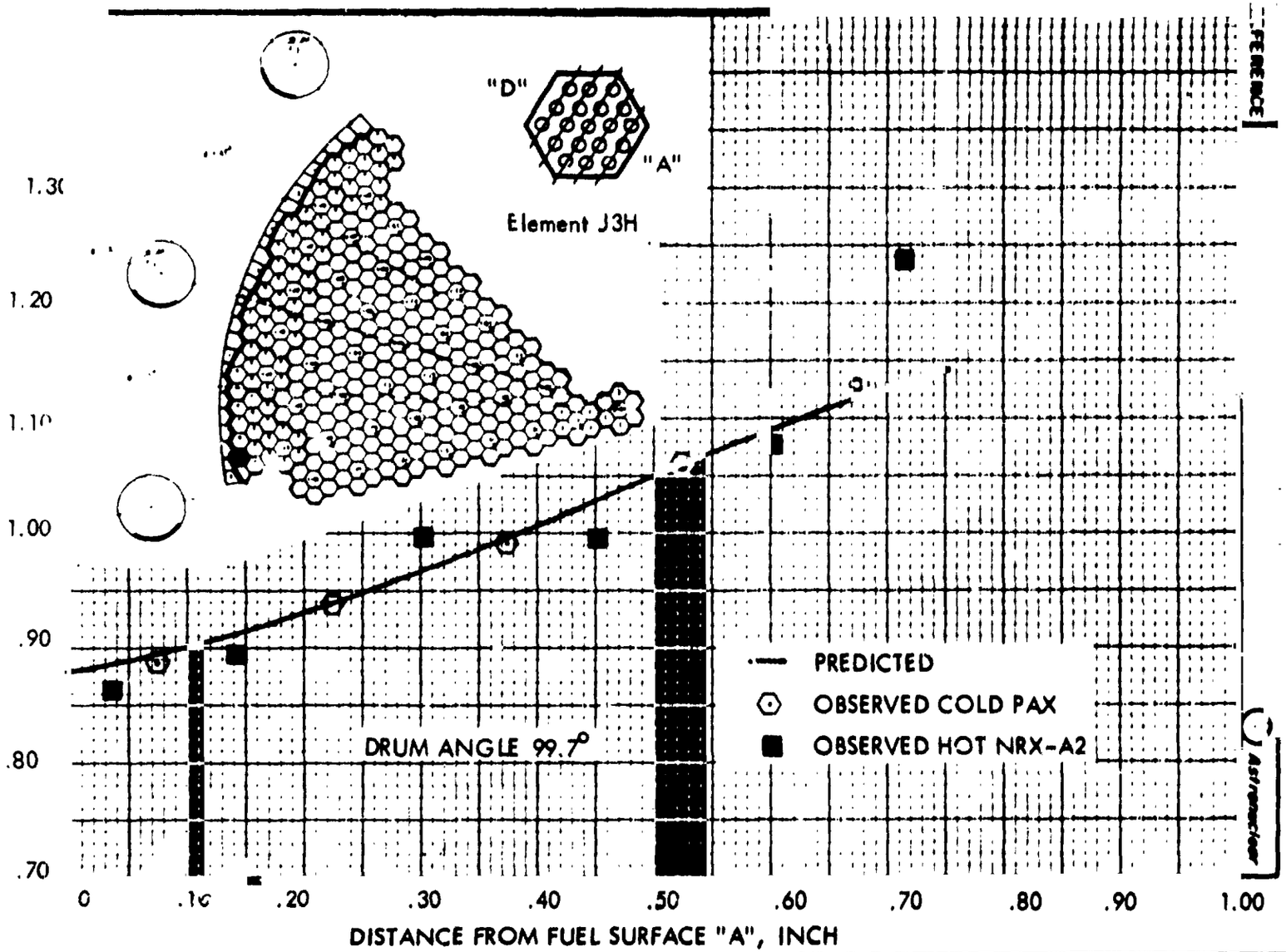

FIGURE NO.	PERIPHERAL ELEMENT POWER GRADIENT, ELEMENT J3H	PREPARED BY	APPROVED BY	CURVE NO.
11-6		R.V.R.		

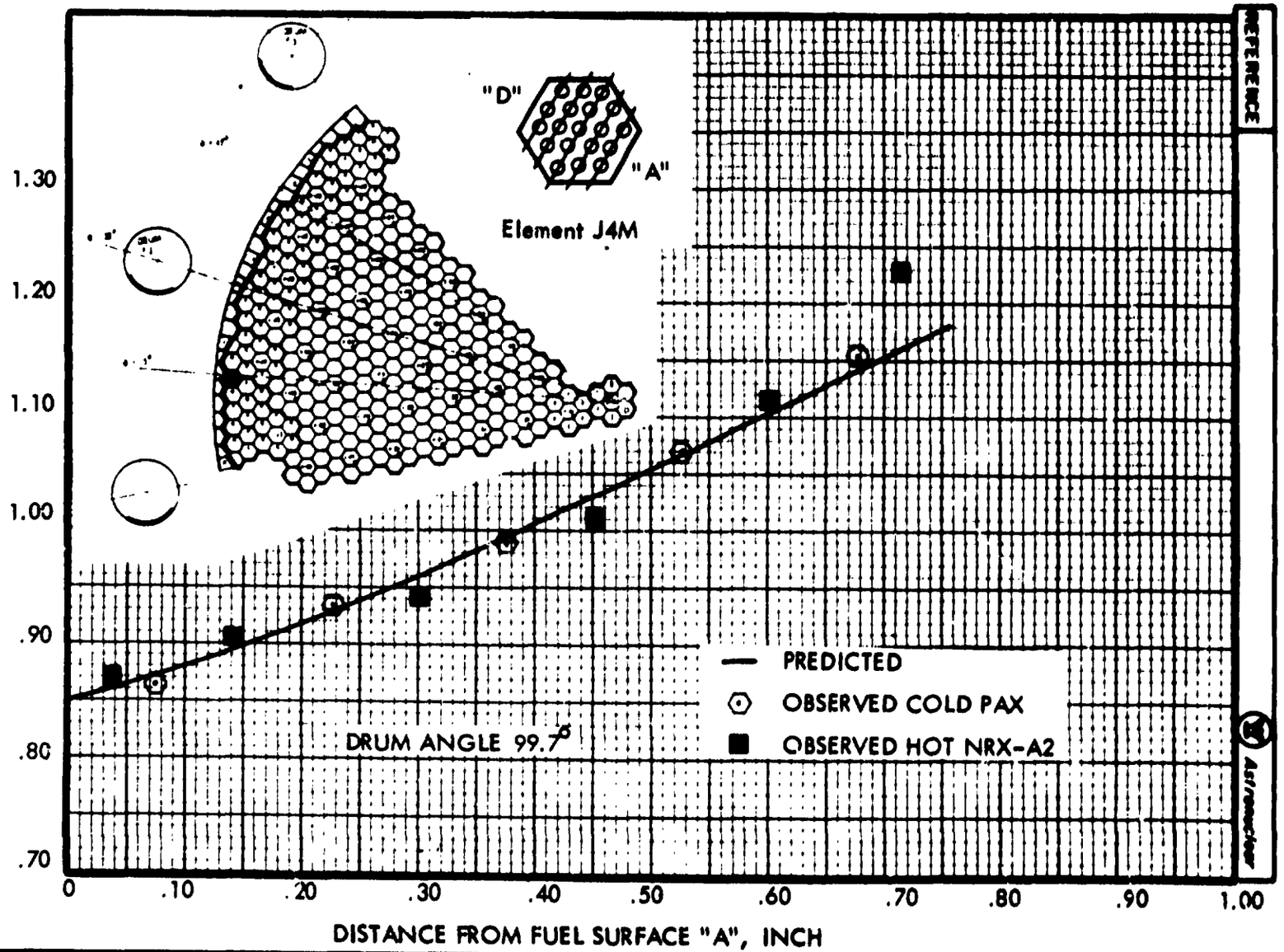

FIGURE NO.	PERIPHERAL ELEMENT POWER GRADIENT, ELEMENT J4M	PREPARED BY	APPROVED BY	CURVE NO.
9-12		R.V.R.		

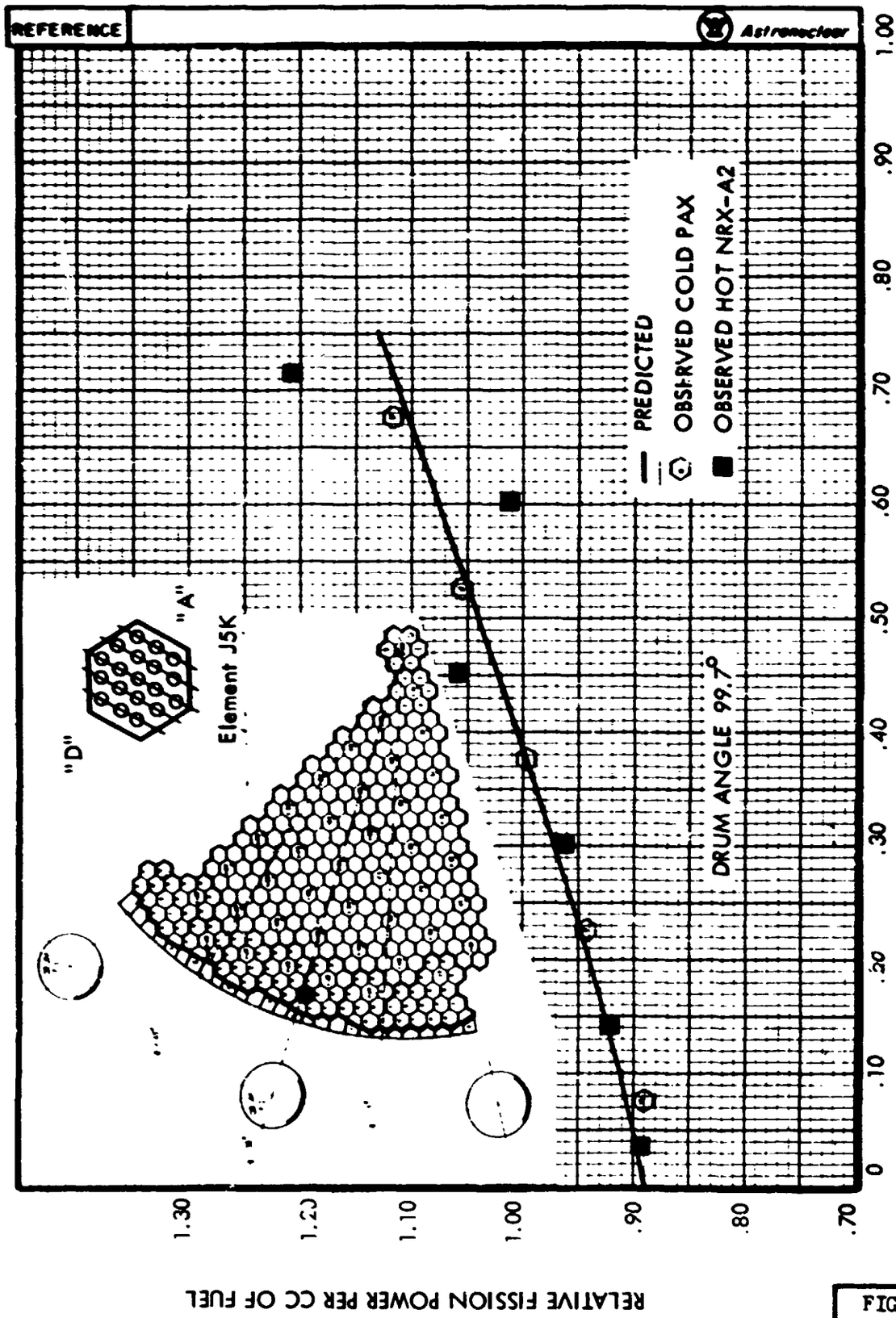

PERIPHERAL ELEMENT POWER GRADIENT, ELEMENT J5K

PREPARED BY	APPROVED BY	CURVE NO.
R.V.R.		

FIGURE NO. 9-13

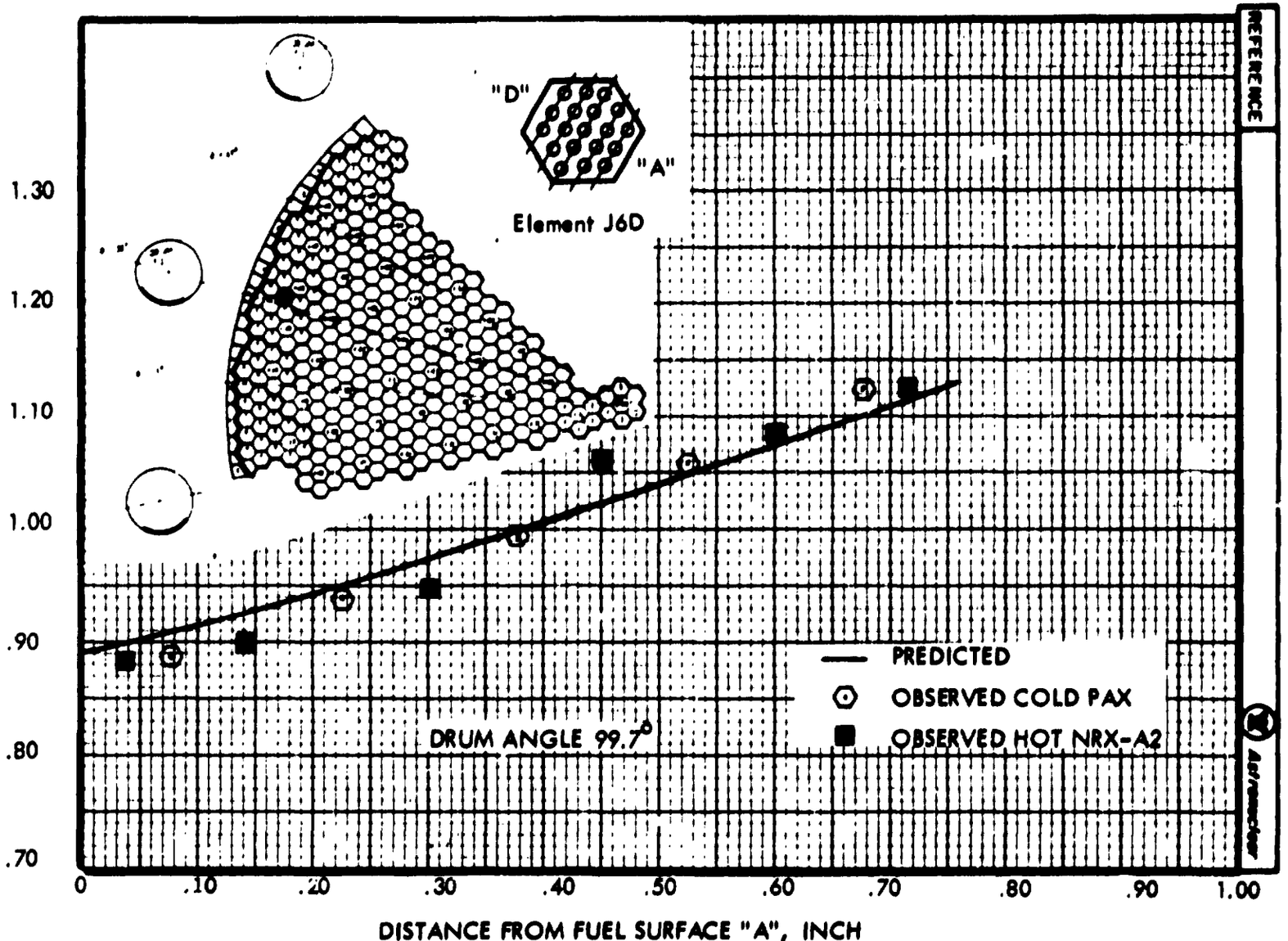

FIGURE NO.	PERIPHERAL ELEMENT POWER GRADIENT, ELEMENT J6D	PREPARED BY	APPROVED BY	CURVE NO.
9-14		R.V.B.		

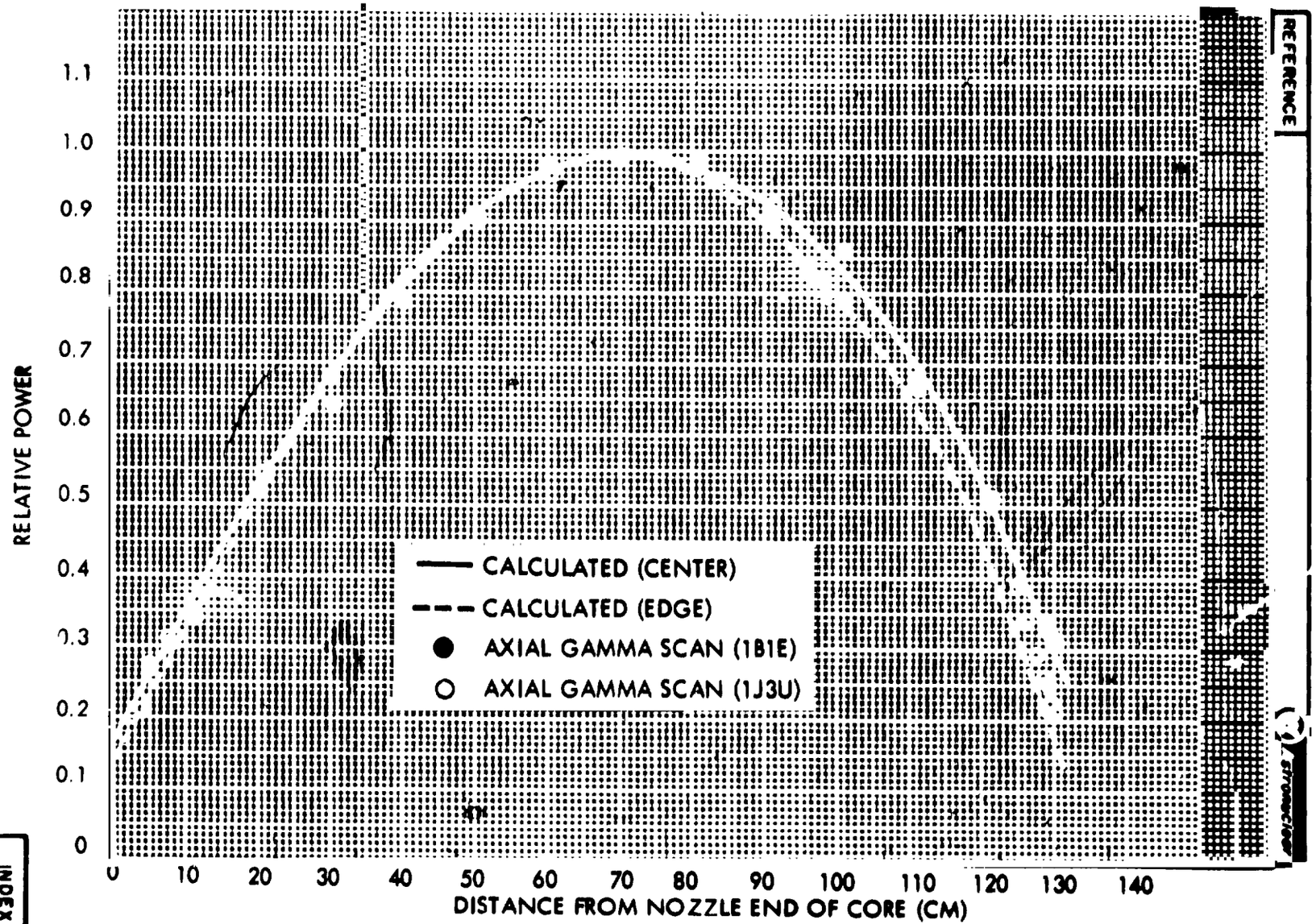

INDEX NO.	COMPARISON OF THE MEASURED AND PREDICTED AXIAL POWER DISTRIBUTIONS	PREPARED BY	APPROVED BY	CURVE NO.
6-15		R.V.R.		

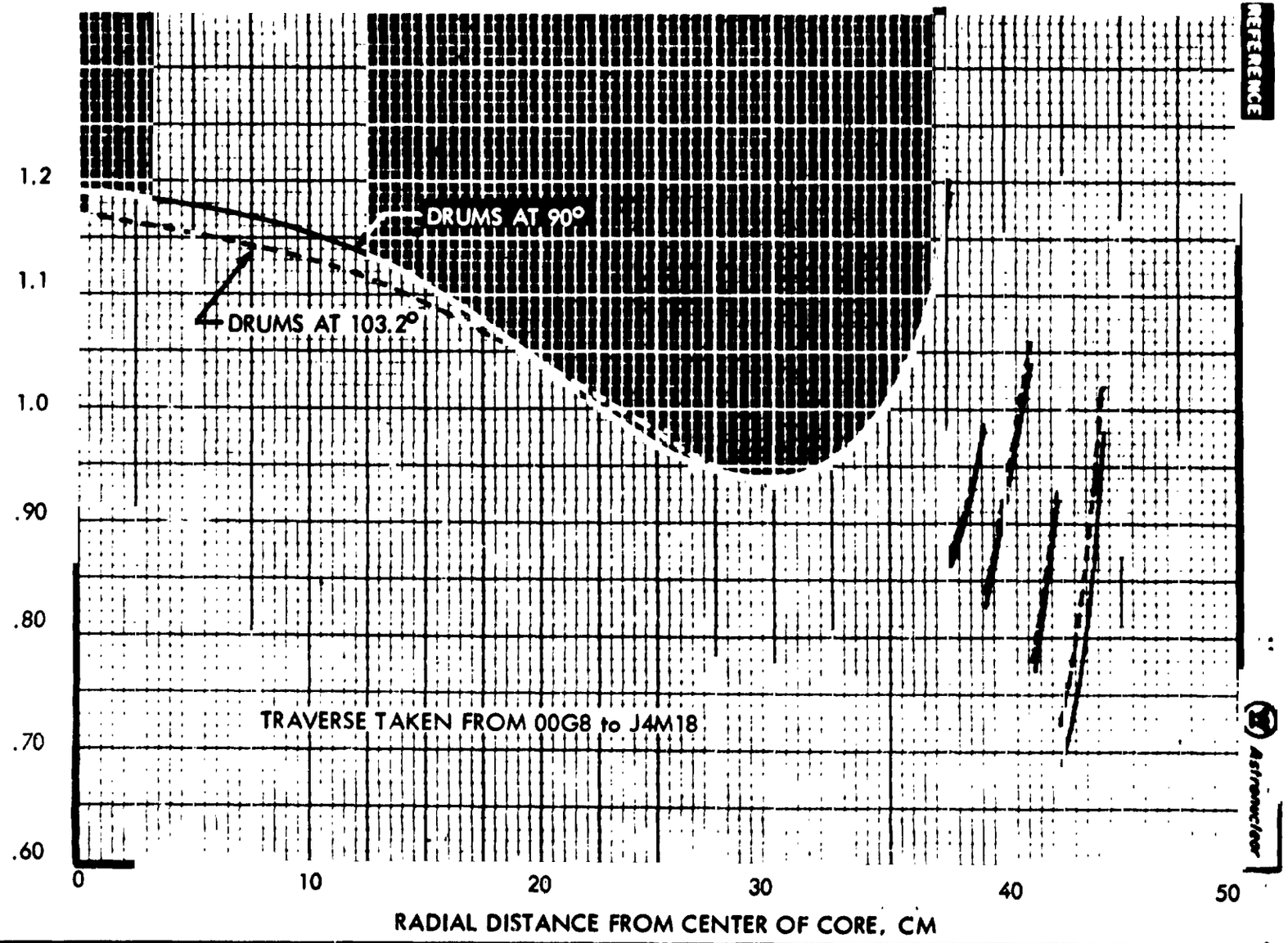

FIGURE NO.	PREDICTED RADIAL FISSION DISTRIBUTION AT 90° AND 103.2°	PREPARED BY	APPROVED BY	CURVE NO.
9-16		R.V.R.		

basis presented in WANL-TME-840[1], the maximum integrated radiation exposures for neutrons (E > 1.0 mev) and gamma rays were computed for the major reactor components. The data are presented in table 9-1. Figure 9-17 is a sketch showing where the major reactor components tabulated in table 9-1 are located in the reactor configuration. Since no experimental radiation levels on major components were obtained during the tests, the data in table 9-1 still contains uncertainties of the type associated with radiation analysis. For this reason the data in table 9-1 is probably accurate to within ± 50 percent.

CORE ELEMENT EXAMINATION

Summary of Core Element Corrosion

Detailed examination and analysis of the corrosion found on the fuel elements continues. These results will be incorporated into a supplement to this report. At this time only a general picture of the fuel element corrosion will be presented.

INTERNAL FUEL ELEMENTS

The corrosion on the outside surfaces of the fuel elements. removed from the vicinity of the core instrumentation and the element with the uncoated coolant channel, was found to be very mild upstream of core station 51 inches. The evident corrosion generally occurred in axial streaks extending between core station 26 and 30 inches, approximately. Although no depth measurements have been obtained on the element faces, visual observation indicated that these depths are of the order of 1 mil or less. Accurate measurements, therefore, would be extremely difficult to perform.

Heavy corrosion curred on element faces in vicinity of the station 32 inch thermocouples. Corrosion also occurred near the station 20 inch and station 45 inch thermocouples, but to a much lesser extent. One element, 5F4F, was found to have corroded through to the outside surface from the No. 3 flow hole for a considerable length of the element. It has been definitely established that this flow channel was uncoated prior to the test. As a

1 WANL-TME-840, Reactor Analysis Data Book, Reactor Analysis Staff, July 31. 1964

TABLE 9-1

MAXIMUM INTEGRATED RADIATION EXPOSURES FOR NEUTRONS (E > 1.0 mev) AND GAMMA RAYS FOR MAJOR REACTOR COMPONENTS

Region No.	Region Description	Neutron NVT E > 1.0 mev n/cm^2	Gamma Ergs/Gm-carbon
1	Core Support Blocks	2.3×10^{17}	5.1×10^{10}
2	Active Core Region	1.5×10^{18}	3.6×10^{11}
3	Filler Strips	6.0×10^{17}	1.9×10^{11}
4	Lateral Support (Inner Reflector)	5.1×10^{17}	1.6×10^{11}
5	Beryllium Reflector	2.1×10^{17}	5.7×10^{10}
6	Pressure Vessel Cylinder	1.6×10^{16}	1.6×10^{10}
7	Reflector-Nozzle Interface Region	4.1×10^{16}	2.5×10^{10}
8	Reflector Support Structure (Nozzle End)	2.2×10^{16}	1.3×10^{10}
9	Cluster Plate Region	3.3×10^{17}	8.3×10^{10}
10	Core Support Plate	2.7×10^{17}	7.2×10^{10}
11	Core Support Ring, Etc.	1.2×10^{17}	4.8×10^{10}
12	Dome End Support Ring	5.4×10^{16}	1.8×10^{10}
13	Drum Drive Shaft Region	4.9×10^{16}	1.7×10^{10}
14	Flow Screen and Support	4.0×10^{16}	1.3×10^{10}
15	Aluminum Mockup Shield	3.8×10^{16}	1.2×10^{10}
16	Pressure Vessel Dome	1.8×10^{15}	6.0×10^{8}

See figure 9-17 for region locations.

Exposures are based on the EP IVA and EP V reactor runs for NRX-A2. Gamma exposures include gamma rays liberated after shutdown due to fission fragment decay. Total fissions for EP IVA and EP V = 1.3×10^{22} fissions.

REFERENCE

Astronuclear

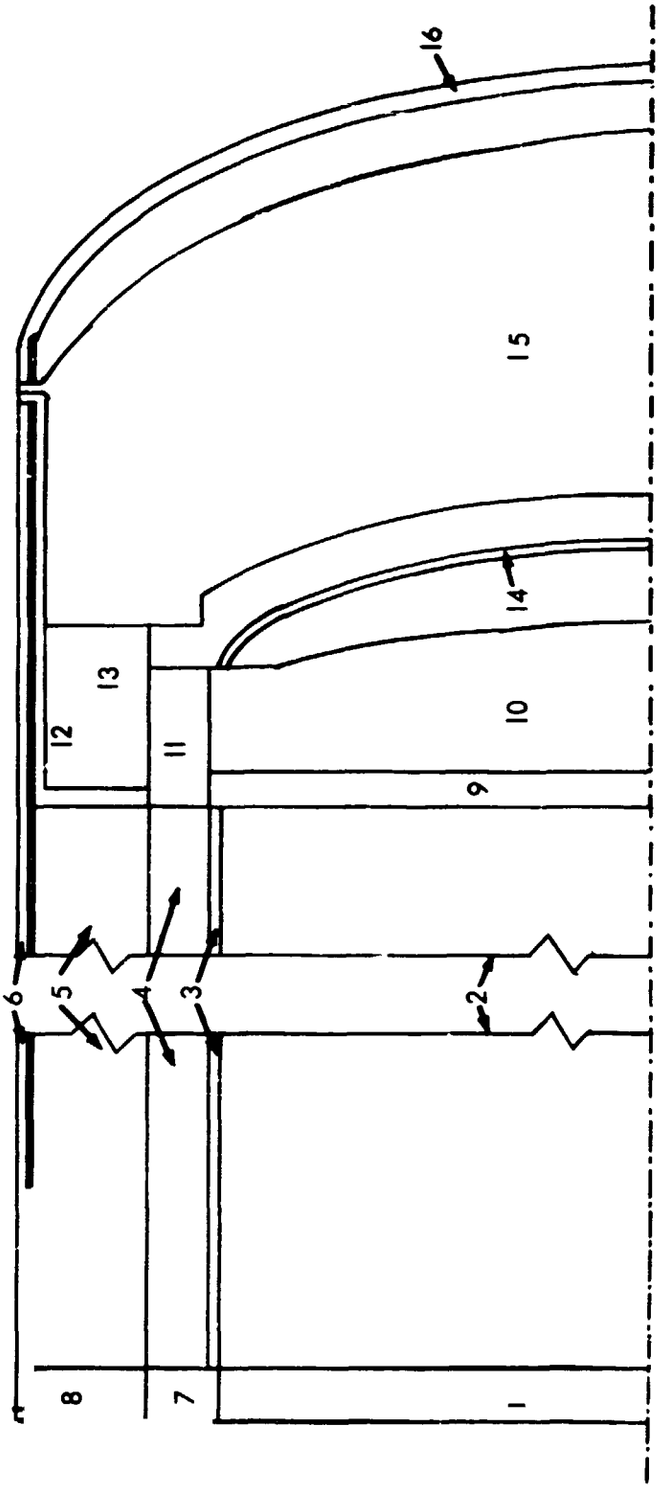

PREPARED BY	APPROVED BY	CURVE NO.

NRX-A2 REGION DESCRIPTION SHOWING MAJOR COMPONENTS

Figure No. 9-17

consequence of this, element faces in the vicinity showed heavy corrosion and some liner exposure.

A whitish deposit was found to exist in a band from about 23 inches to 26 inches from the core inlet. Chemical analyses of samples are being performed and will be reported in the supplemental report.

At the nozzle end of the fuel elements, in the undercut region, heavy corrosion occurred where the niobium carbide coating was absent. The corrosion was sufficient to expose the coolant channel liners in many cases. In addition, the end corners of the elements were generally rounded off due to corrosion in the absence of coating protection. Liners here were exposed in pencil fashion in the more severe instances.

PERIPHERAL FUEL ELEMENTS

The peripheral fuel elements exhibited mild to severe corrosion on the faces adjacent to the pyrographite insulating tiles. This corrosion occurred in discrete circumferential bands starting at approximately core station 23 inches. These bands correspond to the locations of the small plenums formed by the fuel elements, filler strip ledges, and insulating tiles. Although the peripheral faces were severely corroded in these bands, there was no unusual amount of corrosion found on the adjacent radial faces of the same elements. The corrosion bands, in many cases were sharply defined, and in others blurred by an edge feathering extending either upstream and/or downstream. One peripheral element had a flash coating of niobium carbide and this element did not have any appreciable corrosion. Detailed dimensional measurements have been performed on peripheral elements from each of two sectors (3 and 5, respectively). This data is being analyzed and will be incorporated into the supplemental report.

UNFUELED ELEMENTS

The central unfueled instrumented elements showed external surface corrosion in the vicinity of the thermocouples and thermal capsules. As in the rest of the core, the heaviest corrosion occurred at the station 32 inch thermocouples with milder corrosion at the station

20 inch and 45 inch thermocouples. The external surfaces of the uninstrumented central elements conformed, in general, to that of the rest of the core elements.

Corrosion on the ID of the central hole was found to exist in bands about 1/4 inch wide. These bands correspond to the junction of the pyrographite liner tubes and started about 24 inches from the core inlet. Depth measurements performed to date indicate a maximum depth of 14 mils.

Summary of Cluster and Seal System Component Examination

SUPPORT BLOCKS

The external surfaces of the support blocks were found to be in rather good condition. In several cases, chipped areas were found, but these areas were small and did not appear corroded. Many of the upstream faces of the support blocks showed evidence of coating transfer from the ends of the fuel elements. The uncoated central hole was found in several instances to be corroded at both ends with the area between unaffected. Dimensional measurements of this phenomenon are being analyzed and will be reported in the supplemental report.

PYROGRAPHITE INSULATING SLEEVES

The outside surface of the sleeves was found to have a dark deposit. This deposit could not be easily rubbed off the outside surface. The deposit was in the form of a swirl-shaped pattern coinciding with corrosion on the central bore of the unfueled element. In some cases, the pattern was continuous from one sleeve to the next and in others it was not.

PYRO CUPS, STAINLESS STEEL LINER TUBES, CLUSTER PLATES, TIE RODS, AND ORIFICES

Post-operative inspection revealed no significant damage or corrosion to either the insulating cups or washers although the former were found to have lost most of the niobium carbide coating on the outside surface, and in about a dozen instances, all of the coating

from the cup rim.

Cluster plates exhibited no damage. Some cluster plates appeared darker than others and the causes for this are being investigated.

Tie rods, except for those damaged during disassembly, were in good condition. The orifices were undamaged. However, inspection of plugged orifices and channels was hampered by the great quantity of debris resulting from the support plate cutting the inner reflector cylinder slitting operations. It did not appear that any of the orifices or channels were plugged or blocked during the power runs and any particles found have been attributed to the above causes.

APPENDIX A

REACTIVITY CALCULATIONS

A derivation of the methods used for reactivity calculations in this report appears in WANL-TME-936. A summary of the more significant effects and key nuclear parameters is shown in table A-1. Note that during steady state operation the terms R_D, R_C, R_H, and R_T must sum to zero. The last three terms are determined by the fluid flow and temperature characteristics of a particular reactor condition. The term R_D permits the calculation of the drum angle for equilibrium operation.

TABLE A-1
NRX-A2 REACTIVITY EQUATIONS

NRX-A2 Reactivity At Steady State $= R_D + R_C + R_H + R_T = 0$

Control Drum Position	$R_D = -4.5(1+\cos\theta) + 4.5$
Carbon Loss	$R_C = .055\ M_{CL}$
Hydrogen Reactivity Contribution	$R_H = (1+A)\ (W_C + W_{LS} + W_{Be}$
Core Worth	$W_C = 4.0\ \bar{\rho}_1 + 10.5\ \bar{\rho}_2 + 4.6\ \bar{\rho}_3$
Lateral Support Worth	$W_{LS} = (0.968 - 10^{-4}\ \bar{T}_C)\ \bar{\rho}_{LS}$
Be Reflector Worth	$W_{Be} = 0.040\ \bar{\rho}_{Be}$
Temperature Reactivity Contribution	$R_T = \left[-1.039(\bar{T}_C - 528)\ \ 0.943(\bar{T}_{Be} - 528)\right] \times 10^{-3}$

Where

R_i	=	Reactivity, dollars (i is D, C, H or T)
θ	=	Control drum bank position, degrees
M_{CL}	=	Mass of carbon lost, kilograms
A	=	Fraction of diffused hydrogen (0.12 used)
ρ_1, ρ_2, ρ_3	=	Average hydrogen densities in the upper, middle, and lower thirds of the core, lb/ft^3
ρ_{LS}	=	Average hydrogen density in the lateral support, lb/ft^3
ρ_{Be}	=	Average hydrogen density in the beryllium reflector, lb/ft^3
$\bar{T}_C$	=	Average core temperature, ^oR
$\bar{T}_{Be}$	=	Average beryllium reflector temperature, ^oR

APPENDIX B

TEST CELL A LH_2 FLOW METERS

The LH_2 flow meters are nozzle - venturis with the inlet conforming to the definition of an ASME long radius nozzle and the pressure taps placed according to ASME requirements.* Details of the meters required to calculate the flow coefficients are as follows:

Nozzle-venturi	FE-7 Discharge	FE-4 Inlet
Throat diameter at ambient	3.626 in.	3.641 in.
Pipe diameter at ambient	7.981 in.	8.329 in.
Thermal contraction ambient to LH_2 temperature	3.1 mils/inch	3.1 mils/inch
Material	303 SS	303 SS
Discharge Coefficient*	0.995	0.99[illegible]
Compressibility effects (1/2%)	neglect	neglect

On the basis of the information above the following applies to flow rate calculations for Test Cell A.

* ASME Fluid Meters Their Theory and Application, 1959

For the pump inlet venturi, FE-4.

$$W = 7.01 \sqrt{\rho \Delta P} \qquad \frac{2\ LB}{S} < \dot{W}$$

$\dot{W}$ in lb/sec

ρ in lb/ft^3

ΔP in psid

The input data for FE-4 are:

SP-125-L LH_2 ΔP inlet venturi

SP-044-L LH_2 pressure upstream of inlet venturi

ST-020-N LH_2 temperature upstream of inlet venturi

SP-125 gives the ΔP for equation 1 and SP-044 and ST-020-N give the pressure and temperature required to obtain the density in equation B-1.

For the pump discharge venturi, FE-7.

$$W = 6.98 \sqrt{\rho \Delta P} \qquad \frac{2\ LB}{S} < \dot{W}$$

The input data for FE-7 are:

SP-126-L LH_2 ΔP discharge venturi

SP-05[illegible] LH_2 pressure upstream of discharge venturi

ST-018-N LH_2 temperature upstream of discharge venturi

APPENDIX C

ORIFICE SLEEVE PRESSURE DROP

The prediction of core pressure drop under ambient flow conditions involves primarily on analysis of a choked-flow condition existing across the flow channels of the core. For the most part, critical flow (sonic velocity) will exist through the orifices at the inlet of the core. This stems from the fact that the combined orifice flow area is less than the nozzle cross sectional throat area, i.e., 28 in.^{2}-orifices and 58 in.^{2} - nozzle throat. Consequently under ambient conditions choked flow will occur first in the orifices when sufficient flow is passed to result in a critical pressure ratio between core inlet and outlet conditions. At this early stage, the nozzle is not yet operating full (choked) so that the core exit pressure is nearly equal to atmospheric. Nozzle flow is defined isotropically, *

$$W = AP_0 \sqrt{\frac{g}{T_0 R}\left(\frac{2\gamma}{\gamma-1}\right)} \left(\frac{P}{P_0}\right)^{\frac{1}{\gamma}} \sqrt{1-\left(\frac{P}{P_0}\right)^{\frac{\gamma-1}{\gamma}}} \qquad \text{(C-1)}$$

This relationship is applicable to the definition of choked orifice behavior using a characteristic discharge coefficient (C_D). Under choked conditions the above equation reduces to:

$$W = C_D A P_0 \sqrt{\frac{\gamma g}{RT_0}} \left(\frac{2}{\gamma+1}\right)^{\frac{\gamma+1}{2(\gamma-1)}} \qquad \text{(C-2)}$$

---

* Symbols are defined at the end of this appendix.

As the flow through the reactor is increased, core inlet pressure is dictated principally by the behavior through the choked orifices coupled with friction choking in those channels which have the larger orifice sizes. Core inlet conditions with choked flow as such are independent of the conditions in the nozzle. With heat addition to the coolant in the core, channel pressure drop increases as well as core exit gas temperature so that choking in the orifices and channels becomes relieved when core exit temperature approaches a value that is less than four times the core inlet temperature. See the nozzle equation. Above a certain orifice size the flow is channel limited due to the frictional characteristics of the channel. This situation is identified by the comparison of critical flow calculated for a channel with a flow obtained for a given installed orifice size, i.e., calculated critical flow in the channel is less than through the orifice. In the assessment of core pressure drop under ambient conditions the combined flows limited by the orifices in the fuel elements, tie rod orifices and channels establishes a resulting core inlet pressure level. Limited flow in the channel is dependent on inlet Mach number and for adiabatic conditions is related by,

$$4\bar{f}\left(\frac{L\,max}{D}\right) = \frac{1-M^2}{\gamma M^2} + \frac{1-M^2}{\gamma M^2} + \frac{\gamma+1}{2\gamma}\ln\left[\frac{(\gamma+1)M^2}{2\left(1+\frac{\gamma+1}{2}M^2\right)}\right] \qquad \text{(C-3)}$$

Wher the channel is controlling the flow, the orifice is not choked and then it is necessary to use orifice parametric data which in turn gives a Mach number that is consistent with orifice and channel behavior. To define the flow conditions across the orifices, use is made of orifice test data. These orifice test data are presented in figure C-1 in terms of a generalized flow parameter and pressure ratio that is formulated from the nozzle flow equation. This parameter is defined by:

$$\frac{\omega}{AP_0}\sqrt{\frac{T_0 R}{g}} = \left(\frac{2\gamma}{\gamma-1}\right)^{1/2}\left(\frac{P}{P_0}\right)^{1/\gamma}\left[1-\left(\frac{P}{P_0}\right)^{\frac{\gamma-1}{\gamma}}\right]^{1/2} \qquad \text{(C-4)}$$

Orifice tests are conducted under conditions of reactor inlet design conditions.* Orifice tests were also conducted at different conditions of temperature, flow and pressure to confirm the validity of the generalized parameter. Consequently figure C-1 is useful to define orifice behavior at reactor off-design conditions. The generalized orifice parameter is also dependent on specific heat ratio so that there is a difference when the data is used for helium which has a specific heat ratio of 1.67. The isentropic nozzle relationship for helium is also shown in figure C-1.

Essential to the ambient pressure drop evaluation is utilization of the as-built orifice distribution. For instance if there is a greater proportion of large orifice sizes, there will be more channels affected by frictional considerations corresponding to higher core inlet pressure values. In this light ambient core pressure drop calculations are initiated prior to completion of core assembly and consequently an orifice distribution must be estimated for the prediction analysis. The predicted core pressure drop under ambient conditions is then verified at the conclusion of core assembly using the actual as-built orifice distribution.

* WANL-TME-871, NRX-A Core Orificing, J. C. Guzek, September 1964

REFERENCE		PREPARED BY	APPROVED BY	Astronuclear

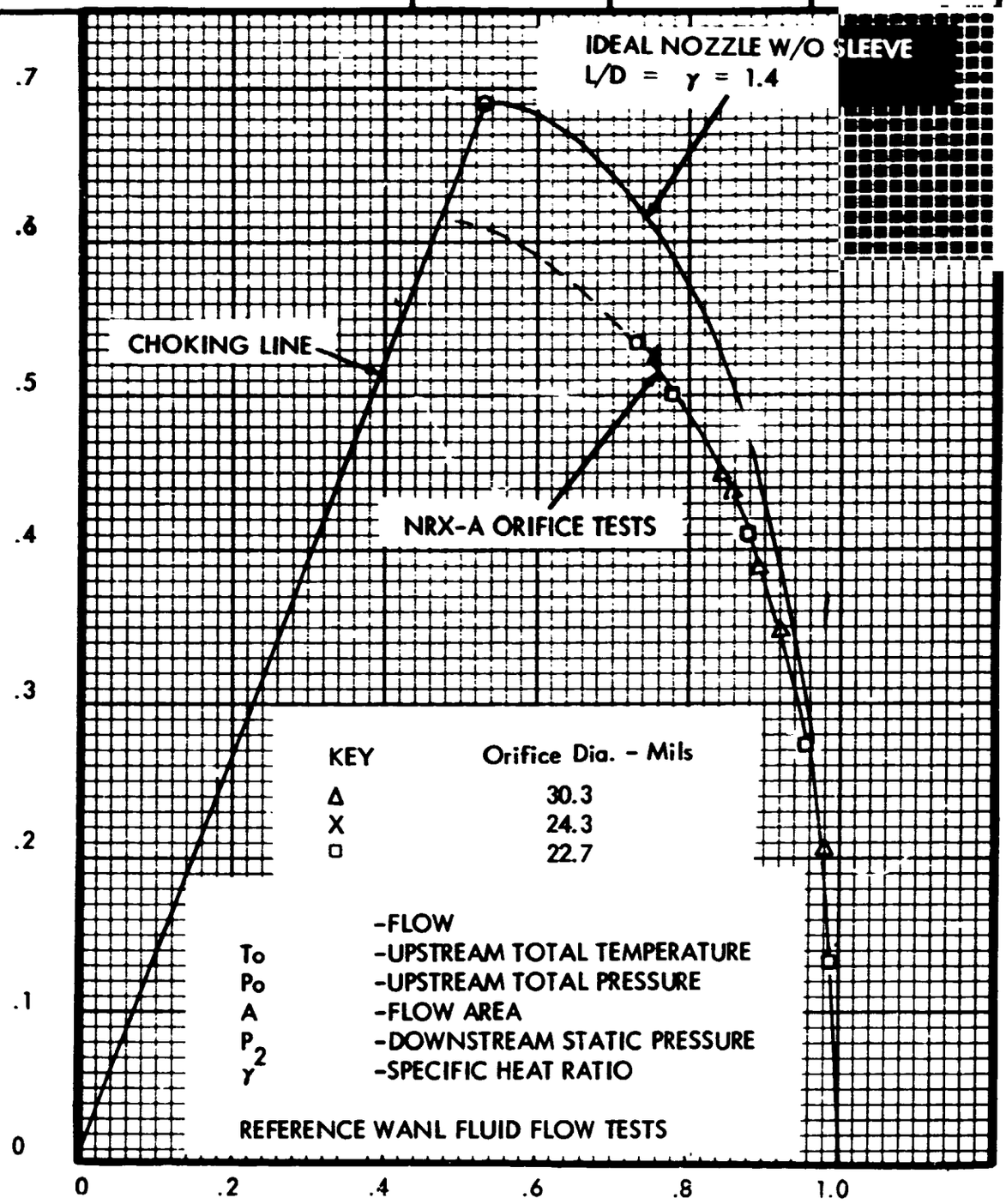

CURVE NO.	FIGURE NO.
	C-1

SYMBOL IDENTIFICATION

A	Cross section flow area - in.^{2}
C_D	Discharge coefficient - dimensionless
D	Channel diameter - inches
$\bar{f}$	Average friction factor - dimensionless
L	Channel length - inches
M	Mach number - dimensionless
P	Static pressure - lb/in.^{2} absolute
P_o	Total pressure - lb/in.^{2} absolute
T_o	Total temperature - Degrees Rankine
W	Gas flow - lb/sec
α	Specific head ratio - dimensionless

Constants

g	Gravitational constant - 32.2 ft/sec^2
R	Gas constant - ft/$^\circ$R

Thus,

$$T_c = 3815 \pm 215 \ ^\circ R$$

c. Thermal power calculation

From the equation in chapter 4

$$PWR = W(h_c - h_r)\,10^{-6}\,1055 + C$$

and the power was calculated to be 1096 MW at CRT 14085 using the values listed in table 4-6. To determine the 2σ error of the calculated power it is necessary to write the equation in terms of the measured variables (for which the 2σ error is known). Thus,

$$PWR = W(C\rho_c\ T_c - C\rho_r\ T_r)\,10^{-6}\,1055 + C \qquad \text{G-7}$$

Using equation (G-5) for Tc,

$$PWR = \left(C\rho_c\ \frac{(KAP_c)^2}{W} - C\rho r\ T_r W\right)10^{-6}\,1055 + C \qquad \text{G-8}$$

Now equation (G-1) is applied to the function for PWR given in (G-8). This leads to the relation,

$$\sigma_{PWR} = .001055\left\{\left(2\,h_c\ W\frac{\sigma KA}{KA}\right)^2 + \left(2h_c W\frac{\sigma\rho}{P_c}\right)^2 + \left(-h_c\sigma_w\right) + \left(-h_r W\frac{\sigma T_r}{T_r}\right)^2 + \left(\frac{\sigma_c}{.001055}\right)^2\right\}^{\frac{1}{2}}$$

Substituting the numerical values from table 4-6,

$$2\sigma_{PWR} = .001055\left\{(2 \times 13991 \times 75.6 \times 01)^2 + \left(2 \times 13991 \times 75.6 \times \frac{10.2}{581}\right)^2 + (13991 \times 1.4)^2 + \left(287 \times 75.6 \times \frac{5}{136}\right)^2 + \left(\frac{.2}{.001055}\right)^2\right\}^{1/2} = 49.5 \text{ MW}$$

Thus,

$$PWR = 1096 \pm 50 \text{ MW}$$

APPENDIX D

AGC U-TUBE NOZZLE S/N 9 DATA

The U-tube S/N 9 geometrical and heat transfer data supplied by Aerojet as input to the TNT code are tabulated in the following table. The first five columns contain, respectively: the nozzle area ratio, tube length measured from aft end of nozzle, tube hydraulic diameter, tube flow area, and tube heat transfer area. Column 6, RADN, contains the thermal radiation view factor between the core and nozzle. Finally, column 7, CG, contains the gas side Cg values. These values are used in a modified Bartz equation as follows:

$$Hg = Cg\left(\frac{\mu}{D}\right)^{0.2} \frac{Cp}{Pr^{0.6}} \left(\frac{4\,W_t\,T_b}{\pi D^2\,T_b}\right)^{0.8}$$

where

Hg	=	heat transfer coefficient
Cg	=	variable correlation given in Column 7
μ	=	viscosity
D	=	tube diameter
W_t	=	tube flow rate
T_b	=	bulk temperature
T_w	=	wall temperature
T_f	=	film temperature, $\frac{T_b + T_w}{2}$
Cp	=	specific heat
Pr	=	Prandt number

TK2	8.9999999E-03	A1E	1.0000000	AT	50.600000	XIT	22.000000
XIT1	17.000000	XNT1	180.00000	XNT2	360.00000	CLNI	1.0000000
CLNO	1.0000000	GPMULT	1.6000000	CMULT	1.0000000		

	AR	DIST	DE	AF	AS	DK	TK3	RADN	CG	HR	VELM
1	11.60	0	0.530	0.258	1.360	0.298	0.175E-01-0		0.470E-01-0		4.090
2	9.900	4.900	0.502	0.225	2.430	0.280	0.175E-01-0		0.400E-01-0		3.920
3	8.400	9.100	0.470	0.195	2.000	0.271	0.179E-01-0		0.365E-01-0		3.750
4	7.900	13.20	0.428	0.166	1.880	0.271	0.190E-01-0		0.352E-01-0		3.680
5	5.500	17.40	0.380	0.136	1.660	0.270	0.203E-01-0		0.280E-01-0		3.280
6	4.400	21.70	0.326	0.104	1.380	0.244	0.219E-01-0		0.220E-01-0		2.930
7	2.500	26.00	0.268	0.730E-01	0.923	0.228	0.232E-01-0		0.145E-01-0		2.420
8	1.800	28.00	0.240	0.580E-01	0.792	0.222	0.245E-01-0		0.117E-01-0		2.060
9	1.100	30.30	0.206	0.450E-01	0.311	0.218	0.270E-01-0		1.000E-02-0		1.390
10	1.060	31.50	0.195	0.400E-01	0.208	0.220	0.290E-01-0		1.000E-02-0		1.280
11	1.000	32.50	0.175	0.380E-01	0.204	0.227	0.200 -0		0.200E-01-0		1.000
12	1.100	33.70	0.190	0.430E-01	0.231	0.216	0.195	0.900E-01	0.170E-01-0		0.690
13	1.250	34.90	0.205	0.480E-01	0.261	0.205	0.191	0.170	0.168E-01-0		0.550
14	1.500	36.10	0.220	0.530E-01	0.290	0.194	0.188	0.170	0.164E-01-0		0.430
15	2.000	37.50	0.237	0.600E-01	0.489	0.181	0.183	0.175	0.165E-01-0		0.300
16	3.200	40.00	0.267	0.710E-01	0.835	0.158	0.206	0.180	0.183E-01-0		0.180
17	4.900	42.40	0.295	0.810E-01	1.560	0.135	0.230	0.180	0.227E-01-0		0.120
18	10.55	48.50	0.220	0.540E-01	1.520	0.175	0.310	0.240	0.370E-01-0		0.500
19	15.40	53.70	0.255	0.660E-01	1.520	0.151	0.348	0.392	0.467E-01-0		0.400
20	17.20	58.10	0.283	0.740E-01	1.420	0.135	0.500	0.300	0.506E-01-0		0.350
21	17.20	62.10	0.283	0.740E-01	1.420	0.135	0.500	0.400	0.572E-01-0		0.350
22	17.20	65.90	0.283	0.740E-01	0.710	0.135	0.500	0.600	0.636E-01-0		0.350
Column No.	1	2	3	4	5			6	7		

Astronuclear

INDEX NO.

TABLE D-1 - "U"-TUBE S/N 9 GEOMETRICAL AND HEAT TRANSFER DATA SUPPLIED BY AEROJET

PREPARED BY	APPROVED BY	CURVE NO.

APPENDIX E

EFFECT OF LEAKAGE AROUND STATION 32 THERMOCOUPLES

All NRX-A2 thermocouples at station 32 with one exception indicated temperatures as much as 1200°R lower than what would be expected on the basis of temperatures at other stations. Post-run observations indicated the potting had failed around the suspect thermocouples thus allowing flow in the channel through which the thermocouple was inserted. An analysis was made to determine if the low temperature readings could be attributed solely to leakage flow.

A model of the unfueled element with a 0.036 inch OD thermocouple in a 0.100 inch channel was constructed. The 0.100 inch channel was assumed to exhaust at the 32 inch length to a core interstitial pressure of 632 psia. This assumes no pressure buildup due to increased interstitial flow. The boundary conditions at the ID of the pyro sleeves were imposed consistent with converged tie rod-fuel element thermal and hydraulic solutions. The exterior surfaces of the unfueled element were assumed to be at fuel element temperature. Under normal operating conditions heat flow is from the unfueled element to the fueled element. With leakage around the station 32 thermocouple there is heat flow from the fueled to unfueled element in the local area around the thermocouple channel, however, the total heat transferred from the fueled element is not large enough to significantly affect the isothermal boundary assumption.

Based on the above assumptions the analysis was made using the TOSS-MCAP thermal-hydraulic code to determine the temperature distributions at several axial stations in the unfueled element as well as the coolant temperature and flow rate around the thermocouple.

The temperature distribution in the unfueled element at station 32 is shown in figure D-1. This temperature distribution is for a control room time of 14885 during EP IV. Figure D-1 shows a minimum material temperature of 3137°R and a maximum material temperature of 3650°R. The analysis indicated the coolant flow rate around the thermocouple was 2.7×10^{-3} lb/sec and the coolant temperature at station 32 was 2736°R. At this control room time the good station 32 thermocouple was reading 3870°R and the others read between 2450°R and 3800°R. It can generally be concluded that the station 32 thermocouples were probably reading the temperature which they saw during EP IV.

REFERENCE	PREPARED BY	APPROVED BY
	[redacted]	[redacted]

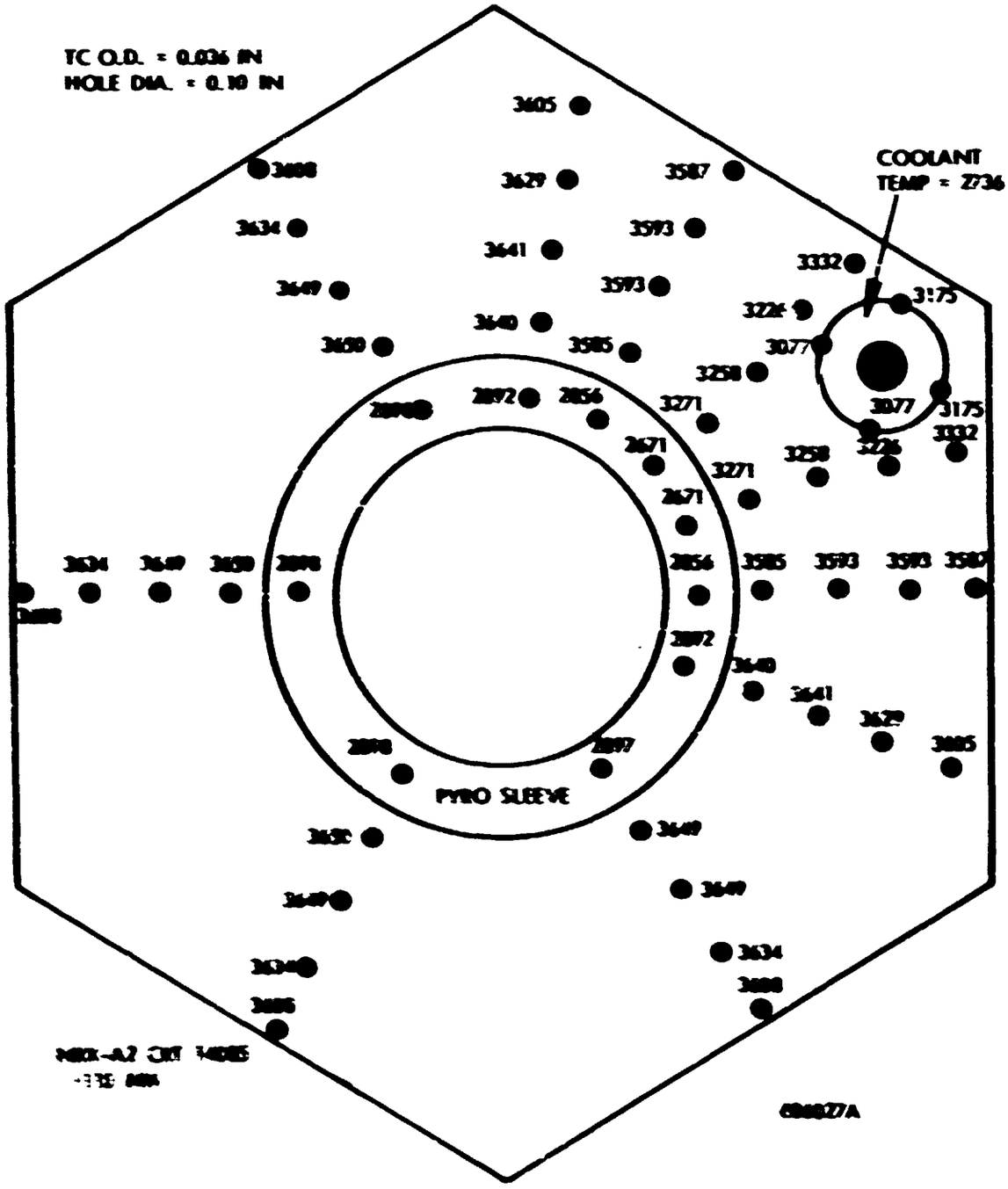

TEMPERATURE DISTRIBUTION IN UNFUELED ELEMENT AT STATION 32 WITH FLOW AROUND THERMOCOUPLE

FIGURE NO.

E - 1

APPENDIX F

METHOD USED IN MULTIPLE REGRESSION CODE

The multiple regression code develops a correlation between the measured dependent variable and those independent variables which have physical significance to the problem. The deviation of the measured values of the dependent variable from the correlation can then be analyzed as random variations.

All independent variables which may affect the dependent variables are input quantities to the code. The order in which variables are entered into the correlation depends on the value of the correlation coefficient. The independent variable with the highest correlation coefficient with the dependent variable is entered first. After each new variable is entered a new correlation is developed using the method of least squares.

After each least squared fit an "F" level is determined for the last variable entered. The "F" level is a measure of how much the new variable adds to the correlation. The "F" level for the first variable entered is described by the equation:

$$F = \frac{\dfrac{\sum_i^N (Y_i - \bar{Y})^2}{N-1} - \dfrac{\sum_i^N (Y_i - \hat{Y}_{1i})^2}{N-2}}{\dfrac{\sum_i^N (Y_i - \hat{Y}_{1i})^2}{N-2}}$$

where,

Y_i = measured value of dependent variable

$\bar{Y}$ = average measured value of dependent variable

$\hat{Y}_{ii}$ = $a + b \times (1)$

N = Number of data points

X = Independent variable

for the k th term entered the F level is described as

$$F_K = \frac{\dfrac{\sum_i^N (Y_i - \hat{Y}_{(k-1)_i})^2}{N-k} - \dfrac{\sum_i^N (Y_i - \hat{Y}_{k_i})^2}{N-(k+1)}}{\dfrac{\sum_i^N (Y_i - \hat{Y}_{k_i})^2}{N-(k+1)}}$$

where,

$$\hat{Y}_{k-1} = a + b \times (1) + c \times (2) + --- L \times (k-1)$$

$$\hat{Y}_k = a + b \times (1) + c \times (2) + --- L \times (k)$$

The "F" level indicates the degree of physical significance of the variable under consideration. If a variable has an "F" level above a certain value it has physical significance to the problem and is entered into the correlation, below a certain value it does not have physical significance and is not entered in the correlation. The proper "F" levels for entering and removing variables were determined from the Table of the "F" Distribution. The "F" level of a variable may change as other variables are entered into the correlation. For this reason the "F" level of each variable is checked after a new variable is added and if the "F" level has become too low the variable is dropped from the correlation.

APPENDIX G

NRX-A2 TEST CELL A DATA ACCURACY AND EXAMPLES

A consistent method of handling the error in the NRX-A2 test data was established and is described in part 1 of this appendix. Part 2 contains examples of the 2σ deviation or error of composite functions calculated from individual independent data channels according to probability theory. The examples selected are the calculation of reactor flow rate, nozzle chamber temperature, and total reactor power at the maximum power hold (CRT 14085 seconds).

Part 1 - NRX-A2 Test Data Estimated Error. Based on WANL analysis of data of 15 channels of low level multiplex data, the following are the results of a statistical analysis:

Type Error	Standard Deviation in % of Full Scale
System Error	0.675
Zero Error	0.206
Drift Error	0.680
Combined Error	0.97

For 95% (2σ) confidence level, the error is 2.145 times the 15 sample standard deviation, i.e., 2.145 x 0.97% = 2.08%, for the data acquisition system. Allowing a 1/2% reading error from plotted data the error is 2.14% of full scale, i.e., $(2.08^2 + 0.5^2)^{1/2} = 2.14$.

In addition to the data acquisition system error a transducer error of 1% of full scale for pressures and temperatures was applied. This led to the overall error for the low level multiplex data of 2.4% of full scale, i.e., $(2.14^2 + 1.^2)^{1/2} = 2.4$.

For 95% (2σ) confidence level the error was assumed to be 2.4% of full scale for all individual pressure and temperature transducer data collected during the test and plotted on the Calcomp plotter.

The 2σ deviation of a function of several of the individual data channel measurements was obtained by combination of the individual channel errors according to probability theory. For X, an arbitrary function of independent random variables X1, X2, X3, ''', Xn, the deviation of X defined as σ is given by,*

$$\sigma^2 = \sum_{i=1}^{N} \left(\frac{\partial X}{\partial X_i}\right)^2 \sigma_i^{\,2} \qquad \text{G-1}$$

where σ_i = the deviation of Xi (in same units as Xi)

Part 2 - Calculation of flow, chamber temperature, power, and their deviation at Maximum Power Hold.

a. Flow rate calculation

From Appendix B the equation for the calculation of discharge venturi (FE-7) flow is,

$$W = k\,(\rho \Delta P)^{1/2} \qquad \text{G-2}$$

and the following data was used to calculate flow rate at the high power hold, DRT 14085 seconds

Symbol	Channel	Designation	Value	Full Range	(2.4% of Full Range)
P	SP-057-L	LH_2 pressure upstream FE-7	922 psia	1000 psig	24 psi
T	ST-018-N	LH_2 temperature upstream FE-7	47.2°R	54°R	1.3°R
ΔP	SP-126-L	FE-7 venturi ΔP	26.1 psid	50 psid	1.2 psid
ρ			4.50 $\frac{lb}{ft^3}$		
K		Coefficient in Eq. G-2	6.98		±1%

Thus, for the discharge venturi FE-7,

$$W = (6.98)(4.5 \times 26.1)^{1/2} = 75.8\ \frac{LB}{SEC}$$

In order to determine the accuracy of the flow, equation (G-1) is applied to the relation for W in equation (G-2).

---

* All symbols are defined on last page of this appendix.

$$\frac{\partial W}{\partial k} = \rho^{1/2} \Delta P^{1/2}$$

$$\frac{\partial W}{\partial \Delta P} = k \quad \rho^{1/2} \Delta P^{-1/2} (.5)$$

$$\frac{\partial W}{\partial T} = \frac{\partial W}{\partial} \frac{\partial \rho}{\partial T} = k \quad \Delta P^{1/2} \rho^{-1/2} (0.5) \frac{\partial \rho}{\partial T}$$

$$\frac{\partial W}{\partial P} = \frac{\partial W}{\partial \rho} \frac{\partial \rho}{\partial P} = k \quad \Delta P^{1/2} \rho^{-1/2} (0.5) \frac{\partial \rho}{\partial P}$$

Substituting these derivatives into equation (G-1) and using the definition of W in equation (G-2) gives,

$$\text{G-3} \quad \left(\frac{\sigma W}{W}\right)^2 = \frac{1}{4}\left(\frac{\sigma \Delta P}{\Delta P}\right)^2 + \frac{1}{4}\left(\frac{\sigma_T}{\rho} \frac{\partial \rho}{\partial T}\right)^2 + \frac{1}{4}\left(\frac{\sigma P}{\rho} \frac{\sigma P}{\rho} \frac{\partial \rho}{\partial P}\right)^2 + \left(\frac{\sigma k}{k}\right)^2$$

$\frac{\sigma \rho}{\sigma T} \cong 0.07 \frac{lb}{Ft^3 \cdot R}$ AND $\frac{\sigma \rho}{\sigma P} \cong .00045 \frac{lb}{Ft^3 \text{ psi}}$ from property tables.

Inserting these values and the numerical values of W, ΔP, ρ, and the 2σ's from the preceding tabulation gives the numerical value of the 2σ limit on W.

$$2\sigma W = 75.8 \frac{lb}{sec} \left\{ \frac{1}{4}\left(\frac{1.2}{26.1}\right)^2 + \frac{1}{4}\left(\frac{1.3}{4.5} \cdot .07\right)^2 + \frac{1}{4}\left(\frac{24}{4.5} .00045\right)^2 + (0.1)^2 \right\}^{\frac{1}{2}}$$

$$2\sigma = 2.05 \frac{lb}{sec}$$

Thus, $W = 75.8 \pm 2.05 \frac{lb}{sec}$

Similarly the flow and flow accuracy was calculated for the pump inlet venturi,

$$W = 75.4 \pm 2.10 \frac{lb}{sec}$$

Taking the average of the two measurements the error is further reduced,

$$W = 75.6 \pm 1.5 \frac{lb}{sec} \qquad \left[\left(\frac{2.05}{2}\right)^2 + \left(\frac{2.10}{2}\right)^2\right]^{1/2} = 1.5$$

b. Nozzle chamber temperature calculation

The equation for choked nozzle flow is given in chapter 4 as,

$$W = \frac{K A P_c}{T_c^{1/2}} \qquad \text{G-4}$$

or

$$T_c = \frac{K^2 A^2 P_c^2}{W^2} \qquad \text{G-5}$$

and the following data is used at the high power hold, CRT 14085 seconds

Symbol	Channel	Designation	Value	Full Range	2 and source
Pc	P-122	Nozzle chamber pressure	579 psia	600 psia	14.4 psia
Pc	P-124	Nozzle chamber pressure	584 psia	600 psia	14.4 psia
Pc		Average nozzle chamber pressure	581.5 psia	-	10.2 psia $(\frac{14.4}{\sqrt{2}})$
A		Flow area at operating conditions	59.0 in^2		.59 in^2 (1% accounts for product KA)
K		Nozzle coefficient	0.136 $\frac{^oR}{sec}$		(Included in 2σ for A above)
W		Flow Rate	75.6 $\frac{lb}{sec}$		1.4 lb (this appendix)
					$1.5\sqrt{sec}$

Thus

$$T_c = \left(\frac{(59)\ (.136)\ (581.5)}{(75.6)}\right)^2 = 3815^\circ R$$

In order to determine the accuracy of the chamber temperature, equation (G-1) is applied to the relation for Tc in equation (G-5) and,

$$\frac{\partial Tc}{\partial W} = -2\frac{Tc}{W}$$

$$\frac{\partial Tc}{\partial (KA)} = 2\frac{Tc}{KA}$$

$$\frac{\partial Tc}{\partial Pc} = 2\frac{Tc}{Pc}$$

These derivatives are substituted into equation (G-1),

$$\left(\frac{\sigma T}{Tc}\right)^2 = \left(2\frac{\sigma\omega}{W}\right)^2 + \left(2\frac{\sigma KA}{KA}\right)^2 + \left(2\frac{\sigma p}{Pc}\right)^2 \qquad \text{G-6}$$

Substituting the values from the tabulation above leads to,

$$2\sigma Tc = 3815\left\{\left(2\frac{1.4}{75.6}\right)^2 + (2 \times .01)^2 + \left(2\frac{10.2}{581.5}\right)^2\right\}^{\frac{1}{2}} = 215\,°R$$

Thus,

$$T_c = 3815 \pm 215 \ ^\circ R$$

c. Thermal power calculation

From the equation in chapter 4

$$PWR = W(h_c - h_r)\,10^{-6}\,1055 + C$$

and the power was calculated to be 1096 MW at CRT 14085 using the values listed in table 4-6. To determine the 2σ error of the calculated power it is necessary to write the equation in terms of the measured variables (for which the 2σ error is known). Thus,

$$PWR = W(C\rho_c\ T_c - C\rho_r\ T_r)\,10^{-6}\,1055 + C \qquad \text{G-7}$$

Using equation (G-5) for Tc,

$$PWR = \left(C\rho_c\ \frac{(KAP_c)^2}{W} - C\rho r\ T_r W\right)10^{-6}\,1055 + C \qquad \text{G-8}$$

Now equation (G-1) is applied to the function for PWR given in (G-8). This leads to the relation,

$$\sigma_{PWR} = .001055\left\{\left(2\,h_c\ W\frac{\sigma KA}{KA}\right)^2 + \left(2h_c W\frac{\sigma\rho}{P_c}\right)^2 + \left(-h_c\sigma_w\right) + \left(-h_r W\frac{\sigma T_r}{T_r}\right)^2 + \left(\frac{\sigma_c}{.001055}\right)^2\right\}^{\frac{1}{2}}$$

Substituting the numerical values from table 4-6,

$$2\sigma_{PWR} = .001055\left\{\left(2 \times 13991 \times 75.6 \times 01\right)^2 + \left(2 \times 13991 \times 75.6 \times \frac{10.2}{581}\right)^2 + \left(13991 \times 1.4\right)^2 + \left(287 \times 75.6 \times \frac{5}{136}\right)^2 + \left(\frac{.2}{.001055}\right)^2\right\}^{1/2} = 49.5 \text{ MW}$$

Thus,

$$PWR = 1096 \pm 50 \text{ MW}$$

W	Reactor flow rate, lb/sec
ρ	Hydrogen density upstream of venturi, lb/ft^3
ΔP	Venturi ΔP, psid
T	Temperature upstream of venturi, ^oR
P	Pressure upstream of venturi, psia
K	Coefficient in nozzle equation, $^oR/sec$
A	Nozzle throat area at operating conditions, in^2
Pc	Nozzle chamber pressure, psia
Tc	Nozzle chamber temperature, ^oR
PWR	Total reactor thermal power, MW
hc	Nozzle chamber enthalpy, Btu/lb
hr	Reflector inlet enthalpy, Btu/lb
C	Gamma heating in nozzle and thermal radiation heat transfer to nozzle, MW
Cp_c	Specific heat hydrogen in nozzle chamber, defined as hc/Tc, Btu/lb^oR
Cp_r	Specific heat of hydrogen at reflector inlet, defined as hr/Tr, Btu/lb^oR
X, Xi	Defined as discussion of equation (G-1), this appendix
σy	The standard deviation or error of a variable y given in same units as y.

~~CONFIDENTIAL~~
~~RESTRICTED DATA~~

Astronuclear Laboratory

TECHNICAL FILM

A motion-picture film supplement WANL-MP65-1, carrying the same classification as the report, is available on loan. Requests will be filled in the order received. You will be notified of the approximate date scheduled.

The film (16 mm, 28 min, color and black and white, sound) shows the complete power test and restart.

Requests for the film should be addressed to:

H. F. Faught
NERVA Program Management
Post Office Box 10864
Pittsburgh, Pennsylvania - 15236

NOTE: The handling of requests for this classified film will be expedited if application for the loan is made by the individual to whom this copy of the report was issued. In line with established policy, classified material is sent only to previously designated individuals. Your cooperation in this regard will be appreciated.

Date _____

Please send, on loan, copy of film supplement WANL-MP65-1 to:

_____
Name of organization

_____
Street number

_____
City and State Zip Code

Attention*: Mr. _____

Title _____

*To whom copy of the WANL-TNR-199 was issued

~~CONFIDENTIAL~~
~~RESTRICTED DATA~~